

University of Strathclyde  
Department of Biomedical Engineering  
A Cystic Fibrosis Infection Monitor

Andrew Ward MEng(Hons)

A thesis presented in the fulfilment of the requirements for the  
degree of Doctor of Engineering

2015

This thesis is the result of the author's original research. It has been composed by the author and has not been previously submitted for examination which has led to the award of a degree.

The copyright of this thesis belongs to the author under the terms of the United Kingdom Copyright Acts as qualified by University of Strathclyde Regulation 3.50. Due acknowledgement must always be made of the use of any material contained in, or derived from, this thesis.

Signed:

## ABSTRACT

*P. aeruginosa* causes chronic infections in people with the inherited disorder, cystic fibrosis (CF). These chronic infections result in a high rate of morbidity and mortality. Once established, the infections are almost impossible to eradicate. Pulmonary exacerbations, thought to be caused by *P. aeruginosa*, result in further damage that leads to deterioration in lung performance. A sensor that would allow rapid, near patient testing of sputum samples would be a valuable addition to CF care by enabling more proactive identification of lung infections.

In this study, a sensor has been developed using low cost screen printing in conjunction with electrochemical impedance spectroscopy for the detection of *P. aeruginosa*. Screen printed electrodes were developed and characterised. An impedance normalisation approach, developed in previous work, was used to identify characteristic changes in the impedance signature during the growth of *P. aeruginosa*. Changes in the normalised impedance were observed under aerobic conditions in standard laboratory media and also under conditions more representative of the CF airway. Specifically, testing was carried out in a number of different scenarios, culminating in tests in an artificial sputum medium that show *Pseudomonas aeruginosa* can be detected in the presence of *Staphylococcus aureus*, *Haemophilus influenzae* or *Candida albicans*.

Investigations using mutant strains of *P. aeruginosa* PA14 demonstrate that the changes in impedance are largely related to the production of redox active phenazine compounds, including pyocyanin. Slight changes in the impedance were observed with *S. aureus* and *H. influenzae*, but were not the same as those observed with *P. aeruginosa*. This suggests that the sensor could be clinically useful for the detection of *P. aeruginosa* in patients with CF.

After gaining the appropriate ethics approval, a pilot study was also carried out in human sputum samples from CF patients. This study involved further development of the electrode and anecdotally suggests that the presence of *P. aeruginosa* could be detectable in sputum from patients.

Future development should focus upon the optimisation of the device through effective integration into a sample pot which could include an increase in the number of electrodes used per sample, adjustment of the potential for more sensitive detection of pyocyanin and improvements in the consistency achieved between sensors.

## **ACKNOWLEDGEMENTS**

My thanks go to both my supervisors, Trish and Nick, for their help, guidance and useful discussion over the course of the project. My thanks also to those who worked in the Wolfson and for their many helpful suggestions, including Brain Cartlidge, Katie Henderson and Stephen Milne. Without the help of the following scientists from the Hay laboratory, I would still be learning how to pour agar plates and use a pipette, so I am enormously grateful to the following people for teaching me the tools of microbiology: Paul Herron, Paul Hoskisson, Lewis Stewart, Alison MacFadyen, Jana Hiltner, Leena Nieminen, James McSorley and Kirsty Robb.

I'd like to acknowledge the funding provided by the EPSRC and in particular the structure of the Doctoral Training Programme, which provided the basis and flexibility to enable this study to take place.

Finally, I want to thank my family for all the support they have provided, since the day I decided to leave my job to pursue a new ambition. Last but certainly not least, I want to thank Selina for her love and wisdom, and for keeping me sane throughout my thesis write up.

## LIST OF PUBLICATIONS

The following publications resulted from the work in this thesis:

1. Ward AC, Connolly P, Tucker NP (2014) *Pseudomonas aeruginosa* can be detected in a polymicrobial competition model using impedance spectroscopy with a novel biosensor. PLoS ONE 9:e91732
2. Ward AC, Tucker NP, Connolly P (2014) Development of a diagnostic device to detect different *Pseudomonas aeruginosa* phenotypes in medically relevant contexts. 2014 36th Annual International Conference of the IEEE Engineering in Medicine and Biology Society (EMBC) 2757–2760

## SYMBOLS

$\Delta\Phi$	Interface potential
$\Delta\Phi_e$	Potential when interface is at equilibrium
A	Absorbance
A	Area
<i>a</i>	Particle radius
b	Light path-length
B	Susceptance
$\beta$	Function of the number of relaxation times within a dielectric
$\beta$	Transfer co-efficient
C	Molar concentration
$c_0$	Ion concentration of electrolyte
$c_i$	Concentration of species <i>i</i>
C	Capacitance
$C_{dl}$	Double layer capacitance
$C_{GC}$	Gouy-Chapman capacitance
$C_H$	Helmholtz capacitance
<i>CPE</i>	Constant phase element
$C_s$	Faradic series pseudocapacitance
$C_S$	Stern capacitance
$C_{series}$	Series capacitance
<i>D</i>	Diffusion coefficient
d	Distance
$e_0$	Electron charge ( $1.6 \times 10^{-19}$ C)
$\varepsilon$	Extinction coefficient
$\varepsilon^*$	Complex permittivity
$\varepsilon'$	Real permittivity
$\varepsilon''$	Imaginary permittivity
$\varepsilon_0$	Permittivity of Free Space
$\varepsilon_r$	Relative permittivity
<i>F</i>	Faraday constant ( $9.6472 \times 10^4$ Cmol <sup>-1</sup> )
$f_r$	Frequency of maximum dielectric loss

$\vec{F}$	Vector of applied force
G	Conductance
g	Grams
Hz	Hertz
I	Current
$i_0$	Exchange current
$i_{an}$	Net anodic current
$i_{cath}$	Net cathodic current
j	Imaginary unit ( $\sqrt{-1}$ )
$j_i$	Current density
$J_i$	Diffusion flux of species $i$
$J_T$	Total current density
K	Magnitude of CPE
$k$	Boltzmann's constant ( $1.380 \times 10^{-23} \text{ J K}^{-1}$ )
$\kappa^{-1}$	Debye- Hückel reciprocal length
l	Litres
m	Mass of ion
M	Molar
N	Number of collisions
$N_A$	Avogadro constant ( $6.0221 \times 10^{23} \text{ mol}^{-1}$ )
$\eta$	Viscosity
$n_i^0$	Bulk concentration of ion species $i$
$\rho$	Resistivity
$\psi_0$	Outer potential at the electrode
$\psi_M$	Potential at the electrode interface
$\psi_x$	Potential at point $x$
$r$	Radius of ion
R	Real gas constant
R	Resistance
$R_{ct}$	Charge transfer resistance
$R_f$	Faradic resistance
$R_n$	Normalised resistance

$R_{series}$	Series resistance
$R_{sol}$	Solution resistance
$\theta$	Phase angle (degrees)
$\sigma$	Conductivity
$\Omega$	Ohms
T	Temperature
t	Time elapsed
$t_i$	Transport number of ion species $i$
$\tau$	Mean time between collisions
$\tau$	Characteristic relaxation time
$\bar{\mu}_{abs}$	Ion mobility
$\mu_{conv}$	Ion mobility in applied electric field
V	Volts/Voltage
$\vec{v}$	Velocity vector
$v_d$	Drift velocity
$\omega$	Angular frequency
$\omega_{max}$	Frequency in rad/sec at top of arc in complex plane
$x$	Distance
X	Force of applied electric field
Y	Admittance
Z	Complex impedance
$ Z $	Impedance modulus
$Z'$	Resistance
$Z''$	Reactance
$z_i$	Charge number of ion $i$
$Z_{pt}$	Impedance of individual platinum electrodes
$Z_{spt}$	Solution resistance
$Z_{Tp}$	Platinum-platinum pair impedance
$Z_w$	Warburg impedance
$Z_x$	Unknown electrode impedance
$z_i$	Valance of ion species $i$



## ABBREVIATIONS

ABPA	Allergic Bronchopulmonary Aspergillosis
AC	Alternating Current
Ag-AgCl	Silver-Silver Chloride
ASM	Artificial Sputum Media
Bcc	<i>Burkholderia cepacia</i> complex
CDC	Centre for Disease Control
CE	Counter Electrode
CF	Cystic Fibrosis
CFTR	Cystic Fibrosis Transmembrane Regulator
CFU	Colony Forming Units
CLSM	Confocal Laser Scanning Microscopy
CPE	Constant Phase Element
CRP	C-reactive Protein
CV	Crystal Violet
CV	Coefficient of Variance
DC	Direct Current
DNA	Deoxyribonucleic acid
DTT	Dithiotheritol
EIS	Electrochemical Impedance Spectroscopy
ELITE	EarLy Inhaled Tobramycin for Eradication
EPS	Extra Polymeric Substances
EtOH	Ethanol
FEV	Forced Expiratory Volume
GFP	Green Fluorescent Protein
HF	High Frequency
HTA	Haemophilus Test Agar
HTM	Haemophilus Test Media
ITO	Indium Tin Oxide
LB	Luria Bertani
LF	Low Frequency
MeOH	Methanol
MFC	Microbial Fuel Cell
MHA	Mueller Hinton Agar
MHB	Mueller Hinton Broth
MSA	Mannitol Salt Agar
NaCl	Sodium Chloride

NHS	National Health Service
OCP	Open Circuit Potential
OD	Optical Density
PAB	Pseudomonas Agar Base
PBS	Phosphate Buffered Saline
PE	Polyethylene
PIA	Pseudomonas Isolation Agar
POCT	Point of care testing
PQS	<i>Pseudomonas</i> quinolone signal
Pt	Platinum
QS	Quorum sensing
Rad/sec	Radians per second
RCT	Randomised Control Trial
RE	Reference Electrode
RMS	Root mean square
RNS	Reactive Nitrogen Species
ROS	Reactive Oxygen Species
SD	Standard Deviation
SEM	Scanning Electron Microscopy
SPCE	Screen Printed Carbon Electrode
TSB	Tryptone Soy Broth
TSB-YE	Tryptone Soy Broth with Yeast Extract
UV	Ultraviolet
V	Volts
VOC	Volatile Organic Chemical
WE	Working Electrode
YE	Yeast Extract

## **GLOSSARY OF TERMS**

Anaerobic grow	Growth of a microorganism in the complete absence of oxygen.
Anodic current	Involves the transfer of electrons from the electrolyte to the electrode, in conjunction with oxidation within the electrolyte.
Bacteriophage	A virus that infects bacterial cells.
Bio-affinity	A protein or recognition element attached to a sensor, which has a high affinity for the analyte.
Biofilm	Growth of bacteria or fungi in colonies protected from destruction by a self produced extra polymeric matrix.
Biofilm matrix	The protective layers of material surrounding microbial cells in a biofilm, that afford the organisms protection from antimicrobial attack.
Capacitance	The storage of energy in an electric field, generally resulting from the turning of dipoles within the dielectric.
Cathodic current	Involves the transfer of electrons from the electrode to the electrolyte, in conjunction with reduction within the electrolyte.
Charge Transfer	The transfer of electrons across an electrode-electrolyte interface.
Ciprofloxacin	Antibiotic that inhibits DNA gyrase which is most effective in Gram negative organisms.
Colistin	Antibiotics with detergent action, that function by disrupting phospholipids in the cell membrane.
Commensal	A microorganism living on or in a host without causing infection or disease.
C-reactive Protein	Acute phase systemic protein released by the liver in response to inflammation.
Death phase	Decline of microorganism population in the long term absence of nutrients.

Dielectric spectroscopy	Analysis of the dielectric properties of a sample through its impedance spectrum. The dielectric properties relate to the charging current resulting from the rotation of dipoles within the sample.
Dipoles	Polar molecules that turn to orient themselves in an electric field, thus leading to energy storage.
DNA profiling	Use of molecular techniques to identify the presence of microorganisms or genes by looking for sequences of DNA.
Double layer	The capacitance between the electrode and the layer of molecules adsorbed to the electrode surface.
Electroactive secondary metabolites	Compounds secreted by microorganisms near the end of exponential growth, that are also redox active.
Electrode	The component within an electrochemical cell that interfaces directly with the electrolyte.
Electrode active area	The area of an electrode that can participate in chemical reactions and affect the performance of the electrode.
Electrolyte	The solutions in an electrochemical cell that connects the electrodes.
Faradaic current	Current that results from the transfer of charge across an electrode-electrolyte interface.
Fastidious organism	An organism with a strict set of growth requirements.
Fermentation	Metabolic production of ATP through substrate level phosphorylation.
Fimbria	Filamentous structures on the outside of bacterial cells, often present in large numbers. May play a role in cell-surface attachment.
Flagellum	Tail like appendage used for motility.

Gram negative	The group of bacteria with one cell membrane surrounded by a thick peptidoglycan cell wall.
Gram positive	The group of bacteria with an inner and outer cell membrane, with a thin peptidoglycan cell wall in between.
Lag phase	Microorganism cell repair and recovery in the presence of abundant nutrients, prior to log phase growth.
Log phase	Constant cell division of bacteria or microorganisms when there is an abundance of required nutrients.
Microaerophilic	Microbial growth in an environment in with a lower oxygen concentration than atmospheric.
Morphological	Observed characteristics of growth of a particular microorganism, covering aspects such as shape and size of colonies (on agar plates), growth colour, growth rate.
Mutant	The strain of a species that has a genetic change, possibly resulting in a different phenotype to the wild type strain.
Non-Faradaic current	Charging current that results from the capacitive component of the electrochemical cell, and does not involve charge transfer.
Non-motile	A phenotype characterised by a lack of movement from an organism, for example because it is not expressing motility genes such as those required for flagella or pili.
Normalisation	In the context of this thesis, normalisation means division of an impedance parameter at a given timepoint against the same measurement at the first timepoint.
Phase Angle	The angle formed between the resistive and reactive measurements of the impedance, when viewed on a complex plane plot.
Phenotype	Collection of a specific set of characteristics of a species.

Pilus	Small bacterial appendage used for a variety of functions, including movement across a surface and toxin injection into eukaryotic cells.
Planktonic	Single free floating microbial cell, not surface attached.
Proton motive force	A concentration gradient of protons created on the outside of bacterial cells, which is used for cellular functions (such as ion transport and flagella rotation).
Pyocyanin	Phenazine small molecule secondary metabolite produced and excreted by <i>P. aeruginosa</i> .
Quorum sensing	Intercellular chemical communication mechanism used by bacteria to sense cell density and subsequently regulate gene expression.
Reactance	The out of phase component of impedance resulting from capacitive or inductive elements within the circuit.
Respiration	Catabolic reactions that product ATP through an electron transport chain with organic or inorganic compounds as the final electron acceptors.
Sessile	Non motile bacteria cell, often attached to a surface.
Stationary phase	Existence of bacteria or other microorganism when insufficient nutrients exist to support further cell division.
Swarming motility	Movement across a surface, such as agar, through the use of flagella.
Tobramycin	An aminoglycoside antibiotic that works by inhibiting protein synthesis.
Virulence factor	Protein or other compound produced by microorganisms which cause host damage or stimulate an immune response.
Volatile organic compounds	Compounds with a high vapour pressure that readily evaporated at room temperature.

Wild type	The natural strain of a species, with no genetic modification or mutation.
Working electrode	The electrode of interest in an electrochemical cell, where reactions are monitored.

## CONTENTS

<b>ABSTRACT.....</b>	<b>iii</b>
<b>ACKNOWLEDGEMENTS .....</b>	<b>iv</b>
<b>LIST OF PUBLICATIONS .....</b>	<b>v</b>
<b>SYMBOLS.....</b>	<b>vi</b>
<b>ABBREVIATIONS.....</b>	<b>ix</b>
<b>GLOSSARY OF TERMS.....</b>	<b>xi</b>
<b>CONTENTS.....</b>	<b>xvi</b>
<b>1 LITERATURE REVIEW.....</b>	<b>1</b>
1.1 Introduction.....	2
1.2 Cystic fibrosis and CF airway infection.....	4
1.2.1 Introduction.....	4
1.2.2 Cystic fibrosis airway microbiome .....	5
1.2.3 <i>P. aeruginosa</i> adaptation to the CF airway.....	7
1.2.4 <i>S. aureus</i> and the CF airway .....	8
1.2.5 <i>H. influenzae</i> and the CF airway .....	8
1.2.6 <i>Burkholderia cepacia</i> complex and the CF airway .....	8
1.2.7 Other important microorganisms within the CF airway.....	9
1.2.8 Pulmonary exacerbations .....	10
1.2.9 <i>P. aeruginosa</i> eradication therapy.....	10
1.2.10 Early detection of <i>P. aeruginosa</i> infection .....	11



1.2.11	CF sputum composition .....	11
1.2.12	Clinical practices for the identification of microorganisms in CF sputum ....	12
1.3	Rapid techniques for the identification of microorganisms .....	13
1.3.1	Immunochemistry devices .....	14
1.3.2	DNA diagnostic devices.....	15
1.3.3	Volatile organic compounds signature devices.....	15
1.4	Electrochemical changes mediated by microbial growth.....	16
1.4.1	Direct microbial changes caused by cell-electrode mechanisms .....	16
1.4.2	Indirect electrode-electrolyte changes caused by microbial mechanisms.....	24
1.5	Conclusion .....	29
1.6	Objectives of this study.....	31
1.6.1	Research goal .....	31
1.6.2	Research questions.....	31
<b>2</b>	<b>ELECTROCHEMISTRY AND MICROBIOLOGY THEORY .....</b>	<b>32</b>
2.1	Electrical theory .....	33
2.2	Electrochemical theory .....	37
2.2.1	Introduction: Fundamental electrochemical processes and impedance spectroscopy.....	37
2.2.2	Properties of electrolytes.....	38
2.2.3	Properties of the electrode-electrolyte interface.....	47
2.2.4	Randles equivalent circuit.....	54
2.3	Microbiology fundamentals and biofilm formation.....	57

2.3.1	Prokaryotic cells.....	57
2.3.2	Microbial growth.....	59
2.3.3	Microbial respiration and fermentation.....	60
2.3.4	Quorum sensing in microorganisms.....	62
2.3.5	Secondary metabolites produced by <i>P. aeruginosa</i> .....	64
2.3.6	Biofilm fundamentals.....	66
<b>3</b>	<b>MATERIALS AND METHODS .....</b>	<b>69</b>
3.1	Introduction.....	70
3.2	Media, buffers and microbial strains.....	72
3.2.1	Microbial strains .....	72
3.2.2	Media and buffers .....	73
3.2.3	Stock cultures and microorganism storage .....	77
3.3	Electrode design and production.....	78
3.3.1	Electrode patterns.....	79
3.3.2	Electrode screen printing .....	80
3.3.3	Electrode assembly: <i>in vitro</i> experiments .....	82
3.3.4	Electrode assembly: human sputum experiments .....	84
3.4	Electrode characterisation .....	84
3.4.1	Contribution to impedance made by each electrode .....	85
3.4.2	Selection of optimum measurement voltage .....	89
3.4.3	Electrode preconditioning .....	89

3.5	Impedance measurements with microorganisms .....	89
3.5.1	Overnight cultures.....	90
3.5.2	Impedance measurements .....	90
3.5.3	<i>In situ</i> impedance measurements .....	91
3.5.4	<i>Ex situ</i> impedance measurements.....	91
3.5.5	Microbial measurements in cystic fibrosis model environment.....	92
3.5.6	Monoculture and polymicrobial experiments .....	93
3.6	Investigations into the role of phenazines in impedance .....	94
3.6.1	UV-Vis spectrum and associated protocol.....	94
3.6.2	Calculation of pyocyanin concentration.....	95
3.6.3	Sterile pyocyanin measurement .....	95
3.6.4	Exogenous pyocyanin measurements .....	95
3.6.5	Growth experiments with mutant strains of <i>P. aeruginosa</i> .....	95
3.7	Investigations into microbial attachment on the electrode surface .....	96
3.7.1	Crystal violet assays.....	96
3.7.2	Microscopy of the electrode surface .....	98
3.8	Impedance data analysis.....	100
3.8.1	Data handling .....	100
3.8.2	Impedance normalisation .....	101
3.8.3	Peak detection algorithm.....	101
3.8.4	Equivalent circuit analysis .....	104

3.8.5	<i>P. aeruginosa</i> detection algorithm .....	104
3.9	Measurements with clinical sputum samples .....	105
3.9.1	<i>In vitro</i> measurement of <i>P. aeruginosa</i> in sputasol.....	105
3.9.2	Ethical consent .....	105
3.9.3	Measurement of sputum samples one and two .....	106
3.9.4	Measurement of remaining sputum samples.....	106
3.9.5	Electrode chamber modifications for use with human sputum .....	106
3.9.6	Microbiological analysis of sputum samples .....	107
3.9.7	Measurement of sputum samples with final electrode assembly .....	108
<b>4</b>	<b>ELECTRODE CHARACTERISATION, PERFORMANCE ASSESSMENT AND OPTIMISATION .....</b>	<b>109</b>
4.1	Introduction.....	110
4.2	Initial impedance measurements in microbial broth .....	112
4.2.1	Performance of carbon electrode .....	112
4.2.2	Performance of Ag-AgCl/carbon electrode .....	118
4.3	Electrode optimisation .....	121
4.3.1	Selection of measurement voltage .....	121
4.3.2	Electrode conditioning .....	124
4.3.3	Electrode characterisation .....	126
4.4	Impedance measurements with conditioned electrodes .....	129
4.4.1	<i>In situ</i> growth of <i>P. aeruginosa</i> PA14 with conditioned electrodes .....	129
4.4.2	Growth of <i>P. aeruginosa</i> clinical isolates with carbon electrodes .....	131

4.5	Microbial attachment on the electrode surface .....	138
4.5.1	Crystal violet staining .....	138
4.5.2	Epifluorescent microscopy of the carbon electrode surface following growth in LB media.....	141
4.6	Summary .....	146
<b>5</b>	<b>MEASUREMENT IN CF SPUTUM MODEL ENVIRONMENT AND IMPEDANCE MEASUREMENT OF DIFFERENT MICROBIAL STRAINS .....</b>	<b>147</b>
5.1	Introduction.....	148
5.2	Impedance analysis with <i>P. aeruginosa</i> incubated in ASM.....	149
5.3	Impedance analysis with polymicrobial cultures .....	153
5.3.1	Impedance analysis with <i>S. aureus</i> cultures.....	153
5.3.2	Impedance analysis with <i>H. influenzae</i> cultures .....	163
5.3.3	Impedance measurements with <i>C. albicans</i> cultures .....	175
5.4	Investigation into role of pyocyanin in <i>P. aeruginosa</i> mediated change in impedance .....	184
5.4.1	Identification of pyocyanin within the media .....	184
5.4.2	Impedance assessment of pure pyocyanin added to ASM .....	186
5.4.3	Exogenous addition of pyocyanin to overnight cultures.....	188
5.4.4	Investigation of impedance changes due to phenazine production in mutant strains of <i>P. aeruginosa</i> .....	191
5.5	SEM analysis of electrode surface following <i>P. aeruginosa</i> growth in ASM .....	197
5.6	Summary .....	202

<b>6</b>	<b>DETECTION OF <i>P. AERUGINOSA</i> IN HUMAN SPUTUM SAMPLES AND FURTHER STUDIES OF ELECTRODE SENSITIVITY.....</b>	<b>204</b>
6.1	Introduction.....	205
6.2	Measurements of <i>P. aeruginosa</i> overnight culture in sputasol.....	206
6.3	Electrode performance in human sputum samples and experimental development 208	
6.3.1	Sputum samples one and two.....	208
6.3.2	Design two electrode assembly.....	213
6.3.3	Testing sputum samples three, four and five.....	214
6.3.4	Sputum sample six.....	218
6.3.5	Design three electrode assembly development.....	220
6.3.6	Sputum sample seven and eight.....	221
6.4	Application of <i>P. aeruginosa</i> detection algorithm.....	225
6.5	Repeated measurement with electrode developments embodied.....	230
6.5.1	Summary.....	234
6.6	Performance assessment of final electrode assembly.....	235
6.7	Summary.....	239
<b>7</b>	<b>DISCUSSION.....</b>	<b>241</b>
7.1	Introduction.....	242
7.2	Electrode pattern rationale and future development.....	243
7.3	<i>In vitro</i> assessment of electrode developed.....	245
7.3.1	Analysis of electrode performance.....	245

7.3.2	<i>P. aeruginosa</i> growth in standard laboratory media .....	258
7.3.3	Impedance changes with related CF microorganisms in ASM .....	267
7.3.4	Impedance changes in the normalised impedance spectrum following growth of <i>P. aeruginosa</i> .....	269
7.3.5	Investigation into phenazine production and impedance .....	279
7.3.6	Conclusions on <i>in vitro</i> studies of <i>P. aeruginosa</i> detection.....	281
7.4	Assessment of the electrode with human sputum samples .....	282
7.4.1	Development of the electrode assembly .....	282
7.4.2	Findings in CF sputum samples .....	283
7.5	Assessment of electrode sensitivity .....	287
7.5.1	Electrode performance contrasted to other electrochemical pyocyanin sensors 287	
7.5.2	Electrode sensitivity in the context of CF airway infection .....	289
7.6	Summary and conclusions .....	291
7.6.1	Introduction.....	291
7.6.2	Findings in the context of the research questions .....	291
7.6.3	Recommendations for future research .....	293
<b>8</b>	<b>REFERENCES.....</b>	<b>296</b>
<b>9</b>	<b>APPENDIX.....</b>	<b>311</b>
9.1	Appendix A: Biorepositroy Ethics Approval Form .....	312
9.2	Appendix B: Published Papers.....	313

## TABLES

Table 1-1: Principal techniques and technologies for rapid detection of microorganisms. ...	13
Table 2-1: Corresponding relationships between key terms .....	35
Table 2-2: Categorisation of microorganisms based upon respiratory properties .....	62
Table 2-3: Metabolites produced and secreted by <i>P. aeruginosa</i> .....	65
Table 3-1: Strains used in this project.....	73
Table 3-2: Identification and verification of different species of microorganism .....	78
Table 3-3: Electrode dimensions.....	80
Table 3-4: Impedance measurements carried out with electrode pairs. ....	87
Table 3-5: Average contribution to impedance from each electrode at 1 Hz .....	88
Table 3-6: Parameters used for peak and trough detection .....	102
Table 3-7: Example of data output from phase data peak and trough detection .....	103
Table 4-1: Comparison of impedance data at a fixed frequency of 1 Hz when negative control media is aspirated and replaced with 48 hour old <i>P. aeruginosa</i> supernatant.....	116
Table 4-2: Application of the peak detection algorithm to identify peaks in the impedance phase and normalised resistance data from the first two experiments. ....	117
Table 4-3: Analysis of current at the two perturbation voltages measured.....	124
Table 4-4: Identification of peaks in the normalised resistance data. ....	131
Table 4-5: Mean change in impedance modulus at low frequency for each strain. ....	134
Table 4-6: Application of the peak detection algorithm to normalised resistance data for clinical isolates.....	135
Table 4-7: Final <i>P. aeruginosa</i> cell densities determined through drop plate colony counting. ....	138



Table 4-8: Test of difference between CV staining of samples and negative control.....	139
Table 4-9: CV staining assay for microbial attachment using electrode coupons .....	141
Table 5-1: Peak normalised resistance data from aerobic and microaerophilic growth conditions.....	152
Table 5-2: Mean impedance modulus at 0.1 Hz for PA14 grown in aerobic and microaerophilic conditions in ASM.....	153
Table 5-3: Indicative cell densities of planktonic cells at the end of the experiment and timepoints during the experiment. ....	162
Table 5-4: Indicative cell densities of planktonic cells at the end of the experiment. ....	174
Table 5-5: Identification of peaks in <i>P. aeruginosa</i> monoculture at 48 Hours.....	182
Table 5-6: Indicative cell densities of planktonic cells at the end of the experiment .....	183
Table 6-1: Microbiological analysis of sputum samples.....	212
Table 6-2: Microbiological analysis of samples 3, 4 and 5.....	218
Table 6-3: Microbiological analysis of sample 6.....	220
Table 6-4: Microbiological analysis of samples 7 and 8.....	225
Table 6-5: Microbiological analysis of human sputum samples after storage at -80°C.....	233
Table 6-6: Mean pyocyanin concentration of supernatant at later timepoints .....	238
Table 7-1: Comparison of electrode impedance with other investigators.....	247
Table 7-2: Measurement of $R_{ct}$ and $C_{dl}$ , determined using ZView fit circle function.....	251
Table 7-3: Analysis of data from PA14 measurement in LB with Kim et al. (2011) equivalent circuit. ....	261
Table 7-4: Reported redox potentials for phenazines produced by <i>P. aeruginosa</i> .....	280
Table 7-5: Distribution of phenazine concentrations between stages of disease severity...	290

## FIGURES

Figure 1-1: Potential end use for <i>P. aeruginosa</i> detection system explored within this thesis.	2
Figure 1-2: Overview of the topics covered in chapter 1 and 2. ....	3
Figure 1-3: Cystic fibrosis lung infections in 2012.....	5
Figure 1-4: Simplified summary of CF airway infection.....	6
Figure 1-5: Equivalent circuit used by Yang et al. (2003).....	17
Figure 1-6: Equivalent circuit used by Muñoz-Berbel et al. (2006). ....	17
Figure 1-7: Equivalent circuit used by (Muñoz-Berbel et al. 2008c).....	18
Figure 1-8: Equivalent circuit used by Muñoz-Berbel et al. (2008). ....	18
Figure 1-9: Equivalent circuit model used by Ben-Yoav et al. (2011). ....	22
Figure 1-10: De-adsorption of metabolites from the electrode surface .....	25
Figure 1-11: Principal proposed mechanisms affecting impedance as a result of microbial material .....	30
Figure 2-1: Fundamental Principles of Capacitance. ....	33
Figure 2-2: Example plot of impedance vector.....	36
Figure 2-3: Relationship between time domain and complex plot .....	37
Figure 2-4: Fundamental electrochemical processes. ....	38
Figure 2-5: Cole-Cole plot for a dielectric with multiple relaxations. ....	44
Figure 2-6: Example of the equivalent circuit for a two phase material .....	45
Figure 2-7: Major Dispersions in Biological Tissues .....	47
Figure 2-8: Origins of charge distribution across a phase boundary .....	48
Figure 2-9: Distribution of ions at the electrode-electrolyte boundary.....	49

Figure 2-10: Anode and cathode reactions .....	52
Figure 2-11: The Randles equivalent circuit.....	55
Figure 2-12: Example complex plane impedance plot of the Randles equivalent circuit. ....	56
Figure 2-13: An example of a typical Gram negative rod prokaryote. ....	57
Figure 2-14: Differences between Gram-negative and Gram-positive bacteria. ....	58
Figure 2-15: Typical microbial growth cycle.....	60
Figure 2-16: Aerobic respiration.....	61
Figure 2-17: Anaerobic respiration.....	61
Figure 2-18: <i>P. aeruginosa</i> quorum sensing network.....	64
Figure 2-19: Typical biofilm lifecycle.....	68
Figure 3-1: Research roadmap for this study. ....	71
Figure 3-2: Electrode patterns used in this study.....	79
Figure 3-3: Summary of screen printing process. ....	81
Figure 3-4: General assembly showing.....	82
Figure 3-5: Completed carbon electrode and assembly. ....	83
Figure 3-6: Cartoon of the electrode, showing the foil cover used to keep the electrodes sterile.....	83
Figure 3-7: Example of electrode chambers at the end of an experiment with <i>P. aeruginosa</i> strains. ....	84
Figure 3-8: ZPlot screen used to control SII260 impedance analyser.....	85
Figure 3-9: Total measured impedance from a platinum-platinum electrode pair.....	86
Figure 3-10: Impedance of a single platinum electrode.....	87

Figure 3-11: Picture of the microaerophilic chamber used in these experiments. ....	93
Figure 3-12: Summary of CV staining assay .....	97
Figure 3-13: Configuration of the electrode coupon used in the positive control.....	98
Figure 3-14: Electrode coupon pattern used for SEM microscopy .....	99
Figure 3-15: Example of raw data signal and equivalent normalised signal. ....	101
Figure 4-1: Example of normalised peaks detected in phase data from an experiment with <i>S. aureus</i> over 16 hours using screen printed Ag-AgCl electrodes.....	110
Figure 4-2: Impedance of <i>P. aeruginosa</i> PAO1 RHL GFP grown for 24 hours in LB media. ....	113
Figure 4-3: Measurement of PAO1 RHL GFP to 0.1 Hz over 48 hours.....	115
Figure 4-4: Growth of <i>P. aeruginosa</i> PA14 in LB media using the Ag-AgCl/carbon electrode.....	120
Figure 4-5: Assessment of different measurement potentials. ....	123
Figure 4-6: Example of an initial impedance signature inconsistent with other electrodes. ....	125
Figure 4-7: Impedance changes as a result of electrode conditioning .....	126
Figure 4-8: Baseline performance of the carbon electrodes.....	128
Figure 4-9: Impedance modulus of the Ag-AgCl counter electrode.....	128
Figure 4-10: <i>P. aeruginosa</i> PA14 in LB media over 72 hours with carbon electrodes after conditioning. ....	130
Figure 4-11: Clinical <i>P. aeruginosa</i> isolates from CF patients.....	132
Figure 4-12: Normalised resistance peaks in <i>P. aeruginosa</i> early isolates (C1426 and J1385) and late isolates (C1433 and J1532). ....	133
Figure 4-13: Comparison of the mean normalised phase angle between non-mucoid and mucoid pairs.....	136

Figure 4-14: Time plot of the normalised phase angle at 100 Hz for each of the non-mucoid/mucoid pairs.....	137
Figure 4-15: CV assay for PA14, showing the change in concentration of CV as a function of growth.....	139
Figure 4-16: CV staining assay using electrode coupons incubated in a 24 well plate .....	140
Figure 4-17: Epifluorescent microscopy of carbon electrode coupons following 24 hour incubation with <i>P. aeruginosa</i> PA14.....	142
Figure 4-18: Example of biofilm on electrode sample of <i>P. aeruginosa</i> PA14.....	143
Figure 4-19: Typical finding from epifluorescent microscopy of the carbon coupons following incubation of PA14 after 48 hours.....	144
Figure 5-1: Measurement of <i>P. aeruginosa</i> PA14 in aerobic and microaerophilic conditions.....	151
Figure 5-2: <i>In situ</i> growth of <i>S. aureus</i> RN4220 in TSB.....	155
Figure 5-3: Example of <i>S. aureus</i> turbid growth.....	156
Figure 5-4: <i>Ex situ</i> impedance of overnight culture of <i>S. aureus</i> RN4220 .....	158
Figure 5-5: Application of peak detection algorithm to the impedance signatures found during <i>ex situ</i> growth of <i>S. aureus</i> RN4220.....	159
Figure 5-6: <i>In situ</i> impedance changes following growth of <i>S. aureus</i> RN4220 in ASM. ..	160
Figure 5-7: <i>In situ</i> polymicrobial measurement of <i>S. aureus</i> RN4220 and <i>P. aeruginosa</i> PA14.....	161
Figure 5-8: <i>In situ</i> measurement of <i>H. influenzae</i> HI680 in HTM.....	164
Figure 5-9: <i>In situ</i> measurement of <i>H. influenzae</i> in HTM over 48 hours.....	165
Figure 5-10: <i>Ex situ</i> measurement of <i>H. influenzae</i> HI680 in HTM.....	167
Figure 5-11: Application of the peak detection algorithm to the identification of the peak in the normalised resistance data.....	168

Figure 5-12: <i>Ex situ</i> measurement of <i>H. influenzae</i> in ASM supplemented with essential growth factors, hemin and NAD .....	170
Figure 5-13: <i>Ex situ</i> measurement of <i>H. influenzae</i> HI680 in ASM media after 72 hours ..	172
Figure 5-14: <i>Ex situ</i> measurement of <i>P. aeruginosa</i> PA14 and <i>H. influenzae</i> HI680 .....	173
Figure 5-15: Example of <i>C. albicans</i> growth, showing both filamentous and yeast forms.	176
Figure 5-16: <i>In situ</i> measurement of <i>C. albicans</i> SC5314 in TSB-YE over 72 hours .....	177
Figure 5-17: Boxplot showing the difference between <i>C. albicans</i> and the negative control in normalised phase data at 5 kHz.....	178
Figure 5-18: Boxplot showing the difference between <i>C. albicans</i> and negative control in normalised resistance data at 500 Hz.....	178
Figure 5-19: <i>In situ</i> measurement of <i>C. albicans</i> SC5314 in ASM over 72 hours. ....	180
Figure 5-20: <i>In situ</i> polymicrobial measurement of <i>P. aeruginosa</i> and <i>C. albicans</i> in ASM media over 72 hours.....	181
Figure 5-21: Positive control measurement of <i>P. aeruginosa</i> PA14 in ASM.....	182
Figure 5-22: Colour change in media resulting from growth of three different strains of <i>P. aeruginosa</i> .....	184
Figure 5-23: UV-Visible spectrum for pure pyocyanin at different concentrations .....	185
Figure 5-24: Measurement of the UV-visible spectrum for supernatant .....	186
Figure 5-25: Measurement of purified pyocyanin in ASM.....	187
Figure 5-26: Boxplot of phase angle at 1 Hz as a result of the addition of pyocyanin to the culture. ....	188
Figure 5-27: The effect of exogenous addition of pyocyanin on the impedance of <i>P. aeruginosa</i> PA14. ....	189
Figure 5-28: The effect of exogenous addition of pyocyanin on the impedance of <i>S. aureus</i> RN4220.....	190

Figure 5-29: Media colour change following exogenous addition of pyocyanin to overnight cultures.....	191
Figure 5-30: Impedance changes caused by the <i>P. aeruginosa</i> PA14 $\Delta$ phzM mutant.....	193
Figure 5-31: Impedance changes caused by the <i>P. aeruginosa</i> PA14 $\Delta$ phzS mutant. ....	194
Figure 5-32: Measurement of <i>P. aeruginosa</i> PA14 $\Delta$ phzA1-G1/A2-G2 double mutant.....	196
Figure 5-33: Example SEM images of biofilm formation by <i>P. aeruginosa</i> PA14 on the positive control samples.....	198
Figure 5-34: Example SEM images of negative control showing electrode surface .....	199
Figure 5-35: First example of SEM images of <i>P. aeruginosa</i> PA14 sample, incubated at the bottom of a 24 well plate .....	200
Figure 5-36: Second example of SEM images of <i>P. aeruginosa</i> PA14 sample, incubated at the bottom of a 24 well plate.....	201
Figure 6-1: Measurement of <i>P. aeruginosa</i> PA14 before and after the addition of sputasol, normalised against sterile ASM .....	207
Figure 6-2: Measurement of <i>P. aeruginosa</i> PA14 in sputasol, normalised against sterile sputasol .....	208
Figure 6-3: Individual baseline measurements of electrodes used for testing of first two human sputum samples .....	209
Figure 6-4: Measurement of first two human sputum samples, blanked against sputasol...	211
Figure 6-5: Cartoon of electrode assembly, showing where small quantities of residual ethanol after sterilisation may have affected the impedance. ....	213
Figure 6-6: Cartoon of design two electrode assembly.....	214
Figure 6-7: Electrode assembly development.....	214
Figure 6-8: Impedance measurements in NaCl prior to sputum measurements .....	215

Figure 6-9: Impedance measurement of second set of sputum samples, blanked against 0.9% w/v NaCl .....	217
Figure 6-10: Impedance measurement of sputum sample 6, blanked against 0.9% w/v NaCl .....	219
Figure 6-11: Cartoon of design three electrode.....	221
Figure 6-12: Bijou tube electrode assembly used for measurement of samples seven and eight. ....	221
Figure 6-13: Impedance measurement of sample 7 blanked against 0.9% w/v NaCl.....	223
Figure 6-14: Impedance measurement of sputum sample 8, blanked against 0.9% w/v NaCl .....	224
Figure 6-15: Pictorial summary of the evolution of electrode assemblies during testing with human sputum samples. ....	226
Figure 6-16: Mean normalised resistance peak frequency, found using the peak detection algorithm. ....	228
Figure 6-17: Summary of normalised phase and resistance data from human sputum samples .....	229
Figure 6-18: <i>P. aeruginosa</i> detection algorithm retrospectively applied to measured sputum samples.....	230
Figure 6-19: Measurement of all sputum samples using design 3 electrodes (without conditioning).....	232
Figure 6-20: Impedance measurement of <i>P. aeruginosa</i> PA14 grown in LB media over 9 hours.....	236
Figure 6-21: Time based analysis of impedance and growth curves. ....	237
Figure 7-1: Example electrode configurations with a distributed arrays of working electrodes. ....	244



Figure 7-2: Complex plane plot of impedance of <i>P. aeruginosa</i> PAO1 RHL GFP over 24 hours.....	249
Figure 7-3: Screen shot of the ZView output from circle fit tool. ....	250
Figure 7-4: Complex plane plots of impedance using data from second experiment with <i>P. aeruginosa</i> PAO1 RHL GFP .....	252
Figure 7-5: Impedance measurements on <i>P. aeruginosa</i> PA14 carried out using a carbon electrode.....	255
Figure 7-6: Analysis of coefficient of variation for experiments with Ag-AgCl/Carbon electrodes.....	257
Figure 7-7: Munoz-Berbel et al. (2006) basic equivalent circuit .....	259
Table 7-8: Analysis of data from PA14 measurement in LB with Munoz-Berbal et al. equivalent circuit.....	260
Figure 7-9: Kim et al. (2011) equivalent circuit. ....	261
Figure 7-10: Complex plot of sterile grid electrode and grid electrode after 1 and 2 weeks of biofilm cultivation, taken from Dheilily et al. (2008). ....	264
Figure 7-11: CLSM images of electrode surface at 72 Hours .....	266
Figure 7-12: Example of PAO1 wild type biofilm formation in flow cell with minimal media .....	266
Figure 7-13: Peak detection algorithm applied to normalised phase peak data. ....	271
Figure 7-14: Peak detection algorithm applied to normalised phase trough data. ....	272
Figure 7-15: Current path at high frequencies. ....	273
Figure 7-16: Current paths at intermediate frequencies. ....	274
Figure 7-17: Peak detection algorithm applied to the normalised resistance data. ....	275
Figure 7-18: Current path at low frequencies. ....	276

Figure 7-19: Peaks and troughs identified in the normalised phase and resistance data applied to the <i>P. aeruginosa</i> PA14 <i>phzA1G1/A2G2</i> mutant.....	277
Figure 7-20: Analysis of data from four separate experiments, normalised against 0.9% w/v NaCl preconditioning measurements .....	286
Figure 7-21: <i>in vitro</i> normalised resistance peak data. ....	287

## **1 LITERATURE REVIEW**

## 1.1 Introduction

Chronic lung infections caused by *Pseudomonas aeruginosa* are widely recognised as the leading cause of morbidity and mortality in patients with cystic fibrosis (CF). Once people with CF have been colonised with *P. aeruginosa*, the infections are almost impossible to eradicate. Pulmonary exacerbations in colonised patients result in further lung deterioration. As discussed in this thesis, early identification of *P. aeruginosa* or pulmonary exacerbations could help clinicians intervene sooner and improve patient quality of life.

This thesis explores the use of electrochemical impedance spectroscopy (EIS), in conjunction with a low cost electrode for the specific detection of *P. aeruginosa*. The ability to miniaturise the electronics required to conduct EIS and the low cost of the electrodes could lead to a portable, point of care testing (POCT) device (Figure 1-1). The scope of the work described here focuses upon the detection of *P. aeruginosa* with EIS, in the context of the CF airway microbiome.

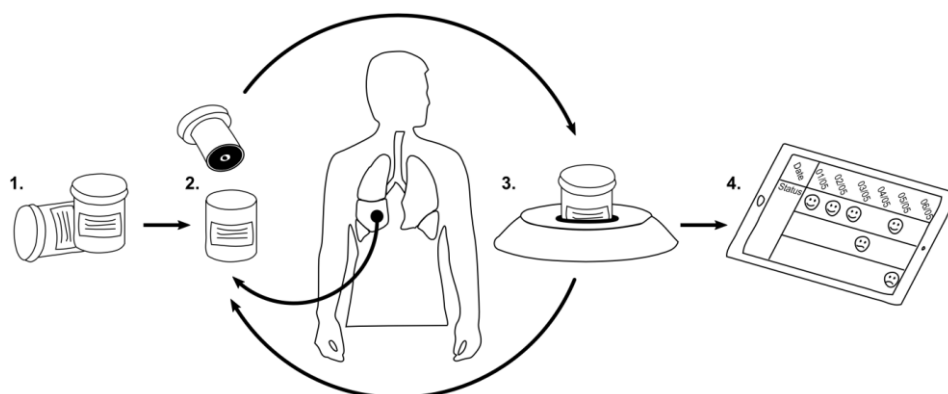


**Figure 1-1: Potential end use for *P. aeruginosa* detection system explored within this thesis. (1) Low cost, disposable sensors integrated in sample pot are provided to patient for daily use. (2) Sputum produced by patient is placed into sample pot. (3) Sensor is used in conjunction with affordable portable device to test for *P. aeruginosa*. After testing, sample pot containing sputum and sensor is discarded. (4) Sample monitored daily for changes indicating colonisation or pulmonary exacerbation.**

A review of the literature is given in this chapter. The first section provides a summary of the CF airway microbiome and associated problems in the clinical context. The second section describes electrochemical detection of microorganisms (with a focus on EIS) and recent findings on the electrochemical properties of microorganisms. The literature reviewed in this chapter is used to form the basis of a set of research questions and a research hypothesis that is investigated within this thesis. These research questions are outlined at the

end of the chapter. For readers unfamiliar with either microbiology or electrochemistry, a review of the underpinning theory is provided in chapter 2 (Figure 1-2).

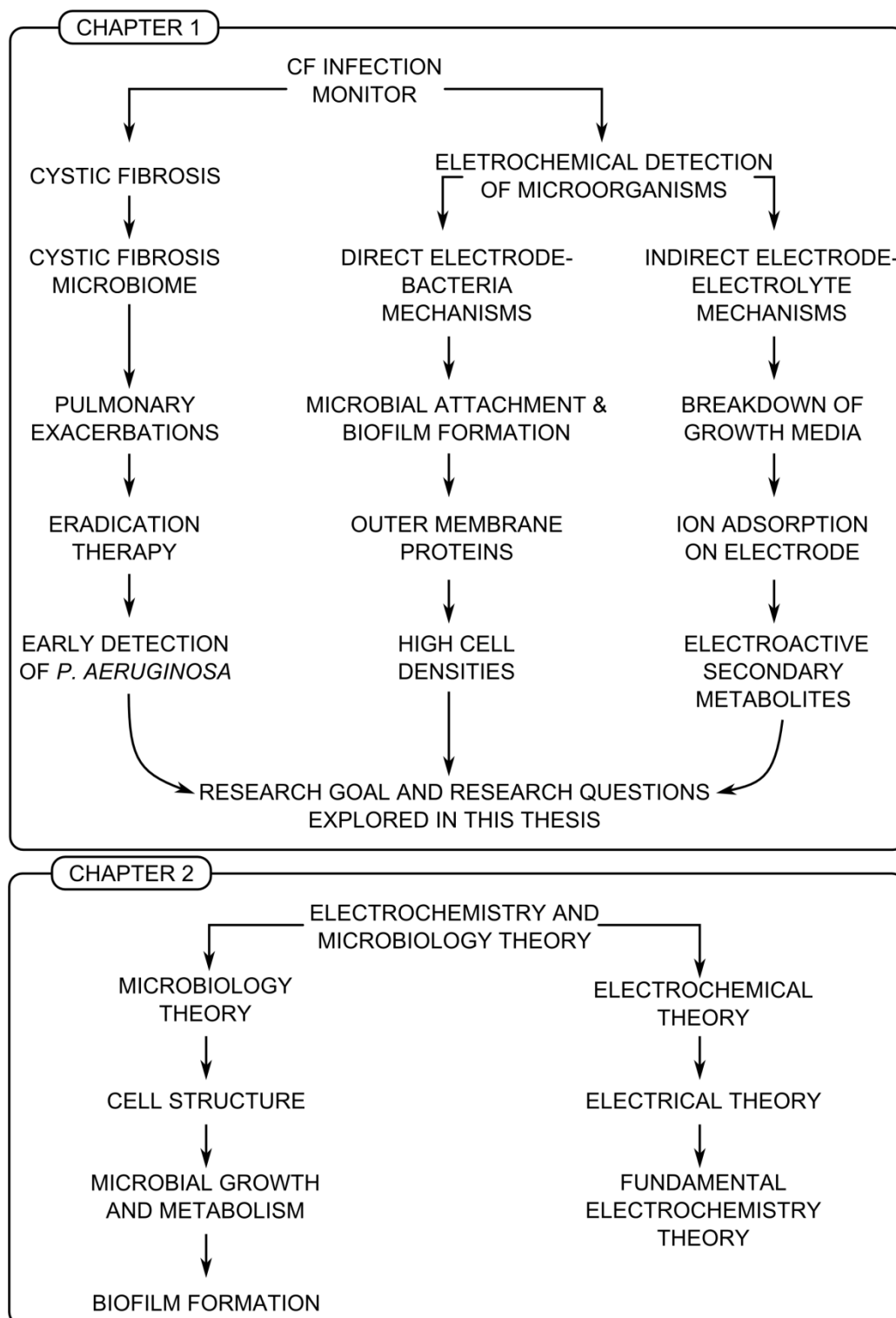


**Figure 1-2: Overview of the topics covered in chapter 1 and 2.**

## **1.2 Cystic fibrosis and CF airway infection**

### **1.2.1 Introduction**

CF is the most common life shortening recessive genetic disease in people of European origin (Rosenstein and Zeitlin 1998). It is caused by a mutation in the Cystic Fibrosis Transmembrane Regulator (CFTR) gene leading to either a non-existent or a dysfunctional membrane bound protein (Rosenstein and Zeitlin 1998; Greger 2000). CF is a systemic disease, manifesting itself in all tissues where cells normally express the CFTR protein, including sweat glands, airway epithelia, gut, pancreas and exocrine glands, reproductive organs, the bile duct and gall bladder (Greger 2000). Within the CF airway, production of sticky, viscous mucus leads to infections and consequently lung damage. More specifically, lung disease is the leading cause of morbidity and mortality in CF patients and generally results from colonisation of the airway by *P. aeruginosa* (Harrison 2007; Hassett et al. 2009; Langton Hewer and Smyth 2009).

In the UK, over 10, 000 people are registered with CF (Cystic Fibrosis Trust 2013) and over 27, 000 people in the US have CF (Cystic Fibrosis Foundation 2012). The life expectancy of patients with CF continues to rise, but is still low, with a median predicted age of survival in the US of 41.1 years (Cystic Fibrosis Foundation 2012). The lifetime costs associated with CF care have recently been estimated at US \$306, 000, with the greatest costs associated with hospital inpatients followed by pharmaceuticals (van Gool et al. 2013).

### 1.2.2 Cystic fibrosis airway microbiome

The CF airway comprises a complex microbiome consisting of several different organisms, with *Staphylococcus aureus*, *Haemophilus influenzae*, *P. aeruginosa* and *Burkholderia cepacia* complex (Bcc) commonly cultured from CF sputum (Harrison 2007; Sibley et al. 2011; Cystic Fibrosis Trust 2013; McGuigan and Callaghan 2014). Initially, *H. influenzae* and *S. aureus* are the most prevalent organisms found in sputum. Over time however, the ecology of the airway changes and chronic colonisation with *P. aeruginosa* occurs (Figure 1-3). Once *P. aeruginosa* is present, the bacteria are thought to adapt rapidly to the conditions within the CF airway, changing from a planktonic non-mucoid phenotype to a sessile, biofilm forming mucoid phenotype. This results in a chronic infection that cannot be eradicated (Ratjen and Döring 2003; Hassett et al. 2009). Chronic lung infections with *P. aeruginosa* are therefore associated with a poor prognosis and increased mortality in CF patients (Littlewood 2004). The changes that occur in the CF airway over time are summarised in Figure 1-4.

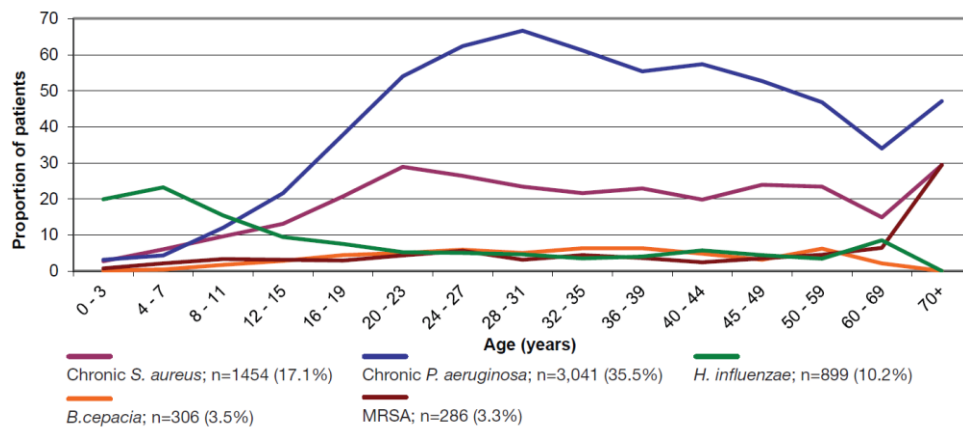
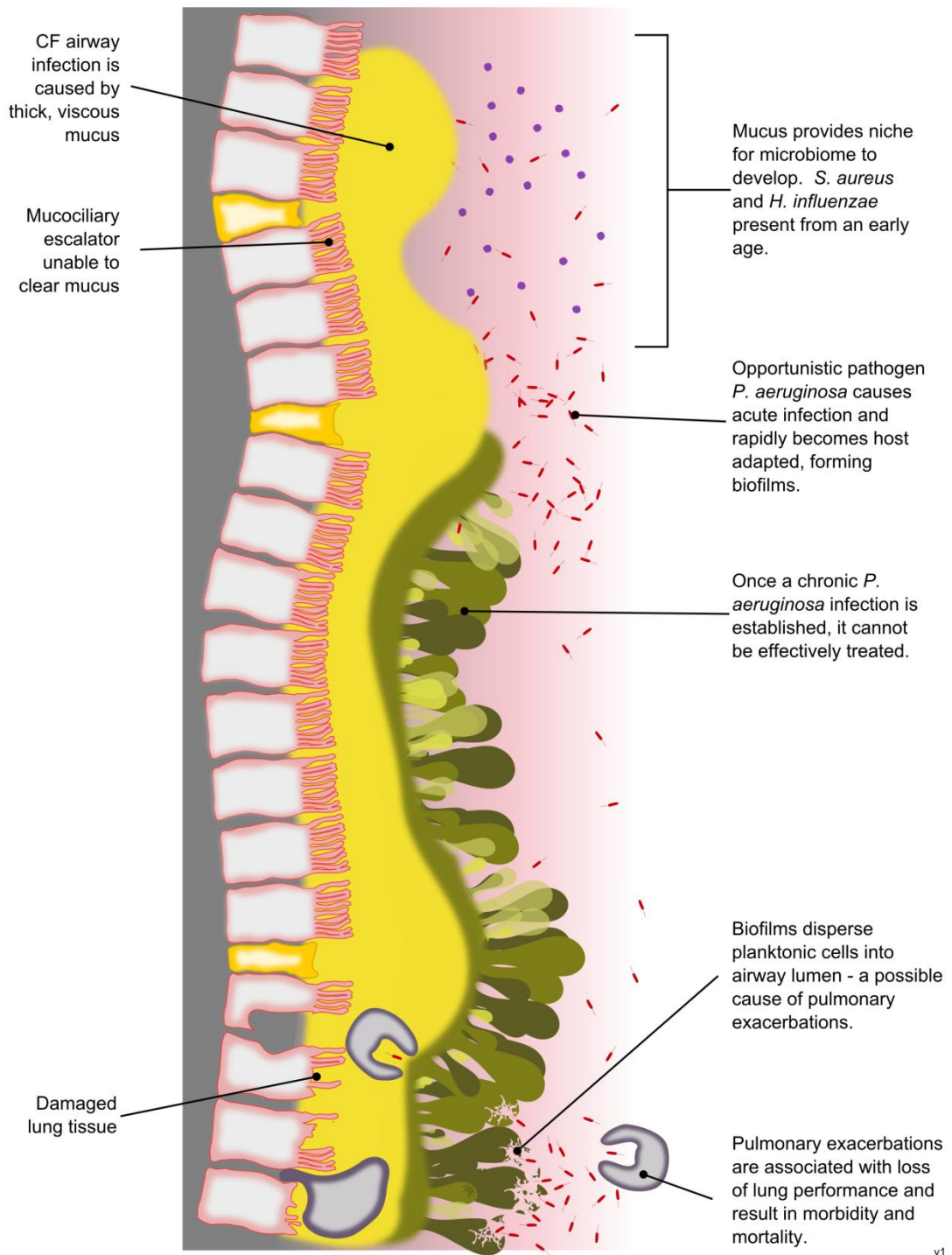


Figure 1-3: Cystic fibrosis lung infections in 2012 (Cystic Fibrosis Trust 2013).



**Figure 1-4: Simplified summary of CF airway infection. Dysfunctional CFTR protein results in thick, viscous mucus which is difficult to clear. This provides a niche for a complex microbiome, eventually leading to chronic infections with *P. aeruginosa*. Periodically, patients experience pulmonary exacerbations, which could be caused by a change in the state or density of the bacteria within the airway.**



### 1.2.3 *P. aeruginosa* adaptation to the CF airway

As described above, *P. aeruginosa* is known to adapt to the conditions within the CF airway to establish chronic infections. Mutations caused by reactive oxygen species (ROS) and reactive nitrogen species (RNS) from the host immune system are thought to drive an advantageous evolution of *P. aeruginosa* (Hasset et al. 2009). Some of the common changes seen in *P. aeruginosa* over time are the production of polysaccharide alginate, failure to express virulent appendages such as flagella or pili (Hasset et al. 2009), the appearance of small colony variants, antibiotic resistance and a decreased production of virulence factors (Harrison 2007). Furthermore, *P. aeruginosa* may be able to use intracellular communication between oropharyngeal microflora leading to the up-regulation of specific genes relating to pathogenesis (Harrison 2007). Morphological differences can often be seen between clinical isolates and laboratory strains. In the case of mucoid phenotypes, these differences are thought to be related to the mutation of genes that control the alginate biosynthesis pathway (Hasset et al. 2009). There is also evidence that *P. aeruginosa* grows anaerobically in the CF airway as a consequence of the low oxygen tension and is different to growth observed *in vitro* (Yoon et al. 2002; Hasset et al. 2009).

Other studies highlight the presence of virulence factors produced by *P. aeruginosa*. Fothergill et al. (2007) isolated endemic strains of *P. aeruginosa* and found that they produced large quantities of exoproducts. Hunter et al. (2012) found that the concentration of pyocyanin in sputum from CF patients was negatively correlated with FEV<sub>1</sub>. In particular, pyocyanin and other phenazines have been related to quorum sensing in *P. aeruginosa* and *in vitro* are produced in early stationary phase in response to *Pseudomonas* quinolone signal (PQS) (Price-Whelan et al. 2007). In other *in vitro* studies, pyocyanin has been found to have several toxic effects on the host, including inhibition of cell respiration and ciliary beating, inactivation of catalase and  $\alpha$ 1-protease and depletion of cellular glutathione (Lau et al. 2004).

The resulting chronic CF airway infections caused by the host adapted *P. aeruginosa* involve growth of the bacteria in a biofilm phenotype, which has been indicated by both morphological and chemical evidence (Costerton 2001). Interestingly, biofilm formation in the CF airway has been shown to differ in terms of genetics, morphology and physiology to that found in other surface attached biofilms (Hasset et al. 2009).

#### **1.2.4 *S. aureus* and the CF airway**

The commensal organism, *S. aureus* is also commonly found in CF sputum. *S. aureus* is a ubiquitous Gram positive bacterium especially found in the anterior nares and skin creases of healthy individuals (Archer et al. 2011; Goss and Muhlebach 2011; Krishna and Miller 2012; Pantosti and Venditti 2009). The bacterium is known to colonise the CF airway from an early age (Mahenthiralingam et al. 2008; Madeira et al. 2013). Several studies have shown that the presence of *S. aureus* in the absence of *P. aeruginosa* predicts longer term survival in patients over the age of 18 years (Lyczak et al. 2002). Furthermore, it has been suggested that patients taking antistaphylococcal therapy show higher rates of *P. aeruginosa* acquisition (Lyczak et al. 2002). More recently, however, a longitudinal study has shown that lower respiratory tract infection with *S. aureus* in infants is associated with a greater decline in lung function than patients with no infection (Pillarisetti et al. 2011). Small colony variants of *S. aureus* can also appear within the CF lung and are associated with higher rates of antimicrobial resistance and more advanced lung disease (Goss and Muhlebach 2011).

#### **1.2.5 *H. influenzae* and the CF airway**

*Haemophilus influenzae*, another commensal bacteria of the upper respiratory tract, has been reported as the most common pathogen in CF patients less than 1 year old (Cystic Fibrosis Trust 2010). *H. influenzae* is a fastidious, non-motile Gram negative bacilli which grows best at 35-37 °C under microaerophilic conditions (World Health Organisation 2011) and whose only natural host is humans (Fleischmann et al. 1995). The genome of *H. influenzae* is relatively small and was the first complete self replicating organism to be sequenced in 1995 (Fleischmann et al. 1995).

#### **1.2.6 *Burkholderia cepacia* complex and the CF airway**

Bcc represents an important group of microorganisms associated with the CF lung. Bcc consists of a group of nine phenotypically similar bacteria widely isolated from the environment (Chiarini et al. 2006). Whilst all nine members of the Bcc family have been isolated from the CF airway, *B. cenocepacia* and *B. multivorans* are most commonly found (Chiarini et al. 2006), with *B. multivorans* now more prevalent in the UK CF population than *B. cenocepacia* (Mahenthiralingam et al. 2008). Studies have shown that infection with *B.*

*ceenocepica* is associated with poor prognosis and accelerated decline in lung function (Mahenthiralingam et al. 2008; Madeira et al. 2013). “Cepacia syndrome” affects approximately 10% of patients infected with *B. ceenocepica* and results in rapid, fatal clinical decline (Mahenthiralingam et al. 2008). Once a chronic infection with any strain of Bcc has become established, treatment is challenging due to the group’s resistance to antibiotics (Chiarini et al. 2006; Mahenthiralingam et al. 2008).

### **1.2.7 Other important microorganisms within the CF airway**

The microbiome of the CF airway extends well beyond the commonly found species highlighted above. Other bacteria including *Stenotrophomonas maltophilia*, *Achromobacter xyloaozidans*, *Cupriavidus species* and *Pandora species* (generally associated with nosocomial infections or not associated with human infection) have also been reported in the CF airway (Hassett et al. 2009; LiPuma 2010). In addition, the fungi *Aspergillus* has been found within the CF airway, particularly *Aspergillus fumigatus* (Balfour-Lynn and Elborn 2007). *A. fumigatus* can result in allergic bronchopulmonary aspergillosis (ABPA), which has been reported to result in clinical deterioration (Shoseyov 2006), although the European Epidemiologic Registry of CF does not indicate a longitudinal decline in FEV when divided into severity subgroups (Balfour-Lynn and Elborn 2007). An increasing prevalence of non-tuberculosis mycobacterium has also been reported in patients with CF (LiPuma 2010). Specifically, the prevalence of *Mycobacterium abscessus* is increasing, with some evidence to suggest that indirect cross contamination between patients occurs (Bryant et al. 2013). *C. albicans* is a eukaryotic yeast organism and is also often recovered from the lungs of patients with CF, in conjunction with *P. aeruginosa* (Bakare et al. 2003; Sudbery 2011). Secreted factors produced by *C. albicans* have an effect upon *P. aeruginosa*, resulting in loss of swarming motility and enhanced biofilm formation (Peleg et al. 2010).

More recently, through the use of molecular DNA profiling techniques, a number of studies have suggested that the CF airway microbiome is even more diverse and complex than previously thought (Rogers et al. 2003; Cox et al. 2010; Lynch and Bruce 2013; Lim et al. 2014). However, the sampling technique used could also affect the microbial complexity. In contrast to studies highlighting a diverse microbiome, the lower CF airway has been shown to only contain a limited number of organisms, typical of those traditionally associated with CF (Goddard et al. 2012). This was found by analysing DNA isolated from paired sputum samples and samples of removed lung tissue from patients that had just undergone lung transplantation (Goddard et al. 2012). In another investigation, deep throat swabs were

compared to sputum samples and showed that the oropharyngeal microbiome did not appear to drive the microbial community composition of the sputum sample (Cox et al. 2010).

Other investigators argue that microbes found in the oral cavity could colonise the lungs and should therefore be considered as part of the community (Lim et al. 2014).

### **1.2.8 Pulmonary exacerbations**

Pulmonary exacerbations are the most important cause of morbidity in CF patients chronically infected with *P. aeruginosa* and typically occur three to four times a year (Balfour-Lynn and Elborn 2007; Lapin and Pryor 2007). Clinically, pulmonary exacerbations have been defined as a need for additional antibiotic treatment resulting from a change in at least two of the following: change in sputum volume or colour; increased cough; increase malaise, fatigue or lethargy; anorexia or weight loss; decreased pulmonary function by 10% or more, or radiographic changes; and increased dyspnoea (Bilton et al. 2011). The underlying cause of pulmonary exacerbations in adults has not been firmly established. However, *P. aeruginosa* is thought to play an important role and antibiotic treatment for exacerbations typically target *P. aeruginosa* (Reid et al. 2013). In contrast, *S. aureus*, *H. influenzae* are most commonly isolated in pulmonary exacerbations during infancy and childhood (Bhatt 2013), however respiratory viruses may also play an important role in these infections too (Reid et al. 2013).

Some studies have found that the concentration of *P. aeruginosa* cells does not change in the lead up to a pulmonary exacerbation, with typical values of  $10^8$  to  $10^9$  CFU/ml reported (Stressmann et al. 2011; Reid et al. 2013). Reid et al. (2013) suggest that this could indicate changes in the bacterial behaviour or dynamics of bacterial communities are responsible for exacerbations. There is consensus across studies, however, that the concentration of *P. aeruginosa* decreases as a result of antibiotic treatment after an exacerbation (Regelmann et al. 1990; Smith et al. 1999; Stressmann et al. 2011; Reid et al. 2013). Another study found that the same clonal strain of *P. aeruginosa* was present throughout a pulmonary exacerbation, suggesting that the exacerbations are not caused by new strains of the bacteria (Aaron et al. 2004).

### **1.2.9 *P. aeruginosa* eradication therapy**

As discussed above, early strains of *P. aeruginosa* are planktonic and non-mucoid (Hassett et al. 2009). Antibiotic eradication therapy has therefore been explored as a strategy to prevent chronic infection (Schelstraete et al. 2013). Langton Hewer and Smyth (2014) conducted a

systemic review of the evidence eradication therapy and found that significantly more children with CF showed clearance of *P. aeruginosa* after two months of antibiotic therapy compared to a placebo group. However, the authors also highlight the lack of well designed and executed studies to establish whether eradication therapy delays chronic infection and results in appreciable benefit without causing harm (Langton Hewer and Smyth 2014). In the EarLy Inhaled Tobramycin for Eradication (ELITE) trial, it was found that inhaled tobramycin taken for 28 days or 56 days resulted in eradication rates of *P. aeruginosa* of 66% and 69% respectively one month after the end of treatment (Ratjen et al. 2010). More recently, an multi centre RCT trial found that 66% of patients taking inhaled colistin and oral ciprofloxacin and 65.2% of patients taking inhaled tobramycin and oral ciprofloxacin were *P. aeruginosa* negative after 6 months (Taccetti et al. 2012). Whilst several studies show that rapid treatment of *P. aeruginosa* infections can increase the length of time before chronic colonisation, none demonstrate a 100% success (Schelstraete et al. 2013). The reasons for this could include delays in detection of *P. aeruginosa* and the use of insensitive detection techniques (Schelstraete et al. 2013).

#### **1.2.10 Early detection of *P. aeruginosa* infection**

At present, no practical system exists that allows checking for infection with *P. aeruginosa* on a daily basis. Whilst current guidelines highlight that microbiological surveillance should occur on every clinical visit, routine appointments can be every two to three months for a stable patient (Cystic Fibrosis Trust 2011) providing long periods of time between appointments in which chronic infections could develop. Daily airway clearance exercises and chest physiotherapy form a key part of patient care and can help to prevent infection and lung deterioration (Lapin and Pryor 2007).

#### **1.2.11 CF sputum composition**

CF sputum is composed of mucin, lipids, proteins, amino acids, ions, DNA, filamentous actin, proteoglycans, biofilms, bacteria and inflammatory cells (Voynow and Rubin 2009). In the airways the mucins found are primarily MUC5A, secreted from goblet cells and MUC5B, secreted from submucosal cells (Rubin 2007). Evidence suggests that CF sputum contains almost no intact mucin when compared to normal airway mucus (Voynow and Rubin 2009). This may be caused by proteolytic degradation, or be due to the presence of large quantities of other molecules diluting the relative concentration of mucins (Voynow and Rubin 2009). CF sputum is also associated with higher levels of amino acids, which

have been found to promote the growth of *P. aeruginosa* (Barth and Pitt 1996). Furthermore, a greater concentration of amino acids was associated with CF samples containing auxotrophic strains of *P. aeruginosa* (Barth and Pitt 1996). Some investigators have developed laboratory based artificial sputum for assessment of the growth of *P. aeruginosa* (Kirchner et al. 2012; Sriramulu et al. 2005). These typically contain mucin, amino acids and DNA.

#### **1.2.12 Clinical practices for the identification of microorganisms in CF sputum**

Clinically, the detection of bacteria within sputum samples is achieved by conventional culturing of samples on selective agar media after homogenising in a DTT solution, such as Sputasol (Cystic Fibrosis Trust 2010). The principle behind this approach is to use the properties of the given microorganism to enable growth of the organism of interest whilst preventing the growth of other organisms. For *P. aeruginosa*, this can be achieved through the use of *Pseudomonas* selective agar, whereby *Pseudomonas* agar base is supplemented with Cefrimide and Nalidixic acid, with the aim of specifically isolating *Pseudomonas* species from other species within the sputum. In contrast, the isolation of *S. aureus* is achieved through the use of mannitol salt agar, which has a high salt content. The peptidoglycan wall of Gram positive bacteria can resist the osmotic pressure resulting from the high salt concentration within the media that causes Gram negative species, such as *P. aeruginosa* to lyse.

### 1.3 Rapid techniques for the identification of microorganisms

A number of detection approaches have been developed for the rapid detection of bacteria in a point of care scenario. Rapid point of care testing predominantly relies on one of three fundamental processes (Table 1-1). Each of these techniques are described briefly below, to provide a context for the succeeding detailed review of the literature relating to the use of reagentless and labelless impedance spectroscopy for bacterial detection.

**Table 1-1: Principal techniques and technologies for rapid detection of microorganisms.**

Principle	Immunochemistry	DNA Detection	Volatile Organic Compounds Signatures
<b>Description</b>	Antibodies capture analyte, which can then be detected using a number of enabling technologies.	Extraction and amplification or direct identification of DNA strands specific to the species of interest.	Volatile Organic Compounds released by the sample are interrogated for the identification of biomarkers or patterns of biomarkers.
<b>Example enabling technologies</b>	Electrochemical Photonic Nanoparticles Magnetic beads ELISA LFI	Microfluidics PCR reagents Electrochemical Photonic	Microfluidics FAIMS MALDI-TOF Solid state ion selective devices
<b>Commercialised Examples</b>	Quidel QuickVue Alere BinaxNOW Alere Affinion	Cepheid GeneXpert BD BDMax	Owlstone
<b>Advantages</b>	Mature, well developed technology. High specificity.	Can be tailored to detection of any strand of DNA PCR principles well established	Reduced/no requirement for reagents or consumables
<b>Drawbacks</b>	Antibodies expensive to produce and store	Contamination and DNA extraction are problematic	Interference is a potential problem Relies on production and release of diagnostically useful VOCs from sample

### 1.3.1 Immunochemistry devices

Immunochemistry devices rely upon the immobilisation of antibodies specific to a particular protein produced either by the host during infection or by the pathogen to be detected. Several devices have been developed, some of which are fully commercialised, whereas other, more novel approaches are still in the early stages and take advantage of recent enabling technologies.

Li et al. (2011) have developed a paper based immunochemistry device capable of detecting *S. aureus* or *P. aeruginosa* between cell concentrations of 500 to 5000 CFU/ml. Gold nanoparticles are used to produce a colour change in the test strip that indicates the presence of pathogen of interest. Impedance spectroscopy approaches have also been employed for the detection of pathogens using aptamers and antibodies (Muñoz-Berbel et al. 2008b). An example of this is the system developed by Bekir et al. (2015). In this system, anti *S. aureus* antibodies were immobilised on a gold electrode. Using impedance spectroscopy and cyclic voltammetry in conjunction with a redox probe, the investigators demonstrated that stressed *S. aureus* cells could be detected down to a concentration of 10 CFU/ml.

A number of well established commercial devices are also available, such as those based upon lateral flow immunochromatography (LFI), which rely on a fluid sample absorbed onto a solid substrate. Market leading individual cartridge tests are provided by Alere (BinaxNOW) for *Legionella*, *S. aureus* and *Streptococcus pneumoniae* infections, in addition to a number of viral and malaria tests. LFI tests are also available from Quidel (QuickVue) for *Legionella* and Streptococcal pharyngitis. Clinical studies highlight that a key limitation of these tests is the interpretation of the result, which can lead to false negatives (Moore et al. 2013). Furthermore, the tests require the use of reagents with expiry dates and require trained personnel for their use. Also, only a limited number of bacteria are detectable via these tests, and each species requires a different cartridge.

An alternative approach using LFI tests is to screen for inflammatory biomarkers produced by the host. In particular, LFI tests are available for the detection of CRP, an inflammatory marker of infection. Point of care tests measuring CRP is a well established market with several suppliers (e.g. Alere Affinion). The tests are widely used to support decision making for antibiotic prescription in Scandinavian countries. They have been found to be cost effective and are believed to be part of the reason for the reduced levels of antibiotic



resistance seen (Oppong et al. 2013; Hunter et al. 2015). The main drawback of this approach is that once CRP is expressed and detectable, the infection is already present and established.

### **1.3.2 DNA diagnostic devices**

Molecular diagnostic devices are based upon the detection of small molecules, indicative of a particular pathogen, such as short DNA sequences or specific biomarkers. Several different innovative approaches have been developed, at different levels of maturity, including microfluidic molecular devices (Wu et al. 2013). Numerous systems have also been developed that use impedance spectroscopy to detect the presence of PCR product. For example, by immobilising short strands of peptide nucleic acid (PNA) on the surface of a gold electrode, Corrigan et al. (2012) were able to detect down to 10 pM of DNA from the *MecA* gene in *S. aureus* using impedance spectroscopy. Several steps were required to prepare the electrodes and sample, but a change in the charge transfer resistance could be seen after 2-3 minutes of adding the *mecA* gene to the electrode. Commercially available devices currently rely on the detection of DNA sequences and are aimed at the small laboratory user, rather than the GP or patient at home. This is partly due to the need for significant sample preparation, instrument operation and results interpretation. Molecular systems related to infection detection are currently available from Cepheid (GeneXpert) for the detection of *S. aureus* (including MRSA) and *C. difficile*, in addition to a number of virus targets. A system is also produced by BD, BDMax, for the detection of hospital acquired infection pathogens: *C. difficile*, MRSA and *S. aureus*.

### **1.3.3 Volatile organic compounds signature devices**

Much research effort has been put into the detection of disease through breath analysis and the detection of other volatile compounds. These technologies are attractive because of the minimally invasive nature of a breath sample. In practice however, it is susceptible to interference. For example, *P. aeruginosa* produces hydrogen cyanide (HCN), a detectable volatile compound, but *Helicobacter pylori* (a stomach pathogen) also produces HCN (Sethi et al. 2013). A novel spinout company called Owlstone entered the VOC market for detection of explosives with a reprogrammable microchip sensor. They are moving into the medical device market, and have demonstrated the ability to identify TB but their approach and technology is yet to be conclusively proved in the detection of lung pathogens.

## **1.4 Electrochemical changes mediated by microbial growth**

This section provides an overview of the literature related to the electrochemical detection of the growth of microorganisms. Electrochemical changes caused by bacteria have been broken down into three broad processes: direct microbial interactions at the electrode-electrolyte interface, changes to the media as an indirect effect of microbial growth, and the production of electroactive compounds as a consequence of microbial growth. Each of these are discussed in detail below, with a focus on the detection of changes using impedance spectroscopy. A large proportion of the research relating to the electrochemical detection of microorganisms focuses upon the use of bio-affinity agents for the specific detection of the analyte (Varshney and Li 2009). As the focus of this project relates to the detection of microorganisms using a reagentless, labelless sensor, this review focuses upon those studies that do not use specific chemical targets such as antibodies, DNA probes or aptamers for detection.

### **1.4.1 Direct microbial changes caused by cell-electrode mechanisms**

#### **1.4.1.1 Microbial attachment and biofilm formation**

Several studies have demonstrated the use of interdigitated microelectrodes to detect the presence of microorganisms within a sample. These systems are advantageous because their small size allows a greater rate of reactant supply, effective cycling of ionic species and therefore improved sensitivity (Varshney and Li 2009). Yang et al. (2003; 2004) studied the detection of *Salmonella tyhimurium* using impedance spectroscopy. In two separate studies, one with a gold working electrode (Yang et al. 2003) and one with an indium tin oxide (ITO) electrode (Yang et al. 2004) they used basic series RC circuit models to interpret the observed impedance signatures and found that the capacitance of the double layer increased, attributable to presence of more ionic compounds as the media was broken down by the bacteria (Figure 1-5). In the gold electrode system, they found that the charge transfer resistance increased as a result of cells impeding the flow of current (Yang et al. 2003). An increase in the corrected resistance (after taking into account solution conductivity) was also thought to occur in the case of the ITO electrode system (Yang et al. 2004). In this case, the microbial cells themselves were not thought to directly affect the double layer because the electrode-cell surface gap is greater than the double layer thickness, instead impeding the current immediately adjacent to the electrode.

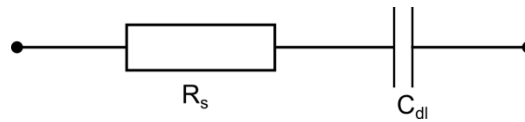


**Figure 1-5: Equivalent circuit used by Yang et al. (2003).**

Muñoz-Berbel et al. (2006) also used gold microelectrodes with a simple series equivalent circuit to characterise the attachment of *P. aeruginosa*. A constant phase element related to the double layer capacitance was found to drop after 80 hours growth, resulting in an increase in the impedance. The authors attribute this change to the attachment of cells and biofilm formation (microbial attachment was observed by microscopy at 50 hours) reducing the electrode active area.

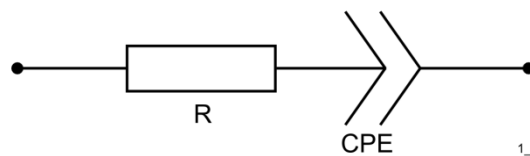


**Figure 1-6: Equivalent circuit used by Muñoz-Berbel et al. (2006).**

Characterisation of *E. coli* at platinum electrodes was also thought to result in a drop in the interface capacitance (Muñoz-Berbel et al. 2007). In this study, the attachment of bacterial cells to the working electrode was detectable after 40 minutes. Furthermore, larger concentrations of bacteria resulted in larger changes to the calculated interfacial capacitance parameter (Muñoz-Berbel et al. 2007). Developing this concept further, the investigators went on to explore whether it was possible to detect microbial attachment over relatively short time periods (Muñoz-Berbel et al. 2008c). Using *E. coli*, they observed an initial increase in the interface capacitance (using a CPE in an equivalent circuit - Figure 1-7) thought to be due to the counter ion effects of the attachment of small numbers of microbial cells to the electrode surface (Muñoz-Berbel et al. 2008c). In addition, a capacitance related to the AgAgCl reference electrode was also included in the measurement ( $C_{ref}$ ), although the investigators don't report the rationale for including the capacitance of the reference electrode, or why it is placed in parallel with the working electrode. A subsequent drop in the CPE occurred, resulting from the maturation of the biofilm during which the electrode surface becomes coated with extrapolsacchrude matrix and bacteria cells with a low capacitance.

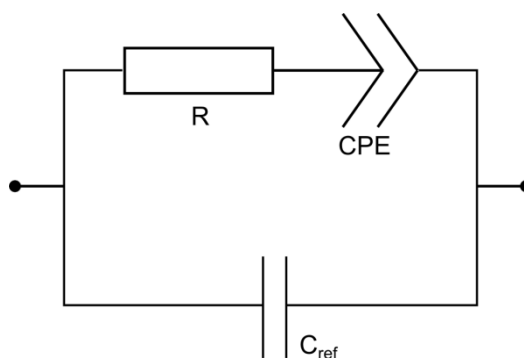


**Figure 1-7: Equivalent circuit used by (Muñoz-Berbel et al. 2008c).  $C_{ref}$  is related to a capacitance associated with the reference electrode and did not change throughout the experiment.**

The system described above was subsequently applied to the detection of bacteriophages in *E. coli* and *P. putida* biofilms (Muñoz-Berbel et al. 2008a). In this study, a more sophisticated equivalent circuit was used (Figure 1-8), with a capacitive parameter to describe the porosity of the biofilm ( $C_{biofilm}$ ). This was found to increase throughout the first 5 days of the experiment.  $C_{biofilm}$  dropped as a result of bacteriophage infection of the biofilm, whereas the double layer component of the equivalent circuit remained the same. The impedance results suggested that the biofilm structure changed as a result of infection, but that the inner cells remained attached to the electrode surface.

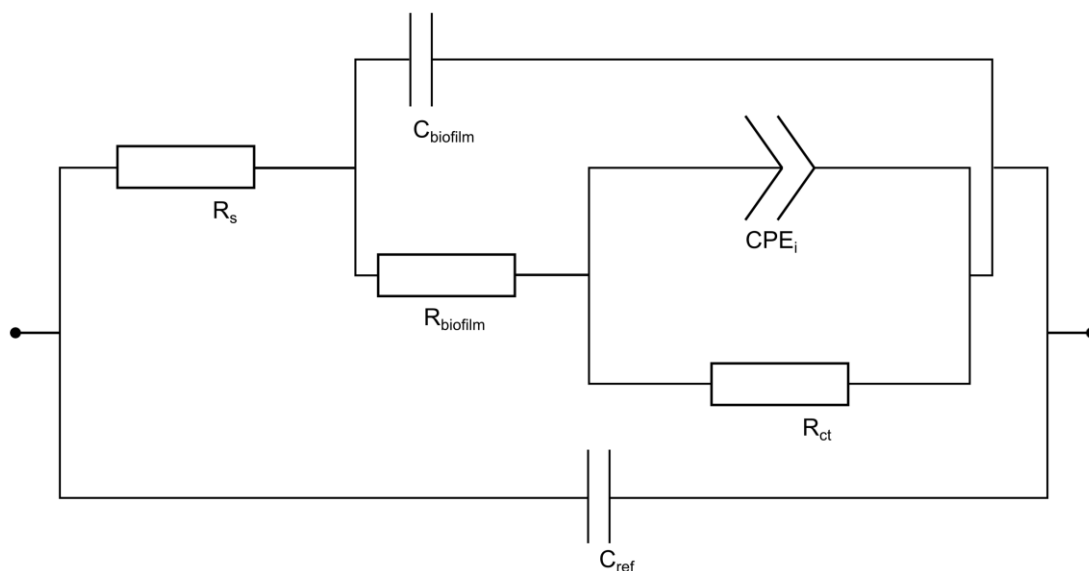


**Figure 1-8: Equivalent circuit used by Muñoz-Berbel et al. (2008).**

*In situ* biofilm formation of *S. epidermidis* has been studied with gold electrodes printed onto a silicon oxide wafer (Paredes et al. 2012). In this investigation, real-time labelless monitoring of biofilms was carried out using an adapted version of the centre for disease control (CDC) bioreactor. The electrodes consisted of 20  $\mu\text{m}$  fingers separated by a distance of 30  $\mu\text{m}$ . Changes to the impedance were thought to be caused by a change in the composition of the media and deposition of cells and biofilm matrix onto the sensor surface. The greatest changes to the impedance occurred at lower frequencies (<1 kHz) where the investigators found that microorganism concentration was directly related to an increase in the capacitance. Furthermore, over the course of the experiment, there was a relative drop in the impedance magnitude, with characteristic changes appearing in the series resistance and capacitance data over the course of the experiment. Paredes et al. (2013) adapted the interdigitated electrodes to characterise the attachment and growth of *S. aureus* and *S. epidermidis* strains in 96 well microtitre plates. The aim was to evaluate the sensors for possible use in intravascular catheters. The greatest change in the impedance was again observed at lower frequencies, as an increase in the resistance and capacitance (Paredes et al. 2013). These were thought to be related to the deposition of cells on the electrode surface, which caused a greater impedance change than metabolic processes. Additionally, the initial inoculation volume affected the rate at which the measured resistance and capacitance parameters changes, with higher initial inoculation volumes resulting in greater changes to the impedance. A similar result to this was also observed by Zikmund et al. (2010) with *E. coli*, where they found a 10% increase in the impedance of a Tantalum-Nikel-Platinum electrode following 24 hours of *E. coli* growth.

Using larger electrodes, the impedance properties of *P. aeruginosa* biofilms grown on platinum discs have been explored. Interestingly, the results of Kim et al. (2011) show consistency with other studies (Yang et al. 2003, 2004; Muñoz-Berbel et al. 2007). It was found that initial microbial attachment to the electrode surface resulted in a decrease in the double layer capacitance, caused by bacteria and associated material reducing the electrode active area (Kim et al. 2011). In order to specifically study the effect of biofilm formation, the investigators replaced the media with fresh electrolyte to perform the spectroscopy measurements. A PA14 $\Delta$ *wspF* mutant was also tested, which overproduces EPS biofilm material, thus creating thicker biofilm structures. A drop in the double layer capacitance was observed throughout the experiment, which was related to the formation of biofilm across the electrode surface. However, only a slight difference in the impedance existed between the wild type and the mutant strain. In a related study, the double layer capacitance

was found to drop as a result of the attachment of *P. aeruginosa* cells to an interdigitated microelectrode (Kim et al. 2012) . These changes were thought to result from cellular appendages such as flagella, fimbriae and pili attached to the electrode surface reducing the electrode surface area. A slight change was also observed in the charge transfer resistance however this did not vary significantly from the negative control (Kim et al. 2012).

Pires et al. (2013) used gold electrodes in conjunction with a microfluidic device to measure cellular respiration and biofilm formation caused by *P. aeruginosa*. They report that the impedance modulus increased as a consequence of *P. aeruginosa* growth. Furthermore, using the amperometric system they had developed, they found that it was possible to detect respiration activity within the biofilm, which disappeared when treated with sodium azide (known to be an effective biocidal compound). The electronic system used to measure the impedance was also produced by the group and was based upon a microcontroller, indicating that a low cost impedance measurement system for monitoring microorganisms is achievable.

Dheilly et al. (2008) studied the formation of a biofilm by two different microorganisms (*P. aeruginosa* PAO1 and *Bacillus subtilis*) on stainless steel working electrodes. They also observed an increase in charge transfer resistance as a result of biofilm formation (verified through the use of SEM and CSLM). Furthermore, they found that the thickness of the biofilm affected the charge transfer resistance. The authors argue that the growth of cells on the surface of the electrode interferes with the electron transfer process and consequently leads to an increase in the measured resistance.

Some investigators have reported changes to the charge transfer upon initial attachment of microbial cells to an electrode surface. These transient charge transfer effects have been reported in *Staphylococcus epidermidis*, *Streptococcus salivarius* and *Actinomyces naeslundii* (Poortinga et al. 1999, 2001). Indium tin oxide and titanium oxy nitride electrodes were used to measure the change in potential as a consequence of microbial attachment over two hours (Bayouhd et al. 2008). During this time, the potential of the electrodes dropped, an effect thought to be related to the transfer of surface charge from the bacterium. Impedance spectroscopy was also used to detect the presence of *P. stutzeri* and *S. epidermidis* to ITO electrodes (Bayouhd et al. 2008). The intrinsic conducting and dielectric properties of the bacterial cells were found to decrease the charge transfer resistance at the electrode-electrolyte interface (Bayouhd et al. 2008).

A screen printing approach was used to produce electrodes for the detection of *S. aureus*, with a sensor that could be integrated into a POCT product such as a wound dressing. Farrow (2010) investigated the use of carbon and Ag-AgCl screen printed electrodes for detection of biofilm formation in chronic wounds (such as a diabetic leg ulcer) in order to detect the presence of infection-causing bacteria. In this study, electrode material and electrolyte selection were assessed in terms of their ability to inhibit growth and biofilm formation of *S. aureus* and also their ability to allow the detection of the bacteria using electrical impedance. Analysis was carried out by normalising the electrode impedance, a procedure which involves dividing the impedance measured at time  $n$  against the starting impedance (Connolly and Shedden 2010). This can be done for the measured value of the resistance, reactance, phase and magnitude. It removes the individual differences found between electrodes and allows changes between the starting signature and subsequent signatures to be easily identified. In these experiments, a shift in the phase angle peak and the peak magnitude frequency could be observed using Ag-AgCl electrodes at a concentration above  $8.5 \times 10^6$  CFU/ml (Farrow 2010; Farrow et al. 2012). During biofilm experiments, microscopic analysis of the electrode surface was carried out and indicated that few cells grew on the electrode surface. On the Ag-AgCl electrode, this was thought to be related to silver ions released into the adjacent electrolyte inhibiting the growth of cells.

Biofilm formation has also been characterised on ITO electrodes integrated into a flow cell device (Ben-Yoav et al. 2011). An equivalent circuit model for the analysis of impedance has also been presented (Figure 1-9), with an anomalous diffusion parameter to characterise the porosity of the biofilm on an ITO electrode (Ben-Yoav et al. 2011). Interestingly, the impedance characteristics of the biofilm formed on the electrode surface were dependent upon the DC bias potential across the electrode, with a DC bias of 600 mV correlated to biofilm growth. Applying their equivalent circuit model, they found that the capacitance of the biofilm increased over a deposition time of 120 minutes, whereas the biofilm resistance (as defined by their equivalent circuit) decreased.

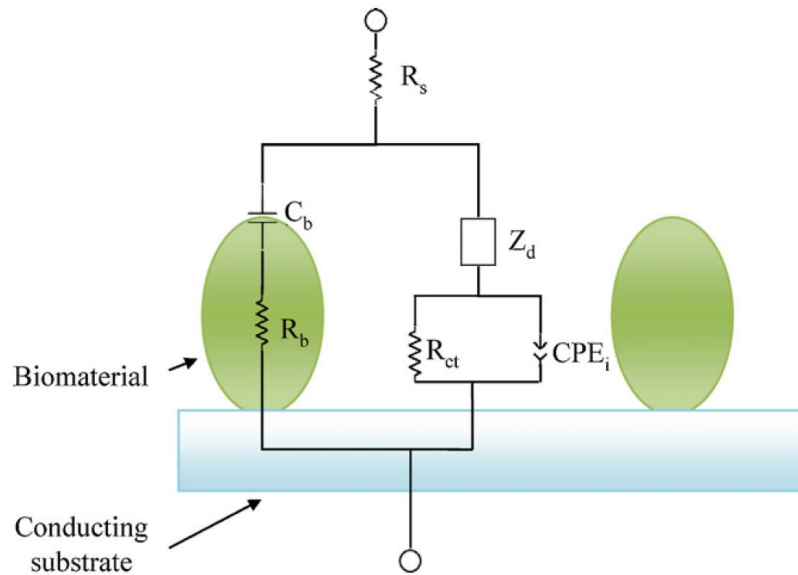


**Figure 1-9: Equivalent circuit model used by Ben-Yoav et al. (2011).  $R_s$  is the solution resistance,  $C_b$  is the biomaterial capacitance,  $R_b$  is the biomaterial resistance,  $Z_d$  is the anomalous diffusion type Warburg impedance element,  $CPE_i$  is the constant phase element of the solution electrode interface and  $R_{ct}$  is the charge transfer resistance. (Taken from Ben-Yoav et al. 2011).**

Biofilm matrix resulting from the growth of bacteria on the electrode surface is believed to affect the electrochemical characteristics of the electrode-electrolyte interface by changing both the capacitive and electron transfer properties. Conductive biofilms have been found in *Geobacter sulfurreducens*, in contrast to other bacteria where the biofilm matrix is thought to have insulating properties (Lovley 2008). *G. sulfurreducens* anode biofilms were shown to possess a discharge current when grown in the presence of a polarisation potential (Schrott et al. 2011). This was believed to result from cytochrome-c present in the biofilm matrix capable of acting as an electron acceptor shunt when the anode was at OCP. On re-polarisation of the anode, the stored charge within the biofilm was released (Schrott et al. 2011). Mechanisms of this nature suggest that biofilm structures produced by some bacteria could be electrically conductive.

#### 1.4.1.2 Impedance changes caused by high cell densities

High cell densities could affect the conductivity and dielectric properties of the sample and the electrode interface. Applying principles of dielectric spectroscopy, Harris et al. (1987)



were able to show that it is possible to quantify the mass of yeast cells that existed in a fermentation process. Their measurement was carried out using screened platinum electrodes at frequencies ranging between 100 kHz and 10 MHz. By measuring the impedance (and specifically the capacitance) in the frequency range associated with the beta dispersion, the investigators were able to identify a linear relationship between the capacitance and the mass of cells present. The greatest change in the capacitance measured was observed at the lower range of the frequency spectrum measured (300 kHz). Furthermore, they identified that the conductivity of the extracellular media varies only a small degree at high concentrations. When calcium carbonate was added to the medium during the impedance test (to represent artefact), it did not affect the measured capacitance. This meant that it would theoretically be possible to measure microbial mass from 0.2 mg/ml up to 100 mg/ml.

#### **1.4.1.3 Electrochemical changes mediated by outer membrane proteins**

In some microbial species, electron transfer may be facilitated through a direct contact pathway (Hernandez and Newman 2001). Reguera et al. (2005) used conducting probe atomic force microscopy and found that pilus-like nanowires produced by *Geobacter* species were electrically conductive, whilst no conductivity was found in *S. oneidensis* or *P. aeruginosa* species. From this, they proposed a model for extracellular electron transfer through the pilus from electron donors in the periplasm or outer membrane electron transfer proteins (Reguera et al. 2005). The role of conductive pilus has also been implicated in the long range transfer of electrons during *G. sulfurreducens* biofilm growth through the production of a network of nanowires (Reguera et al. 2006). In a separate study a different approach was adopted using scanning tunnelling microscopy and spectroscopy to identify conductive nanowires in *S. oneidensis* in response to electron acceptor limitations (Gorby et al. 2006). Importantly, Gorby et al. 2006 report that a cyanobacterium (*Synechocystis* spp) and a thermophilic fermentative bacterium (*Pelotomaculum thermopropionicum*) also produce conductive nanowires, which suggests that this mechanism is not limited to metal-reducing bacteria. These studies demonstrate the flexibility of bacteria to use multiple mechanisms to facilitate electron transfer over large distances.

## **1.4.2 Indirect electrode-electrolyte changes caused by microbial mechanisms**

### **1.4.2.1 Microbial breakdown of growth media**

A number of impedance based microbial growth measurement techniques were developed in the 1970s and 1980. The basis of these approaches was the monitoring of impedance during microbial growth in different media. During growth, the bacteria within the media break down nutrients into charged particles, which are subsequently detectable through the changes they cause to the bulk conductivity. Specifically, the increased number of charged molecules, along with their smaller size lead to increased motility and result in a higher conductivity within the medium (Cady 1975). These techniques resulted in the development of commercial devices, such as the Bactometer® and the Malthus Microbiological Growth Analyser (Firstenberg-Eden and Eden 1984).

Cady (1975) produced a system consisting of gold electrodes and sterile media to detect the relative changes in impedance between a reference and sample well. After inoculation, the system was placed into a shaking incubator to ensure adequate mixing of the media and bacteria along with adequate aeration. Through measurement of microbial growth in a number of different media at the same time, Cady (1975) was able to determine a specific signature for different species of bacteria. In another series of experiments, by controlling the level of salt through the choice of media used, the sensitivity of the sensor could be improved. For example, the detection of red blood cell lysis was possible through the use of a low salt medium. The rapid detection of *E. coli* was also facilitated through the use of a low salt medium. The changes observed between the inoculated cell and the control cell indicate a fall in the overall impedance, thought to be due to an increase in the dielectric constant and an increase in the number of charged, highly mobile ions. Furthermore, a link was postulated between the bacterial growth and metabolite accumulation on the electrode surface. A charged layer was thought to develop at the electrode surface, which could be removed over time when the electrode cell was washed and flooded with sterile media (Figure 1-10). It is interesting that the impedance rose over a long period in fresh media, rather than immediately upon removal from the inoculated media. This may suggest that the charged layer on the electrode surface had been chemically adsorbed.

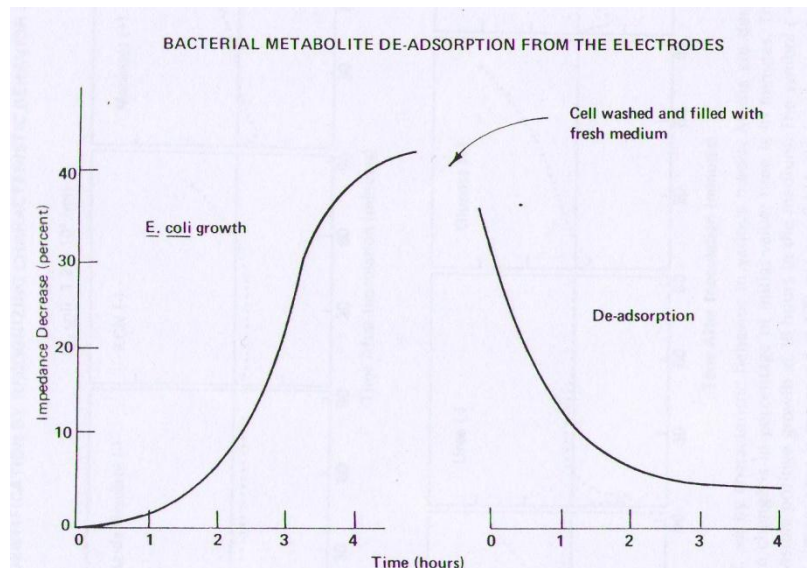


**Figure 1-10: De-adsorption of metabolites from the electrode surface following flooding of measurement cell with sterile media. (Cady 1975)**

Through the measurement of conductivity, Richards et al. (1978) showed that it was possible to detect the presence of *E. coli* bacteria and conducted a series of experiments to prove the validity of their results. In their experimental system, wire electrodes fabricated from platinum were fused into test tubes. The cell was then filled with media and the whole assembly autoclaved prior to inoculation. Measurement of impedance focused exclusively on the conductivity of the media, as a consequence of the authors' observations that the capacitance was subject to significant random fluctuations (Richards et al. 1978).

Changes in conductivity of an inoculated growth medium were studied extensively by (Firstenberg-Eden and Eden 1984). They suggest some of the pathways through which the nutrients within the media may be broken down. For example, carbohydrates may be broken down into lactate and then carbonic acid or bicarbonate. The authors also highlight the importance of temperature in the measured conductivity. They used the change in temperature to explain the initial sharp rise in conductivity at the start of the experiment, resulting from the start of the incubation period.

#### **1.4.2.2 Ion adsorption on the electrode surface**

Early researchers developed theories of the changes that occur to the double layer as an indirect result of microbial growth (Hause et al. 1981; Noble et al. 1999). Hause et al. (1981) found that an abrupt change in the impedance could be observed between 5 and 10 hours of culture growth. The drop in impedance signature observed was greatest at low frequency suggesting that the effect is due to changes at the electrode surface (Hause et al.

1981). They present a model that shows the phase angle associated with diffusion controlled impedance can fall between 45 and 90 when the proportion of ions participating in electron transfer (for example, as tissue dispersive effects appear). Using this model, the increased angle of the Warburg impedance during the experiment may have been due to adsorbed ions from the media participating in the double layer capacitance. As mentioned above, at least one investigator noticed that the capacitance was subject to unpredictable fluctuation and recommended against its use (Richards et al. 1978). This view highlights the importance of the electrochemical cell design. In their experiment, Richards et al. (1978) used relatively small electrodes with a large distance between them (in contrast to many other studies). This may have led to the detection of artefact (such as stray capacitance) in the measurements taken. It has been reported that the electrode size, configuration and cell geometry have a profound effect upon the measured impedance (Muñoz-Berbel et al. 2008b).

Analysis of the electrode-electrolyte interface properties as a result of microbial growth have been studied theoretically and experimentally by Noble (1999) and Noble et al. (1999). Noble (1999) proposes that the susceptance is defined by the Stern model for the double layer, combined with a series contribution from a passive oxide layer formed on stainless steel electrodes. This model implies a link between the ionic concentration of the media and the measured susceptance, because the diffuse layer described by the Stern model decreases as the ionic concentration of the bulk electrolyte increases. This was supported by their experimental finding (Noble et al. 1999), which showed that an increase in the ion concentration of an electrolyte with low conductivity resulted in an increase in the susceptance, whereas little increase in susceptance was observed for an electrolyte that already had a high conductivity. The hypothesis suggested by (Noble et al. 1999) is also in agreement with the findings of Yang et al. (2004) who suggest that the changes observed in the measured double layer are due to ionic changes in the media, given that there is a gap of between 10 nm to several 100 nm between the electrode and the bacterial cell surface (see section 1.4.1). Noble et al. (1999) suggest that the change observed in the susceptance may also be the result of proton production in bacterial metabolism. In this case, the protons were thought to interact with the oxide passivation layer on the electrode surface, rather than affecting the Stern capacitance. Noble et al. (1999) didn't identify any relationship between the susceptance and the adsorption of organic or inorganic molecules on the electrode surface. However, a drop in the double layer capacitance has been observed in an electrochemical cell when tryptone was added to the electrolyte (Kim et al. 2011).

Felice and Valentinuzzi (1999) attempted to break down the components of the observed frequency into a resistance from the culture medium ( $R_m$ ), an interface reactance ( $X_i$ ) and an interface resistance ( $R_i$ ). They achieved this through a frequency variation measurement and electrode distance variation measurement. The frequency variation was used to calculate the resistance at high frequency where the contribution to the measured resistance from the interface resistance is minimal and then subtracting this value from the measured resistance at low frequency in order to determine  $R_i$ . The interface reactance was calculated as follows:

$$X_t = 2X_i + X_p \quad [1-1]$$

$$X_p = \frac{\omega C_m}{G_m^2 + (\omega C_m)^2} \quad [1-2]$$

Where  $X_t$  is the total reactance,  $X_i$  is the interface reactance,  $X_p$  is the reactance of the media,  $C_m$  is the capacitance of the media,  $\omega$  is the angular frequency and  $G_m$  is the conductivity of the media. From the investigations and subsequent analysis, they conclude that no detectable effects can be seen on the interface reactance or resistance. Instead, they attribute the change in the impedance they observed to the changes in  $R_m$  (i.e. resistance of the culture media) as a result of microbial growth.

### 1.4.2.3 Microbial production of electroactive metabolites

A number of studies have been carried out that suggest electroactive compounds produced by microorganisms could have an electrochemical effect. These mechanisms are distinct from changes in the bulk conductivity of the media, as they allow charge transfer to occur between the electrode and electrolyte and are more specific to particular species of organisms.

Several facultative anaerobic bacteria are known to produce electroactive secondary metabolites. Some of these compounds have been elucidated in the context of microbial fuel cells, particularly in *Shewanella* spp. (Brutinel and Gralnick 2012; Gralnick and Newman 2007; Hernandez and Newman 2001; Marsili et al. 2008a; Newman and Kolter 2000). Riboflavin produced by *Shewanella* has been shown to be redox active and is thought to play a role in extracellular respiration (Marsili et al. 2008a). By replacing the supernatant of the media with fresh media, Marsili et al. (2008) showed that extracellular compounds changed the redox properties of the culture. They went on to relate these changes to riboflavin

adsorbed to the electrode surface. There is evidence to suggest that extracellular flavins secreted into the supernatant transfer electrons through cytochrome outer membrane proteins to insoluble electron acceptors, such as Fe(III) or electrodes (Brutinel and Gralnick 2012).

Whilst much of the work in this field has been carried out on *Shewanella* spp, other microorganisms are also capable of secreting redox active metabolites. It is well known that *P. aeruginosa* produces the phenazine pyocyanin, a known virulence factor in infection (Baron and Rowe 1981; Fothergill et al. 2007; Hassett et al. 1992; Lau et al. 2004; Pierson and Pierson 2010; Ran et al. 2003). Furthermore, the phenazine family of compounds to which pyocyanin belongs have been widely reported as being redox active and implicated in the facilitation of extracellular respiration (Pierson and Pierson 2010; Price-Whelan et al. 2007; Rabaey et al. 2004; Wang et al. 2011).

Another group used an *E. coli* strain which they evolved within an microbial fuel cell (MFC) to produce a higher power output (Zhang et al. 2006, 2008b). The change in power output was possibly caused by the following redox active electron carriers: ethyl 2-aminoacetimidate, methyl 4-ethoxybutanoate and 3-isobutylhexahydropyrrolo[1,2-a]pyrazine-1,4-dione (Zhang et al. 2008b).

Electroactive species have been identified in a *Klebsiella pneumoniae*, strain L17 isolated from forest sediment (Li et al. 2013; Xia et al. 2010; Zhang et al. 2008a). Biofilm formation and nanowires produced by the bacteria could have caused the observed electrochemical changes (Zhang et al. 2008a). A later study suggested that the changes were due to quinone-like substances secreted into the media (Xia et al. 2010).

Two electrochemically active strains of *Clostridium* spp. have also been identified, *C. butyricum* and *C. beijerinckii*, however, the electrochemical change is thought to originate from the breakdown of starches whereas the pathogenic strains (*C. botulinum* and *C. tetanie*) gain their energy through fermentation (Niessen et al. 2004).

Detection of electroactive compounds have also been explored for use in POCT devices. Sharp et al. (2010) used carbon fibre tow to detect the presence of the *P. aeruginosa* secondary metabolite pyocyanin. Their device, which they propose could be adapted for use in a smart bandage, is capable of linear detection of pyocyanin within the physiologically relevant range between 1  $\mu$ M and 100  $\mu$ M. It operates using square wave voltammetry to detect the presence of an oxidation peak at -0.17 volts.

## 1.5 Conclusion

The diverse discipline of electrochemistry provides techniques and tools that can be used to study electrolytes and interfaces. Several investigators have used these tools in order to detect the presence of bacteria with different experimental arrangements. The literature discussed above demonstrates that the use of impedance spectroscopy to detect the presence of bacteria in a reagentless manner is feasible. Most of these detection techniques, however, rely on sophisticated equipment, electrodes that are challenging and expensive to manufacture, or require specialist expertise to operate. Therefore there are several obstacles towards implementation in a POCT context.

It is also worth noting the work that has been carried out in the study of microbial fuel cells. Several species which are also known to be pathogenic such as *P. aeruginosa*, *K. pneumoniae* and *E. coli* have been studied within this context and the literature relating to the mechanisms of charge storage and transfer could be useful as detection strategies in POCT scenarios.

The most common CF airway pathogen is arguably *P. aeruginosa*, which is a major cause of respiratory dysfunction and mortality (Hassett et al. 2009). Recent outcomes relating to eradication therapy suggest that the prompt detection of initial infection with *P. aeruginosa* could help to delay chronic infection and improve patient quality of life. Whilst the trigger event for pulmonary exacerbations has not been clearly elucidated, it is widely acknowledged that treatment with antibiotics reduces symptoms and density of cells. Monitoring *P. aeruginosa* concentration and phenotypic behaviour within sputum samples on a daily basis could allow the detection of a pulmonary exacerbation before the patient becomes symptomatic and also provide important information on the underlying processes.

Whilst *P. aeruginosa* is recognised as an important CF airway pathogen, other pathogens are also found, specifically *Haemophilus influenzae*, *Staphylococcus aureus*, and *Burkholderia cepacia* complex (Harrison 2007). Therefore, sputum samples from patients are likely to be complex, and the specific detection of *P. aeruginosa* against a background of other microorganisms using a reagentless sensor is inevitably challenging.

Impedance spectroscopy could be a useful electrochemical technique within this context, as different electrochemical processes are dominant at different frequencies. As described in the previous sections, a number of bacteria mediated electrochemical processes have been identified, which could have an effect upon an electrode-electrolyte interface that would be

detectable using impedance spectroscopy (Figure 1-11). Some of these processes have been postulated to cause a change in impedance in other studies carried, as described above.

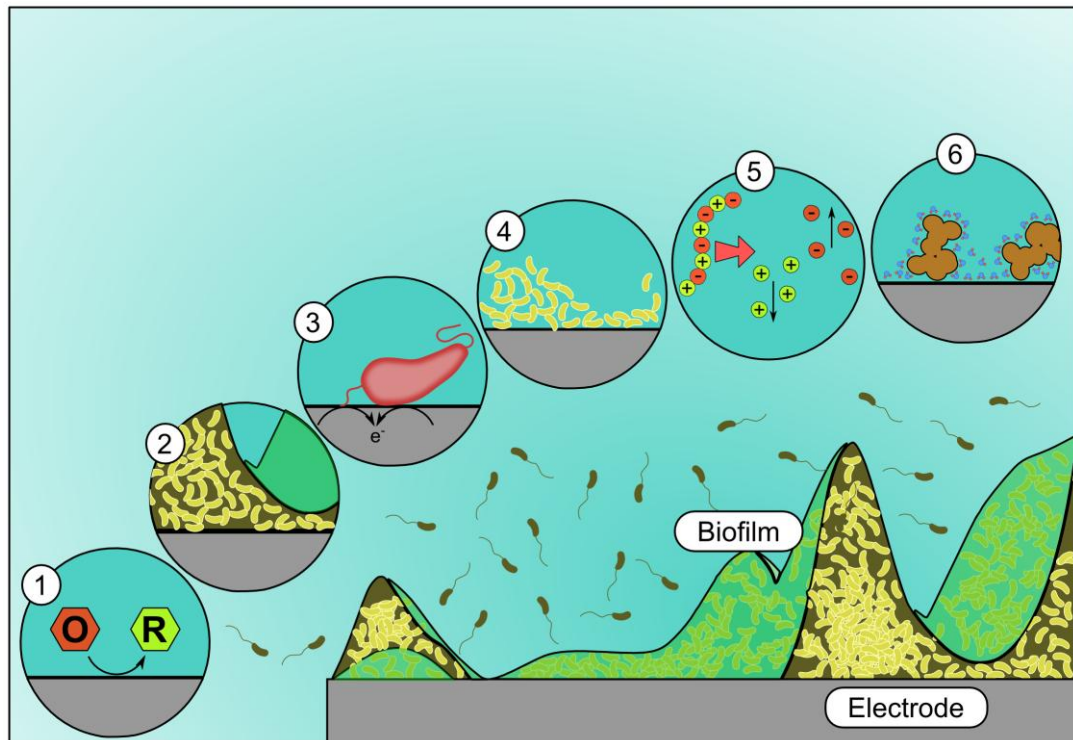


**Figure 1-11: Principal proposed mechanisms affecting impedance as a result of microbial material. (1) Electroactive secondary metabolites facilitate a charge transfer at the electrode/electrolyte interface; (2) Biofilm matrix attached to the electrode surface affects capacitance and/or charge transfer; (3) Direct microbial attachment, through pili, flagella and outer membrane proteins facilitate charge transfer; (4) Outer cell membrane contact at high cell densities affects capacitance; (5) Breakdown of nutrients within the media reduce solution resistance; (6) Protein/macromolecule adsorption on the electrode surface influences double layer capacitance.**



## **1.6 Objectives of this study**

### **1.6.1 Research goal**

The goal of this research is to use a screen printed electrochemical sensor in conjunction with EIS to determine if it is possible to detect the presence of *P. aeruginosa* against a background of other microorganisms commonly found within the CF airway.

### **1.6.2 Research questions**

Within this thesis, the following research questions are explored:

1. Is it possible to detect the growth of *P. aeruginosa* using impedance spectroscopy and a screen printed sensor?
2. Is there a characteristic impedance signature that indicates the presence of *P. aeruginosa* in microbial broths also containing other microorganisms commonly found in the CF airway?
3. Why does the impedance change as a result of microbial growth?
4. Is it possible to link a given impedance signature with a specific metabolite or compound produced by the bacteria?
5. What impact does biofilm formation have on the impedance signature, both directly and indirectly?

## **2 ELECTROCHEMISTRY AND MICROBIOLOGY THEORY**

## 2.1 Electrical theory

Resistance is defined by Ohm's law as the ratio between the voltage and current of a given conductor. In a DC circuit:

$$R = \frac{V}{I} \quad [2-1]$$

Where  $V$  is the potential difference in Volts,  $I$  is the current in Amperes and  $R$  is the resistance in Ohms or  $\Omega$ .

Capacitance relates to a transient increase in the potential difference between conductors that are separated by an insulating material (Figure 2-1).

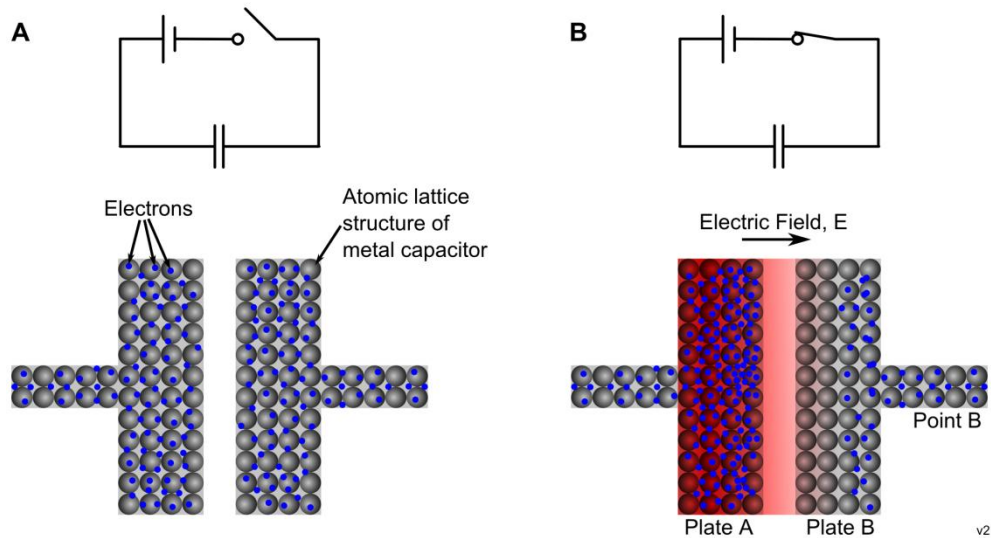


**Figure 2-1: Fundamental Principles of Capacitance. (A) In an open circuit, there is no electromotive force and therefore equal charge density exists on both plates. (B) On application of an electromotive force, electron buildup on plate A results in an electric field large enough to displace electrons on plate B, leading to a flow of current at point B. This continues until the maximum charge density is achieved at plate A then no further current can flow and the maximum potential difference exists between plates A and B.**

In a vacuum, the properties of a capacitor are defined by its area and the distance between the plates:

$$C = \frac{\epsilon_0 A}{d} \quad [2-2]$$

Where  $C$  is the capacitance measured in Farads,  $\epsilon_0$  is the permittivity of free space (i.e. of a vacuum –  $\epsilon_0 = 8.854 \times 10^{-12} \text{ C}^2\text{N}^{-1}\text{m}^{-2}$ ),  $A$  is the area in  $\text{m}^2$  and  $d$  is the distance between the plates in metres. Replacement of the vacuum between the plates by an insulating material containing polar molecules (called dipoles) affects the capacitance.

Dipoles in the dielectric play a key role in the capacitance by turning under the influence of an electric field (Koryta 1991). Orientation of the dipoles within the dielectric partially compensates for the effect of the charge that builds up on the capacitor plates and therefore leads to an increase in the capacitance (Koryta 1991). The effect of the dielectric material on the capacitance is defined by the dielectric constant of the material, which is quoted relative to the permittivity of free space ( $\epsilon_0$ ). Thus:

$$C = \frac{\epsilon_0 \epsilon_r A}{d} \quad [2-3]$$

Where  $\epsilon_r$  is the relative permittivity.

In an AC circuit capacitive and inductive components may impede the flow of current in addition to resistance. The contribution to impedance produced by inductive and capacitive elements is called the reactance, whilst the contribution made by the resistive element is termed the resistance. The term impedance is used to describe the obstruction to current presented by the whole system (i.e. combined contributions from resistance and reactance) and is frequency dependant. In terms of the electrochemistry of biological matter, the capacitive and resistive aspects of the impedance are of most interest as inductance is rarely observed (Muñoz-Berbel et al. 2008). The reciprocal of resistance and reactance are termed the conductance and susceptance (Table 2-1).

**Table 2-1: Corresponding relationships between key terms**

Impedance Term	Admittance Term	Relationship
Impedance (Z)	Admittance (Y)	$Z = 1/Y$
Resistance (R, Z')	Conductance (G)	$R = 1/G$
Reactance (X, Z'')	Susceptance (B)	$X = 1/B$
Resistivity ( $\rho$ )	Conductivity ( $\sigma$ )	$\rho = 1/\sigma$

Impedance can be usefully interpreted through the application of complex numbers where the resistance is treated as the real part and the reactance as the imaginary part, leading to:

$$Z = Z' - jZ'' \quad [2-4]$$

Where  $Z$  is the overall impedance,  $Z'$  is the real (resistive) component,  $Z''$  is the imaginary (reactive) component and  $j = \sqrt{-1}$ . This complex number is related to the phase shift that occurs between the current and voltage in AC circuits with reactive components and can be shown in a complex impedance plot, or Nyquist plot (Figure 2-2). The complex number may also be expressed in polar form as follows:

$$Z = |Z|\angle\theta \quad [2-5]$$

Where  $|Z|$  is the modulus of impedance defined as the vector between the reactance and the resistance (Figure 2-2):

$$|Z| = \sqrt{(Z')^2 + (Z'')^2} \quad [2-6]$$

And  $\theta$  is the phase angle, defined by:

$$\theta = \tan^{-1}\left(\frac{Z''}{Z'}\right) \quad [2-7]$$

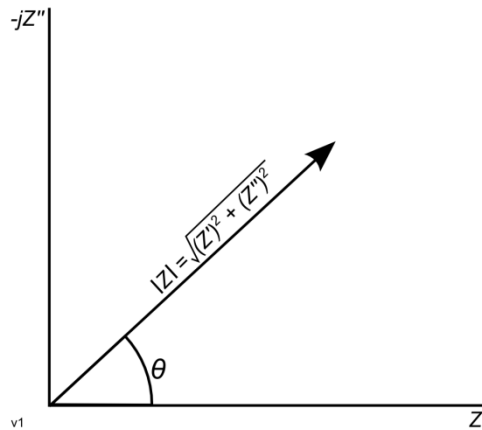


**Figure 2-2: Example plot of impedance vector, showing the relationship between resistance ( $Z'$ ), reactance ( $Z''$ ), impedance magnitude ( $|Z|$ ) and the phase angle ( $\theta$ ).**

In a perfectly capacitive circuit, the current leads the voltage by  $90^\circ$ . The impedance in this instance may be described as:

$$Z_{Pure\ capacitor} = (0 \times Z') - jZ'' \quad [2-8]$$

Therefore, a purely capacitive circuit, (i.e. one in which the current leads the voltage by  $90^\circ$ ) can be described completely by a vector at  $90^\circ$  from the real axis, with a magnitude of  $Z_{Pure\ capacitor}$ . Similarly, in the case of a purely resistive circuit, the current and the voltage are perfectly in phase. Therefore the phase angle is  $0^\circ$ , and:

$$Z_{Pure\ resistor} = Z' - (0 \times jZ'') \quad [2-9]$$

This can be described by a vector located purely on the real axis. A combination of resistive and capacitive components will result in a plot that fall somewhere between these two extremes, whereby:

$$-90 \leq \theta \leq 0$$

A summary of the relationship between the complex plot and the time domain is shown for a purely resistive and purely reactive circuit in Figure 2-3.

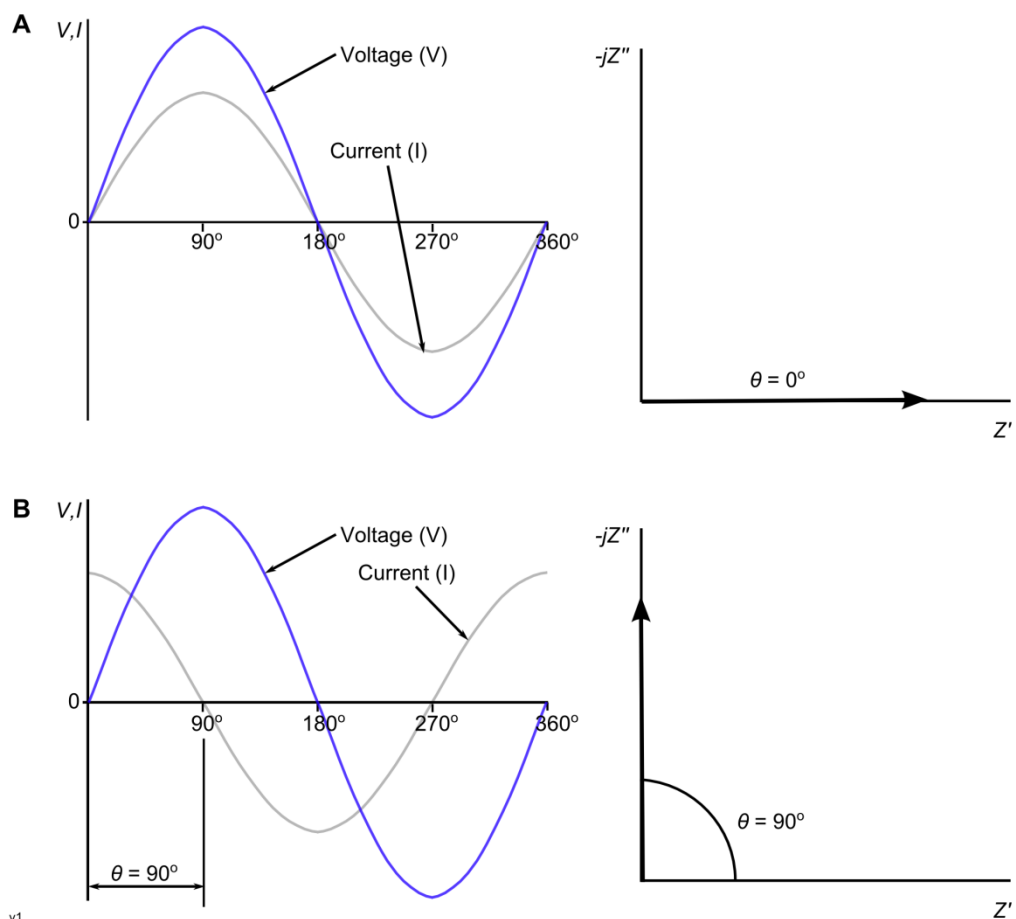


**Figure 2-3: Relationship between time domain and complex plot for (a) a purely resistive circuit and (b) a purely capacitive circuit.**

## 2.2 Electrochemical theory

### 2.2.1 Introduction: Fundamental electrochemical processes and impedance spectroscopy

Several fundamental processes occur at an electrode-electrolyte interface. Impedance spectroscopy measures the resistance and reactance of an electrode in contact with an electrolyte across a spectrum of AC frequencies. A number of electrochemical processes affect these two measurements at different frequencies as shown in Figure 2-4 (Bard and Faulkner 2001; K'Owino and Sadik 2005). The ability of the electrode to exchange electrons with the electrolyte is governed by the electrode material and the composition of the media. For example, if electroactive compounds are present within the electrolyte and the electrode is held at an appropriate redox potential, then a charge transfer is possible that affects the measured impedance. The availability of the electroactive species at the electrode surface also has an impact on the electron transfer rate across the interface and therefore the

impedance in a diffusion dependant manner. Other processes which affect impedance include the dielectric properties of the electrolyte adjacent to the electrode and the resistance of the bulk electrolyte. The former is known as the double layer capacitance and is defined by the relationship between polar and non-polar molecules and structures in very close proximity to the electrode. The latter is defined by the number and size of ions and other charged compounds within the media that convey charge between the electrodes. Solvation of ions will also influence their movement through the media. These fundamental processes are discussed in detail in the following section.

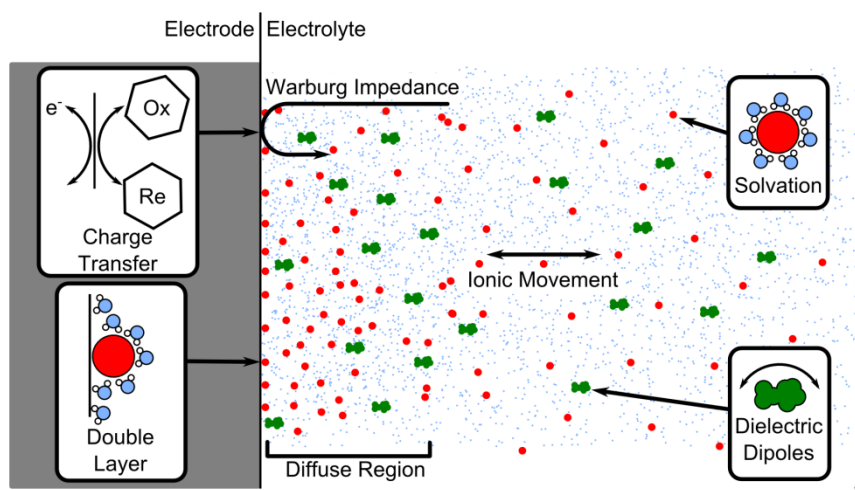


**Figure 2-4: Fundamental electrochemical processes. A number of processes can occur in an electrochemical system, including charge transfer, double layers, diffuse regions, Warburg impedance, ionic movement, solvation and dielectric dipoles.**

## 2.2.2 Properties of electrolytes

### 2.2.2.1 Solvation and hydration

When a salt is placed into a solvent such as water, the water ionises the salt producing an electrically conducting solution (Grimnes and Martinsen 2008). In response to the presence of the ion, a structural organisation of water molecules occur around the ion known as ion solvation or ion hydration if the solvent is water (Koryta 1991). Dipole solvent molecules orientate themselves with the appropriate charged end towards the ion to create a solvent sheath (Bockris and Reddy 1998). In the immediate vicinity of the solvated ion, the solvent molecules are still partly affected by the ion (and associated solvent sheath) and orientate out of the solvent and towards the ion to varying degrees (Bockris and Reddy 1998). These changes are due to van-der-Waals forces acting between the ion and the oppositely charged end of the H<sub>2</sub>O dipole. Ion solvation affects the rate at which the ion moves through the solution. This is because the hydration sheath increases the effective diameter of the moving



particle, resulting in an increase in the viscosity (Grimnes and Martinsen 2008; Koryta 1991).

Whilst the hydration sheath holds ions of opposite charge away from each other, the central ion attracts ions of opposite charge into the same vicinity, resulting in an ionic atmosphere surrounding the reference ion (Grimnes and Martinsen 2008; Koryta 1991). This thickness of this region is called the Debye-Hückel length and is defined as (Bockris and Reddy 1998):

$$\kappa^{-1} = \sqrt{\left(\frac{\epsilon kT}{4\pi \sum_i n_i^0 z_i^2 e_0^2}\right)} \quad [2-10]$$

Where  $\kappa^{-1}$  is the Debye- Hückel reciprocal length,  $n_i^0$  is the bulk concentration of ion species  $i$  and  $z_i$  is valance of ion species  $i$  and  $k$  is Boltzmann's constant.

#### 2.2.2.2 Diffusion of ions and Fick's laws

The process of diffusion and viscous flow are related through the Einstein-Stokes equation, which links the mobility of an ion to its charge and radius (Bockris and Reddy 1998):

$$D = \frac{kT}{6\pi r\eta} \quad [2-11]$$

Where  $D$  is the diffusion coefficient,  $r$  is the radius of the ion and  $\eta$  is the viscosity of the solution.

Fick's laws of diffusion are important because they enable diffusion within a system to be characterised. The first law defines diffusion in a system that is at or near its steady state, whereas the second law is related to a system that is in a transient (i.e. non-steady) state.

Fick's first law states that the *diffusion flux is proportional to the gradient of the concentration between two points*. Therefore, steady state diffusion can be described as:

$$J_i = -D \frac{dc_i}{dx} \quad [2-12]$$

Where  $J_i$  is the diffusion flux of species  $i$ ,  $D$  is the diffusion co-efficient,  $c_i$  is the concentration of species  $i$  and  $x$  is the distance. Fick's first law can be used in the characterisation of systems that do not vary as a function of time. Fick's second law, on the

other hand, states that *the concentration of a species varies with respect to time and space* as follows:

$$\frac{\partial c}{\partial t} = D \frac{\partial^2 c}{\partial x^2} \quad [2-13]$$

### 2.2.2.3 Ion drift and mobility

An applied electric field imparts a force that causes an ion to accelerate. Where the electric field is small, the acceleration of the ion stops each time it collides with other molecules. The ion gradually migrates through the electrolyte towards the region of opposite charge. Following a collision, the ion is subject to two forces: a component from the collision that may occur in any direction and a component resulting from the applied electric field. The force resulting from the applied field can be described as (Bockris and Reddy 1998):

$$\frac{\vec{F}}{m} = \frac{d\vec{v}}{dt} \quad [2-14]$$

Where  $\vec{F}$  is the vector of the applied force,  $m$  is the mass of the ion, and  $\frac{d\vec{v}}{dt}$  is the change in velocity with respect to time. The average time between collisions can be described as:

$$\tau = \frac{t}{N} \quad [2-15]$$

Where  $\tau$  is the mean time between collisions,  $t$  is the time elapsed and  $N$  is the number of collisions. The average drift velocity can thus be determined from equations [2-14] and [2-15]:

$$v_d = \frac{\vec{F}}{m} \tau \quad [2-16]$$

Where  $v_d$  is the drift velocity. A description of the mobility of an ion is defined as follows:

$$\bar{u}_{abs} = \frac{\tau}{m} = \frac{v_d}{\vec{F}} \quad [2-17]$$

Where  $\bar{u}_{abs}$  is the absolute mobility. More specifically, for an applied electric field:

$$(\bar{u}_{conv})_i = \frac{v_d}{\bar{F}} z_i e_0 = \frac{v_d}{X} \quad [2-18]$$

Where  $(\bar{u}_{conv})_i$  is the conventional mobility of species  $i$ ,  $X$  is the force of the applied electric field,  $z_i$  is the charge number of species  $i$  and  $e_0$  is the electron charge constant. Equation [2-16] shows that the higher the force and the fewer the collisions, the greater the drift velocity (Bockris and Reddy 1998). Furthermore, because the mobility (equation [2-17] and [2-18]) of the ion is related to the number of collisions, it is a function of the electrolyte the ion is in, rather than a constant value.

From the concept of absolute mobility, a relation (called the Einstein relation) can be derived to describe the diffusion co-efficient of a particular species,  $D_i$ , which shows the diffusion co-efficient to be concentration dependent (Bockris and Reddy 1998):

$$D_i = \frac{kT}{(\bar{u}_{abs})_i} \quad [2-19]$$

#### 2.2.2.4 Total ionic movement: Combining migration and diffusion

If there is a concentration gradient within an electrolyte and a migration flux caused by an applied electric field, then a combined expression is required to describe the total flux encountered. This can be defined through the Nernst-Planck expression for *independent* flux (Bockris and Reddy 1998):

$$J_i = \frac{D_i}{RT} c_i z_i F X - D_i \frac{dc_i}{dx} \quad [2-20]$$

Where  $J_i$  is the flux density,  $D_i$  is the diffusion coefficient,  $c_i$  is the ion concentration,  $z_i$  is the ion charge and  $X$  is the electric field. Whilst equation [2-20] provides a unified expression for the movement of an ion within a solution (neglecting hydrodynamic forces), the ions within the electrolyte do not behave independently. Within the electrolyte, the interactions between ions result in the formation of ionic atmospheres, which affect diffusion and migration of each ion species. Different ionic species have different radii, and therefore different mobilities as given by (Bockris and Reddy 1998):

$$(u_{conv})_i = \frac{z_i e_0}{6\pi r \eta} \quad [2-21]$$

Where  $\eta$  is the viscosity. The greater the mobility of an ion, the more it contributes to the transport of charge. The transport number can be used to describe the proportion of the current carried by a particular species. An expression for the transport number is:

$$t_i = \frac{j_i}{J_T} = \frac{j_i}{\sum j_i} \quad [2-22]$$

Where  $t_i$  is the transport number of ion species  $i$ ,  $j_i$  is the current density and  $J_T$  is the total current. The current density of a given species can be related to its mobility and concentration through:

$$j_i = z_i F c_i (u_{conv})_i X \quad [2-23]$$

Cations are generally smaller than anions, therefore the transport number of a cation is normally higher. The transport number shows that some species are involved in the transport of current within the electrolyte, whereas other species facilitate the charge transfer reactions at the electrode surface, but have a transport number of zero. These species are not depleted at the electrode surface because the removal of their charge by redox reactions produced a diffusion flux in the vicinity of the electrode, drawing more ions of the given species towards the electrode surface (Bockris and Reddy 1998).

#### 2.2.2.5 Dielectric properties

The dielectric constant of the material and the dielectric loss are related through the Debye equation (Bone and Zaba 1992):

$$\varepsilon^* = \varepsilon' - j\varepsilon'' = \varepsilon_\infty + \frac{(\varepsilon_s - \varepsilon_\infty)}{1 + j\omega\tau} \quad [2-24]$$

Where  $\varepsilon^*$  is the complex permittivity composed of a real part ( $\varepsilon'$ ) representing the permittivity and an imaginary part ( $j\varepsilon''$ ) representing the dielectric loss.  $\varepsilon_s$  is the low frequency permittivity,  $\varepsilon_\infty$  is the permittivity at high frequency,  $\omega$  is the angular frequency, and  $\tau$  is the characteristic relaxation time, defined by (Bone and Zaba 1992):

$$\tau = \frac{1}{2\pi f_r} \quad [2-25]$$

Where  $f_r$  is the frequency of the maximum dielectric loss. For a dielectric with more than one relaxation time, equation [2-24] can be written as (Bone and Zaba 1992):

$$\varepsilon^* = \varepsilon' - j\varepsilon'' = \varepsilon_\infty + \frac{(\varepsilon_s - \varepsilon_\infty)}{1 + (j\omega\tau)^\beta} \quad [2-26]$$

Where  $0 < \beta \leq 1$  and is a function of the number of relaxation times within the dielectric. For a dielectric with an infinite number of relaxation times,  $\beta \rightarrow 0$  and for a system with one relaxation time,  $\beta = 1$ . Equation [2-26] is also known as the Cole-Cole equation and is more appropriate for the measurement of biological tissues, which are heterogenous and contain a distribution of relaxation frequencies (Rigaud et al. 1996).

The above analysis of dielectric relaxation can be represented by a plot of the dielectric permittivity ( $\varepsilon'$ ) against the dielectric loss ( $\varepsilon''$ ), called a Cole-Cole plot (Figure 2-5). The angle between the centre of the semicircle and the intersection between the perimeter and the real axis is defined as  $\alpha\pi/2$  rads. (Bone and Zaba 1992), which is related to the parameter beta as follows:

$$\beta = 1 - \alpha \quad [2-27]$$

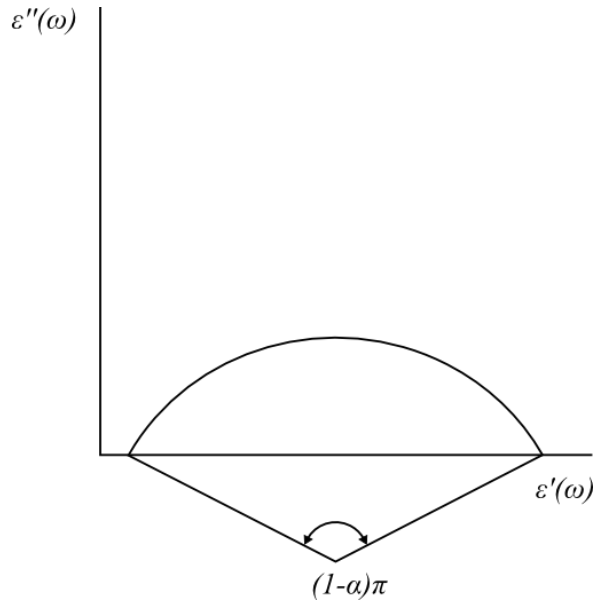


**Figure 2-5: Cole-Cole plot for a dielectric with multiple relaxations. The angle between the centre of the semicircle and the real axis is related to equation [2-26] (Adapted from Bone and Zaba 1992).**

Thus, when the centre of the semi-circle in the Cole-Cole plot falls below the real axis, the dielectric exhibits more than one time constant. As mentioned above, a distribution of relaxation times is characteristic of a biological dielectric (Rigaud et al. 1996). Dielectric properties of biological tissues can be characterised by three different relaxation effects: Dipolar relaxation, Maxwell-Wagner Relaxation and counterion relaxation (Rigaud et al. 1996).

#### 2.2.2.5.1 Dipolar relaxation

The relaxation time of the dipolar molecule can be related to the viscosity and thermal agitation of the electrolyte (Rigaud et al. 1996). For a spherical dipole (Bone and Zaba 1992):

$$\tau = \frac{4\pi\eta r^3}{kT} \quad [2-28]$$

Where  $\eta$  is the viscosity of the solution,  $r$  is the radius of the dipole,  $k$  is Boltzmann's constant and  $T$  is the absolute temperature. Equation [2-28] can be further developed for an ellipsoidal particle, which exhibits a high degree of agreement to experimentally obtained values of  $\tau$  (Bone and Zaba 1992).

### 2.2.2.5.2 Maxwell Wagner relaxation

The Maxwell-Wagner relaxation relates to a heterogenous electrolyte which is composed of more than one phase (Bone and Zaba 1992; Foster and Schwan 1989; Rigaud et al. 1996). The higher rate of ionic movement under the influence of an electric field in one part of the electrolyte will result in the build-up of a charge at a phase boundary (Bone and Zaba 1992). In a simple analysis, the Maxwell-Wagner equation can be developed for two phases adjacent to each other with different dielectric properties using an associated equivalent circuit (Figure 2-6; Rigaud et al. 1996).

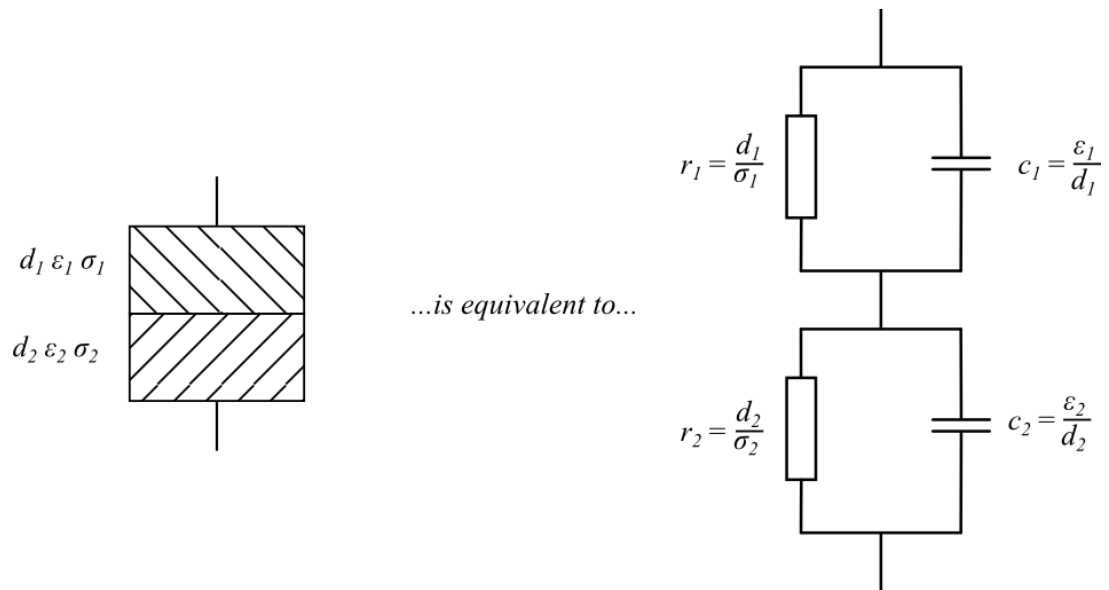


**Figure 2-6: Example of the equivalent circuit for a two phase material, used to determine Maxwell-Wagner relaxation (Adapted from Rigaud et al. 1996).**

For a simple two phase model, the time constant, along with the high and low limits of permittivity can be related through circuit theory and the application of the Debye equation (equation [2-24]). This gives (Rigaud et al. 1996):

$$\tau = \frac{[\varepsilon_0(d_2\varepsilon_1 + d_1\varepsilon_2)]}{[d_2\sigma_1 + d_1\sigma_2]} \quad [2-29]$$

$$\sigma_s = \frac{d\sigma_1\sigma_2}{(d_1\sigma_2 + d_2\sigma_1)} \quad [2-30]$$

$$\varepsilon_s = \frac{[d(\varepsilon_1d_1\sigma_2^2 + \varepsilon_2d_2\sigma_1^2)]}{[d_2\sigma_1 + d_1\sigma_2]^2} \quad [2-31]$$

$$\varepsilon_{\infty} = \frac{d\varepsilon_1\varepsilon_2}{(d_1\varepsilon_2 + d_2\varepsilon_1)} \quad [2-32]$$

Lipid membranes can be studied through the application of the Maxwell-Wagner relaxation, by representing the polar and non-polar regions of the phospholipid as phases with different dielectric properties (Bone and Zaba 1992).

#### 2.2.2.5.3 Counterion relaxation

The counterion relaxation is related to the ion double layer that forms on charged surfaces (such as cells and DNA molecules) when they are placed within a solvent (Bone and Zaba 1992; Foster and Schwan 1989). The dispersion caused by counterion relaxation effects is seen in the frequency range between 15 and 20 kHz and due to coupled electrical and hydrodynamic effects is difficult to study (Foster and Schwan 1989). Schwartz demonstrated that the relaxation time constant for such a system can be described by (Grimnes and Martinsen 2008):

$$\tau = \frac{a^2\varepsilon_0}{2\mu kT} \quad [2-33]$$

Where  $a$  is the particle radius,  $\mu$  is the counterion mobility,  $k$  is Boltzmann's constant and  $T$  is absolute temperature. Counterion relaxation effects have been applied to dielectric data from bacteria by Einolf and Carstensen, taking into account the inside and outside surfaces of the cell wall (Foster and Schwan 1989).

#### 2.2.2.5.4 Dielectric spectra of biological materials

Three major dielectric dispersions are observable in biological material between the low frequencies and 10 MHz (Figure 2-7; Foster and Schwan, 1989). The alpha dispersion appears to be a phenomena relating to cell-membrane and electrolyte interactions, and thus may be considered as a dipolar relaxation of the cell due to the build-up of opposite charge either side of the membrane (Rigaud et al. 1996). At higher frequencies, a beta dispersion results from the capacitive charging of lipid membranes within the sample. The gamma dispersion occurs at much higher frequency (25 GHz) due to the relaxation of water molecules (Foster and Schwan 1989).



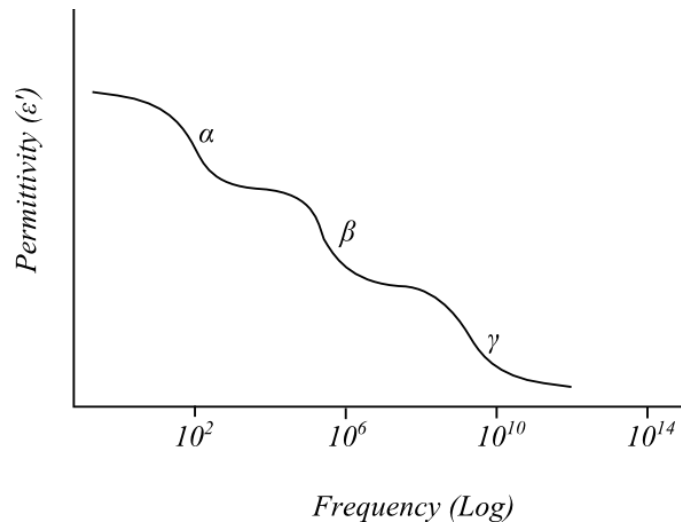


**Figure 2-7: Major Dispersions in Biological Tissues (adapted from Rigaud et al. 1996).**

### 2.2.3 Properties of the electrode-electrolyte interface

#### 2.2.3.1 Electrode-electrolyte interface and the interphase

At an interface, for example between an electrode and the electrolyte, a charge is created in each phase of equal and opposite magnitude (Bockris et al. 2000). Consider the situation of an electrolyte of infinite volume (i.e. unbound by any other phase). In the absence of any external force, the ions and molecules exist in a state of homogenous equilibrium, where the net charge per unit area is zero (Figure 2-8). If another phase (i.e. an electrode) is then introduced into the first phase, this equilibrium at the boundary is unbalanced and the net charge of a unit area overlapping the phases is no longer zero. In order to compensate for this difference, a redistribution of charge occurs at the boundary. The change in the charge distribution at the boundary between phases results in the formation of an electric field and therefore a potential difference (Bockris et al. 2000).

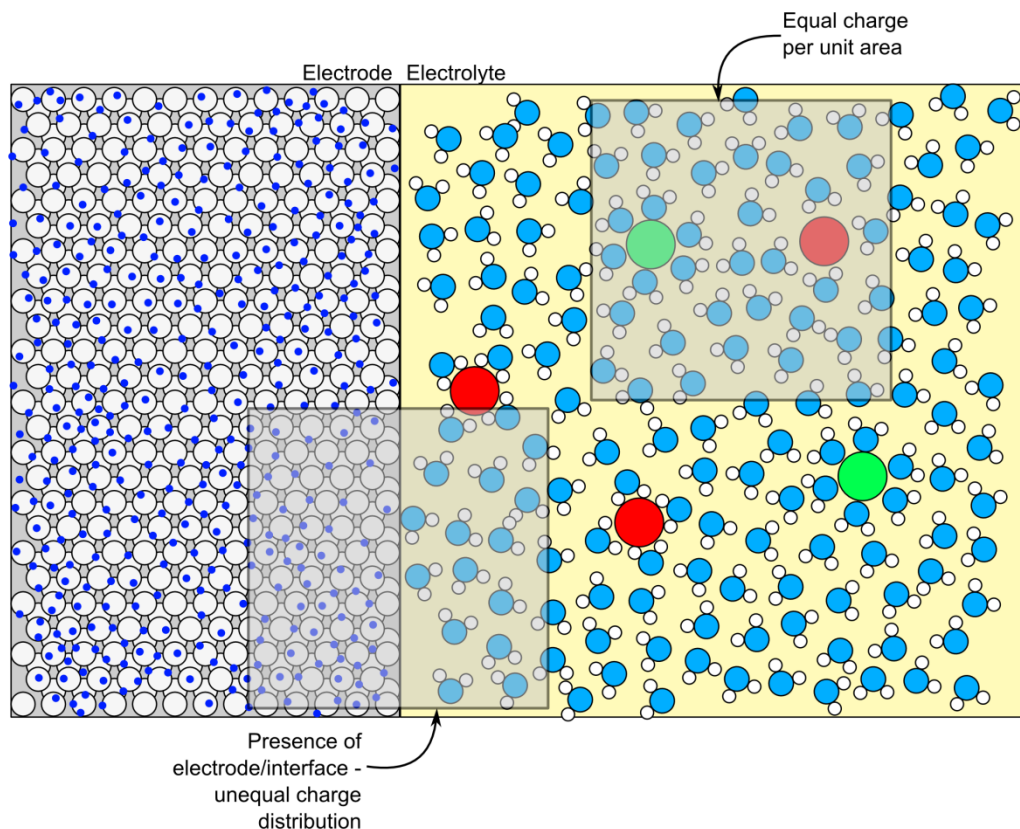


**Figure 2-8: Origins of charge distribution across a phase boundary. The right hand box shows the hypothetical scenario whereby no phase boundary exists and any given unit volume has a net charge of zero. The left hand square shows the situation immediately following the introduction of a second phase (e.g. an electrode), whereby the net charge of a given volume across the interface is no longer zero.**

Assuming the electrolyte solvent is water, immediately adjacent to the phase boundary, a hydration sheath is formed, consisting of a layer of water molecules, with their dipoles oriented to reflect the charge density in the electrode phase. In addition, at the immediate phase boundary, some ions may exist that are specifically adsorbed to the electrode surface, this is known as the Inner Helmholtz Plane. Moving away from the phase boundary towards the bulk electrolyte, a layer of solvated ions is encountered, called the Outer Helmholtz Plane. If the charge between the phases is not compensated by the distribution of ions in the three layers discussed above, a dispersion zone forms to fully counteract the charge density within the electrode phase (Figure 2-9).

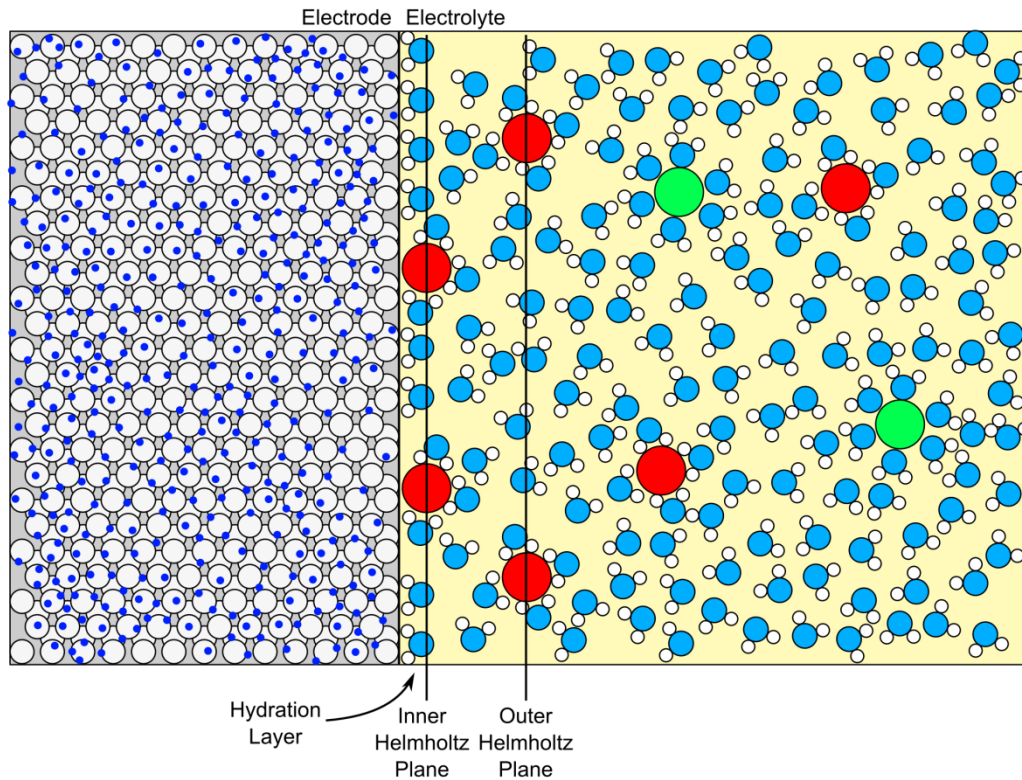


**Figure 2-9: Distribution of ions at the electrode-electrolyte boundary (adapted from Bockris et al. 2000)**

Three classic models exist to describe the capacitive properties of the double layer. The Helmholtz-Perrin model is based upon a single plane of ions adjacent, but not in contact with the electrode surface (Bockris et al. 2000). This model is therefore analogous to a parallel plate capacitor with a very high capacitance because the distance between the electrode surface and the outer Helmholtz plane is very small. The capacitance is linear across this distance. The capacitance of this interface is represented by (Bockris et al. 2000):

$$C_H = \frac{\epsilon}{4\pi d} \quad [2-34]$$

Where  $C_H$  is the Helmholtz capacitance,  $\epsilon$  is the dielectric permittivity of the dipoles between the electrode surface and the outer Helmholtz plane and  $d$  is the distance between the electrode surface and the outer Helmholtz plane. The Helmholtz-Perrin model only proves to be valid where the double layer does not change with applied potential (Bockris and Reddy, 1998).

Gouy-Chapman considered the ions that composed the outer Helmholtz plane to be capable of movement into the electrolyte as a consequence of thermal forces and the random walk

(Bockris et al. 2000). Thus, the electrode is surrounded by an ionic atmosphere similar to that experienced by individual ions and defined through the Debye length. Thus, the potential of the Gouy-Chapman layer drops exponentially as a consequence of distance from the electrode surface (Bockris et al. 2000):

$$\psi_x = \psi_0 e^{-\kappa x} \quad [2-35]$$

Where  $\psi_x$  is potential at point  $x$ ,  $\psi_0$  is the outer potential at the electrode, and  $\kappa$  is the Debye length. The capacitance associated with the Gouy-Chapman model is described by:

$$C_{GC} = \left( \frac{\epsilon z^2 e_0^2 c_0}{2\pi kT} \right)^{1/2} \cosh \frac{ze_0 \psi_M}{kT} \quad [2-36]$$

Where  $C_{GC}$  is the Gouy-Chapman capacitance,  $\epsilon$  is the dielectric constant of Gouy-Chapman diffuse layer,  $c_0$  is the ion concentration of the electrolyte,  $\psi_M$  is the potential at the electrode interface. Equations [2-35] and [2-36] indicate that as the ion concentration of the electrolyte increases, the potential drops more sharply as a function of distance towards the bulk electrolyte. However, the Gouy-Chapman model has limited validity during experimental assessment and is found to only be valid when the ion concentration of the electrolyte is very low (Bockris et al. 2000).

Stern provided the synthesis of the Helmholtz-Perrin and Gouy-Chapman models of capacitance (Bockris et al. 2000). This model recognises that the double layer is influenced by the ionic concentration of the electrolyte (as described by the Gouy-Chapman model), but also that the ions are not point charges and therefore remain a finite distance off the electrode surface, as described by the Helmholtz-Perrin model (Bockris et al. 2000). Thus, the Stern capacitance is described by the Helmholtz-Perrin and Gouy-Chapman capacitance in series:

$$\frac{1}{C_s} = \frac{1}{C_H} + \frac{1}{C_{GC}} \quad [2-37]$$

Equation [2-37] provides an indication of the concentration dependence of the double layer. At high concentrations the Helmholtz-Perrin component of the capacitance is dominant. Conversely, at low concentrations, the Gouy-Chapman component of the capacitance dominates (Bockris et al. 2000).

### **2.2.3.2 Faradaic and non Faradaic current and electrode polarisation**

A Faradaic current results from the transfer of charge between the electrode and the electrolyte. Charge transfer between the electrolyte and the electrode occurs through oxidation or reduction reactions, called redox reactions. In contrast, non-Faradaic current does not involve the transfer of charge across the electrode-electrolyte interface. Electrodes that resist a change in potential at the interface between the electrode and electrolyte are known as non-polarisable, because a charge separation between the two phases cannot build up. This situation occurs when the electrode-electrolyte interface readily allows charge transfer. In a polarisable electrode, no charge can pass between the electrode and the electrolyte and therefore the interface is analogous to that of a capacitor (Bard and Faulkner 2001). No electrode is perfectly polarisable or non-polarisable, with the extent to which an electrode becomes polarised being a function of the both the properties of the electrode (e.g. electrode material and potential) and the electrolyte (e.g. the presence of redox active compounds, compatible with electrode potential and the dielectric properties of the electrolyte).

### **2.2.3.3 Redox reactions**

Reduction and oxidation reactions describe the gain or loss of electrons from one species to another. Reduction refers to the gain of one or more electrons, whereas oxidation relates to the loss of one or more electrons from a species. In addition to redox reactions occurring between species in solution, they can also occur between an electrode and electrolyte. In electrochemistry, half cell reactions can be used to describe these oxidation or reduction reactions (Fifield 2000). Formal potentials are determined by measuring the half cell potential of a redox couple with reference to a normal hydrogen electrode when the ratio of the oxidised and reduced species is unity (Bard and Faulkner 2001).

The terms anode and cathode are used to describe the flow of electrons in an electrochemical system (Figure 2-10). The anode acts as the electron sink, where ions or neutral substances in the electrolyte lose electrons and are oxidised. Conversely, the cathode acts as an electron source, whereby ions or neutral substances gain electrons to become reduced (Grimnes and Martinsen 2008).

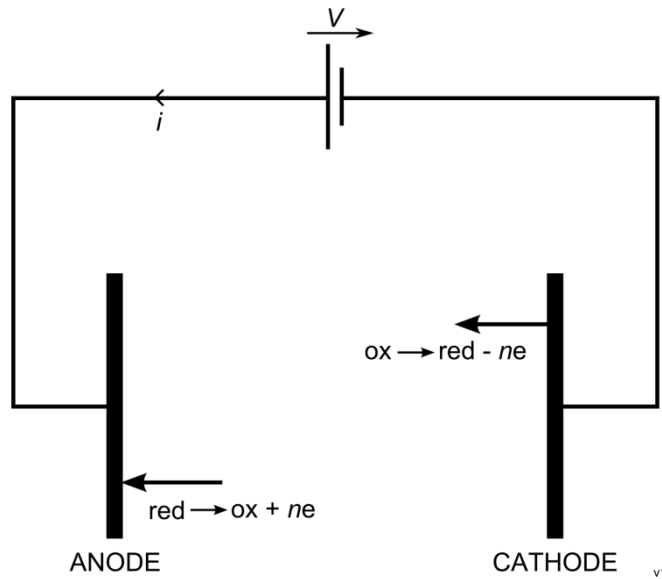


**Figure 2-10: Anode and cathode reactions**

If the activity coefficients of the oxidised and reduced species are the same, then the Nernst equation can be used to determine the potential where the oxidised and reduced concentration of the species differ (Bard and Faulkner 2001):

$$E = E^{0'} + \frac{RT}{nF} \ln \frac{C_O^*}{C_R^*} \quad [2-38]$$

Where  $E$  is the electrode potential,  $E^{0'}$  is the formal electrode potential,  $R$  is the real gas constant,  $T$  is the absolute temperature,  $n$  is the number of electrons transferred,  $C_O^*$  is the bulk concentration of oxidised species and  $C_R^*$  is the bulk concentration of reduced species.

#### 2.2.3.4 Charge transfer

In conditions where Faradaic current exists, redox reactions occur between electroactive species within the electrolyte and the electrode. When the electrode-electrolyte interface is at equilibrium, no current flows through the cell and the reduction and oxidation of the species both occur at equal and opposite rates (Southampton Electrochemistry Group 2001). Therefore, at equilibrium, there is a charge transfer between the electrode and the electrolyte with a net current of zero (Bockris et al. 2000). Thus:

$$\vec{i} = \vec{k}c_M + \exp\left\{\frac{-\beta\Delta\phi_e F}{RT}\right\} = \vec{i}_0 = \vec{k}c_A + \exp\left\{\frac{(1-\beta)\Delta\phi_e F}{RT}\right\} \quad [2-39]$$

Where  $\vec{i}$  is the current density,  $c_M$  is the concentration of metal ions,  $c_A$  is the surface concentration of atoms on the electrode,  $\beta$  is the transfer coefficient,  $i_0$  is the exchange current density,  $\vec{k}$  and  $\vec{k}$  are rate constants, and  $\Delta\phi_e$  is the potential when the interface is at equilibrium. When an external current sink or source (i.e. an electromotive force) is applied to the electrode, the electrode-electrolyte interface is no longer in equilibrium and a change occurs in the electrode potential, expressed in terms of the equilibrium potential as an overpotential (Bockris et al. 2000):

$$\eta = \Delta\phi - \Delta\phi_e \quad [2-40]$$

Where  $\eta$  is the overpotential,  $\Delta\phi$  is the interface potential and  $\Delta\phi_e$  is the potential when the interface is at equilibrium. Thus, when the overpotential is negative, there will be a net cathodic current and when positive a net anodic current (Bockris et al. 2000). The net current flow can be expressed by the Butler-Volmer equation for a net anodic or net cathodic current (Bockris et al. 2000):

$$i_{cath} = i_0 \left( \exp\left\{\frac{-\beta\eta F}{RT}\right\} - \exp\left\{\frac{(1-\beta)\eta F}{RT}\right\} \right) \quad [2-41]$$

$$i_{an} = i_0 \left( \exp\left\{\frac{(1-\beta)\eta F}{RT}\right\} - \exp\left\{\frac{-\beta\eta F}{RT}\right\} \right) \quad [2-42]$$

Where  $i_{cath}$  is the net cathodic current and  $i_{an}$  is the net anodic current. The Butler-Volmer equation is valid where the current is driven by transfer of charge across the electrode-electrolyte interface, and not by diffusion processes bringing species to the electrode (Bockris et al. 2000). In essence, the Butler-Volmer equations indicate that the flow of current across the electrode-electrolyte interface is dependent upon the overpotential and varies in a non-linear manner.

### 2.2.3.5 Warburg impedance

In the situation where electron transfer is sustained, the redox active species available within the electrolyte adjacent to the electrode interface become depleted. The transfer of charge then becomes dependent upon the transport of electroactive species from the bulk electrolyte to the electrode surface (Muñoz-Berbel et al. 2008b). In terms of the resistance and reactance, the Warburg impedance appears as an equal contribution from both components

(thus forming a 45° line on a complex plane plot across a range of frequencies). However, it is important to note that the Warburg impedance may show different behaviours depending upon the electrode geometry and experimental conditions (Muñoz-Berbel et al. 2008b).

#### 2.2.4 Randles equivalent circuit

The Randles equivalent circuit is frequently used to represent an electrochemical cell, as seen in Figure 2-11 (Bard and Faulkner 2001). In this model, the charging capacitance of the electrode-electrolyte interface is represented by a capacitor in parallel with a Faradaic component. These are then placed in series with a solution resistance (Bard and Faulkner 2001). In reality, the electrode-electrolyte interface does not behave like a perfect capacitor and deviates in relation to the surface roughness of the electrode (Muñoz-Berbel et al. 2008b). Therefore, a component called the constant phase element (CPE) is sometimes introduced to describe the charging capacitance (Muñoz-Berbel et al. 2008b):

$$CPE = \frac{1}{K_{CPE}(j\omega)^{n_{CPE}}} \quad [2-43]$$

Where  $K_{CPE}$  is the magnitude of the CPE and is proportional to the capacitance and  $n_{CPE}$  is an index of the surface roughness at the electrode interface.

The Faradaic component in Randles circuit (Figure 2-11) can be represented by a resistor in series with a pseudocapacitance, or by a charge transfer resistance in series with a Warburg impedance reflecting mass transfer processes (Bard and Faulkner 2001).



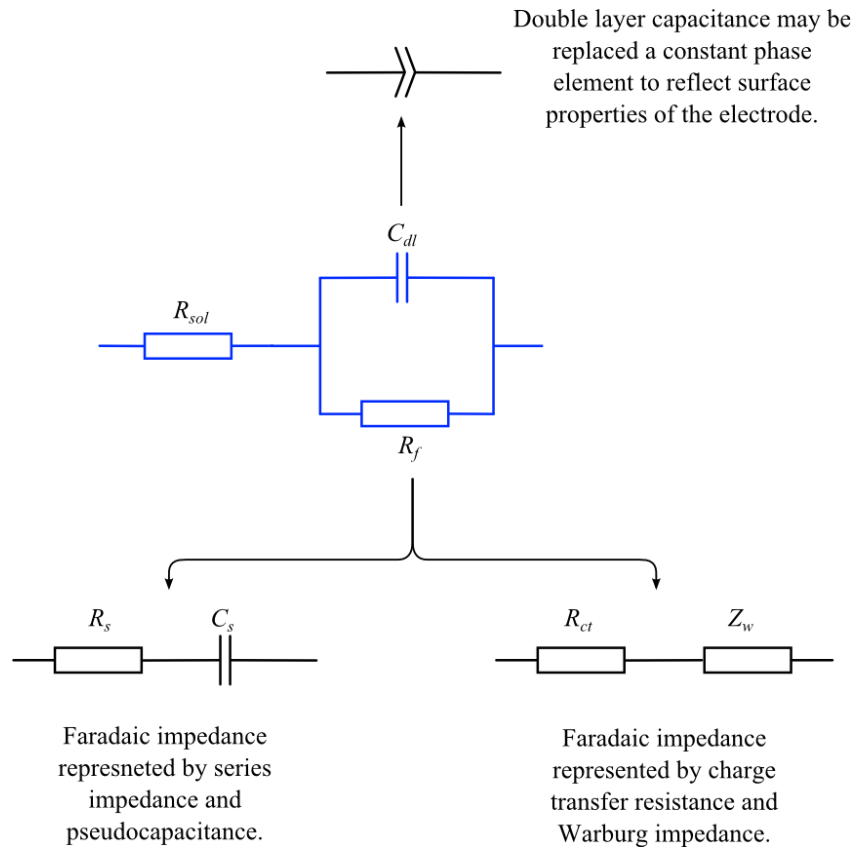


**Figure 2-11: The Randles equivalent circuit and alternative representations for the double layer capacitance ( $C_{dl}$ ) and the Faradaic resistance ( $R_f$ ).  $R_{sol}$  - electrolyte resistance,  $R_s$  - Faradaic series resistance,  $C_s$  - Faradaic series pseudocapacitance,  $R_{ct}$  - charge transfer resistance,  $Z_w$  - Warburg impedance (Bard & Faulkner 2001).**

In an ideal system, the shape of the impedance curve resulting from the Randles equivalent circuit can be used directly to determine the values of the circuit components (Figure 2-12). Measurement of the impedance in an electrochemical cell provides reactance and resistance values that represent the entire system being measured (i.e. assuming the system behaves as described in Figure 2-11, all the circuit elements within the equivalent circuit). It can be shown that a simple equivalent circuit consisting of a resistor and capacitor in parallel both contain portions of the measured resistance and reactance. Therefore, the identification of equivalent circuit values needs to be based upon transformation of equivalent circuits from a series form to a parallel form (Yuan et al. 2010). A series combination of resistance and capacitance:

$$Z = R_s - j \frac{1}{\omega C_s} \quad [2-44]$$

Can be described by the equivalent parallel components as:

$$R_p = R_s \left( \frac{(\omega R_s C_s)^2 + 1}{(\omega R_s C_s)^2} \right) \quad [2-45]$$

$$C_p = \left( \frac{C_s}{(\omega R_s C_s)^2 + 1} \right) \quad [2-46]$$

Many curve fitting approaches can be employed to fit empirical data to an equivalent circuit. With this approach, however, care has to be taken to ensure that the chosen circuit has a valid physical basis as several different circuits can fit the same data (Macdonald 1987).

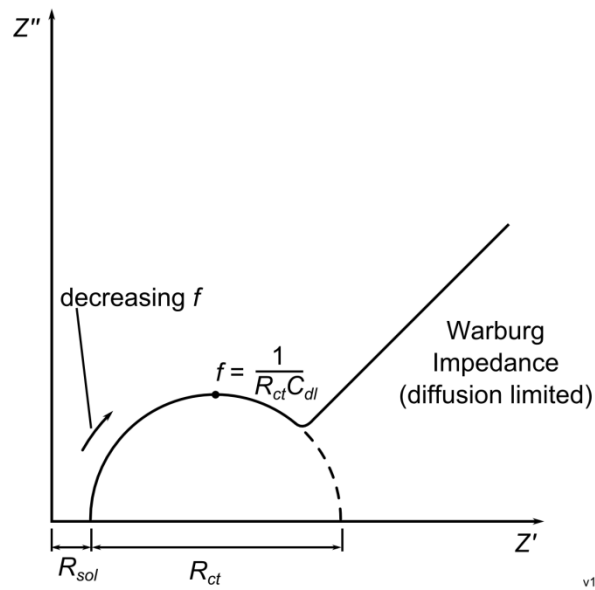


**Figure 2-12: Example complex plane impedance plot of the Randles equivalent circuit.**

**At high frequencies, the impedance is dominated by the solution resistance, as the measurement frequency drops, the charge transfer resistance increasingly plays a role. Eventually the impedance is controlled by the diffusion of redox active compounds to the electrode surface, and thus the impedance plot reflects 45° line, known as the Warburg impedance.**

## 2.3 Microbiology fundamentals and biofilm formation

The following section describes the basic properties of prokaryote organisms with a focus on cell structure, growth and respiration. The later section describes the properties of biofilms and the process of biofilm formation. It also includes a review of the literature on recent findings relating to the difference between *in vitro* and *in vivo* biofilms.

### 2.3.1 Prokaryotic cells

Prokaryotes are found in all environmental niches and are classically defined by their structure (Figure 2-13). As shown, the prokaryote cell consists of a cytoplasmic membrane surrounded by a cell wall.

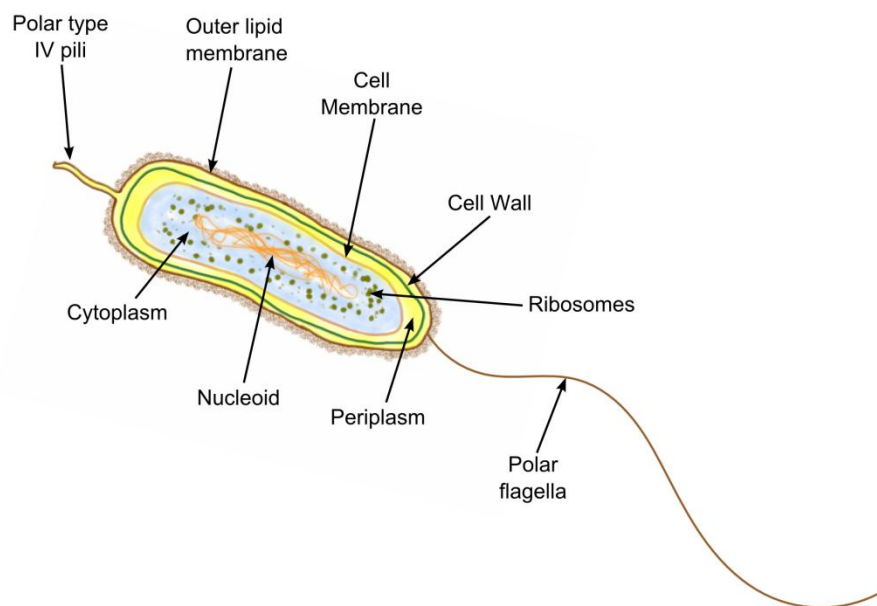


**Figure 2-13: An example of a typical Gram negative rod prokaryote. Drawing is based upon *P. aeruginosa*, which has a polar pili and flagella.**

The cytoplasmic membrane acts as a permeability barrier, protein anchor and provides the charge separation required for the proton motive force (Brock and Madigan 2009). Ions and small molecules are actively transported across the membrane through specific transport proteins, whilst water molecules are able to diffuse across the membrane (although the presence of aquaporins enhances this process; Brock and Madigan 2009). Enclosed within the cytoplasmic membrane is the nucleoid which is a covalently closed and circular double stranded DNA in most prokaryotes (Brock and Madigan 2009). Additionally, the cytoplasm contains macromolecules, organic molecules, inorganic ions, ribosomes and plasmid DNA (Brock and Madigan 2009).

The cell wall protects the bacteria against this osmotic lysis and gives the cell shape and rigidity. It is constructed from several crosslinked layers of peptidoglycan chains, the thickness of which varies depending upon the species of bacteria (Brock and Madigan 2009). In addition to the cell wall, some bacteria also have a second, outer membrane consisting of phospholipids, proteins and lipopolysaccharides. Cells containing an outer membrane have thinner cell walls than those without (Brock and Madigan 2009). The presence of an outer cell membrane is used as a basis to classify prokaryotes as Gram-negative or Gram-positive. Those without an outer membrane are described as Gram-positive, whereas those with an outer membrane are described as Gram-negative (Figure 2-14). In Gram-negative bacteria, a space exists between the inner membrane and outer membrane, called the periplasm, which contains proteins for initial degradation of nutrients, transport and chemotaxis (Brock and Madigan 2009). Prokaryotic cells may also secrete polysaccharides or proteins on their surface, called a capsule or a slime layer. This layer helps in cellular attachment to surfaces, protection from phagocytosis and possibly also resistance from dehydration (Brock and Madigan 2009).

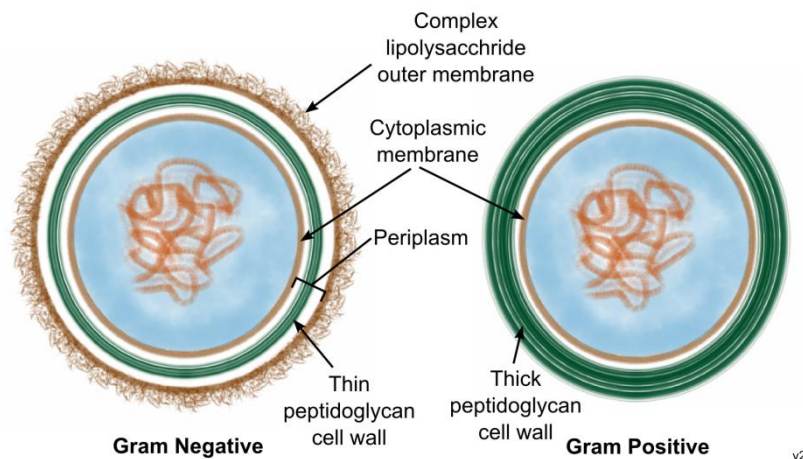


**Figure 2-14: Differences between Gram-negative and Gram-positive bacteria.**

Cellular appendages such as fimbriae can enable attachment to surfaces or tissues, whilst pili are larger appendages which may be involved in the transfer of genetic material between cells and also with cellular motility in the case of type IV pili (Brock and Madigan 2009). Another motility appendage found on some species of bacteria, called the flagella, are long structures that allow the cell move through an aqueous phase in a process called swimming (Brock and Madigan 2009). Finally, some cells are motile through an ability to glide across a surface (Brock and Madigan 2009).

### **2.3.2 Microbial growth**

Microbial growth of prokaryotic cells is described in terms of an increase in the number of cells and is achieved through a process of binary fission, where one cell divides to become two cells (Madigan et al. 2009). In laboratory conditions, microbial growth can be studied in terms of the microbial growth cycle, which typically consists of a lag phase, exponential growth phase, a stationary phase and then finally a death phase (Figure 2-15; Brock and Madigan 2009). The lag phase is defined as the period of time between inoculation of fresh medium with the bacteria and the start of cell division. It occurs due to the time required for the cells to adapt to the new environment, replenish and biosynthesise depleted constituents, and to allow the cells to undertake any repairs that may be necessary prior to cell division. The exponential growth phase is marked by the binary division of the cells within the medium, facilitated by the presence of nutrients. The rate of growth of the culture is governed by the generation time, which is defined as the length of time required for one cell to divide. The generation time varies between species and is also dependent upon the environmental conditions, such as the availability of nutrients and temperature. The depletion of nutrients in the culture and the build-up to toxic waste products eventually brings an end to the exponential growth phase. At this point, the bacteria enter stationary phase where the number of cells dividing balance the number of cells that die in a phenomenon called cryptic growth. Eventually the cells within the culture will die and the population concentration will drop, which is characterised by the death phase. The decline in the cellular population is typically much slower than the exponential growth phase.

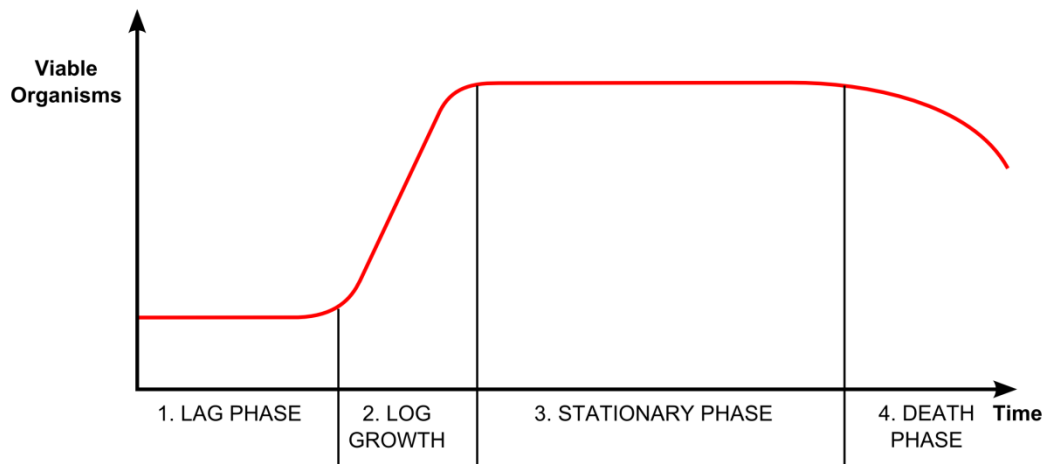


**Figure 2-15: Typical microbial growth cycle. (1) The duration of the lag phase is dependent on the history of the bacteria and the properties of the growth media. The lag period is greater if the cells were previously damaged. (2) The log growth phase covers a period of binary cell division and growth, generally limited by exhaustion of nutrients and accumulation of waste products. (3) In stationary phase, the population growth is zero but cells functions still continue. (4) Eventual death of cells occurs in the final phase, typically at a much slower rate than exponential growth.**

### 2.3.3 Microbial respiration and fermentation

ATP synthesis can be achieved through either fermentation or respiration pathways. Fermentation generates energy through substrate level phosphorylation and generates much less energy than respiration, which requires the presence of an electron donor such as  $O_2$  (Brock and Madigan 2009). Many prokaryotes are capable of using a diverse range of electron acceptors during respiration, in addition to oxygen (Figure 2-16) such as nitrate, nitrite and ferric oxide (Figure 2-17). The phenotype of microorganisms can be classified according to their ability respire aerobically or anaerobically (Table 2-2). Recent research also suggests that bacteria are capable of using solid electrodes, poised at an appropriate potential, as electron acceptors (Gralnick and Newman 2007; Hernandez and Newman 2001; Richardson 2000; Wang and Newman 2008). This approach, known as extracellular respiration, could form the basis for some of the electroactive compounds discussed in section 1.4.2.3.

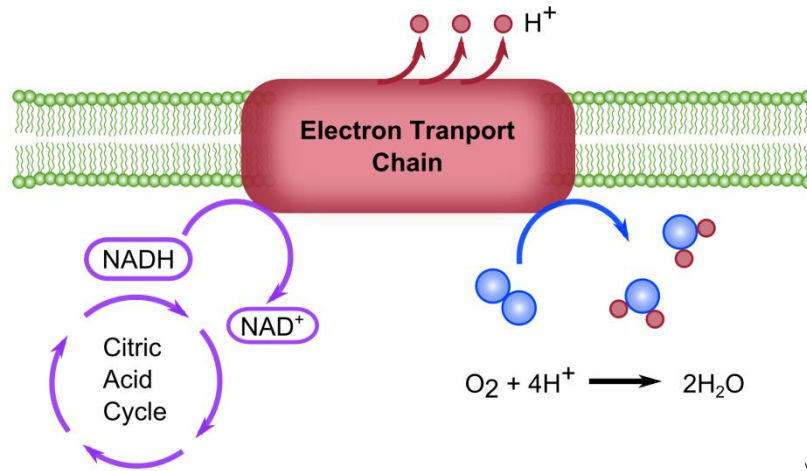


**Figure 2-16: Aerobic respiration uses O<sub>2</sub> as an electron acceptor in generation of the proton motive force.**

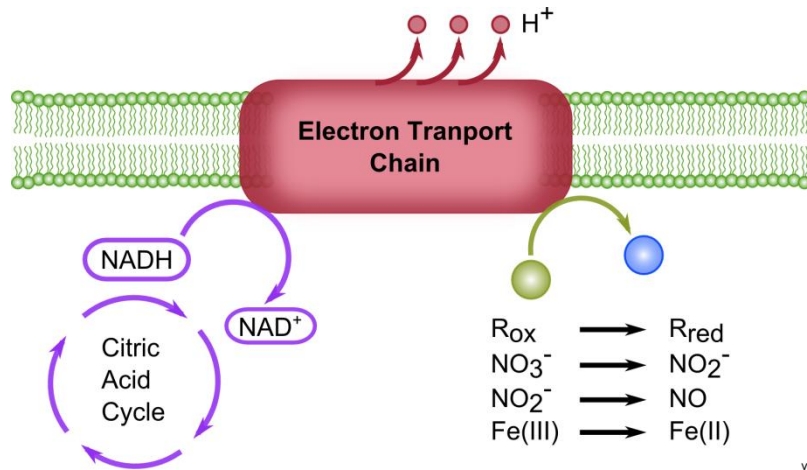


**Figure 2-17: Anaerobic respiration can use a number of different substrates as electron acceptors, including nitrate, nitrite and ferric oxide.**

**Table 2-2: Categorisation of microorganisms based upon respiratory properties  
(Adapted from Brock & Madigan 2009)**

Group	Relationship to O <sub>2</sub>	Type of Metabolism	Examples
Obligate aerobe	Required	Aerobic Respiration	<i>Micrococcus</i> spp.
Facultative aerobe	Not required but growth better with O <sub>2</sub>	Aerobic Respiration Anaerobic Respiration Fermentation	<i>P. aeruginosa</i> <i>E. coli</i> <i>Staphylococcus</i> spp.
Microaerophilic	Required but at levels lower than atmospheric	Aerobic Respiration	<i>Campylobacter</i> spp. <i>Helicobacter</i> spp.
Aerotolerant anaerobe	Not required and growth no better with presence of O <sub>2</sub>	Fermentation	<i>Streptococcus</i> spp.
Obligate anaerobe	O <sub>2</sub> harmful or lethal	Fermentation or anaerobic respiration	<i>Clostridium</i> spp.

#### 2.3.4 Quorum sensing in microorganisms

Quorum sensing (QS) is an intracellular communication strategy employed by organisms to control within species gene expression in a cell density dependent manner (Sifri 2008). QS systems exist in several Gram negative and Gram positive species. There is evidence that the organisms explored in this study utilise QS networks to control gene expression and virulence. A brief description of QS systems in *S. aureus*, *H. influenzae* and *C. albicans* is provided below, followed by a more detailed overview of the QS mechanisms of *P. aeruginosa*.

QS in *S. aureus* is governed by the accessory gene regulator, switches off the expression of several cell surface proteins and turns on the expression of several virulence factors (Yarwood and Schlievert 2003). In non typeable *H. influenzae* the mechanism of QS is thought to promote biofilm formation within the species (Swords 2012). Additionally, it is thought that in a polymicrobial infection with *H. influenzae* and *Moraxella catarrhalis*, *M. catarrhalis* is able to respond to QS signals produced by *H. influenzae*, suggesting that a model for interspecies QS could also exist (Swords 2012). Interestingly, the eukaryote organism *C. albicans* also exhibits a QS system. *C. albicans* is capable of undergoing morphogenesis from a non invasive single cell yeast phenotype to an invasive filamentous



growth, which can be induced in response to several mechanisms (Gow et al. 2012). It been shown that morphogenesis of *C. albicans* can be triggered in a cell dependent manner, suggesting that within species QS also plays a role in this morphogenesis (Kruppa 2009).

*P. aeruginosa* contains at least three QS signal/response systems (Wade et al. 2005; Dietrich et al. 2006a; Price-Whelan et al. 2006; Holm and Vikström 2014). Two of these systems are based upon secreted N-acetyl homoserone lactones (AHL) and are known as the *las* and *rhl* systems (Holm and Vikström 2014). The *las* system governs subsequent activation of the *rhl* system, and also a third system that is mediated by a quinolone signalling molecule, referred to as Pseudomonas Quinolone Signal (PQS) (Déziel et al. 2004). Production of PQS is negatively regulated by the *rhl* system, but positively regulated by the *las* system through the *MvfR* regulator (Wade et al. 2005). The QS molecules from all three systems result in the production and secretion of numerous virulence factors. The *rhl* and *las* systems are known to control the activation of over 300 genes (Holm and Vikström 2014). In addition to the three QS networks described above, a further network, dependent upon the phenazine pyocyanin has also been suggested. Through the protein *SoxR*, this results in the upregulation of a limited number of genes including a proton driven efflux pump and a monooxygenase (Dietrich et al. 2006a). The relation between these systems is shown in Figure 2-18.

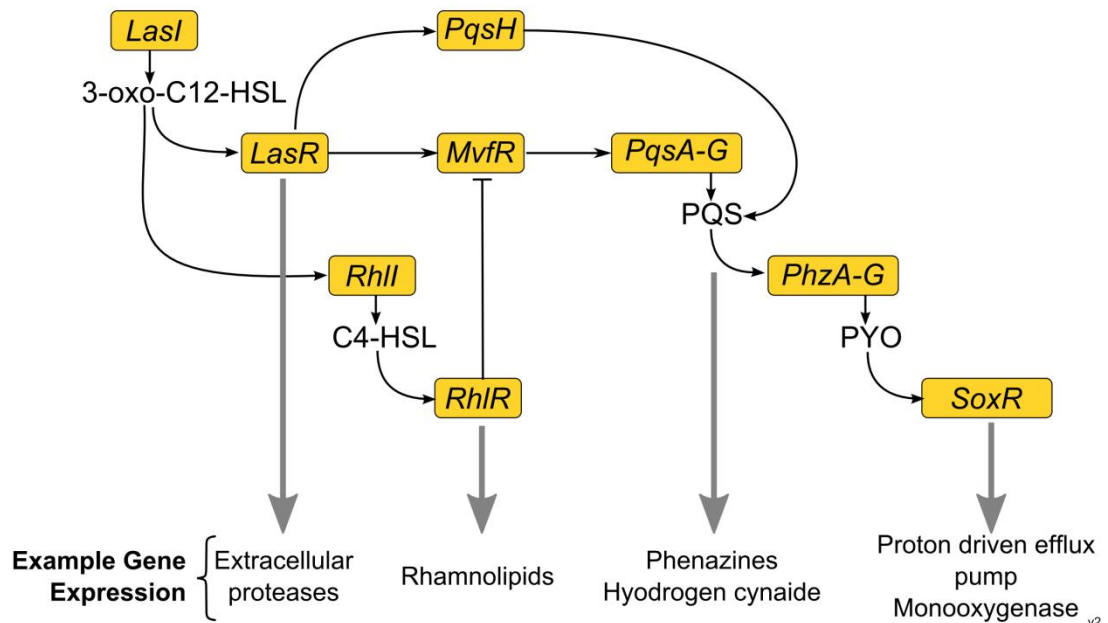


**Figure 2-18: *P. aeruginosa* quorum sensing network. QS molecules are initially produced by the *las* system, which controls the *rhl* system and ultimately the production of PQS. Pyocyanin has also been shown to drive the expression of a limited number of genes. Yellow boxes show proteins, blue boxes show example secreted virulence factors controlled by the QS systems. 3-oxo-C12-HSL = N-3-oxo-dodecanoyl-Homoserine lactone; C4-HSL = N-butyryl-Homoserine lactone; PYO = pyocyanin; PQS = *Pseudomonas* quinolone signal.**

### 2.3.5 Secondary metabolites produced by *P. aeruginosa*

Many of the genes expressed by *P. aeruginosa* in response to secreted QS molecules are known to be virulence factors capable of damaging host tissue, and promotion of infection and inflammation (Holm and Vikström 2014). Furthermore, a key phenotypic change that occurs to *P. aeruginosa* in response to QS molecules is the production of biofilms (de Kievit 2009). In addition to these metabolites, *P. aeruginosa* also produces siderophores such as pyoverdinin and pyochelin. These are expressed and secreted in iron depleted conditions to sequester extracellular iron to allow uptake by the cell for essential metabolism (Brandel et al. 2012). Important metabolites produced and secreted by *P. aeruginosa* are described in Table 2-3.

**Table 2-3: Metabolites produced and secreted by *P. aeruginosa***

Metabolite	Description	Reference
<b>Quorum Sensing Molecules</b>		
N-acyl homoserine lactones	Signalling molecules of the rhl and las QS system.	(Holm and Vikström 2014)
4-Hydroxy-2-alkylquinolines (HAQ)	Intracellular signalling molecules, which play an important role in quorum sensing. Some HAQ are known to have antibacterial properties.	(Déziel et al. 2004; Gross and Loper 2009)
<b>Virulence Factors</b>		
Phenazines (including pyocyanin)	Intracellular signalling molecules with antibiotic and antifungal properties. Have also been implicated in extracellular respiration.	(Price-Whelan et al. 2006)
Hydrogen Cyanide	Inhibition of cytochrome c oxidase and other metalloproteins.	(Gross and Loper 2009)
Elastinolytic and proteolytic enzymes	Impair host defences by degradation of host proteins and breakdown of physical barriers that typically prevent bacterial attachment.	(Kessler and Safrin 2014)
ExoU	Cytotoxic enzyme directly injected into target eukaryotes via type III secretion system.	(Sawa et al. 2014)
Rhamnolipid	Glycolipids with biosurfactant activity that play an important role in establishment and maintenance of biofilms. Numerous actions, including haemolytic activity in human pathogenesis, antimicrobial activity, solubilisation of PQS and promotion of swarming motility.	(de Kievit 2009; Reis et al. 2011)
Extracellular polysaccharides	Secreted during biofilm formation as part of the matrix which holds cells together and allows the formation of three dimensional structures.	(Sharma et al. 2014)
<b>Siderophores</b>		
Pyoverdinin Pyochelin	Sequester Fe(III) from the environment.	(Gross and Loper 2009)

### 2.3.6 Biofilm fundamentals

Bacteria are known to exist in two distinct states: single planktonic cells (thought to make up less than 0.1% of total microbial biomass) and sessile aggregates of cells, known as biofilms (Bjarnsholt 2013). A biofilm was defined by Costerton et al. (1999) as a “structured community of bacterial cells enclosed in a self-produced polymeric matrix, adherent to an inert or living surface”. In hostile environments, biofilms provide protection to bacteria, allowing them to evade antimicrobial attack and therefore survive and grow (Costerton et al. 1999).

Biofilms preferentially develop on inert surfaces, such as dead tissue or medical devices and growth is usually slow with host symptoms taking a long time to develop. The dispersion of planktonic cells appears to occur periodically, causing recurrent acute infection. These planktonic cells are susceptible to antibiotics but the underlying biofilm is not effectively attacked by them (Costerton et al. 1999). Many microorganisms are capable of growing in biofilms, including Gram-positive and Gram-negative, aerobic and anaerobic bacteria, mycobacteria and fungi (Bjarnsholt et al. 2013b).

Biofilm formation can be broken down into a number of stages (Figure 2-19). Prior to the attachment of a cell to the surface, a conditioning layer composed of material in the media forms a substratum upon which the bacteria are able to attach (Garrett et al. 2008). Once a substratum has been formed, bacteria arriving at the surface through either motility or external forces reversibly attach (Costerton et al. 1999; Garrett et al. 2008). Reversible attachment occurs as a result of physical forces such as van der Waals forces, steric interactions and electrostatic interactions. Bacterial adhesion may also be related to the zeta potential of the cell (Bayouhd et al. 2008), collectively known as the Derjaguin and Landau and Verwey and Overbeek (DLVO) theory (Garrett et al. 2008). More recently, it has been suggested that biofilm formation does not require an abiotic or biotic surface for a biofilm to form (Bjarnsholt 2013), as described above.

Following reversible attachment, the bacteria are thought to form microcolonies as a result of attachment between motility appendages, such as flagella or pili (Bjarnsholt 2013; Costerton et al. 1999). However, there is also evidence that microcolony formation is the result *in situ* of microbial growth (Klausen et al. 2003). At some point, those cells that have not been removed from the surface by either repulsive forces or external forces consolidate their

position and irreversibly attach to the surface (Costerton et al. 1999; Garrett et al. 2008). This could be achieved through the use of appendages, overcoming repulsive forces to attach to the conditioning substrate (Garrett et al. 2008). During the attachment phase, the bacteria start to excrete extracellular matrix materials, which provide protection to the microcolonies (Costerton et al. 1999). These extracellular matrix materials are known to consist of polysaccharides, extracellular DNA, other large macromolecules such as proteins, lipid, biosurfactants, flagella and pili (Bjarnsholt 2013). Binary fission of the bacteria also occurs and the microcolonies form into a mature biofilm (Garrett et al. 2008). At high cell densities, intercellular signalling called quorum sensing control the expression of genes related to biofilm growth, such as the production of secondary metabolites (Costerton et al. 1999). The colonies formed by biofilms may assume a classic mushroom shape (Costerton et al. 1999), which is believed to facilitate the passage of nutrients (Garrett et al. 2008). However, biofilm morphology has been found to differ as a function of the media the cells are grown in, as well as the existence of motility appendages (Klausen et al. 2003). Furthermore, the shape and size of *in vitro* biofilms, compared to *in vivo* biofilms has been challenged. Reviewing publications of *in vivo* biofilms, Bjarnsholt et al. (2013a) show that across multiple different types of chronic infection, biofilms ranging from 5 to 200  $\mu\text{m}$  diameter aggregates existed rather than the large, more extensive biofilms found *in vitro*. These differ to *in vitro* model systems which can produce biofilms of several square centimetres.

From the mature biofilm, the sessile microcolonies are capable of giving rise to planktonic bacteria which have motility and are therefore capable of dispersal and rapid multiplication (Costerton et al. 1999). This complete the biofilm cycle and may be the reason that microbial colonisation of the CF airway follows a pattern of exacerbations resulting from acute infection (Costerton et al. 1999).

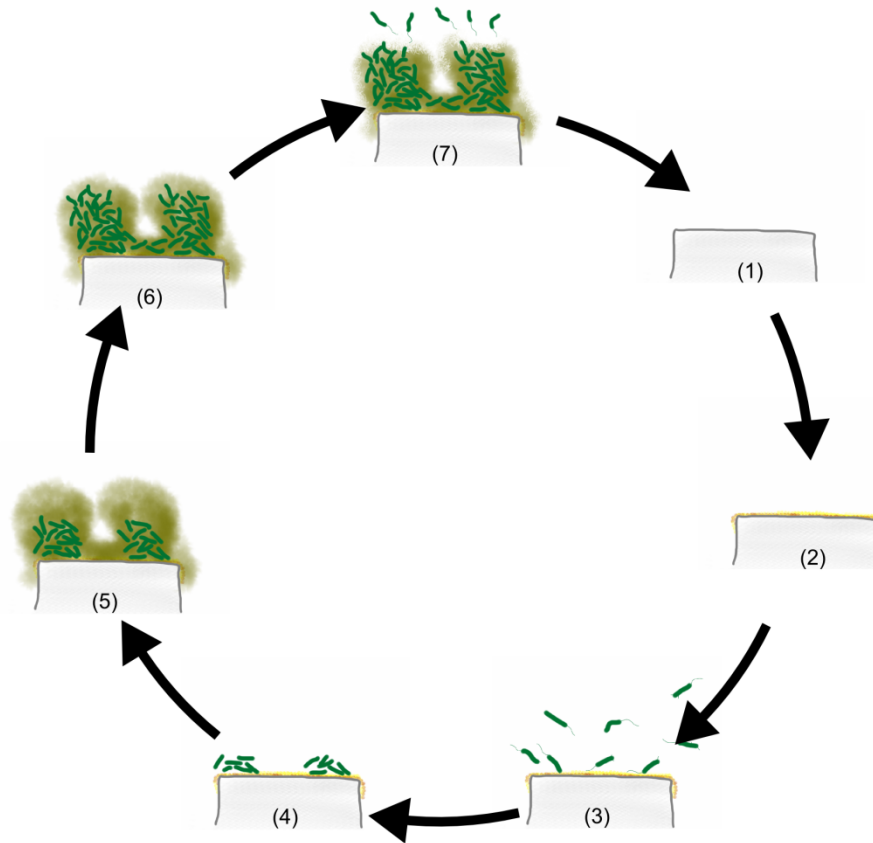


**Figure 2-19: Typical biofilm lifecycle, consisting of (1) target surface, (2) surface conditioning, (3) reversible microbial attachment, (4) irreversible attachment and microcolony formation, (5) growth and biofilm production, (6) biofilm maturation, (7) dispersion of planktonic cells.**

### **3 MATERIALS AND METHODS**

### 3.1 Introduction

As described in chapter 1, this study sets out to determine if it is possible to detect the presence of *P. aeruginosa* using a screen printed electrode and electrochemical impedance spectroscopy. To test the functionality of the sensor further, the specific capability to detect *P. aeruginosa* against a background of other species commonly found in the CF airway was also tested. Although not part of the original study aims, a small series of experiments were also carried out in human sputum samples. The materials and methods used to achieve all of this work are covered in the chapter. In addition, the data analysis approach and techniques used are covered here.

The experiments carried out in this study and the order they have been undertaken in are summarised in Figure 3-1. In the first part of the study, electrodes were developed and manufactured using screen printing techniques and carbon and Ag-AgCl inks. Following electrode development, initial microbial studies were carried out with *P. aeruginosa* to determine whether the bacterium could be detected. Once the ability to detect *P. aeruginosa* was established, development and characterisation of the electrode was performed to optimise consistency between electrodes.

A series of experiments with both *P. aeruginosa* and other microorganisms found in the CF airway were then carried out in an artificial sputum media to determine how useful the device would be in the context of a CF infection. An investigation was performed to identify some of the root causes for changes observed in the impedance spectrum and these were fed into the final part of the project, where the device was tested in a small number of human sputum samples.

The measurements carried out in human sputum required modifications to the electrode assembly. These are described in this chapter and covered in more detail in chapter 6. In the final experiment, the electrode and associated assembly resulting from the human sputum measurement was used in an *in vitro* performance test in order to determine the detection limit of the sensor in terms of cell density and pyocyanin concentration.



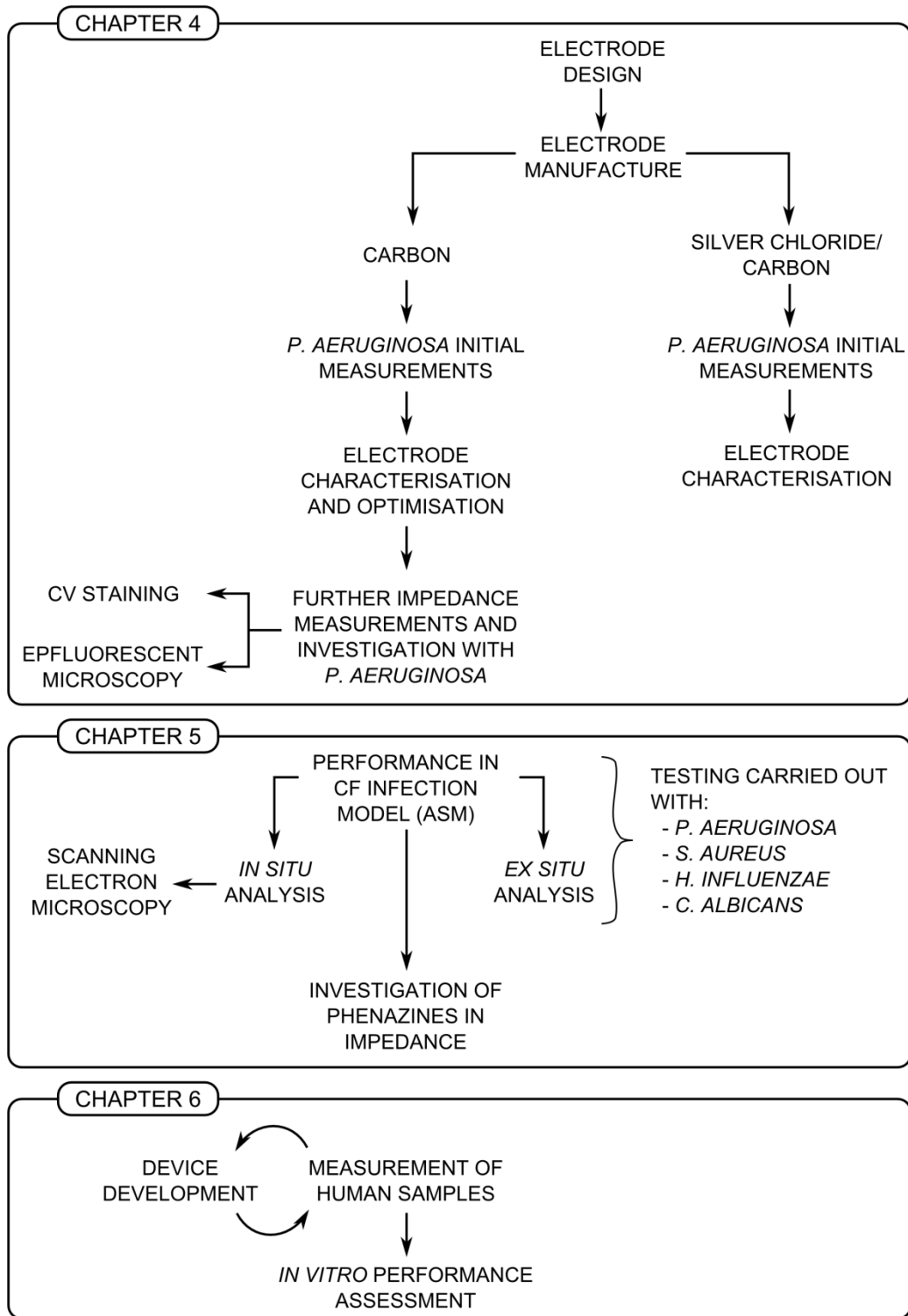


**Figure 3-1: Research roadmap for this study. Chapter numbers relate to presentation of results. The methods for each experiment are described in this chapter.**

## **3.2 Media, buffers and microbial strains**

### **3.2.1 Microbial strains**

The microorganisms used in experiments came from the Tucker laboratory culture stocks, or from the National Collection of Type Culture (Public Health England) as described in Table 3-1. In addition to type strains such as *P. aeruginosa* PA14, a number of well-studied clinical isolates have also been used in this study (i.e. J1385, J1532, C1426 and C1433), originally from John Govan at the University of Edinburgh (Stewart et al. 2013). In some experiments, mutant strains of *P. aeruginosa* PA14 were employed to determine the underlying causes for changes in impedance. These were taken from a copy of the PA14NR set (Liberati et al. 2006) with the exception of the double knockout mutant (PA14 $\Delta$ *phzA1-G1/A2-G2*) which was provided by Dianne Newman at the California Institute of Technology (Dietrich et al. 2006b). All strains were streaked out to single colonies, which were checked for appropriate morphology prior to use, on the appropriate media as indicated in the following sections. Mutant strains from the PA14NR set were initially streaked out onto plates containing gentamicin to ensure that they were not wild type. The stains, along with a reference to their use within the literature are described in Table 3-1. In addition, a cross reference is provided to the results section where they have been used in this study. A description of the storage procedure is provided in section 3.2.3 below.

**Table 3-1: Strains used in this project**

Strain	Comment	Reference	Thesis section where used
PA14WT	<i>P. aeruginosa</i> wild type laboratory strain	(Liberati et al. 2006)	4.4.1;4.2.2; 0; 5.3.1.2; 5.3.2.2; 5.3.3.2; 5.4.3; 5.5; 6.6
PAO1 RHL GFP	<i>P. aeruginosa</i> laboratory strain with GFP protein expression inserted after the RHL operon.	Filloux et al. Imperial College, Personal Communication	4.2.1
J1385	<i>P. aeruginosa</i> non-mucoid CF clinical isolate	(Stewart et al. 2013)	4.4.2
J1385	<i>P. aeruginosa</i> mucoid CF clinical isolate	(Stewart et al. 2013)	4.4.2
C1426	<i>P. aeruginosa</i> non-mucoid CF clinical isolate	(Stewart et al. 2013)	4.4.2
C1433	<i>P. aeruginosa</i> mucoid CF clinical isolate	(Stewart et al. 2013)	4.4.2
RN4220	<i>S. aureus</i> wild type laboratory strain	(Nair et al. 2011)	5.3.1
HI680	<i>H. influenzae</i>	NCTC	5.3.2
SC5314	<i>C. albicans</i>	(Gillum et al. 1984)	5.3.3
PA14 $\Delta$ phzS	<i>P. aeruginosa</i> PA14 mutant from the PA14NR set (gene ID: 44099)	(Liberati et al. 2006)	5.4.4
PA14 $\Delta$ phzM	<i>P. aeruginosa</i> PA14 mutant from the PA14NR set (gene ID: 40343)	(Liberati et al. 2006)	5.4.4
PA14 $\Delta$ phzA1-G1/A2-G2	<i>P. aeruginosa</i> double knockout mutant	(Dietrich et al. 2006b)	5.4.4

### 3.2.2 Media and buffers

The following section describes the media and buffers used in the experiments carried out in this study. Solid agar versions of the media were used to maintain cultures of the microorganisms used (long term storage of strains is described in section 3.2.3) and also for colony counting experiments as described below. Some of the media described below were also used in impedance experiments as indicated in the text. Additionally, this section outlines the recipes for buffers used for electrode conditioning and for microscopy.

#### 3.2.2.1 LB media

LB media was used for the growth of stock culture of *P. aeruginosa* and *C. albicans* strains. Liquid culture was used for initial impedance experiments with *P. aeruginosa*. It was made by mixing 10 g of tryptone (order code: BPE1421, Fisher Scientific, Loughborough, UK), 5

g NaCl (order code: 31434, Sigma Aldrich) and 5g yeast extract (order code: 92144, Fluka) with 1000 ml of w/v dH<sub>2</sub>O. The media was then autoclaved at 121°C for 20 minutes. To make solid media, 5% w/v agar was added prior to autoclaving. Plates were poured once the media cooled to 50°C and left in a laminar flow hood to dry for at least 20 minutes.

#### **3.2.2.2 Mueller Hinton media**

Mueller Hinton Agar (MHA) was used for stock cultures of *S. aureus* and was made by mixing 38 g of MHA media (CM0337, Oxoid) with 1000 ml of dH<sub>2</sub>O. The media was then autoclaved at 121°C for 20 minutes. Plates were poured once the media cooled to 50°C and left in a laminar flow hood to dry for at least 20 minutes. Mueller Hinton Broth (MHB) was used as the base for Haemophilus Test Media and was made by mixing 21 g of MHB (CM0405, Oxoid) to 1000 ml of dH<sub>2</sub>O. The media was then autoclaved at 121°C for 20 minutes.

#### **3.2.2.3 Haemophilus test media**

*Haemophilus* test media (HTM) was used to maintain cultures of *H. influenzae*, for colony counting. Liquid HTM media was also used for impedance experiments with *H. influenzae*. HTM was made by mixing 38 g of MHB (see above) and 5g yeast extract (92144, Fluka) with 1000 ml dH<sub>2</sub>O. The media was then autoclaved at 121°C for 20 minutes. Once cooled to approximately 50°C, NAD (N7004, Sigma-Aldrich) and Hemin (H9039, Sigma-Aldrich) were added to the media to a final concentration of 15 mg/l w/v each. To make solid media, 5% w/v agar was added prior to autoclaving. Plates were poured once the media cooled to 50°C and left in a laminar flow hood to dry for at least 20 minutes.

#### **3.2.2.4 Tryptone soy broth**

Tryptone soy broth (TSB) was used in liquid form for impedance experiments with *S. aureus* and was made by mixing 30 g of TSB media (CM0129, Oxoid) with 1000 ml of dH<sub>2</sub>O. The media was then autoclaved at 121°C for 20 minutes.

#### **3.2.2.5 Tryptone soy broth with yeast extract**

Tryptone soy broth with yeast extract (TSB-YE) was used for impedance growth experiments with *C. albicans* and was produced by mixing 30 g of TSB media (CM0129, Oxoid) with 5 g yeast extract (order code: 92144, Fluka). The media was then autoclaved at 121°C for 20 minutes.

### **3.2.2.6 Muller Hinton agar with salt**

MHA with salt was used for colony counting *S. aureus* in polymicrobial experiments with *P. aeruginosa*. It was made by adding 75 g/l NaCl to 1000 ml of MHA. The media was then autoclaved at 121°C for 20 minutes. Plates were poured once the media cooled to 50°C and left in a laminar flow hood to dry for at least 20 minutes.

### **3.2.2.7 Pseudomonas isolation agar**

*Pseudomonas* isolation agar (PIA) was used for colony counting of *P. aeruginosa* during polymicrobial experiments and was made by mixing 45 g of PIA media (17208, Fluka) with 1000 ml dH<sub>2</sub>O containing 20 ml glycerol (G/0600/17, Fisher Scientific). The media was then autoclaved at 121°C for 20 minutes.

### **3.2.2.8 Pseudomonas agar base with CN supplement**

*Pseudomonas* agar base (PAB) was used for colony counting and to identify the presence of *P. aeruginosa* in human sputum samples and was made by mixing 24.2 g of agar base (CM0559, Oxoid) with 500 ml of dH<sub>2</sub>O and 5 ml of glycerol (G/0600/17, Fisher Scientific) prior to autoclaving at 121°C for 20 minutes. After the media cooled to 50°C, cetrimide and sodium nalidixate (CN) supplement (SR0102, Oxoid) was mixed with 1 ml sterile dH<sub>2</sub>O and 1 ml EtOH and then added to the media prior to pouring into plates.

### **3.2.2.9 Mannitol salt agar**

Mannitol salt agar (MSA) was used for the identification of Gram positive bacteria in human sputum samples and was made by mixing 1 g of lab-lemco power (LP0029, Oxoid), 10 g of peptone (BP1420, Fisher Scientific), 10 g of mannitol (M/2400/53, Fisher Scientific), 75 g of NaCl (31434, Sigma-Aldrich), 0.025 g of phenol red (P3532, Sigma-Aldrich) and 20 g of agar (A/1080/53, Fisher Scientific) to 1000 ml of dH<sub>2</sub>O. The media was then autoclaved at 121°C for 20 minutes. Plates were poured once the media cooled to 50°C and left in a laminar flow hood to dry for at least 20 minutes

### **3.2.2.10 Burkholderia cepecia agar**

*Burkholderia cepecia* ready prepared plates (PO0938, Oxoid) were procured directly from Fisher Scientific as required for the identification of Bcc in human sputum samples.

### **3.2.2.11 Artificial sputum media**

Artificial sputum media (ASM) was produced to simulate human sputum and was used in experiments with strains of *P. aeruginosa*, *S. aureus*, *H. influenzae* and *C. albicans*. 100 ml aliquots of ASM were produced following an adapted version of the protocol by Kirchner et al. (2012). 400 mg DNA from fish sperm (order code: 74782, Sigma-Aldrich) and 500 mg of porcine mucin (order code: M2378, Sigma-Aldrich) were sterilised overnight in 2 ml of 100% EtOH. This was then aseptically poured into 50 ml of sterile dH<sub>2</sub>O. 25 mg each of the following amino acids were mixed together: L-Alanine, L-Arginine, L(+)-Asparagine monohydrate, L(+)-Aspartic acid, L-Cystine, L(+)-Glutamic acid, Glycine, L-Histidine, L-Isoleucine, L-Leucine, L(+)-Lysine monohydrochloride, L-Methionine, L-Phenylalanine, L-Proline, L-Serine, L-Treonine, L(-)-Tryptophan, L-Tyrosine and L-Valine. Prior mixing, L-Tyrosine was added to 2.5 ml 0.5M NaOH and L-Cystine was added to 2.5 ml dH<sub>2</sub>O. The amino acids were then filter sterilised and added to the DNA fish sperm. Following this, 1 ml egg yolk emulsion (order code: 17148, Sigma-Aldrich) and 500 mg NaCl was then added to the DNA and porcine mucin as described (Kirchner et al. 2012). The pH of the media was tested and adjusted to 6.9 by aseptically taking small aliquots of media to measure the pH after adjusting with sterile 1M Tris. Where ASM was used for *H. influenzae*, the media was supplemented with NAD (N7004, Sigma-Aldrich) and Hemin (H9039, Sigma-Aldrich) to a final concentration of 15 mg/l w/v each.

### **3.2.2.12 0.9% w/v NaCl**

0.9% w/v NaCl was used for electrode conditioning and was made in aliquots of 100 ml by mixing dH<sub>2</sub>O with 0.9 g NaCl.

### **3.2.2.13 Cacodylate buffer**

Preparation and use of cacodylate buffer for scanning electron microscopy (SEM) was carried out in fume hood in accordance with the laboratory risk assessment. 0.1 M cacodylate buffer was prepared by adding 2.14 g of sodium cacodylate trihydrate (Sigma, C0250) to 100 ml of 18.2 MOhm/m H<sub>2</sub>O and adjusted to 7.2 pH using paper pH test strips.

### **3.2.2.14 Glutaraldehyde solution for SEM**

Preparation and use of glutaraldehyde fixative for SEM was carried out in fume hood in accordance with the laboratory risk assessment. 2.5% v/v Glutaraldehyde solution was

produced by adding 1 ml of EM grade 25% v/v glutaraldehyde (G5882, Sigma-Aldrich) to 9 ml of cacodylate buffer.

### **3.2.2.15 Sputasol**

Sputasol (SR0233, Oxoid) was prepared by mixing one 7.5 ml vial with 92.5 ml of dH<sub>2</sub>O. Once mixed, Sputasol was stored at 2-8°C and used within 48 hours of preparation.

### **3.2.3 Stock cultures and microorganism storage**

Microorganisms were stored in microbank (PL.170, Pro-Lab Diagnostics) beads at -20°C when not in use. Cultures were streaked out onto solid agar media and incubated overnight at 37°C to select for single colonies. Prior to use, visual verification of colonies was carried out by checking for typical colony morphology (Table 3-2). For *P. aeruginosa* and *C. albicans* strains, LB agar was used, for *S. aureus* LB agar or MHA was used and for *H. influenzae* HTA was used. Streaked plates were retained for a maximum of four weeks and then discarded in accordance with laboratory protocol. If any doubt existed that the organism on a streaked plate was different to that expected (e.g. because of contamination), further tests were carried out using the characteristics described in Table 3-2. Overnight liquid cultures were used to start each experiment and were produced using equivalent liquid media for each species. *H. influenzae* requires microaerophilic conditions for growth. For the purposes of maintaining a stock culture, these were created using a candle jar (World Health Organisation 2011).

**Table 3-2: Identification and verification of different species of microorganism (information collated from Ryan & Ray 2014)**

Species	Identification and growth characteristics
<i>P. aeruginosa</i>	<ul style="list-style-type: none"> <li>• Gram negative rod, 0.9 – 1.5 µm long 0.5 µm wide.</li> <li>• Rough edge colonies (non mucoid).</li> <li>• Round non motile colonies (mucoid).</li> <li>• Produces green coloured pigment that diffuses into the agar</li> <li>• Growth on <i>pseudomonas</i> selective media (e.g. <i>pseudomonas</i> agar base + CN supplement).</li> <li>• Resistant to Triclosan. WT susceptible to gentamicin.</li> <li>• Grows at 20-42°C.</li> </ul>
<i>H. influenzae</i>	<ul style="list-style-type: none"> <li>• Gram negative coccobacilli, 1.0 – 1.5 µm long.</li> <li>• Smooth round white or grey colonies.</li> <li>• Growth only under microaerophilic conditions on chocolate agar or media supplemented with NAD and hemin at 37°C only.</li> </ul>
<i>S. aureus</i>	<ul style="list-style-type: none"> <li>• Gram positive cocci, growth in clusters.</li> <li>• White, round colonies, that turn a golden colour over time growth occurs within 24 hours on rich aerobic media (e.g. blood agar).</li> <li>• Coagulase positive.</li> </ul>
<i>C. albicans</i>	<ul style="list-style-type: none"> <li>• 4-6 µm budding round/oval yeast cells. Can also grow filamentously under certain conditions.</li> <li>• Overnight growth results in smooth white colonies 2-4 mm diameter. Grows on media containing gentamician.</li> <li>• Growth occurs at 25-37°C.</li> <li>• Usually displays tiny projections around base of colony following 24 hours growth (Mahon et al. 2015).</li> <li>• Can also be distinguished from <i>S. aureus</i> by growing on media with a high salt content (e.g. MSA).</li> </ul>

### 3.3 Electrode design and production

Two different types of electrode were produced. The basic pattern for both electrodes differed only in the ink used to print them. The principle applied for the electrodes used in this study was to focus upon the impedance at only one of the electrodes. Thus, the working electrode was used for the detection of *P. aeruginosa*. This was achieved by making the working electrode much smaller than the counter electrode so that the impedance at the working electrode dominated the signature. In order to maintain the simplicity (and therefore cost) of the electrode and device, a reference electrode was not used in this study. In house screen printing was used to produce the electrodes, as described below.



### 3.3.1 Electrode patterns

Two electrode patterns were developed, one consisting of a carbon counter electrode and working electrode and one that consisted of a carbon working electrode and an Ag-AgCl counter electrode. The carbon design was explored because it is low cost to produce and has relatively inert properties which yield consistent impedance characteristics. The findings of experiments carried out with the carbon electrodes are described in sections 4.2.1 and 4.4, and in chapters 5 and 6. The Ag-AgCl/carbon design was explored because it offers the opportunity to achieve lower baseline impedance. The findings of experiments carried out with the Ag-AgCl/Carbon electrodes are described in section 4.2.2. Both designs were based upon the same bipolar electrode pattern, which was used because it would fit within the footprint of a bijou tube with a 12 mm internal diameter (Table 3-3).

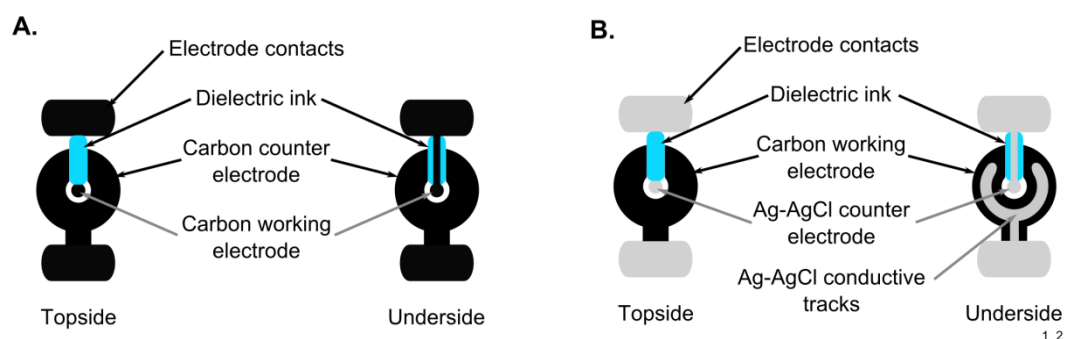


**Figure 3-2: Electrode patterns used in this study. (A) Carbon electrode. (B) Ag-AgCl/carbon electrode. Note that the electrode used as the WE and CE is switched between the two designs.**

The all-carbon electrodes (Figure 3-2 A) were designed to have a small working electrode to counter electrode ratio, thus making it possible to minimise the effects of the counter electrode impedance in the results (Pires et al. 2013; Wegener et al. 1996). When used in conjunction with an electrolyte containing chloride, Ag-AgCl electrodes have non-polarisable properties and relatively low impedance contrasted to carbon. On this basis, a geometrically small CE constructed from Ag-AgCl was used in conjunction with a larger WE printed in carbon, with the aim of reducing the overall electrode impedance (Figure 3-2 B). The impedance of the WE and CE for both the carbon and Ag-AgCl designs were measured separately to check that the WE had a higher impedance as expected (method described in section 3.4.1, results described in section 4.3.3). The same pattern was therefore used for both electrodes with the centre electrode acting as a working electrode in the carbon design. In the Ag-AgCl/carbon design, the centre electrode was made using Ag-

AgCl ink and therefore formed the counter electrode, with the larger, outer electrode being used as the working electrode.

**Table 3-3: Electrode dimensions**

Electrode Design	WE Radius	WE Surface Area	CE Radius	CE Surface Area
Carbon	1 mm	3.142 mm <sup>2</sup>	6 mm	92.65 mm <sup>2</sup>
Ag-AgCl/Carbon	6 mm	92.65 mm <sup>2</sup>	1 mm	3.142 mm <sup>2</sup>

### 3.3.2 Electrode screen printing

The electrodes described above were manufactured using thick film screen printing processes on a DEK 247 semi-automatic screen printing machine. This process starts by producing a mask for each electrode pattern (Figure 3-3). The electrodes were then printed onto glass microscope slides (three electrodes per slide) or onto acetate sheets suitable for a mono laser printer (order code: 9543383, Supplies Team). The printing process was carried out in two layers. For the Ag-AgCl/Carbon electrode design, the tracks for the Ag-AgCl counter electrode and working electrode (Electrodag 6037SS, Acheson) were printed first. Then, after a curing stage in the oven, the carbon ink (Electrodag PF407A, Acheson) was printed on top. For the carbon electrodes, the same process was followed, with the exception that the first print was carried out with carbon ink rather than Ag-AgCl. Following the printing of the conductive inks, a dielectric insulating layer (D2020823D2, Gwent) was used to cover the tracks to the electrodes. The carbon ink was cured at 120°C for 30 minutes in a box oven. The Ag-AgCl ink and dielectric inks were cured at 80°C for 30 minutes in a box oven. Curing was carried out in accordance with the ink manufacturers recommended methods and times.

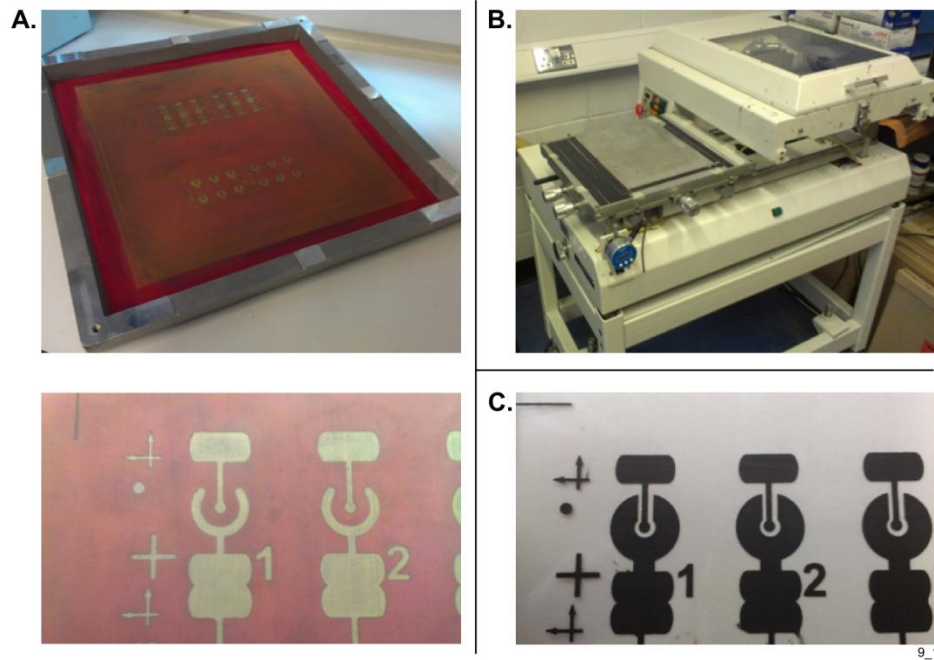


**Figure 3-3: Summary of screen printing process. (A) Mask is produced on a screen impregnated with photo sensitive emulsion. (B) Electrodes were printed in a two layer process using a DEK 247 screen printing machine. (C) The printed electrodes were cured in a box oven as described in the text.**

### 3.3.3 Electrode assembly: *in vitro* experiments

This section describes the electrode assembly used in the experiments outlined in chapters 4 and 5, covering the *in vitro* investigation carried out. After the electrode printing had been completed, a polypropylene tube, cut from a 15 ml centrifuge tube was attached to the glass slide to contain the liquid media (e.g. 0.9% w/v NaCl or culture media) above the electrode (Figure 3-4). Tubes were attached using a small plastic syringe filled with Servisol Adhesive Sealant (Maplin). Care was taken not to touch the electrode surface throughout the printing and assembly processes.

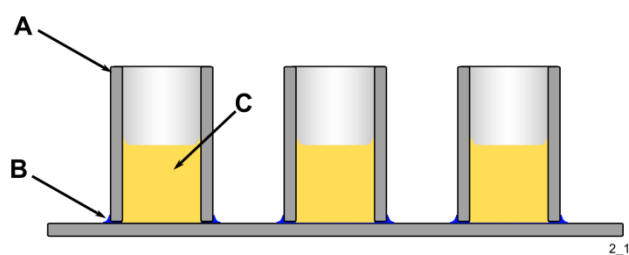


**Figure 3-4: General assembly showing (A) polypropylene tubing, (B) silicone adhesive attaching tubing to electrode base and (C) growth media or electrolyte within container.**

The completed electrode chamber is shown in Figure 3-5. The screen design included two contacts on the outside of the electrode chamber used to connect each electrode to the impedance analyser. For the electrodes printed on acetate, a microscope slide was placed underneath to provide structural support for the chamber. The chambers were covered with a custom made aluminium foil cover to ensure they remained sterile throughout the experiment (Figure 3-6). The cover was sterilised by submerging in 70% v/v ethanol for 10 mins. Figure 3-7 shows an example of the foil cover used, and a typical view of the electrodes at the end of an experiment.

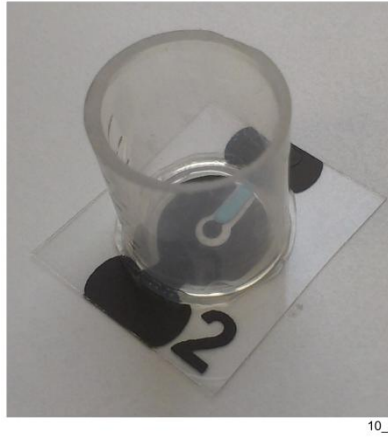


**Figure 3-5: Completed carbon electrode and assembly. The contact pads for connection to the impedance analyser can be seen on the outside of the chamber.**

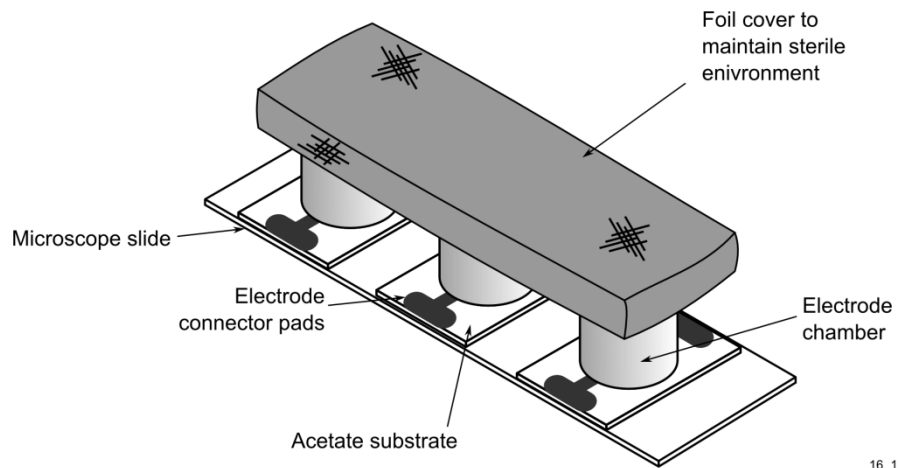


**Figure 3-6: Cartoon of the electrode, showing the foil cover used to keep the electrodes sterile.**



15\_1

**Figure 3-7: Example of electrode chambers at the end of an experiment with *P. aeruginosa* strains. The foil covers used to keep the samples sterile are shown at the bottom of the picture. Electrode assembly: human sputum experiments**

### **3.4 Electrode characterisation**

As described above, the WE was designed such that the impedance would dominate and the effect of the CE impedance could be minimised. In order to verify that this was the case for both the carbon electrode design and the Ag-AgCl/carbon electrode design, an experiment was carried out to confirm the WE impedance was greater than the CE impedance.

### 3.4.1 Contribution to impedance made by each electrode

In order to characterise the impedance of (1) the carbon and (2) the Ag-AgCl/Carbon electrode combination, the WE and CE for each design were analysed by taking measurements using platinum return electrodes as described below. Platinum was used for these measurements because the impedance was lower than the carbon electrodes. Impedance measurements were carried out in 2 ml of 0.9% w/v saline placed into each assembled electrode chamber. The impedance measurements were carried out with a Solartron 1260 impedance analyser (Solartron) from 0.1 Hz to 1 MHz with 0 V dc bias and a perturbation potential of 200 mV<sub>rms</sub>, at room temperature. The impedance analyser was controlled using the ZPlot software package (Scribner Associates) for all the experiments described within this thesis. The ZPlot software provides full control over the impedance analyser and in particular allows the user to define the frequency range, the perturbation amplitude and any DC bias potential (Figure 3-8). Data from each individual sweep is stored by the software in a text file which contains the frequencies measured and the corresponding reactance and resistance measurements.

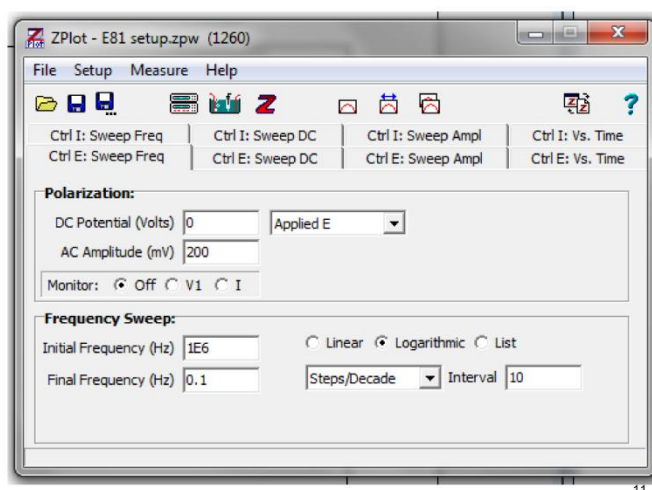
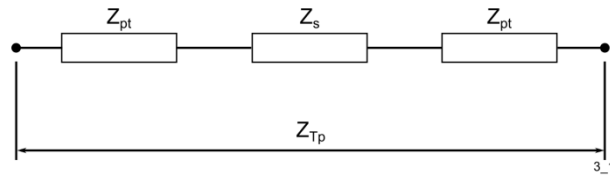


Figure 3-8: ZPlot screen used to control SI1260 impedance analyser, showing the setting used for this study.

#### 3.4.1.1 Characterisation of the platinum electrode

The contribution to the impedance made by the platinum reference electrode was determined by first measuring the impedance of a platinum-platinum electrode pair, where both electrodes are essentially the same. For this, 2 mm platinum rod electrodes (PT007920, Goodfellows), were used with 8 mm submerged in 0.9% w/v saline in the electrode chamber.

This gave a geometric surface area of approximately 50 mm<sup>2</sup>. Then, by treating the observed impedance as three impedances in series (one for each of the electrodes and one for the solution) the contribution of each electrode could be calculated (Figure 3-9).



**Figure 3-9: Total measured impedance from a platinum-platinum electrode pair can be treated as three general impedances in series. Whilst this arrangement does not elicit any information about the charge transfer resistance or double layer capacitance, it makes it possible to assess the contribution to the impedance made by different electrode sizes and materials.**

To determine the impedance contribution, the following procedure was used. An impedance sweep was carried out with the platinum electrode pair, then one of the platinum electrodes was suspended in saline solution in the electrode chamber and submerged to 8 mm. The impedance was then measured in conjunction with each of the electrodes in a circuit experiment. The impedance of one platinum electrode is then subtracted from the total impedance in order to determine the contribution to the impedance made by the working electrode or counter electrode. Mathematically, the impedance of a single platinum electrode is determined from the combined impedances for the platinum pair:

$$Z_{Tp} = Z_{pt} + Z_{spt} + Z_{pt}$$

$$Z'_{Tp} - jZ''_{Tp} = 2Z'_{pt} - j2Z''_{pt} + Z'_{spt} \quad [3-1]$$

Where  $Z_{Tp}$  is the total impedance of the Pt-Pt pair,  $Z_{spt}$  is the solution resistance and  $Z_{pt}$  is the impedance from each of the Pt electrodes.  $Z_{spt}$  was typically 60  $\Omega$ , determined from the complex plane plot at high frequency where the reactance is 0  $\Omega$ . The impedance magnitude of  $Z_{pt}$  was typically found to be 80 K $\Omega$  at 0.1 Hz. Equating the real and imaginary parts of equation [3-1] gives:

$$Z'_{Tp} = 2Z'_{pt} + Z'_{spt}$$



$$Z'_{pt} = \frac{(Z'_{Tp} - Z'_{spt})}{2} \quad [3-2]$$

and:

$$-jZ''_{Tp} = -j2Z''_{pt}$$

$$Z''_{pt} = \frac{Z''_{Tp}}{2} \quad [3-3]$$

### 3.4.1.2 Characterisation of printed electrode impedance

The combined impedance of a platinum electrode with either the working electrode or counter electrode was measured (Table 3-4). Mathematically, this can be modelled in order to determine the impedance of the measured working electrode or counter electrode, excluding the platinum electrode and the solution resistance (Figure 3-10).

**Table 3-4: Impedance measurements carried out with electrode pairs. The Ag-AgCl WE has the same geometry and is made from the same ink as the carbon CE and therefore had the same impedance.**

Electrode Type	Measurement Taken	Parameter Determined
Carbon	Pt-WE	Carbon WE
	Pt-CE	Ag-AgCl WE/Carbon CE
Ag-AgCl/Carbon	Pt-CE	Ag-AgCl CE

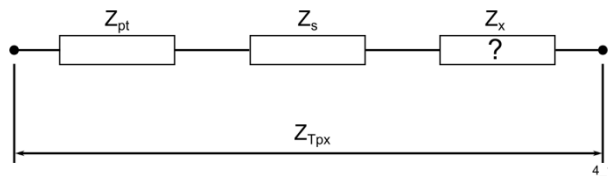


**Figure 3-10: Impedance of a single platinum electrode can be used to determine the impedance of either the working electrode or counter electrode. The unknown electrode impedance is represented here as  $Z_x$ .**

The total impedance for the circuit shown in Figure 3-10 can be described by:

$$Z_{Tpx} = Z_{pt} + Z_{spx} + Z_x$$

$$Z'_{Tpx} - jZ''_{Tpx} = Z'_{pt} - jZ''_{pt} + Z'_{spx} + Z'_x - jZ''_x \quad [3-4]$$

Where  $Z_{Tpx}$  is the impedance of a single platinum electrode in conjunction with the unknown electrode impedance,  $Z_x$ . Equating real and imaginary parts gives:

$$Z'_{Tpx} = Z'_{pt} + Z'_{spx} + Z'_x$$

$$Z'_x = Z'_{Tpx} - Z'_{pt} - Z'_{spx} \quad [3-5]$$

and:

$$-jZ''_{Tpx} = -jZ''_{pt} - jZ''_x$$

$$Z''_x = Z''_{Tpx} - Z''_{pt} \quad [3-6]$$

Equations [3-2], [3-3], [3-5] and [3-6] were used to determine the impedance of the carbon and Ag-AgCl WE and CE. After measuring the impedance contribution from each of the electrodes, the impedance of the platinum pair was measured again to verify that the impedance signature hadn't changed. Average electrode impedance values for printed electrodes are given in Table 3-5. The full results from the measurements shown in section 4.3.3.

**Table 3-5: Average contribution to impedance from each electrode at 1 Hz**

Electrode	$Z'$ ( $\Omega$ )	$Z''$ ( $\Omega$ )
Carbon WE	$7.27 \times 10^4$	$-4.28 \times 10^5$
Carbon CE Ag-AgCl/Carbon WE	$2.31 \times 10^3$	$-1.67 \times 10^4$
Ag-AgCl CE	$3.65 \times 10^3$	-181

### **3.4.2 Selection of optimum measurement voltage**

Previous studies within the research group used a 200 mV<sub>rms</sub> perturbation voltage for impedance measurements (Farrow 2010; Shedden 2008), however this is outside the range where the system would be expected to be approximately linear (Macdonald 1987). Therefore, an experiment was carried out to assess the use of a lower perturbation voltage of 10 mV<sub>rms</sub>. All measurements were made in 1 ml of 0.9% w/v NaCl added directly to the electrode chambers. Impedance measurements were carried out with a Solartron 1260 impedance analyser at room temperature. Two sets of measurements were made, the first at a perturbation voltage of 10 mV<sub>rms</sub> between 0.1 Hz and 1 MHz, the second at 200 mV<sub>rms</sub> across the same frequency range. All measurements were carried out at 0 V dc bias. The results are shown in section 4.3.1 and indicate that when a 10 mV<sub>rms</sub> perturbation voltage is used for the measurement, a large amount of noise occurs at lower frequencies. Therefore 200 mV<sub>rms</sub> was used for all future measurements.

### **3.4.3 Electrode preconditioning**

A conditioning technique was developed based upon Wang et al. (1996) to improve the consistency between carbon electrodes. Activation of the electrode surface in a pre-anodisation step was found to improve the electrochemical activity of the electrodes across a wide range of analytes. The pre-anodisation step was thought to increase surface functionalities and roughness and the removal of surface contaminants (Wang et al. 1996). This approach was adopted here to improve the consistency between electrodes because it could be readily implemented in a future device and was found to slightly lower the baseline impedance and improve the consistency of the electrodes.

1 ml of 0.9% w/v NaCl was added to the electrode chamber at room temperature. Using the Solartron 1260 impedance analyser, in conjunction with a platinum CE, a DC bias of 2 V was placed across both carbon electrodes relative to the platinum CE. This potential was held for three minutes before the potential was reversed to -2 V and held for a further three minutes. Following this, three impedance sweeps were carried out in the same 0.9% w/v NaCl to verify that a consistent baseline signature was present.

## **3.5 Impedance measurements with microorganisms**

This section describes the experiments carried out with the microorganisms described in Table 3-1. For all microorganisms tested, initial experiments were always carried out in the

optimal growth media (see section 3.2.2) prior to any measurements in artificial sputum media. A combination of *in situ* and *ex situ* measurements were performed as part of the study. *In situ* measurements are defined as those where the growth of the microorganism occurred in the presence of the electrode. The *in situ* measurements were used to attempt to identify processes such as biofilm formation and microbial attachment that could affect the electrode impedance. *Ex situ* measurements were also performed, whereby the microorganisms were incubated separately to the electrode and only added for the purpose of the measurement. The *ex situ* measurements were important because the concept behind the infection monitor is that the sputum sample will only be in contact with the electrode for the duration of the measurement. Furthermore some species tested showed lower viability when grown in the presence of the electrode chamber.

### **3.5.1 Overnight cultures**

All overnight cultures were prepared in a laminar downflow hood by picking a single colony from an LB agar plate and inoculating 5 ml of LB media in a 30 ml universal (128C, Sterilin, Thermo Scientific). The culture was then incubated at 37°C, shaking at 150 rpm overnight (15-20 hours). Culture media was checked for turbid growth at this point. The culture media used for each species of microorganism is described in section 3.2.3.

### **3.5.2 Impedance measurements**

All impedance measurements were carried out using a Solartron 1260 impedance analyser with an AC voltage of 200 mV<sub>rms</sub> between 0.1 Hz and 1 MHz. Impedance measurements were carried out at room temperature. Initial measurements were made at the start of the experiment and then every 24 hours during the experiment, unless otherwise stated. Measurements were carried out by removing the electrode chambers from the incubator and attaching the impedance analyser with two crocodile clips to the chamber contacts. A 200 mV<sub>rms</sub> measurement potential was used and measurements were carried out from 0.1 Hz to 1 MHz. Two sweeps were carried out per electrode chamber in order to verify that the impedance remained the same between sweeps. Electrodes not meeting this criterion were typically found to have a leak and were discarded from the experiment. Following the measurement, the electrode chambers were returned to the incubator. Impedance data analysis was carried out using Matlab r2012b (Mathworks). The theory and models of the impedance measurements are explained in section 2.1 and 2.2.

### **3.5.3 *In situ* impedance measurements**

Assembled electrode chambers were sterilised by submerging in 70% v/v ethanol (32221-2.5l, Sigma-Aldrich) prior to the experiments for 10 minutes and then left to dry under a laminar flow hood. 1 ml of sterilised media (selected for the species being tested, as described in section 3.2.3) was then aseptically added to each electrode chamber. Chambers were then inoculated with an overnight culture of the species and strain of interest or left with un-inoculated media as a negative control. Unless otherwise stated, a 1% v/v overnight culture was used for inoculation.

#### **3.5.3.1 Replacement of media to identify microbial attachment**

In order to investigate the role that microbial attachment had upon the impedance when *P. aeruginosa* was grown *in situ* a further step was carried out at the end of experiments (see sections 4.2.1 and 4.4.1 for results). The media within the electrode chamber was carefully aspirated using a 1 ml pipette. Fresh, sterile media was then added to the chamber very slowly down the side wall of the chamber. The first aliquot of media was used to rinse away any remaining unattached culture. The chamber was slowly aspirated before a second aliquot of sterile media was added. Impedance measurements were then carried out as described in section 3.5.2.

### **3.5.4 *Ex situ* impedance measurements**

As described above, *ex situ* measurements were carried out in order to assess the performance of the electrode at detecting *P. aeruginosa* when the bacteria has not been grown in the presence of the electrode. This is important from the perspective of the end use device whereby the human samples will only be in contact with the electrode for the duration of the measurement. A 1% v/v aliquot of overnight media was used to inoculate a 5 ml aliquot of media in a 30 ml universal container and was incubated at 37°C for up to 72 hours. All impedance measurements were carried out at the end of the incubation period. An initial impedance measurement was carried out in 1 ml of sterile media at room temperature. Impedance measurements were carried out using the parameters described in section 3.5.2. Following this, the sterile media was removed and 1 ml of the incubated culture was added to the electrode chamber. A further impedance measurement was carried out using the same procedure as the first measurement.

### **3.5.5 Microbial measurements in cystic fibrosis model environment**

Growth experiments were carried out in artificial sputum media (ASM) to represent the conditions found within the CF airway (Kirchner et al. 2012). To achieve this, electrode assemblies were produced as described above (section 3.3.3) and sterilised in 70% v/v ethanol. 1 ml of sterile ASM (section 3.2.2.11) was then added to each electrode chamber. Chambers were inoculated with the bacteria of interest, either in a mono culture or a polymicrobial culture at equal cell densities. Polymicrobial cultures consisted of *P. aeruginosa* combined with one other species (either *S. aureus*, *H. influenzae* or *C. albicans*) and were used to model basic situations that could occur in the CF airway.

#### **3.5.5.1 Calculation of appropriate starting cell density**

In preparation for the polymicrobial experiments, a standard curve was produced for each bacterial species used, linking OD<sub>600</sub> to CFU/ml. OD<sub>600</sub> is widely used to indirectly determine microbial cell density. Serial dilutions of the overnight culture of each strain were carried out in a 96 well plate and the OD<sub>600</sub> was measured using a plate reader (Spectramax 190, Molecular Devices). The concentration of CFUs in the overnight culture was calculated and used to determine the concentration at each serial dilution. This procedure was used for *P. aeruginosa*, *H. influenzae* and *C. albicans*. For the polymicrobial experiments, the OD<sub>600</sub> of the overnight culture was adjusted to correspond to a starting cell density of  $3 \times 10^8 - 5 \times 10^8$  CFU/ml.

#### **3.5.5.2 Microaerophilic chamber design**

A microaerophilic environment was created by using a lock 'n' lock plastic box (HPL826M, Lock 'n' Lock) modified with two 9 way D-sub connectors mounted through the sidewalls of the box (Order code: 674-0760 and 450-9258, RS components) to enable impedance measurements to be carried out without the need to remove the lid. The D-sub connectors were made airtight by sealing around the connectors on the inside of the box with Servisol silicone adhesive (Figure 3-11).



17\_1

**Figure 3-11: Picture of the microaerophilic chamber used in these experiments. Chamber lid and foil electrode covers removed for clarity.**

### **3.5.6 Monoculture and polymicrobial experiments**

At the start of the experiment, up to nine sterile electrodes were connected, inoculated and placed into each microaerophilic box, with up to 18 electrodes used in any one experiment (i.e. two microaerophilic chambers). The microaerophilic environment was created using a Campygen gas generation pack (order code: 10108012, Fisher Scientific). Electrodes were then incubated at 37°C in a shaking incubator at 75 rpm for up to 72 hours.

#### **3.5.6.1 Impedance measurements**

Impedance measurements were carried out at the start of the experiment and then at least once every 24 hours for the duration of the experiment. The microaerophilic chamber was removed from the incubator and kept at room temperature for the duration of the measurements which typically lasted approximately 45 minutes per chamber and four

minutes per electrode. Impedance measurements were carried out using the parameters described in section 3.5.2.

### **3.5.6.2 Post experiment colony counting**

Colony counting was carried out on the ASM cultures used in the CF model environment. For monoculture experiments, *P. aeruginosa*, *C. albicans* and *S. aureus* colony counting was done on LB agar. For *H. influenzae* colony counting was carried out on HTA. Selective agar was used for polymicrobial colony counting. For *P. aeruginosa*, PIA was used. For *S. aureus* MHA with salt was used, and for *C. albicans* LB agar supplemented with 15 µg/ml gentamicin (G3632-5g, Sigma-Aldrich) was used (see section 3.2.2 for detailed media and buffers).

Colony counting was done using ten-fold serial dilutions in conjunction with the drop plate method (Herigstad et al. 2001). This involved placing 10 µl drops of the diluted broth onto the appropriate solid media at different concentrations. 10 drops were plated for each sample at each concentration. Plates were incubated at 30-37°C overnight. Colonies were then enumerated at the concentration where 3 – 30 colonies existed per drop.

## **3.6 Investigations into the role of phenazines in impedance**

A series of experiments were carried out to determine if pyocyanin, an easily identifiable phenazine metabolite produce by *P. aeruginosa*, was present within the media. Furthermore, given the widely reported electrochemical properties of pyocyanin and associated phenazines, a series of experiments were carried out to determine the role they played in the measured impedance. The results from these experiments are described in section 5.4.

### **3.6.1 UV-Vis spectrum and associated protocol**

UV-Vis spectroscopy was used to determine whether pyocyanin was present in the supernatant from media following the growth of *P. aeruginosa*. At the end of the experiment period, the supernatant was filter sterilised through 0.22 µm syringe filter (Millipore) and then added to an equal volume of methanol to fix the sample. The UV visible spectrum was then measured from 190 nm to 850 nm using a Thermofisher 2000x spectrophotometer. Data analysis of the UV-visible spectrum was carried out in Matlab r2012b (Mathworks).



### 3.6.2 Calculation of pyocyanin concentration

From the UV-vis spectrum, the concentration of pyocyanin was calculated to determine the overall sensitivity of the electrode. The Beer-Lambert equation was used to calculate the concentration of oxidised pyocyanin present within the supernatant at 690 nm. This was achieved by measuring the absorbance using a Thermofisher 2000x spectrophotometer and the applying the following equation:

$$C = \frac{A}{\epsilon b} \quad [3-7]$$

Where  $C$  is the molar concentration,  $A$  is the measured absorbance at 690 nm,  $b$  is the light pathlength (0.1 cm for the Thermofisher 2000x spectrophotometer) and  $\epsilon$  is the extinction co-efficient, which for pyocyanin is  $4310 \text{ M}^{-1}\text{cm}^{-1}$  at pH 7 (Price-Whelan et al. 2007).

### 3.6.3 Sterile pyocyanin measurement

The addition of pyocyanin to sterile ASM media was explored to determine if it resulted in a change in impedance. Pyocyanin purified from *P. aeruginosa* (P0046, Sigma-Aldrich) was solubilised in 100% ethanol to create a stock solution. This was mixed with sterile ASM to create solutions containing different concentrations from 1000  $\mu\text{M}$  to 1  $\mu\text{M}$ .

### 3.6.4 Exogenous pyocyanin measurements

Experiments were also carried out to determine the effect that the addition of pyocyanin to an overnight culture of *P. aeruginosa* and *S. aureus* had upon the impedance. The stock solution described above was mixed with sterile dH<sub>2</sub>O for the measurements carried out using *S. aureus* and *P. aeruginosa*. 1 ml samples of *P. aeruginosa* and *S. aureus* (as monocultures) were grown overnight (20 hours) along with negative controls in 24 well plates. Following this, the samples were removed from the microaerophilic growth chamber and after initial impedance measurements, pyocyanin was added to aliquots of media to a final concentration of 100  $\mu\text{M}$  and 300  $\mu\text{M}$ . An impedance measurement was carried out at each concentration.

### 3.6.5 Growth experiments with mutant strains of *P. aeruginosa*

A series of experiments were carried out to determine the effect that *P. aeruginosa* strains unable to produce phenazines had upon the impedance. These experiments were carried out

by following the monoculture protocol described in section 3.5.5 with mutant strains from the PA14NR set and a double knockout mutant (see Table 3-1 for specific strains used).

### **3.7 Investigations into microbial attachment on the electrode surface**

Biofilm formation and microbial attachment on the carbon electrode surface was investigated through the use of crystal violet (CV) staining and both fluorescent and scanning electron microscopy (SEM). Visualisation of the electrode in this manner was carried out to determine if changes observed in the impedance following the addition of fresh media after the growth of *P. aeruginosa* could be related to microbial attachment and biofilm formation on the electrode surface. CV staining was used because it represented a quantitative method of assessing microbial attachment across the whole electrode. Epifluorescent microscopy and SEM were both used as techniques that facilitated qualitative analysis of the electrode surface following the growth of *P. aeruginosa*. The results are described in section 4.5 (CV staining and epifluorescent microscopy) and section 5.5 (SEM).

#### **3.7.1 Crystal violet assays**

##### **3.7.1.1 Electrode chamber CV staining**

CV staining was carried out using the following procedure (Figure 3-12). Chambers were attached to the electrodes printed on as described in section 3.3.2. After sterilising in 70% v/v ethanol for 10 minutes, 1 ml of sterile LB was then added to each chamber and inoculated with *P. aeruginosa*. The electrode chambers were incubated for up to 72 hours.

At the end of the experiment, CV staining was carried out using an adaptation of the protocol described by Merritt et al. (2005). Chambers were carefully flushed twice with sterile LB media. Following this, 1 ml of an aqueous solution of 0.1% v/v CV was added to each chamber. After 10 minutes, the chambers were aspirated and rinsed with dH<sub>2</sub>O to remove any further loose material. At this point, the base (containing the electrode) was peeled away from the polypropylene tube. Each base was then placed into its own bijoux tube containing 3 ml of 95% v/v ethanol for 10 minutes to solubilise the stain. The electrode was removed after 10 minutes and the absorbance of the ethanol was measured using a Nanodrop 2000c (Thermoscientific) spectrophotometer at 570 nm (Figure 3-12). By using the approach of removing the electrode base from the growth chamber, the background absorbance caused by biofilm attachment at the air-liquid interface and not the electrode could be eliminated.

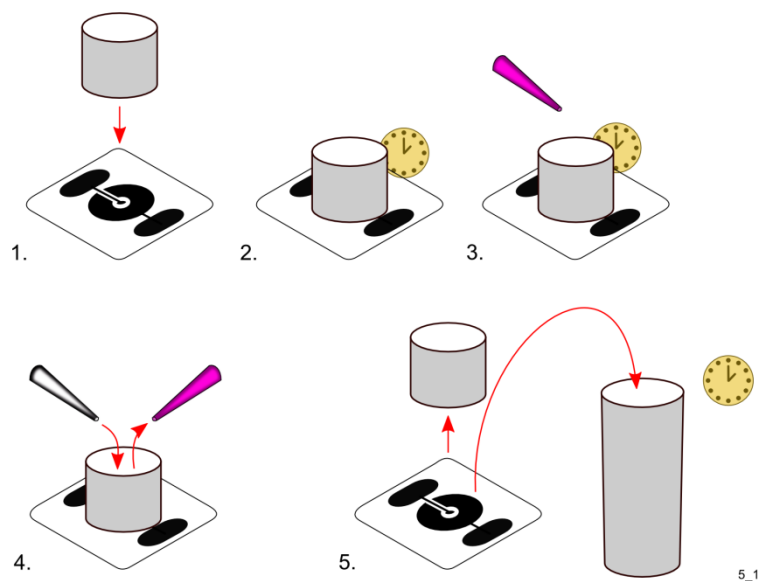


**Figure 3-12: Summary of CV staining assay used to measure microbial attachment and biofilm on the electrode surface. (1) Chamber is attached to electrode. (2) Assembly is sterilised and media is added, inoculated and incubated for required length of time. (3) Chamber is rinsed and CV stain is added. (4) CV removed after 10 mins, chamber rinsed with dH<sub>2</sub>O. (5) Chamber is removed; electrode is placed into ethanol for 10 mins.**

### 3.7.1.2 Electrode coupon CV staining

An alternative version of the CV staining assay was also used, whereby electrode coupons sterilised in 70% v/v ethanol and placed into the bottom of a 24 well plate. This adapted version was carried out remove the problems associated with biofilm attaching to the silicone adhesive sealant used to construct the chambers. The coupons were then left in a laminar down flow hood to allow the ethanol to fully evaporate. 1 ml of sterile LB media was then added to each of the electrode chambers and then inoculated with 2 µl of the *P. aeruginosa* strain of interest and incubated for up to 72 hours.

At the end of the time period, the media from each electrode chamber was removed and replaced with a fresh aliquot of LB to wash away loose biofilm material. The fresh media was then aspirated and replaced with a 0.1% v/v solution of CV in dH<sub>2</sub>O. This was then incubated at room temperature for 10 minutes. The electrode coupons were removed from the CV solution using forceps and dipped in dH<sub>2</sub>O to rinse away any non-attached biofilm and CV stain. The coupon was then placed into a clean 24 well plate containing 1 ml of 95% v/v ethanol and incubated for 10 minutes at room temperature. Following this, the electrode

coupon was removed and the absorbance of the ethanol was measured using a spectrophotometer at 570 nm (Thermofisher, 2000x).

### 3.7.2 Microscopy of the electrode surface

#### 3.7.2.1 Electrode coupon preparation for microscopy

Microscopy of the electrode was carried out in order to understand the extent to which *P. aeruginosa* was able to attach to the electrode. Electrode coupons were printed onto acetate sheets using carbon ink as described in section 3.3.2. These were then cut out and sterilised in 70% v/v ethanol (32221-2.5l, Sigma-Aldrich) for 10 minutes, placed one each into a 24 well plate and left in a laminar flow hood to allow the ethanol to evaporate. Some of the coupons were placed directly into the bottom of the 24 well plate, whereas other were placed perpendicular to the bottom of the plate so that a portion of the electrode would protrude from the media. This enabled a biofilm to form at the air liquid interface and served as a positive control (Figure 3-13).

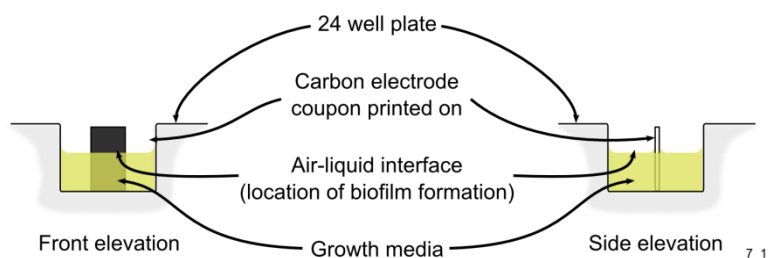


**Figure 3-13: Configuration of the electrode coupon used in the positive control.**

#### 3.7.2.2 Epifluorescent microscopy in LB media

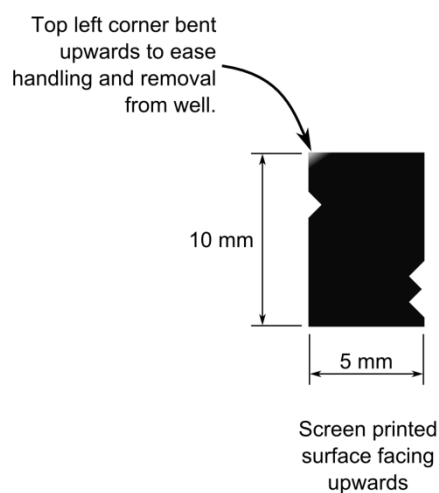
1 ml of sterile LB was added to each well containing a prepared electrode coupon and inoculated with *P. aeruginosa* PA14. The 24 well plate was incubated at 37°C shaking at 75 rpm. Following this, the coupons were aspirated and gently rinsed with 1 ml of normal saline for 5 minutes to remove any loosely attached material.

The coupons were stained by adding 50  $\mu$ l of 5  $\mu$ M SYTO 9 stain in filter sterilised dH<sub>2</sub>O to the surface of the coupon and incubated in darkness for 15 minutes. After the incubation, the coupons were rinsed again in filter sterilised dH<sub>2</sub>O prior to mounting on a glass microscope slide with a coverslip to prevent evaporation. Microscopy was carried out using an epifluorescent microscope (Zeiss Axio Imager Z1). Image analysis was subsequently carried out using the Fiji image processing package (Schindelin et al. 2012).

Positive and negative controls were carried out in conjunction with the experiments. Negative controls were employed in all experiments in order to verify there was no auto-fluorescence on either the electrode surface or within the media. Positive controls were produced as described in section 3.7.2.

### 3.7.2.3 Scanning electron microscopy

SEM was carried out to explore microbial attachment of *P. aeruginosa* in ASM following microaerophilic growth. Modified electrode coupons were made, by cutting out carbon electrodes printed on acetate (section 3.3.2). The electrodes were cut into a specific pattern which would allow the front face and top and bottom of the electrode to be easily identified (Figure 3-14). Following this, the exposed edges and back of the electrodes were hand painted with carbon ink (Electrodag PF407A, Acheson) to ensure that no acetate remained exposed. The carbon ink was cured in a box oven as described in section 3.3.2.



8\_1

**Figure 3-14: Electrode coupon pattern used for SEM microscopy**

The electrode coupons were sterilised in 70% v/v ethanol for 10 minutes, placed into a 24 well plate and left to dry in a laminar flow hood. As described above (section 3.7.2) some of the electrode coupons were placed at right angles to the base of the well in order to allow a biofilm to form at the air liquid interface and thus serve as a positive control. 1 ml of ASM was then added to each electrode chamber. Chambers were inoculated with 1% v/v of an overnight culture of *P. aeruginosa* PA14 ( $OD_{600} = 0.33$ ), which equated to approximately  $2.5 \times 10^6$  CFU/ml final concentration. The 24 well plate was incubated for 72 hours at 37°C shaking at 75 rpm in a microaerophilic environment. The microaerophilic environment was created using a campygen pack (CN0025, Oxoid) placed into a lock n lock airtight container.

Fixation of the biofilm was carried out in a fume cupboard using a protocol adapted from Harrison et al. (2006). Electrode chambers were removed from the incubator and aspirated. 1 ml of sterile saline was added to each well and incubated for 5 minutes at room temperature after which the sterile saline was aspirated from the electrode chambers. 500  $\mu$ l of 2.5% v/v glutaraldehyde solution (section 3.2.2.14) was added to the electrode chamber and incubated (in the fume cupboard with the lid on the plate) at room temperature for 2 hours. To visualise the biofilm structures, the wells were aspirated and rinsed for 10 minutes in 500  $\mu$ l cacodylate buffer (section 3.2.2.13) for 10 minutes. A further rinse was then carried out for 10 minutes in 18.2 M $\Omega$  dH<sub>2</sub>O to remove any remaining salts. Following this, the wells were aspirated and the electrode coupons left to air dry for 120 hours.

To view, they were mounted on stubs and sputter coated using a gold target. Viewing was carried out using a Hitachi TM-1000 table top SEM with an acceleration voltage of 15, 000 V. Once the samples were fixed and air dried, they were stored at room temperature in culture dishes to prevent contamination from dust.

### **3.8 Impedance data analysis**

In the discussion, the electrochemical theory described in section 2.2 is used to explore the results. This section describes the approaches adopted to handle the large quantities of data produced and analysed. Data analysis was also carried out to identify trends and characteristic signals in the impedance data that related to particular species. Finally, a peak detection algorithm was created to allow peaks in the normalised impedance data be easily identified.

#### **3.8.1 Data handling**

Each impedance measurement produced a single text file containing data on the impedance frequency, resistance and reactance measurements. A database was developed in MS Access to allow data from different experiments to be imported and structured for downstream analysis. Once in MS Access, the data could be copied into Matlab where a front end tool was produced to carry out full analysis of the results.

The Matlab front end facilitated easy production of mean impedance data (resistance, reactance, phase, normalised resistance, normalised reactance and normalised phase) and was also used to develop the peak detection algorithm described in section 3.8.3.

### 3.8.2 Impedance normalisation

Impedance data was normalised to detect characteristic changes that could indicate the presence of microorganisms, as described previously (Connolly and Shedden 2010). This was carried out on the resistance and phase data as follows:

$$IPN_{t=n} = \frac{IPA_{t=n}}{IPA_{t=0}} \quad [3-8]$$

Where  $IPN_{t=n}$  is the normalised impedance parameter of interest (i.e. reactance, resistance, impedance modulus or phase) and  $IPA_t$  is the absolute (as measured) impedance parameter. An example of un-normalised and normalised resistance data is shown below in Figure 3-15. This indicates that the normalised process highlights changes in the impedance that are less easily identified by analysis of the raw data.

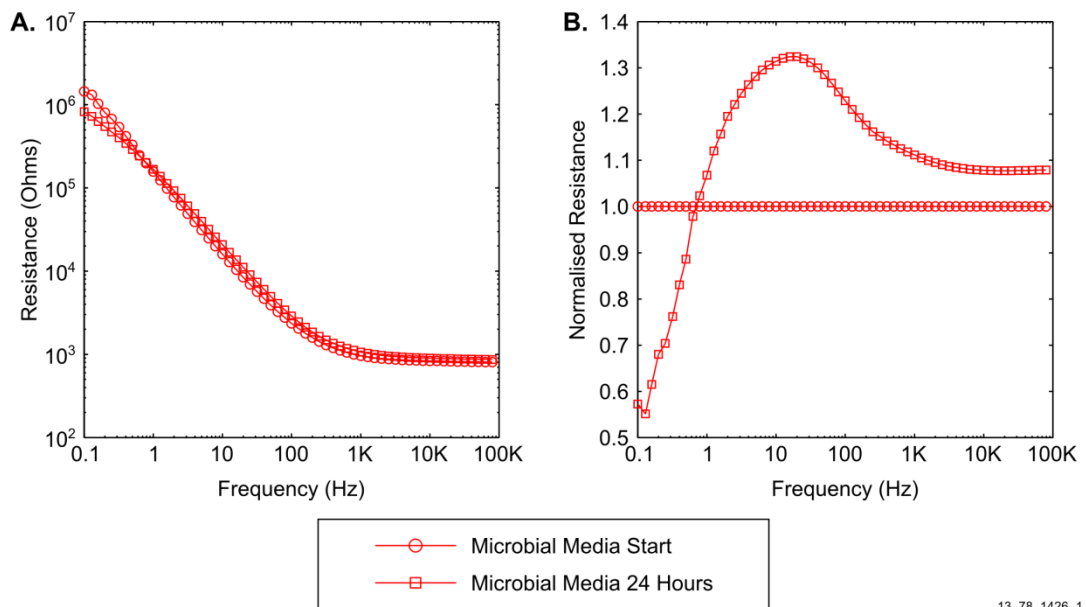


**Figure 3-15: Example of raw data signal and equivalent normalised signal. (A) Measured resistance. (B) Normalised resistance.**

### 3.8.3 Peak detection algorithm

As shown in the results (for example, section 4.4 and Figure 5-11) the presence of *P. aeruginosa* leads to characteristic peaks in the normalised impedance data. Therefore, a simple peak detection algorithm was developed to rapidly and objectively identify peaks and troughs in the phase and normalised resistance data. The algorithm was implemented in

Matlab and analyses impedance data from individual or mean impedance data for peaks and troughs. The algorithm works as follows:

1. The frequency is converted into a linear scale, with divisions set by a user defined parameter called the step size.
2. A spline interpolation is carried out on the y-axis data (i.e. the normalised phase or normalised resistance) to generate a value for each point on the x-axis linear scale.
3. The interpolated data is then fitted using a Savitsky-Golay filter. The polynomial size and frame size used are defined by the user.
4. From the filtered data, a peak is defined as four consecutively increasing datapoints in the y-axis data, followed by four consecutively decreasing datapoints.
5. The peaks and troughs identified in each of the impedance measurements are plotted over the raw data to provide the user with an indication of the quality of the fit. Additionally, a text file can be produced with specific details of the locations of each peak and trough.

The optimum values for the step size, polynomial order and frame size vary for each of the impedance parameters. A set of user defined values were established and used throughout this study. These are shown in Table 3-6. An example of the peak detection algorithm is shown in Table 3-7.

**Table 3-6: Parameters used for peak and trough detection**

<b>Impedance Parameter</b>	<b>Step Size</b>	<b>Polynomial Order</b>	<b>Frame Size</b>
<b>Normalised Resistance</b>	0.1	2	15
<b>Normalised Phase</b>	0.05	3	19



**Table 3-7: Example of data output from phase data peak and trough detection. The graphical plots provide an indication of how well the identified peak fits the data. The text beneath the plots shows the frequency and location of each peak identified.**

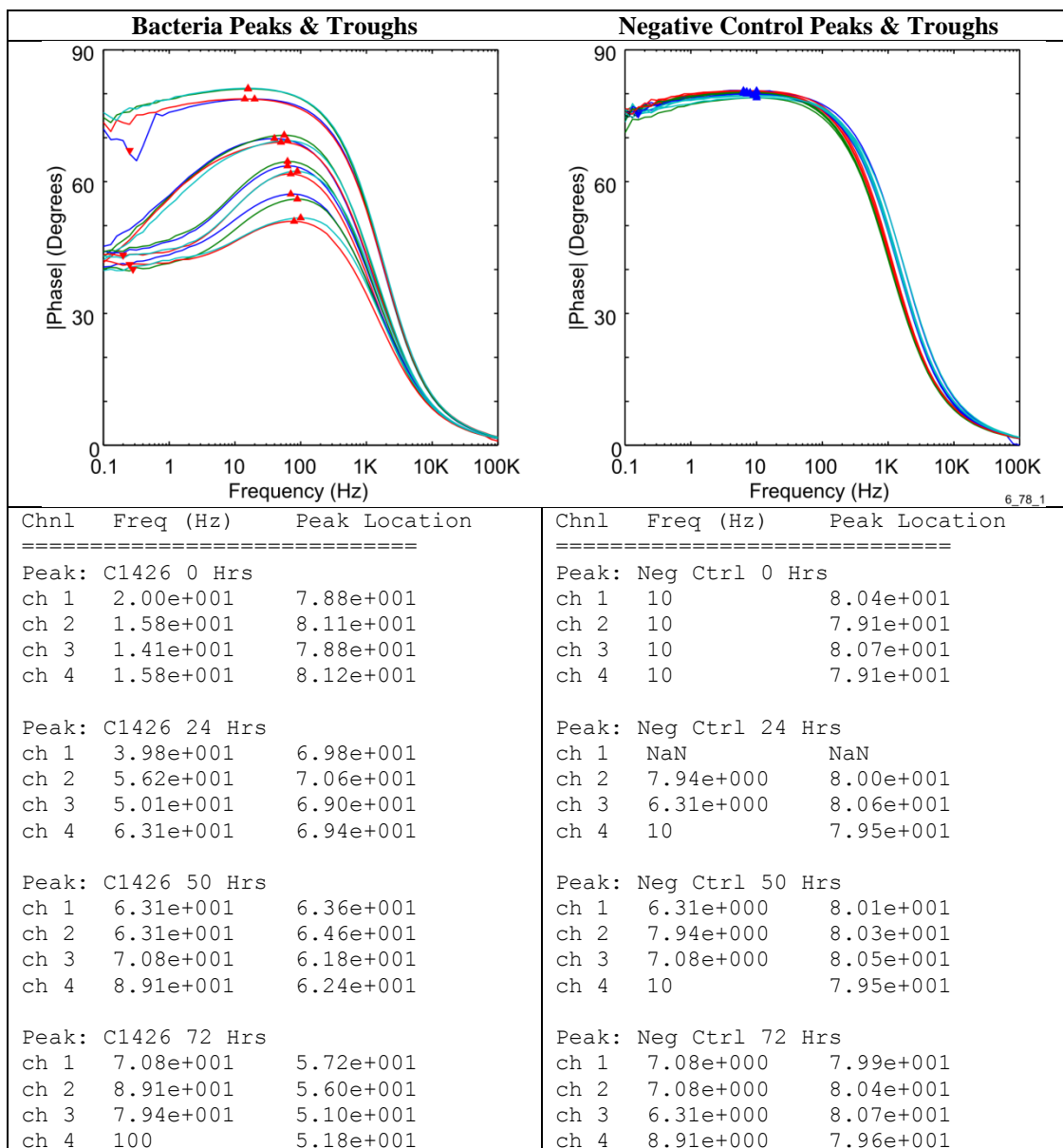


**Table 3-7 continued.**

Bacteria Peaks & Troughs			Negative Control Peaks & Troughs		
Chnl	Freq (Hz)	Trough Location	Chnl	Freq (Hz)	Trough Location
=====			=====		
Trough: C1426 0 Hrs			Trough: Neg Ctrl 0 Hrs		
ch 1	2.51e-001	6.71e+001	ch 1	NaN	NaN
ch 2	NaN	NaN	ch 2	NaN	NaN
ch 3	NaN	NaN	ch 3	NaN	NaN
ch 4	NaN	NaN	ch 4	NaN	NaN
Trough: C1426 24 Hrs			Trough: Neg Ctrl 24 Hrs		
ch 1	NaN	NaN	ch 1	NaN	NaN
ch 2	NaN	NaN	ch 2	NaN	NaN
ch 3	NaN	NaN	ch 3	NaN	NaN
ch 4	NaN	NaN	ch 4	NaN	NaN
Trough: C1426 50 Hrs			Trough: Neg Ctrl 50 Hrs		
ch 1	NaN	NaN	ch 1	NaN	NaN
ch 2	NaN	NaN	ch 2	NaN	NaN
ch 3	2.00e-001	4.33e+001	ch 3	NaN	NaN
ch 4	NaN	NaN	ch 4	1.58e-001	7.54e+001
Trough: C1426 72 Hrs			Trough: Neg Ctrl 72 Hrs		
ch 1	NaN	NaN	ch 1	NaN	NaN
ch 2	2.82e-001	4.01e+001	ch 2	NaN	NaN
ch 3	2.51e-001	4.11e+001	ch 3	NaN	NaN
ch 4	NaN	NaN	ch 4	NaN	NaN

### 3.8.4 Equivalent circuit analysis

Equivalent circuit analysis was carried out using the instant fit tool within the ZView (Scribner Associates) suite. Individual impedance sweeps were fitted to circuit data and average results and SD are reported for comparison with other studies. The equivalent circuits analysed and comparison with other studies is described in detail in section 7.3.2.1.

### 3.8.5 *P. aeruginosa* detection algorithm

A detection algorithm was produced based upon the observation in human sputum samples that a peak in the normalised resistance data appears at a higher frequency when *P. aeruginosa* is present than when absent. The detection score is designed to provide an indication of the likelihood of infection with *P. aeruginosa*, with a positive value indicative of the presence of *P. aeruginosa* and a negative value indicative of a *P. aeruginosa* negative sample. This was applied retrospectively to the data from human sputum samples. The score was calculated by dividing the normalised resistance magnitude at 1000 Hz by the normalised resistance magnitude at 100 Hz. The logarithm to the base 10 of this value was then taken, as follows:

$$Detection\ Score = \log_{10} \left\{ \frac{Rn_{1000}}{Rn_{100}} \right\} \quad [3-9]$$

Where  $Rn_{1000}$  is the normalised resistance at 1000 Hz and  $Rn_{100}$  is the normalised resistance at 100 Hz.

### 3.9 Measurements with clinical sputum samples

A series of measurements were carried out with human sputum samples in order to determine if it is possible to detect the presence of *P. aeruginosa* in the context of infections. These experiments formed the conclusion of the study carried out here. In order to accommodate the different properties of human sputum contrasted to ASM and address fundamental differences in the experiments contrasted to the earlier work, much of this part of the study related to experimental development.

#### 3.9.1 *In vitro* measurement of *P. aeruginosa* in sputasol

Sputasol is a mucolytic agent containing Dithiotheritol (DTT) and is used clinically to help breakdown sputum for microbiological analysis. DTT is an electroactive compound, therefore the impact it had upon the impedance was assessed using an overnight culture of *P. aeruginosa* grown in ASM. 1 ml aliquots of sterile ASM media were placed into a 24 well plate and inoculated with an overnight culture of *P. aeruginosa* optically adjusted to a concentration of  $2.5 \times 10^8$  CFU/ml (see section 3.5.5.1). These were incubated microaerophilically using a campygen pack (CM0025, Oxoid) for 48 hours. Following the incubation, impedance measurements were carried out using four conditioned electrodes using the settings described in section 3.5.2. Measurements were made firstly in sterile ASM, then in the inoculated ASM (after incubation) and finally in ASM after the addition of 50% v/v sputasol. The media was then incubated for a further 60 minutes at room temperature, before a final impedance measurement was taken in order to determine whether the sputasol had a longer term effect upon the impedance measurement.

#### 3.9.2 Ethical consent

Ethical consent was gained from the Greater Glasgow NHS trust biorepository for the use of clinical sputum samples to assess the performance of the electrode (application number 139, Appendix A). Approval was also gained from the University Ethics Committee for the handling of sputum samples at the University of Strathclyde.

### **3.9.3 Measurement of sputum samples one and two**

Sputasol was used to perform a baseline measurement and break down the first two sputum samples tested. Sputasol was prepared following the manufacturer's instructions (see section 3.2.2.15). The design one electrode assembly (described in section 3.3.3) was used for this experiment. After conditioning (described in section 3.4.3), electrode chambers were sterilised in 70% v/v ethanol and then a blanking measurement was carried out using sputasol and the impedance settings described in section 3.5.2. Following this, the electrode chambers were rinsed with dH<sub>2</sub>O and the human sputum samples were placed into the electrode chamber, and the impedance measurement taken. A further impedance measurement was then taken after dilution of the sample in 50% v/v sputasol using the sample electrodes. All measurements were carried out in a class II biological safety cabinet. The methods described in this section are best understood when read in conjunction with results chapter 6.

### **3.9.4 Measurement of remaining sputum samples**

Following ambiguous results when sputasol was used with human samples, 0.9 % v/v NaCl was used to perform baseline blanking measurement prior to measurements in human sputum samples for the rest of the samples tested. Electrodes were prepared as described in section 3.3.4. Where described in the results, electrodes were conditioned (see section 3.4.3) and then a blanking measurement was taken in 0.9% w/v NaCl immediately prior to measurements in human sputum samples (see section 3.5.2). For the blanking measurements, the electrodes were applied to a 5 ml aliquot of saline in a 30 ml universal container. Measurements with the human sputum samples were carried out by applying the electrode directly to the sputum sample in the pot used for collection. The electrode assembly was held in position during the impedance measurements using a test tube clamp. All measurements were carried out in a class II biological safety cabinet.

### **3.9.5 Electrode chamber modifications for use with human sputum**

The following sections describe the changes made for the design two and three electrodes, which were used for measurement in human sputum samples. Electrode design one was the same as that used in the *in vitro* experiments (see section 3.3.3). The modifications were made to the assembly in order to allow the developed electrode to easily be applied to the human sputum samples.

### **3.9.5.1 Assembly design two**

Electrodes were cut out and a length of wire was attached to each electrode connector. A reliable conductive path to these was achieved cementing the connection in place with carbon ink (Electrodag PF407A, Acheson) and curing in the oven at 120°C for 30 mins. Following this, polyethylene was fixed over the top of the connectors and over the top of the track leading up to the working electrode. The electrode was then integrated into the lid of a 15 ml centrifuge tube (430790, Corning). To achieve this, two parallel slots were cut in the lid of the tube, approximately 12 mm apart and just deep enough to break through to the underside of the lid. Two 2 mm holes were then cut into the side walls of the tube, approximately 15 mm from the top. The electrode assembly was then fed through the slots in the lid and the wires through the holes in the tube. The lid was screwed on to the tube to complete the assembly (a cartoon of the assembly is shown in Figure 6-6).

### **3.9.5.2 Assembly design three**

Electrodes were assembled by cutting out and attaching wires as described in section 3.9.5.1 above. In addition to the carbon ink, dielectric ink was painted over the contacts and the exposed portion of wire (D2020823D2, Gwent) and cured at 80°C for 30 minutes in a box oven. Following this, a PE substrate was fixed over the electrode contacts and track leading up to the working electrode. The assembly was then attached to the bottom of a 7 ml bijou tube using a length of the PE substrate. The assembled electrodes were each stored in a 30 ml universal container prior to use. This reduced exposure to the atmosphere and protected the assembly from mechanical damage. The end of a 15 ml centrifuge tube was pushed into the top of the bijou tube to allow the assembly to be held in a test tube clamp prior to measurement (a cartoon of the assembly is shown in Figure 6-11Figure 6-12).

### **3.9.6 Microbiological analysis of sputum samples**

After impedance measurements, microbiological analysis of sputum samples was carried out in order to determine the number of colony forming units of *P. aeruginosa* and Gram positive bacteria. Prior to impedance measurements, a small aliquot of sputum was removed and placed into a pre-weighed microcentrifuge tube. The mass of the tube was measured before and after the addition of the sputum and an equivalent quantity of sputasol was added to the sample. This was homogenised by incubating at room temperature for 20 minutes and pipetting vigorously with a 1 ml pipette. Tenfold serial dilutions were then carried out in sterile 0.9% w/v NaCl and the drop plate method (described in section 3.5.6.2) was used in

conjunction with selective media. For enumeration of *P. aeruginosa*, PAB+CN was used (see section 3.2.2.8). For enumeration of Gram positive bacteria, MSA was used (see section 3.2.2.9).

### **3.9.7 Measurement of sputum samples with final electrode assembly**

LB media was prepared as described in section 3.2.2.1. 100 ml of prepared media was then placed into three 250 ml conical flasks and autoclaved for 15 mins at 121°C. The flasks were kept sterile by placing a foam bung in the mouth of the flask prior to autoclaving. 1 ml of an overnight culture of *P. aeruginosa* PA14 grown in LB media was used to inoculate each of the three flasks, after an aliquot of sterile media had been taken. The flasks were then incubated at 37°C shaking at 250 rpm.

Three of the design three electrodes assembled as described in section 3.9.5.2 were used for the impedance measurements, one for each flask. Impedance measurements were carried out (see section 3.5.2) once every hour by aseptically removing 5 ml of media. Electrodes were held in place using a test tube stand. The initial aliquot of media taken prior to inoculation was measured at the start of the experiment, prior to any measurements carried out with inoculated media as a blanking measurement.

At the same time as the impedance measurements were carried out, a small aliquot of media was taken and used to perform hourly colony counts in accordance with the drop plate method described in section 3.5.6.2, using LB agar. In addition, a 1 ml cuvette was filled with the media at the given time point and the absorbance was measured at 600 nm using a Thermofisher 2000x spectrophotometer. The media taken between the fifth and ninth hours was also used to determine the concentration of pyocyanin by measuring the UV-visible spectrum as described in section 3.6.2.

In order to assess the effect of changes to the media or the electrodes over the course of the experiment, the impedance measurements were repeated on sterile LB media under the same conditions. Specifically, three conical flasks containing sterile LB media were incubated for 8 hours with impedance measurements taken every two hours.

## **4 ELECTRODE CHARACTERISATION, PERFORMANCE ASSESSMENT AND OPTIMISATION**

## 4.1 Introduction

Comparison of the impedance signature between an initial measurement and measurements at subsequent time point allows relative changes in the electrode-electrolyte interface to be readily identified. In a previous study, differences have been seen in the impedance of a microbial broth in which *S. aureus* has grown. Peaks observed following the impedance measurement of *S. aureus* on a screen printed carbon electrode have shown that it is possible to detect growth of the bacteria after 4-8 hours as shown in Figure 4-1 (Farrow et al. 2012).

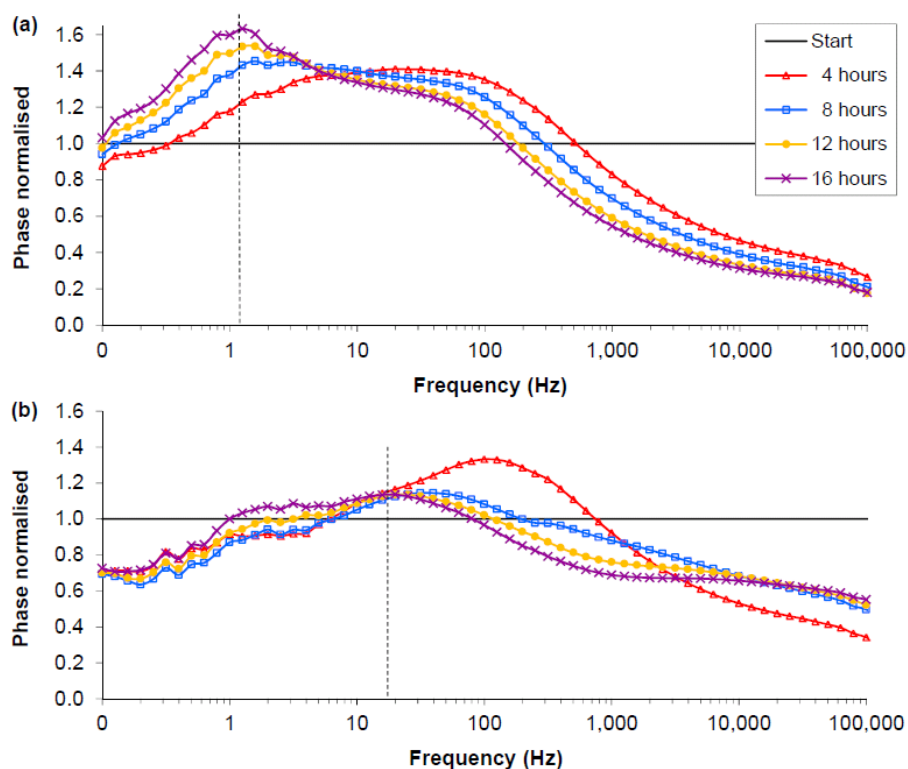


**Figure 4-1: Example of normalised peaks detected in phase data from an experiment with *S. aureus* over 16 hours using screen printed Ag-AgCl electrodes. (A) Negative control containing MHB growth media only. (B) Culture of *S. aureus* RN4220. Dotted lines show location of frequency peak. From Farrow et al. (2012).**

In this chapter, the electrode described in section 3.3.3 is studied to determine if characteristic peaks can be determined in the same manner for *P. aeruginosa*. Normalised data were compared with negative control electrode chambers to determine if changes in the normalised impedance spectrum could be related to the growth of the bacteria. The main impedance parameters explored were the phase, the real part of the measured impedance



(referred in the results as the resistance), and impedance modulus, across the frequency spectrum from 0.1 Hz to 100 kHz.

A set of initial experiments were carried out with *P. aeruginosa* over 24 and 48 hours with both screen printed carbon and screen printed carbon/silver-chloride electrodes. As discussed in this chapter, the baseline impedance of the carbon electrodes was high and the consistency between individual electrodes was sometime poor. To address these issues, an electrode conditioning procedure was developed. The impedance contribution of the working and counter electrodes were then characterised to understand the relative contribution from each electrode. Finally, measurements were carried out with the conditioned electrodes with a total of five different strains of *P. aeruginosa* to identify changes in the impedance as a result of microbial growth.

As described in section 1.4.1, microbial attachment and biofilm formation at the electrode surface could be key drivers to changes in the impedance. Therefore, crystal violet (CV) staining and epifluorescent microscopy of the electrode surface were undertaken to determine the extent of microbial attachment possible on the electrode over the same time periods used for the impedance measurement.

## 4.2 Initial impedance measurements in microbial broth

### 4.2.1 Performance of carbon electrode

The carbon electrode described in section 3.3.1 (and shown in Figure 3-5) was assessed to determine its ability to detect the presence of *P. aeruginosa* during incubation in LB media. As described in section 3.3.1, the bipolar electrode was asymmetric consisting of a central working electrode, surrounded by a counter electrode that was approximately 30 times larger in geometric area, allowing the effects at the working electrode to dominate the impedance measurement (Bockris et al. 2000). The pattern was initially printed using carbon ink on a glass microscope slide, as described in section 3.3.2. Carbon has been widely used as a choice material for biosensors because of its relative chemical inertness, large range of working potentials and low residual currents (Morrin et al. 2003). Furthermore, carbon ink is relatively low cost, contrasted to other commonly used electrode materials such as platinum, gold or Ag-AgCl.

A drawback, however, of the carbon ink was the high baseline impedance observed (e.g. impedance modulus of 4.1 M $\Omega$  with a phase angle of 79.1° at 1 Hz; and 3.7 k $\Omega$  with a phase angle of 2.9° at 100 kHz). Such high baseline impedances could mask electrochemical processes that might affect the electrode interface as a result of microbial growth, attachment and biofilm formation.

To test this directly, the impedance of the electrode in the presence of media inoculated with *P. aeruginosa* was tested over 24 hours and 48 hours at 37°C. After sterilising the electrode chambers, 2  $\mu$ l *P. aeruginosa* PAO1 RHL GFP overnight culture was used to inoculate 1 ml of LB media in a sterile electrode chamber. At the end of the experiment, the media within each electrode chamber (both PAO1 RHL GFP and negative control) was slowly aspirated and replaced with a sterile aliquot of LB, to determine if any changes had occurred to the electrode surface that could be detected using impedance.

The results indicate that the growth of *P. aeruginosa* causes a discernible change in all the measured impedance parameters. A number of peaks were observable in the phase data, normalised phase data and the resistance data (Figure 4-2 A, B and C). A drop in the

impedance was also observable in the impedance modulus data (Figure 4-2 D). The greatest changes in the phase and impedance modulus were observed at the low frequency end of the spectrum, therefore the experiment was repeated across a wider frequency spectrum from 1 MHz down to 0.1 Hz.

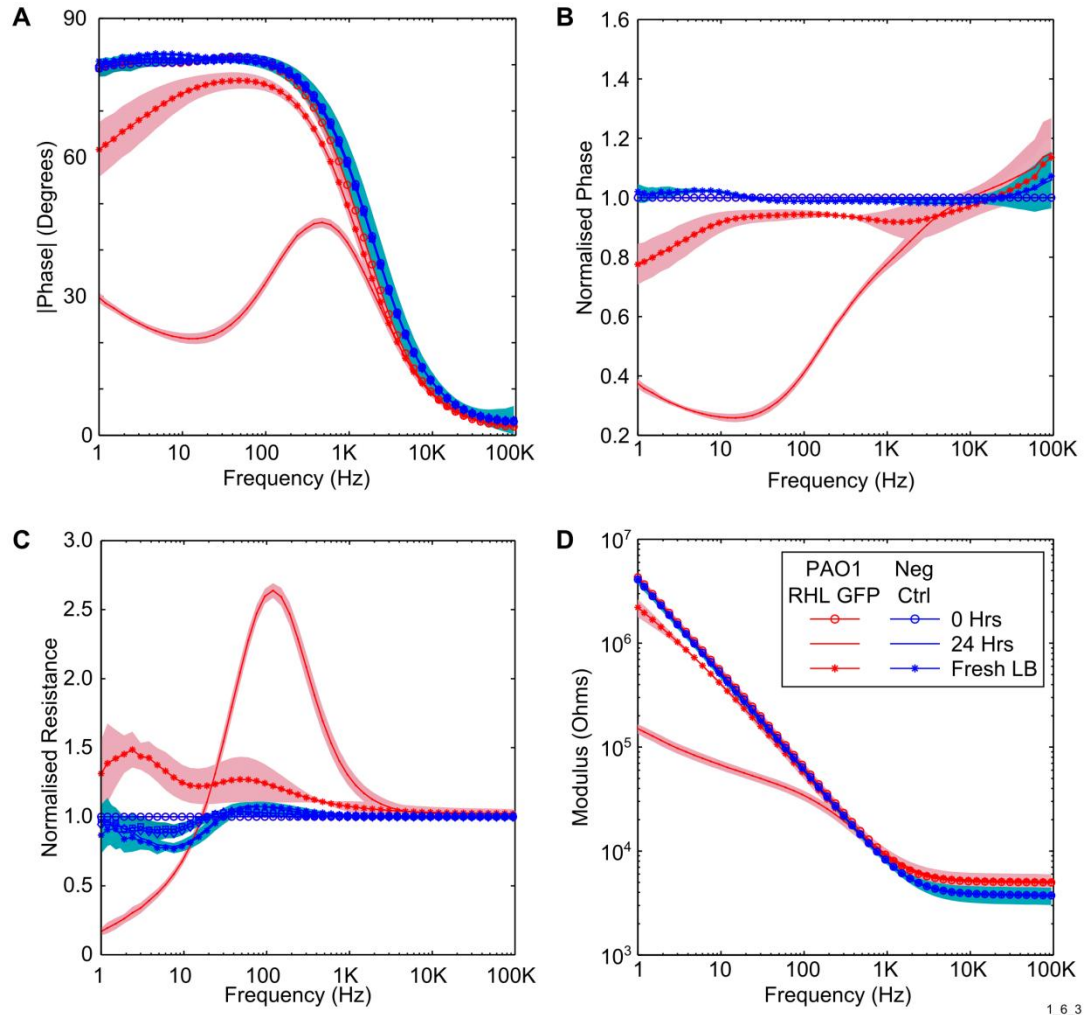


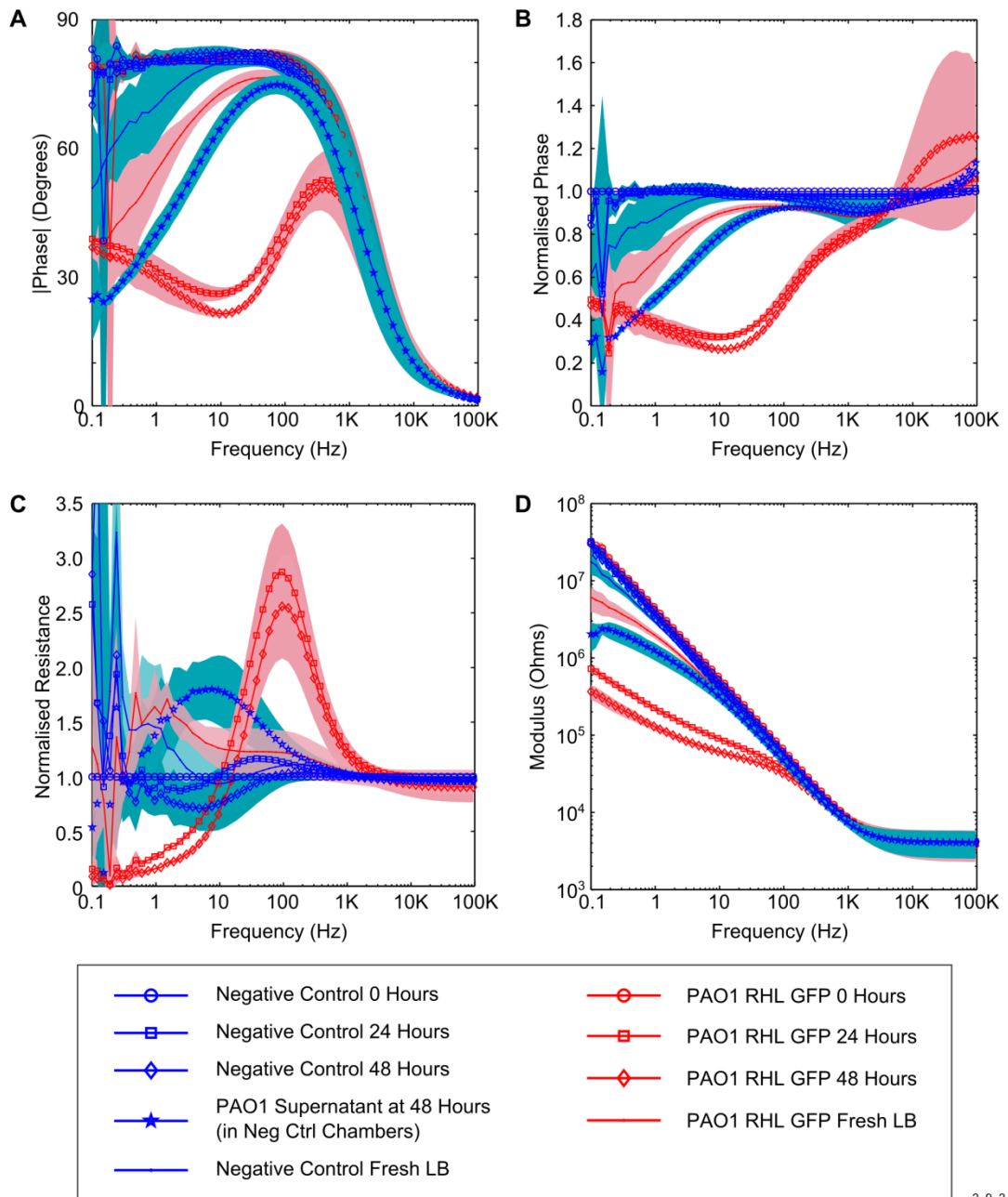
**Figure 4-2: Impedance of *P. aeruginosa* PAO1 RHL GFP grown for 24 hours in LB media. (A) A drop in the phase angle occurs below 3 kHz. (B) The changes are also reflected in the normalised phase data. (C) Peaks are clearly visible in the normalised resistance data. (D) The impedance modulus shows an overall drop in the impedance at the end of the experiment. Error bars represent  $\pm 1$  SD,  $n = 4$ .**

Following the results of the first experiment, a second experiment was carried out over a longer time period of 48 hours in order to see if further changes occurred to the impedance signature in the samples containing *P. aeruginosa*. Additionally, measurements were carried out down to a lower frequency of 0.1 Hz. At the end of the second experiment, the supernatant from the samples containing *P. aeruginosa* was removed and added to the negative control electrode chambers. This was done to try and determine if the impedance

changes were related to direct microbial interaction at the electrode surface, or a change in the properties of the media caused by *P. aeruginosa*.

Changes in the impedance signature were similar to those observed in the first experiment. The starting impedance phase angle was consistent with the first experiment and was close to 90° at lower frequencies. However, at frequencies less than 1 Hz the normalised resistance impedance signature was largely obscured by noise (Figure 4-3 A, B and C). This could have been due to instrument error. The performance specification for the SI1260 impedance analyser indicates that above an impedance of 1 MΩ, the instrument error is +/- 1% and above 10 MΩ the error is +/- 10% (Solartron 1996). It can be seen from Figure 4-3 that at 0.1 Hz, the negative control impedance modulus is greater than 10 MΩ, resulting in a noisy signal when the resistance data is normalised.

Between 24 and 48 hours, there was little change in the impedance signature across the phase, normalised phase, normalised resistance or impedance modulus. However, when the electrode chambers containing *P. aeruginosa* were aspirated and an aliquot of fresh media was added to them, a pronounced change could be observed in the normalised phase angle at low frequency, contrasted to the negative control. In the first experiment at 24 hours, the normalised phase value when fresh media was added to the electrode was 0.8 units at 1 Hz (Figure 4-2 B). In contrast, the mean normalised phase in fresh media was 25% lower in the second experiment at 48 hours (0.6 units at 1 Hz), suggesting a time dependent change in the electrode surface as a consequence of *P. aeruginosa* growth (Figure 4-3 B).



2\_9\_2

**Figure 4-3: Measurement of PAO1 RHL GFP to 0.1 Hz over 48 hours. (A) A drop is observable in the phase angle, at low frequencies. (B) Similar changes can be seen in the normalised phase angle. (C) Peaks are also observable in the normalised resistance data. (D) A drop in the impedance modulus is also seen. It is interesting to note that the impedance modulus measurement at 0.1 Hz is approximately one order of magnitude higher than it is at 1 Hz. Shading represents +/- 1SD,  $n = 4$ .**

The aspirated media from the electrode chambers containing *P. aeruginosa* was filter sterilised and added to the negative control electrodes. A change in the measured impedance parameters contrasted to the negative control was observed at frequencies below 100 Hz. Analysis of the impedance phase, modulus, normalised phase and normalised resistance at 1

Hz shows that these changes are significantly different, contrasted to the negative control (Table 4-2). Furthermore, the peak normalised resistance shifts from 100 Hz in the electrode chambers where *P. aeruginosa* is grown to 10 Hz when this media is added to the negative control electrode (Figure 4-3 C).

**Table 4-1: Comparison of impedance data at a fixed frequency of 1 Hz when negative control media is aspirated and replaced with 48 hour old *P. aeruginosa* supernatant. *P* values were calculated using two tailed Mann-Whitney test (*n* = 4 for each sample).**

Impedance Parameter	Changes in Media at 1 Hz		
	Negative Control 48 Hrs	Conditioned Media 48 Hrs	Negative Control vs. Conditioned Media Mann-Whitney Test
Phase (degrees)	81.01 (SD 2.20)	39.67 (SD 3.39)	0.0304
Modulus (ohms)	$3.58 \times 10^6$ (SD $2.97 \times 10^5$ )	$1.26 \times 10^6$ (SD $3.21 \times 10^5$ )	0.0304
Normalised Phase	1.09 (SD 0.02)	0.49 (SD 0.04)	0.0304
Normalised Resistance	0.79 (SD 0.14)	1.38 (SD 0.36)	0.0304

As noted in the first experiment, peaks were identified in the phase and normalised resistance data. The peak detection algorithm described in section 3.8.3 was used to determine the location of the peaks in the normalised resistance data and normalised phase data from the two experiments described (Table 4-2). Peaks were only included between 1 Hz and 10 kHz, and a peak was only considered to exist when it appeared in the same location in all four samples (i.e. peak frequency within a factor of ten of each other). From Table 4-2, it can be seen that, for the phase angle, peaks were consistently detected in the samples containing *P. aeruginosa*. Where peaks were also detected in the negative control data, they were significantly different from the *P. aeruginosa* samples, with the exception of the measurements taken at the start of the experiment. In contrast, fewer peaks were consistently detected in the normalised resistance data, with no peaks being detected when the fresh media was measured.

**Table 4-2: Application of the peak detection algorithm to identify peaks in the impedance phase and normalised resistance data from the first two experiments. Peaks were identified between 1 Hz and 10 kHz. Only peaks identified in the same region across all four samples were averaged and included in the table below. n.t. = not tested; n.d. = not detected in every replicate. The two-tailed Mann-Whitney test was used by pooling individual data points from both experiments for each timepoint.**

Time point (Hours)	Peaks identified in first experiment				Peaks identified in second experiment				Pooled Mann-Whitney test results	
	Specimen (n = 4)		Neg Ctrl (n = 4)		Specimen (n = 4)		Neg Ctrl (n = 4)			
	Freq	Amp	Freq	Amp	Freq	Amp	Freq	Amp	Freq	Amp
<b>Phase angle peaks</b>										
<b>0</b>	38.73	81.43	43.75	81.73	38.65	82.38	32.80	82.40	0.9164	0.7527
<b>24</b>	460.50	45.90	6.33	82.25	404.75	52.85	n.d.		-	-
<b>48</b>	n.t.		n.t.		428.00	50.98	n.d.		-	-
<b>Fresh media</b>	46.53	76.65	5.96	82.43	47.00	76.55	28.13	80.68	0.0101	0.0009
<b>Supernatant</b>	n.t.		n.t.		78.33	74.93	-		-	-
<b>Normalised resistance peaks</b>										
<b>24</b>	119.50	2.55	85.63	1.08	94.85	2.79	51.18	1.17	0.0101	0.0009
<b>48</b>	n.t.		n.t.		106.50	2.48	n.d.		-	-
<b>Fresh media</b>	n.d.		n.d.		n.d.		n.d.		-	-
<b>Supernatant</b>	n.t.		n.t.		6.63	1.86	-		-	-

In summary, the initial experimental results with *P. aeruginosa* indicate that the growth of the bacteria in the electrode chambers causes a change to the impedance, contrasted to the negative control. Peaks that appear to be characteristic of the growth of *P. aeruginosa* were observed in the phase data and the normalised resistance data. Changes to the impedance contrasted to the negative control were seen when the electrode chambers containing *P. aeruginosa* were aspirated and fresh media was added. A change was also seen in the impedance when the supernatant was placed into the negative control electrode chambers and measured. These results suggest that *P. aeruginosa* interacts with the electrode through two different mechanisms. Firstly, by modifying the electrode surface during growth, and secondly by changing the properties of the media, thus causing changes to the impedance

contrasted to the negative control. Next, the performance of the Ag-AgCl/carbon electrodes was tested to determine if similar changes to the impedance spectrum occurred in the presence of *P. aeruginosa*.

#### 4.2.2 Performance of Ag-AgCl/carbon electrode

As mentioned in section 4.2.1 above, the impedance modulus of the carbon electrodes at the start of the experiment at 0.1 Hz was in the order of 10 M $\Omega$ . This high starting impedance could mask other characteristic changes relating to the growth of *P. aeruginosa* that have not been observed. To address this, an Ag-AgCl counter electrode was used, as described in section 3.3.1. The aim was to produce a hybrid electrode that overall had a lower starting impedance whilst still using carbon for the working electrode. Although the Ag-AgCl counter electrode was now much smaller than the carbon counter electrode, the non-polarisable properties of Ag-AgCl were expected to result in lower impedance across the frequency spectrum. Therefore, it was anticipated that with a much larger carbon working electrode the total impedance of the electrode would be lower. Both the carbon and Ag-AgCl/carbon electrodes are characterised in detail later in this chapter (section 4.3.3).

As expected, the Ag-AgCl /carbon electrodes had lower baseline impedance than any of the carbon electrodes. The impedance modulus was typically in the range of 288 k $\Omega$  at 0.1 Hz, contrasted to 10 M $\Omega$  at 0.1 Hz observed with the carbon electrodes. Furthermore, the phase angle peaks at 60° at 20 Hz before dropping at lower frequencies, in contrast to the carbon electrodes where the phase angle plateaus at approximately 80° across the entire low frequency spectrum (Figure 4-4A). To assess the Ag-AgCl/carbon electrode in the context of changes resulting from the growth of *P. aeruginosa*, the experiment described in section 4.2.1 was repeated.

As before, electrode chambers were sterilised and filled with 1 ml of LB media and half were then inoculated with 2  $\mu$ l of *P. aeruginosa* PAO1 RHL GFP from an overnight broth before incubating again for 48 hours. In the earlier experiments, it was noted that evaporation of the media from the electrode chamber occurred, particularly over longer periods of time. This was addressed by incubating the chambers in a high humidity environment, produced using two plastic trays placed together with inside surfaces facing. Some damp paper towels were placed in this enclosure to create a humid environment for the incubation of the

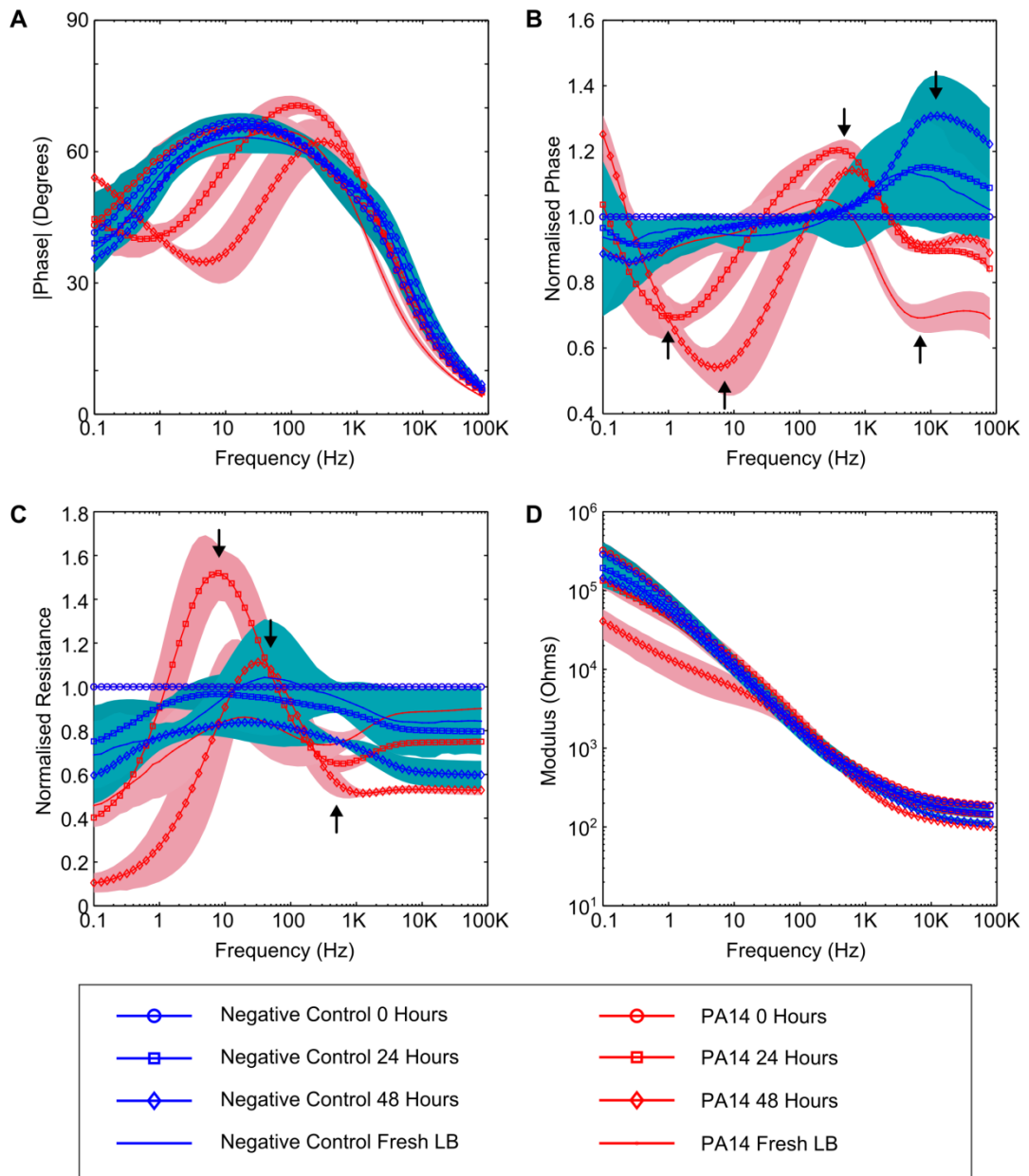


electrodes. The media within the electrode chambers was kept sterile by the custom made covers, shown in Figure 3-7.

Changes in the impedance signatures as a result of the growth of *P. aeruginosa* PAO1 RHL GFP can be seen after 24 hours (Figure 4-4). The impedance signature is similar, but not the same as that observed with the carbon electrodes. The phase angle shows a slight trough at 1 Hz (24 hours), which shifts to a higher frequency of 100 Hz at 48 hours (Figure 4-4 A).

Similar troughs to those observed with the carbon electrodes can also be seen in the normalised phase data (Figure 4-4 B). In addition, the normalised phase data shows changes at higher frequencies not visible in the impedance measurements from the carbon electrodes. A peak in the normalised phase is also observable in the higher frequency data that wasn't present in the impedance measurements from the carbon experiments. Similar peaks can be observed in the negative control data, although these occur at a higher frequency (Figure 4-4 B). These peaks indicate that, with the Ag-AgCl/carbon electrode changes also occur to the negative control throughout the experiment. It is interesting to note that such changes were not observed in the impedance signatures from the carbon electrodes, and could suggest that there is a conditioning effect not seen previously due to the high impedance of the carbon. Overall, therefore, it is also conceivable that the differences between the Ag-AgCl electrodes and carbon electrodes in the *P. aeruginosa* positive chambers occur because they are not masked by the high starting impedance observed with the carbon electrodes.

The normalised resistance data shows peaks similar to those observed in the carbon electrodes (Figure 4-4 C). As with the normalised phase, changes could be seen at higher frequencies that weren't visible in the carbon electrodes. In contrast, the impedance modulus only showed a change at 48 hours (Figure 4-4 D). These changes were much less pronounced than those found with the carbon electrodes, where an impedance change could be seen after 24 hours (Figure 4-4 D). This suggests that, although the carbon electrode has a high starting impedance, the normalised resistance parameter is more sensitive to changes caused by *P. aeruginosa* than the Ag-AgCl/carbon electrode. A complete discussion of the advantages and disadvantages of the carbon electrode and Ag-AgCl/carbon electrode is provided in section 7.3.1.4.



3\_17\_2

**Figure 4-4: Growth of *P. aeruginosa* PA14 in LB media using the Ag-AgCl/carbon electrode. (A) The phase angle exhibits a broad peak from the outset, but there is still little change in the negative control throughout the experiment. (B) Peaks and troughs are clearly visible in the inoculated chambers, note also that a high frequency peak can be seen in the negative control. (C) The normalised resistance data shows similar peaks to the carbon electrode. However, there is also some fluctuation in the negative control. (D) A drop of one order of magnitude is observable in the impedance modulus. Shading represents  $\pm 1$  SD,  $n = 4$ .**

### 4.3 Electrode optimisation

The initial results described above indicate that the carbon electrodes had a high starting impedance modulus, particularly at low frequencies, whereas the Ag-AgCl/Carbon electrode had a lower total impedance. In this section, the optimisation of the electrode design is described, followed by characterisation of the electrodes. Firstly, the selection of AC perturbation voltage of 200 mV<sub>rms</sub> is reviewed and verified as appropriate, and then the results of electrode conditioning are presented. The section then ends with the characterisation of the impedance of both the carbon and Ag-AgCl/carbon electrodes.

During the early experiments, it was noted that, over long time periods (in excess of 48 hours), the electrode could detach from the glass microscope substrate. This was further confirmed by the fact that the ink could easily be scraped from the surface of the slides. In order to ensure that this did not cause a problem in future experiments, the printing substrate was changed to acetate. The adherence to this substrate was greater, and it was not possible to scrape either the carbon or Ag-AgCl inks off.

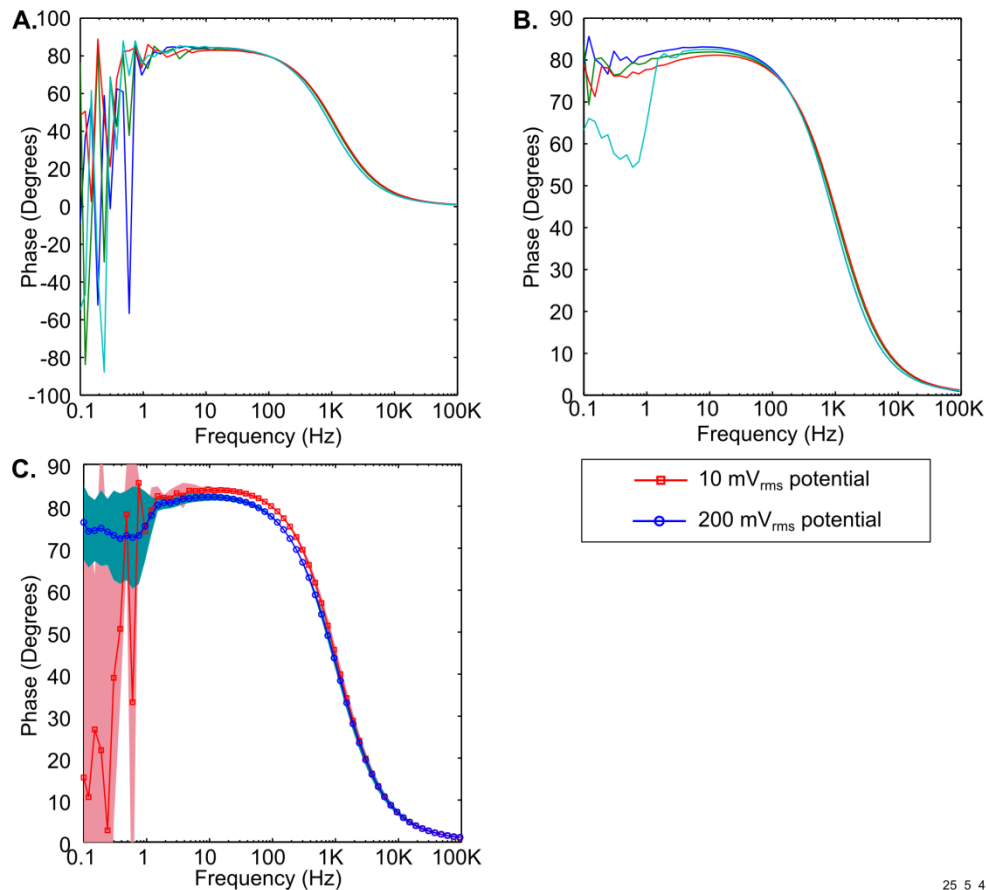
#### 4.3.1 Selection of measurement voltage

A perturbation voltage of 200 mV<sub>rms</sub> was selected for the impedance experiments described above. Previous investigations within the research group have used this measurement potential and have demonstrated that it is possible to characterise both mammalian and bacterial cells (Farrow 2010; Shedden 2008). 200 mV<sub>rms</sub> is sufficiently small to avoid large electrochemical or electric field effects on cells, yet large enough to take measurements out of the noise range at low frequencies in particular. In contrast, several studies that have used impedance spectroscopy to detect the presence of bacteria employed perturbation voltages less than 50 mV (Bayouhdh et al. 2008; Ben-Yoav et al. 2011; Marsili et al. 2008a; Muñoz-Berbel et al. 2006, 2008a; Paredes et al. 2012; Pires et al. 2013; Kim et al. 2012; Yang et al. 2003, 2004). One reason commonly cited for the selection of a low perturbation voltage is that it ensures the response of the system is approximately linear (Macdonald 1987).

Given the high impedance of the carbon electrode at low frequencies in particular, described in section 4.2.1, it was anticipated that a lower perturbation voltage would be below the detection limit of the SI1260 instrument. However, a brief experiment was carried out in order to explore the effect that a lower perturbation voltage would have upon the impedance with the carbon electrodes developed as part of this study. A measurement was carried out

in 0.9% w/v NaCl at 10 mV<sub>rms</sub> and 200 mV<sub>rms</sub> potentials (see section 3.4.2 for more detail on the method).

When measurements were carried out at 10 mV<sub>rms</sub>, it was found that below 1 Hz, the impedance signature was dominated by noise (Figure 4-5 A). The noise observed when a perturbation voltage of 10 mV<sub>rms</sub> was used is a direct result of very low fields around the electrode and across the double layer, resulting in poor diffusion gradients and drift profiles, and therefore a less stable electron exchange. In contrast, a consistent impedance signature resulted from the measurement at 200 mV<sub>rms</sub>, except at low frequencies, where a consistent signature existed for three out of four electrodes (Figure 4-5 B and C). One of the electrodes showed a sudden drop in the phase angle below 1 Hz. The reasons for this are discussed in more detail in the next section on electrode conditioning. Briefly, it is thought to result from residual solvents left behind during the curing stage of the ink and the silicone adhesive used to mount the chamber above the electrode.



25\_5\_4

**Figure 4-5: Assessment of different measurement potentials. (A) when a measurement potential of 10 mV<sub>rms</sub> was used, the impedance signature became noisy at less than 1 Hz for all four electrodes measured. (B) a more consistent impedance signature could be seen at low frequencies when 200 mV<sub>rms</sub> was used. (C) Mean results from 10 mV<sub>rms</sub> and 200 mV<sub>rms</sub> superimposed. Shading represents +/- 1SD, *n* = 4.**

The other increase in noise with a perturbation voltage of 10 mV<sub>rms</sub> is likely to result from the measured current being below the accurate detection limit of the impedance analyser (Table 4-3). With a perturbation voltage of 10 mV<sub>rms</sub> or 200 mV<sub>rms</sub>, the resulting current for the impedance magnitude at 1 Hz is beyond the detection limit of the SI1260 instrument. The 10 mV<sub>rms</sub> perturbation voltage is over two orders of magnitude beyond the detection limit, whereas at 200 mV<sub>rms</sub> the perturbation voltage is half an order of magnitude beyond the detection limit. This partly explains why the results at 200 mV<sub>rms</sub> are less noisy than at 10 mV<sub>rms</sub>. Therefore, as expected, 200 mV<sub>rms</sub> measurement potential was more consistent and was used for all the future impedance measurements. However, even at 200 mV<sub>rms</sub>, the detection limit is above that of the impedance analyser. Therefore, to lower the impedance

further and increase the consistency of the electrodes, electrode conditioning was carried out, as described in the following section.

**Table 4-3: Analysis of current at the two perturbation voltages measured. The error is calculated from the Solartron specification chart, showing the measurement performance of the instrument (Solartron 1996).**

Perturbation Voltage ( $V_{rms}$ )	Impedance modulus at 0.1 Hz ( $\Omega$ )	Corresponding current (Amps)	Corresponding current ranges across SI1260 performance specification for a perturbation voltage of 1V (Amps)			
			0.1%/0.1° (10 < Z < 100K)	0.2%/2° (100K < Z < 1M)	1%/1° (1M < Z < 10M)	10%/10° (10M < Z < 100M)
$1 \times 10^{-2}$	$1 \times 10^7$	$1 \times 10^{-9}$	$0.1 - 1 \times 10^{-5}$	$1 \times 10^{-5} - 1 \times 10^{-6}$	$1 \times 10^{-6} - 1 \times 10^{-7}$	$> 1 \times 10^{-7}$
$2 \times 10^{-1}$		$2 \times 10^{-8}$				

### 4.3.2 Electrode conditioning

In some circumstances when performing baseline measurements with the carbon electrodes, a different impedance signature was observed, characterised by large, low frequency drop in the phase angle, and a corresponding drop in the impedance magnitude. This was observed a below approximately 100 Hz (Figure 4-6 and Figure 4-5) and, although it did not affect all electrodes, it was present in a large enough sample of the electrodes to require a resolution. Possible reasons for this impedance signature include the effect of residual solvents present in the electrode ink prior to curing and solvent left behind from the silicone adhesive used to mount the chambers.

To address these problems and to lower the baseline starting impedance so that the measurements would be within the detectable range for the Solartron SI1260 impedance analyser, the conditioning approach described in section 3.4.3 was employed. This would allow electrodes to be consistently produced with the same baseline impedance. It involved biasing the DC potential of the electrode at 2 V for three minutes and then at -2 V for a further three minutes, using a platinum electrode as the counter electrode in a 0.9% w/v NaCl electrolyte. Following this, three impedance sweeps were carried out across the electrode, to ensure the signature was consistent.

It was found that in most cases the conditioning process removed the problems associated with the large low frequency drop and resulted in a consistent signature across all electrodes (Figure 4-6). Occasionally, electrodes were still found with the peculiar signature after

conditioning. A quality control step was therefore included during the baseline measurements whereby these electrodes were discarded and replaced with ones that had a consistent baseline. In addition to addressing the problems associated with electrode consistency, conditioning resulted in a drop in the impedance magnitude of 44% at 0.1 Hz and a drop in the phase angle at lower frequencies (Figure 4-7). Thus, the conditioning process was expected to improve the sensitivity of the carbon electrodes by slightly reducing the masking of changes to the impedance caused by the high baseline impedance, and bringing the measurements into the detectable range for the SI1260 instrument.

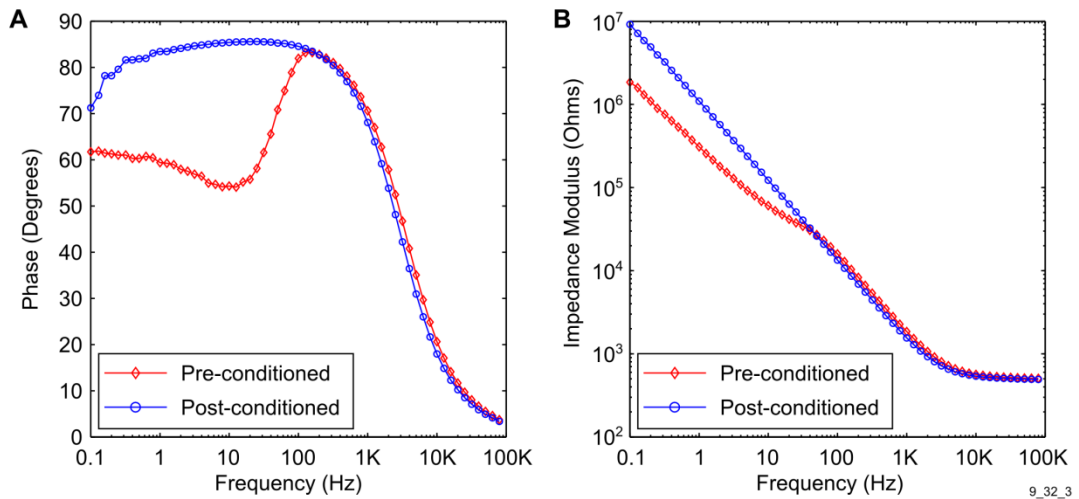


**Figure 4-6: Example of an initial impedance signature inconsistent with other electrodes showing (A) phase plot and (B) impedance modulus before and after conditioning. Application of the conditioning procedure ensured that all electrodes had the same baseline impedance signature.**

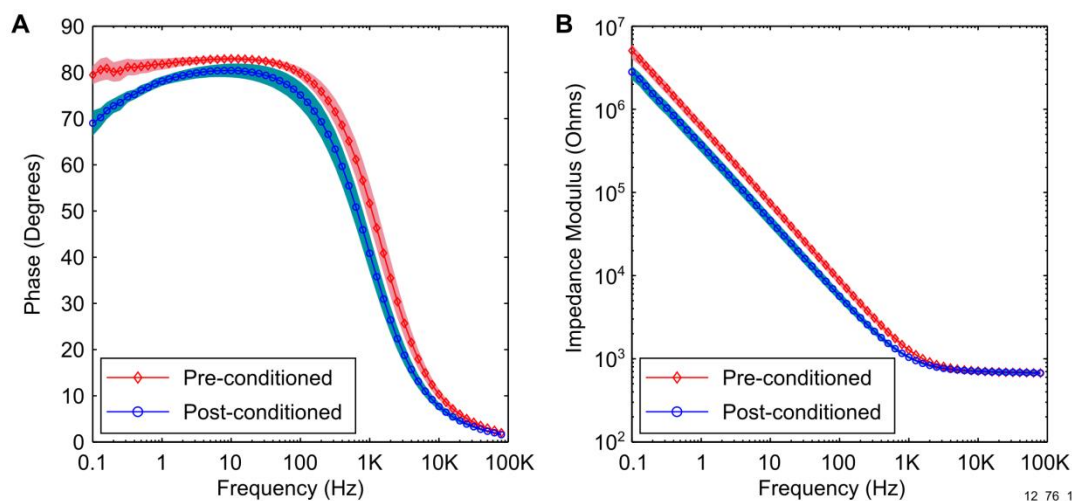


**Figure 4-7: Impedance changes as a result of electrode conditioning. (A) A slight drop in the phase angle can be seen at lower frequencies. (B) From 1 kHz, there is a slight but consistent drop in the modulus of the impedance. Shading represents +/- 1 SD,  $n = 4$ .**

### 4.3.3 Electrode characterisation

To understand how the electrode area (print area and surface roughness) and material affects the overall impedance, an experiment was carried out in order to determine the relative contribution made by each of the electrodes to the total impedance measured in a 0.9% v/v NaCl solution. A complete description of the procedure is described in section 3.4.1. Briefly, this involved the use of two platinum electrodes constructed from 2 mm diameter platinum rods. An impedance measurement was carried out with both the platinum electrodes to ascertain their value, followed by an impedance measurement with a single platinum electrode in conjunction with either the working electrode or counter electrode. Subtracting the low value platinum impedance from the measurement gives the impedance of either the working electrode or counter electrode, depending which was used in the experiment. Finally, a measurement was carried out with the platinum pair again to verify there was no change in the platinum impedance during the experiment. The contribution to the impedance made by one of the platinum electrodes used with the carbon electrode and the electrolyte resistance was then mathematically removed from the results in order to determine the contribution to the impedance from a single electrode (i.e. the carbon working electrode, carbon counter electrode and the Ag-AgCl counter electrode).

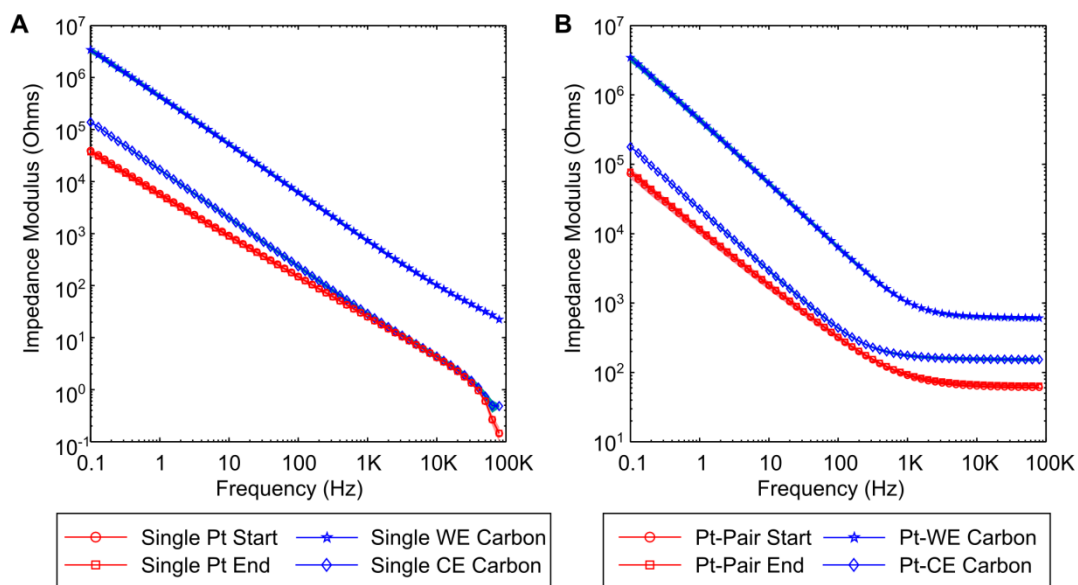
The results are shown in Figure 4-8 and indicate that the large area carbon counter electrode (geometric area of 92.65 mm<sup>2</sup>) makes a contribution to the impedance that is similar to the impedance of a single platinum electrode (geometric area of 50 mm<sup>2</sup>), except at low



frequencies where an increase in impedance magnitude of the carbon electrode can be seen (98.2 k $\Omega$  at 0.1 Hz). Platinum is well known for its low impedance (Geddes 1972); however it is interesting to note that the impedance of the carbon electrode is comparable at high frequencies. This could be explained by the relative surface areas of the two electrodes. The carbon electrode is over 45% larger in surface area compared to the platinum electrode and therefore the platinum would have lower impedance on a comparable geometric area.

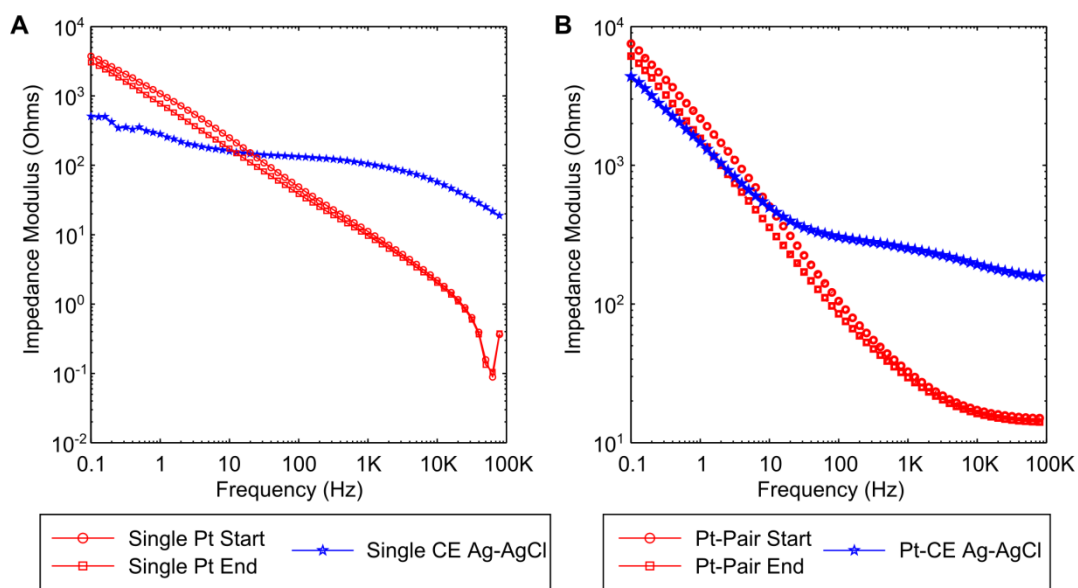
The large area counter electrode has an impedance 1.5 orders of magnitude lower when compared to the impedance signature of the working electrode across the whole frequency spectrum (Figure 4-8A). This indicates that during the experiment, changes to the impedance of the small area working electrode (geometric area of 3.14 mm<sup>2</sup>) will dominate the observed signature, indicating that the growth of the bacteria on this electrode might be observable as an impedance change, through one or more of the mechanisms described in the literature review (section 1.4).

In contrast to the carbon electrode, the impedance of the Ag-AgCl counter electrode at 0.1 Hz is 507  $\Omega$  and therefore much lower than either the carbon working electrode (3.39 M $\Omega$  at 0.1 Hz) or the carbon counter electrode (139 k $\Omega$  at 0.1 Hz; Figure 4-8). The impedance signature of the Ag-AgCl electrode across the impedance spectrum differs from that of the platinum electrode and carbon electrodes, due to the different properties of the electrode materials. Unlike the carbon and platinum materials, the Ag-AgCl undergoes an electrochemical reaction with chloride ions within the electrolyte enabling the oxidation or reduction of the silver and therefore facilitating the flow of a faradic current (Grimnes and Martinsen 2008). This results in the Ag-AgCl being relatively non-polarisable and explains lower impedance seen in section 4.2.2.



10\_76\_4

**Figure 4-8: Baseline performance of the carbon electrodes. (A) The impedance modulus of each electrode when the contribution of a single platinum electrode and electrolyte resistance has been removed. (B) The “raw” impedance modulus for comparison. Shading represent +/- 1 SD,  $n = 4$ .**



11\_16\_3

**Figure 4-9: Impedance modulus of the Ag-AgCl counter electrode. Ag-AgCl is non-polarisable, therefore faradic current flows more readily than in the platinum or carbon electrodes. (A) The impedance modulus of the counter electrode when the contribution of a single platinum electrode and the electrolyte resistance has been removed. (B) The “raw” impedance modulus for comparison.**

## 4.4 Impedance measurements with conditioned electrodes

### 4.4.1 *In situ* growth of *P. aeruginosa* PA14 with conditioned electrodes

Once the conditioning approach described above had been implemented and the electrodes had been characterised, a set of experiments was carried out in LB media to determine whether *P. aeruginosa* influenced the impedance of the electrodes during growth in a consistent manner that might allow the signature to be used as a detection mechanism. This also provided the opportunity to test the standard laboratory strain of *P. aeruginosa*, PA14 (see Table 3-1).

The results show that with the conditioned carbon electrodes, *P. aeruginosa* causes a characteristic change in the impedance (Figure 4-10). Interestingly, the changes to the impedance over the frequency range differ to those found with the *P. aeruginosa* strain, PAO1 RHL GFP. The change in phase angle during growth is not as pronounced (Figure 4-10 A). However, a clear trough was evident in the normalised phase at high frequency (Figure 4-10 B).

In general, the normalised resistance signature was similar to that previously seen for the *P. aeruginosa* strain PAO1 RHL GFP with a large peak visible between approximately 10 Hz and 100 Hz (Figure 4-10 C). The peak detection algorithm described in section 3.8.3 was applied to the data from the experiment described here (Table 4-4). This shows that a peak can be consistently identified in all five of the chambers where PA14 was growing between 24 and 72 hours. In contrast, slight peaks were detected in some of the negative control channels, but not consistently and generally at a higher frequency. When the electrode chambers were aspirated and replaced with fresh media, a single peak was present in the normalised resistance at 500 Hz in the chambers where *P. aeruginosa* PA14 was grown. Interestingly, the double peaks observed in the normalised resistance data at approximately 1 Hz and 10 Hz in the first two experiments did not develop as in Figure 4-2 C and Figure 4-3 C. The reasons for changes in the normalised impedance spectrum are fully explored in discussion section 7.3.4. At this stage, it is useful to note that the differences could be related to: phenotype differences between the two strains; an effect caused by the electrode conditioning; or the fact that the experiment with *P. aeruginosa* PA14 was performed over a longer time period than the first two experiments discussed at the start of the chapter (i.e. 72 hours). The modulus of impedance shows that there is a drop of approximately one order of magnitude in the impedance (Figure 4-10 D), which is less than the drop in impedance

observed in the second experiment with PAO1 RHL GFP, where a change in the impedance magnitude of two orders was seen at 0.1 Hz (see Figure 4-2 and Figure 4-3).

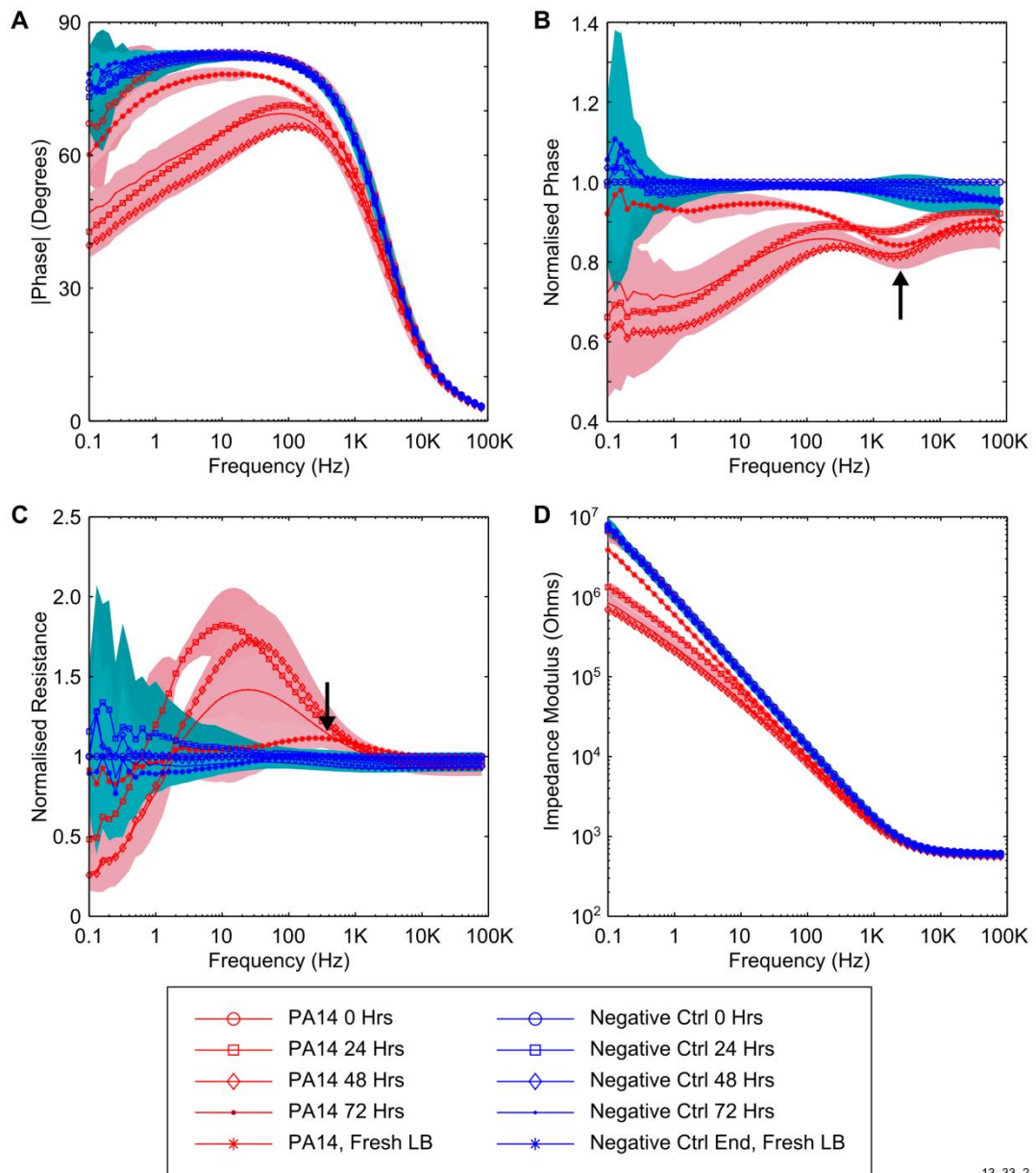


**Figure 4-10: *P. aeruginosa* PA14 in LB media over 72 hours with carbon electrodes after conditioning. (A) a change is clearly observable in the phase impedance signature after 24 hours. (B) the normalised phase shows a trough at 4 kHz (black arrow) which is not visible in the un-normalised phase data and persists in an aliquot of fresh, sterile, LB. (C) a series of peaks are clearly observable in the normalised resistance data, a small peak at different frequency can also be observed when the media is replaced with an aliquot of fresh, sterile LB at the end of the experiment (black arrow). (D) The normalised reactance indicates that significant changes occur in the measured reactance data throughout the experiment. Shading represents +/- 1 SD,  $n = 3$ .**

**Table 4-4: Identification of peaks in the normalised resistance data. The table shows that peaks were only detectable in all replicates when PA14 was grown in LB media. Sporadic peaks were also visible in the negative control data, but never in all replicates at the same timepoint. PA14  $n = 5$ ; Neg ctrl  $n = 4$ . Ten measurements were performed per frequency decade, therefore the range of the peaks detected at high frequencies is greater than the range at lower frequencies.**

Strain	Time point	No. of channels peaks observed in	Peak freq – Hz (SD)	Peak amp (SD)
PA14	24	all	10.43 (4.95)	1.83 (0.22)
	48	all	28.32 (7.62)	1.72 (0.23)
	72	all	21.50 (11.85)	1.44 (0.21)
	Fresh LB	4	419.50 (157.11)	1.09 (0.02)
	Fresh LB	3	2.60 (3.22)	1.27 (0.13)
Neg Ctrl	24	1	0.25	1.65
	24	2	63.12 (62.87)	1.00 (0.04)
	48	1	0.25	1.42
	48	2	94.55 (44.48)	0.97 (0.04)
	72	3	76.50 (25.08)	0.96 (0.04)
	Fresh LB	1	0.32	1.02
	Fresh LB	4	251.75 (104.65)	1.01 (0.04)

#### 4.4.2 Growth of *P. aeruginosa* clinical isolates with carbon electrodes

The strains of *P. aeruginosa* that initially colonise the CF airway have been found to differ from isolates taken at later timepoints (Harrison 2007; Hassett et al. 2009). As described fully in the literature review (section 1.2.3), early isolates are typically non-mucoid, virulent and planktonic, whereas late isolates have a host adapted phenotype, often characterised by the production of large quantities of polysaccharides, giving rise to the so called mucoid strain. Late isolates readily form biofilms that are almost impossible to eradicate. An experiment was carried out with the conditioned carbon electrodes in order to explore the differences in the impedance between two pairs of clinical isolates (defined in Table 3-1). As shown in Figure 4-11, each of the pairs are isogenic and were isolated from the same patient at different timepoints, one strain being an early isolate and the other a host adapted isolate (Stewart et al. 2013). The isolates were originally collected by the CF Microbiology Consortium at Edinburgh University.

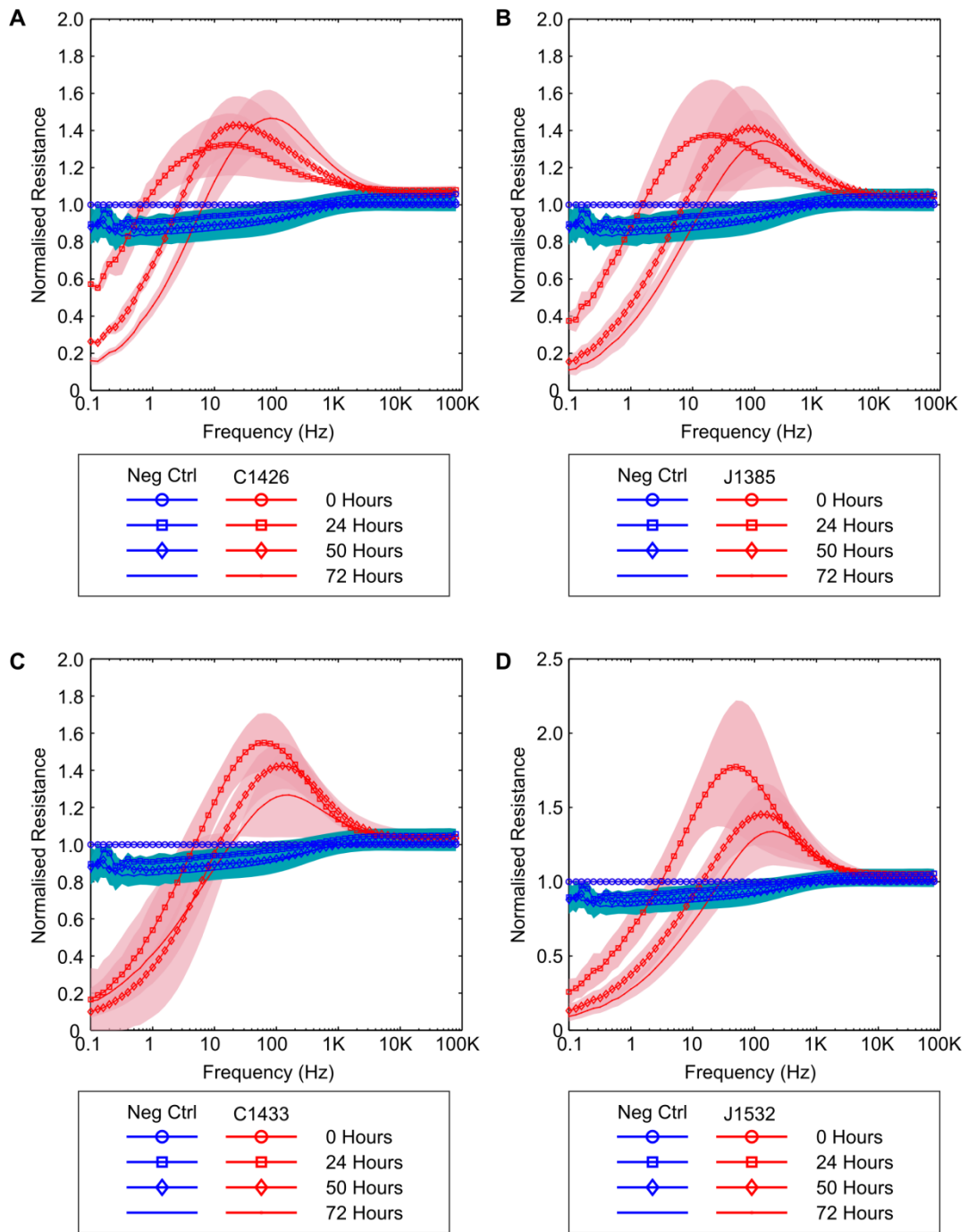


**Figure 4-11: Clinical *P. aeruginosa* isolates from CF patients.**

An impedance experiment was carried out with the J1385/J1532 and C1426/C1433 strains in order to identify any differences in the impedance signature between early *P. aeruginosa* isolates from the CF airway and late isolates. Sterile media was added to the electrode chambers and inoculated with one of the four *P. aeruginosa* strains outlined in Figure 4-11 or left sterile as a negative control.

The electrode chambers were then incubated at 37°C for 72 hours. After 24 hours, all strains of *P. aeruginosa* produced a change in the impedance resistance, reactance and associated normalised impedance parameters, when contrasted against the negative controls. Characteristic impedance peaks occurred in the normalised resistance data for both the early and late isolates after 24 hours (Figure 4-12). These peaks were analysed using the peak detection algorithm described in section 3.8.3.

The results show that the normalised resistance peak occurs at similar frequencies and amplitudes for each of the four strains tested, comparable to those observed in previous experiments in this chapter (Table 4-6). Additionally, a significant drop in the impedance modulus at low frequency could be seen with each of the strains contrasted against the negative control, indicating a decrease in the impedance of the electrode as a consequence of the growth of *P. aeruginosa* ( $P < 0.05$ , measured with the two tailed Mann-Whitney test, Table 4-5).



14\_78\_3

**Figure 4-12: Normalised resistance peaks in *P. aeruginosa* early isolates (C1426 and J1385) and late isolates (C1433 and J1532). (A) and (B) show the normalised resistance for the early isolates. (C) and (D) show the normalised resistance for the late isolates (C1433 and J1532). Shading represents  $\pm 1$  SD,  $n = 4$ .**

**Table 4-5: Mean change in impedance modulus at low frequency for each strain. Values marked \* are significantly different to the negative control (P<0.05, measured with the two tailed Mann-Whitney test).**

Strain	Impedance Modulus at 0.1 Hz ( $\Omega$ )			
	0 Hours	24 Hours	50 Hours	72 Hours
Neg Ctrl	$4.51 \times 10^6$	$4.39 \times 10^6$	$4.20 \times 10^6$	$4.09 \times 10^6$
C1426	$5.27 \times 10^6$	$1.13 \times 10^6$ *	$5.28 \times 10^5$ *	$3.04 \times 10^5$ *
C1433	$4.73 \times 10^6$	$3.03 \times 10^5$ *	$2.00 \times 10^5$ *	$2.47 \times 10^5$ *
J1385	$4.98 \times 10^6$	$7.33 \times 10^5$ *	$2.95 \times 10^5$ *	$2.10 \times 10^5$ *
J1532	$5.58 \times 10^6$	$5.35 \times 10^5$ *	$2.87 \times 10^5$ *	$2.14 \times 10^5$ *



**Table 4-6: Application of the peak detection algorithm to normalised resistance data for clinical isolates.  $n = 4$  for all samples. Ten measurements were performed per frequency decade, therefore the range of the peaks detected at high frequencies is greater than the range at lower frequencies. For comparison, the peak detection results from the experiment with *P. aeruginosa* PA14 (Table 4-4) are included below with a grey background.**

Strain	Time	Number of channels peak detected in	Peak freq – Hz (SD)	Peak amplitude (SD)
J1385	24	all	31.84 (32.2)	1.38 (0.29)
	24	1	316	1.08
	50	all	106.63 (43.40)	1.42 (0.22)
	72	all	177.25 (64.02)	1.35 (0.16)
J1532	24	all	41.95 (15.71)	1.78 (0.44)
	50	all	139.50 (48.73)	1.45 (0.21)
	72	all	243.75 (114.93)	1.34 (0.23)
C1426	24	all	20.00 (8.31)	1.33 (0.16)
	50	all	23.83 (2.55)	1.43 (0.16)
	72	all	86.98 (27.13)	1.47 (0.15)
C1433	24	all	65.43 (18.73)	1.55 (0.15)
	50	all	122.35 (32.36)	1.43 (0.12)
	72	3	152.67 (50.21)	1.36 (0.13)
	72	1	6.31	1.16
	72	1	1260	1.01
PA14 (from Table 4-4)	24	all	10.43 (4.95)	1.83 (0.22)
	48	all	28.32 (7.62)	1.72 (0.23)
	72	all	21.50 (11.85)	1.44 (0.21)
Neg ctrl	24	2	7125.00 (1152.58)	1.07 (0.04)
	24	1	10	0.92
	50	2	4085 (1308.15)	1.01 (0.07)
	72	2	3245 (1039.45)	1.01 (0.07)
Neg ctrl (from Table 4-4)	24	1	0.25	1.65
	24	2	63.12 (62.87)	1.00 (0.04)
	48	1	0.25	1.42
	48	2	94.55 (44.48)	0.97 (0.04)
	72	3	76.50 (25.08)	0.96 (0.04)

The normalised phase impedance signatures from each of the isogenic pairs were compared to determine if it is possible to detect any difference between the early *P. aeruginosa* isolates

and the host adapted, late isolates. Comparison of the mean data shows that a clear peak and trough pair are present in the phase data from both the early isolates (J1385 and C1426) around 100 Hz, with a trough present between 1 kHz and 2.5 kHz (Figure 4-13 A). In contrast, only one peak is observable at 100 Hz for one of the host adapted strains, seen in the data for C1433 at 72 hours (Figure 4-13 B). It is interesting that the differences between the early and late isolates are consistent across the two pairs. The changes therefore appear to be related to the phenotype.

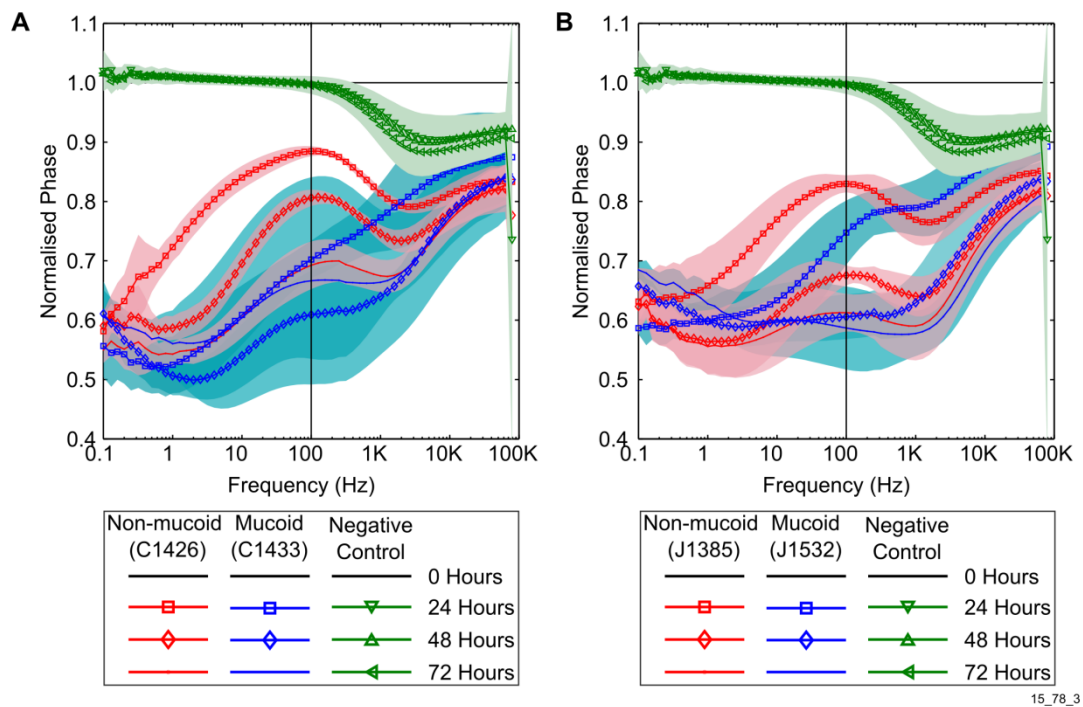


**Figure 4-13: Comparison of the mean normalised phase angle between non-mucoid and mucoid pairs. (A) Isogenic strains, C1426 and C1433, showing a clear peak at approximately 100 Hz and a trough between 1 kHz and 2.5 kHz. (B) Similar behaviour for the other two isogenic strains, J1385 and J1532, peak and trough pairs. Shading represents +/- 1 SD,  $n = 4$ .**

Further analysis of the normalised phase angle against time at 100 Hz shows that a clear difference is observable between the early and late isolates. Specifically, it can be seen that the early isolates have a higher normalised phase angle than the late isolates (Figure 4-14). Furthermore, when the data from the two early isolates and the data from the two late isolates are pooled, there is a significant difference in the normalised phase angle at 24 hours and 48 hours ( $P = 0.0014$  and  $P = 0.0039$  respectively, two tailed Mann-Whitney test), but not at the final timepoint of 72 hours. It is possible that the production of virulence factors by the early isolates (J1385 and C1426) causes a change in the impedance which differs to

that observed in the late strain. Furthermore, the large quantity of polysaccharides produced by the late isolates could have an impact upon the impedance in a more direct manner by encouraging microbial attachment to the electrode surface.

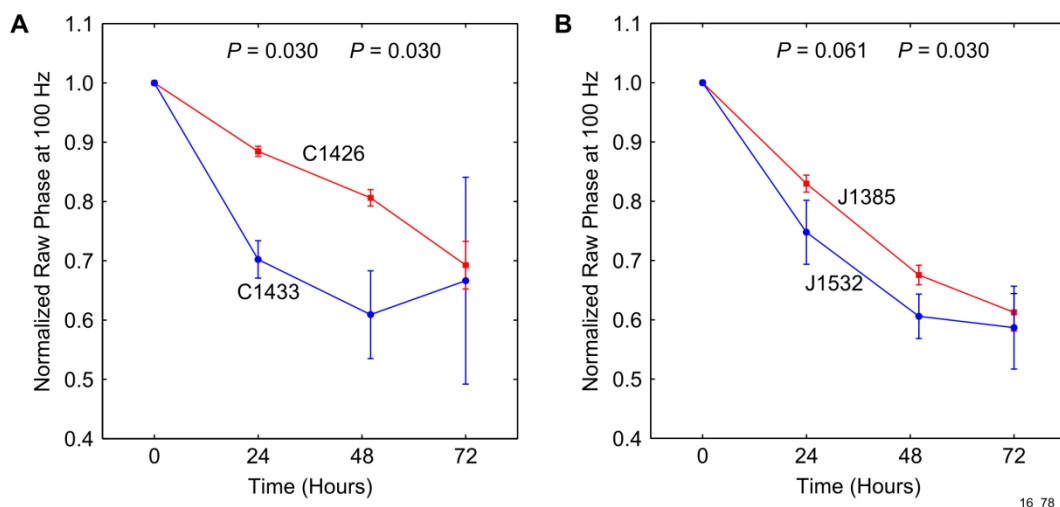


**Figure 4-14: Time plot of the normalised phase angle at 100 Hz for each of the non-mucoid/mucoid pairs. (A) Non mucoid strain C1426 contrasted to mucoid strain C1433. (B) Non mucoid strain C1385 contrasted to mucoid strain C1532. *P* values calculated using two tailed Mann-Whitney test. Error bars represent +/- 1SD, *n* = 4.**

Colony counting was carried out at the end of the experiment in order to determine the *P. aeruginosa* cell density within each of the electrode chambers. A similar concentration of cells was found across all strains, in the region of  $10^9$  CFU/ml (Table 4-7), with the exception of J1532, where a slightly lower cell concentration was counted. This could have been related to the viscous media present at the end of the experiment which made it difficult to homogenize the sample and perform serial dilutions equally, thus leading to an underestimate of the number of viable cells present. The number of cells counted at the end of the experiment are typical for *P. aeruginosa* under these growth conditions (i.e. stationary phase in rich media).

**Table 4-7: Final *P. aeruginosa* cell densities determined through drop plate colony counting,  $n = 4$  for each different strain.**

Strain	<i>P. aeruginosa</i> cell density at 72 Hours (CFU/ml)		
	Mean	Min	Max
<b>C1426</b>	$5.96 \times 10^9$	$5.20 \times 10^8$	$1.65 \times 10^{10}$
<b>C1433</b>	$6.80 \times 10^9$	$1.68 \times 10^9$	$2.00 \times 10^{10}$
<b>J1385</b>	$5.28 \times 10^9$	$1.55 \times 10^8$	$1.27 \times 10^{10}$
<b>J1532</b>	$4.60 \times 10^8$	$7.00 \times 10^6$	$1.63 \times 10^9$

#### 4.5 Microbial attachment on the electrode surface

To investigate the foundation for changes in the impedance further, the capacity for *P. aeruginosa* to attach to the carbon electrode surface and form microcolonies and biofilms was explored. In LB media, this was achieved using a simple CV assay to quantify the formation of microcolonies on the carbon electrode surface. Epifluorescent microscopy was also used to visualise the extent of microbial attachment on the electrode surface.

##### 4.5.1 Crystal violet staining

The crystal violet assay described in section 3.7.1.1 was used to quantify the amount of microbial attachment on the carbon electrode surface at the end of an experiment. Briefly, this is achieved by aspirating the electrode chamber, adding a 0.1% v/v CV in dH<sub>2</sub>O solution and incubating for 10 minutes at room temperature. Following this, the CV was removed, the chamber was rinsed with dH<sub>2</sub>O and the stain was solubilised using 95% v/v ethanol for a further 10 mins. CV stains the peptidoglycan cell wall of the bacteria, which is then removed by the ethanol. By measuring the absorbance of the solubilised dye from the attached bacteria only, it was possible to assess the degree of microbial attachment to the electrode surface (Merritt et al. 2005).

CV staining was carried with *P. aeruginosa* PA14 (Figure 4-15). The results show that there is an increase in the amount of staining throughout the experiment, but at 24 hours, there is no significant difference between the inoculated chambers and the negative control (Table 4-8). These results suggest that the formation of microcolonies occurs on the carbon electrode surface, but only significantly over periods greater than 24 hours.

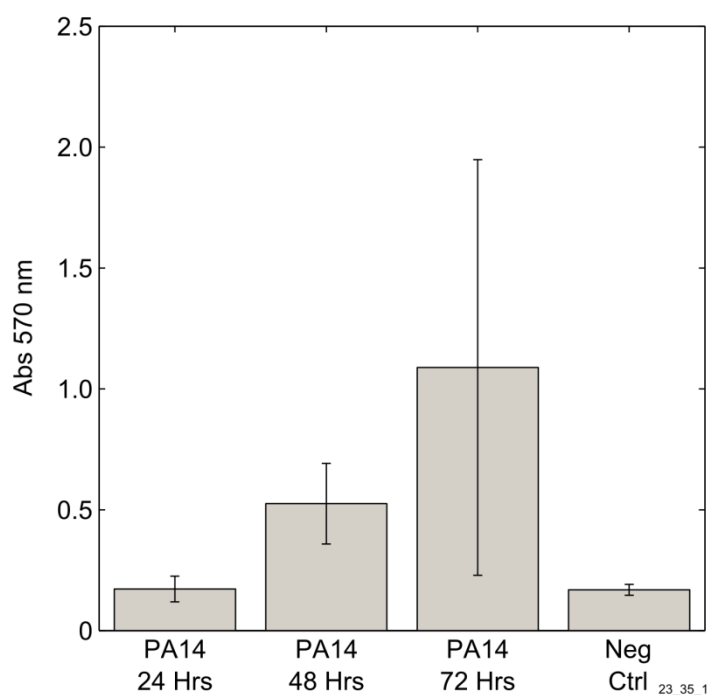


**Figure 4-15: CV assay for PA14, showing the change in concentration of CV as a function of growth. There is no significant change in the concentration of CV after 24 hours of incubation. Error bars represent +/- 1 SD. PA14 24 Hr  $n = 5$ ; PA14 48 Hr  $n = 5$ ; PA14 72 Hr  $n = 6$ ; Neg Ctrl  $n = 6$ .**

**Table 4-8: Test of difference between CV staining of samples and negative control. Calculated using two tailed Mann-Whitney test.**

	PA14 24 Hrs ( $n = 5$ )	PA14 48 Hrs ( $n = 5$ )	PA14 72 Hrs ( $n = 6$ )
Negative Ctrl ( $n = 6$ )	0.8551	0.0081	0.0051

A potential weakness of the approach used for CV staining is that the silicone adhesive used to mount the electrode chambers could have provided a substrate that the *P. aeruginosa* cells readily colonised. If this was the case, microbial attachment to the silicone, not the electrode surface could dominate the CV staining results. To address this problem, a refined version of the CV staining assay was employed to measure the quantity of stain from experiments with the *P. aeruginosa* strains J1385 and J1532 (Table 3-1). In this experiment, electrode coupons made out of carbon ink with a 10 mm diameter were cut out of acetate and incubated in 1 ml of LB media inoculated with J1385 or J1532 in a 24 well plate.

Staining on the inoculated electrodes was significantly different between the negative control and also the positive controls. There is a steady increase in the concentration of CV over time from the non-muroid strain contrasted to the muroid strain. A possible reason for this could be the sloughing off of large quantities of biofilm material at later timepoints with the muroid strain which is known to produce a larger quantity of extracellular matrix. Furthermore, given that these differences are seen on the acetate positive control in addition to the carbon coupons, this suggests that they are not related to the electrode material.

In summary the CV staining assay suggest that there may be some microbial attachment on the surface of the electrodes. The extent to which microbial attachment occurred was explored further through epifluorescent microscopy.

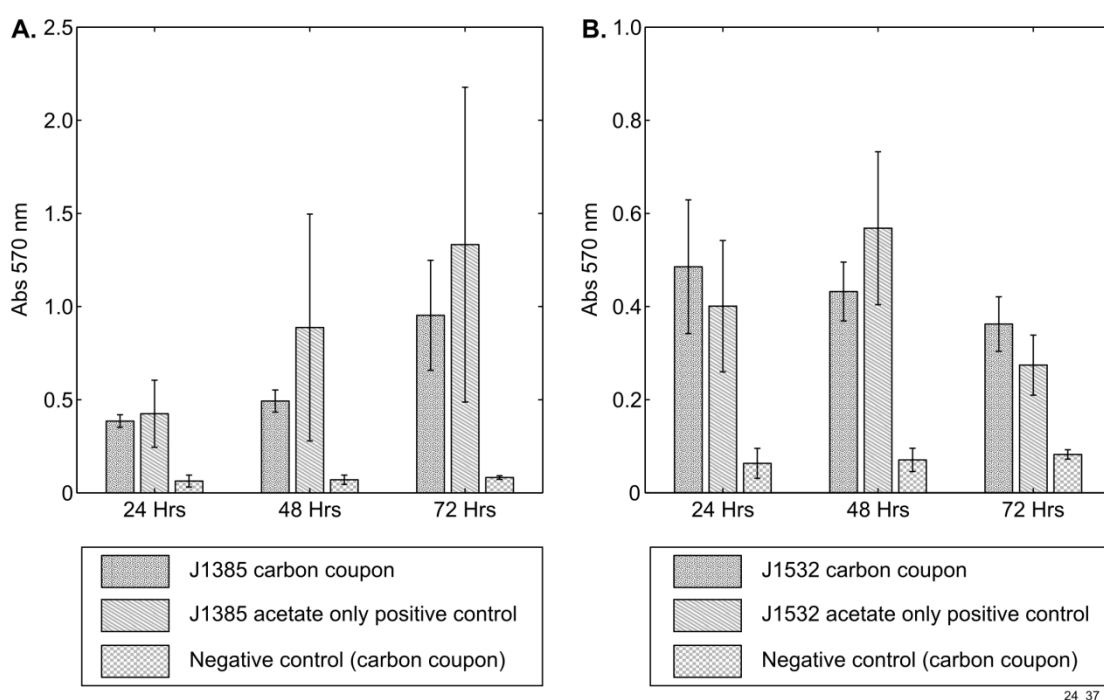


**Figure 4-16: CV staining assay using electrode coupons incubated in a 24 well plate. (A) non-muroid (J1385) strain of *P. aeruginosa*. (B) muroid (J1532) strain of *P. aeruginosa*. Error bars +/- 1 SD. J1385  $n = 4$  (except at 48 hrs where  $n = 2$ ), J1385 positive control  $n = 4$ , J1532  $n = 4$ , J1532 positive control  $n = 4$ , negative control  $n = 4$ .**

**Table 4-9: CV staining assay for microbial attachment using electrode coupons incubated in a 24 well plate showing significance of changes between negative control and *P. aeruginosa* clinical isolates. Calculated using two tailed Mann-Whitney test,  $n = 4$  for all samples except J1385 at 48 hours where  $n = 2$ .**

J1385 vs. Negative Control			
	J1385 24 Hrs	J1385 48 Hrs	J1385 72 Hrs
Neg Ctrl	0.0304	0.1052	0.0304
J1532 vs. Negative Control			
	J1532 24 Hrs	J1532 48 Hrs	J1532 72 Hrs
Neg Ctrl	0.0304	0.0304	0.0304

#### **4.5.2 Epifluorescent microscopy of the carbon electrode surface following growth in LB media**

To explore the extent of *P. aeruginosa* attachment and biofilm formation on the carbon electrode surface, epifluorescent microscopy was carried out. As described in section 3.7.2.3, small coupons of electrode material were sterilised and incubated in LB. In experiments with CV staining it was noted that biofilm formation is always greatest at the air-liquid interface (shown in Figure 3-13). Some electrode coupons were incubated vertically in 24 well plates for 24 and 48 hours in order to allow a biofilm to form at the air liquid interface. These served as a positive control and an indicator of the extent to which *P. aeruginosa* would attach to the carbon electrode material. Following incubation, the electrode coupons were rinsed, placed onto a microscope slide and stained with 5  $\mu$ M concentration of SYTO9, sufficient to cover the surface of the electrode. SYTO9 is a membrane permeable stain with an absorbance peak around 450 nm and an excitation peak around 500 nm when bound to DNA. The electrode coupons were rinsed again prior to microscopy.

After incubation for 24 hours and staining with SYTO9, small quantities of microbial attachment were seen across the electrode coupon (Figure 4-17 A and B). Some regions of the coupon surface also had small biofilm like structures, although this was not typical across the samples (Figure 4-18). In contrast, a large quantity of biofilm formation was evident on

the electrode surface in the positive control samples at the air-liquid interface (Figure 4-17 C and D). Growth is known to be greater at the air liquid interface due to the abundance of oxygen from above and nutrients from below (Koza et al. 2009).

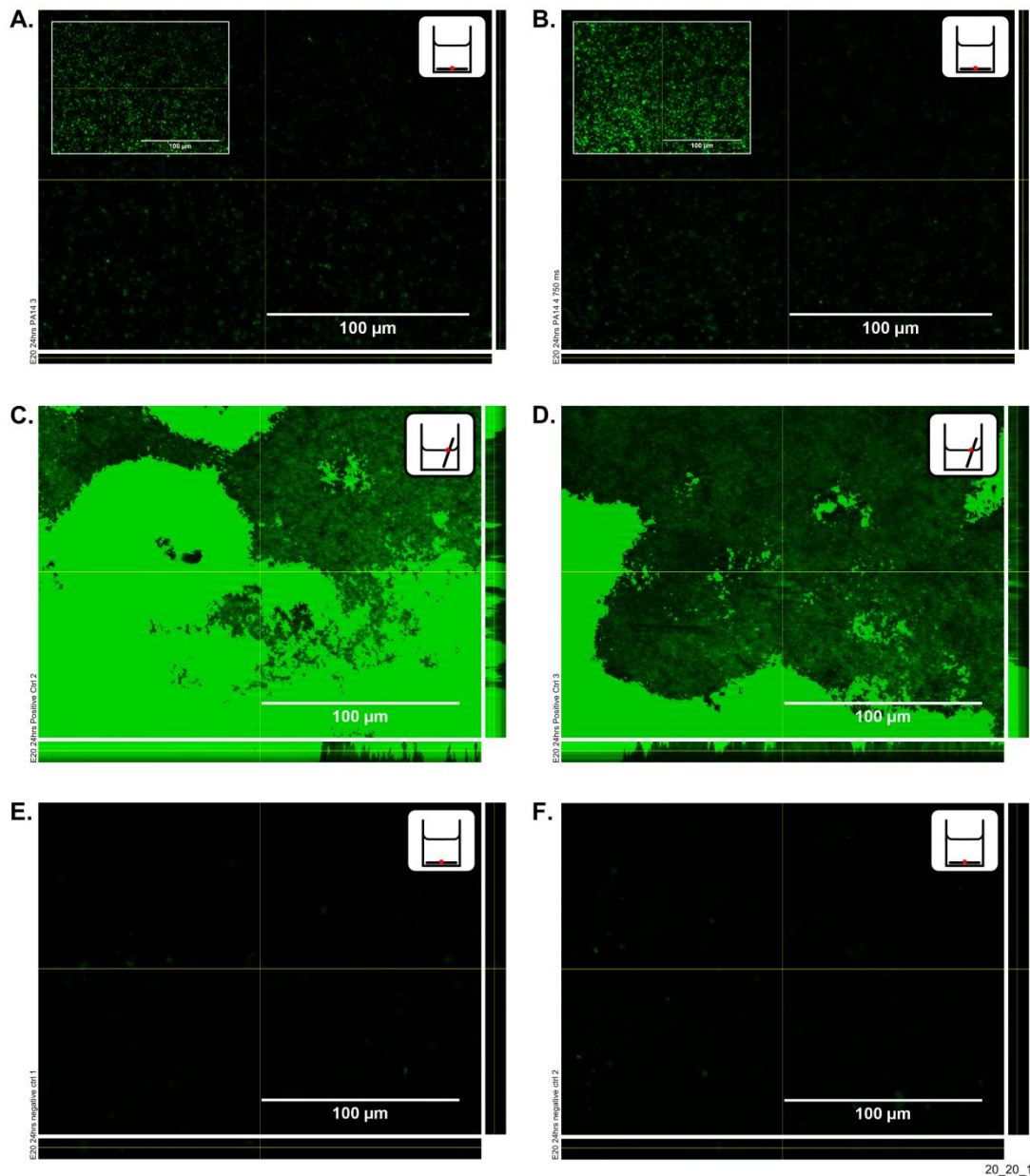
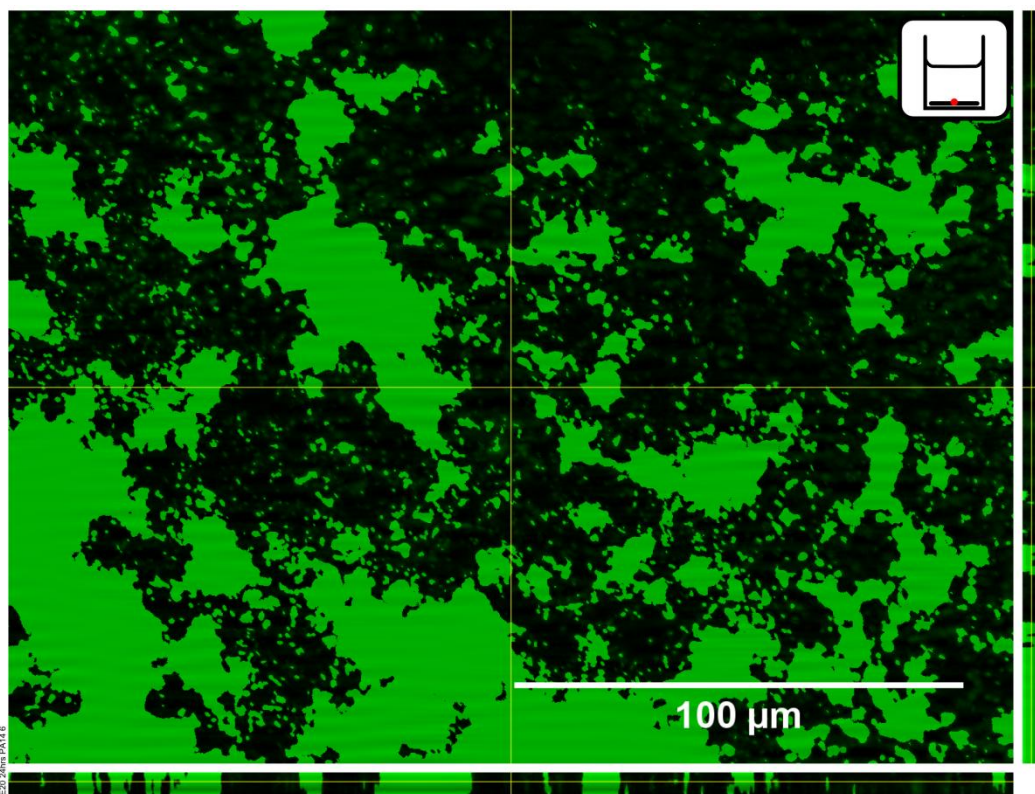


**Figure 4-17: Epifluorescent microscopy of carbon electrode coupons following 24 hour incubation with *P. aeruginosa* PA14. (A) and (B) PA14 on coupon at bottom of 24 well plate. Insets in (A) and (B) show the same images with brightness and contrast maximised. (C) and (D) positive control showing biofilm formation and growth of PA14 at air-liquid interface. (E) and (F) negative control showing that the carbon electrode surface doesn't auto fluoresce. Exposure time 750 ms for all images.**

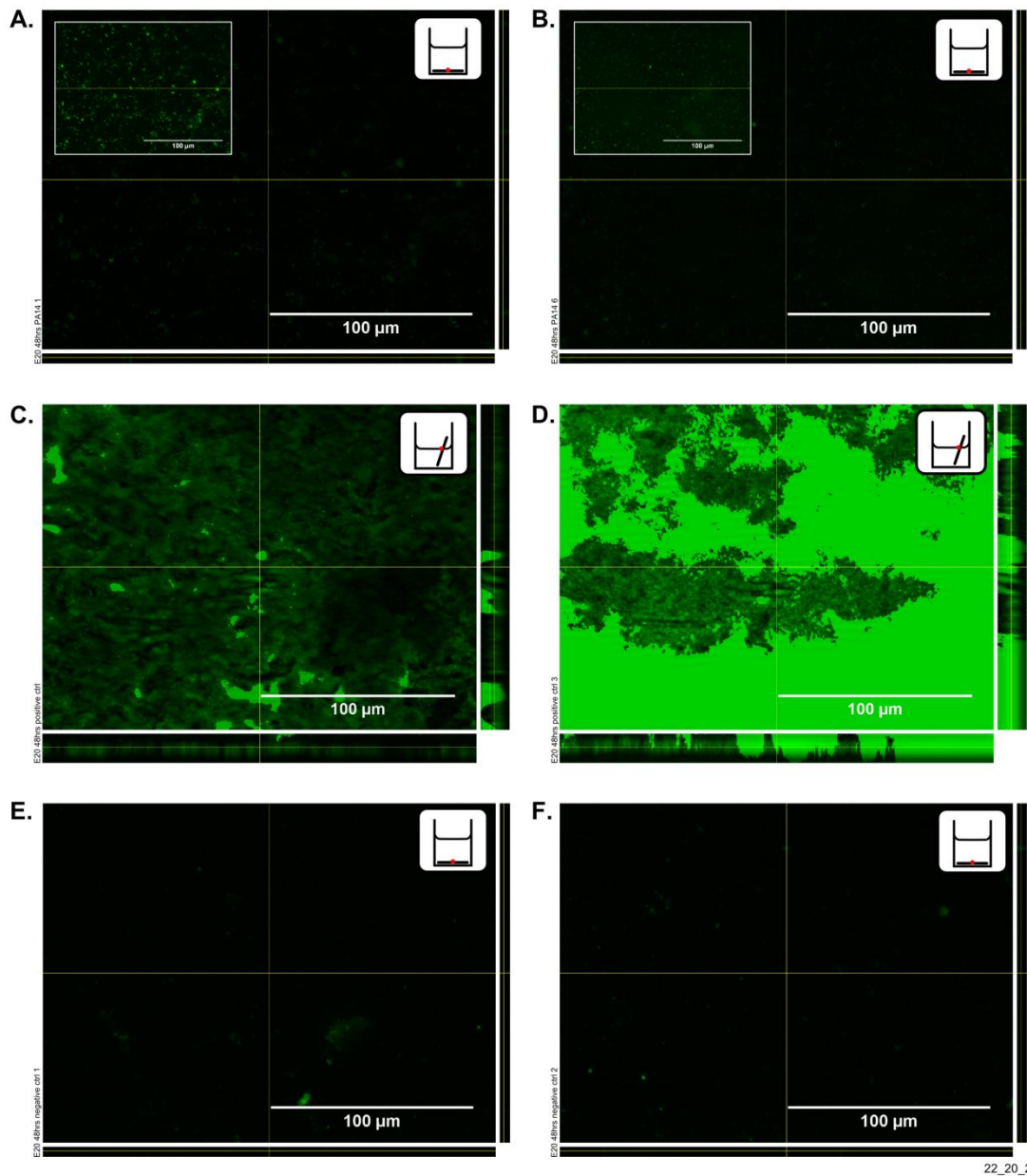




21\_20\_1

**Figure 4-18: Example of biofilm on electrode sample of *P. aeruginosa* PA14. This was not typical of most of the electrode surface, however it demonstrates that some biofilm formation does appear to occur on the electrode surface.**

Interestingly, microscopy of the electrode coupons located at the bottom of the electrode chamber at 48 hours showed less microbial attachment than that found at 24 hours (Figure 4-19 A and B). It was noticed when removing the coupons from the electrode chamber that the media was very viscous and sticky, probably as a result of the large quantity of extra polymeric substances secreted from the *P. aeruginosa* cells in stationary phase as part of the formation of biofilms. Furthermore, the incubation was carried out in conditions where the bacteria were not subjected to large shear forces. Therefore, it is possible that when removing the coupons from the wells, the viscous nature of the media resulted in the removal of biofilm from the electrode coupon and its retention in the bulk media.



22\_20\_2

**Figure 4-19: Typical finding from epifluorescent microscopy of the carbon coupons following incubation of PA14 after 48 hours. (A) and (B) *P. aeruginosa* PA14 on coupon at bottom of 24 well plate. Insets in (A) and (B) show the same image with brightness and contrast maximised. (C) and (D) positive control showing biofilm formation and growth of PA14 at air-liquid interface. (E) and (F) negative control showing that the carbon electrode surface doesn't auto fluoresce. Whilst there is some artefact present in (E), this is markedly different to the biofilm structures seen in the positive controls. Exposure time 750 ms for all images.**

The microscopy of the electrode surface demonstrates that biofilm formation is possible on the carbon electrode, suggesting that none of the substances within the electrode ink inhibit

attachment and growth of *P. aeruginosa*. It is important to note, however, that the extent of biofilm formation at the bottom of the well is more limited than at the air liquid interface. The optimum location for microbial growth in the context of these experiments is at the air liquid interface where there is an abundance of both nutrients and oxygen. This could be because most of the media within the well is used by the bacteria located at the air-liquid interface, resulting in well developed biofilm structures after 24 hours, once the media is spent.

## 4.6 Summary

In this chapter, a carbon screen printed electrode and a Ag-AgCl/carbon electrode have been tested to determine if a characteristic signature can be found when *P. aeruginosa* is incubated with the electrode. Specifically, it was hypothesised that characteristic impedance signatures may exist in the normalised impedance spectrum, produced using the approach described in section 3.8.2. The baseline impedance of the electrode was also assessed and a conditioning approach was employed to lower the impedance of the carbon electrode and improve the consistency between electrodes. In order to investigate possible causes for the change observed in the impedance, analysis of the electrode surface was carried out with *P. aeruginosa* using CV staining and epifluorescent microscopy. This was to determine if microbial attachment and biofilm formation could have an impact upon the impedance.

Initial experiments carried out with *P. aeruginosa* demonstrate a characteristic change in the normalised impedance can be seen with both the carbon and Ag-AgCl/carbon electrode developed in this study. Inconsistencies between the baseline impedance of the carbon electrodes were addressed through the use of a conditioning approach. The conditioning approach helped to address inconsistencies between carbon electrodes by removing contaminants from the electrode surface and lowering the starting impedance.

In total, impedance measurements with six different strains of *P. aeruginosa* were carried out using the carbon electrodes, and all showed that characteristic changes in the normalised impedance spectrum could be seen. The most prominent change observed was a peak in the normalised resistance data, but changes could also be seen in the normalised phase data. Furthermore, significant differences existed in the normalised phase data between early and late clinical isolates. This result is important because it suggests that the electrodes developed here can detect phenotypically different strains of *P. aeruginosa*.

The extent of microbial attachment on the carbon electrode surface revealed some interesting information about the electrode surface and biofilm formation. The investigation confirmed that under optimal conditions, biofilm formation on the carbon surface occurred at the air liquid interface. Limited biofilm formation was also seen at the bottom of the electrode chambers, possibly caused by some of the biofilm being removed during the aspiration process.

In the next chapter, the carbon electrode-electrolyte interface is explored further, under growth conditions more representative of the CF airway.

**5 MEASUREMENT IN CF SPUTUM MODEL ENVIRONMENT AND  
IMPEDANCE MEASUREMENT OF DIFFERENT MICROBIAL STRAINS**

## 5.1 Introduction

In the previous chapter, an electrode was designed, developed and tested for the detection of *P. aeruginosa* within LB media (which is a rich medium for the growth of *P. aeruginosa*). This resulted in a carbon screen printed electrode with consistent impedance signatures when used in conjunction with the conditioning procedure described in section 3.4.3. The results indicated that under simple and optimal testing conditions, the growth of *P. aeruginosa* led to a characteristic impedance signature.

In this chapter, the electrode is evaluated more comprehensively. A CF airway model is used, consisting of an artificial sputum media (ASM) in conjunction with a microaerophilic environment (Kirchner et al. 2012) to test if *P. aeruginosa* remains detectable in sub-optimal conditions. In addition, a series of studies are carried out, testing the performance of the electrode with three other microorganisms common to the CF lung. *S. aureus* and *H. influenzae* are tested in optimal growth media and in the CF airway model. Whilst less common, the yeast *C. albicans* is also a CF pathogen and was tested. This allowed the performance of the electrode in the presence of a eukaryote microorganism to be evaluated. Each of the species described here was also grown together in a co-culture with *P. aeruginosa* to determine if an impedance signature for *P. aeruginosa* remained detectable.

Later in the chapter, the underlying mechanisms for the changes in impedance caused by *P. aeruginosa* are explored. This part of the investigation was carried out in order to determine the effect that a set of exogenously produced, electroactive compounds had upon the impedance. The experiments focused upon the use of mutant strains from the *P. aeruginosa* PA14 non-redundant library (Liberati et al. 2006) and a double knockout mutant (Dietrich et al. 2006b). Finally, a small scanning electron microscopy investigation is described, that reveals topographical changes to the electrode surface as a result of the growth of *P. aeruginosa*.

## 5.2 Impedance analysis with *P. aeruginosa* incubated in ASM

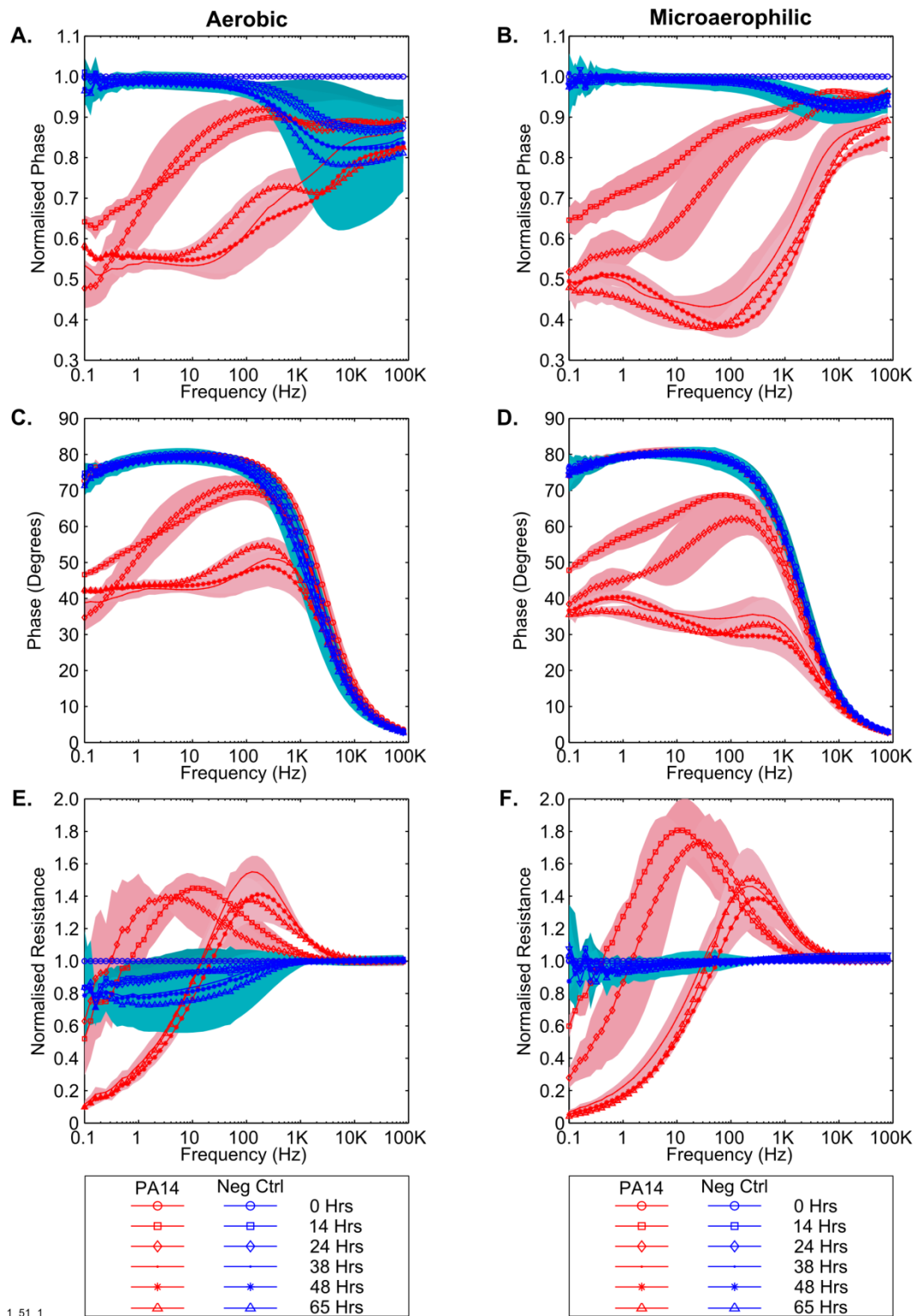
Impedance experiments were carried out in ASM with conditioned carbon electrodes (see section 3.4.3 for conditioning method) in a model CF environment (see section 3.5.5) to determine if similar impedance signatures to those described in section 4.4 could be achieved. As described in section 4.4, when *P. aeruginosa* was grown in LB media over 24-72 hours, characteristic peaks were observed in the phase angle, normalised phase angle and normalised resistance, which were not present in the negative control data. If peaks like this are also visible in an environment more representative of the CF airway, they could be used to identify the presence of *P. aeruginosa* in human sputum samples.

Many of the microorganisms present within the CF airway are believed to grow microaerophilically (Hassett et al. 2009). Therefore, in the first experiment, some samples were incubated aerobically and others microaerophilically to determine the impact this had upon impedance. The approach used is described in section 3.5.5. Briefly, electrode chambers were sterilised and filled with 1 ml of ASM. Then the samples were inoculated with 10 µl of PA14 at a concentration of  $7.5 \times 10^8$  CFU/ml (final pre-incubation sample concentration of  $7.5 \times 10^6$  CFU/ml). This concentration was calculated by measuring the OD<sub>600</sub> against a previously produced standard curve. Following this, half of the electrode chambers (including negative controls) were incubated microaerophilically and the other half aerobically. Both sets of samples were incubated at 37°C, shaking at 75 rpm (Kirchner et al. 2012).

The results show that it is possible to detect the presence of *P. aeruginosa* in both aerobic and microaerophilic conditions (Figure 5-1). The impedance signature for the normalised resistance, normalised phase and phase angle follow the same basic shape, regardless of whether the bacterial culture was incubated aerobically or microaerophilically. However, the relative changes in the impedance for those strains incubated in microaerophilic conditions is greater than those incubated aerobically. To explore this further, the peak detection algorithm described in section 3.8.3 was used to determine the location of individual peaks. Whilst the peaks in the microaerophilic data appeared to be larger, no significant difference existed between the microaerophilic and aerobic peak frequencies or peak normalised resistances (Table 5-1). The algorithm also detected the presence of some small peaks within the negative control data in both the microaerophilic and aerobic conditions. Some of these peaks appear at similar peak frequencies to the sample data whereas the peak amplitude is always at least 1.2 units above the negative control peaks. This suggests that

regardless of microaerophilic or aerobic growth conditions, the peak resistance amplitude could be a useful indicator of the presence of *P. aeruginosa*.





1\_51\_1

**Figure 5-1: Measurement of *P. aeruginosa* PA14 in aerobic and microaerophilic conditions. The data shows that there are differences in the impedance spectrum between the two growth conditions. (A) and (B) normalised phase angle; (C) and (D) phase angle before normalisation; (E) and (F) normalised resistance. Shading represents +/- 1 SD,  $n = 3$  for all samples.**

**Table 5-1: Peak normalised resistance data from aerobic and microaerophilic growth conditions. P values calculated using the two tailed Mann-Whitney test ( $n = 3$  for both aerobic and microaerophilic conditions). Ten measurements were performed per frequency decade, therefore the range of the peaks detected at high frequencies is greater than the range at lower frequencies.**

Time Hours	Aerobic		Microaerophilic		Mann-Whitney Test	
	Freq Hz (SD)	Resistance Normalised Units (SD)	Freq Hz (SD)	Resistance Normalised Units (SD)	Frequency	Resistance
14	12.97 (6.85)	1.46 (0.06)	11.25 (4.08)	1.81 (0.18)	1.00	0.08
24	4.87 (4.75)	1.49 (0.06)	28.64 (19.34)	1.85 (0.1)	0.19	0.08
38	128 (29.05)	1.55 (0.09)	241.67 (79.41)	1.46 (0.15)	0.12	0.51
48	172 (24.25)	1.41 (0.08)	343.33 (47.34)	1.38 (0.16)	0.08	0.66
65	117.33 (15.01)	1.37 (0.13)	255.67 (58.14)	1.5 (0.18)	0.08	0.38

Changes in the impedance modulus are also similar between the *P. aeruginosa* growth in aerobic and microaerophilic conditions (Table 5-2). Interestingly, as can be seen in Table 5-2, the rate of change of the impedance modulus where *P. aeruginosa* is grown microaerophilically is greater than during aerobic growth. This is seen in the change at 24 hours, where the impedance magnitude in the aerobic chamber drops to  $1.45 \times 10^6 \Omega$  at 10 Hz, whereas in the microaerophilic chambers the modulus drops lower, to  $8.49 \times 10^4 \Omega$ . During this time period the negative control remains similar for both the aerobic and microaerophilic chambers ( $4.51 \times 10^6 \Omega$  and  $5.89 \times 10^6 \Omega$  respectively) therefore the observed changes are likely to be due to changes in the behaviour of *P. aeruginosa* in response to the microaerophilic conditions. For example, the changes could lead to earlier expression of genes relating to biofilm formation, or the production of protective compounds and proteins that also affect the impedance.

**Table 5-2: Mean impedance modulus at 0.1 Hz for PA14 grown in aerobic and microaerophilic conditions in ASM. The values in bold font show that the change in the impedance modulus is more rapid in the microaerophilic electrode chambers. Numbers in brackets are SD,  $n = 3$ .**

Time (Hrs)	Impedance modulus ( $\Omega$ )			
	Aerobic		Microaerophilic	
	PA14	Neg Ctrl	PA14	Neg Ctrl
0	$6.46 \times 10^6$ ( $8.67 \times 10^5$ )	$5.69 \times 10^6$ ( $3.65 \times 10^5$ )	$5.00 \times 10^6$ ( $1.63 \times 10^6$ )	$6.24 \times 10^6$ ( $1.08 \times 10^6$ )
14	$1.44 \times 10^6$ ( $3.01 \times 10^5$ )	$4.94 \times 10^6$ ( $6.50 \times 10^5$ )	$1.17 \times 10^6$ ( $1.72 \times 10^5$ )	$5.91 \times 10^6$ ( $1.45 \times 10^6$ )
24	<b><math>1.45 \times 10^6</math></b> <b>(<math>7.13 \times 10^5</math>)</b>	$4.51 \times 10^6$ ( $7.74 \times 10^5$ )	<b><math>4.66 \times 10^5</math></b> <b>(<math>8.49 \times 10^4</math>)</b>	$5.89 \times 10^6$ ( $1.49 \times 10^6$ )
37	$2.83 \times 10^5$ ( $5.76 \times 10^4$ )	$3.94 \times 10^6$ ( $3.16 \times 10^5$ )	$1.12 \times 10^5$ ( $2.58 \times 10^4$ )	$5.85 \times 10^6$ ( $1.19 \times 10^6$ )
48	$2.53 \times 10^5$ ( $4.93 \times 10^4$ )	$3.94 \times 10^6$ ( $4.07 \times 10^5$ )	$8.56 \times 10^4$ ( $1.08 \times 10^4$ )	$5.82 \times 10^6$ ( $1.46 \times 10^6$ )
69	$2.52 \times 10^5$ ( $1.39 \times 10^4$ )	$4.06 \times 10^6$ ( $8.97 \times 10^5$ )	$6.52 \times 10^4$ ( $1.03 \times 10^4$ )	$5.58 \times 10^6$ ( $1.47 \times 10^6$ )

### 5.3 Impedance analysis with polymicrobial cultures

The changes observed in the impedance as a result of the growth of *P. aeruginosa* could be due to mechanisms independent of this bacterium (see section 1.3 for a full background of the potential mechanisms that could cause changes in the impedance). The electrode was therefore tested to ensure that similar changes to the impedance did not occur as a result of growth of other pathogens commonly found within the CF airway. If specific changes are observed that can be attributed directly to the presence of *P. aeruginosa* then a device could be developed for specific detection against a background of other microorganisms.

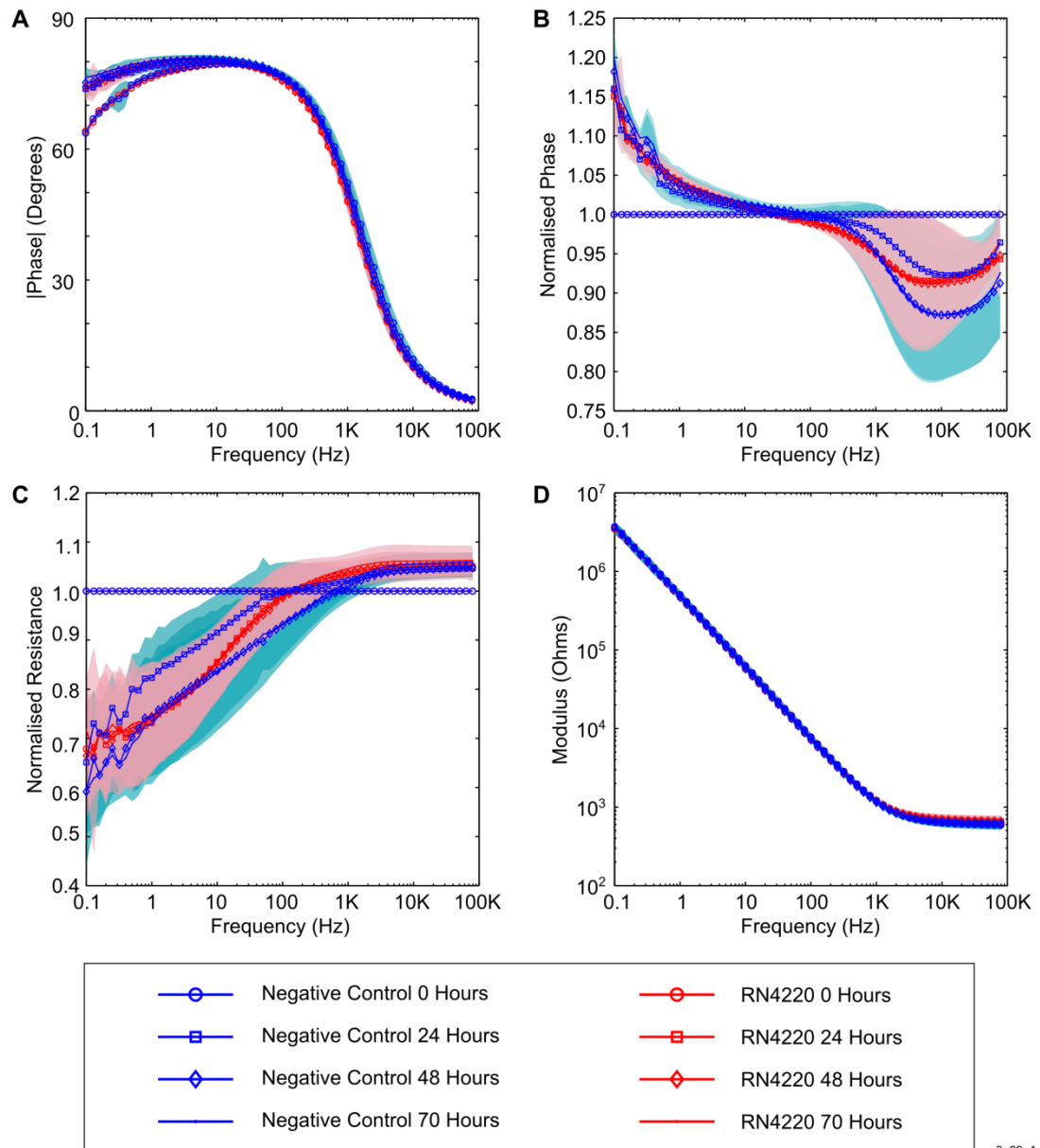
#### 5.3.1 Impedance analysis with *S. aureus* cultures

As shown in Figure 1-3, *S. aureus* is the most common CF pathogen present in the airways of young patients and generally present before colonisation with *P. aeruginosa* (Harrison 2007). Therefore, a series of tests were carried out to determine the changes in impedance caused by *S. aureus* and to find out if these were the same as those caused by *P. aeruginosa*. Experiments were firstly carried out in TSB, which is an optimal growth media for *S. aureus*, followed by experiments in ASM. Furthermore, some of the experiments carried out in ASM were done as a co-culture to determine if the presence of *P. aeruginosa* remained detectable when *S. aureus* was also present.

### 5.3.1.1 Impedance analysis with *S. aureus* grown in TSB media

Impedance measurements were carried out using *S. aureus* strain RN4220, from the NCTC in order to determine if a change similar to that found with *P. aeruginosa* occurred (see section 3.5.3). In brief, the experiment was prepared by filling sterilised electrode chambers with 1 ml of TSB and inoculating them with 10  $\mu$ l of overnight *S. aureus* RN4220 culture. These were then incubated in air (i.e. aerobically) for 72 hours.

The results indicate that no notable impedance changes that can distinguish *S. aureus* from controls are present when grown in TSB media. Specifically, no drop occurs in the phase angle (Figure 5-2 A), no peaks exist in the normalised resistance (Figure 5-2 C) and there is no change in the impedance modulus (Figure 5-2 D). Furthermore, there was no discernible difference between the negative control data and inoculated samples. The baseline impedance modulus at 0.1 Hz at the start of the experiment was  $5 \times 10^6 \Omega$  and therefore similar the starting impedance modulus in LB media (see Table 4-5).



3\_69\_1

**Figure 5-2: *In situ* growth of *S. aureus* RN4220 in TSB. (A) Phase angle, (B) normalised phase angle, (C) normalised resistance, (D) modulus. Shading represents +/- 1SD,  $n = 4$  for negative control and for RN4220.**

In order to determine the cell density of *S. aureus* at the end of the experiment, colony counting was carried out on the media using during the growth of RN4220 within the electrode chambers (see section 3.5.6.2 for details of protocol used). The final cell density was found to be  $5.5 \times 10^7$  CFU/ml, which was low contrasted to experiments carried out with *P. aeruginosa*, which were typically found to be around  $5 \times 10^9$  CFU/ml (see Table 4-7). Furthermore, impedance changes in a broth containing *P. aeruginosa* often occurred at cell densities around  $10^9$  CFU/ml. This suggests that the concentration of *S. aureus* in the experiment carried out above was below the detection limit.

To explore the effect that growth in the electrode chamber could have had upon the bacteria, an experiment was carried out whereby *S. aureus* RN4220 was inoculated in 1 ml aliquots of TSB in a 24 well plate and in the electrode chambers, in order to determine if a difference in CFU/ml existed after 72 hours. Prior to colony counting, a pipette was used to disturb the media in the electrode chambers five to six times and resulted in the media becoming turbid, suggesting that the *S. aureus* cells settle to the bottom of the chamber during the course of the experiment (see Figure 5-3 for an example of turbid growth with *S. aureus* contrasted to a negative control). 20  $\mu$ l aliquots were removed every 24 hours and used for colony counting. The results indicate that growth was slightly higher in the 24 well plate in contrast to the electrode chambers, after 72 hours ( $8.93 \times 10^9$  CFU/ml and  $2.28 \times 10^9$  CFU/ml respectively). Interestingly, it was noted that the media in the electrode chambers appeared clear and not turbid at the end of the experiment.

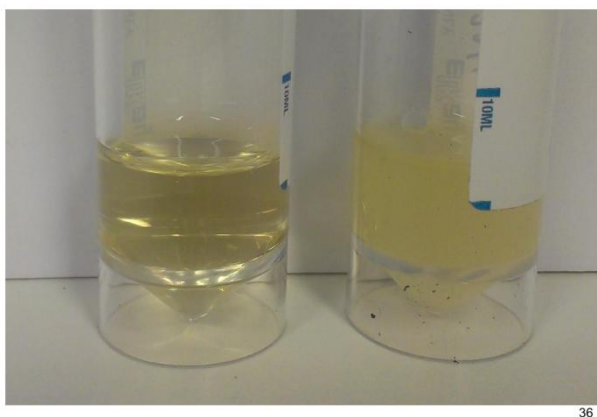
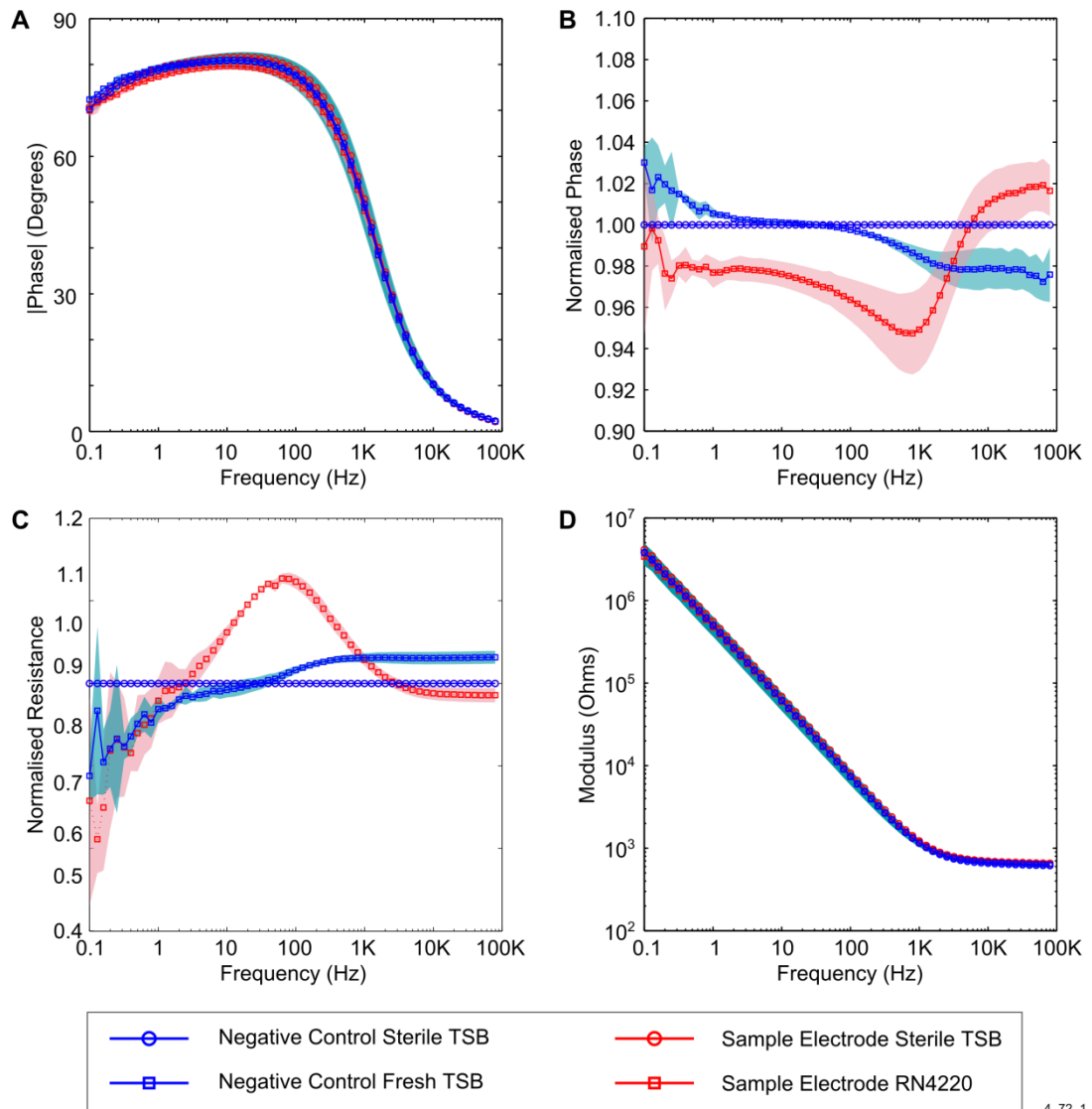


**Figure 5-3: Example of *S. aureus* turbid growth. The universal on the left shows sterile LB media, whereas the universal on the right shows *S. aureus* following 24 hours incubation at 37°C.**

The lower number of viable cells observed in the *in situ* impedance experiment with *S. aureus* could have been caused by three different factors. Firstly, unlike *P. aeruginosa*, *S. aureus* do not have flagella and are non motile. Therefore, the *S. aureus* cells may have clumped together and settled during growth within the electrode chamber, contrasted to a universal shaking at 150 rpm and when plated would have been counted as a single CFU. Secondly, *S. aureus* biofilm formation could have encapsulated a larger proportion of the cells contrasted to the *P. aeruginosa*, resulting in fewer cells being removed in the aliquot of media taken. Thirdly, the electrode material, the substrate or the adhesive silicone sealant used could have compromised the viability of *S. aureus* and inhibited growth, resulting in lower cell densities.

In order to verify the results found with *S. aureus* grown *in situ*, a further experiment was carried out using an overnight, *ex situ* culture of *S. aureus* grown in a 20 ml universal (incubated at 37°C, shaking at 150 rpm). For this experiment, a total of six electrodes were used, three to measure two sterile aliquots of TSB (first one as a reference measurement) and three electrodes were used to measure 1 ml aliquots of sterile TSB (as reference measurements) followed by measurements of a 24 hour culture of *S. aureus*. At the end of the experiment, cell density of the culture media was found to be  $1.1 \times 10^9$  CFU/ml.

The results from this experiment show that in fact a small difference in the impedance contrasted to the negative control is seen (Figure 5-4). Firstly, a trough is clearly visible in the normalised phase angle. Application of the peak detection algorithm shows that the trough can be readily identified in the electrode chambers containing *S. aureus* RN4220 but in only one of the negative control chambers (Figure 5-5). The mean location of the peak in the chambers containing *S. aureus* is 695 Hz. Therefore, this was used as a reference point to determine if the negative control differs significantly from the chambers containing *S. aureus*. The mean normalised phase value of the chambers containing *S. aureus* at 630 Hz, the closest measured point to 695 Hz, was 0.948 and for the negative control it was 0.988. This was not significantly different when the Mann-Whitney U test was used ( $P = 0.0809$ ), which could have been related to the small sample size. Secondly, a peak similar to those identified in *P. aeruginosa* experiments is visible in the normalised resistance data. A peak is also observed in the normalised resistance data at a mean of 68.4 Hz, and amplitude of 1.12. This is comparable to those peaks observed in the normalised resistance data for *P. aeruginosa* when grown in LB media (see Table 4-2). This is interesting because it raises the possibility that the appearance of a peak in the resistance data is caused by changes to the electrode-electrolyte interface, common to both *P. aeruginosa* and *S. aureus*.



4\_72\_1

**Figure 5-4: *Ex situ* impedance of overnight culture of *S. aureus* RN4220 added to electrode for measurement. (A) and (D) no significant different can be seen in the phase angle or impedance modulus. (B) and (C) differences are visible in the normalised phase and resistance data. Shading represents +/- 1SD,  $n = 3$ .**



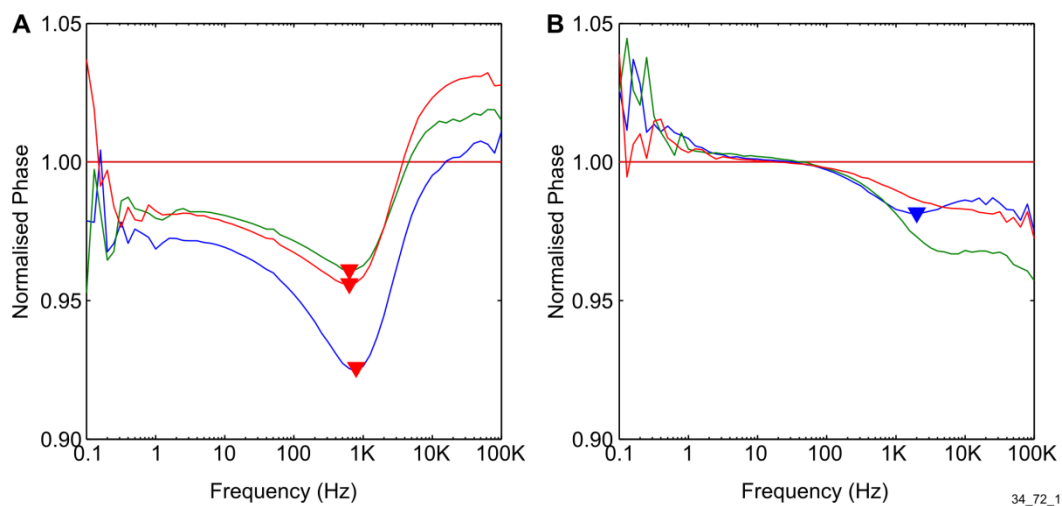
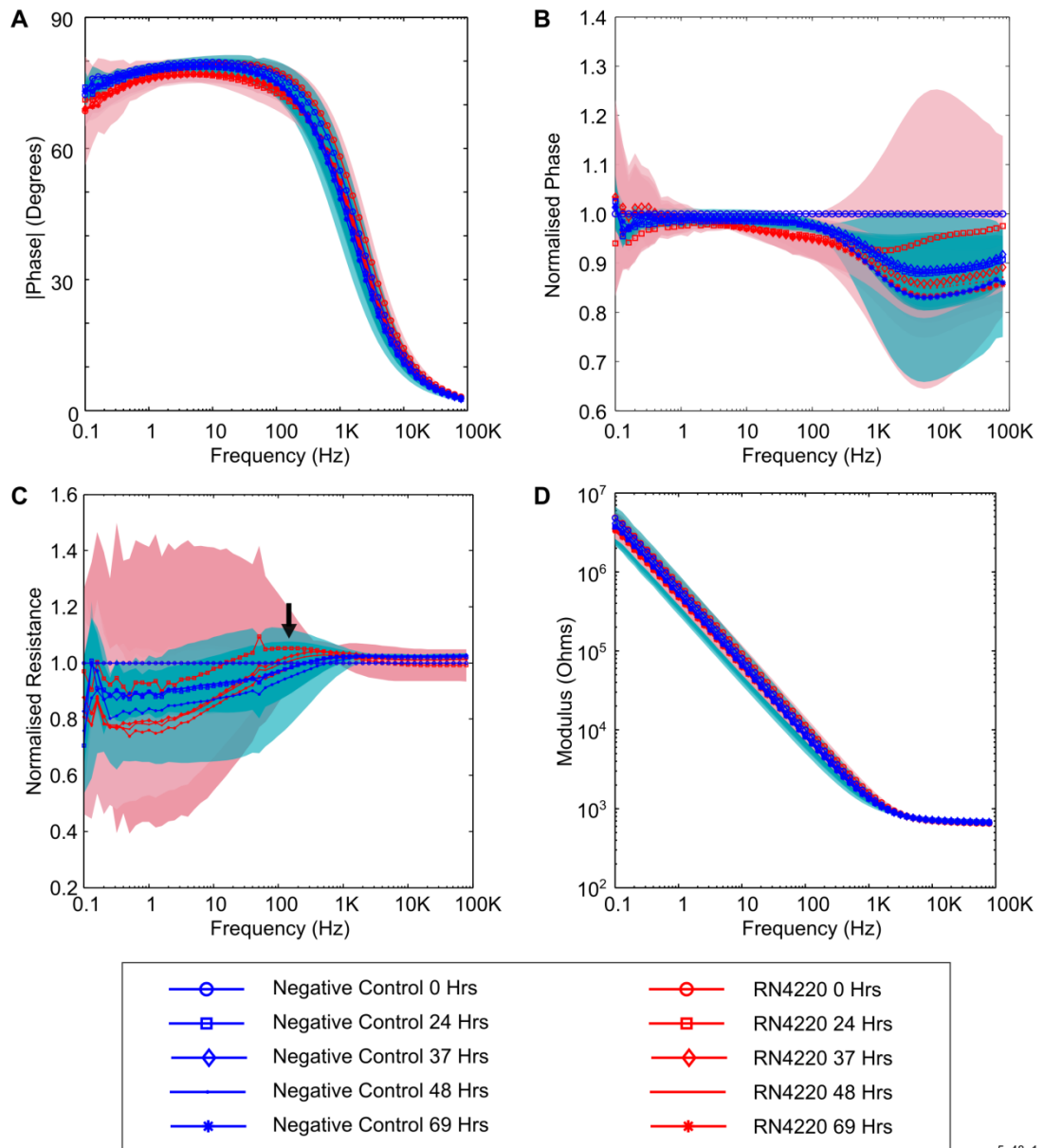


**Figure 5-5: Application of peak detection algorithm to the impedance signatures found during *ex situ* growth of *S. aureus* RN4220.**

### 5.3.1.2 Impedance measurements with *S. aureus* in ASM and polymicrobial investigation with *P. aeruginosa* and *S. aureus*

Following growth experiments carried out in TSB, and confirmation that growth in the electrode chambers does appear to adversely affect the density of *S. aureus* cells, the impedance of *S. aureus* RN4220 incubated alone and in the presence of *P. aeruginosa* within the CF model environment was tested. *S. aureus* was grown *in situ* in ASM in the electrode chamber to ensure that any effects resulting from longer term electrode, electrolyte interaction could also be captured. It was found that the interface did not change significantly throughout the experiment, compared to the negative control, for either the raw impedance data or any of the normalised impedance parameters (Figure 5-6). Interestingly, the trough at 695 Hz seen in the normalised phase data from the *ex situ* experiment with *S. aureus* RN4220 in TSB did not appear after 69 hours of growth in this experiment (see Figure 5-5). However, the normalised resistance plot shows that the samples containing *S. aureus* differ in their impedance curve compared to the negative control, with a slight peak visible after 37 hours at 400 Hz (Figure 5-6 C). A more sensitive electrode with lower baseline impedance might be more sensitive to these changes and enable a unique signature to be identified. The final cell densities contrasted to *P. aeruginosa* are discussed below.

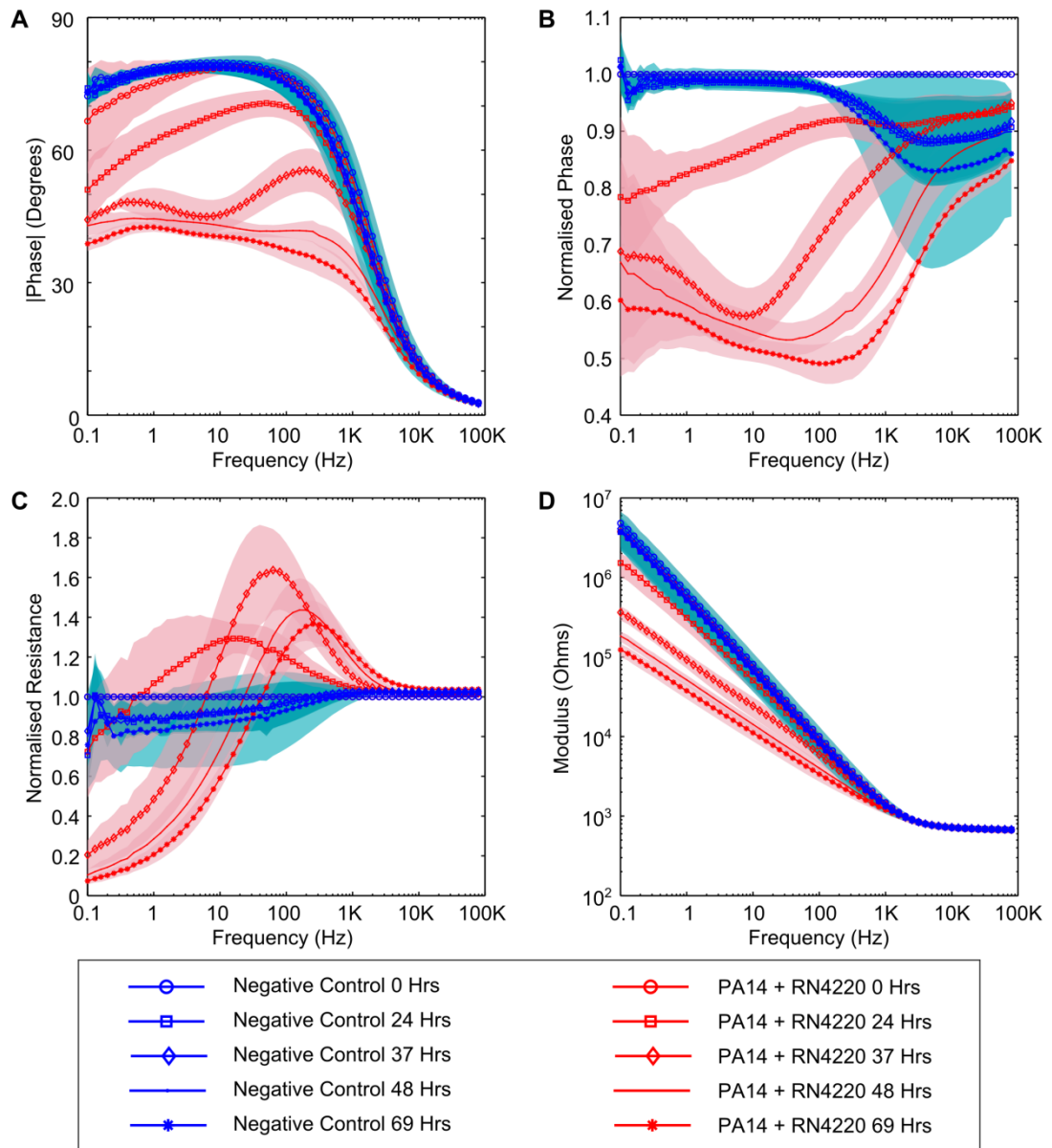


5\_48\_1

**Figure 5-6: *In situ* impedance changes following growth of *S. aureus* RN4220 in ASM. There is no discernible different in (A) the phase, (B) the normalised phase, (C) the normalised resistance and (D) the modulus. The arrow in (C) indicates a slight peak at 125 Hz at 24 hours moving to 400 Hz at later timepoints. Background shading represent +/- 1 SD. RN4220  $n = 4$ ; Neg Ctrl  $n = 5$ .**

In order to test the performance of the electrode in the context of a polymicrobial infection, *P. aeruginosa* PA14 and *S. aureus* RN4220 were also grown together at equal starting densities in the same electrode chamber, under microaerophilic conditions in ASM. As with the microaerophilic monoculture of *P. aeruginosa* alone (Figure 5-1 B, D and F), changes in the impedance between the negative control and the polymicrobial infection were observable after 24 hours in the impedance phase and modulus data (Figure 5-7 A and D). These

changes were similar to those observed with PA14 alone. Furthermore, at the end of the experiment, the polymicrobial infection model and PA14 monoculture had a similar impedance curve. The normalised resistance data was also similar, suggesting that PA14 was responsible for the changes seen in the impedance (Figure 5-7 C).



14\_48\_1

**Figure 5-7: *In situ* polymicrobial measurement of *S. aureus* RN4220 and *P. aeruginosa* PA14. (A) Phase, (B) normalised phase, (C) normalised resistance and (D) normalised modulus. Shading represents +/- 1 SD, PA14+RN4220  $n = 5$ , neg ctrl  $n = 5$**

To further understand the dynamics of the polymicrobial model, colony counting was carried out on an aliquot of the samples taken at 37 hours and 69 hours (Table 5-3). From this, it can be seen that *P. aeruginosa* PA14 outcompetes RN4220 by the 69 hour timepoint, where *S. aureus* RN4220 could no longer be cultured from the electrode chambers. This supports other work that found *P. aeruginosa* results in reduced numbers of Gram positive bacteria in a polymicrobial infection model (Korgaonkar et al. 2013). At the 37 hour timepoint, it can also be seen that fewer viable RN4220 cells exist within the polymicrobial samples than in the monocultures. Specifically, at 37 hours  $3.65 \times 10^5$  CFU/ml were present for *S. aureus* RN4220, indicating that some viable cells remained in the presence of *P. aeruginosa* PA14, but no growth occurred. In general, the concentrations of both *P. aeruginosa* and *S. aureus* were a factor of approximately 10 and 20 respectively less than the typical values in optimal growth media (recall that typical CFU/ml for both species were around  $1 \times 10^9$  CFU/ml). This is probably due to the more challenging growth conditions imposed by the microaerophilic conditions and the minimal ASM media. Clearly, *P. aeruginosa* thrives more in the model CF environment than *S. aureus*.

**Table 5-3: Indicative cell densities of planktonic cells at the end of the experiment and timepoints during the experiment.**

Sample Type	Cell Concentration (CFU/ml)		
	Initial (0 hrs)	37 Hrs mean (range)	69 Hrs mean (range)
PA14 Mono	$3-5 \times 10^6$	$6.5 \times 10^8$ ( $5.4 \times 10^8 - 7.3 \times 10^8$ )	$2.1 \times 10^8$ ( $6.5 \times 10^7 - 3.3 \times 10^8$ )
RN4220 Mono	$3-5 \times 10^6$	$1.6 \times 10^7$ ( $1.1 \times 10^7 - 2.9 \times 10^7$ )	$3.1 \times 10^7$ ( $4.9 \times 10^6 - 7.2 \times 10^7$ )
PA14 Poly	$3-5 \times 10^6$	$6.0 \times 10^8$ ( $4.1 \times 10^8 - 7.2 \times 10^8$ )	$8.5 \times 10^7$ ( $5.9 \times 10^6 - 1.0 \times 10^8$ )
RN4220 Poly	$3-5 \times 10^6$	$3.7 \times 10^5$ ( $6.8 \times 10^4 - 1.4 \times 10^6$ )	0

In summary, the experiments in this section have tested the ability of the carbon electrode to detect the presence of *S. aureus* in a number of different conditions. The initial experiments demonstrated that the presence of *S. aureus* RN4220 *in situ* couldn't be detected, but an overnight culture added to the electrode to carry out an impedance measurement was detectable. The polymicrobial infection model demonstrates that the impedance within the

electrode chambers changes in the presence of *S. aureus* in a manner that is specific to the growth of *P. aeruginosa*. Further investigation is required to understand the reasons for the changes in the impedance of an *S. aureus* monoculture and why these changes only appear to occur in the *ex situ* culture and not the *in situ* culture, however this is outside the scope of the current study.

### **5.3.2 Impedance analysis with *H. influenzae* cultures**

To progress the study further, a similar set of experiments to those carried out with *S. aureus* were also conducted with *H. influenzae*. Like *S. aureus*, *H. influenzae* is highly prevalent in the CF airway and has been reported as the most common CF pathogen in patients less than 1 year old (Cystic Fibrosis Trust 2010). Therefore, it is important that any infection monitor is able to detect the presence of *P. aeruginosa* against a background of *H. influenzae*. As described in section 1.2.5, *H. influenzae* is a fastidious non-motile Gram negative bacilli (World Health Organisation 2011).

#### **5.3.2.1 Impedance measurements with *H. influenzae* grown in HTM**

Measurement of *H. influenzae* was carried out in Haemophilus Test Media (HTM) initially, in order to determine if any changes occurred in the impedance under optimal growth conditions. *H. influenzae* strain HI680 was incubated microaerophilically in HTM (i.e. under optimal growth conditions) for 72 hours, shaking at 75 rpm (see section 3.5.3 for method). The incubation period was started with a 10 µl aliquot of overnight culture of *H. influenzae* HI680 added to 1 ml of HTM in a sterilised electrode chamber. The mean data indicates that a slightly deeper trough exists in the inoculated electrode chambers at 10 kHz, contrasted to the negative control (Figure 5-8), although identification of specific differences is difficult.

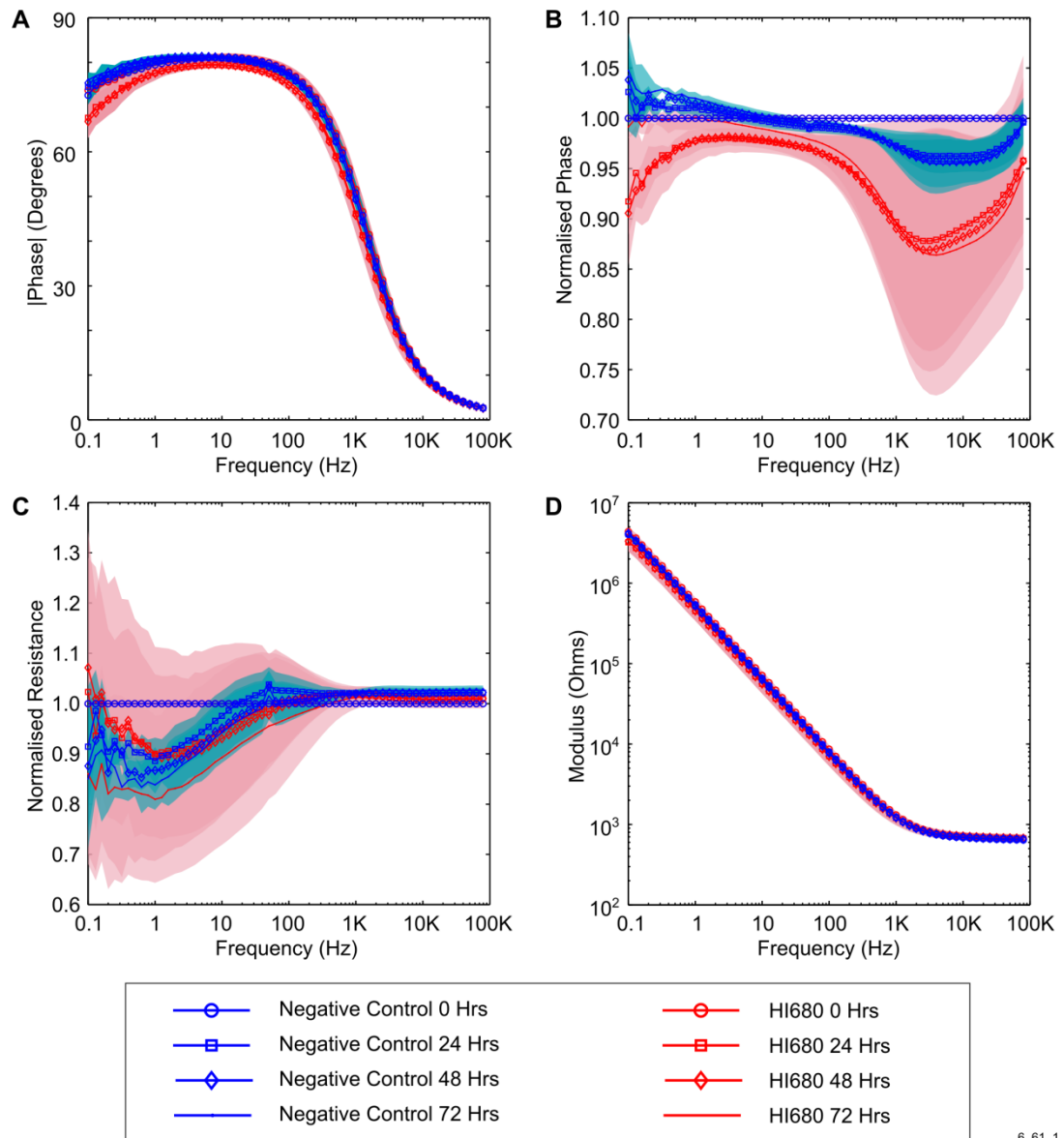


**Figure 5-8: *In situ* measurement of *H. influenzae* HI680 in HTM. Showing (A) Phase, (B) normalised phase, (C) normalised resistance, and (D) modulus. Background shading represents  $\pm 1$  SD, neg ctrl  $n = 4$ ; HI680  $n = 5$ .**

At the end of the experiment, the media within the electrode chamber was clear, suggesting that there was no growth of *H. influenzae* during the experiment. It appears that the cells in the culture could have survived for some time, but were no longer viable by 72 hours. To explore this further, the experiment was repeated and stopped after 48 hours. After the experiment, an aliquot of the media was cultured on *Haemophilus* Test Agar (HTA) to determine if there were any viable cells.

No *H. influenzae* could be cultured from the inoculated chambers after the 48 hour growth period, suggesting the bacteria lose viability early on in the experiment. Furthermore, the

impedance data indicates that there is no change between inoculated electrode chambers and the negative control, for any of the measured impedance parameters (Figure 5-9).

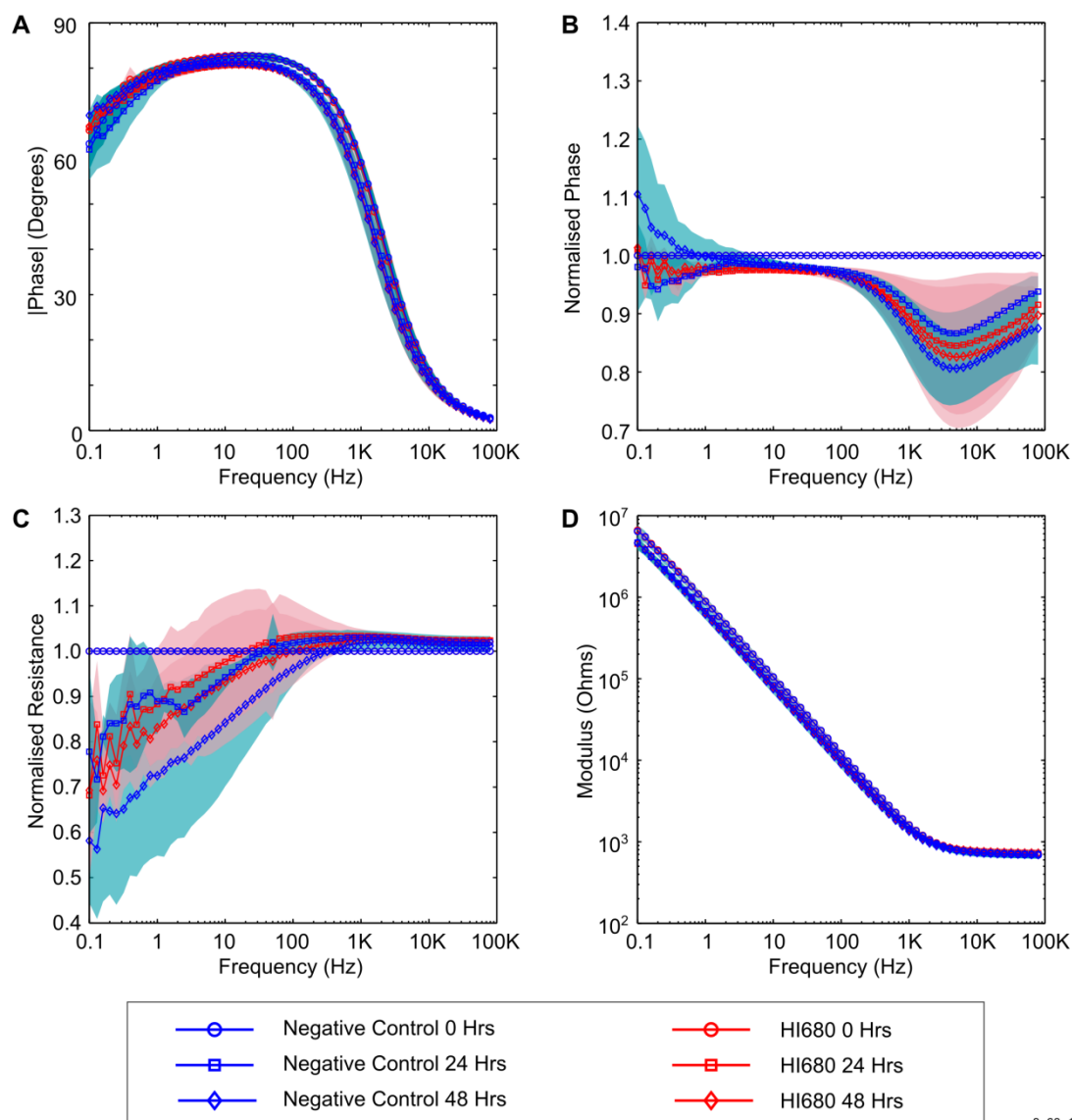


**Figure 5-9: *In situ* measurement of *H. influenzae* in HTM over 48 hours. (A) Phase, (B) normalised phase, (C) normalised resistance and (D) modulus. Background shading represents +/- 1 SD,  $n = 3$  for both samples and negative controls.**

To overcome the lack of viability during the incubation of *H. influenzae* within the electrode chamber, a further experiment was carried out by incubating the bacteria *ex situ* in a 24 well plate incubated under microaerophilic conditions and adding an aliquot of the culture to the electrode for the measurement (see section 3.5.4). Four electrodes were used for the measurement, with an initial blanking measurement carried out in HTM, followed by a

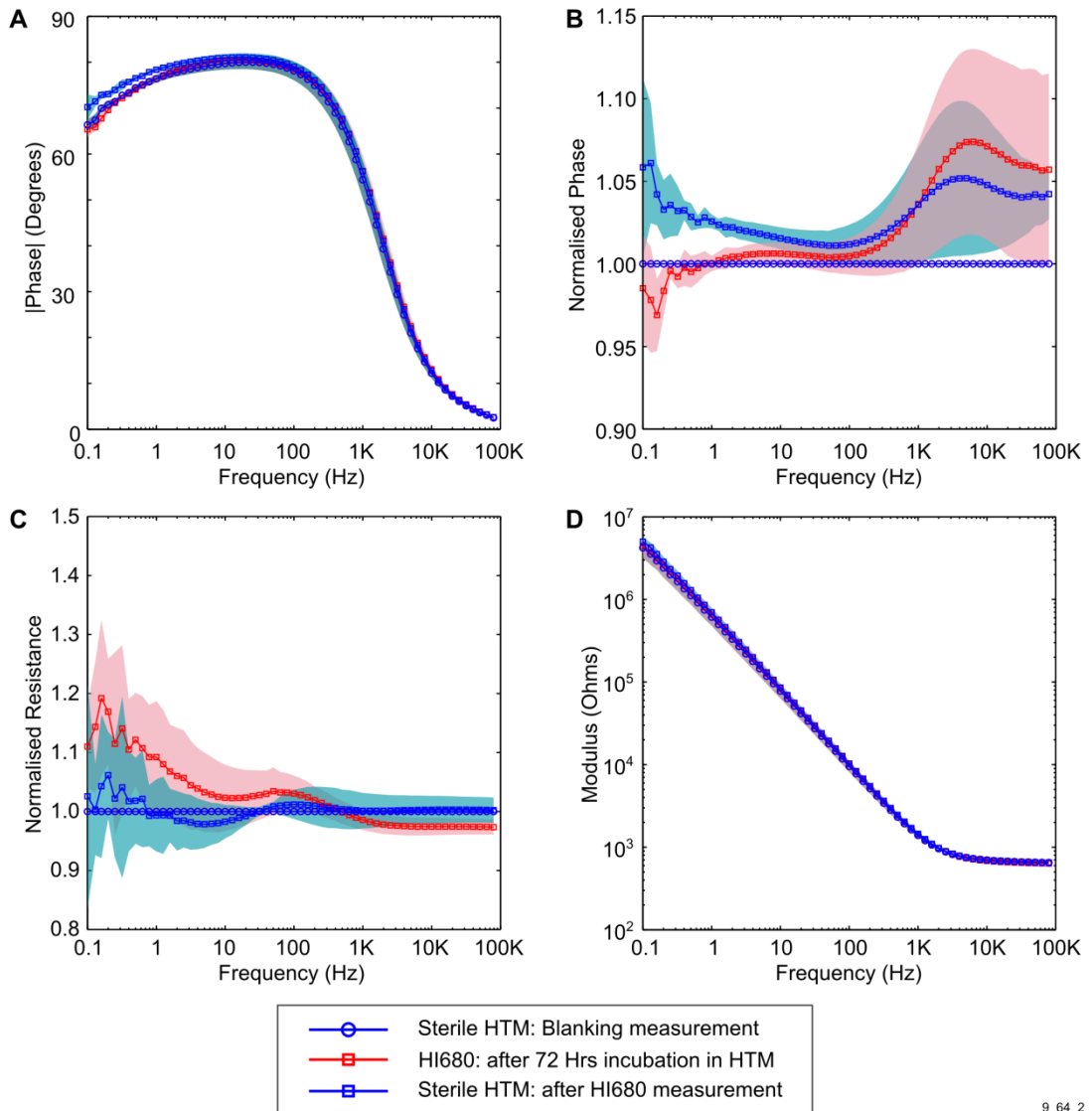
measurement of the media containing the incubated *H. influenzae*. At the end of the experiment, the media within the inoculated electrode chambers was clearly cloudy, indicating that growth had occurred. Typically, the number of viable cells from *H. influenzae* in stationary phase in HTM was found to be  $2.67 \times 10^9$  CFU/ml.

Whilst no peaks are visible within the data, there is a small drop in the phase angle (Figure 5-10 B) at lower frequencies between the inoculated samples and the negative control. The Mann-Whitney test was used to determine that this was significantly different at 1 Hz ( $P = 0.0304$ , two tailed Mann-Whitney test,  $n = 4$  for both negative control and inoculated chambers). No significant changes were seen in the other impedance parameters contrasted to the negative control (Figure 5-10 A, C and D). Application of the peak detection algorithm to the normalised resistance showed that the slight peak present in the normalised phase data for the inoculated chambers could not be readily identified, with the principal peak of interest being found in only two of the four electrodes containing the inoculated culture (Figure 5-11A). Furthermore, it is interesting to note that several peaks and troughs were identified in the negative control data (Figure 5-11B), suggesting that HTM could have a different effect upon the impedance, contrasted to LB or TSB media. Another reason for the partial detection of peaks in the negative control data shown in (Figure 5-11B) is because the negative control measurements were taken with the same electrodes, by aspirating and rinsing the chamber after measurement of the inoculated *H. influenzae* and replacement with a fresh aliquot.

In summary, the results under optimal growth conditions show that *H. influenzae* does not cause the same changes in the impedance seen with *P. aeruginosa* when grown *ex situ*. Interestingly, however, some differences were observed in the impedance. Further investigation is carried out with *H. influenzae* in the next section to explore polymicrobial growth in ASM with *P. aeruginosa*.

The use of alternative electrode materials, such as platinum, with a lower starting impedance would result in more sensitive measurements and therefore could yield changes in the impedance not observed with the all carbon electrode used in this study. However, extensive investigation with *H. influenzae* on alternative electrode materials is beyond the scope of the current study.





9\_64\_2

**Figure 5-10: Ex situ measurement of *H. influenzae* HI680 in HTM. (A) Phase; (B) normalised phase; (C) normalised resistance; (D) modulus. Background shading represents +/- 1 SD,  $n = 4$ .**

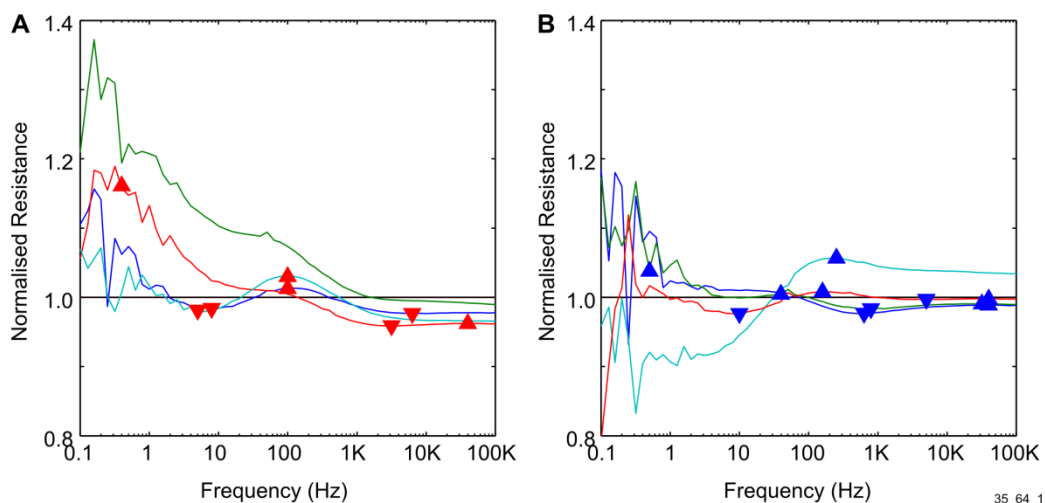


**Figure 5-11: Application of the peak detection algorithm to the identification of the peak in the normalised resistance data. (A) measurements from media inoculated with *H. influenzae* HI680; (B) negative control measurements. The plot of the inoculated chambers shows that a slight peak was identified at 100 Hz, but only in two of the four electrode chambers.**

### 5.3.2.2 Impedance measurements with *H. influenzae* grown in ASM and polymicrobial investigation with *P. aeruginosa* and *H. influenzae*

#### 5.3.2.2.1 First ASM impedance measurement experiment with *H. influenzae* grown *ex situ*

A series of experiments were carried out to assess changes in the impedance caused by *H. influenzae* in the CF model environment (see section 3.5.5). In contrast to the experiment carried out using HTM as the growth media, this experiment was done using a set of electrodes for the measurement of *H. influenzae* HI680 and a separate set for the negative control measurement. By doing this, it was possible to ensure that any negative control measurements taken were not affected by the media from the electrode chambers.

*H. influenzae* was incubated in a 24 well plate in order to ensure viability would not be compromised by the electrode chambers. As described in section 3.2.2.11, ASM was supplemented with NAD and hemin to support growth of *H. influenzae* which requires these two growth factors (World Health Organisation 2011). During colony counting after the experiment, it was found that two of the four wells inoculated with *H. influenzae* were contaminated; therefore these were omitted from the following results.

It can be seen from this experiment that similar changes to the impedance occur to those identified when *H. influenzae* was grown *ex situ* in HTM media (Figure 5-12). Specifically, there is a greater drop in the normalised phase angle at low frequencies compared to the negative control (Figure 5-12 B). The same characteristics were seen in the normalised phase data when *H. influenzae* was incubated in HTM (Figure 5-10 B); i.e. a peak exists in the phase angle for both the negative control and the inoculated electrodes at high frequency. The slight increase in phase angle contrasted to the negative control suggests that at lower frequencies, there is an increase in the capacitance of the interface, relative to the resistance.

When the normalised resistance data is analysed, the mean impedance signature for *H. influenzae* is greater than that for the negative control, although the difference is marginal (Figure 5-12 C). The same trend was also observed when *H. influenzae* was incubated in HTM (Figure 5-10 C). Colony counting carried out on the wells inoculated with *H. influenzae* HI680 but not contaminated confirmed that viable cells were present ( $5 \times 10^5$  CFU/ml and  $4.4 \times 10^6$  CFU/ml). These concentrations are low; suggesting that survival of *H. influenzae* in ASM is more limited than it is in HTM.

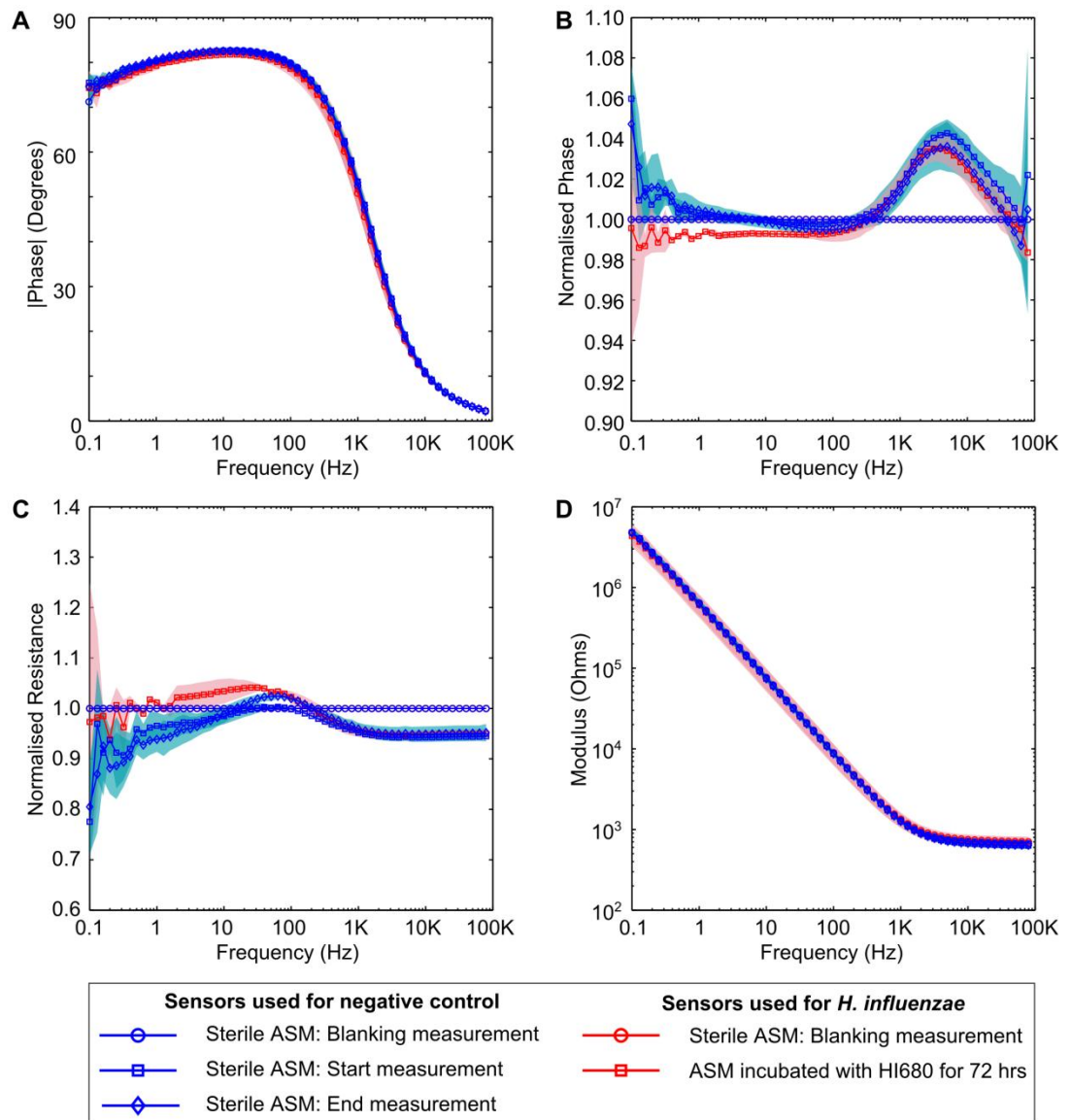


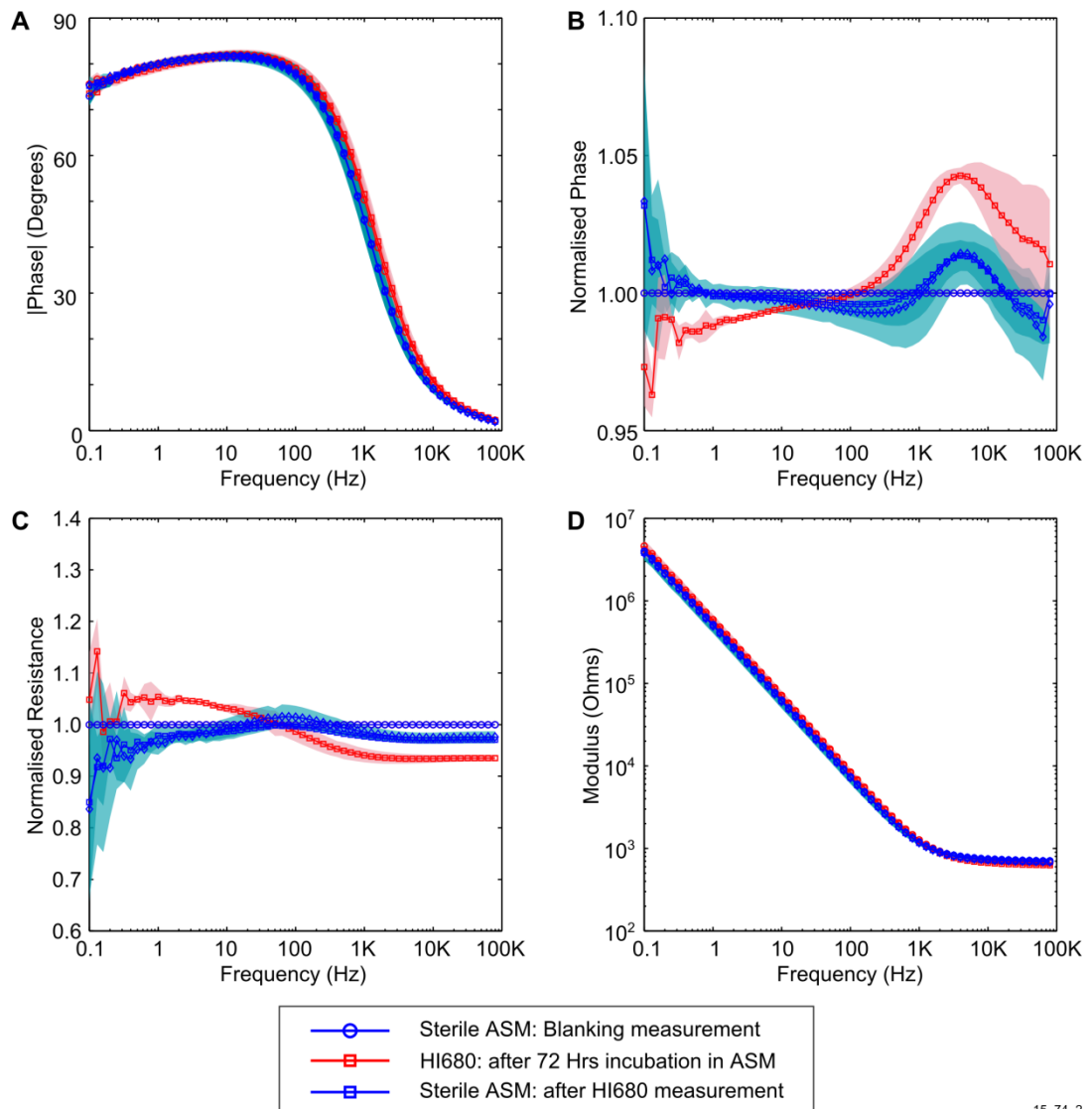
**Figure 5-12: *Ex situ* measurement of *H. influenzae* in ASM supplemented with essential growth factors, hemin and NAD. (A) phase angle; (B) normalised phase, showing differences in impedance at low frequency; (C) normalised resistance showing small impedance differences at low frequency; (D) modulus. Background shading represents +/- 1SD, HI680  $n = 2$ ; neg ctrl  $n = 4$ .**

### 5.3.2.2.2 Second ASM impedance measurement experiment with *H. influenzae ex situ* with and without *P. aeruginosa*

An additional experiment was carried out to determine the behaviour of *H. influenzae* when grown in the presence of *P. aeruginosa*. In addition to the polymicrobial measurements, monocultures of *H. influenzae* were incubated in order to determine if the changes observed

with the two uncontaminated chambers from the experiment above were repeatable. Monocultures of *P. aeruginosa* were also carried out in ASM media, under microaerophilic conditions using a 24 well plate for the incubation as described above. This also provided the opportunity to verify that *P. aeruginosa* caused a change in the impedance when not incubated in the presence of the electrode. After an initial blanking measurement in sterile ASM, measurement of a monoculture of *H. influenzae* HI680 was carried out, followed by the polymicrobial culture. Separate electrodes were used for the measurement of the negative control (sterile ASM) carried out at the start of the experiment and again at the end.

Similar changes were observed in the impedance as those seen with the previous measurements carried out *ex situ* in HTM and in ASM (Figure 5-10 and Figure 5-12). Specifically, these consisted of a high frequency peak in the normalised phase data and slightly higher normalised resistance contrasted to the negative control. Interestingly, the peak observed in the normalised phase at high frequency is larger when the inoculated media was measured, contrasted to the negative control (Figure 5-13 B). Also, the low frequency portion of the normalised phase shows the same trend seen previously, with a greater drop contrasted to the negative control (contrast Figure 5-10 B and Figure 5-12 B).



15\_74\_2

**Figure 5-13: Ex situ measurement of *H. influenzae* HI680 in ASM media after 72 hours. (A) Phase, (B) normalised phase, showing similar impedance trends to those seen previously, (C) normalised resistance and (D) modulus. Shading represents +/- 1 SD. HI680  $n = 3$ ; neg ctrl  $n = 4$ .**

Growth of *P. aeruginosa* and *H. influenzae* together results in a large change in the impedance, similar to that observed when *P. aeruginosa* is grown alone (Figure 5-14). It is interesting to note, however, that the extent of the change in impedance is not as great as that observed when *S. aureus* is grown alongside *P. aeruginosa* (Figure 5-7). Some of these changes could have been due to the difference between the experiments being carried out *in situ* (in the case of *S. aureus*) and *ex situ* (in the case of *H. influenzae*) suggesting that the

mechanisms affecting the electrode impedance differ between *in situ* and *ex situ* experiments.

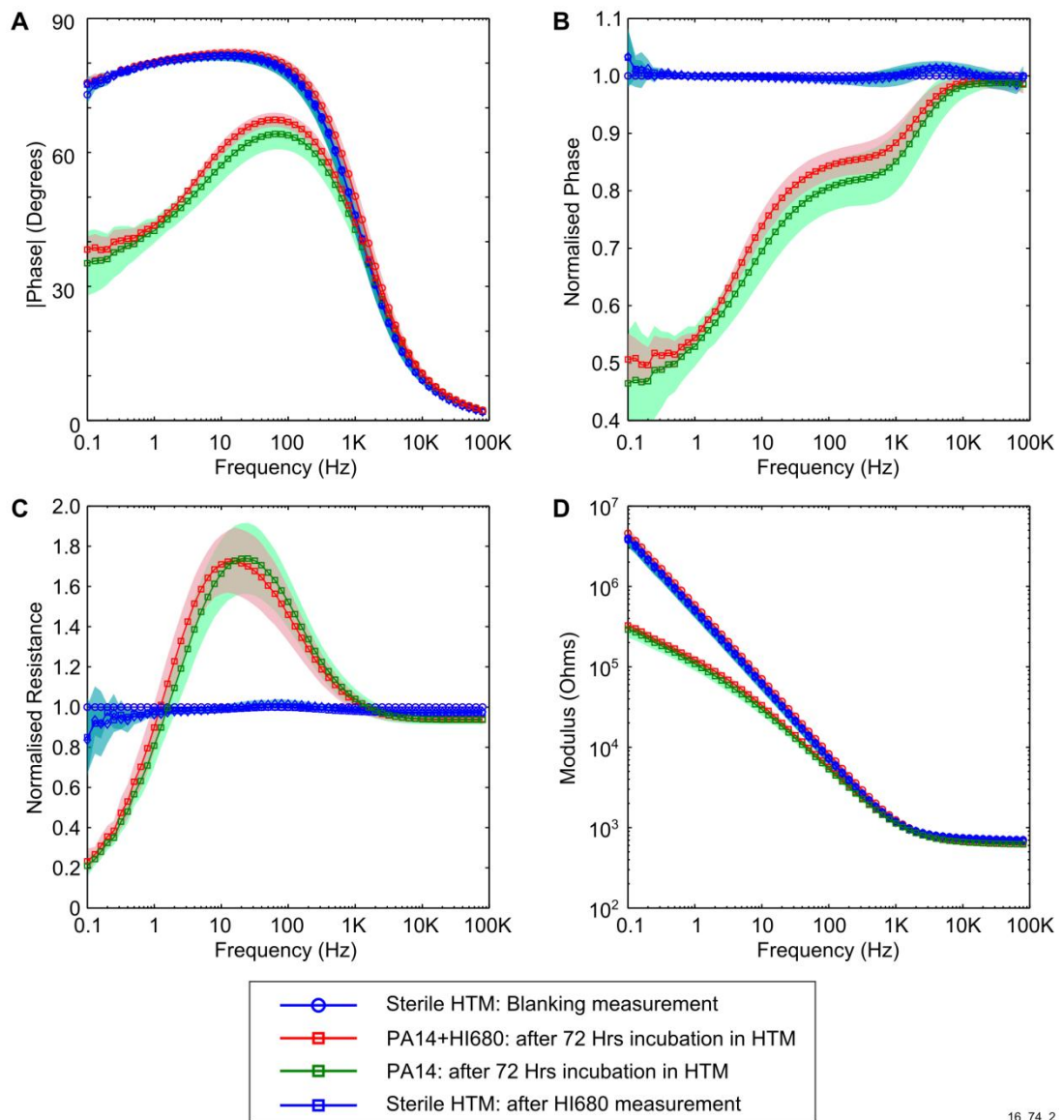


**Figure 5-14: *Ex situ* measurement of *P. aeruginosa* PA14 and *H. influenzae* HI680 grown together in ASM media for 72 hours. (A) Phase, (B) normalised phase, (C) normalised resistance, (D) modulus. Shading represents +/- 1SD, polymicrobial  $n = 4$ ; neg ctrl  $n = 4$ .**

Colony counting was carried out to establish the concentration of *H. influenzae* and *P. aeruginosa* in the monoculture experiments (Table 5-4). For the *H. influenzae* monocultures, a mean concentration  $2.9 \times 10^6$  CFU/ml was seen at the end of the experiment, which is similar to the growth of *H. influenzae* seen in ASM in section 5.3.2.2.1 above. The

concentration of *P. aeruginosa* was also determined within the polymicrobial cultures. An agar media that was selective for *H. influenzae* whilst inhibiting *P. aeruginosa* couldn't be identified; therefore determine the number of viable *H. influenzae* cells at the end of the polymicrobial culture wasn't possible.

**Table 5-4: Indicative cell densities of planktonic cells at the end of the experiment.**

Sample Type	Cell Concentration (CFU/ml)	
	Initial (0 hrs)	72 Hrs mean (range)
PA14 Mono	$3.4 \times 10^6$	$1.93 \times 10^9$ ( $9.0 \times 10^8 - 5.0 \times 10^9$ )
HI680 Mono	$1.25 \times 10^6$	$2.9 \times 10^6$ ( $1.5 \times 10^6 - 4.3 \times 10^6$ )
PA14 Poly	$3.4 \times 10^6$	$3.1 \times 10^9$ ( $6.1 \times 10^8 - 7.1 \times 10^9$ )

### 5.3.2.2.3 Impedance measurements following *in situ* and *ex situ* incubations with *P. aeruginosa*

It can be seen that when the impedance of the *P. aeruginosa* monoculture is measured, the changes to the *ex situ* culture differ from that of the *in situ* culture at the three day time point (contrast Figure 5-1 to Figure 5-14). Firstly, when *P. aeruginosa* is grown microaerophilically *in situ*, a large trough develops in the normalised phase after three days, whereas in the *ex situ* culture, a shoulder appears at the same frequency and the impedance change is not as great. Application of the peak detection algorithm shows that the trough from the 65 hour timepoint of the *in situ* experiment with *P. aeruginosa* occurs at a mean frequency and amplitude of 50.8 Hz and 0.37. In contrast, when the peak detection algorithm was applied to the *ex situ* normalised phase data at 72 hours, troughs were not readily identified across all of the four measurements. A trough was identified in two of the *P. aeruginosa* positive channels, but these occurred at a much lower frequency (mean frequency of 285 mHz with a mean amplitude of 0.541). The causes for these peaks are discussed fully in the discussion in section 7.3.4.

Another interesting difference can be seen in the resistance peak, which occurs at a lower frequency when the media is incubated *ex situ* contrasted to the *in situ* measurement. When the peak detection algorithm is used to locate the *in situ* peaks in the normalised resistance at



65 hours, peaks are found at a mean frequency of 255 Hz with mean amplitude of 1.5. In contrast, the *ex situ* peaks are found at a mean frequency of 22 Hz with a mean amplitude of 1.7. These signatures are interesting because they suggest that different mechanisms could be at play when *P. aeruginosa* is grown *in situ* with the electrode and when grown *ex situ* and only added to the electrode during the measurement period. If the impedance technique and electrode discussed here changes in response to multiple electrode-microbe interactions, then it raises the possibility that a unique signature could be elucidated for different microbial species. Furthermore, it also raises the possibility that the electrode would be able to detect bacteria in different phenotypic states, which could be indicative of infection.

### **5.3.3 Impedance measurements with *C. albicans* cultures**

*C. albicans* is a eukaryotic yeast organism and as such differs largely from the previous three prokaryote organisms studied. As described in section 1.2.7, *C. albicans* is capable of growth as a unicellular organism and also with a filamentous phenotype (Figure 5-15). It is also commonly cultured from sputum of patients with CF. For example, in one study Bakare et al. (2003) report finding *C. albicans* in 59% of sputum samples collected. Additionally, *C. albicans* can exist as part of a polymicrobial infection with *P. aeruginosa*, increasing the severity of infection (Peleg et al. 2010). To explore the impact that a eukaryote microorganism would have upon the electrode impedance, a series of experiments were undertaken with *C. albicans* SC5314, measuring the impedance *in situ* (see section 3.5.3 for method).

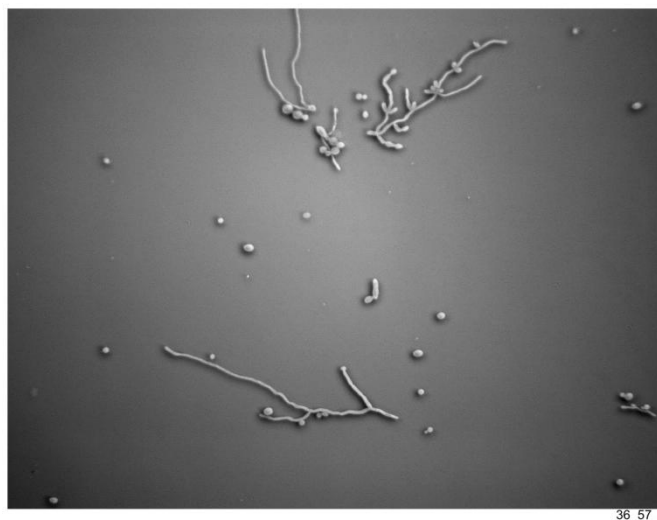
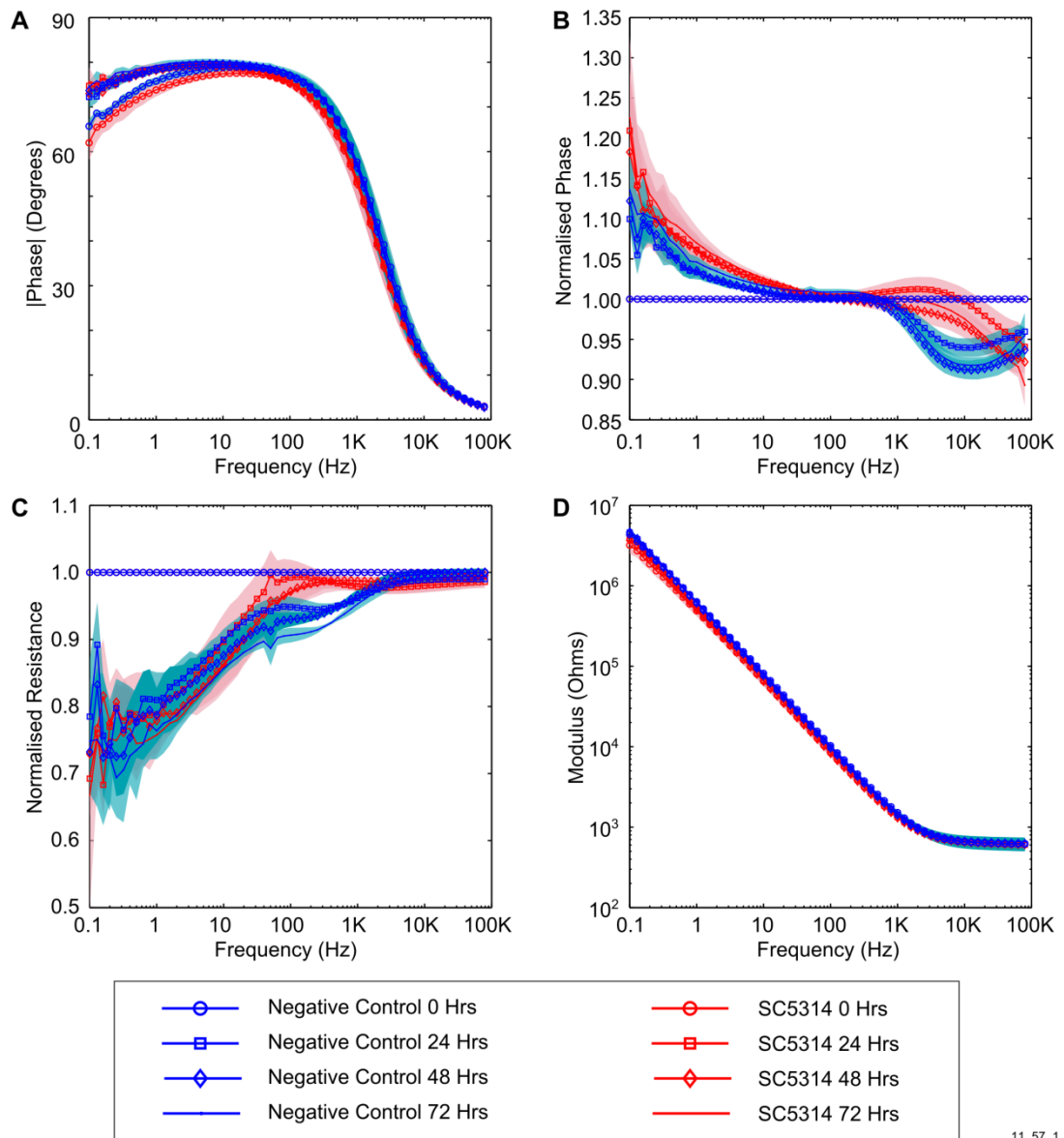


**Figure 5-15: Example of *C. albicans* growth, showing both filamentous and yeast forms.**

### **5.3.3.1 Impedance measurements with *C. albicans* incubated in TSB-YE**

To explore the effect that *C. albicans* had on the impedance, 10  $\mu$ l of strain SC5314 was inoculated into sterilised electrode chambers containing 1 ml of TSB-YE and incubated for 72 hours. Six electrode chambers were used, with three inoculated with SC5314 and three kept sterile as a negative control. Impedance measurements were carried out at the start and subsequently every 24 hours.

The results show that changes in the impedance throughout the experiment are different to those observed with *P. aeruginosa*. The phase angle and the impedance modulus do not show any significant change in the impedance contrasted to the negative control at each timepoint (Figure 5-16 A and D). Interestingly, two small changes are visible in the normalised phase data (Figure 5-16 B) and the normalised resistance data (Figure 5-16 C). At high frequencies the normalised phase angle increases relative to the starting angle for inoculated chambers, in contrast to the negative control where the phase angle drops (Figure 5-17), however, the change is not significantly different ( $P>0.05$ ). Additionally, it was also noted that the normalised resistance is higher in the inoculated chambers than in the negative control channels at 500 Hz (Figure 5-18), but not significantly different ( $P>0.05$ ). Colony counting carried out at the end of the experiment indicated that the final density of *C. albicans* cells was approximately  $1.5 \times 10^7$  CFU/ml.



11\_57\_1

**Figure 5-16: *In situ* measurement of *C. albicans* SC5314 in TSB-YE over 72 hours. (A) Phase, (B) normalised phase, showing different signature in the inoculated chambers at high frequency, (C) normalised resistance showing a small change in the impedance at intermediate frequencies. Background shading +/- 1 SD,  $n = 3$ .**

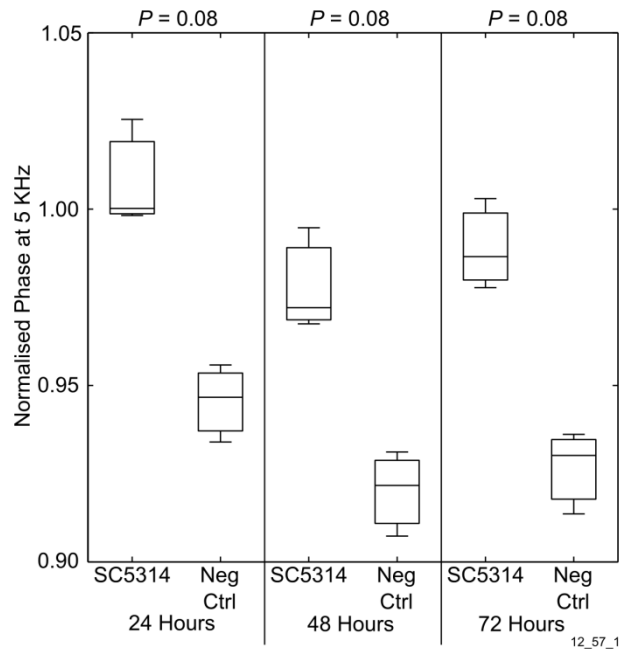


**Figure 5-17: Boxplot showing the difference between *C. albicans* and the negative control in normalised phase data at 5 kHz. Central box lines represent the median value, lower and upper bounds the 25<sup>th</sup> and 75<sup>th</sup> percentile and the whiskers represent the most extreme datapoints. *P* values were calculated using the two tailed Mann-Whitney test. *n* = 3 for both negative control and SC5314 samples.**

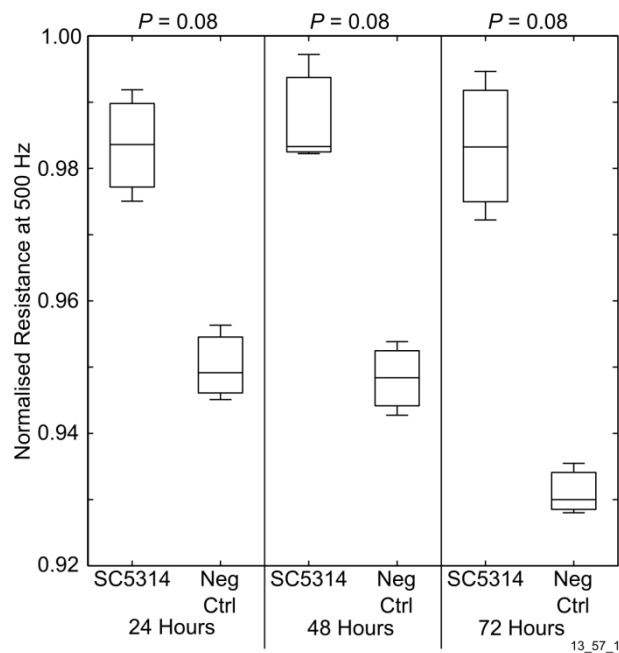
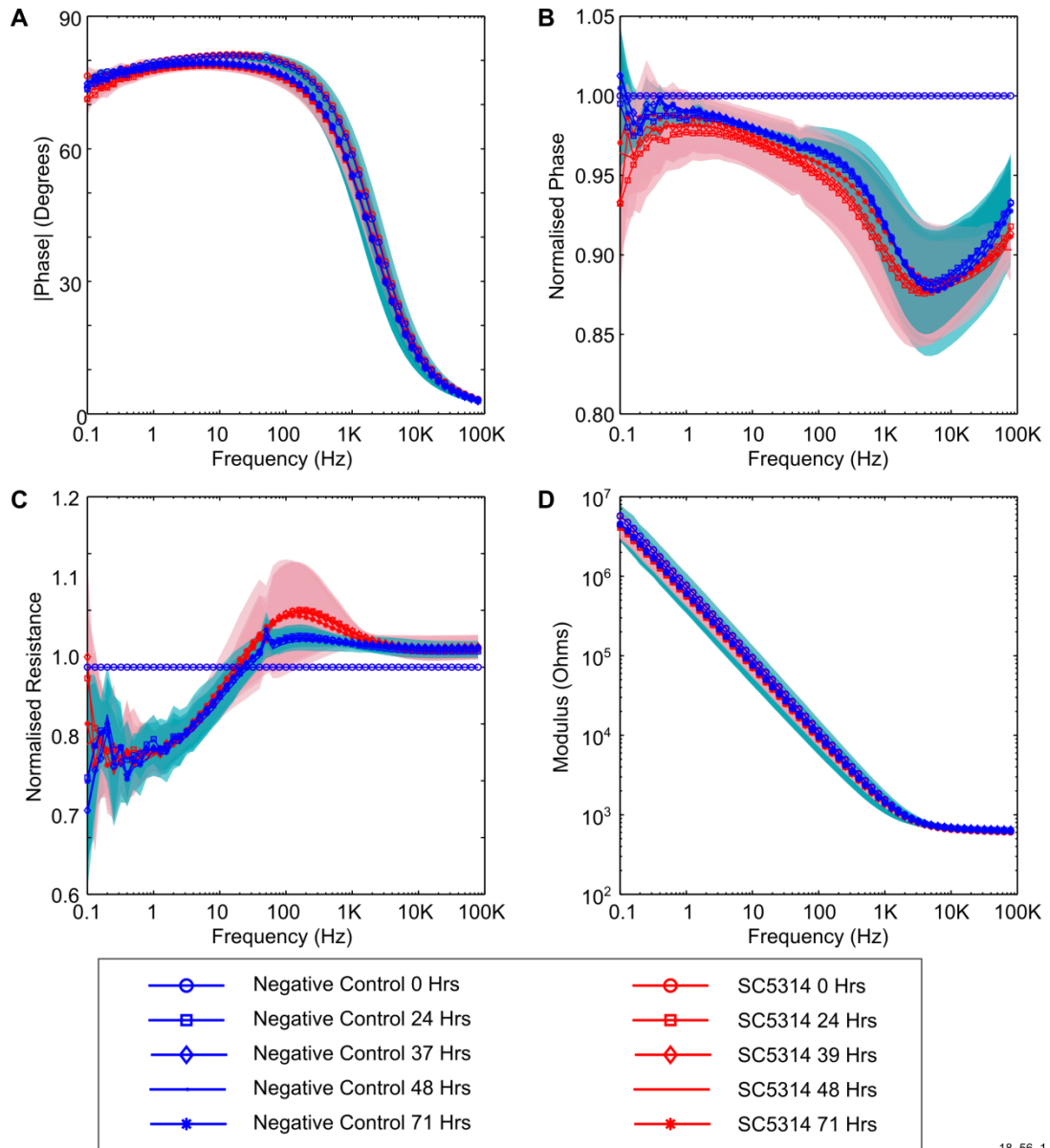


**Figure 5-18: Boxplot showing the difference between *C. albicans* and negative control in normalised resistance data at 500 Hz. Central box lines represent the median value, lower and upper bounds the 25<sup>th</sup> and 75<sup>th</sup> percentile and the whiskers represent the most extreme datapoints. *P* values were calculated using the two tailed Mann-Whitney test. *n* = 3 for both negative control and SC5314 samples.**

### 5.3.3.2 Impedance measurement with *C. albicans* in ASM and polymicrobial impedance investigation with *P. aeruginosa* and *C. albicans*

*C. albicans* was incubated in ASM media to explore the performance of the electrode at detecting the microorganism within the model CF environment. As with the previous experiments involving the ASM model, *C. albicans* was grown *in situ* in five electrode chambers over 72 hours under microaerophilic conditions (see section 3.5.5 for detailed method). In addition, four chambers were inoculated with a polymicrobial culture consisting of *P. aeruginosa* and *C. albicans* together, started at an equal cell densities.

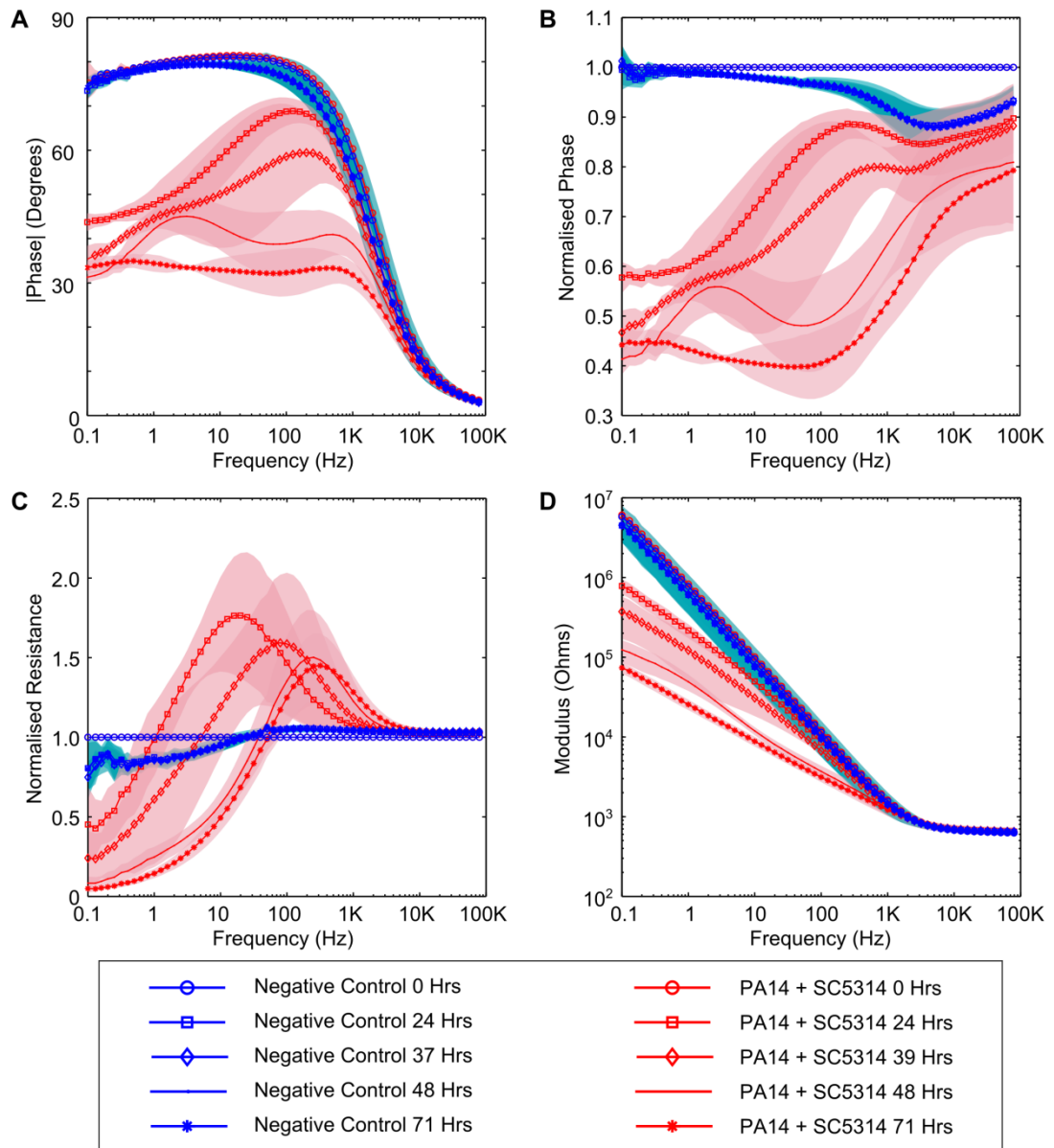
In the impedance signature, few differences were identified between the negative control and the electrode chambers inoculated with *C. albicans*. A small peak is present in the normalised resistance data. The results indicate that there is no significant difference in the impedance as a result of the growth of *C. albicans* in a monoculture (Figure 5-19). The mean normalised resistance data suggests that a peak exists at 200 Hz where *C. albicans* is grown, although this is not significantly different to the negative control. Application of peak detection algorithm did not reveal any consistent peaks in the normalised resistance data. A peak was consistently observed in four of the five chambers inoculated with *C. albicans*, at around 200 Hz with amplitude of around 1.1. However, peaks were also sporadically detected in the negative control data at similar frequencies and amplitudes. A different electrode, designed with a lower impedance, may enable such features to be identified more consistently and a specific signature of *C. albicans* to be elucidated.



18\_56\_1

**Figure 5-19: *In situ* measurement of *C. albicans* SC5314 in ASM over 72 hours. (A) Phase, (B) normalised phase, (C) normalised resistance and (D) modulus. Shading represents  $\pm 1$  SD, SC5314  $n = 5$ , neg ctrl  $n = 4$**

Analysis of the results from electrode chambers containing a polymicrobial culture with *P. aeruginosa* showed similar impedance changes to those seen in the other polymicrobial experiments with *S. aureus* and *H. influenzae*. These include a drop in the phase angle (Figure 5-20 A) and similar peaks to those found in the normalised resistance data when *P. aeruginosa* was grown alone (Figure 5-20 C).



17\_56\_2

**Figure 5-20: *In situ* polymicrobial measurement of *P. aeruginosa* and *C. albicans* in ASM media over 72 hours. (A) Phase, (B) normalised phase, (C) normalised resistance and (D) modulus. Shading represents +/- 1SD, polymicrobial  $n = 5$ ; neg ctrl  $n = 4$ .**

Interestingly, at 48 hours, a pronounced second peak in the phase angle appeared in both the polymicrobial chambers and also the *P. aeruginosa* monoculture (Figure 5-21). This second peak has been seen previously in other experiments under microaerophilic conditions with PA14 (see for example Figure 5-1). The results suggest that subtle differences in the experiment could have an impact upon the observed impedance. For example, if the composition of the ASM used in this experiment differed slightly from previous batches, it may have caused a slight change in the phenotypic behaviour of *P. aeruginosa* which led to an additional change in the impedance. The transient nature of the change also suggests that

it could have been due to a different growth rate, which resulted in the double peak being measured whereas in previous experiments, it was caused by a metabolite which changed in the impedance being only briefly present. Analysis of the two phase peaks from the *P. aeruginosa* monoculture shows that they are both readily detected by the peak detection algorithm (Table 5-5).

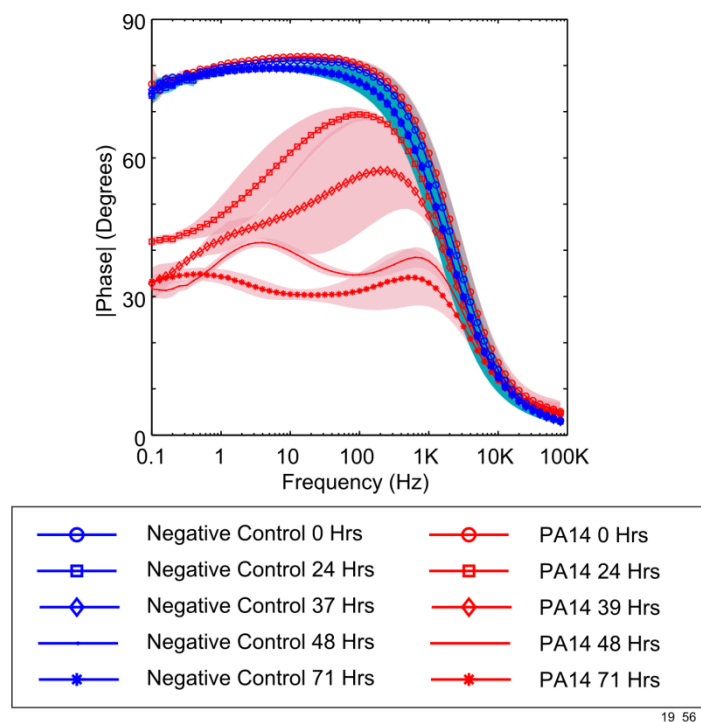


**Figure 5-21: Positive control measurement of *P. aeruginosa* PA14 in ASM, showing similar peaks at 48 hours to those seen in the polymicrobial model with *C. albicans*. Background shading represents +/- 1 SD,  $n = 4$  for both PA14 and negative control.**

**Table 5-5: Identification of peaks in *P. aeruginosa* monoculture at 48 Hours. The location of the high frequency and low frequency peaks were determined using the peak detection algorithm. Only one peak was identified in each of the negative control channels. Ten measurements were performed per frequency decade, therefore the range of the peaks detected at high frequencies is greater than the range at lower frequencies.**

Peak Location	PA14		Negative Ctrl	
	Mean Peak Frequency Hz (SD)	Mean Peak Amplitude Degrees (SD)	Mean Peak Frequency Hz (SD)	Mean Peak Amplitude Degrees (SD)
High Frequency	3.83 (0.8)	41.73 (0.95)	9.75 (12.32)	79.68 (0.68)
Low Frequency	673.75 (99.91)	38.50 (2.12)		



Colony counting was performed out at the end of the experiment in order to determine the number of viable cells in both the polymicrobial cultures and the monocultures. The results indicate that *P. aeruginosa* out-competes *C. albicans* by the end of the experiment (Table 5-6). Additionally, the concentration of *C. albicans* viable cells at the end of the experiment in the monoculture was low. There are two possible reasons for this. Firstly, the cells could have formed pellets during the experiment and fallen to the bottom of the electrode chamber. This is plausible because at the end of each experiment with *C. albicans*, the media appeared clear until it was disturbed by pipetting. When colony counting was carried out, a pellet of cells could have been counted as a single cell. The second reason relates to the ability of the ASM to support the growth of SC5314. This would imply that no growth occurred and the overall viability of the observed cells is lower.

**Table 5-6: Indicative cell densities of planktonic cells at the end of the experiment (nd. = not detected).**

Sample Type	Cell Concentration (CFU/ml)	
	Initial (0 hrs)	72 Hrs mean (range)
PA14 Mono	$1.36 \times 10^7$	$1.02 \times 10^9$ ( $9.5 \times 10^8 - 1.25 \times 10^9$ )
SC5314 Mono	$1.6 \times 10^6$	$2.0 \times 10^3$ (n.d. - $9.7 \times 10^3$ )
PA14 Poly	$1.36 \times 10^7$	$5.14 \times 10^8$
SC5314 Poly	$1.6 \times 10^6$	n.d.

In summary, the experiments with *C. albicans* indicate that the presence of *P. aeruginosa* in a polymicrobial context still causes a change in the impedance. The results also suggest that slight changes could be observed in the normalised resistance as result of *C. albicans* growth in a monoculture. These were not conclusively defined in the experiments carried out here, therefore further work is required to elucidate them more completely. In this study, the focus now shifts toward an exploration of the possible mechanisms behind the impedance changes caused by *P. aeruginosa*, starting with the role that phenazines such as pyocyanin play.

## 5.4 Investigation into role of pyocyanin in *P. aeruginosa* mediated change in impedance

After growth of *P. aeruginosa* in both LB media and ASM, it was noted that there was a colour change when the media was exposed to air (Figure 5-22). *P. aeruginosa* is known to produce a number of coloured secondary metabolites such as pyoverdinin and pyocyanin. In particular pyocyanin, an electroactive secondary metabolite produced by *P. aeruginosa*, changes from blue to clear when it is reduced, and from clear to blue when oxidised and has widely reported electroactive properties (Price-Whelan et al. 2006, 2007; Wang and Newman 2008). Given the well reported redox properties of pyocyanin and other phenazines further investigation was carried out, firstly to confirm that pyocyanin was produced by the strains studied and also to understand the role it plays in impedance.

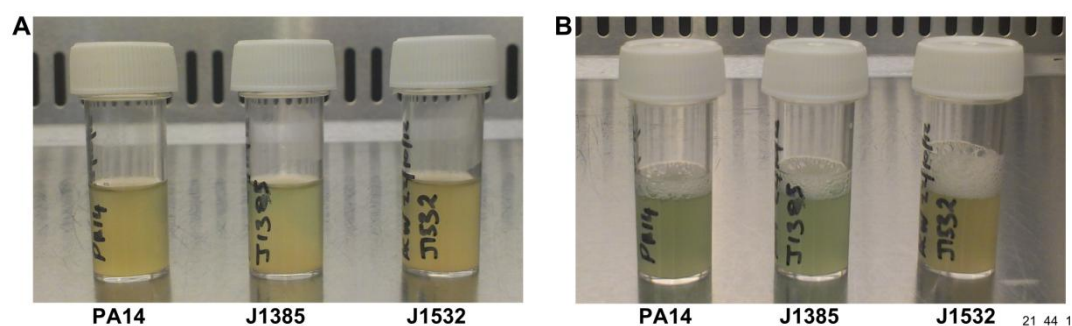
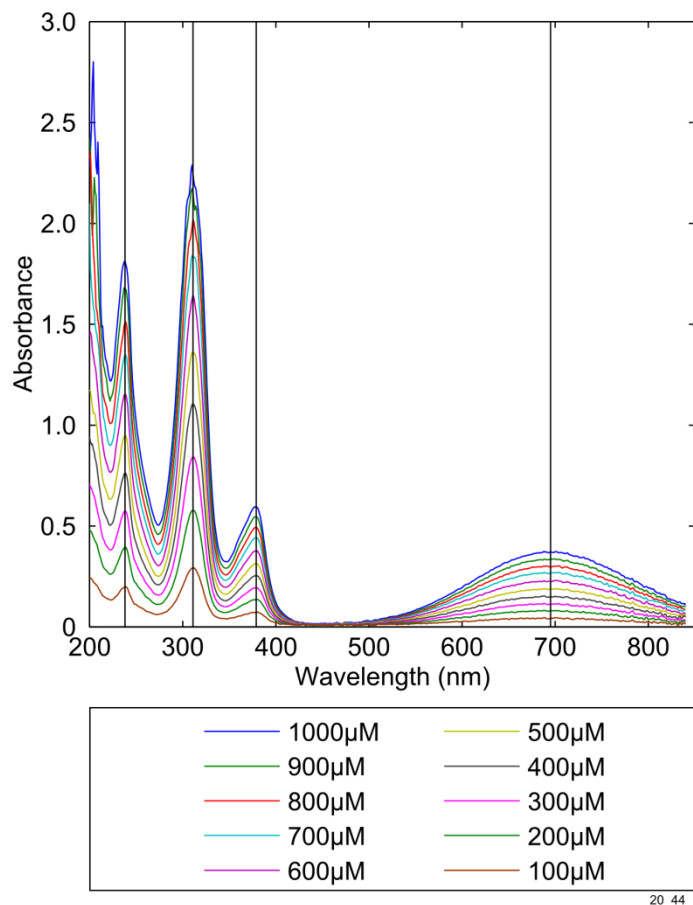


**Figure 5-22: Colour change in media resulting from growth of three different strains of *P. aeruginosa*. (A) Colour of media after 24 hours. (B) Colour of media when air in the headspace is refreshed and culture is agitated.**

### 5.4.1 Identification of pyocyanin within the media

Purified pyocyanin was used to determine the location of the peaks that existed within the UV spectrum. Analysis of the UV visible spectrum showed that peaks were present at 238 nm, 311 nm, 379 nm and 695 nm (Figure 5-23), which was consistent with other findings in the literature (Watson et al. 1986).



20\_44\_1

**Figure 5-23: UV-Visible spectrum for pure pyocyanin at different concentrations, showing peaks at 238 nm, 311 nm, 379 nm and 695 nm.**

The supernatant UV-visible spectrum from spent media after experiments carried out in ASM was measured to determine if pyocyanin was being produced by *P. aeruginosa* (see section 3.6). Peaks below 300 nm were obscured by other compounds, such as amino acids and proteins, present in the media. However, the results show that a similar pattern of peaks exist in the UV-visible spectrum to those found with pure pyocyanin (Figure 5-24). These results suggest that *P. aeruginosa* strain J1532 produces more pyocyanin than strains PA14 and J1385. The concentration can be estimated from the UV-visible spectrum by measuring the absorbance at 690 nm and calculating the concentration using the absorbance coefficient (Price-Whelan et al. 2007), as described in section 3.6.2. In ASM under microaerophilic conditions, these were found to be between 197 μM and 600 μM, after 72 hours depending upon the strain measured.

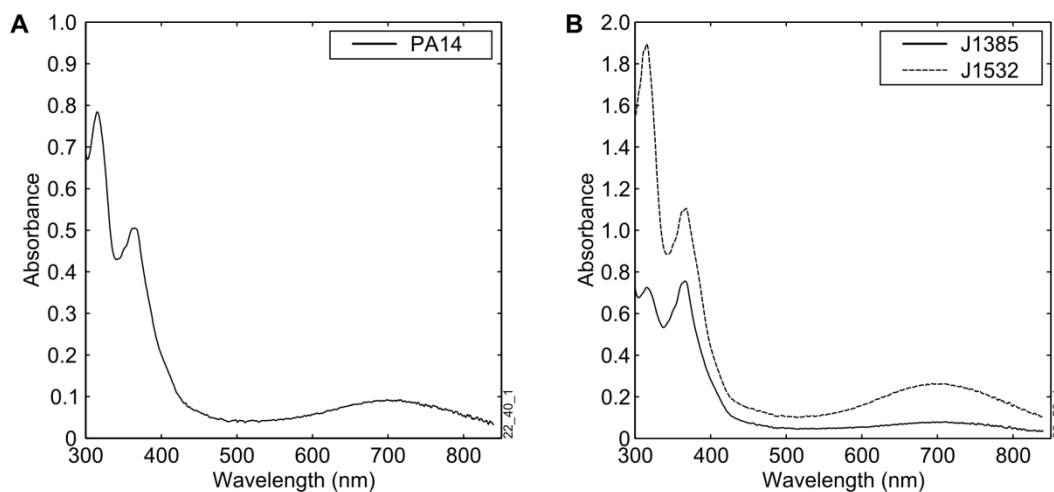
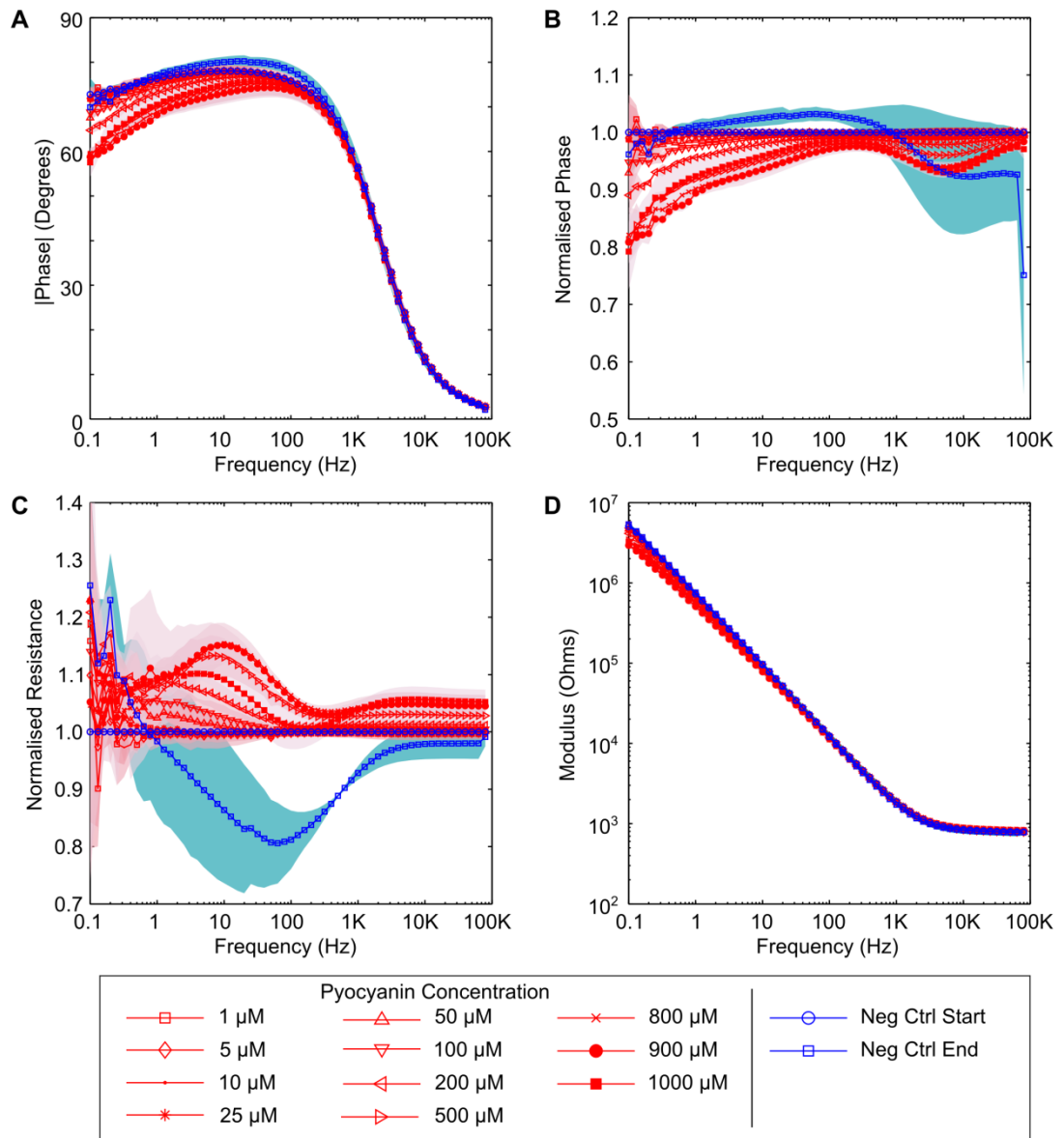


**Figure 5-24: Measurement of the UV-visible spectrum for supernatant following microaerophilic growth in ASM. (A) PA14 supernatant and (B) Supernatant from J-strains (see section 4.4.2 for a description of the J-strains). Spectra (A) and (B) are from separate experiments.**

#### 5.4.2 Impedance assessment of pure pyocyanin added to ASM

Given the electroactive properties of pyocyanin, the effect that purified pyocyanin had on the impedance was investigated. Impedance measurements were taken before and after purified pyocyanin was added to sterile ASM (section 3.6.3). Different concentrations of pyocyanin from 1000  $\mu\text{M}$  to 1  $\mu\text{M}$  were used to determine if changes similar to those observed with *P. aeruginosa* occurred. Recall from above that the typical *in vitro* concentration of pyocyanin found after 72 hours was between 200  $\mu\text{M}$  and 600  $\mu\text{M}$ .

The results show only a slight change in the impedance, unrepresentative of the changes observed when *P. aeruginosa* is grown in either LB media (see for example, Figure 4-10) or in ASM with similar concentrations of pyocyanin (see for example, Figure 5-1). There was little change in the phase angle (Figure 5-25 A), normalised phase (Figure 5-25 B) or the modulus of impedance (Figure 5-25 D). Interestingly, some changes could be seen in the normalised resistance at low frequencies, with similar peaks seen to those at early timepoints in experiments with *P. aeruginosa* (Figure 5-25 C). The greatest changes were seen at low frequencies and high concentrations of pyocyanin (1000  $\mu\text{M}$  to approximately 500  $\mu\text{M}$ ). However, they were unrepresentative of the changes observed when the impedance of a culture containing PA14 (alone or polymicrobial) was measured (Figure 5-26).



23\_44\_2

**Figure 5-25: Measurement of purified pyocyanin in ASM. (A) Phase, (B) normalised phase, (C) normalised resistance and (D) modulus. Shading represents +/- 1 SD,  $n = 3$ .**

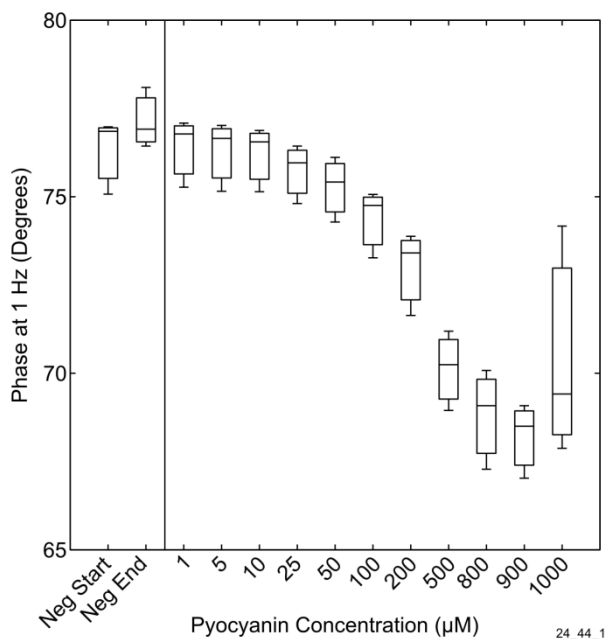


**Figure 5-26: Boxplot of phase angle at 1 Hz as a result of the addition of pyocyanin to the culture. The greatest changes occur when concentrations of more than 100 µM are used.  $n = 3$ .**

### 5.4.3 Exogenous addition of pyocyanin to overnight cultures

The interaction between exogenous pyocyanin and *P. aeruginosa* could explain why there was little change in the impedance in sterile ASM. Specifically, it could be because in the sterile ASM experiments, pyocyanin exists in its oxidised form and therefore no reduced pyocyanin was available to balance the redox reaction at each electrode. Alternatively, pyocyanin could have been just one of multiple electroactive compounds produced by the bacteria that transferred electrons in a chain, with the compounds at an appropriate redox potential compared to the electrode, thus causing a change in the impedance.

A more representative situation was explored, where pyocyanin was added directly to a late log culture of *P. aeruginosa* and *S. aureus* in order to assess the effect it had on the impedance (section 3.6.4). Cultures of *P. aeruginosa* (PA14) and *S. aureus* (RN4220) were grown in ASM microaerophilically overnight to late log phase in 24 well plates. After measuring the impedance of the media, and the impedance of the late log phase cultures, pyocyanin was added to the cultures at concentrations of 100 µM and 300 µM. The results indicated a clear change in the impedance for each of the samples of *P. aeruginosa* (Figure

5-27) and *S. aureus* tested (Figure 5-28). These were more representative of the changes observed when *P. aeruginosa* was grown in either LB media or ASM.

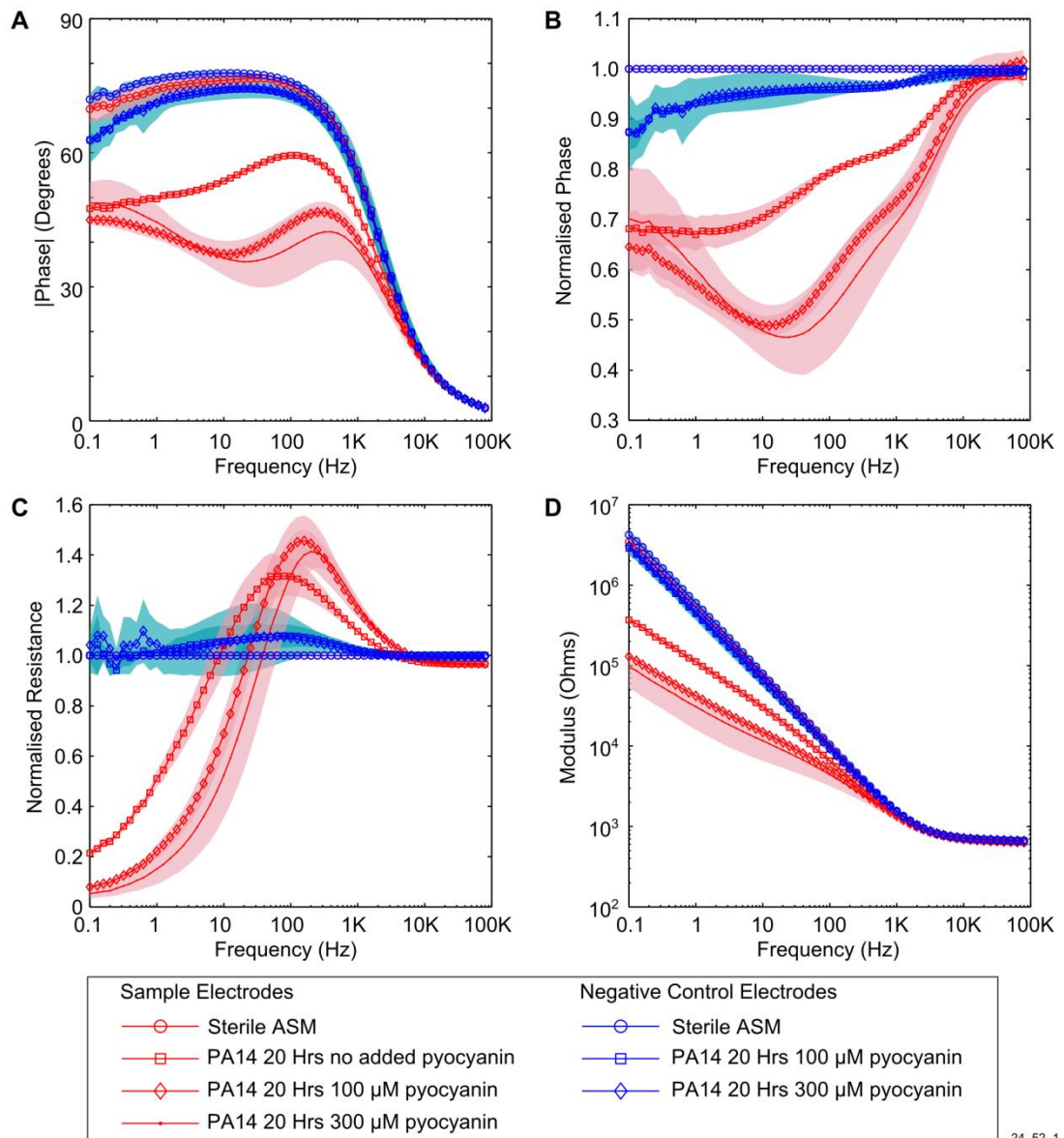


**Figure 5-27: The effect of exogenous addition of pyocyanin on the impedance of *P. aeruginosa* PA14. (A) Phase, (B) normalised phase, (C) normalised resistance, (D) modulus. Shading represents +/- 1 SD,  $n = 3$  for both PA14 and neg ctrl.**

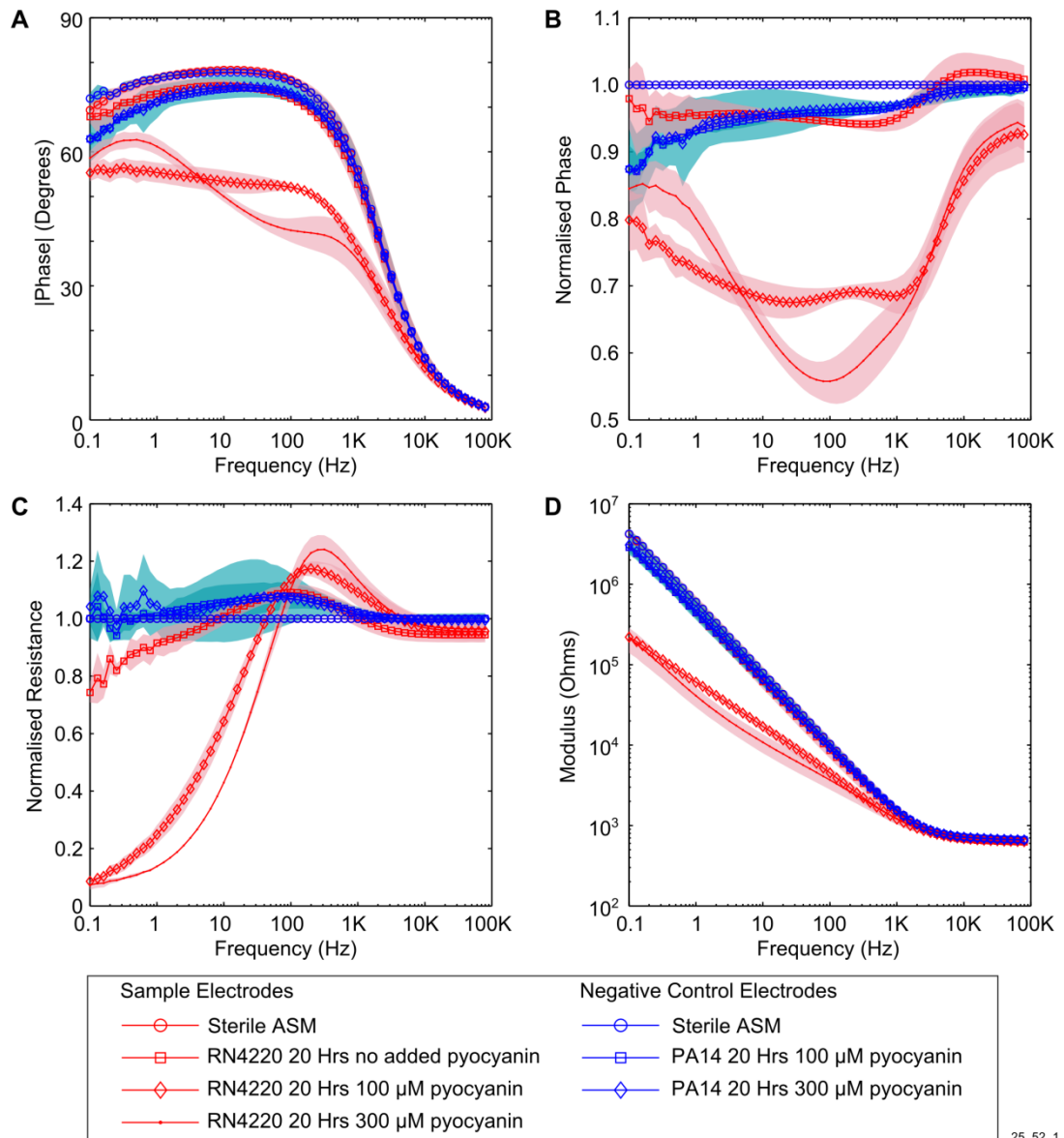


**Figure 5-28: The effect of exogenous addition of pyocyanin on the impedance of *S. aureus* RN4220. (A) Phase, (B) normalised phase, (C) normalised resistance, (D) modulus. Shading represents +/- 1 SD,  $n = 3$  for both PA14 and neg ctrl.**

It was noted when similar experiments were carried out in LB media that the blue pigment resulting from the addition of pyocyanin changed to clear in all but the top layer of each of the cultures (Figure 5-29). As mentioned above, and consistent with cultures of *P. aeruginosa*, on shaking the pyocyanin was rapidly oxidised and returned to its original blue pigment, before gradually being reduced again. This was apparent after five minutes for the culture of *S. aureus* while *P. aeruginosa* took longer to lose its pigment and did so to a lesser degree. These results indicate that pyocyanin plays a role in the observed impedance of



PA14 when grown microaerophilically in ASM. Furthermore, it is clear that the presence of *S. aureus* leads to the reduction of pyocyanin in some manner and a consequent change in the impedance signature.

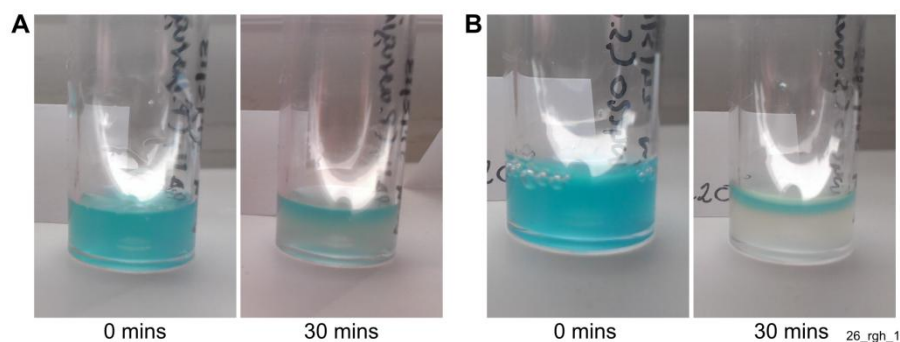


**Figure 5-29: Media colour change following exogenous addition of pyocyanin to overnight cultures of (A) *P. aeruginosa* PA14 and (B) *S. aureus* RN4220.**

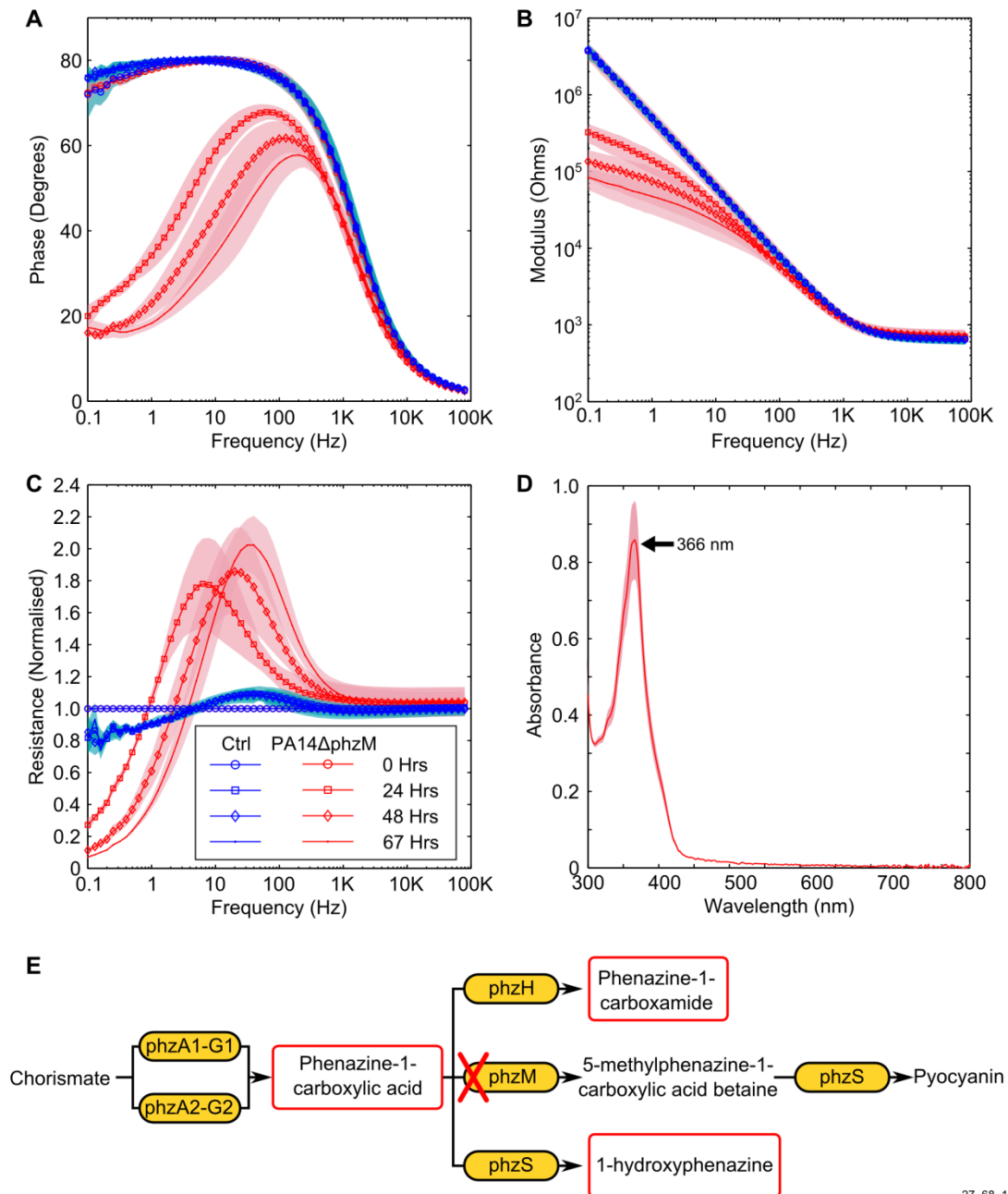
#### **5.4.4 Investigation of impedance changes due to phenazine production in mutant strains of *P. aeruginosa***

The biosynthesis pathway of pyocyanin in *P. aeruginosa* is also responsible for the production of other phenazines, such as phenazine-1-carboxylate (the precursor to pyocyanin), 1-hydroxyphenazine, and phenazine-1-carboxamide (Winsor et al. 2011). Like pyocyanin, these phenazines are redox active (Wang and Newman 2008) and therefore could also have an impact upon the measured impedance.

In order to explore the changes that a culture of *P. aeruginosa* unable to produce pyocyanin would have, the impedance signature of mutant strains of PA14 from the PA14NR set (Liberati et al. 2006) and also the impedance of a double knockout mutant (Dietrich et al. 2006b) were investigated. PA14 $\Delta$ *phzM* is a mutant that produces phenazine-1-carboxylic acid and 1-hydroxyphenazine and PA14 $\Delta$ *phzS* is a mutant that produces phenazine-1-carboxylic acid and 5-methylphenazine-1-carboxylic acid betaine (Mavrodi et al. 2001).

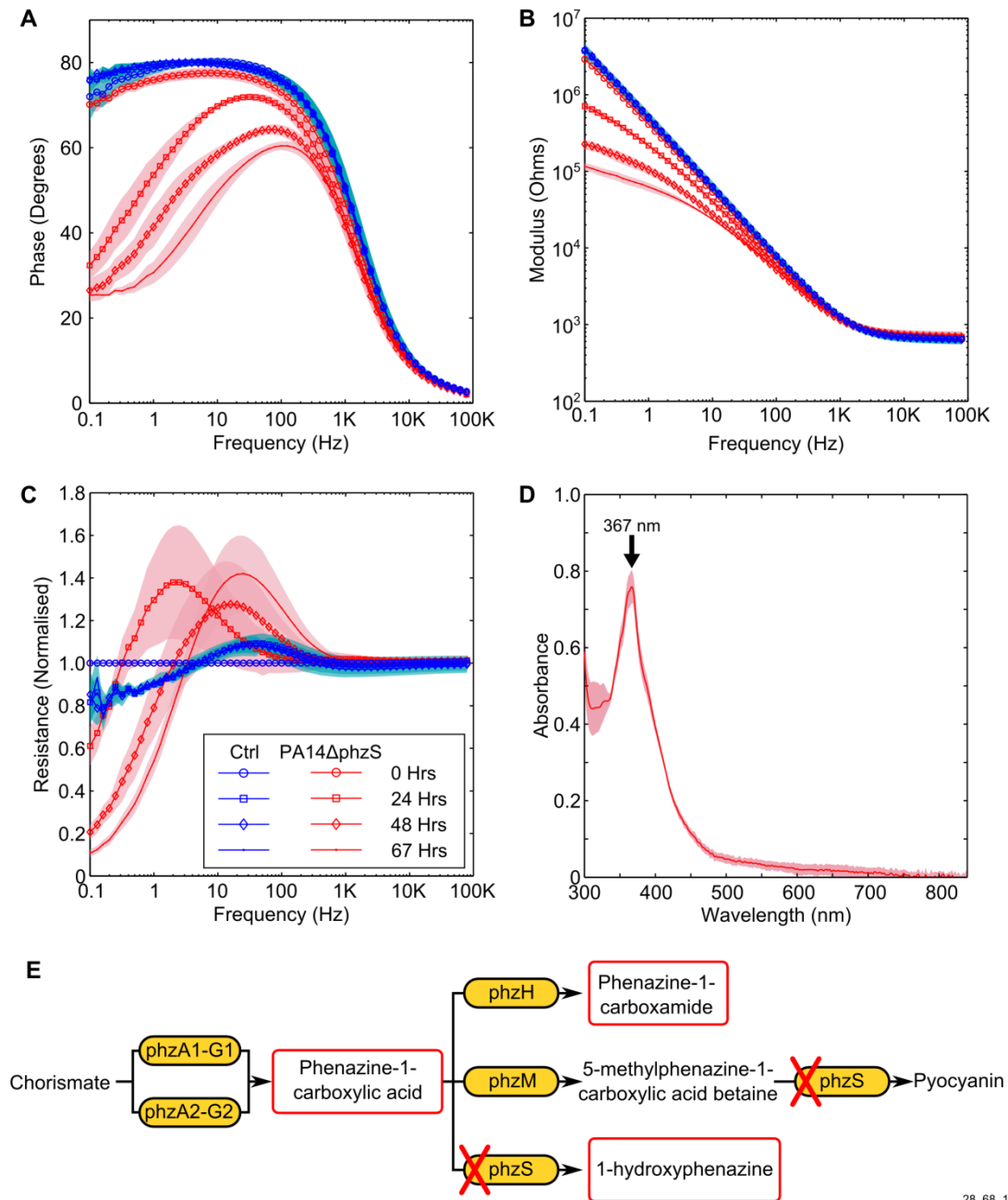
Whilst both PA14 $\Delta$ *phzM* and PA14 $\Delta$ *phzS* were able to produce phenazines, neither of the strains was able to produce pyocyanin. Changes in the impedance phase angle and modulus, and a peak in the normalised resistance were observed in data for both the PA14 $\Delta$ *phzM* and PA14 $\Delta$ *phzS* strains (Figure 5-30 A-C and Figure 5-31 A-C). The UV-visible spectrum shows a peak clearly visible at 366 nm, suggesting the presence of phenazine-1-carboxylic acid (Mavrodi et al. 2001). No peak is present at 698 nm, confirming that no pyocyanin was

produced (Figure 5-30 D and Figure 5-31 D). Although the PA14 $\Delta$ *phzM* and PA14 $\Delta$ *phzS* strains followed the same basic pattern as the wild type strain, a different impedance signature can clearly be seen, particularly in the phase angle and the normalised resistance. This shows that different combinations of phenazine compounds influence the electrode/electrolyte interface (Figure 5-30 E and Figure 5-31 E).



27\_68\_1

**Figure 5-30: Impedance changes caused by the *P. aeruginosa* PA14Δ*phzM* mutant.** Changes to the impedance spectrum can be clearly observed when a mutant of *P. aeruginosa*, unable to produce pyocyanin is measured. Changes to the (A) phase, (B) modulus and (C) normalised resistance are similar to those found in the PA14 wild type. (D) the UV-visible spectrum shows a peak at 367 nm, suggesting the presence of phenazine-1-carboxylic acid. (E) Indicates the biosynthesis pathway for phenazines and shows the effect that the *phzM* knockout is anticipated to have. Background shading represent +/- 1 SD. PA14Δ*phzM* *n* = 3; Neg Ctrl *n* = 3.

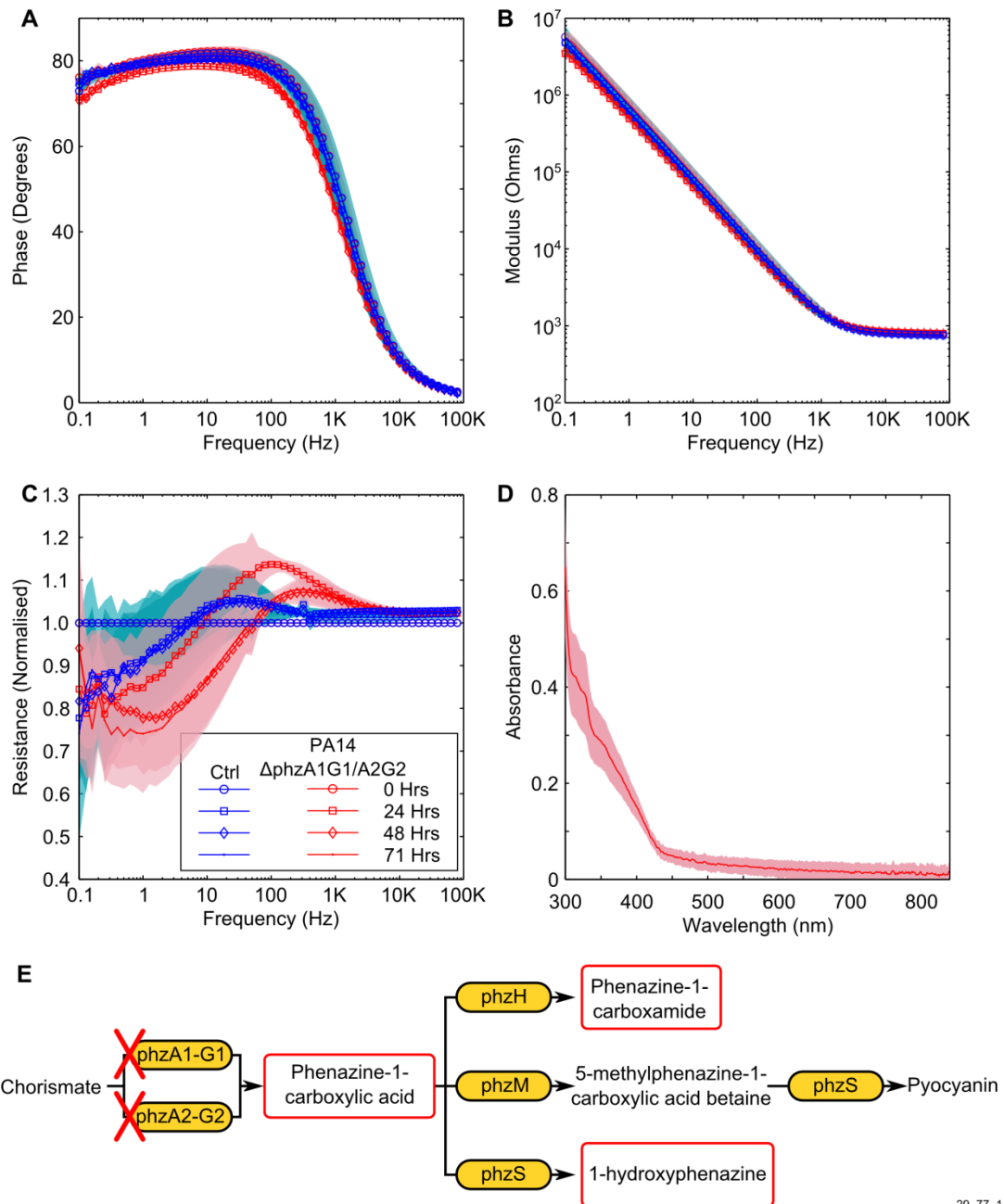


28\_68\_1

**Figure 5-31: Impedance changes caused by the *P. aeruginosa* PA14 $\Delta$ phzS mutant. Similar changes are observable in the (A) phase, (B) modulus and (C) normalised resistance to the wild type and the PA14 $\Delta$ phzS mutant. (D) the presence of phenazine-1-carboxylic acid can also be seen. (E) Indicates the biosynthesis pathway for phenazines and shows the effect that the *phzS* knockout is anticipated to have. Background shading represent +/- 1 SD. PA14 $\Delta$ phzS  $n = 3$ ; Neg Ctrl  $n = 3$ .**

In addition to the two mutants described above, a third double knockout mutant was studied that did not produce any phenazines at all. In this strain, the *phzA1-G1* and *phzA2-G2*

operons have been deleted and therefore the bacteria cannot produce any phenazines (Dietrich et al. 2006b). Unlike the other two mutants, the PA14 $\Delta$ *phzA1-G1/A2-G2* mutant did not result in a significant impedance change in the phase and modulus data (Figure 5-32 A and Figure 5-32 B). A small peak in the normalised resistance data different to the negative control is clearly visible after 24 hours, although this is not of the same magnitude as the wild type or other mutants tested. This suggests a process other than electroactive transfer mediated by phenazines.



29\_77\_1

**Figure 5-32: Measurement of *P. aeruginosa* PA14 $\Delta$ phzA1-G1/A2-G2 double mutant. (A and B) no significant different can be seen in the phase or modulus of the impedance. (C) a small difference in the normalised resistance can be seen, contrasted to the negative control. (D) The UV-visible spectrum indicates that the phenazines present in the wild type or other mutants tested are no present. (E) Indicates the point on the biosynthesis pathway that the double knockout is anticipated to affect. Background shading represent  $\pm 1$  SD. PA14 $\Delta$ phzA1-G1/A2-G2  $n = 4$ ; Neg Ctrl  $n = 4$ .**

## 5.5 SEM analysis of electrode surface following *P. aeruginosa* growth in ASM

In order to explore the interactions between the electrode surface and *P. aeruginosa*, SEM was performed on the electrode surface, as described in section 3.7.2.3. Briefly, electrode coupons were incubated in ASM in 24 well plates microaerophilically over 72 hours. Some of the electrode coupons were incubated perpendicular to the base of the well in order to allow a biofilm to form at the air-liquid interface. This served as a positive control and builds upon the evidence in section 4.5 that *P. aeruginosa* attaches to the carbon electrode.

The positive control shows extensive biofilm at the air-liquid interface. Biofilm-like structures are visible, which appear dehydrated and cracked in places, probably caused by the fixing method (Figure 5-33 A and B). However, microbial attachment is clearly visible, with some cells covered by what is likely to be biofilm matrix. Channel-like structures are also visible within the biofilm (Figure 5-33 C). In contrast, the negative control demonstrates that the electrode surface is porous with several flake-like structures which are probably graphite (Figure 5-34).

Electrode coupons located at the bottom of a 24 well plate were incubated in 1 ml of ASM inoculated with 10  $\mu$ l of *P. aeruginosa* PA14. Consistent with the findings of the epifluorescent microscopy, small groups of colonies were visible on the electrode surface, rather than the extensive biofilm formation seen at the air liquid interface (Figure 5-35 and Figure 5-36). As previously mentioned, the negative control shows the electrode surface consists of a porous structure containing flakes of graphite (Figure 5-34). In contrast, the porous structure was less clearly defined in the samples containing *P. aeruginosa*, incubated at the bottom of the electrode chamber. This suggests that although biofilm formation is more limited at the bottom of the electrode chamber, deposition of extrapolymeric substances could still be taking place.

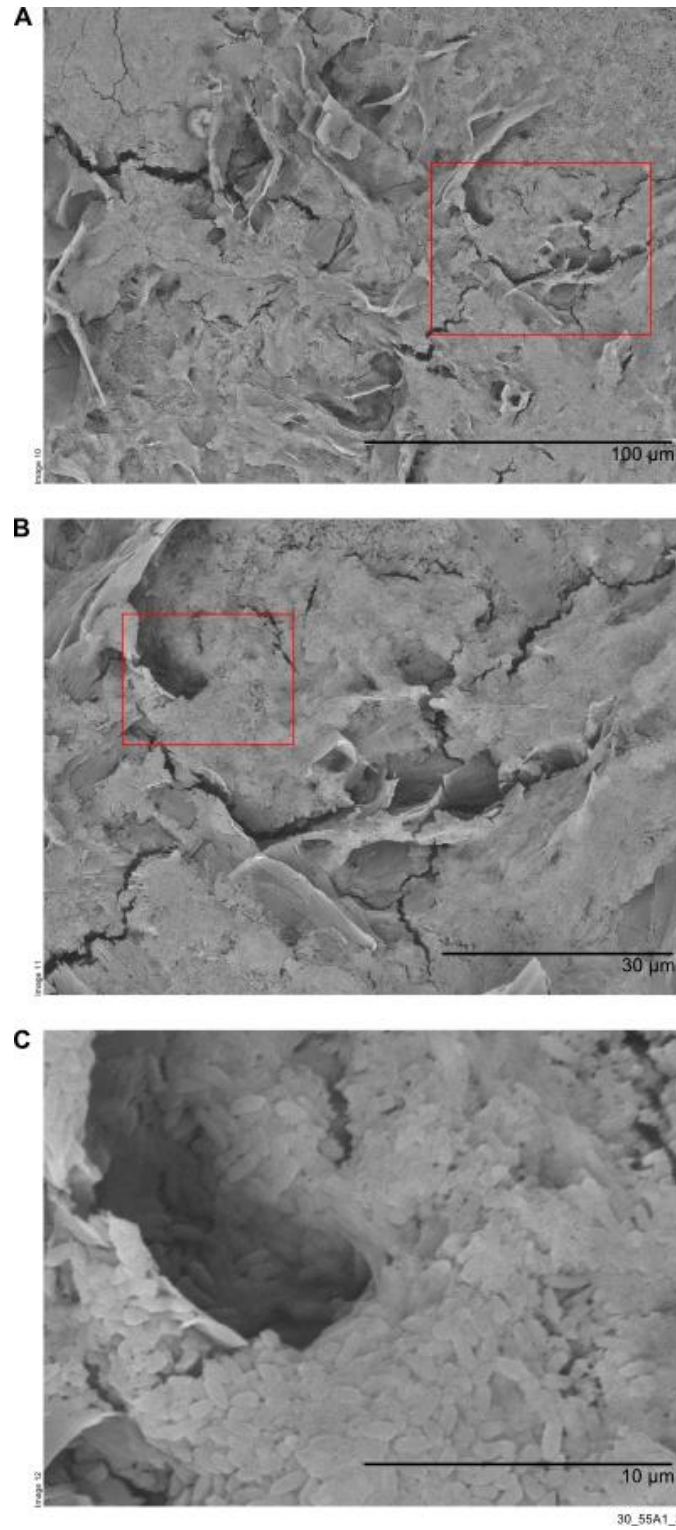


**Figure 5-33: Example SEM images of biofilm formation by *P. aeruginosa* PA14 on the positive control samples. (A) and (B) show dehydrated biofilm structure, (C) shows possible biofilm water channel. Red squares indicate magnified region.**



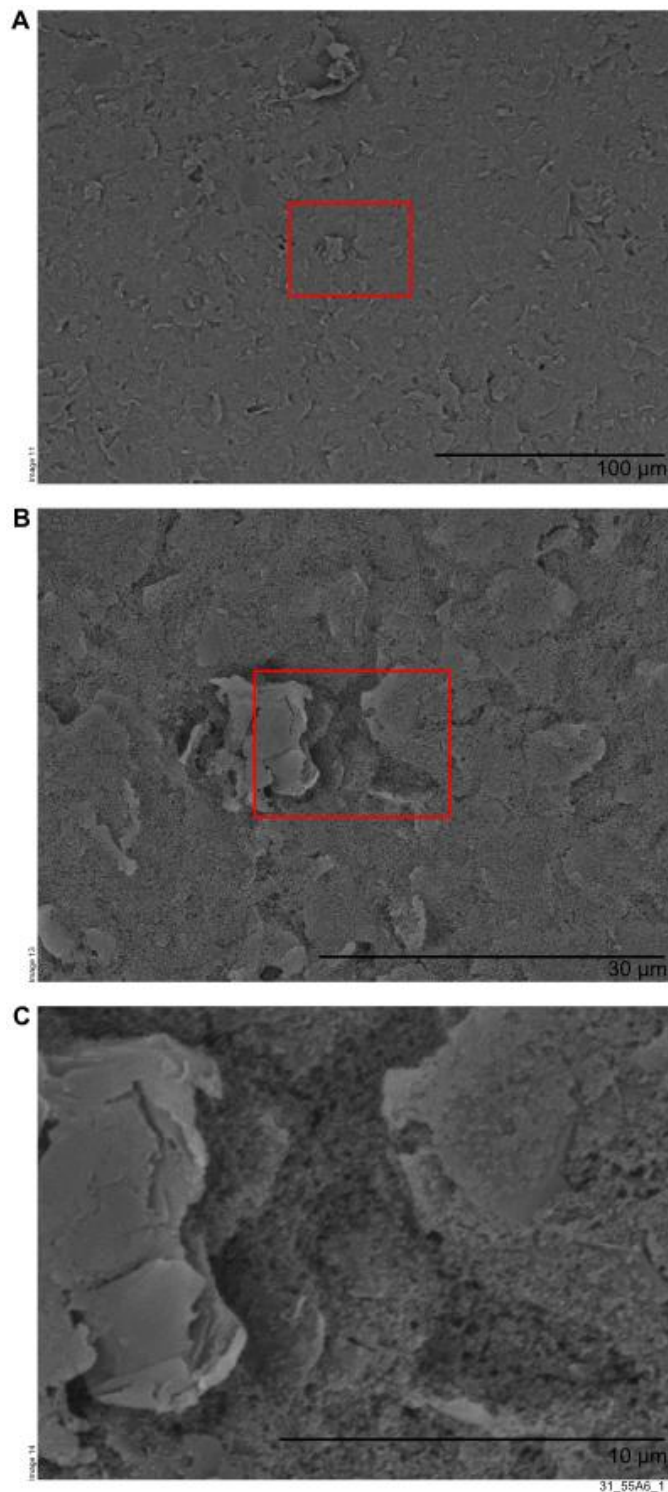


**Figure 5-34: Example SEM images of negative control showing electrode surface. The electrode has a porous surface with large flakes within it, which are probably graphite. Red boxes show magnified regions.**

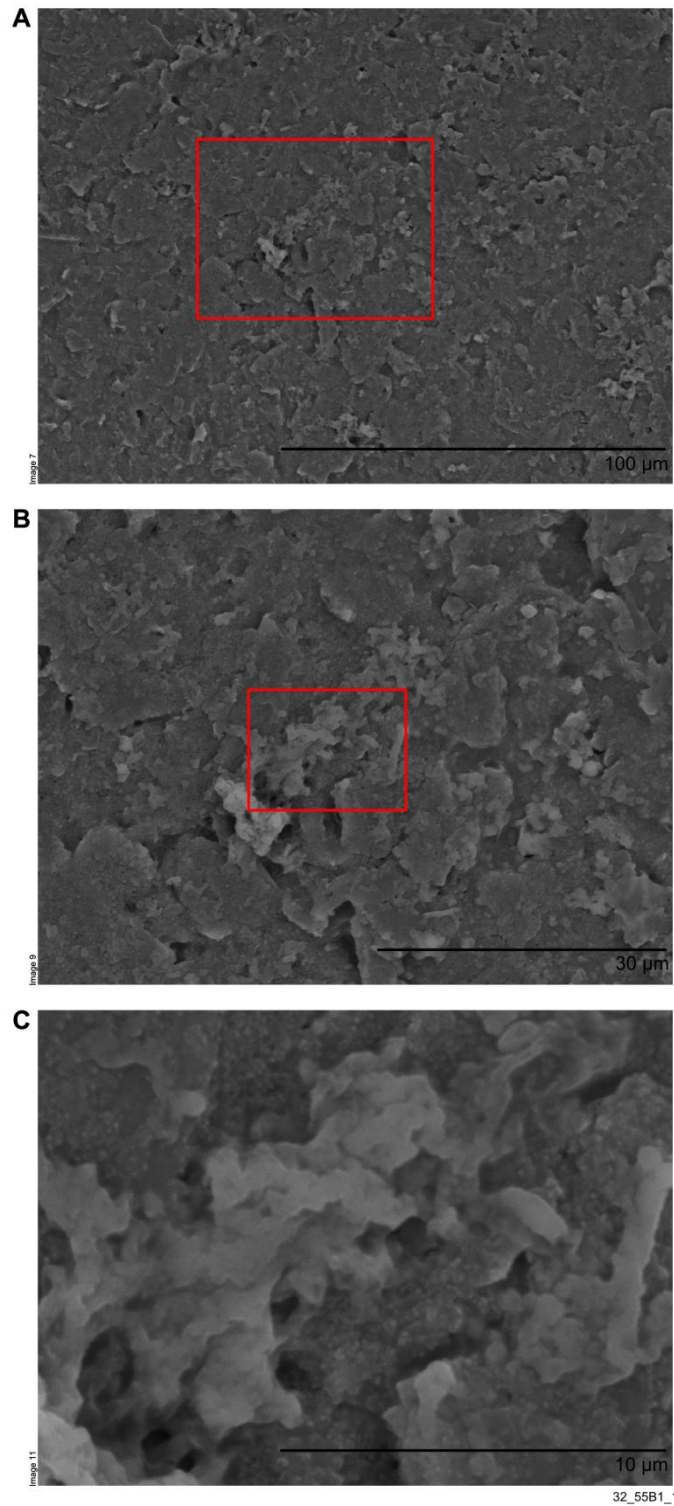


**Figure 5-35: First example of SEM images of *P. aeruginosa* PA14 sample, incubated at the bottom of a 24 well plate. Less biofilm structure exists than is present in the negative control, but small clusters of cells were still evident. Red boxes represent magnified area.**

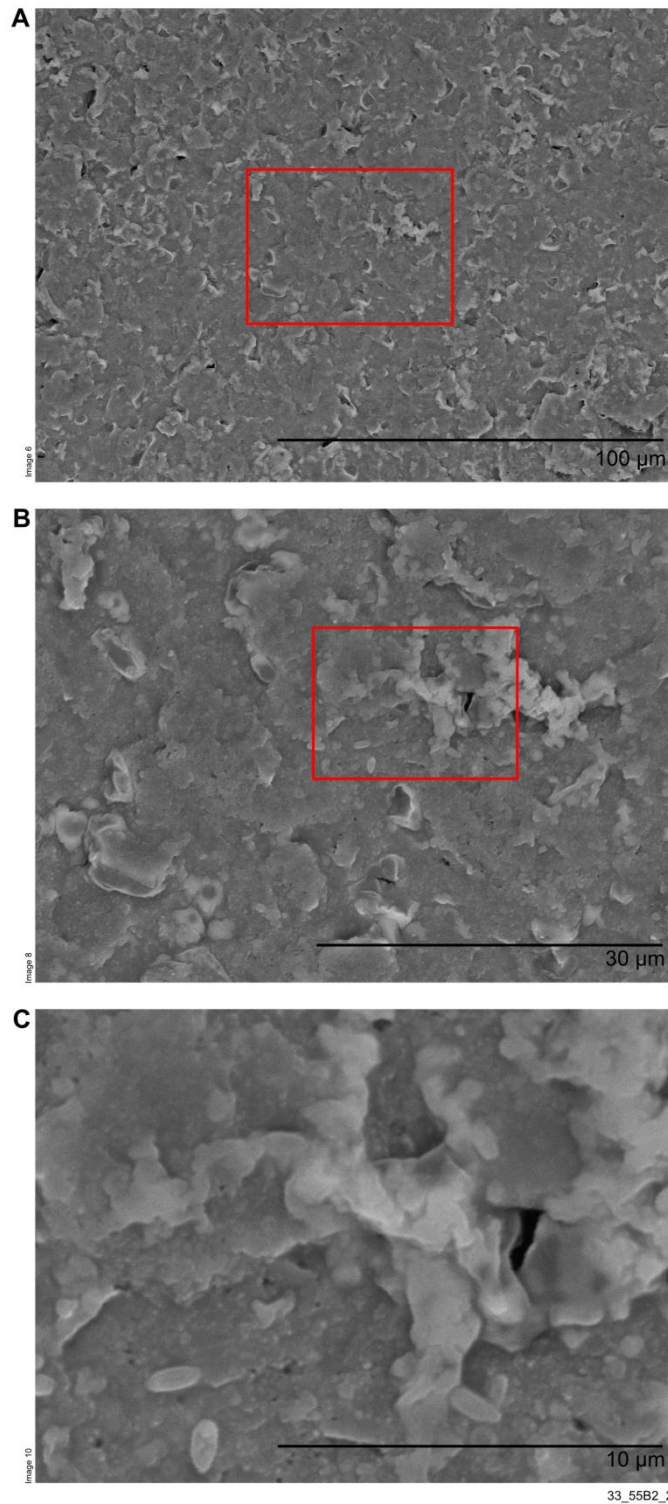


**Figure 5-36: Second example of SEM images of *P. aeruginosa* PA14 sample, incubated at the bottom of a 24 well plate. Less biofilm structure exists than is present in the negative control, but small clusters of cells were still evident. Red boxes represent magnified area.**

## 5.6 Summary

In this chapter, the carbon electrode developed in section 4 was investigated further to determine if *P. aeruginosa* could be detected in an environment representative of the CF airway. As described in section 1.2, CF patients are colonised with a complex microbiome (Harrison 2007). Therefore, a series of studies were carried out with three other species common within the CF airway. The chapter concluded with a study into the underlying mechanisms that could drive changes to the impedance.

The results show that *P. aeruginosa* remains detectable on the carbon electrodes used for this study in conditions designed to be more representative of the CF airway (Kirchner et al. 2012). Interestingly, different changes were seen in the impedance when the other three species of bacteria were studied in both optimal and sub-optimal conditions. *S. aureus* led to small changes in impedance when an aliquot of overnight culture (grown in LB media) was added to the electrode after growth in a universal container. The key changes seen were a peak in the normalised resistance data around 100 Hz and a through in the normalised phase angle at 1 kHz. Some changes to the impedance were found as a consequence of *H. influenzae* growth, *ex situ*. A greater drop in the normalised phase angle contrasted to the negative control at low frequency. This was observed across three out of five of the experiments carried out and suggests that electrode optimisation could allow a signature for *H. influenzae* to be elucidated. Experiments with *C. albicans* did not yield any significantly different changes to the impedance contrasted to the negative control. However, further development of the electrode could allow some of the small changes seen in the impedance to be elucidated. In summary, therefore, further studies are required to fully explore the impedance changes caused by *S. aureus*, *H. influenzae* and *C. albicans*.

None of the changes observed in the impedance were the same as those found with *P. aeruginosa*. Throughout all of these experiments, *P. aeruginosa* resulted in higher cell densities than the other microorganisms tested, even when they were tested under optimal conditions. This could suggest that *P. aeruginosa* causes impedance changes because it is better adapted to conditions within the electrode chamber and grows to higher cell densities. However, investigation of the underlying causes for the changes in impedance with *P. aeruginosa* suggests that this is not the primary reason.

In the next section of this chapter, the ability of phenazine secondary metabolites to drive a change in the impedance was explored. By making use of the *P. aeruginosa* PA14 non

redundant mutant library and a double knockout mutant, it was demonstrated that the production of redox active secondary metabolites caused a large change in the impedance of *P. aeruginosa*. Furthermore, the ability of the electrode to detect these changes in a labelless and reagentless manner could make it useful as a diagnostic tool for *P. aeruginosa* infections in a number of different contexts.

The work with phenazine mutants also re-opened another question raised at the outset of this project: does microbial attachment and biofilm formation cause a change to the impedance? Specifically, the use of the double knockout mutant showed that there is still a small change in the impedance even when no phenazines are produced. This implies that other impedance-changing mechanisms could be at play.

This chapter concludes with SEM study of the electrode surface following growth in ASM. This shows that microbial attachment and biofilm formation are possible on the electrode surface, although to a much lesser degree at the bottom of an electrode chamber or well, presumably because of the disadvantageous position in the competition for oxygen, contrasted to the air liquid interface (even under microaerophilic conditions). Nevertheless, extrapolymeric substances and microcolonies can still be seen on the electrode surface in this location and these could have an impact upon the observed changes in impedance. Further investigation is clearly required to elucidate more about the impedance changes resulting from biofilm formation on screen printed electrodes, including experimentation with electrodes that have a lower starting impedance than those used here to accurately elucidate changes.

**6 DETECTION OF *P. AERUGINOSA* IN HUMAN SPUTUM SAMPLES AND  
FURTHER STUDIES OF ELECTRODE SENSITIVITY**

## 6.1 Introduction

In the previous two results chapters, an impedance signature characteristic of *P. aeruginosa* has been identified. Additionally, experiments with other microorganism common to the CF airway showed that the changes related to the impedance are specific to *P. aeruginosa* within the context of the other species tested.

The investigation was taken further to determine if it is possible to detect the presence of *P. aeruginosa* within human sputum samples. After gaining ethics approval through the Glasgow and Greater Clyde Biorespository scheme (reference number: 139), and the university ethics committee, a total of eight human samples from inpatients were received and tested.

In this chapter, the effect that the widely used mucolytic agent sputasol has upon the impedance was explored. Following this, the device was tested with clinical samples. As a consequence of this initial testing, a number of improvements to the electrode assembly were identified. These are highlighted and described throughout the course of the chapter, along with developmental changes made to the electrode assembly to address these challenges. Following this, clinical samples were used to iteratively test and develop the electrode, resulting in design improvements and changes in the impedance that may anecdotally suggest that *P. aeruginosa* can be detected.

The chapter concludes with the results of a brief experiment that was carried out on the sensitivity of the electrode developed throughout this project. This *in vitro* growth curve experiment was done in order to understand the minimum detection threshold of the electrode in terms of CFU/ml of *P. aeruginosa* under laboratory conditions.

## 6.2 Measurements of *P. aeruginosa* overnight culture in sputasol

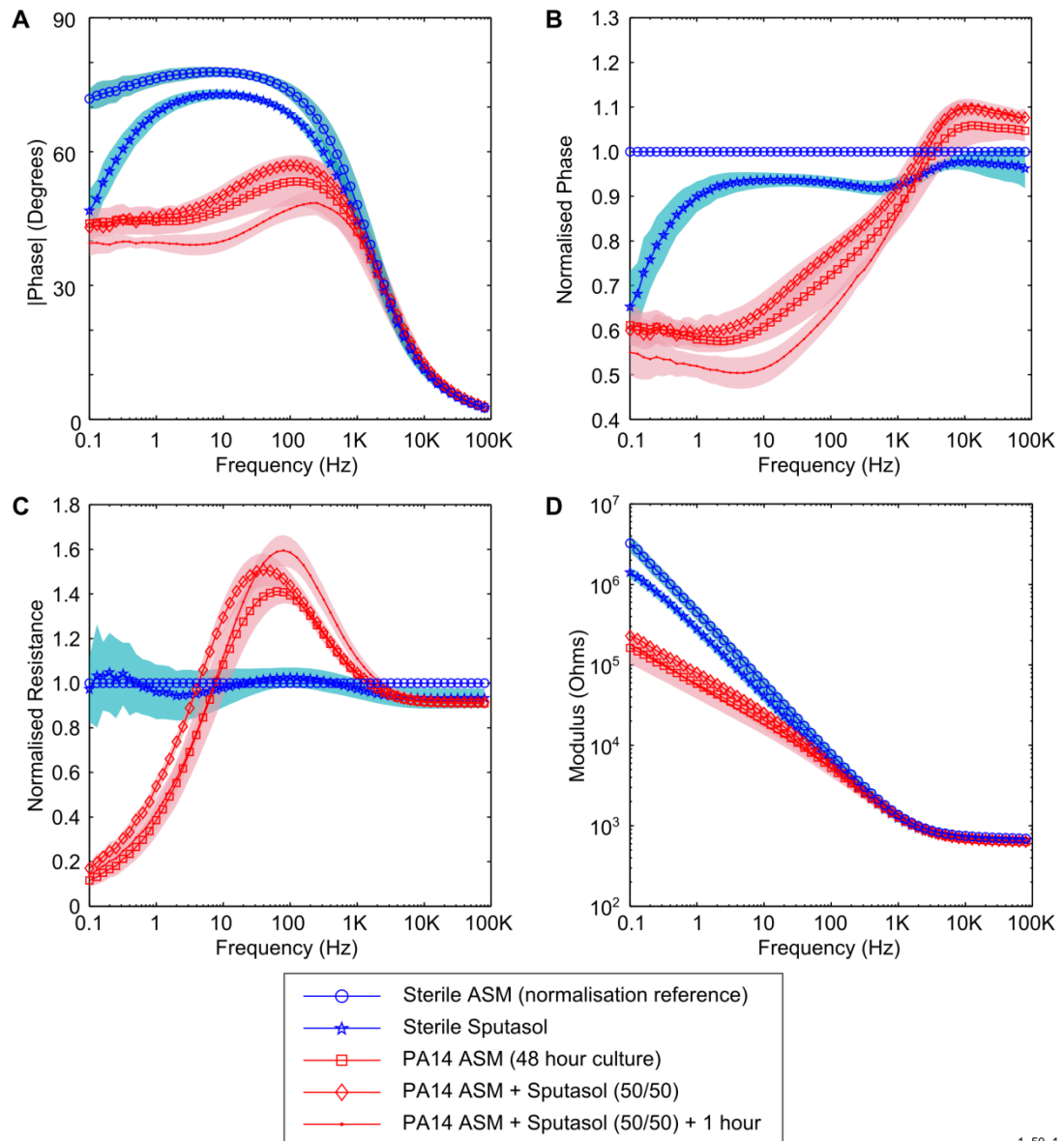
A frequent problem observed with CF sputum samples is the sticky, viscous and heterogeneous properties of the sample. In order to address this, Clinical Microbiologists use mucolytic reagents containing Dithiothreitol (DTT) to allow the dilution of sputum and the retrieval of microorganisms (Cystic Fibrosis Trust 2010). Given the viscous, heterogeneous properties of sputum, a commonly used mucolytic agent (called sputasol, containing DTT) was explored as a tool to help break down the sputum and make *P. aeruginosa* detectable in clinical samples.

DTT is a reducing agent and therefore it could interfere electrochemically with the electrode and affect the detection of *P. aeruginosa*. Therefore, an *in vitro* experiment was carried out in advance of receiving any sputum samples to investigate what effect the addition of sputasol had on a microbial culture. This was achieved by measuring the change in the impedance of aliquot of *P. aeruginosa* (incubated for 48 hours in ASM) when sputasol was added at the concentration recommended by the manufacturer.

It can be seen that there is little change to the impedance signature of *P. aeruginosa* PA14 as a result of adding sputasol to the media (Figure 6-1). Following the addition of sputasol, the culture was incubated for a further hour at room temperature and then the impedance was measured again, to ensure that no longer term changes in the composition of the culture occurred that could negatively affect the signature. Again, the results show that the impedance remains very similar. In fact, the *P. aeruginosa* normalised phase (Figure 6-1A) and the normalised resistance (Figure 6-1C) appear to be slightly more pronounced after one hour.

Interestingly, changes to the negative control as a result of adding sputasol are more pronounced in the phase, normalised phase and impedance modulus data (Figure 6-1 A, B and D). However, only a marginal change between sterile ASM and sputasol is seen in the normalised resistance data (Figure 6-1 C). The greater change to the negative control impedance contrasted to the inoculated culture could be explained by the higher impedance of the control culture contrasted to the inoculated culture which, as described in section 5.4, contains several electroactive species.



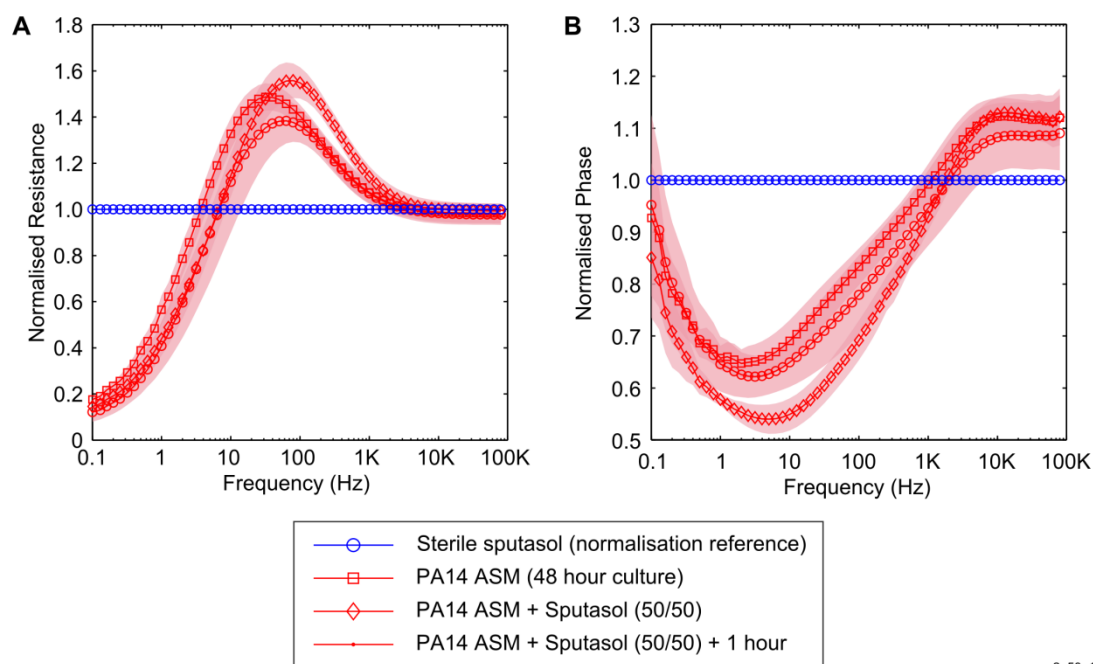


1\_50\_1

**Figure 6-1: Measurement of *P. aeruginosa* PA14 before and after the addition of sputasol, normalised against sterile ASM. (A) Phase, (B) normalised phase, (C) normalised resistance, (D) modulus. Background shading represents  $\pm 1SD$ ,  $n = 4$ .**

Further analysis of the change in the baseline impedance following the addition of Sputasol was carried out to determine the impact that the presence of sputasol would have if it was present in the starting normalisation measurement. To achieve this, the data from the above experiment were normalised against the sterile sputasol measurement (Figure 6-2A). This helped to determine if it was appropriate to include sputasol in the blanking media in experiments with human samples. The results indicate that the normalised resistance signature for *P. aeruginosa* PA14 remains very similar, to that normalised against sterile

ASM, with a peak still present between 100 Hz and 1 kHz. In contrast, there are some low frequency changes to the shape of the normalised phase data, as would be expected from the change in the phase angle in sputasol at low frequencies (Figure 6-2B). On the basis of these measurements, it was decided to use sputasol to carry out a blanking measurement on the first set of human sputum samples received. As discussed in the next section, the use of sputasol was important in the first set of experiments with human samples, because it ensured that the sputum could be placed effectively into the electrode chamber.



2\_50\_1

**Figure 6-2: Measurement of *P. aeruginosa* PA14 in sputasol, normalised against sterile sputasol. (A) normalised resistance, (B) normalised phase. Background shading represents  $\pm 1$  SD  $n = 4$ .**

## 6.3 Electrode performance in human sputum samples and experimental development

### 6.3.1 Sputum samples one and two

Initially, two human sputum samples were received and measured. On receipt of the samples, it was found that they were difficult to handle and, without the use of sputasol, it was not possible to fit them into the electrode chambers. Therefore following the collection of the samples blanking measurements were carried out in sputasol on a set of six electrodes, conditioned as previously described (see section 3.4.3). Prior to blanking and

measurement of the sputum samples, the electrodes were sterilised in 70% v/v ethanol for 10 minutes. After an impedance sweep in sputasol, each sample was measured by placing an aliquot into the electrode chamber. After this measurement, samples were homogenised in sputasol and impedance measurements were repeated.

The electrodes were successfully conditioned in 0.9% w/v NaCl the day before the experiment, and had highly consistent signatures (Figure 6-3 A). However, when the blanking measurements were carried out in sputasol immediately prior to the measurement with the sputum samples, some of the electrodes were found to have inconsistent signatures, unlike those expected and seen previously in sputasol (Figure 6-3 B). Therefore, only data from electrodes 1, 4 and 5 is analysed below. It was noted that even for these electrodes, the baseline impedance measurement was different and not as consistent as described in the *in vitro* experiment above (section 6.2).

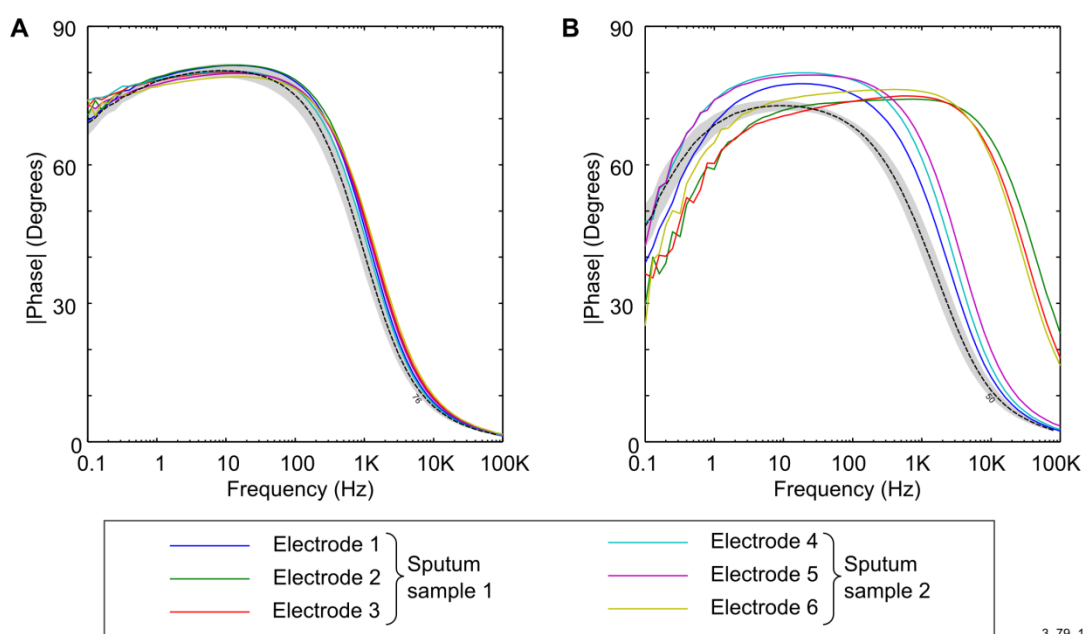
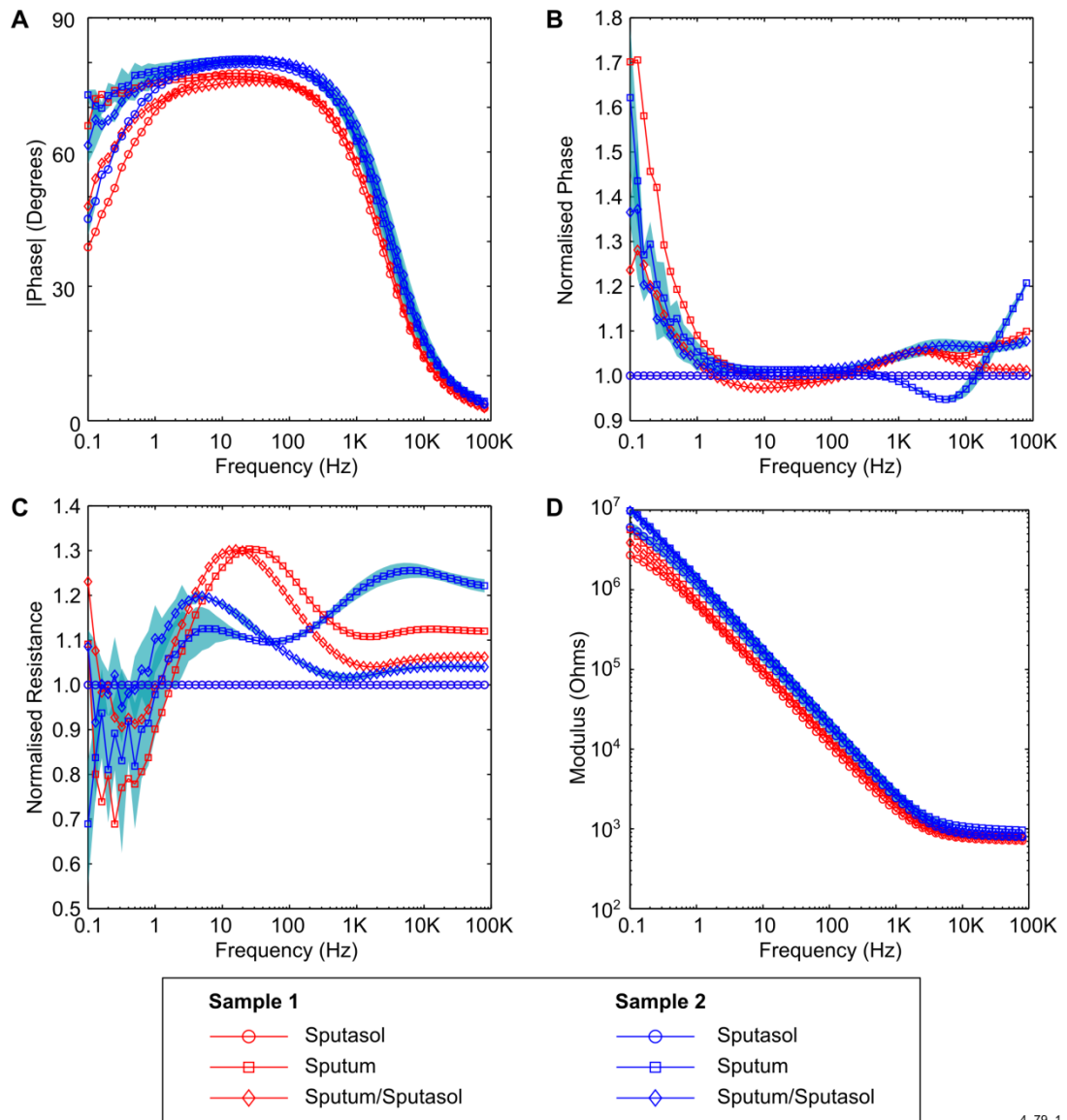


**Figure 6-3: Individual baseline measurements of electrodes used for testing of first two human sputum samples. (A) Baseline measurements carried out in 0.9% w/v NaCl and (B) baseline measurements carried out in sputasol. The black dashed line represents mean data for equivalent baseline measurements from a different experiment, for these, the SD is shown as grey shading,  $n = 4$  for NaCl and  $n = 3$  for sputasol.**

As described above, both sputum samples were thick and viscous, which made handling them challenging and in particular made it difficult to get the sample into the electrode chamber. In the first sample, the sputum was covered by a large quantity of saliva.

Therefore it was unlikely that the sputum itself was in contact with the electrode. The impedance results were blanked against sweeps carried out in sterile sputasol. The phase data shows that there is little difference between the sputasol negative control and the sputum/sputasol mixture (Figure 6-4 A). Additionally, from the phase data, the same changes that were present within the culture experiments with *P. aeruginosa* are not evident. When both sputum samples have been treated with sputasol, it is clear that they appear the same as each other whereas prior to this, each had a unique signature. This can be seen at high frequency in the normalised phase angle (Figure 6-4 B) and also across the entire normalised resistance frequency spectrum (Figure 6-4 C). Specifically, it can be seen from the normalised resistance spectrum that there is a difference in the peak frequency between the two samples before they are treated with sputasol.



4\_79\_1

**Figure 6-4: Measurement of first two human sputum samples, blanked against sputasol. (A) Phase, (B) normalised phase, showing differences in unmodified sputum between samples at high frequency, (C) normalised resistance showing differences in the locations of peaks in unmodified sputum, (D) modulus. Background shading represents  $\pm 1$  SD, sample 1,  $n = 1$ ; sample 2  $n = 2$ .**

After impedance testing, microbial analysis of the samples was carried out as described in section 3.9.6. Briefly, colony counting was carried with an aliquot of sputum on Pseudomonas Agar Base with CN supplement (PAB + CN) and Gram positive bacteria using Mannitol Salt Agar (MSA) (Table 6-1). The results indicate that for sample 1, only one CFU was cultured on PAB+CN. In contrast, the results for sample 2 show a higher

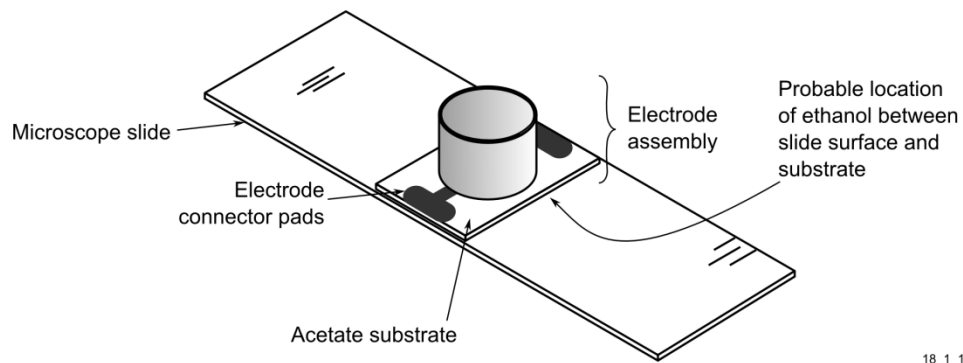
concentration of CFU/ml. Growth on MSA indicates that both samples were populated with a number of Gram positive bacteria.

**Table 6-1: Microbiological analysis of sputum samples**

Selective Agar	Colony forming units per ml	
	Sample 1	Sample 2
<i>PAB + CN supplement</i> (for <i>P. aeruginosa</i> )	< 1	3 x 10 <sup>5</sup>
MSA (for Gram negative)	1.12 x 10 <sup>6</sup>	3.65 x 10 <sup>5</sup>

Testing with the first two sputum samples suggests that differences exist in the normalised resistance signature between the un-modified sputum samples. However, both samples have a similar impedance signature when mixed with sputasol. This suggests that the addition of sputasol could mask small changes in the impedance caused by *P. aeruginosa*. This is likely given that the large changes in impedance observed when *P. aeruginosa* is grown in a monoculture were not seen (see Figure 5-1 for example of *P. aeruginosa in vitro* experiment in ASM). Initial testing also shows that the thick, viscous nature of the sputum samples made it difficult to get them into the electrode chamber and in contact with the electrode.

The baseline performance of the electrodes was dramatically different and far more inconsistent than that found in any previous experiment, with very little consistency across electrodes. The cause of these problems (Figure 6-3) was difficult to identify. The only treatment the electrode received prior to the impedance measurement was with 70% v/v ethanol for sterilisation. This could have caused the impedance inconsistencies. If the ethanol had not fully evaporated on the underside of the electrode chamber (Figure 6-5), it would have affected the impedance by providing an alternative current path, resulting in erroneous results. Prior to collecting further sputum samples, these issues were addressed.

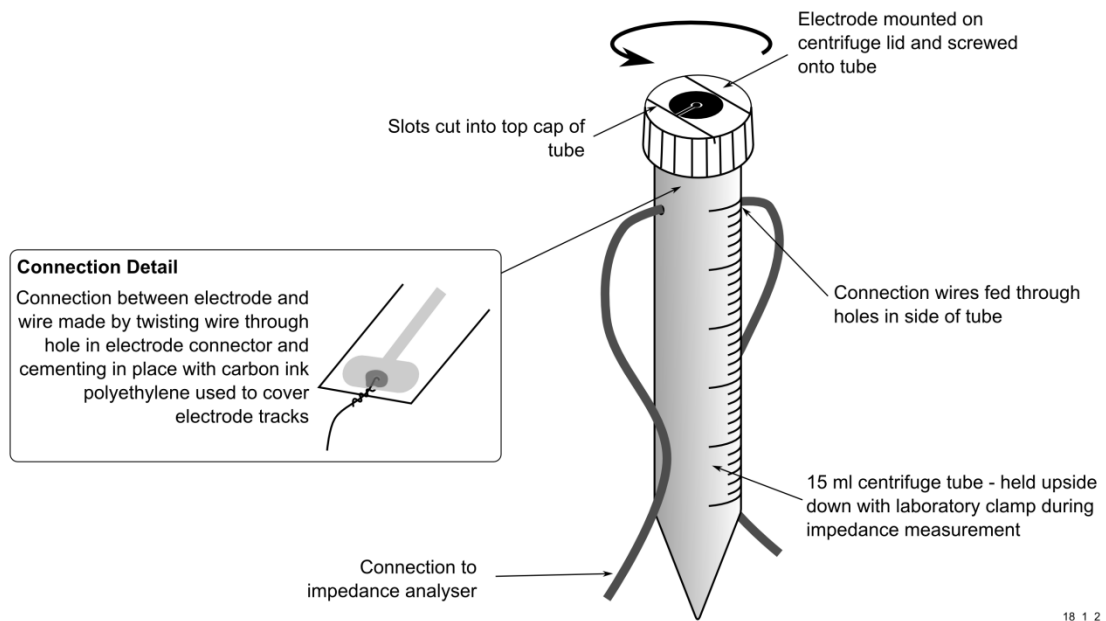


18\_1\_1

**Figure 6-5: Cartoon of electrode assembly, showing where small quantities of residual ethanol after sterilisation may have affected the impedance.**

### 6.3.2 Design two electrode assembly

As described above, some development of the electrode was carried out to make it more practical for the testing and measurement of human samples. The electrode assembly was adapted to make it possible to apply directly to a sputum sample in a 60 ml specimen container, which was the same type of container that the samples were typically provided in (Figure 6-6). This was achieved by integrating the electrode into the lid of a 15 ml centrifuge tube (see section 3.9.5.1 for full description of assembly). In addition, adhesive backed polyethylene was used to cover the track leading up to the electrode, instead of dielectric paste. This was done to prevent problems associated with the dielectric paste cracking when the electrode was flexed, potentially exposing the electrode track to the sample and affecting the impedance. With the modified assembly, the electrode could be pushed down onto the sputum sample and held in place on the sample with a test tube stand (Figure 6-7). This approach had the benefit of removing the need to use sputasol to homogenise the samples as the electrode could be more precisely applied to the sample. Immediately prior to the measurement on sputum, an impedance sweep was carried out in normal saline to verify that no changes had occurred to the electrode since the electrode conditioning process.



18\_1\_2

**Figure 6-6: Cartoon of design two electrode assembly.**

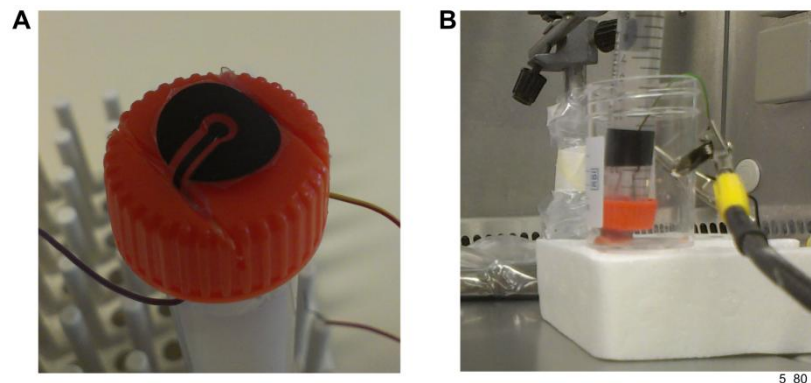


**Figure 6-7: Electrode assembly development. (A) View of electrode surface integrated into 15 ml centrifuge tube, (B) electrode applied to sputum sample in an experiment.**

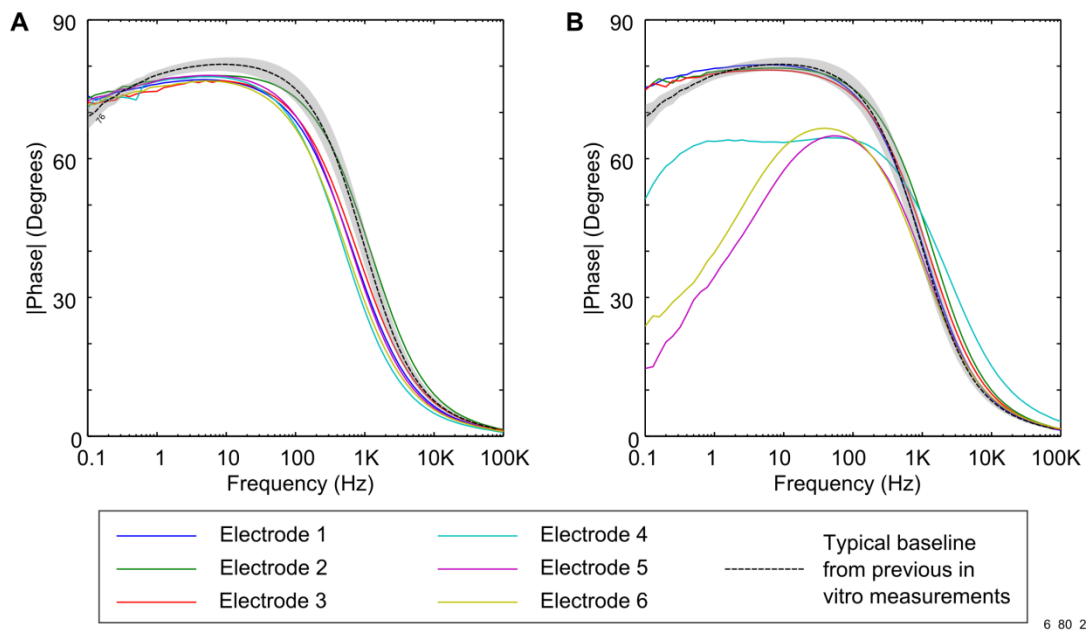
### 6.3.3 Testing sputum samples three, four and five

After modifications had been made to the electrode assembly, six electrodes were conditioned in preparation for receipt of the next sputum samples. Although all the electrodes were conditioned successfully, the impedance signature differed to that found in previous experiments (Figure 6-8 A). The pre-sweep carried out in saline immediately prior



to measurement in sputum appeared spurious (Figure 6-8 B). To identify the problem, one of the electrodes that gave the spurious result was dismantled and traces of ethanol were found around the connection between the wire and the electrode. Given the similarity of the spurious results with those observed in section 6.3.1, it appears that a similar problem affected the impedance.

Given the clear problems caused by sterilisation in ethanol, particularly with the new assembly, future electrodes were not sterilised prior to measurement of the sputum samples. This was considered acceptable given that the electrode only remains in contact with the sample for a brief period of time. To ensure that the microbiological analysis remained valid, an aliquot of the sputum was aseptically removed prior to the impedance measurement being carried out.

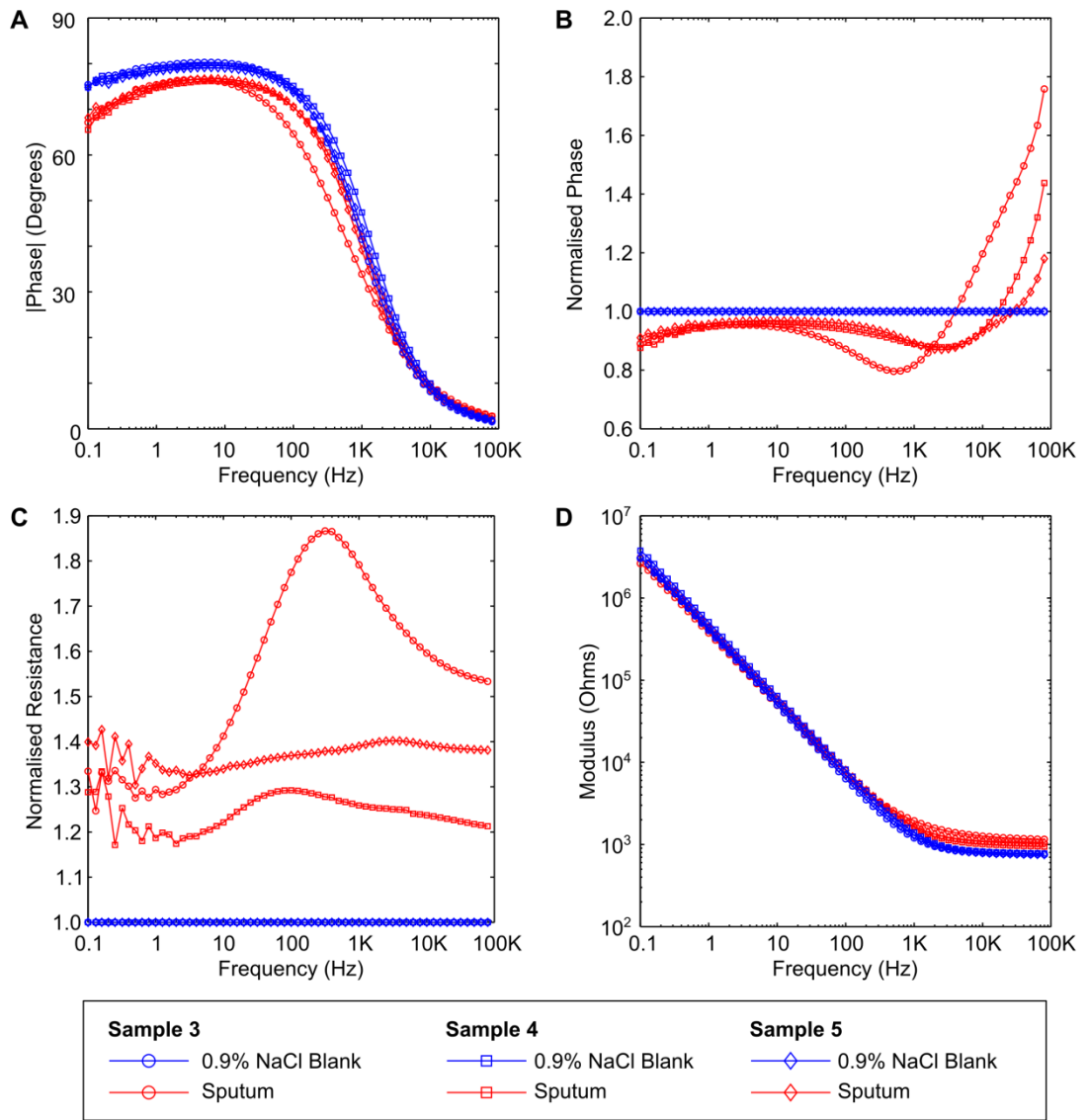


6\_80\_2

**Figure 6-8: Impedance measurements in NaCl prior to sputum measurements (A) measurement immediately after conditioning, (B) measurement immediately prior to measurement in human sputum.**

Given the problems encountered with electrodes 4, 5 and 6 (highlighted in Figure 6-8), they were discarded and not used in the rest of the study with the second set of sputum samples because of their unsatisfactory performance. Three sputum samples were received therefore one electrode was used to measure each sample. The impedance measurements were blanked against the normal saline immediately prior to taking a measurement with the sputum.

The results demonstrate that there are differences between all three of the samples. The phase angle at low frequency for all three samples is lower than the blanking measurement. Interestingly, sample 3 shows a slightly greater trough in the normalised phase angle contrasted to samples 4 and 5 (Figure 6-9 B). The most pronounced change however, is seen in the normalised resistance data with a very large peak present in sample 3 contrasted to the other two samples (Figure 6-9 C). Microbiological analysis of the samples using selective agar also provided interesting results (Table 6-2). These suggest that sample 3 contains the highest concentration of CFU/ml on PAB + CN. Colony forming units were also identified in sample 4 on PAB + CN ( $2.48 \times 10^5$  CFU/ml). However, no pigmentation was seen in these colonies, suggesting they were not *P. aeruginosa*. Bcc was also identified in sample 4 and was found to grow on PAB + CN, therefore the growth observed on this media could have been Bcc.



7\_80\_1

**Figure 6-9: Impedance measurement of second set of sputum samples, blanked against 0.9% w/v NaCl. (A) Phase, (B) normalised phase, (C) normalised resistance and (D) modulus.**

**Table 6-2: Microbiological analysis of samples 3, 4 and 5. Growth on PAB+CN supplement was observed for sample 4, but this could have been Bcc, as the colonies observed were not pigmented.**

Selective Agar	Colony forming units per ml		
	Sample 3	Sample 4	Sample 5
<i>PAB + CN supplement</i> (for <i>P. aeruginosa</i> )	$1.6 \times 10^8$	Unknown	$6.8 \times 10^5$
MSA (for Gram negative)	$6.75 \times 10^3$	$9.5 \times 10^3$	Not detected
<i>Burkholderia cepacia</i> agar (for Bcc)	Negative	Positive	Negative

In summary, the electrodes used for the second impedance measurement were an improvement upon the original electrode chamber design (Figure 3-4) because they removed problem associated with handling the sputum and effectively placing it onto the electrode. Furthermore, these results identified a possible explanation for the consistency problems found with the electrodes used for the first impedance measurement.

Some changes in the impedance signature were observed, in particular with the normalised resistance data, which suggest that a high frequency peak is more prominent and visible in the sample that appeared to be positive for *P. aeruginosa*. It is difficult to know whether sample 4 contained any *P. aeruginosa* in addition to Bcc.

#### 6.3.4 Sputum sample six

In preparation for the third set of human sputum samples, a further set of electrodes were produced using the electrode assembly tested on the second set of samples. After the conditioning process, 2 out of 12 of the electrodes conditioned showed inconsistencies. Specifically, this was seen as a drop in the low frequency phase angle. A possible cause of this was related to a twisting action on the electrodes as the lid of the tube was screwed on. Only one sample was received, therefore this was tested with the three electrodes that provided the most consistent signature during the post conditioning sweep in normal saline. The results indicate a low frequency drop occurs in the phase angle (Figure 6-10 A). Also, a peak is evident in the normalised phase at low frequency (Figure 6-10 C). Microbiological analysis did not yield any growth on PAB + CN (Table 6-3), but testing on *Burkholderia cepacia* agar indicated the presence of Bcc.

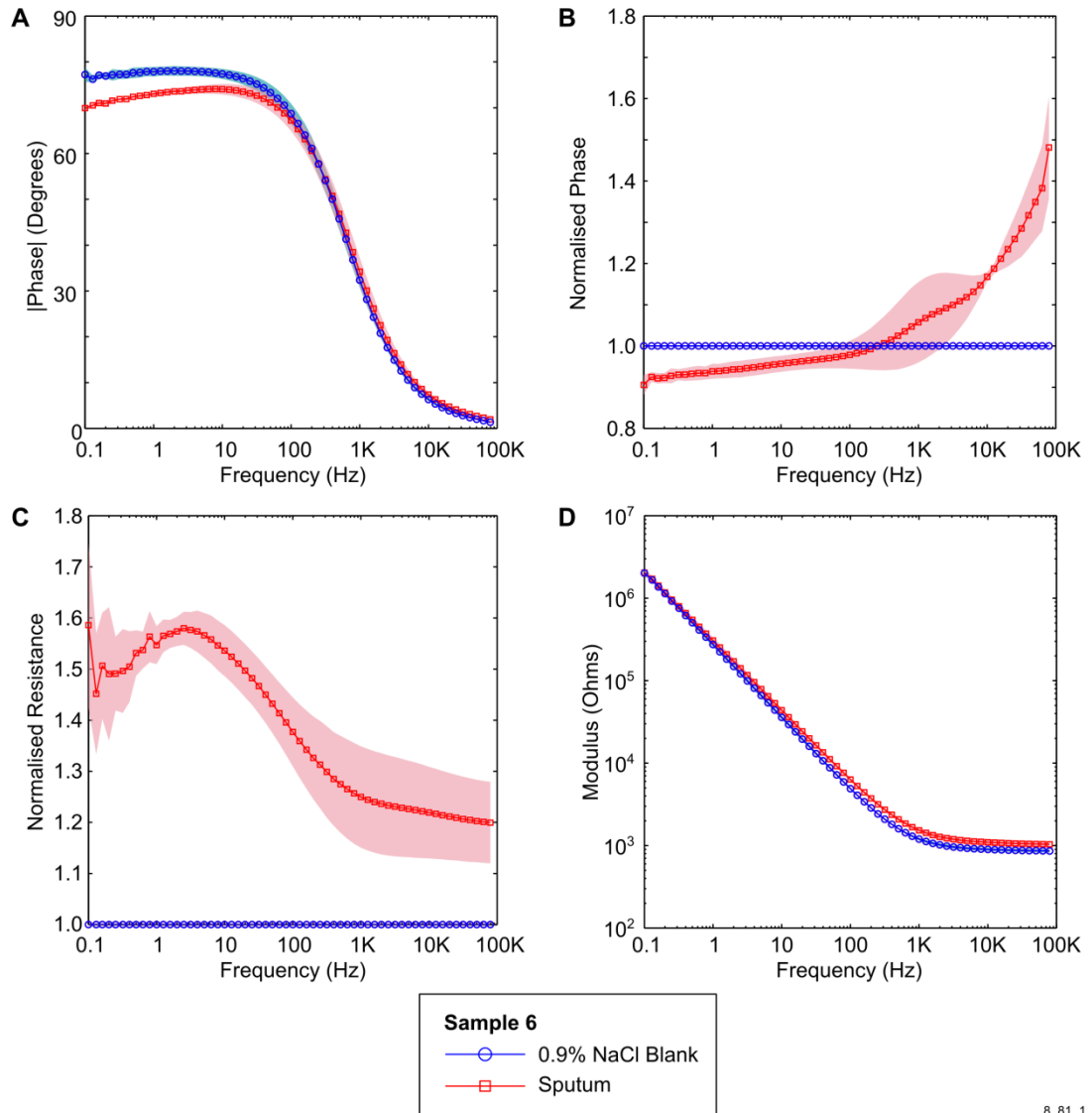


**Figure 6-10: Impedance measurement of sputum sample 6, blanked against 0.9% w/v NaCl. (A) Phase, (B) normalised phase, (C) normalised resistance, (D) modulus. Background shading represents +/- 1SD,  $n = 3$ .**

**Table 6-3: Microbiological analysis of sample 6**

	Colony forming units per ml
<b>Selective Agar</b>	<b>Sample 6</b>
<i>PAB + CN supplement</i> (for <i>P. aeruginosa</i> )	Not detected
MSA (for Gram negative)	1.93 x 10 <sup>6</sup>
<i>Burkholderia cepacia</i> agar (for Bcc)	Positive

### 6.3.5 Design three electrode assembly development

To improve the electrode further and address the challenges associated with conditioning, a further adaptation was made to the electrode assembly, as shown in Figure 6-11 (see section 3.9.5.2 for a detailed description of the changes to the assembly). By mounting the chamber on the outside of a bijou tube, less mechanical stress was placed on the screen printed ink, which appeared to help maintain the consistency between electrodes (Figure 6-12). Additionally, both dielectric ink and PE plastic were used to seal the connection with the measurement wires to ensure that no fluid could contact the connection between the wire and the electrode, and affect the impedance.

An additional challenge encountered with the conditioning of the revised electrode design related to the use of the platinum counter electrode. It was difficult to locate this electrode a consistent distance from the carbon electrodes and appeared to affect the consistency of the result. Therefore, in order to attempt to maintain electrode consistency, the conditioning process described in section 3.4.3 was not used with these electrodes.

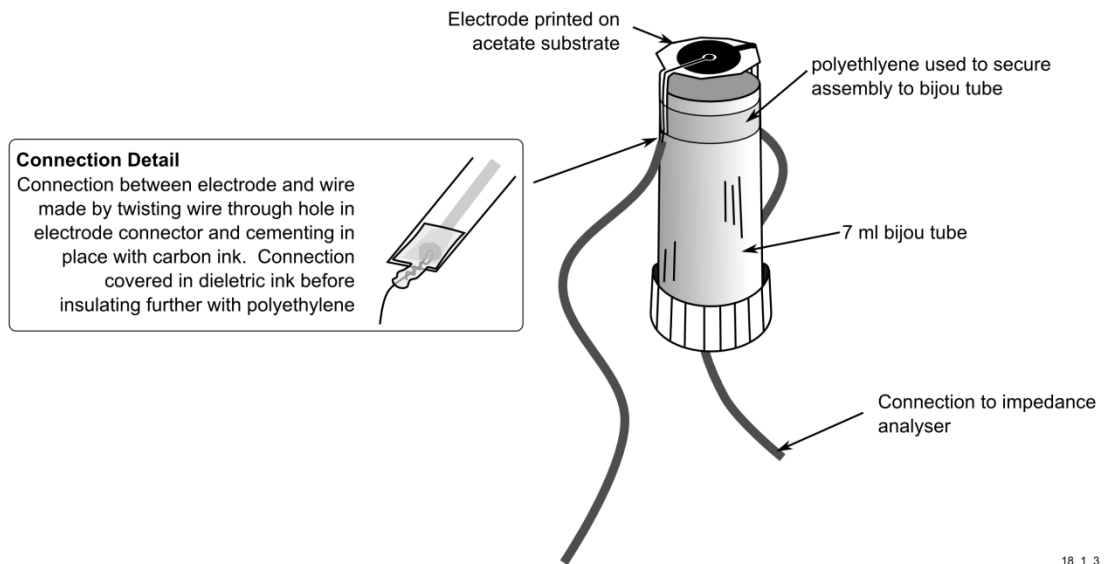


**Figure 6-11: Cartoon of design three electrode.**

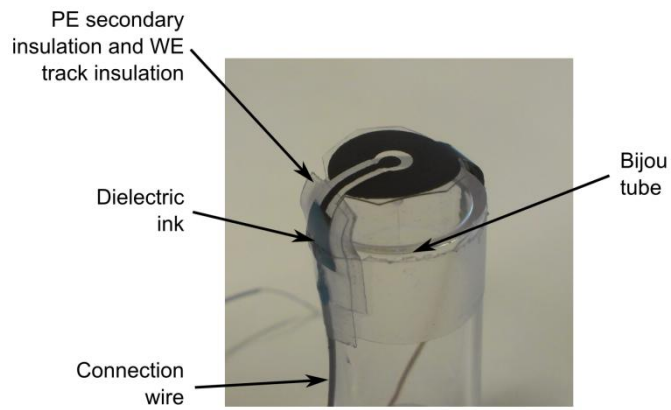


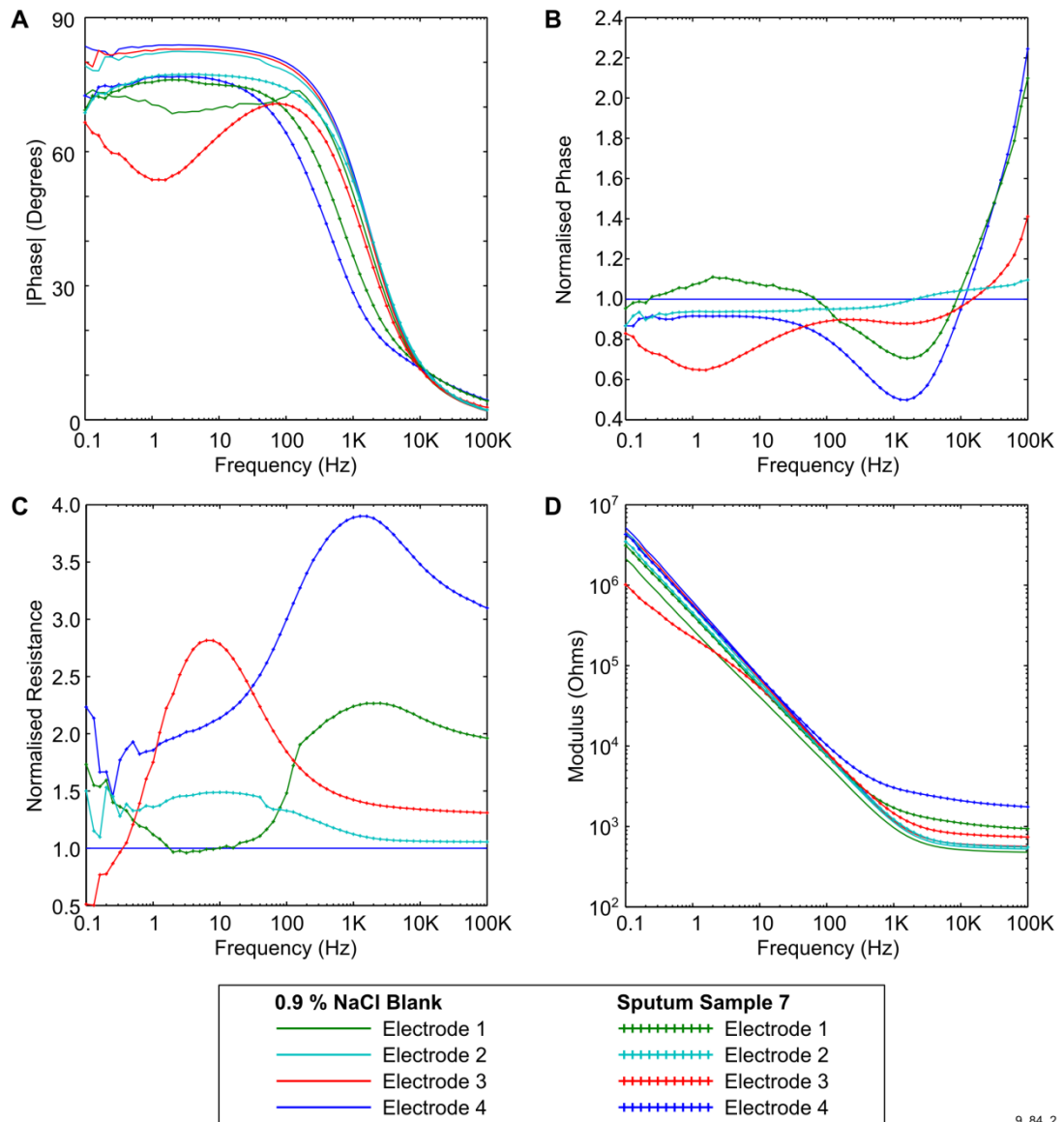
**Figure 6-12: Bijou tube electrode assembly used for measurement of samples seven and eight.**

### 6.3.6 Sputum sample seven and eight

During measurement of the sputum sample 7, several inconsistencies occurred to the electrodes used for the measurements. Electrode 1 had an inconsistent signature during the pre-sweep in saline, observed as a drop in the phase angle at lower frequency and was probably a consequence of not pre-conditioning the electrodes (Figure 6-13 A). In contrast, the saline pre-sweep carried out with the other three electrodes was more consistent. However, during the measurements, electrode 3 suffered mechanical damage by being

pushed too far into the sputum sample, causing the printed ink tracks leading to the electrodes to be bent. This clearly affected the impedance signature seen in the phase angle (Figure 6-13 A), and may also have had an impact upon the normalised resistance (Figure 6-13 C). Electrodes 2 and 4 had a consistent impedance signature when measured in saline and no problems occurred during the impedance measurements undertaken. It is interesting to note, therefore that the impedance signature for both these electrodes differs. This could have been caused by the heterogeneous nature of the sample. Specifically, there was a large quantity of saliva also present that could have affected the measurement. Therefore a possible explanation for the difference is that one of the working electrodes was in direct contact with saliva whilst the other one was in contact with sputum thus resulting in fundamentally different electrochemical characteristics.





9\_84\_2

**Figure 6-13: Impedance measurement of sample 7 blanked against 0.9% w/v NaCl. (A) Phase, (B) normalised phase, (C) normalised resistance and (D) modulus.**

On collection, it was reported that sample 8 had been collected the day before testing and stored at 7 °C. In contrast to sample 7, the electrodes used for sample 8 demonstrated a high degree of consistency and four electrodes used had a highly consistent baseline signature when blanked in saline. When measurements were carried out in sputum, consistent changes were seen in the normalised impedance spectrum across all of the electrodes. The results show that no trough was visible in the normalised phase data (Figure 6-14 B) and the peak in the normalised resistance data occurred at a lower frequency (Figure 6-14 C).

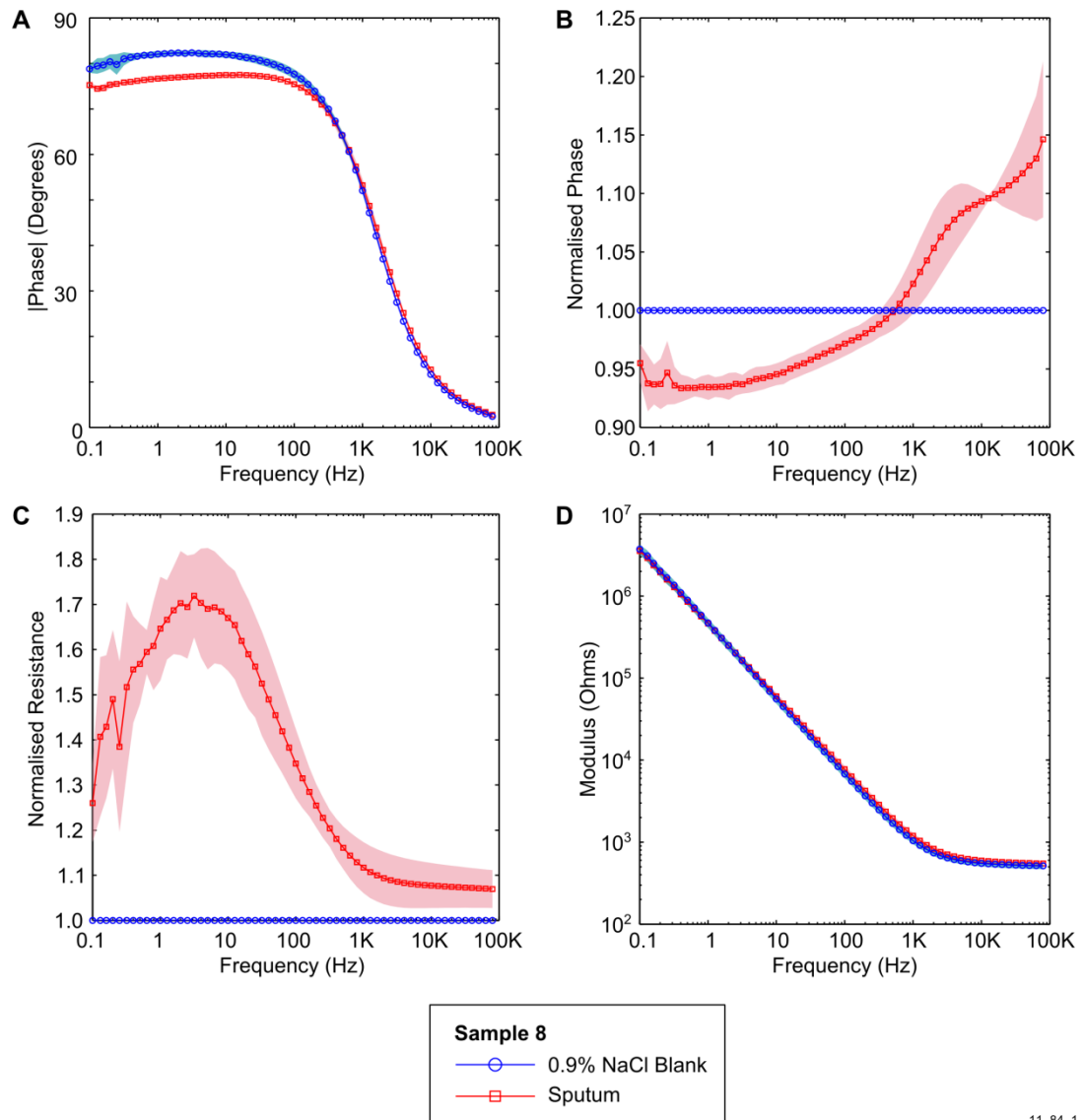


**Figure 6-14: Impedance measurement of sputum sample 8, blanked against 0.9% w/v NaCl. (A) Phase, (B) normalised phase, (C) normalised resistance, (D) modulus. Background shading represents +/- 1SD,  $n = 4$ .**

As with the other samples, microbiological analysis was carried out on selective media to identify the number of viable CFUs present (Table 6-4). For sample seven, growth occurred on both PAB + CN and MSA, whereas sample eight appeared negative for all bacteria other than Bcc. In the next section, the results across all eight sputum samples received are analysed to determine if there are trends in the impedance that could suggest the presence of *P. aeruginosa*.

**Table 6-4: Microbiological analysis of samples 7 and 8**

Selective Agar	Colony forming units per ml	
	Sample 7	Sample 8
<i>PAB + CN supplement</i> (for <i>P. aeruginosa</i> )	8.76 x 10 <sup>5</sup>	Not detected
MSA (for Gram negative)	2.22 x 10 <sup>6</sup>	Not detected
<i>Burkholderia cepacia</i> agar (for Bcc)	Negative	Positive

#### **6.4 Application of *P. aeruginosa* detection algorithm**

As described above, several changes were made to the electrode assembly in order to increase the consistency of the impedance sweeps carried out in human sputum. A summary of the electrode designs used for these experiments are shown in Figure 6-15 below. Although several changes were made to the electrode, the carbon ink, electrode substrate and perturbation voltage were kept the same. Therefore, in this section, the impedance results produced during the experiments with human sputum are analysed to look for trends that would indicate the difference between *P. aeruginosa* positive and negative samples. The outcome of this analysis is clearly limited due to the changes made to the electrode design, however, it is intended to serve as a useful first step in understanding the impedance results in human samples.

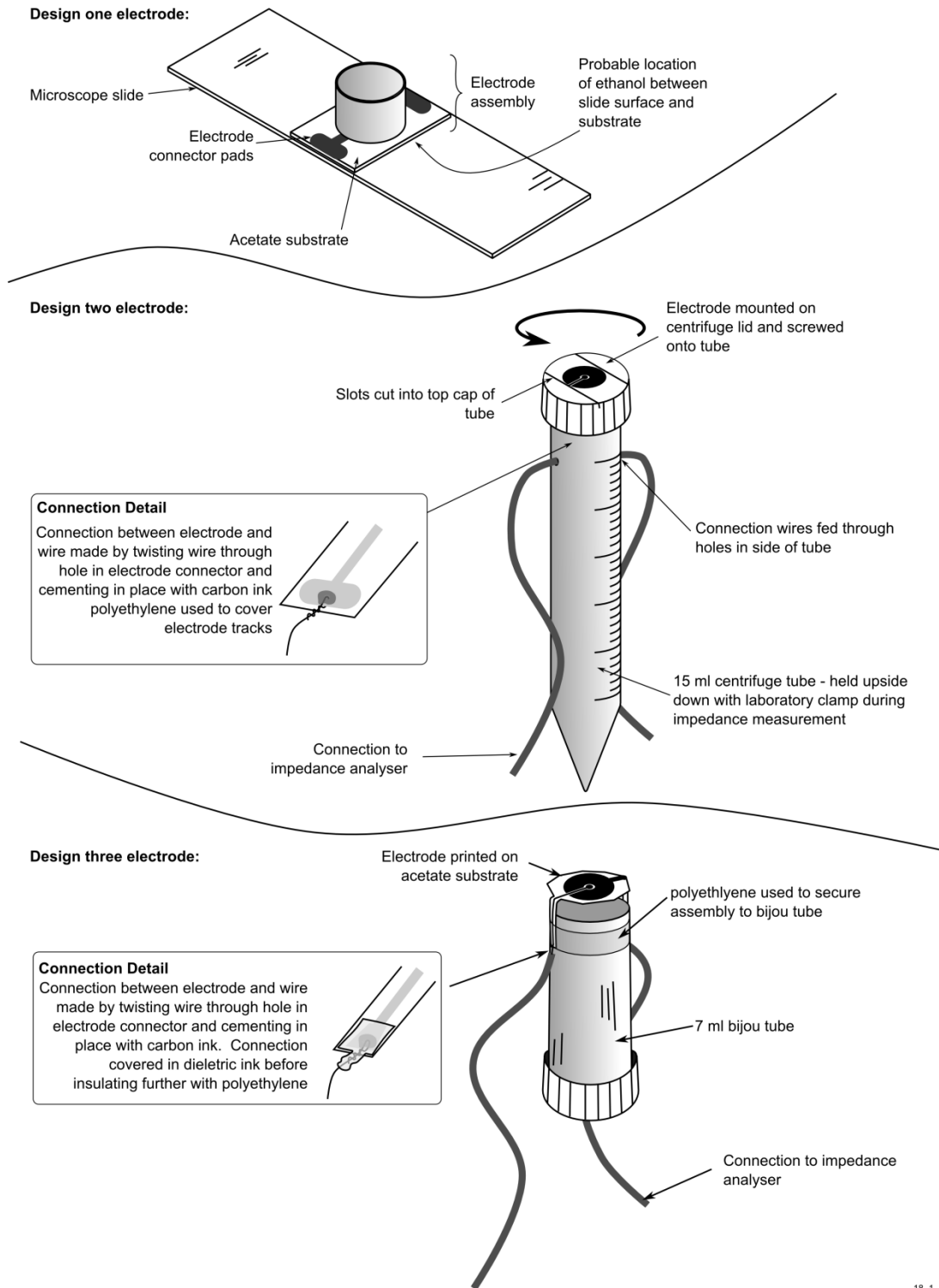
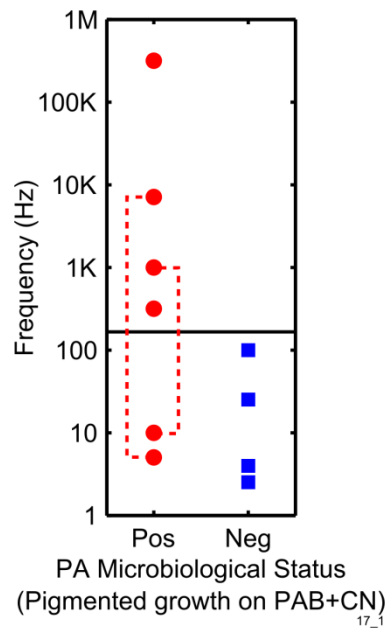


**Figure 6-15: Pictorial summary of the evolution of electrode assemblies during testing with human sputum samples.**

It is immediately obvious from the experiments above that the large changes in phase angle seen during the growth of *P. aeruginosa* (as described in the previous chapters) were not present in any of the samples tested here. Furthermore, the *in vitro* experiments described in chapters 4 and 5 with *P. aeruginosa* indicate that a peak always appeared in the normalised resistance data. In contrast, measurements in human sputum samples show that peaks in the normalised resistance data are a common feature of all the measurements taken, not just samples that are *P. aeruginosa* positive. This probably relates to the use of saline to carry out the pre-sweep, whereby large differences between the saline and the sputum which results in peaks being present in the normalised impedance for negative samples. A more complete discussion with evidence for this is described in the discussion (section 7.4.2). These challenges meant that close analysis of the data was required to identify any anecdotal changes in the impedance that suggest a characteristic signature exists for *P. aeruginosa*.

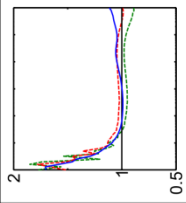
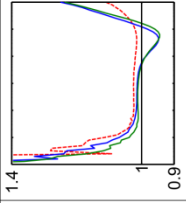
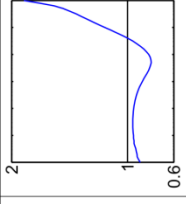
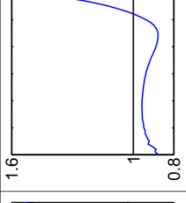
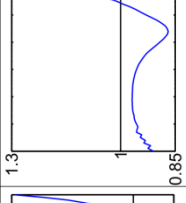
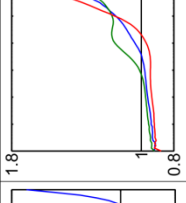
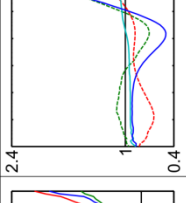
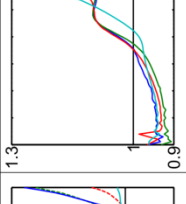
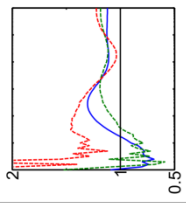
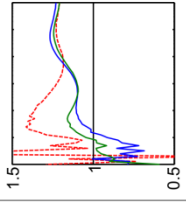
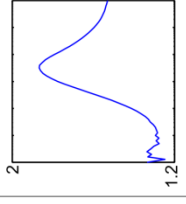
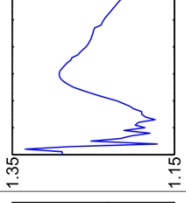
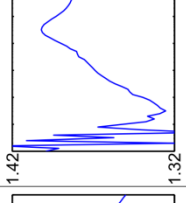
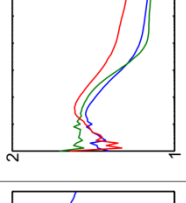
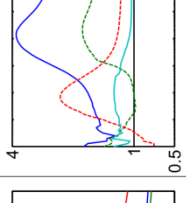
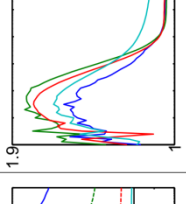
In the human sputum samples, the location of peaks in the normalised resistance data appear at a higher frequency in those samples found to be *P. aeruginosa* positive, contrasted to negative samples. This was found using the peak detection algorithm (described in section 3.8.3), through which the normalised resistance peak frequencies were identified.

Interestingly in some samples, two normalised resistance peaks can be seen: one at a high frequency and one at a lower frequency. When the mean normalised resistance data from each of the eight samples above was analysed, it was apparent that the peak at higher frequency only existed in *P. aeruginosa* positive sputum (Figure 6-16 and Figure 6-17). This observation was used to produce a simple algorithm that was then retrospectively tested on the data from the sputum samples measured.



**Figure 6-16: Mean normalised resistance peak frequency, found using the peak detection algorithm. Note that in sample believed to be *P. aeruginosa* positive, a peak always appeared above 100 Hz. In two of the positive samples, a second peak also appeared at a lower frequency, denoted by the dotted lines.**

Briefly, the detection algorithm developed operates by comparing the normalised resistance data at a high frequency and a low frequency (section 3.8.4). The logarithm of the ratio between these two frequencies is taken to provide a *P. aeruginosa* risk index based upon the location of the peak. The logarithm is taken to achieve an equal magnitude either side of the origin, based upon the location of the resistance peak, and therefore the likelihood of infection. A positive index then indicates a *P. aeruginosa* positive sample and a negative index would indicate a negative sample. Using the data resulting from the sputum samples measured in this experiment, it was possible to consistently identify a *P. aeruginosa* positive and negative culture using the algorithm (Figure 6-18). Obviously, further sputum samples are required to test the algorithm prospectively and assess its performance for the detection of *P. aeruginosa* within sputum samples.

Sample Number	Sample 1	Sample 2	Sample 3	Sample 4	Sample 5	Sample 6	Sample 7	Sample 8
Normalised Phase								
Normalised Resistance								
Electrode Design	Design 1	Design 1	Design 2	Design 2	Design 2	Design 2	Design 3	Design 3
Blanking Medium	Sputasol	Sputasol	0.9% NaCl	0.9% NaCl	0.9% NaCl	0.9% NaCl	0.9% NaCl	0.9% NaCl
PA Status (CFU/ml)	< 1	$3 \times 10^5$	$1.6 \times 10^8$	Negative	$6.8 \times 10^5$	Negative	$8.76 \times 10^5$	Negative

12\_7864\_2

**Figure 6-17: Summary of normalised phase and resistance data from human sputum samples. Normalised data for each individual channel has been plotted. Plots with dotted lines indicate channels that were found to have an irregular baseline impedance signature (in sterile Sputasol for samples 1 and 2; in 0.9% w/v NaCl for samples 3 to 8). It can be seen that in *P. aeruginosa* positive samples, a trough is often seen in the normalised phase data at high frequency and the normalised resistance peak also appears at a higher frequency. PA = *P. aeruginosa*.**

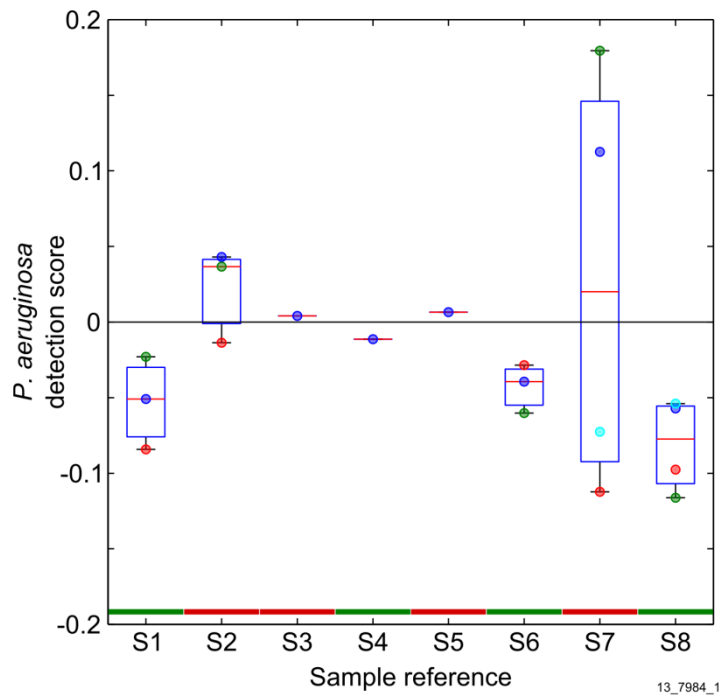


**Figure 6-18: *P. aeruginosa* detection algorithm retrospectively applied to measured sputum samples. Coloured dots correspond to the individual data channels shown in Figure 6-17. Red bars at bottom indicate *P. aeruginosa* positive samples, green bars indicate negative sample.**

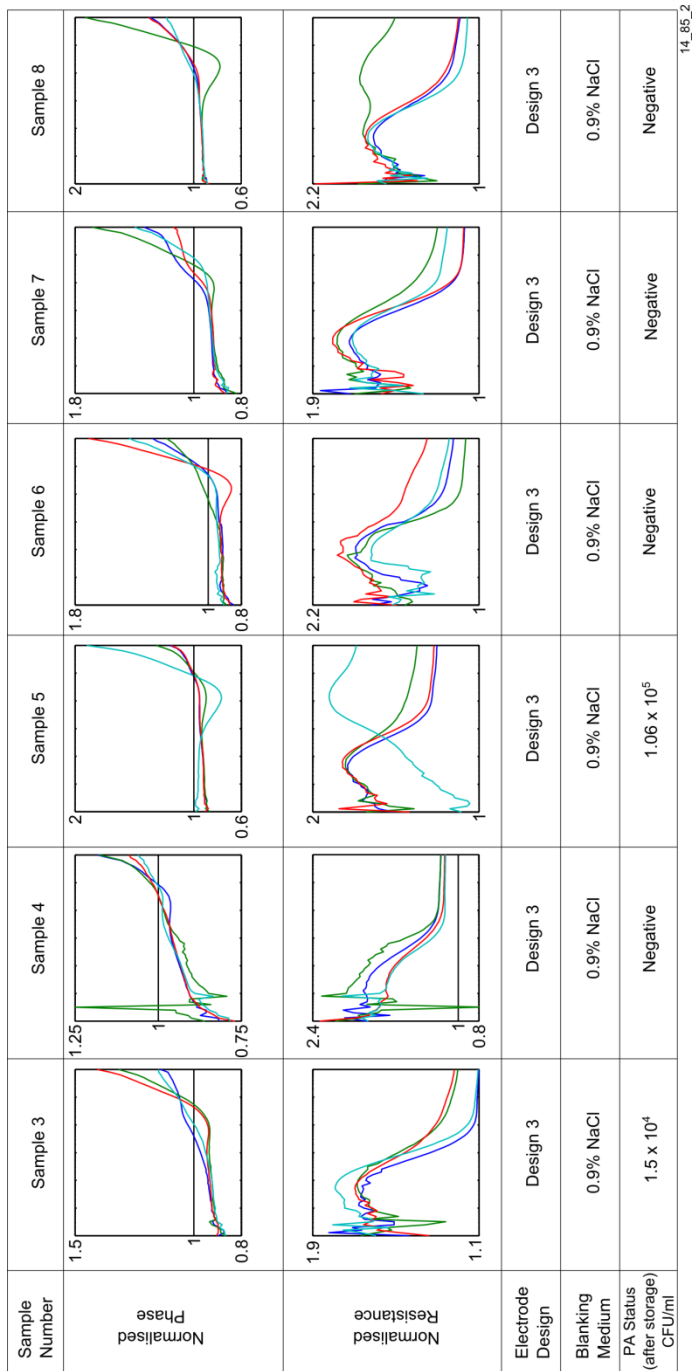
## 6.5 Repeated measurement with electrode developments embodied

One of the key weaknesses of the data shown above relates to the design development changes made to the electrode interface. Furthermore, the detection algorithm is based upon a retrospective analysis of the data. After each experiment, the samples were archived by storing at  $-80^{\circ}\text{C}$ . This provided the opportunity to test the samples with a set of electrodes that embodied the design developments described earlier in this chapter. Therefore, the final electrode design was used to measure the impedance of samples three to eight again in order to determine if the same trends were identifiable. The first two samples were excluded from this measurement because they had already been mixed with sputasol.

The results indicate that the high frequency changes observed in sputum samples containing *P. aeruginosa* were not the same as those observed during individual measurements (Figure 6-19). Instead, the electrodes showed a higher degree of consistency between the measurements, suggesting that the performance of the final electrode assembly was good. A possible reason for the lack of change in the *P. aeruginosa* positive samples could be caused by freeze thaw lysis of the bacterial cells within the sample affecting pyocyanin redox



homeostasis. As seen in the experiments with exogenous pyocyanin, the impedance changes most when pyocyanin is added to an overnight culture of cells (see section 5.4.3). If freeze-thaw lysis affected the viability of the bacteria within the sample, the presence of pyocyanin and other phenazines could have had an undetectable effect on the impedance. To explore this further, colony counting was repeated on samples 3-8 to compare cell viability.



14\_85\_2

**Figure 6-19: Measurement of all sputum samples using design 3 electrodes (without conditioning). The samples were removed from storage at -80oC and allowed to warm to room temperature prior to the measurement being carried out. Unlike measurements with the original samples, almost all measurements were the same regardless of *P. aeruginosa* status. PA = *P. aeruginosa*.**

As observed earlier (see 3.6.3) this could be due to fewer viable cells within media, possibly caused by the -80°C storage conditions.

The results of the second colony count indicate that the overall viability of *Pseudomonas* spp following freezing of the samples at -80°C is reduced (Table 6-5). In sample 4,  $1.03 \times 10^3$  CFU/ml were counted on the pseudomonas agar and in sample 8,  $3.0 \times 10^7$  CFU/ml were counted. These colonies did not have the green coloured pigment typical of *P. aeruginosa* and given the earlier finding of these samples being Bcc positive, the cultures on the plates are also likely to be Bcc.

**Table 6-5: Microbiological analysis of human sputum samples after storage at -80°C. \*represent samples suspected to contain Bcc rather than PA. Results from the first count are collated from the tables in the previous section to ease comparison. n.d. = not detected.**

Sample Number	CFU/ml <i>P. aeruginosa</i>		% decrease in cell viability (1-(second count/first count))*100
	First Count (pre -80°C)	Second count (post -80°C)	
3	$1.6 \times 10^8$	$1.5 \times 10^4$	99.99
4*	n.d.	n.d.	-
5	$6.8 \times 10^5$	$1.06 \times 10^5$	84
6	n.d.	n.d.	-
7	$8.76 \times 10^5$	n.d.	100
8*	n.d.	n.d.	-

### 6.5.1 Summary

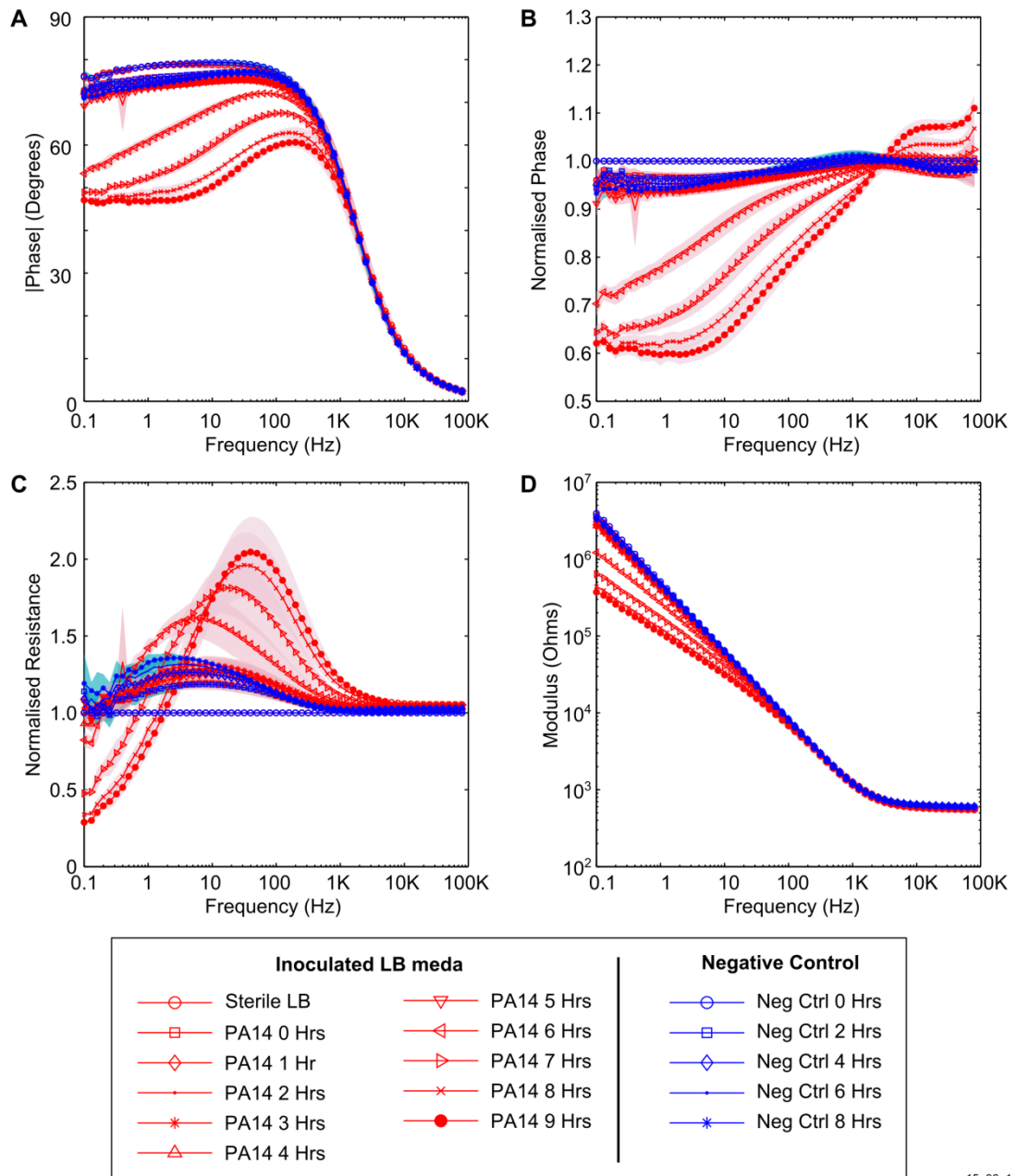
Results carried out with human sputum samples highlighted numerous challenges not seen during the *in vitro* experiments carried out in the previous chapters. This viscous nature of the sputum made it difficult to handle and indicated that the previous electrode chamber was unsuitable. The adaptations made to the chamber highlighted several other problems, including complications from poorly insulated connections to the electrode and also the implications mechanical stress could have on the screen printed carbon electrode. The results indicate that further investigation is still required in order to determine and fully assess the detection capability of the electrode, taking into account the following points from the experimental development carried out here:

- The electrode should be applied to the sample, rather than being integrated into the bottom of a device.
- Sputasol affects the impedance and could compromise any potential ability to be able to detect *P. aeruginosa*. However, it was also noted that the normalised resistance was less sensitive to the addition of sputasol.
- Connections to the impedance analyser or measurement equipment need to be kept dry to avoid confounding the results with artefact.
- The screen printed carbon tracks leading up to the electrodes are very delicate and easily damaged, potentially affecting the impedance.
- Freezing sputum samples for storage could affect the impedance and may possibly compromise the ability to detect the presence of *P. aeruginosa*.

## 6.6 Performance assessment of final electrode assembly

A final experiment was carried out to assess the overall sensitivity of the electrode assembly developed for sputum measurement (section 3.9.7). Briefly, this was achieved by measuring the growth of *P. aeruginosa*, PA14 in LB media in conical flasks for 9 hours. In addition to taking an hourly impedance measurement on an aliquot of media, colony counting and OD<sub>600</sub> were also measured. From five hours onwards, the supernatant was taken, mixed with 50% v/v methanol and then the UV visible spectrum was measured, to determine the concentration of pyocyanin. Following the experiment, a new set of three electrodes were used to repeat the impedance measurements in sterile LB (incubated in conical flasks in the same manner) in order to assess the extent of changes caused to the negative control.

The results show a large drop in the phase angle and normalised phase angle after 6 hours (Figure 6-20 A and B), peaks in the normalised resistance data (Figure 6-20 C) and a drop in the impedance modulus (Figure 6-20 D). The negative control remained similar throughout the experiment and did not exhibit the same large changes in impedance seen in the inoculated media after five hours. Interestingly, a small broad peak was visible in the normalised resistance data for the negative control after two hours incubation, suggesting that the similar peak visible over this time in the inoculated media is not related to the growth of *P. aeruginosa*.



15\_86\_1

**Figure 6-20: Impedance measurement of *P. aeruginosa* PA14 grown in LB media over 9 hours. (A) Phase, (B) normalised phase, (C) normalised resistance and (D) modulus. Shading represents  $\pm 1$  SD,  $n = 3$ .**

To investigate the number of viable *P. aeruginosa* cells the electrode is capable of detecting, a growth curve was produced alongside the impedance measurements. The optical density of the media was measured every hour, in addition to colony counting using the drop plate method. The results indicate a sharp rise in the normalised resistance occurs at 100 Hz (Figure 6-21 A) in addition to a sharp drop in the normalised phase at 10 Hz (Figure 6-21 B)

and a drop in the modulus at 0.1 Hz (Figure 6-21 C). Colony counting reveals that this equates to a point well into the growth phase of the *P. aeruginosa* with a cell density of  $1.2 \times 10^9$  CFU/ml.

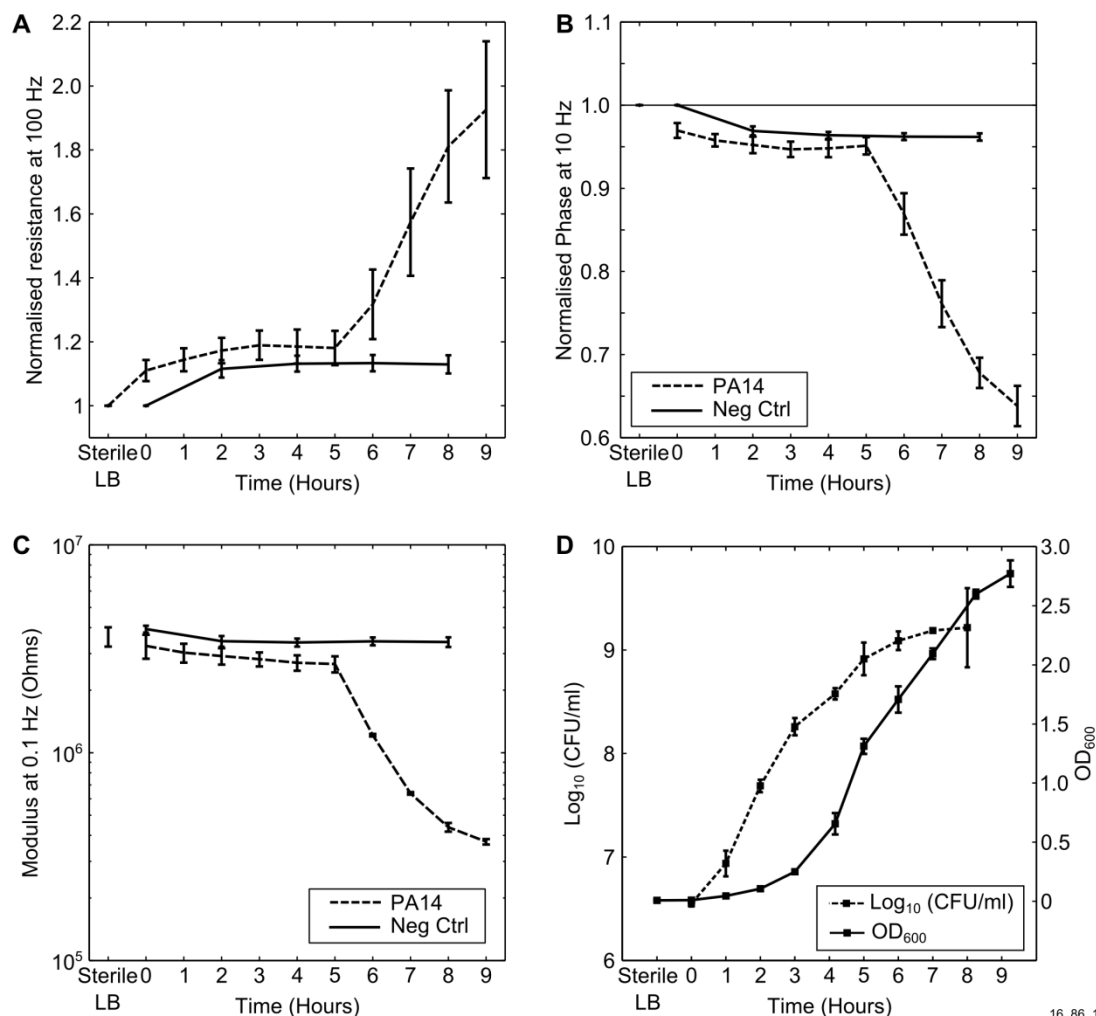


**Figure 6-21: Time based analysis of impedance and growth curves. (A) Normalised resistance at 100 Hz, (B) Normalised phase at 10 Hz, (C) modulus at 0.1 Hz, (D) growth curves, showing the change in optical density and number of colony forming units against time. Error bars represent  $\pm 1$  SD,  $n = 3$ .**

To investigate the role of pyocyanin, the supernatant from timepoints 5 to 9 was taken and mixed with 50% v/v MeOH. The absorbance was then measured at 690 nm and using the extinction coefficient for pyocyanin, the concentration was calculated (section 3.6.2). This indicated that the mean concentration of oxidised pyocyanin present in the original culture at 6 hours was  $34 \mu\text{M}$  (Table 6-6), which increased over the following three hours to  $106 \mu\text{M}$ .

**Table 6-6: Mean pyocyanin concentration of supernatant at later timepoints .  $n = 3$ .**

<b>Time point (hours)</b>	<b>Pyocyanin concentration (<math>\mu\text{M}</math>)</b>	<b>SD</b>
5	21.66	7.09
6	34.03	2.68
7	58.78	7.09
8	88.17	0
9	106.73	23.20



## 6.7 Summary

In this chapter, the carbon electrode investigated in the previous two chapters was developed further for testing in clinical sputum samples. The first experiment was carried out *in vitro* with *P. aeruginosa* PA14 in order to determine whether sputasol would affect the impedance signature. This showed that the baseline impedance is affected to the greatest extent in terms of the phase angle, but also that the measured resistance was less affected. The results demonstrated that it was still possible to determine the presence of the bacterium when sputasol was added to a two day culture of *P. aeruginosa* grown in ASM media. Further, little change was seen in the shape of the normalised resistance peak.

The electrode as developed was then applied to the measurement of human sputum. Clear parallels did not exist between the human samples and the *in vitro* testing carried out in the previous chapters. Therefore, *P. aeruginosa* detection in the context of human sputum is clearly more challenging. Three key findings resulted from the study with human sputum samples. Firstly, the thick, viscous nature of the sputum made it difficult to handle and place inside the small electrode chamber. Mixing the sample with sputasol helped to reduce the challenges associated with this. However, given that the impedance changes were very small, there is a concern that the use of sputasol could mask a particular signature indicative of the presence of *P. aeruginosa*. These problems were addressed by adjusting the electrode assembly so that the electrode could be applied directly to the sputum samples. This led to the second key finding that the electrode tracks are very delicate. It appears that when the electrode tracks are mechanically stressed (e.g. by bending over a sharp angle) the impedance signature is affected and can result in spurious measurements. Future development of the device needs to cater for this to ensure that users cannot damage the electrode in the process of testing a sample.

The final finding of the study with clinical sputum relates to the ability to be able to detect the presence of *P. aeruginosa* within sputum using the normalised resistance measurements. Anecdotally, the results gained with sputum throughout the device development suggest that a higher frequency peak might exist in the normalised resistance data as a consequence of the presence of *P. aeruginosa*. However, when the samples were tested with the final electrode design, the changes observed during development were not seen, suggesting that storage of samples at  $-80^{\circ}\text{C}$  could compromise the effectiveness of the electrode, possibly by reducing the number of viable cells within the sample or that a high frequency peaks previously observed are an artefact resulting from the different electrode designs tested.

The electrode developed for the measurement of clinical samples was also assessed for overall sensitivity in order to determine the detection threshold in terms of pyocyanin and the number of viable cells. The results of this brief study indicate that in standard laboratory media under optimal conditions, detection of *P. aeruginosa* occurs during the middle to late portion of the exponential growth phase. This coincides with the point at which *P. aeruginosa* starts to produce phenazines.

## **7 DISCUSSION**

## 7.1 Introduction

At the outset of this thesis, a number of research questions were posed, relating to the use of a low cost, screen printed electrode for the identification of *P. aeruginosa* within growth cultures and an explanation for any underlying mechanisms responsible for these impedance changes (section 1.6). This chapter considers the results described in the previous three chapters and synthesises them to answer the original research questions posed.

The first section explores baseline impedance of the electrode in comparison to other literature where microorganisms were successfully detected. Following this, an analysis is carried out on the raw data resulting from the initial experiments with *P. aeruginosa*, applying basic electrochemical theory to understand some of the processes underway during the growth of the organism. Some key research from the literature is then contrasted to the results from this study, where impedance spectroscopy has been applied specifically to the detection of *P. aeruginosa* (Dheilly et al. 2008; Kim et al. 2011; Muñoz-Berbel et al. 2006; Pires et al. 2013). Specifically, the results carried out with the conditioned, screen printed carbon electrodes are contrasted to the literature by applying equivalent circuit analysis in the same manner as that used by other investigators.

Microbial attachment to the electrode surface could play an important role in the measured impedance. The microbial attachment observed in this study is contrasted to other studies, and the implications discussed in the context of possible mechanisms that could lead to changes in the impedance.

Throughout this study, much has been made of the normalised impedance spectrum and a characteristic signature for *P. aeruginosa*. Therefore, a meta analysis is carried out in this chapter, whereby the trends in the normalised impedance spectrum are contrasted across all of the *in vitro* experiments performed. Discussion is included on the key characteristics that are present at high, intermediate and low frequencies, and the possible causes of these changes.

After a discussion of the results from human sputum samples, the capabilities of the electrode sensitivity for the detection of pyocyanin is discussed, contrasting the findings here with those of recent studies in the literature. The last section of the discussion, and this thesis, concludes with a review of the research questions posed in section 1.6 and how they have been answered in this work.

## 7.2 Electrode pattern rationale and future development

The all carbon electrode described in section 3.3.1 was designed with an asymmetric pattern in order to allow changes at only the work electrode to be studied. As seen in Figure 4-8, this resulted in the impedance magnitude for the working electrode that was approximately 300 times greater than that of the counter electrode. The greater contribution to the impedance from the working electrode means that impedance spectrum would be dominated by interface changes from this electrode. The initial design intent of the electrode was to fit within the footprint of a standard bijou tube with a diameter of approximately 12 mm. Therefore, the working electrode had a diameter of 2 mm. This was selected as a trade-off between achieving a high counter electrode to working electrode ratio and an overall size that was compatible with thick film screen printing technology. A suggested resolution for screen printed features has previously been reported as 230  $\mu\text{m}$  for a polyester screen mesh (Mandon et al. 2010). Furthermore, it is reported that reproducible direct screen printing in the  $\mu\text{m}$  range is difficult to achieve (Honeychurch 2012). Given that the 2 mm diameter working electrode was much larger than the  $\mu\text{m}$  size, a good degree of consistency between individual electrodes was achievable.

Another advantage of adopting an asymmetric electrode design was that it provided a smaller working area upon which to study microbial attachment and biofilm formation. Whilst a smaller working electrode would have resulted in a greater change in the impedance in response to the formation of a biofilm, it would also have been more difficult to consistently produce, for the reasons described above. Furthermore, a smaller working electrode would have had a larger baseline impedance, which was already approaching the detection limit of the instrument (a discussion of the impedance analyser resolution is provided in section 4.3.1).

A potential limitation of the electrode designed in this study relates to the largest biofilm features observed. Figure 5-35 and 5-36 show that the biofilm features on the electrode surface were typically 10-15  $\mu\text{m}$  in length. In order to fully characterise microbial growth on the electrode surface, the electrode dimensions would have to be comparable in size to this. Alternatively, a larger biofilm could be grown by adjusting other aspects of the experimental design, for example, by positioning the electrode at the air-liquid interface, as seen in Figure 5-33. Whilst features in the  $\mu\text{m}$  size are outside the resolution of direct electrode screen printing, two strategies could be employed to improve the resolution achieved and allow a higher resolution to be printed. A heat shrinkable substrate was used by Mandon et al.

(2010) created features up to 100  $\mu\text{m}$  in width. This was achieved through the use of Polyshrink(TM) polystyrene, which shrinks by 60% when heated to 163°C. Alternatively, Permberton et al. (2009) created a screen printed microband electrode with dimensions of 20  $\mu\text{m}$  x 3 mm. This was achieved by cutting vertically through screen printed electrode, which had been coated with a dielectric, effectively creating an electrode using the cross sectional area of the printed ink. In the context of this study, the shrinkable polymer used by Mandon et al. (2010) could be an attractive future option, because the shrinking process was also found to result in a rougher carbon electrode surface, which increased the electroactive surface area.

In terms of microbial attachment and biofilm formation, an electrode design which utilises a distributed array of electrodes could also be considered in the future. One potential approach would be the use of a common counter electrode, along with a series of working electrodes around the perimeter which could be individually measured against the counter electrode (Figure 7-1). This approach would increase the volume of the sample in contact with a working electrode and therefore the likelihood that microbial attachment and biofilm formation could be detected.

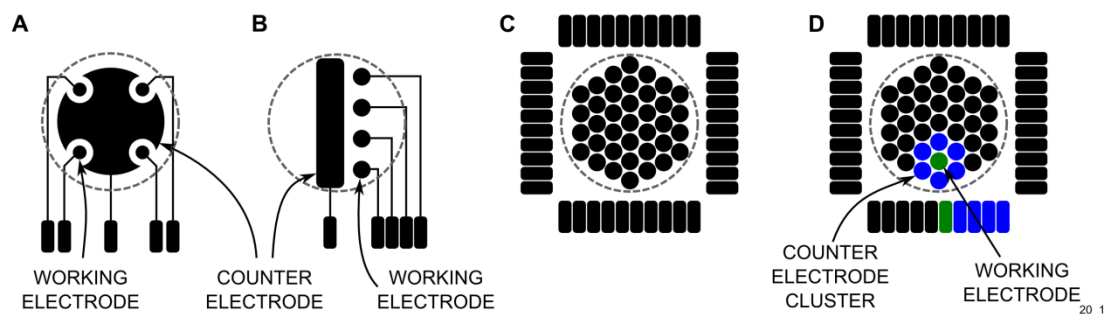


**Figure 7-1: Example electrode configurations with a distributed arrays of working electrodes. (A) a large common counter electrode is available for use with four working electrodes. (B) a smaller counter electrode with four separate working electrodes. (C) an array of individually addressable working electrodes. (D) Each electrode could be used as a working electrode, with the six adjacent electrodes used as a counter electrode. The complexity of this electrode pattern would make it more costly and difficult to implement, but it would also allow a greater level of information about the sample to be determined.**

### **7.3 In vitro assessment of electrode developed**

#### **7.3.1 Analysis of electrode performance**

In this section, the baseline performance of the screen printed carbon electrode developed is contrasted to other studies carried out. This is important to understand because the starting impedance of the electrode developed within this study was very high.

##### **7.3.1.1 Baseline performance of carbon electrodes**

Measurements in LB media indicated that the unconditioned carbon electrodes have a high starting impedance, with a typical impedance modulus at 1 Hz of  $4.09 \times 10^6 \Omega$ . Whilst this is within the detection limit of the Solartron 1260 impedance analyser (section 4.3.2), the impedance of the electrodes used in this study is high compared to other investigators who have used reagentless and label free impedance spectroscopy to detect the presence of microorganisms (Table 7-1). Several of these studies used electrodes constructed from ITO, gold or platinum manufactured by lithography to produce high resolution micro-electrodes. Out of all the label free, reagentless impedance studies conducted for characterisation of bacteria, two used carbon based working electrodes.

The study most closely related to this work was carried out by Farrow (2010). The baseline impedance from the screen printed carbon electrodes investigated in this study was initially high. However, Farrow (2010) found that the impedance modulus could be reduced 100 fold from  $12 \times 10^6 \Omega$  to  $1.2 \times 10^5 \Omega$  (at 0.1 Hz) by using a conditioning procedure whereby a square wave with an amplitude of 10 V and period of 120 seconds was applied to the electrode for 20 minutes. In addition to reducing the impedance magnitude, this also improved the consistency between electrodes.

The consistency of the screen printed carbon electrodes used in this study after the electrode conditioning process was high (Figure 4-8). As discussed later, initial testing with *P. aeruginosa* indicated that the bacteria could be detected without the need to reduce the baseline electrode impedance. However, the conditioning approach employed by Farrow et al. (2010) indicates a useful approach to reduction of the baseline impedance.

Marsili et al. (2008b) used glassy carbon electrodes to measure the impedance of an electrochemical cell in a vitamin free minimal media and showed an impedance magnitude of  $150 \Omega$  and 1 Hz. In the study by Marsili et al. (2008b) a sophisticated electrochemical configuration, consisting of the glassy carbon electrode, a saturated calomel reference

electrode and a platinum wire counter electrode was used. The preparation procedure for glassy carbon electrode involved extensive polishing to a mirror finish followed by sonication and overnight soaking in 1 N HCl, rinsing in acetone and then storage in deionised H<sub>2</sub>O prior to use. All these procedures were appropriate for their experimental investigation, where the aim was to determine the electrochemical properties of a *G. sulfurreducens* biofilm. In contrast, the application of a low cost screen printed carbon electrode for near patient testing would preclude many of these preparation procedures and the sophisticated electrochemical setup used. Furthermore, screen printed carbon ink has a low carbon content (Wang et al. 1996) and the small size of the working electrode used in this study means it would be difficult to achieve baseline impedance similar to that found by Marsili et al. (2008b).

Low baseline impedance may play an important role in the detection of microorganisms, given that the studies highlighted in Table 7-1 have all successfully detected the presence of the target bacteria. However, the key drivers of cost and portability in a near patient testing device arguably mean that a compromise is required between electrode performance and production costs. The screen printed carbon electrodes described here are low cost, easy to manufacture and are designed to avoid the need for a sophisticated set up consisting of specialist counter and reference electrodes. The compromise is that the high impedance of the carbon electrode could mask some of the changes to the electrode/electrolyte interface or electrode resulting from the growth of *P. aeruginosa*.



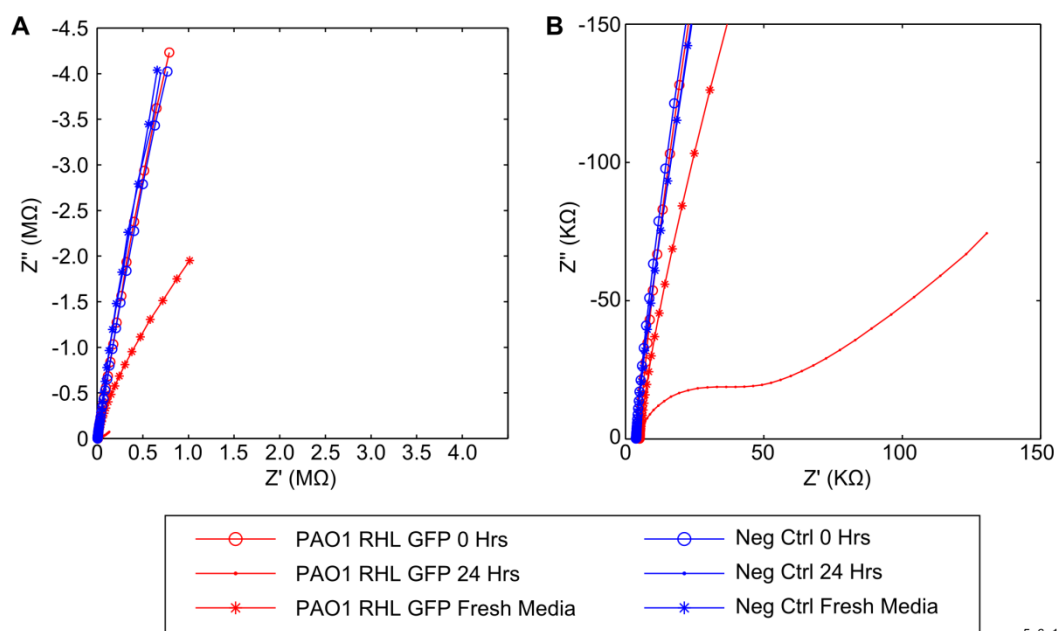
**Table 7-1: Comparison of electrode impedance with other investigators. Taken from studies where baseline impedance data is provided and sorted by working electrode material and then studies with greatest impedance modulus first. (n.s. not specified.)**

Investigator	Electrode size and configuration	Electrolyte	AC Potential	Frequency (Hz)	Z  ( $\Omega$ )	Phase  (Degrees)	Comments
Yang et al. 2004	ITO interdigitated microelectrode	Selenite-Cystine Broth	5 mV	1 MHz	$3 \times 10^3$	n.s.	
				1 Hz	$5.0 \times 10^5$	n.s.	
Bayouhd et al. 2008	ITO WE, Calomel RE, Pt CE	150 mM PBS	10 mV	0.01 Hz	$1.43 \times 10^4$	85.94	DC polarisation potential of $-600 \text{ mV}_{\text{dc}}$ used
Ben-Yoav et al 2011	ITO WE, Ag-AgCl RE	LB media	50 mV	137 mHz	$6.5 \times 10^5$	82.78	Measurements taken from experiment using DC potential of $50 \text{ mV}_{\text{dc}}$ vs Ag-AgCl
Yang et al. 2003	Gold WE, Ag-AgCl RE, Pt CE	PBS + 0.01M $\text{Fe}(\text{CN})^{3-}$ and $\text{Fe}(\text{CN})^{4-}$	5 mV	1 MHz	250	n.s.	
				10 Hz	$6.66 \times 10^4$	n.s.	
Munoz-berbel et al. 2006	Gold WE, Pt CE	Physiological serum	25 mV	10 Hz to 1kHz	$3.35 \times 10^4$	n.s.	Frequency shown not specified.
Paredes et al. 2012	Gold interdigitated microelectrode	TSB + 5% Glucose	50 mV	10 Hz	$4.9 \times 10^4$	85	Measurements estimated from plot after 2 hr inoculation.
				100 kHz	25	35	
Paredes et al. 2013	Gold interdigitated microelectrode	TSB + 5% Glucose	100 mV	10 Hz	$1.5 \times 10^5$	87	
				100 kHz	40	32	
Kim et al. 2012	Gold interdigitated microelectrode	M9 minimal salts media	10 mV	1 Hz	$4.77 \times 10^5$	51	

Investigator	Electrode size and configuration	Electrolyte	AC Potential	Frequency (Hz)	Z  ( $\Omega$ )	Phase  (Degrees)	Comments
Piers et al. 2013	Gold WE and CE	BHI broth	40 mV <sub>p-p</sub>	1.3 kHz	2.0 x 10 <sup>3</sup>	n.s.	
Munoz-berbel, Garcia et al 2008	Pt WE and CE; Ag-AgCl RE	5 mM KCl	25 mV	10 Hz	1.50 x 10 <sup>5</sup>	n.s.	
This study	Screen printed carbon electrodes pre-conditioned	LB media	200 mV <sub>rms</sub>	1 Hz	4.09 x 10 <sup>6</sup>	79	
This study	Screen printed carbon/Ag-AgCl electrode	LB media	200 mV <sub>rms</sub>	1 Hz	7.72 x 10 <sup>4</sup>	57	
Farrow 2010	Screen printed carbon electrode	MHB	200 mV <sub>rms</sub>	0.1 Hz	1.2 x 10 <sup>5</sup>	57	
Marsili et al. 2008	Glassy Carbon WE, Pt CE, Calomel RE	Vitamin free minimal media	10 mV	0.01 Hz	1.0 x 10 <sup>4</sup>	77	DC potential of -160 mV <sub>dc</sub> vs SHE used.
				1 Hz	150	67	
Farrow 2010	Screen printed Ag-AgCl electrode	MHB	200 mV <sub>rms</sub>	0.1 Hz	6.0 x 10 <sup>3</sup>	21	

### 7.3.1.2 Analysis of initial impedance measurements with *P. aeruginosa*

During initial measurements with *P. aeruginosa* PAO1 RHL GFP, clear changes were seen in the impedance spectrum (Figure 4-2 and Figure 4-3). The greatest change in the impedance occurred at low frequencies, where the properties of the interface go from highly polarised, supporting little faradic current to an interface where electron transfer was possible. This can be seen in the complex plane (Figure 7-2). A near vertical plot (as seen in the negative control data and at the start of the experiment in the inoculated electrodes) is indicative of a purely capacitive interface, whereas the presence of a semicircular arc at high frequency indicates an RC circuit where a faradic path exists in parallel to the charging current (Brett and Brett 1993).



5\_6\_1

**Figure 7-2: Complex plane plot of impedance of *P. aeruginosa* PAO1 RHL GFP over 24 hours, using data from the first experiment (see section 4.2.1) over the frequency range 1 Hz – 1 MHz. (A) Shows the complete frequency spectrum of the negative control and initial measurements at 0 Hrs. (B) Shows the inoculated electrodes at 24 Hrs. A semicircular arc is clearly visible in the inoculated chambers indicating the presence of a charge transfer resistance. Plots represent mean data,  $n = 4$  for both *P. aeruginosa* PAO1 RHL GFP and negative controls.**

To investigate the electrode-electrolyte interface further, the fit circle function was used in ZView (Scribner Associates) to estimate the charge transfer resistance and double layer capacitance of the interface following the growth of PAO1 RHL GFP in the first two

experiments. An example of the application of this function, and the key parameters that result is shown in Figure 7-3. The omega max parameter, which is defined as the frequency in rad/sec at the top of the arc, calculated by the ZView circle fitting tool can be used to determine the double layer capacitance in conjunction with the charge transfer resistance (Bard and Faulkner 2001):

$$\omega_{max} = \frac{1}{R_{ct}C_{dl}} \quad [7-1]$$

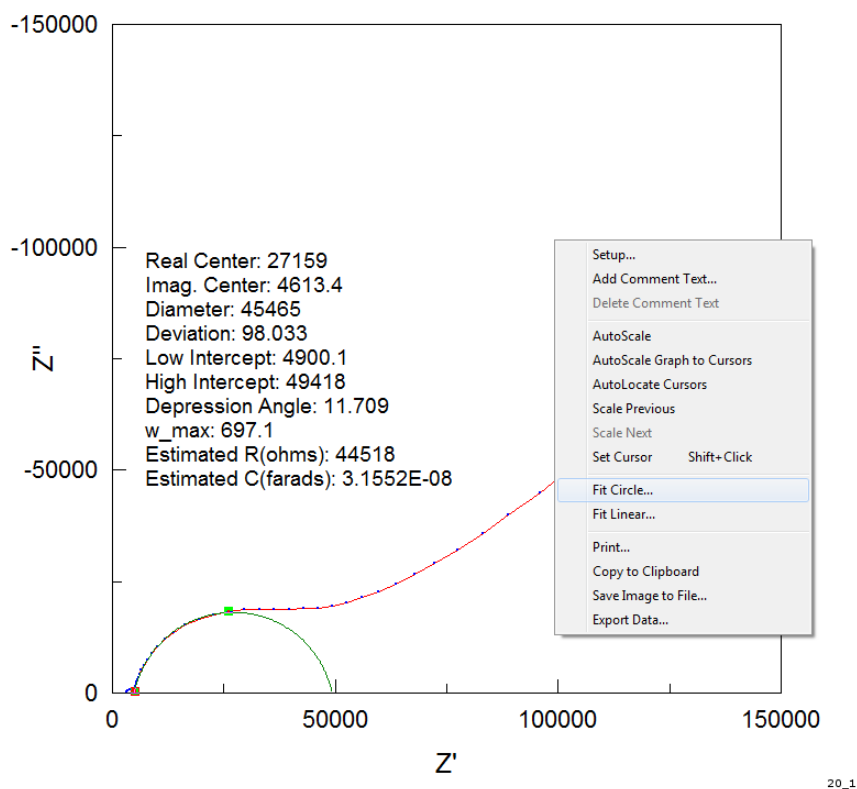


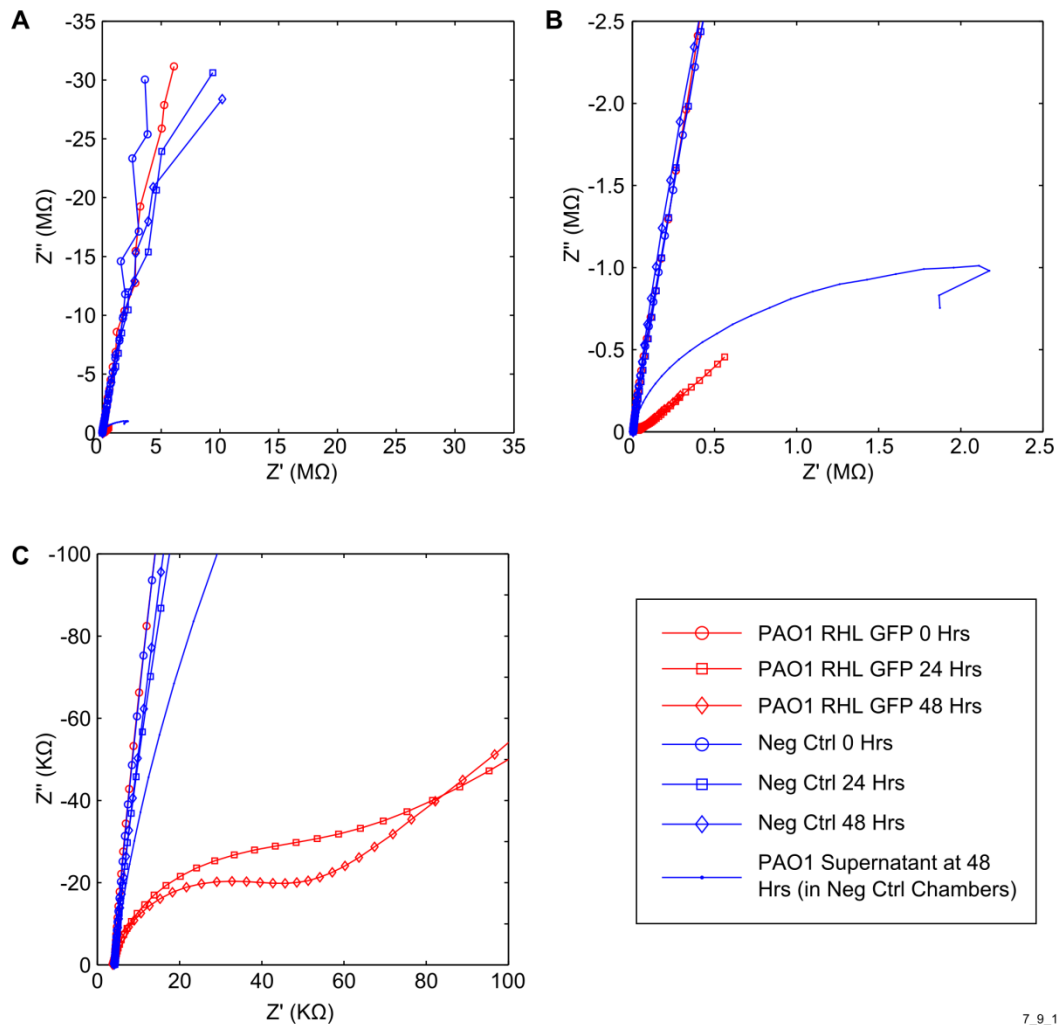
**Figure 7-3: Screen shot of the ZView output from circle fit tool. The images shows parameters produced by the fit circle function and the menu option selected. This data was calculated from individual impedance traces and then averaged to determine the values shown in Table 7-2.**

**Table 7-2: Measurement of  $R_{ct}$  and  $C_{dl}$ , determined using ZView fit circle function. The circle was fitted using datapoints between 120 Hz and 20 kHz, where the complex plot had a clear arc. SD is shown in brackets ( $n = 4$ ).**

Exp #	Time point (Hrs)	$\omega_{max}$ (Rad/Sec)	Depression Angle (Degrees)	$R_{ct}$ ( $\Omega$ )	$C_{dl}$ (F)
1	24	693.61 (44.17)	11.83 (0.91)	$4.47 \times 10^4$ ( $3.95 \times 10^3$ )	$3.26 \times 10^{-8}$ ( $3.65 \times 10^{-9}$ )
2	24	408.09 (33.98)	11.31 (1.73)	$6.16 \times 10^4$ ( $5.3 \times 10^3$ )	$4.00 \times 10^{-8}$ ( $1.08 \times 10^{-9}$ )
2	48	491.94 (86.57)	11.92 (2.44)	$4.88 \times 10^4$ ( $4.5 \times 10^3$ )	$4.25 \times 10^{-8}$ ( $5.22 \times 10^{-9}$ )
2	Fresh Media	6.71 (3.01)	10.51 (1.57)	$1.35 \times 10^6$ ( $4.08 \times 10^5$ )	$1.28 \times 10^{-7}$ ( $3.88 \times 10^{-8}$ )

Fresh media was added to the electrode chamber after both the first and second *P. aeruginosa* experiments. This shows that there is still a change in the impedance as a consequence of the growth of *P. aeruginosa*. Although a large dispersion existed in the phase angle (Figure 4-3) when fresh media was added to the electrode chamber, the semi-circular arc in the complex plane plot disappeared (Figure 7-2 A), suggesting that the mechanism causing the electron transfer was altered when the spent media was removed. Changes to the impedance did still exist when fresh media was added to the electrode chamber, therefore some residual effect from the growth of the bacteria *in situ* (Figure 4-3) clearly remains.

To understand the effect that adding the supernatant had upon the impedance, the *P. aeruginosa* PAO1 RHL GFP culture was filter sterilised and placed into the negative control electrode chambers. The results showed that a significant difference was observed in the impedance and a large semicircular arc was visible in the impedance data, as shown in the complex plane plot (Figure 7-4 B). In contrast to the measurements with *P. aeruginosa* PAO1 RHL GFP, the charge transfer resistance is more than 27 times greater than it is in the electrode chambers at 48 hours (Table 7-2). Interestingly, an increase of approximately one order of magnitude is also seen in the double layer capacitance, although a change still exists in the depression angle. These results suggest that a combination of both the supernatant and the *P. aeruginosa* cells are required to observe the maximum change in impedance.



7\_9\_1

**Figure 7-4: Complex plane plots of impedance using data from second experiment with *P. aeruginosa* PAO1 RHL GFP over the frequency range from 0.1 Hz to 1 MHz. (A) Shows the complete frequency spectrum of the negative control and initial measurements at 0 Hrs. (B) Shows the same plot on a larger scale, indicating the semi circular arc in the impedance from the PAO1 RHL GFP filter sterilised supernatant. (C) Shows the same plot at a much larger scale indicating the semicircular arcs resulting from the impedance measurements.**

It is interesting to note that the centre of the arc discussed in this section is located below the x-axis, whereas the impedance of an ideal capacitor and resistor in parallel describes a semicircular arc with a centre located on the x-axis (Bard and Faulkner 2001). The concept of a constant phase element (CPE) has been created to explain this anomaly. Between the 1920s and 1950s the CPE was believed to relate to the ion selectivity of cell membranes, as a depressed semicircle was observed in several biological systems (Schanne and Ruiz 1978). It has subsequently been shown that CPE is caused by a distribution of time constants, which

can be caused by surface roughness and heterogeneities, electrode porosity, variation of coating composition, slow adsorption reactions and non-uniform potential and current distribution (Jorcin et al. 2006). Therefore, the CPE can be quite non-specific and difficult to interpret. Figure 5-34 shows an SEM image of the surface of the negative control electrode. This indicates that graphite flakes present in the electrode binder material are all orientated at different angles. Furthermore, the non-uniform distribution of carbon within the electrode is likely to have an effect upon the local current distribution and potential. It is anticipated that these will have an impact upon the capacitance of the electrode, potentially resulting in the depression angle highlighted in Table 7-2. Despite these limitations, the CPE has been widely used in microbiological impedance studies as a key element in equivalent circuits to fit empirical data (Muñoz-Berbel et al. 2006, 2008a, 2008a; Ben-Yoav et al. 2011; Kim et al. 2011, 2012). Further discussion of the use of the CPE in equivalent circuit measurements is made in future sections.

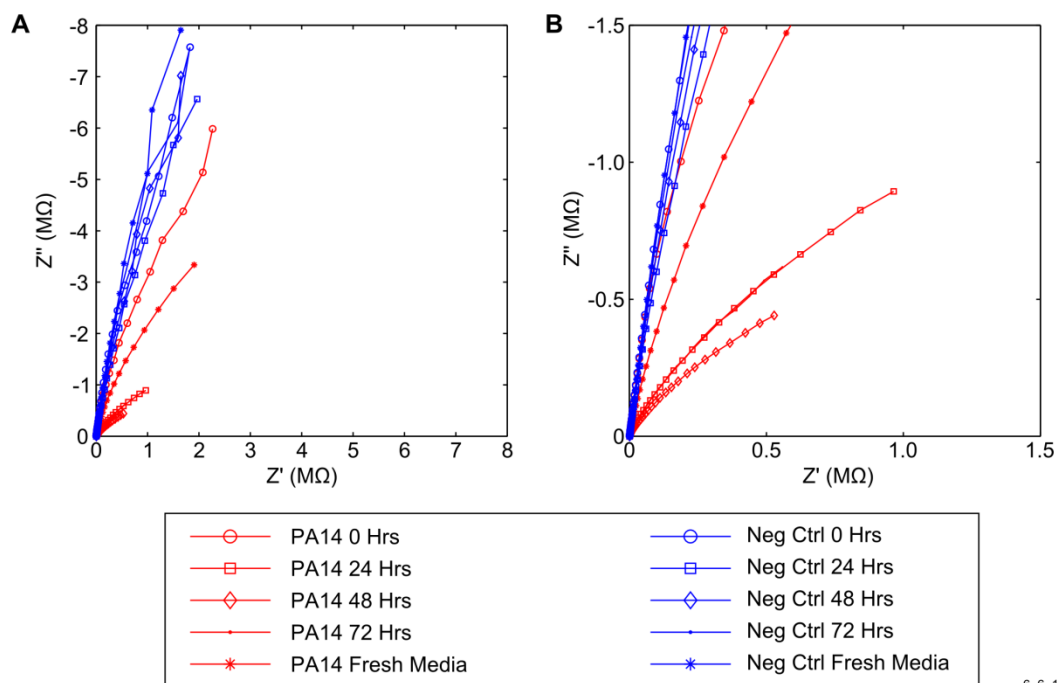
### 7.3.1.3 Analysis of results post conditioning

As described in section 7.3.1.1, conditioning was employed to improve the consistency between the electrodes and give a reduction in the baseline impedance. When the strains *P. aeruginosa* PA14, J1385, J1532, C1426 and C1433 were grown as monocultures in LB media (see section 4.4), the impedance changed in a similar manner to that seen in the initial experiments. Unlike previously however, no semicircular arc was observed in the complex plane (Figure 7-5).

The lack of a semicircular arc could have been due to phenotypic behaviour associated with the strain *P. aeruginosa* PAO1 RHL GFP, which may have caused greater, more prominent impedance changes contrasted to the other *P. aeruginosa* strains tested. Significant differences were still visible in the impedance for all these strains contrasted to the negative controls, therefore a characteristic signature could still be defined for *P. aeruginosa*. The lack of a semicircular arc could also have been related to the conditioning process. Although the process should have increased the electroactive area and improved charge transfer (Wang et al. 1996), the complex impedance plot suggests that the interface is predominately capacitive, suggesting that it has been affected in a different manner to that proposed by Wang et al. (1996). These differences could have been related to other factors such as the ink curing temperature or the electrolyte used for the conditioning.

Despite the changes relating to the semicircular arc, the electrode conditioning used appears to deliver some clear benefits. Firstly, the noise observed in the measurements at lower frequencies (see Figure 4-3 compared to Figure 4-12) was less when the conditioned electrodes. Another advantage of the conditioned electrode related to the problems associated with consistency in the phase angle (Figure 4-6), which rarely occurred at low frequency with the conditioned electrodes.





6.6\_1

**Figure 7-5: Impedance measurements on *P. aeruginosa* PA14 carried out using a carbon electrode. Data from first experiment with PA14, showing the frequency spectrum from 0.1 Hz to 1 MHz. (A) Shows the complete frequency spectrum of the negative control and initial measurements at 0 Hrs. (B) Shows PA14 data at 24, 48 and 72 Hrs. The plot at 72 Hrs is partially obscured by the 24 Hr plot. Data represents the mean of the measurements taken.  $n = 3$  for both PA14 and negative control.**

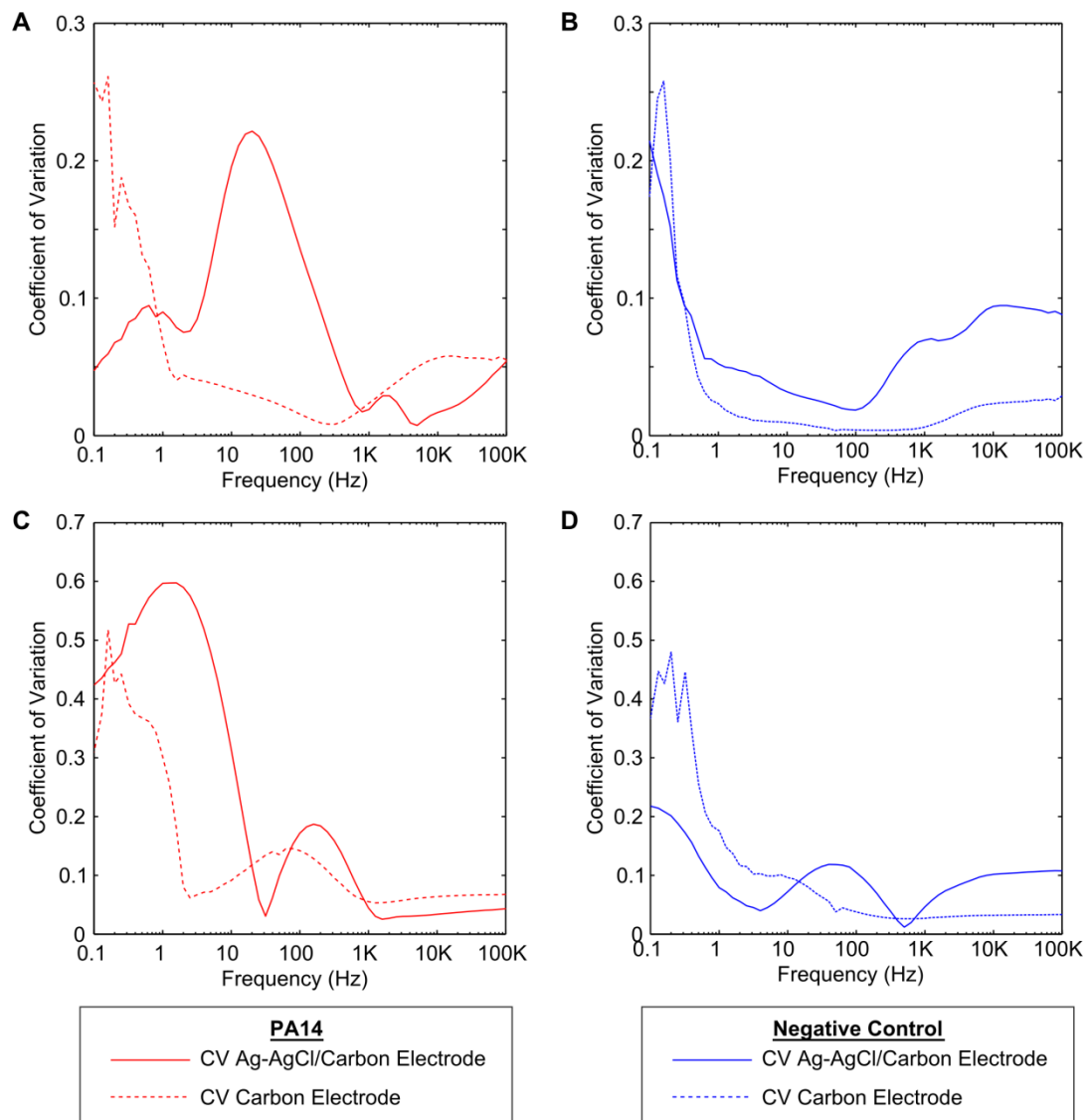
#### 7.3.1.4 Analysis of the results from measurements carried out with the Ag-AgCl/carbon electrodes

The experiment carried out in section 4.2.2 describes the measurement of *P. aeruginosa* PA14 with a larger carbon working electrode and Ag-AgCl counter electrode (Figure 3-2). The rationale behind this design was that the use of Ag-AgCl for the counter electrode would lower the overall impedance, and improve the sensitivity of the carbon working electrode. In turn, the larger carbon working electrode would have a lower impedance and would therefore make the overall electrode more sensitive. The growth experiment carried out in section 4.2.2 shows that the impedances changes associated with *P. aeruginosa* PA14 are different to the negative control. However, the consistency between individual electrodes appeared to be lower than that seen with the carbon electrodes in earlier experiments, and in the measurement of *P. aeruginosa* PA14 with the preconditioned carbon electrodes (section 4.4.1).

The consistency between replicates of carbon electrodes and Ag-AgCl/carbon electrodes was quantified by calculating the coefficient of variance (CV). This was achieved by dividing

the measured standard deviation at each frequency with the mean measurement for the normalised phase and resistance data at 48 hours. With this approach, the coefficient of variation for the impedance signatures from comparable experiments with both electrode designs could be contrasted. This was done to confirm which of the two electrodes had the greatest variability. The experiments used for this are described in section 4.4.1 (for the experiment with the carbon electrode) and section 4.2.2 (for the experiment with the Ag-AgCl/carbon electrode).

Following the growth of *P. aeruginosa* PA14, the results indicate that at certain frequencies the Ag-AgCl/carbon electrode had a CV much larger than the carbon electrode. This was particularly seen in the normalised phase angle between 10 Hz and 100 Hz (Figure 7-6A) and also in the normalised resistance below 10 Hz (Figure 7-6 C). In contrast, the carbon electrode had a lower CV across the same parameters, which indicates the consistency between electrodes is greater. The CV between carbon and Ag-AgCl/carbon electrodes for the negative controls were lower across the frequency spectrum and were similar across the frequency spectrum (Figure 7-6 B and D). This shows that the greatest variation in impedance between Ag-AgCl/carbon electrodes occurs in the presence of *P. aeruginosa*. This could be explained by toxicity of silver ions towards bacteria, as described below.



10\_17\_33\_1

**Figure 7-6: Analysis of coefficient of variation for experiments with Ag-AgCl/Carbon electrodes and carbon electrodes. (A) CV from normalised phase for *P. aeruginosa* PA14 samples, (B) CV from normalised phase for negative control samples, (C) CV from normalised resistance for PA14 samples and (D) CV from normalised resistance for negative control samples.  $n = 4$  for all samples except PA14 on carbon where  $n = 5$ .**

The release of free silver ions into the media could have caused a high rate of variability between electrode chambers due to the toxicity of heavy metals to bacteria (Lemire et al. 2013). Silver is widely recognised as an antimicrobial agent. Although all the mechanisms of action are not fully understood, it is believed to affect cell viability by interfering with protein synthesis, leading to dysfunctional proteins, inhibiting uptake of nutrients and impairing membrane functions (Lemire et al. 2013). Farrow et al. (2010) found that when

screen printed Ag-AgCl incubated in cultures of *S. aureus* and regular impedance measurements were carried out, the cell viability of cultures was much lower. Instead of achieving cell densities of  $1 \times 10^9$  CFU/ml for the control chambers, densities of  $1 \times 10^3$  CFU/ml were commonly found when the screen printed electrodes were present (Farrow, 2010). This suggests that the Ag-AgCl screen printed ink has the capacity to release silver ions into the media. Findings in other studies demonstrate that silver can affect the growth and viability of *P. aeruginosa* (Ip et al. 2006), therefore the use of Ag-AgCl in the electrode design could have an effect upon the overall viability of the electrodes.

Development of an electrode using a Ag-AgCl electrode could be advantageous in indwelling devices, particularly if it was possible to use a device to both detect the presence of the bacteria and then release silver ions from an electrode to kill them. However, CV also shows that the carbon electrodes achieve a higher degree of consistency when grown in the presence of *P. aeruginosa*. Therefore, the carbon electrode design formed the focus of the remainder of the study.

### **7.3.2 *P. aeruginosa* growth in standard laboratory media**

#### **7.3.2.1 Equivalent circuit analysis**

As described in section 1.3, several investigators have used equivalent circuit analysis to explore and explain impedance changes on reagentless and labelless electrodes, as a result of the growth of *P. aeruginosa*. In this section the data from experiments carried out with *P. aeruginosa* PA14 are applied to comparable equivalent circuit models and contrasted to related investigations. In this part of the discussion, the results from this study are contrasted to comparable published studies.

Muñoz-Berbel et al. (2006) found a drop in the CPE of an equivalent circuit used to monitor adhesion of *P. aeruginosa* to a gold microelectrode. The equivalent circuit used in this study consisted of a CPE in series with a resistance. The CPE represented the electrode-electrolyte double layer and the resistance represented the solution resistance (Figure 7-7). At 80 hours, a drop of 20% was observed in the  $K_{CPE}$  parameter with fresh saline pumped over the electrode surface, as defined using the ZView software package. The investigators linked this to microbial attachment and biofilm formation on the electrode surface.

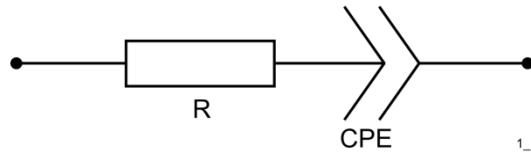


**Figure 7-7: Munoz-Berbel et al. (2006) basic equivalent circuit to model microbial attachment and biofilm formation of *P. aeruginosa*.**

In order to contrast this to the electrode developed in this study, the equivalent circuit used by Muñoz-Berbel et al. (2006) was applied to an early experiment carried out with *P. aeruginosa* PA14 (see section 4.4). The change in the CPE element over time was calculated as follows (this equation has also been used by Kim et al. 2011):

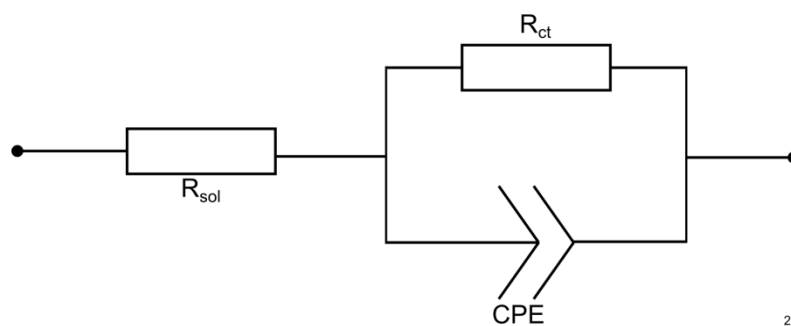
$$K_{CPE\ Diff} = \left( \frac{K_{CPE\ t} - K_{CPE\ t0}}{K_{CPE\ t0}} \right) \times 100 \quad [7-2]$$

Where  $K_{CPE\ Diff}$  is the relative increase in the modelled  $K_{CPE}$  parameter,  $K_{CPE\ t0}$  is the starting value and  $K_{CPE\ t}$  is the value at the specific timepoint contrasted to the starting measurement. Comparison of the measurements carried out in fresh media following the growth of *P. aeruginosa* to the initial measurement indicate that an increase in  $K_{CPE\ Diff}$  of over 85% occurs following the growth of *P. aeruginosa* PA14. This differs from the results found by Muñoz-Berbel et al. (2006). In their study, a drop in  $K_{CPE}$  of 20% was observed.

**Table 7-8: Analysis of data from PA14 measurement in LB with Munoz-Berbal et al. equivalent circuit. The data shows that an increase of over 85% occurs in the  $K_{CPE}$  parameter when fresh LB is added to the electrode at the end of the experiment. This is in contrast to the results of Muñoz-Berbal et al. (2006) where a drop of 20% was observed.  $K_{CPEdiff}$  was calculated using equation [7-2].  $n_{CPE}$  is a measure of the electrode roughness from equation [2-43] and  $R$  is the series resistance described in Figure 7-7.**

Condition	$K_{CPE}$ (error %)	$n_{CPE}$ (error %)	$R$ ( $\Omega$ ) (error %)	$K_{CPE Diff}$ (%)
Neg Ctrl 0 Hrs	$1.79 \times 10^{-7}$ (0.79)	0.93 (0.15)	608.2 (0.63)	-
Neg Ctrl 72 Hrs	$1.93 \times 10^{-7}$ (0.63)	0.93 (0.12)	566.5 (0.51)	7.82
Neg Ctrl Fresh Media	$1.93 \times 10^{-7}$ (0.49)	0.93 (0.09)	603.4 (0.4)	7.82
PA14 0 Hrs	$1.93 \times 10^{-7}$ (1.47)	0.92 (0.28)	589 (1.17)	-
PA14 72 Hrs	$1.10 \times 10^{-6}$ (3.5)	0.75 (0.85)	497.5 (2.64)	469.95
PA14 Fresh Media	$3.58 \times 10^{-7}$ (1.66)	0.88 (0.35)	587 (1.31)	85.50

In another study, Kim et al. (2011) employed a different equivalent circuit and found similar results to Muñoz-Berbal et al. (2006). In these experiments, Kim et al. (2011) used a platinum disc electrode to measure impedance of *P. aeruginosa* PA14. Application of an equivalent circuit similar to the Randles model (Figure 7-9) was used to demonstrate that a drop in  $K_{CPE}$  of 12.5% was seen after 72 hours. Kim et al. (2011) attributed the change in the impedance to microbial attachment reducing the electrode active area. Using the ZView instant fit tool, the model shown in Figure 7-9 was applied in order to determine if similar changes to those observed by Kim et al. (2011) could be seen following the measurement of *P. aeruginosa* PA14 (see section 4.4.1). Interestingly, the results show that there is an increase in the CPE of over 81% when fresh media is added to the electrode chambers (Table 7-3).



2\_1

**Figure 7-9: Kim et al. (2011) equivalent circuit. The circuit used is similar to the Randles circuit, with the double layer capacitance replaced by a CPE to reflect the capacitive properties of the electrode-electrolyte interface.**

**Table 7-3: Analysis of data from PA14 measurement in LB with Kim et al. (2011) equivalent circuit. The data shows that an increase of 81% occurs in  $K_{CPE}$  at the end of the experiment when fresh LB media is added to the electrode. This is in contrast to the results of Kim et al. (2011) where a drop of 12.5% was observed.  $K_{CPE\ Diff}$  calculated using equation [2-19]. The relationship between  $R_{sol}$  and  $R_{ct}$  and CPE is defined in Figure 7-9. The parameters  $K_{CPE}$ ,  $K_{CPE\ Diff}$  and  $n_{CPE}$  are defined in equations**

Condition	$R_{sol}$ ( $\Omega$ ) (error %)	$K_{CPE}$ (error %)	$n_{CPE}$ (error %)	$R_{ct}$ ( $\Omega$ ) (error %)	$K_{CPE\ Diff}$ (%)
Neg Ctrl 0 Hrs	610.4 (0.37)	$1.76 \times 10^{-7}$ (0.48)	0.93 (0.09)	$4.44 \times 10^7$ (5.74)	-
Neg Ctrl 72 Hrs	568.1 (0.22)	$1.89 \times 10^{-7}$ (0.28)	0.93 (0.05)	$4.90 \times 10^7$ (3.96)	7.39
Neg Ctrl Fresh Media	604.5 (0.25)	$1.91 \times 10^{-7}$ (0.28)	0.93 (0.06)	$7.28 \times 10^7$ (6.84)	8.52
PA14 0 Hrs	594.8 (0.52)	$1.84 \times 10^{-7}$ (0.68)	0.93 (0.13)	$1.94 \times 10^7$ (3.89)	-
PA14 72 Hrs	517.3 (1.54)	$8.94 \times 10^{-7}$ (2.45)	0.78 (0.54)	$1.37 \times 10^6$ (5.34)	385.87
PA14 Fresh Media	595.8 (0.45)	$3.34 \times 10^{-7}$ (0.61)	0.89 (0.12)	$9.40 \times 10^6$ (3.12)	81.52

A number of factors could explain the impedance differences between this study and those carried out by Muñoz-Berbel et al. (2006) and Kim et al. (2011). In particular, the electrochemical configuration used in this study was different to that employed by the other two investigators. The use of carbon as the electrode material and the different electrode

design could explain some of the difference seen in the modelled results. Specifically, the screen printed carbon electrodes have a large area contrasted to the smaller gold electrodes used by Muñoz-Berbel et al. (2006). Therefore, one reason for the differences between the impedance observed in this study, and that observed in the study by Muñoz-Berbel et al. (2006) and by Kim et al. (2011) could relate to the extent of biofilm formation on the electrode surface. The smaller gold electrodes could have resulted in the *P. aeruginosa* cells covering a greater proportion of the electrode and therefore changing the impedance through a different mechanism to that observed in the study carried out here (for example, through an insulating biofilm, as suggested by the investigators). Also, the surface topography is likely to have had an effect. The gold electrodes used by Muñoz-Berbel et al. (2006) were fabricated using a sputtering and electroplating approach, and the platinum electrodes used by Kim et al. (2011) were fabricated by polishing platinum discs. In contrast, the surface roughness of the screen printed carbon electrodes would have been much higher. Therefore, in addition to the electrochemical differences between gold, platinum and carbon, the *P. aeruginosa* cells within the inoculated media will have encountered a different topology, which could have changed electrode-bacteria interaction. These differences are discussed further in section 7.3.2.3 below.

#### **7.3.2.2 Direct comparison of measured impedance parameters**

In addition to interpretation of the data from impedance measurements with the use of equivalent circuits, two further studies are reported on the characterisation of *P. aeruginosa* growth using EIS. Both studies rely on direct analysis of data without the use of equivalent circuits. Below a comparison is provided on the differences between these two studies and the same experiments as those used in section 7.3.2.1 for the equivalent circuit analysis.

Pires et al. (2013) studied *P. aeruginosa* biofilm formation on gold electrodes and determined that the impedance modulus increased by 400  $\Omega$  at 1300 Hz as a result of the growth of a biofilm on the electrode surface. Over longer time periods, it was found that the impedance modulus increased further to 2 k $\Omega$  after 3 days and 3 k $\Omega$  after 6 days. The investigators related these to changes on the electrode surface as a consequence of biofilm formation. In this study, no changes between the negative control and inoculated channels were visible at 1259 Hz (the closest measurement made to 1300 Hz) for any of the five different strains of *P. aeruginosa* studied in LB media. The reason that no change in the impedance was detected in this study could be related to the use of screen printed carbon as an electrode material, and the high baseline impedance highlighted in section 7.3.1.1. Pires



et al. (2013) didn't measure the impedance across the entire frequency spectrum, therefore it isn't possible to determine if similar trends to those observed here occur across the entire frequency spectrum. Another reason for the drop in impedance observed as part of this study could relate to the growth conditions used by Pires et al. (2013), which may have prevented or limited the expression of electroactive secondary metabolites. The effect electroactive secondary metabolites had upon the impedance measured in this study is discussed later, in section 7.3.5.

In the final study reviewed, Dheilly et al. (2008) incubated *P. aeruginosa* PAO1 GFP with a stainless steel electrode and concluded that there was an increase in the charge transfer resistance as a consequence of biofilm formation on the electrode surface, this was based upon the measured resistance data. In their experimental setup, Dheilly et al. (2008) used a redox probe in the media for the measurement of the impedance, therefore it is logical that biofilm formation on the electrode surface would increase the charge transfer resistance, by reducing the amount of the redox probe capable of interacting with the electrode. As described above, the results of the experiments in this study suggest that the charge transfer resistance *decreases* as a consequence of the growth of *P. aeruginosa*. Interestingly, the complex impedance plot from the study by Dheilly et al. (2008) appears to show a similar trend to that seen in the experiments carried out in this study, over the first week of the experiment. Therefore, a further analysis based upon this plot is provided below.

The complex plane plot shown in the study by Dheilly et al. (2008) was analysed to estimate the change in impedance following one week of growth of *P. aeruginosa* PAO1 GFP (Figure 7-10). The measurement after one week was analysed because it was closest to the three day time period used in the studies carried out here. From the figure, it appears that there is a drop in the impedance modulus from 15.59 k $\Omega$  to 8.06 k $\Omega$ , and phase angle from 81° to 67° as a consequence of the growth of *P. aeruginosa* PAO1 GFP, which follows the same general trend as the results found in this study. After two weeks, it appears that the charge transfer value increases from that seen in the first week, as described by the authors. The results of this study suggest that at least two different effects are seen, one related to changes that lead to an initial increase in the rate of charge transfer, followed by another event that sees the charge transfer drop in the longer term. As described by the authors, the increase in charge transfer resistance was believed to relate to biofilm formation. In the short term (i.e. 1 week) therefore, it appears that the results from the study by Dheilly et al. (2008) are consistent with the general trend observed in this project. Further experiments are

clearly required to reveal the whole story, and determine if the screen printed carbon electrodes follow the same trend after 2 weeks growth.

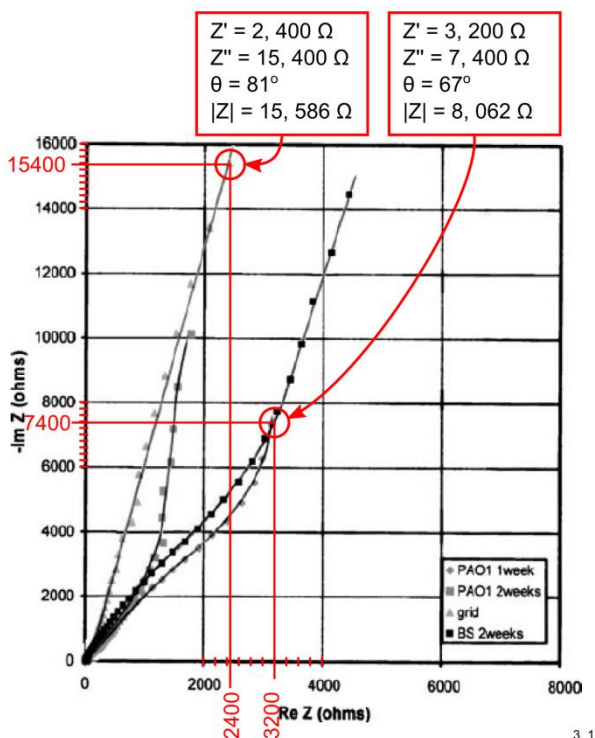


**Figure 7-10: Complex plot of sterile grid electrode and grid electrode after 1 and 2 weeks of biofilm cultivation, taken from Dheilly et al. (2008). The plot has been analysed to determine the phase angle and impedance modulus of the negative control (grid) and electrode containing PAO1 biofilm. Annotation is shown in red. It can be seen from the analysis that there is a drop in the impedance modulus and phase as a consequence of the growth of PAO1. BS represents data from biofilm formation on a separate electrode by *Bacillus subtilis* and is not discussed further here.**

### 7.3.2.3 *P. aeruginosa* impedance changes and microbial attachment

A common theme throughout the above studies is the formation of *P. aeruginosa* biofilm on the electrode surface impeding or inhibiting the transfer of charge across the electrode-electrolyte interface and also decreasing the double layer capacitance (Dheilly et al. 2008; Kim et al. 2011; Muñoz-Berbel et al. 2006; Pires et al. 2013). In this project, microscopy was carried out on biofilms produced by *P. aeruginosa* PA14 grown in both LB media (section 4.5) and ASM (section 5.5). This section takes microscopy results from the above impedance studies with *P. aeruginosa* and contrasts them to the microscopy findings in this study. A brief summary of the microscopy findings from this study are provided, and then contrasted to the literature.

In general, the outcome of the crystal violet (CV) staining carried out indicates that microbial attachment occurs on the screen printed carbon electrode surface as a consequence of the growth of *P. aeruginosa* (see section 4.5.1). It can be seen that the general trend across the CV staining experiments is that regardless of the *P. aeruginosa* strain tested, the quantity of CV is always higher than the negative control at the end of the experiment. Epifluorescent microscopy and SEM provided further insight to the extent of microbial attachment.

Extensive biofilm formation on the electrode surface was only observed when the electrode was located at the air liquid interface (Figure 4-17 C & D and Figure 5-33). These structures are consistent with other reported studies of *in vitro* biofilm formation and suggest that at the air liquid interface channel structures are present, thought to facilitate the circulation of nutrients (Costerton et al. 1999). However, at the bottom of the electrode chamber where impedance measurements were carried out, the extent of biofilm formation appears to be limited to microcolony formation (Figure 4-17 A & B and Figure 5-35). Therefore, the microscopy results from this study appear to indicate that the extent of biofilm formation at the bottom of the electrode chambers (i.e. where the impedance measurements were taken) was limited contrasted to other studies (Dheilly et al. 2008; Kim et al. 2011; Muñoz-Berbel et al. 2006; Pires et al. 2013).

More specifically, Kim et al. (2011), show that extensive biofilm exists on the electrode during measurement (Figure 7-11 A), and Dheilly et al. (2008) show large quantities of biofilm formation on the electrode surface (Figure 7-11 B). Muñoz-Berbel et al. (2006) also showed that biofilm formed on the surface of the electrode after 80 to 150 hours of incubation, although this appears to a lesser extent than the other studies discussed. Pires et al. (2013) also shows that there is extensive biofilm formation on the surface of the electrode, although much of this contained non-viable cells due to treatment with a biocide. The more extensive biofilm formation observed in these studies could explain some of the reasons why the impedance findings are different to those observed here.

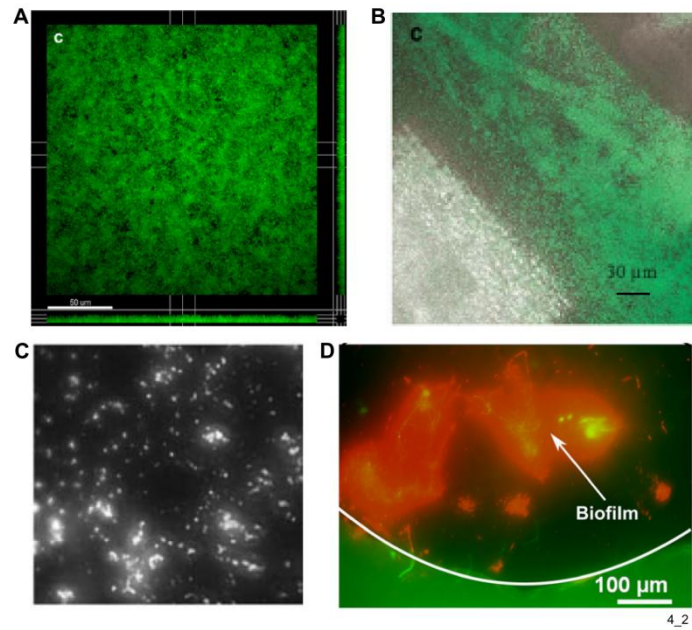


**Figure 7-11: CLSM images of electrode surface at 72 Hours from studies by (A) Kim et al. (2011) with *P. aeruginosa* PA14, bar represents 50  $\mu\text{m}$ , (B) Dheilly et al. (2008) with *P. aeruginosa* PAO1 GFP, bar represents 30  $\mu\text{m}$ , (C) Muñoz-Berbel et al. (2006) with *P. aeruginosa* (taken with 40x objective). (D) Pires et al. (2013) *P. aeruginosa* UCBPP-PA14, bar represents 100  $\mu\text{m}$ .**

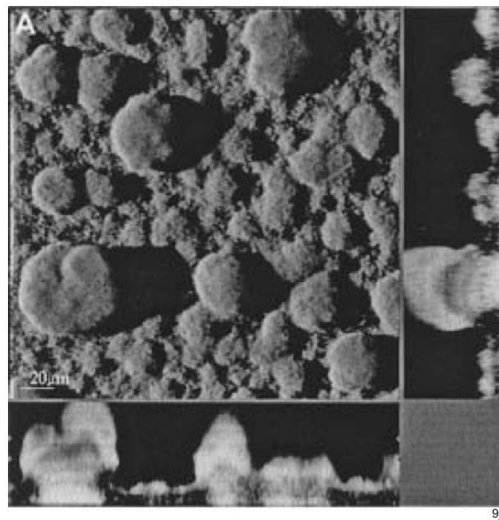


**Figure 7-12: Example of PAO1 wild type biofilm formation in flow cell with minimal media , showing large, three dimensional biofilm structures (taken from Klausen et al. 2003)**

### 7.3.3 Impedance changes with related CF microorganisms in ASM

As described in section 1.2, the CF airway is colonised by a complex microbiome from an early age. A typical situation within the CF airway is a polymicrobial infection consisting of several different microorganisms. Specifically, *S. aureus* and *H. influenzae* are present from an early age, and before *P. aeruginosa* (Cystic Fibrosis Trust 2013). Therefore, these two organisms were tested in a number of different experiments in section 5.3.1 and section 5.3.2 to determine if the changes found in the impedance were related specifically to *P. aeruginosa* or were general changes also observed with other microorganisms. Additionally, impedance measurements were carried out with *C. albicans* to investigate a eukaryotic species also often cultured from sputum (Sudbery 2011).

Whilst the laboratory media used in the experiments discussed above was appropriate for initial investigation and provided a good basis for comparison with the literature, it is not representative of the CF airway. To investigate the growth of *P. aeruginosa* in an environment more representative of the CF airway, artificial sputum media was used in conjunction with a microaerophilic environment to mimic conditions within the lungs (Kirchner et al. 2012). This section focuses upon a discussion of these results and contrasts the impedance data from experiments carried out with *S. aureus* to those reported in the literature (no comparable impedance experiments with *H. influenzae* and *C. albicans* were identified from the literature).

#### 7.3.3.1 Impedance changes resulting from *S. aureus*

*S. aureus* resulted in some small changes in the impedance, mainly seen as a peak in the normalised phase when the bacteria was grown in TSB media and only added to the electrode for the purpose of the measurement. As described in section 5.3.1.1, this could have been due to the higher cell density that appeared to result from growth outside the electrode chamber ( $1.1 \times 10^9$  CFU/ml *ex situ* vs.  $5.5 \times 10^7$  CFU/ml in the chamber). Interestingly, the large drop in phase angle observed when *P. aeruginosa* was grown did not occur with *S. aureus*. This suggests that a different impedance signature exists between the two species, implying that *P. aeruginosa* could be detected against a background *S. aureus* infection.

The changes observed in the impedance are comparable to Paredes et al. (2013) who found that a relative increase in the measured resistance value of 14 % occurred at 100 Hz after incubation of *S. aureus* on an interdigitated gold microelectrode for 20 hours. This is similar

to the results found in section 5.3.1.1 where the peak normalised resistance at 24 hours was 10% higher than the initial measurement. The key differences between this study and Paredes et al. (2013) are the electrode material and the proximity of the electrode during the incubation period. In the study carried out here, the peak normalised resistance was found to be higher when the bacteria was incubated *ex situ*, whereas for the study carried out by Paredes et al. (2013), the bacteria were incubated *in situ*. All the measured frequencies from Paredes et al. (2013) show that there is an increase in the relative resistance, therefore it is unlikely that a peak similar to the one found during this project existed within their data. This again suggests that the different electrode material, electrochemical configuration and *S. aureus* strain used have an impact upon the impedance.

In another study, Farrow (2010) investigated the use of screen printed carbon electrodes to detect the presence of *S. aureus* and found it was difficult to directly identify the bacteria with the screen printed carbon electrodes used. However, in the same study, when *S. aureus* was grown in a suspension of MHB with 5% w/v glucose, a peak in the impedance magnitude of a 20% increase was observed at approximately 5 kHz. These results were seen with Ag-AgCl electrodes, rather than carbon electrodes and indicate that changes in the electrode material and design impacts the ability to detect *S. aureus* (Farrow, 2010).

### **7.3.3.2 Impedance changes resulting from *H. influenzae***

The results with *H. influenzae* grown in HTM show a similar trend to the *S. aureus* experiments. When *H. influenzae* is grown in the presence of the electrode, it was found that no viable cells could be cultured from the media. Therefore, the viability of the bacteria appears to be compromised by the presence of the carbon electrode or by the silicone adhesive used to assemble the electrode chambers. However, results *ex situ* across three separate experiments show that two changes occur in the impedance spectrum. Firstly, there is a relative drop in the low frequency phase angle contrasted to the negative control. This can be seen under ideal growth conditions (i.e. microaerophilic growth in HTM, in a 24 well plate) and also in ASM media supplemented with NAD and hemin (figure 5-11 and 5-12). There are no reported studies of the measurement of *H. influenzae* using impedance spectroscopy in a labelless manner, therefore these results are difficult to interpret in the context of other literature.

### **7.3.3.3 Impedance changes resulting from *C. albicans***

Impedance experiments were carried out with *C. albicans* in order to determine if any characteristic changes in impedance could be observed. This microorganism is particularly interesting to study as it is a eukaryote rather than a prokaryote and therefore fundamentally different. The results in both TSB-YE media and in ASM did not reveal a clear impedance signature for *C. albicans*, although a slight deviation in the normalised resistance was seen at 1 kHz and in the normalised phase at 10 kHz contrasted to the negative control when grown in TSB-YE. Further analysis is clearly required to explore the impedance of *C. albicans* further, possibly with a different electrode material to determine if a trend can be identified.

### **7.3.3.4 Impedance changes resulting from polymicrobial co-cultures with *P. aeruginosa***

For each of the experiments carried out with the *S. aureus*, *C. albicans* and *H. influenzae*, polymicrobial measurements were also carried out with *P. aeruginosa* (sections 5.3.1.2, 5.3.2.2 and 5.3.3.2). The results indicate that it remains possible to detect the presence of *P. aeruginosa* even when one of the other species is present. Furthermore, the impedance signature changes are similar to those observed when *P. aeruginosa* is grown alone.

### **7.3.4 Impedance changes in the normalised impedance spectrum following growth of *P. aeruginosa*.**

Trends are observable in the normalised impedance data resulting from *in vitro* growth experiments with *P. aeruginosa*. In order to fully assess the sensitivity of the electrode developed for the detection of *P. aeruginosa*, particularly in the context of other microorganisms, the peak detection algorithm was used to perform a meta analysis of the mean data for each impedance measurement carried out. This was carried out with data from all of the mono-culture and polymicrobial experiments described in chapter 4 and chapter 5. The raw results following the application of the peak detection algorithm to each impedance sweep are described in Appendix C.

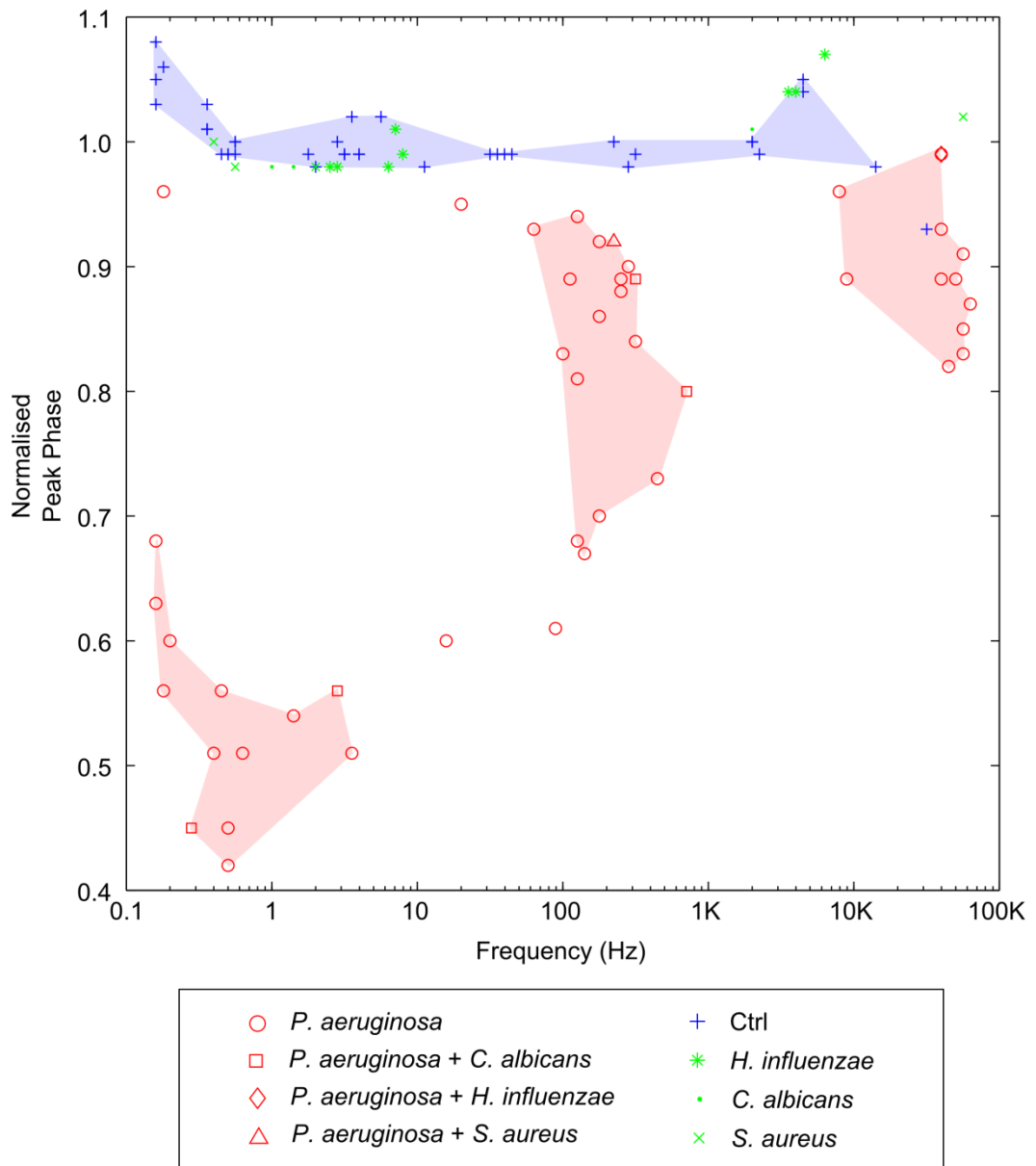
The peak detection algorithm can be used to detect peaks and troughs in the normalised impedance data (see section 3.8.3 for full description of algorithm). It was noted across the experiments carried out that peaks and troughs were frequently present in both the normalised phase and normalised resistance data. In contrast, peaks and troughs were rarely

seen in the normalised reactance and normalised modulus data. Therefore, this section focuses upon normalised phase and resistance peaks and troughs.

Both peaks and troughs were readily identified in the normalised phase data from all the impedance sweeps carried out, regardless of species or whether the electrode chamber was a negative control. However, it was clear from the experiments that the peaks and troughs observed in chambers where *P. aeruginosa* was present differed from those seen in chambers where *P. aeruginosa* was not present. In general, this trend related to a drop in the phase angle, which was greater at low frequencies than at high frequencies. This large drop in the normalised phase can be explained by the production of electroactive phenazine compounds, which are discussed in detail in the next section. However, beyond the overall drop in the impedance is a trend for local peaks and troughs. As can be seen Figure 5-1 A, these often occurred close to each other.

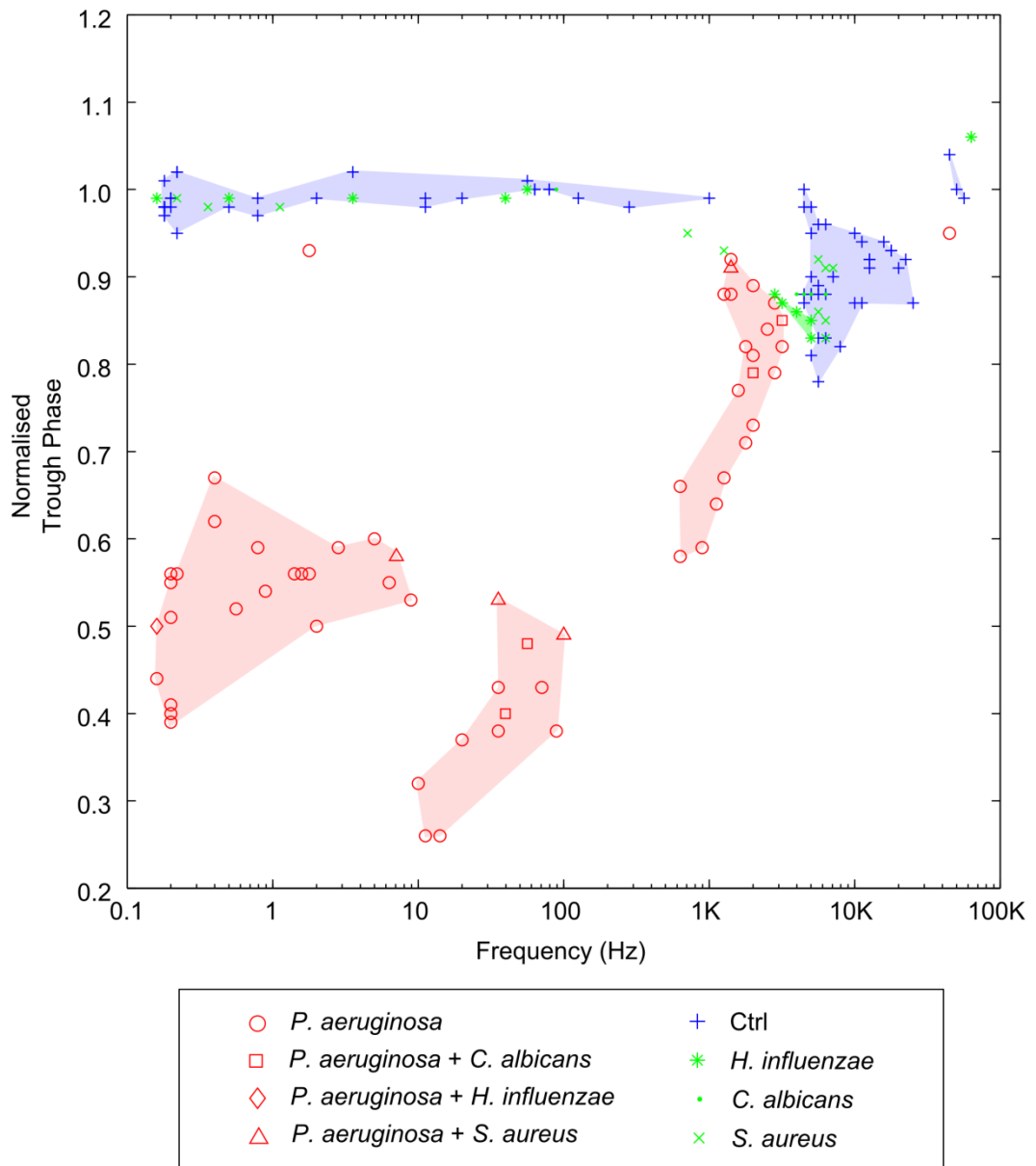
Interestingly, the peaks and troughs appeared to collect within three different frequency regions (depicted as shaded regions in Figure 7-14 and Figure 7-20). These were: below 10 Hz, between 10 Hz and 10 kHz, and above 10 kHz. As previously discussed in section 1.3 and section 2.2, different effects dominate the electrode-electrolyte interface at different frequencies. The small peaks and troughs observed suggest that, in addition to the large change in the electrode-electrolyte interface seen as a drop in phase angle across the impedance spectrum, other processes could be affecting the impedance. Each of these frequency ranges is discussed in detail in the following sections.





12\_d\_1

**Figure 7-13: Peak detection algorithm applied to normalised phase peak data. Ten measurements were performed per frequency decade, therefore the absolute resolution of the peaks identified at higher frequencies could be increased if more measurements were performed at these frequencies.**



13\_d\_1

**Figure 7-14: Peak detection algorithm applied to normalised phase trough data.**

**Ten measurements were performed per frequency decade, therefore the absolute resolution of the peaks identified at higher frequencies could be increased if more measurements were performed at these frequencies.**

### 7.3.4.1 Impedance changes at high frequencies

At high frequencies (e.g. above 10 kHz), the interface is dominated by the solution resistance and the capacitance of the double layer. Therefore, the high frequency peaks and troughs observed could be related to adsorption of macromolecules onto the electrode surface. As suggested in previous studies, ion adsorption to the electrode surface could be responsible for some of the high frequency changes in impedance (Hause, 1981). Changes to the media conductivity could also have an impact at the higher frequencies (Figure 7-15).

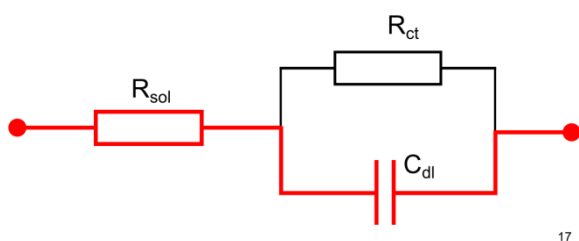


**Figure 7-15: Current path at high frequencies. The predominant current path at high frequency is shown in red.**

Clear differences can be seen between *P. aeruginosa* positive impedance signatures and the negative control in the high frequency normalised phase angle. The most interesting differences exist in the normalised phase trough, where *P. aeruginosa* positive electrodes exhibit a trough that occurs at a slightly lower frequency than the negative control. Furthermore, the *H. influenzae* positive impedance signatures also appear to exhibit a trough in between the *P. aeruginosa* positive and negative chambers (Figure 7-14). These results suggest that compounds adsorbing to the electrode over longer periods of time have an impact on the impedance. Characteristic changes to the impedance may result from these processes that allow particular organisms to be identified.

### 7.3.4.2 Impedance changes at intermediate frequencies

At the intermediate frequencies, the double layer starts to become fully charged, and an interplay exists whereby charge transfer is via the double layer capacitance and in part by electron transfer (Figure 7-16). These transfer mediators could be present in such small quantity that their contribution to the impedance changes are only visible during the change over from a purely capacitive to purely resistive interface, thus causing an undulation in the phase angle, which is observed as a peak or trough when the signature is normalised.

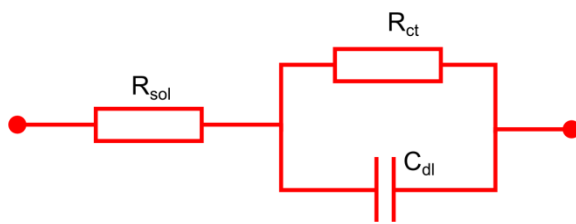
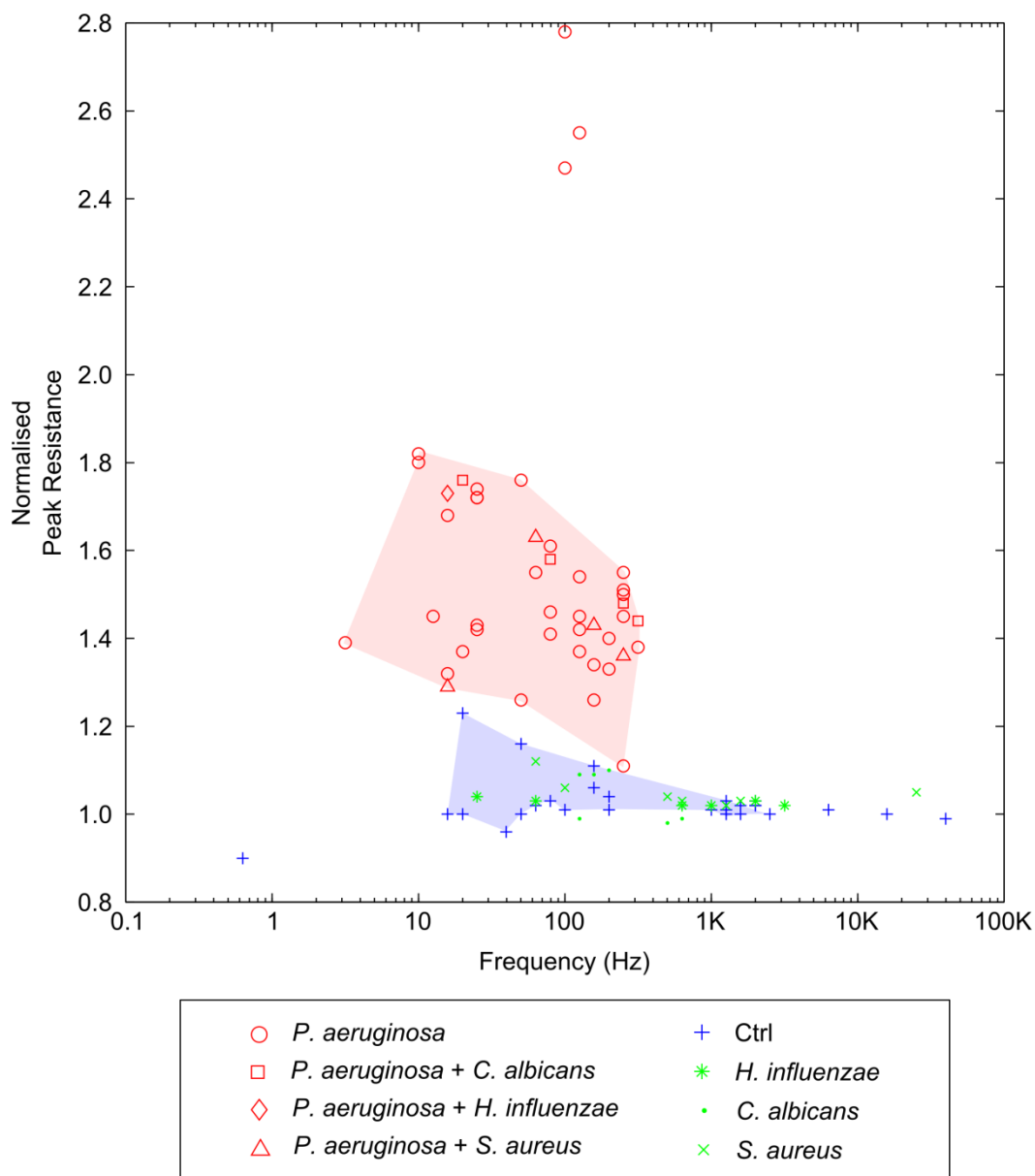


**Figure 7-16: Current paths at intermediate frequencies. At intermediate frequencies, portions of the current follow both paths.**

In the context of this study, the small peaks and troughs observed in the normalised phase could be related to the presence of charge transfer mediators capable of rapid charge transfer produced by the bacteria. Examples of these charge transfer mechanisms could include electroactive metabolites (Brutinel and Gralnick 2012; Gralnick and Newman 2007; Newman and Kolter 2000; Marsili et al. 2008a; Hernandez and Newman 2001), biofilm material containing charge transfer proteins such as cytochrome C (Schrott et al. 2011) and direct microbial attachment with nanowires (Gorby et al. 2006; Reguera et al. 2006).

The capacitive nature of the interface could also be affected by the presence of the bacteria within the sample. As shown in Figure 2-7, an alpha dispersion is seen in biological material between 100 and 1000 Hz. This is thought to be related to the cell membrane-electrolyte interactions (Rigaud et al. 1996). Therefore, microorganisms adsorbed to the electrode surface could cause the changes in the impedance seen at the intermediate frequencies. Cells attached to the electrode surface could transiently provide an alternative charge transfer path at a specific range of frequencies. Other investigators have reported that the presence of cells within the media result in a drop in the interface capacitance due to the presence of protons, produced by metabolically active bacteria, balancing more charge on the electrode than other ions (Noble et al. 1999).

At intermediate frequencies, prominent peaks were also observed in the normalised resistance in the presence of *P. aeruginosa* (Figure 7-17). As discussed in section 2.2.4, an increase in the measured resistance does not directly relate to  $R_{ct}$  and is influenced by the solution resistance, the interface capacitance and the frequency (see equation [2-45]).



11\_d\_1

**Figure 7-17: Peak detection algorithm applied to the normalised resistance data. The datapoints on the plot represent the mean peak observed for each time point from all of the *in vitro* experiments under taken with wild type strains. Ten measurements were performed per frequency decade, therefore the absolute resolution of the peaks identified at higher frequencies could be increased if more measurements were performed at these frequencies.**

### 7.3.4.3 Impedance changes at low frequencies

The perturbation wavelength at lower frequencies is longer and therefore the bulk of the charge transfer must occur through electron transfer across the interface (Figure 7-18). As described in section 2.2, electron transfer is dependent upon the electrode redox potential,

the perturbation amplitude, the presence of charge transfer mediators and their diffusion profile close to the electrode surface.

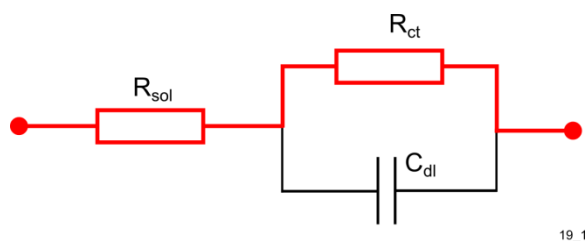


**Figure 7-18: Current path at low frequencies. The predominant current path at low frequencies is shown in red.**

Given the results relating to the presence of phenazine secondary metabolites, the changes observed at these frequencies are most likely to be related to an abundance of pyocyanin and related phenazines. In addition to electroactive mediators, protein adsorption has been shown to have an effect upon the measured impedance at lower frequencies. For example, protein adsorption onto gold electrodes has previously been shown to cause a decrease in the capacitance of the interface, dependant on the type of protein adsorbed to the electrode surface (Moulton et al. 2004). Increases to the electron transfer resistance were also observed, believed to be related to the formation of a proteinaceous layer on the electrode surface. These results were seen with human serum albumin and human immunoglobulin G (Moulton et al. 2004). In this study, given the large impact on the impedance caused by secondary metabolites the more subtle processes related to protein adsorption underway at the electrode surface are not seen directly, but could be responsible for the small peaks and troughs seen at these frequencies. Additionally, the high baseline impedance of the carbon electrodes is likely to have a masking effect on many of these processes. These problems are in part addressed by the experiment carried out with the double knockout mutant, which is discussed in the next section.

#### **7.3.4.4 Peak detection algorithm applied to double knockout mutant**

From the discussion above, it is clear that the presence of the phenazine secondary metabolites play a large role in the impedance changes observed at low and intermediate frequencies. In order to review the impedance changes caused by *P. aeruginosa* when no phenazines are present, the peak detection algorithm was applied to the impedance measurements taken with the double knockout mutant, as described in section 5.4.4. The peaks and troughs identified were superimposed onto the figures presented above as part of the peak-trough trend analysis (Figure 7-13, Figure 7-14 and Figure 7-17). Interestingly, the high frequency troughs observed in the normalised phase trough data were in locations

comparable to those seen with the wild type strain of *P. aeruginosa* PA14 (Figure 7-19 A). The other normalised impedance parameters did not result in a peak location different to the negative control (Figure 7-19 B and Figure 7-19 C), although positive peaks in the normalised resistance were on the boundary of the typically observed negative control values.

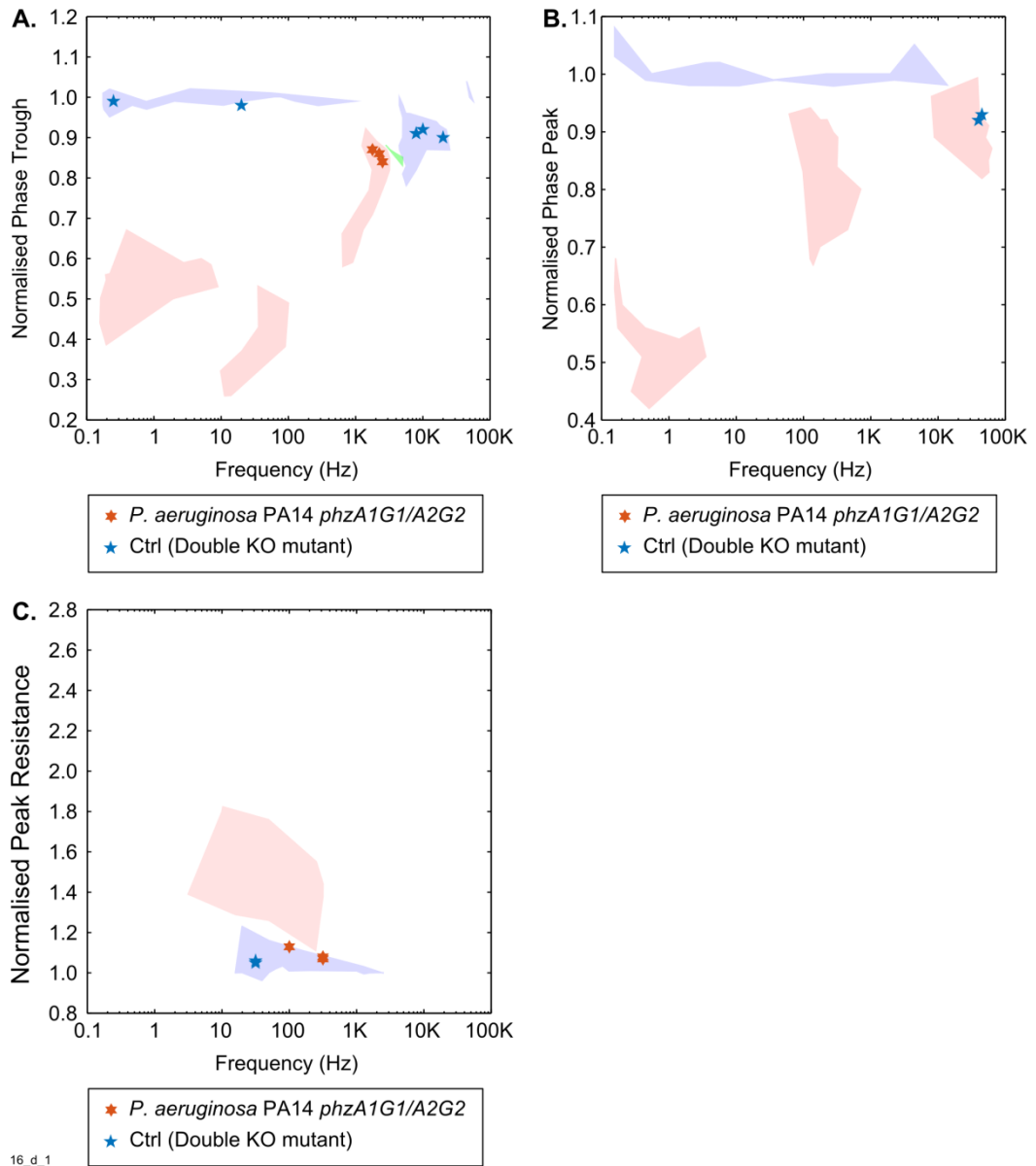


**Figure 7-19: Peaks and troughs identified in the normalised phase and resistance data applied to the *P. aeruginosa* PA14 *phzA1G1/A2G2* mutant. (A) Normalised phase trough, (B) Normalised phase peaks, (C) normalised resistance peaks. Background shading is taken from Figure 7-13, Figure 7-14 and Figure 7-17, and represents the regions where peaks and troughs were previously identified. Blue = negative control; Red = *P. aeruginosa*; Green = *H. influenzae*.**

This could be related to small quantities of biofilm formation found on the electrode surface (Figure 5-35 and Figure 5-36). As discussed in section 1.3, it is possible that changes to the electrode surface are caused by small microcolonies attached to the electrode surface. Poortinga et al. (1999, 2001) highlighted that charge transfer can occur during initial attachment to an electrode and Bayoudh et al. (2008) drew similar conclusions using an ITO electrode and impedance spectroscopy. Once attached to the electrode surface, the biofilm produced could have conductive properties, as described previously, through the excretion of cytochrome-c (Schrott et al. 2011) and also as a consequence of other redox active compounds adsorbed to the electrode surface, such as riboflavin (Marsili et al. 2008a).

Clearly, further investigation is required to fully understand the peaks observed with the double knockout mutant. However, the result suggests that changes to the electrode occur by more than just electroactive secondary metabolites. Furthermore, the fact that a change is observed at higher frequencies, where the overall electrode impedance is lower, could again imply that an electrode with a lower baseline impedance would be sensitive to further changes, beyond the production of electroactive metabolites.



### 7.3.5 Investigation into phenazine production and impedance

Pyocyanin and related phenazines have widely reported redox active properties (Friedheim and Michaelis 1931; Price-Whelan et al. 2006; Sharp et al. 2010; Sismaet et al. 2014; Wang and Newman 2008). Friedheim and Michaelis (1931) studied the normal potential of purified pyocyanin and found that the colour of the pigment changes based upon the solvent pH and its reduced or oxidised state. At low pH, the compound was found to exist in three states, a wine-red oxidised state, a green state and a colourless reduced state. At neutral and higher pH, the compound appeared blue when oxidised and colourless when reduced. The results in section 5.4.1 show that pyocyanin can be identified within the media from this experiment. From the results, it is also interesting to note that the colour change in the oxidised media is green, rather than blue (compare Figure 5-22 which shows an overnight *P. aeruginosa* culture to Figure 5-29 showing purified pyocyanin). Alternatively, colour difference could have been caused by the presence of other coloured compounds produced by *P. aeruginosa*, giving the green appearance. For example, siderophores such as pyoverdins are also produced by *P. aeruginosa* and have a yellow-green colour (Cox and Adams 1985). Other phenazines have different colours including orange, yellow and green (Price-Whelan et al. 2006).

In the experiments carried out in section 5.4, the effect that pyocyanin had upon the impedance of a sterile culture was explored. To achieve this, the impedance of pyocyanin alone in ASM at different concentrations, from 1000  $\mu\text{M}$  to 10  $\mu\text{M}$  was measured (section 5.4.2). Only a slight change in the impedance was seen at low frequencies and high concentrations of pyocyanin (1000  $\mu\text{M}$  to approximately 500  $\mu\text{M}$ ), which were unrepresentative of the changes observed when the impedance of a culture containing *P. aeruginosa* PA14 (alone or polymicrobial) was measured (Figure 5-25, section 5.4.2 contrasted to Figure 5-1, section 5.2). This could be because the pyocyanin existed in its oxidised form and therefore no reduced pyocyanin was available to balance the redox reaction at each electrode.

On the pyocyanin biosynthesis pathway, there are a number of phenazines produced by *P. aeruginosa* (Mavrodi et al. 2001). Therefore, pyocyanin could have been just one of multiple electroactive compounds that transferred electrons in a chain, with the compounds at an appropriate redox potential compared to the electrode causing the change in impedance. The synthesis pathway of pyocyanin in *P. aeruginosa* is also responsible for the production

of phenazine-1-carboxylic acid, 1-hydroxyphenazine, phenazine-1-carboxamide and 5-methylphenazine-1-carboxylic acid betaine (Dietrich et al. 2006b; Mavrodi et al. 2001; Price-Whelan et al. 2006; Winsor et al. 2011). The range of different redox active compounds present within the media could explain why results with pure pyocyanin don't cause a change in the impedance. The range of redox potentials covered by the phenazines produced by *P. aeruginosa* (Table 7-4) suggest more than one redox reaction may take in order to facilitate charge transfer at the electrode surface.

**Table 7-4: Reported redox potentials for phenazines produced by *P. aeruginosa* reported by Wang and Newman (2008) in aqueous solution at pH 7.**

Compound	Potential (vs. NHE)
Pyocyanin	- 40 mV
Phenazine-1-carboxylate	-116 mV
Phenazine-1-carboxamide	-140 mV
1-hydroxyphenazine	-174mV

In section 5.4.3, pyocyanin was added directly to a late log culture of *P. aeruginosa* and *S. aureus* in order to assess the effect it had on the impedance of these cultures. When 100  $\mu\text{M}$  or 300  $\mu\text{M}$  of pyocyanin was added, changes in the impedance were observed that were similar to the changes in phase observed through the growth of PA14 and the polymicrobial infection model (figure 5-25 and figure 5-26). These results indicate that pyocyanin plays a role in the observed impedance of *P. aeruginosa*. It has been shown previously that pyocyanin is capable of non-enzymatically oxidising NADH in a  $2e^-$ ,  $2H^+$  reaction (Kito et al. 1974), releasing iron from the protein transferrin (Cox 1986) and facilitating extracellular respiration through electron shuttling (Price-Whelan et al. 2007). It was hypothesised that these mechanisms could explain why a change in impedance was only observed when pyocyanin was added to a microbial culture. The experiments carried out with the mutants from the PA14 non-redundant library (Liberati et al. 2006) indicate that phenazines along the biosynthesis pathway contribute to the impedance in addition to *P. aeruginosa* (section 5.4.4). This shows that the impedance changes are not just caused by pyocyanin, but by a collection of redox active secondary metabolites belonging to the phenazine family.

### 7.3.6 Conclusions on *in vitro* studies of *P. aeruginosa* detection

The results from the studies carried out indicate that the impedance of the screen printed carbon electrodes produced here is affected by the growth of *P. aeruginosa*. Furthermore, in this study it has been shown that impedance changes are caused by the presence of phenazine secondary metabolites. Given the pronounced changes in impedance observed through this series of experiments, it is interesting to note that other investigators discussed above studying reagentless and labelless impedance for characterisation of *P. aeruginosa* have not identified pyocyanin as a causal agent in impedance changes. This could be explained by the focus given to microbial attachment and biofilm formation in many of these studies (Dheilly et al. 2008; Kim et al. 2012; Muñoz-Berbel et al. 2006; Pires et al. 2013). The use of a flow cell whereby the media is constantly replaced could remove redox active phenazine pigments and therefore prevent the detection of the cells. Alternatively, electrode material and electrochemical configuration used in the study here could have led to a detectable change caused specifically by phenazine production which masked changes observed in other studies. Additionally, the high impedance of the electrodes used here could also have affected the sensitivity of the electrodes and masked the changes observed in other studies. The relatively inert and unreactive properties of the screen printed carbon electrode would mean that when phenazines are present, they provide almost all of the electron transfer observed, fundamentally changing the electrode-electrolyte interface from completely polarised to being capable of supporting charge transfer. In related studies (Dheilly et al. 2008; Kim et al. 2011, 2012; Muñoz-Berbel et al. 2006) the starting electrode impedance is much lower, suggesting that the capacitive and charge transfer properties of the electrode-electrolyte interface differ. Thus, the presence of phenazine metabolites produced by *P. aeruginosa* could cause a smaller change in the impedance than those observed in this study, explaining why this often isn't identified as one of the reasons for a change in the impedance.

Testing of other species of bacteria in both optimal and suboptimal growth conditions demonstrates that *P. aeruginosa* remains specifically detectable in conditions that to a certain extent reflect those identified within the CF airway. This indicates that the electrode might be capable of specifically detecting the presence of *P. aeruginosa* in CF sputum samples. The final section of the discussion will explore the findings of initial tests carried out in human sputum samples, and make recommendations for future investigations.

## 7.4 Assessment of the electrode with human sputum samples

The final part of this study relates to initial development work carried out to test the infection monitoring device in human sputum samples from CF patients. The results from this part of the study are described in section 6.3. Here, key points of the electrode that should be taken forward into a near patient device for CF infection monitoring are discussed first. Following this, the patterns observed in the impedance data between *P. aeruginosa* positive and negative samples are discussed and limitations of the approach adopted highlighted. The final experiment carried out as part of this study related to the *in vitro* sensitivity of the device. The results of this are discussed in the context of the literature to assess the likelihood that the device can detect lung infections or pulmonary exacerbations caused by *P. aeruginosa* in CF patients.

### 7.4.1 Development of the electrode assembly

The results from testing carried out in human sputum were different to those observed *in vitro*. As described in chapter 6, this difference could have been caused by the challenges associated with placing sputum into the original electrode assembly (Figure 3-4). The small size of the electrode chamber and relative ease of production made it well suited to the *in vitro* experiments carried out. However, it was quickly realised that the chamber was not appropriate for the measurement of heterogeneous sputum samples. Furthermore, samples were often received containing sputum coated in large quantities of saliva. In addition to the difficulties associated with getting the sample into the original electrode chamber, the saliva rather than sputum often appeared to be in contact with the electrode surface. This could have reduced the sensitivity of the electrode. Sputasol was found to be effective at homogenising the first two samples, making it much easier to add them to the electrode chamber. However, this also appeared to change the normalised resistance signal in the sample that contained *P. aeruginosa* (Figure 6-4). This change could suggest that the DTT in the sputasol affected the pyocyanin-electrode interaction and masked the effect that *P. aeruginosa* present within the sample had on the impedance.

In a practical sense, a further problem with the use of sputasol relates to the implementation of a device for near patient testing. Sputasol must be stored in a refrigerator and once mixed to its working concentration, used within 48 hours (Oxoid 2014). Therefore, an additional step would have to be carried out by the device user (e.g. the patient) in order to mix the sputasol and sputum prior to the measurement. Both the challenges discussed above could

be avoided if the electrode was inverted and pushed onto the sample. This would have the benefit ensuring the sample is in contact with the electrode. Furthermore, for many heterogenous samples containing sputum and saliva, pushing the electrode into the sample could displace the saliva to ensure the electrode is in contact with the sputum where the highest concentration of *P. aeruginosa* is likely to be found.

The first development of the electrode assembly for testing in human sputum (where the electrode was integrated into the lid of a centrifuge tube – see section 6.3.2) was not successful and some of the problems associated with consistency of the electrode were identified. Specifically, the mechanical stresses placed upon the electrode during the assembly process appeared to compromise integrity of the electrodes and make them inconsistent. When the second electrode assembly for testing in human sputum (section 6.3.5) was developed, these problems were addressed and the consistency of the electrodes much improved. A future device for the measurement of sputum within a sample should embody the above points.

#### **7.4.2 Findings in CF sputum samples**

The issues described in the previous section make it difficult to conduct a meta analysis across all of the impedance measurements carried out in the previous section. Therefore, this section discusses some of the potential changes that could be related to the presence of *P. aeruginosa*, by linking the results in human sputum samples with an analysis previously carried out *in vitro* in ASM with the *ex situ* experiments.

The impedance measurements carried out with human sputum samples did not resemble the *in vitro* experiments carried out in ASM or LB media. Instead of a drop in the phase angle across a large range of frequencies (as in Figure 5-1 for example) there was little change in the phase angle even in samples suspected of being *P. aeruginosa* positive. In contrast, it is interesting to note that regardless of the properties of the sample, a peak always appeared in the normalised resistance data, regardless of whether *P. aeruginosa* was identified in the sample during microbiological analysis (Figure 6-17). This differed from the *in vitro* experiments, where a large peak in the normalised resistance data indicated the presence of *P. aeruginosa*. One explanation for the presence of the peak in human sputum samples that were negative could relate to the use of 0.9% w/v NaCl as the blanking medium. For the *in vitro* experiments carried out in the earlier part of this study, the negative control and initial measurement were taken in the same media as that used for incubation and growth of *P.*

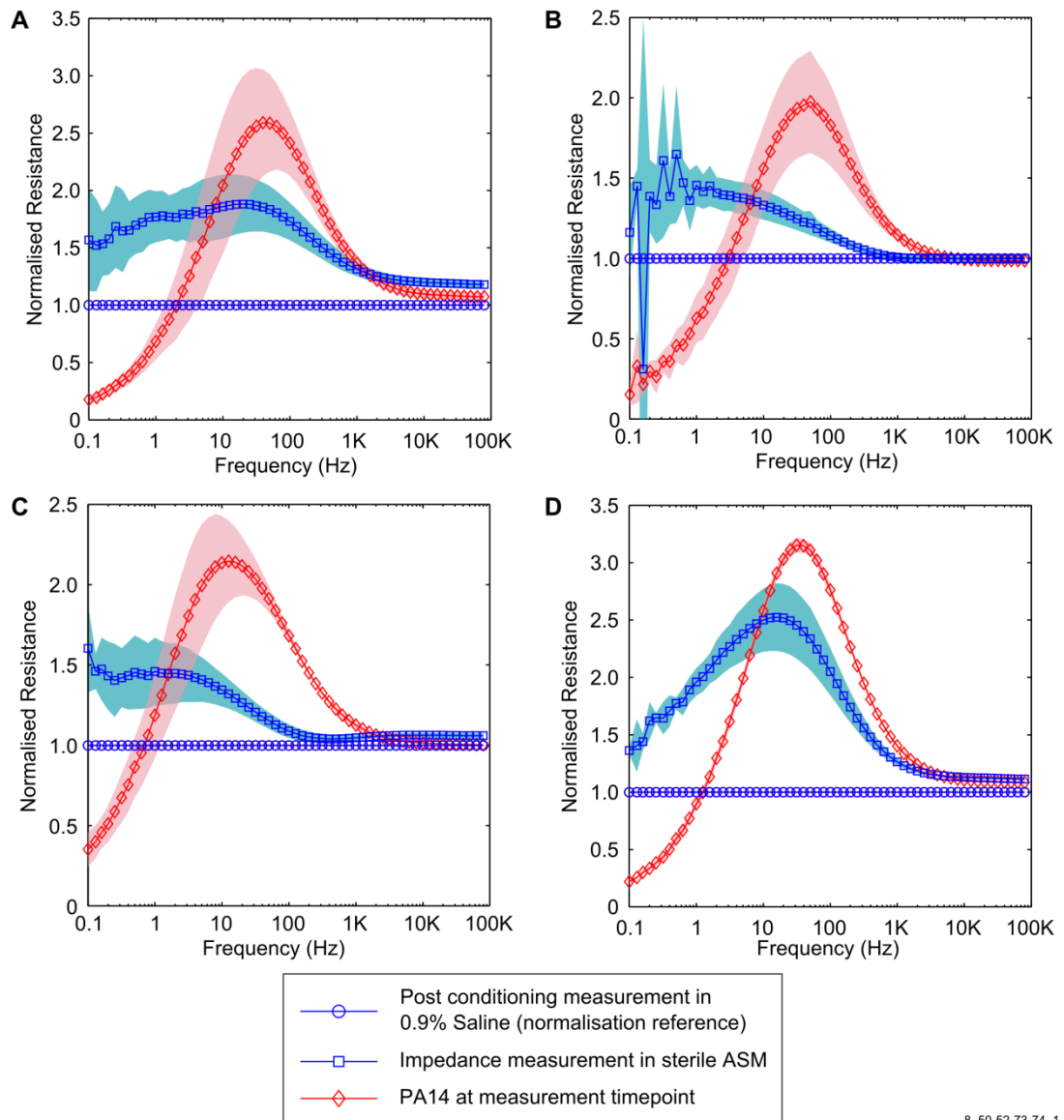
*aeruginosa*. Because of this, only impedance changes directly related to the growth of the organism, or related to small changes caused by media-electrode interactions were seen. In contrast, 0.9% w/v NaCl was used as a blanking media in the experiments carried out with human sputum. This was selected as the blanking media because it contains minimal ingredients and can be made rapidly (and therefore consistently between batches). Additionally, given its use throughout the project, it allowed the electrode baseline performance to be checked to ensure that it was consistent with all previous measurements carried out.

Given that 0.9% w/v NaCl was used for the preconditioning exercises for each of the *in vitro* experiments discussed earlier in the study (section 3.4.3), it is possible to contrast the *in vitro* results to the findings in human sputum. To explore this, data from four *ex situ* experiments carried out *in vitro* have been normalised against an impedance sweep carried out in 0.9% w/v NaCl as part of the conditioning process. When measurement in sterile ASM are normalised against the measurements after conditioning in 0.9% w/v NaCl with the same electrodes, the results show that an increase in the normalised resistance occurs at low frequencies, across each experiment (Figure 7-20). This is comparable to the normalised resistance peak observed in the data from the experiments with real sputum (Figure 6-17), where a peak is visible in the negative control data. It is particularly noteworthy that there is a large peak in the negative control data from one of these experiments when 0.9% w/v NaCl is used as the blanking media (Figure 7-20 D). This suggests that the device is less sensitive *in vitro*, when 0.9% w/v NaCl is used as the blanking media. Interestingly, the *in vitro* normalised resistance peak occurs at a frequency of more than 10 Hz (Figure 7-21), whereas the peak frequency for *P. aeruginosa* positive human sputum samples is 100 Hz (Figure 6-16). These differences could be explained by the properties of laboratory growth media contrasted to sputum. Further investigation is clearly required to understand these small differences more. The presence of the peak in the negative control normalised resistance data when blanked against 0.9% w/v NaCl clearly requires addressing. This would probably be most effectively achieved through the device implementation concept.

As shown in Figure 1-1, the concept behind the CF infection monitoring device is to measure the impedance of a sample on a daily basis. Therefore, the impedance signature from the latest sputum sample tested could be normalised against a previous reference sample from the same patient known to be *P. aeruginosa* negative. This would help to increase the

sensitivity of the device and result in impedance signatures similar to the *in vitro* ones seen earlier in this study.

The variability between the electrodes used in this study could also have had an influence on the overall sensitivity of the device. Future testing should focus upon reducing this variability to ensure that small changes in the impedance can be meaningfully interpreted. This may lead to observations such as those seen in Figure 7-14, where high frequency changes in the normalised phase are observable. Electrode manufacturing and production methods would go some way to addressing this.



8\_50-52-73-74\_1

**Figure 7-20: Analysis of data from four separate experiments, normalised against 0.9% w/v NaCl preconditioning measurements instead of measuring against sterile ASM. (A) Results from *ex situ* experiment with PA14 after 48 hours microaerophilic growth ( $n = 4$ ), (B) and (C) results from two separate experiments showing PA14 after 72 hours microaerophilic growth (B:  $n = 4$ , C:  $n = 3$ ), (D) results from PA14 *ex situ* growth after 20 hours ( $n = 3$ ).**



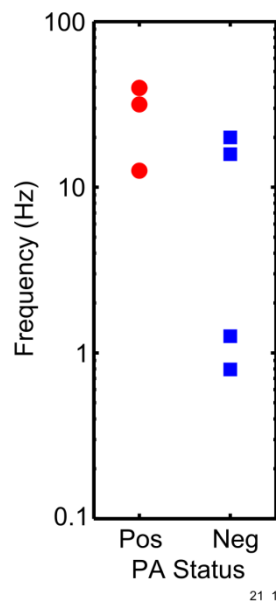


**Figure 7-21: *in vitro* normalised resistance peak data. Detected using the peak detection algorithm from the *in vitro* data presented in Figure 7-20.**

## 7.5 Assessment of electrode sensitivity

### 7.5.1 Electrode performance contrasted to other electrochemical pyocyanin sensors

The final section discusses the sensitivity of the electrode in standard laboratory media and compares this to the reported concentrations of *P. aeruginosa* and pyocyanin typically found within the CF airway. As described in section 6.6, the results of this experiment demonstrate that under these conditions, detection of *P. aeruginosa* is possible after 5 hours, when the cell density reaches between  $8.2 \times 10^8$  and  $1.2 \times 10^9$  CFU/ml. At 5 hours, the pyocyanin concentration was estimated to be 21.66  $\mu\text{M}$  (SD: 7.09) using UV-visible spectroscopy. Two other studies have been carried out that use carbon electrodes to detect and quantify pyocyanin concentration using square wave voltammetry.

Sharp et al. (2010) achieved a limit of detection of 0.030  $\mu\text{M}$  of purified pyocyanin with an unmodified carbon fibre tow electrode. This was achieved using an electrochemical set up which consisted of a carbon fibre tow working electrode, an Ag-AgCl reference electrode and Pt wire counter electrode. The investigators highlight the redox potentials of pyocyanin as -0.18 V and -0.25 V using cyclic voltammetry. Interestingly, when this sensor was used to determine the concentration of pyocyanin within cultures of different strains of *P. aeruginosa*, production didn't occur until approximately 72 hours and reached a maximum

of 25  $\mu\text{M}$  in 100 hours. This was measured with the carbon fibre sensor and independently using chloroform extraction and UV spectroscopy (Sharp et al. 2010).

Another investigation recently used a screen printed carbon sensor to measure the concentration of pyocyanin for more rapid detection of *P. aeruginosa* within laboratory cultures (Sismaet et al. 2014). In this study, different amino acids were used to accelerate the production of pyocyanin by *P. aeruginosa*. The sensor had a similar performance to that developed by Sharp et al. (2010) with a limit of detection of 0.048  $\mu\text{M}$  in Trypticase Soya Broth (TSB). In these experiments, the investigators observed low levels of pyocyanin production over the course of 10 hours, with the maximum recorded value of 2.25  $\mu\text{M}$  in TSB supplemented with 17.6 mM of valine, or 16 mM of tyrosine (Sismaet et al. 2014). A standard curve was produced using media spiked with known concentrations of pyocyanin in order to determine limit of detection of the sensor and was then employed to determine the concentration observed during the incubation period with *P. aeruginosa*. However, no independent method was used to verify that the concentration of pyocyanin measured by the screen printed sensor.

In the study carried out here, the pyocyanin concentrations over the nine hour course of the experiment were much higher than that observed in the studies by Sharp et al. (2010) and Sismaet et al. (2014). The concentration of pyocyanin observed in this study increased above 30  $\mu\text{M}$  within six hours of incubation (Table 6-6). This is similar to that observed in other studies *in vitro* (Hunter et al. 2012; Price-Whelan et al. 2007). This discrepancy could be caused by a number of different factors. Firstly, the strains of *P. aeruginosa* used by Sharp et al. (2010) were different to those employed in other studies reported in the literature (Hunter et al. 2012; Price-Whelan et al. 2007) and could have had a phenotype that resulted in lower pyocyanin production. However, Sismaet et al. (2014) used the same strain of *P. aeruginosa* as the study carried out here (i.e. PA14) so a phenotypic difference does not explain the lower pyocyanin production rates. Secondly, different media was used in the experiments carried out by Sharp et al. (2010), who used *Pseudomonas aeruginosa* broth (PAB), and Sismaet et al. (2014), who used TSB or M63 media. It is possible that the media affected the rate at which pyocyanin was produced and therefore the differences in final concentrations observed, contrasted to the study here. Using a similar technology to Sismaet et al. (2014), Webster et al. (2014) recently applied commercial screen printed carbon electrodes to detect the presence of *P. aeruginosa* in spiked human samples using square wave voltammetry. They demonstrated that it is possible to detect concentrations of

pyocyanin between 2  $\mu\text{M}$  and 20  $\mu\text{M}$  after 24 hours growth of *P. aeruginosa* in human BAL, blood, sputum and urine samples.

Sismaet et al. (2014) used a screen printed sensor to achieve the low limits of detection described above. Although square wave voltammetry was used for the measurements carried out in their study, which is a different technique to impedance spectroscopy, it demonstrates that the use of an electrode produced through screen printing could achieve a low limit of detection for pyocyanin. If the DC bias voltage used in this study was adjusted to match the redox potential for pyocyanin with the electrode system developed here, then the concentration of pyocyanin at which a change is observed in the impedance could be lower.

### **7.5.2 Electrode sensitivity in the context of CF airway infection**

Pyocyanin is widely reported as a virulence factor produced by *P. aeruginosa in vivo* (Hunter et al. 2012; Lau et al. 2004; Mowat et al. 2011; Price-Whelan et al. 2006; Wilson et al. 1988). In this section, other studies that have been carried out to quantify the concentration pyocyanin *in vitro* and *in vivo* are discussed in the context of the concentrations detectable with the electrode developed here.

*P. aeruginosa* strains PA14 and PAO1 were found to excrete phenazines *in vitro* during early stationary phase (Dietrich et al. 2006b). In aerobic LB media, the concentration of pyocyanin has been found to be between 30  $\mu\text{M}$  (Dietrich et al. 2006b) and 100  $\mu\text{M}$  (Price-Whelan et al. 2007) after 15 hours. In contrast, Fothergill et al. (2007) studied several isolates of *P. aeruginosa* from CF sputum and identified that many exhibited overproduction of pyocyanin during early rather than late phase exponential growth. A similar finding was also observed by Hunter et al. (2012) who found that *P. aeruginosa* isolates taken from patients with an FEV1 > 100 produced more pyocyanin *in vitro* than those isolated from patients with an FEV1 < 100. These results suggest that the electrode developed here could be more sensitive to the strains of *P. aeruginosa* if they over express pyocyanin. Mowat et al. (2011) found that the proportion of overproducing pyocyanin isolates found in sputum during a pulmonary exacerbation were higher than those found in stable samples. In summary, the findings in the literature suggest that the production of virulence factors and in particular pyocyanin is related to poor prognosis and pulmonary exacerbations.

The concentration of pyocyanin has also been measured from sputum samples in patients with CF and bronchiectasis. Wilson et al. (1988) found that the concentrations of pyocyanin

as high as 27 µg/ml (equivalent to 128 µM) in bronchiectasis sputum and 16 µg/ml (equivalent to 76 µM) in CF sputum. However, pyocyanin concentrations as low as 0.9 µg/ml (equivalent to 4.28 µM) were also found in some CF sputum samples (Wilson et al. 1988). To determine if these concentrations of pyocyanin can be identified with the electrode developed in this study further investigation is required to accurately establish the limit of detection. In a separate study, Hunter et al. (2012) show that the concentration of pyocyanin and other phenazine pigments is related to the FEV<sub>1</sub>. They showed that as FEV<sub>1</sub> drops, phenazine concentration increases. As shown in Table 7-5, the phenazine concentration during moderate obstruction was found to be 25.7 µM, suggesting that pyocyanin within the range detectable by the electrode described here. These findings suggest that the electrode described in this study is within range to be able to detect clinically relevant concentrations of pyocyanin and implicitly other phenazine pigments.

**Table 7-5: Distribution of phenazine concentrations between stages of disease severity (from Hunter et al. 2012)**

Obstruction	FEV1 (%)	<i>n</i>	Age in years (average)	Average total PHZ (µM)	Average PYO (µM)	Average PCA (µM)
Normal	> 90	13	31.4 ± 9.3	12.9 ± 3.8	7.7 ± 2.9	5.2 ± 1.3
Mild	70-89	5	34.8 ± 12.2	30.3 ± 12.6	10.5 ± 3.0	19.7 ± 11.6
Moderate	40-69	19	36.5 ± 10.4	42.7 ± 5.9	25.2 ± 3.7	17.5 ± 4.1
Severe	< 40	10	33.0 ± 10.9	86.8 ± 18.0	46.8 ± 8.5	39.9 ± 11.5

## 7.6 Summary and conclusions

### 7.6.1 Introduction

As described in chapter 1, chronic infections caused by *P. aeruginosa* are the leading cause of morbidity and mortality in patients with CF (Littlewood 2004). In this thesis, a low cost, screen printed carbon electrode was developed and investigated for the detection of *P. aeruginosa* in CF sputum samples (Figure 1-1). Daily monitoring of the sputum composition with respect to *P. aeruginosa* could be clinically useful in three ways. Firstly by identifying the initial onset of infection, secondly by detecting phenotypic changes that could indicate the onset of a pulmonary exacerbation, and thirdly by verifying that infections with *P. aeruginosa* have been successfully eradicated or suppressed. In the final section, the results from this project are discussed in the context of the research questions posed at the end of chapter 1 (section 1.6.2) and makes recommendations on future activities that could be undertaken in this research area.

### 7.6.2 Findings in the context of the research questions

The first two research questions posed related to the detection of *P. aeruginosa* using low cost screen printed electrodes and EIS. Specifically, these questions were:

1. Is it possible to detect the growth of *P. aeruginosa* using impedance spectroscopy and a screen printed electrode?
2. Is there a characteristic impedance signature that indicates the presence of *P. aeruginosa* in microbial broths also containing other microorganisms commonly found in the CF airway?

In chapter 4, impedance measurements carried out with five different strains of *P. aeruginosa* indicate that it is possible to detect the presence of the bacterium in standard laboratory media. Further investigation (chapter 5) showed that it was also possible to detect the presence of *P. aeruginosa* in ASM in conditions more representative of the CF airway. A key aspect of the research, as indicated by research question two above was whether *P. aeruginosa* could be detected in the presence of other microorganisms. This is important in the context of a CF infection monitor, whereby the omnipresence of other microorganisms could mask the presence of *P. aeruginosa*. To test this, experiments were carried out with *S. aureus*, *H. influenzae* and *C. albicans*, in both monocultures and co-cultures with *P.*

*aeruginosa*. The results indicated that changes observed in the impedance with *P. aeruginosa* were not also caused by mechanisms present in other microorganisms (sections 5.3.1, 5.3.2 and 5.3.3). These investigations answered the second research question and led on to the next two research questions, which were related to the underlying causes for the change in impedance:

3. Why does the impedance change as a result of microbial growth?
4. Is it possible to link a given impedance signature with a specific metabolite or compound produced by the bacteria?

As shown in the discussion (section 7.3.2), analysis of the early results highlights that a drop in the charge transfer resistance occurs as a consequence of *P. aeruginosa* growth. Therefore, the changes in impedance appeared to be related to a mechanism that facilitates electron transfer across the interface. Pyocyanin is a well reported example of an electroactive phenazine secondary metabolite produced by *P. aeruginosa* and its redox active properties and implied a role in changing the impedance. Investigations were carried out with both exogenous pyocyanin (sections 5.4.2 and 5.4.3) and with mutant strains of *P. aeruginosa* PA14 (section 5.4.4). These investigations show that pyocyanin and other related phenazine metabolites are largely responsible for the changes exclusively observed in the impedance signatures when *P. aeruginosa* is cultured. Experiments with a PA14 double knockout mutant that doesn't produce any phenazine metabolites helps to partially answer the final research question:

5. What impact does biofilm formation have on the impedance signature, both directly and indirectly?

Epifluorescent microscopy and SEM were used to understand the extent to which *P. aeruginosa* would attach to the carbon electrode surface and go on to form biofilm structures (sections 4.5.2 and 5.5 respectively). Small microcolonies and biofilm formation were observed on the electrodes located at the bottom of a 24 well plate, and much more extensive biofilm was seen at the air-liquid interface. These results indicate that *P. aeruginosa* has the capacity to attach to the screen printed carbon electrode surface and form biofilms. As mentioned above, the measurements carried out with the double knockout mutant show that small changes in the impedance are still observable. Section 1.4.1 and 1.4.2 highlight a

number of mechanisms that could facilitate electron transfer between biofilm bacteria and electrodes. These mechanisms are discussed further in the context of the results in section 7.3.4. Further investigation is required to explore this more fully, possibly with an experimental setup that facilitates the creation of a large biofilm on the electrode surface.

Although not intended as part of the original study, a small investigation was carried out to analyse the performance of the electrode for the detection of *P. aeruginosa* in human sputum samples. This part of the study tackled some of the more practical issues related to the electrode. One of the key challenges related to the development of the electrode assembly that facilitated the application of the electrode onto sputum (Figure 6-15) and the need to protect the electrode contacts from liquid (e.g. ethanol or 0.9% w/v NaCl) or from mechanical damage (section 6.3.5). Furthermore, this part of the study also highlights potential detection problems that could result from the use of 0.9% w/v NaCl as a blanking media (section 7.4). In an *in vitro* scenario, the use of 0.9% w/v NaCl led to a peak in the normalised resistance at low frequency in the negative control electrodes, a characteristic not seen when the measurements are normalised against the experiment media. These key points should be taken forward in a future electrode in order to improve the sensitivity with which the presence of *P. aeruginosa* can be detected.

The results from the final *in vitro* experiment assess the detection threshold of the carbon electrode for presence of *P. aeruginosa* PA14. The results from this indicate that this threshold occurs at a cell density of  $1.2 \times 10^9$  CFU/ml, well into logarithmic growth phase (section 6.5). This point equates to a normalised resistance peak which occurs at 6.31 Hz with an amplitude of 1.62.

In conclusion, the results from this research prove that *in vitro* detection of *P. aeruginosa* is possible using a low cost screen printed carbon electrode, in conjunction with EIS. The findings in human sputum samples suggest that it could also be possible to detect the presence of *P. aeruginosa* in the scenario, but clearly further investigation is required to demonstrate this. The next section makes some recommendations on testing that could be carried out.

### **7.6.3 Recommendations for future research**

On a fundamental level, a study should be carried out to fully understand the role that biofilm formation has on the electrode surface. In this study, it has been shown that *P. aeruginosa* is capable of microbial attachment and biofilm formation at the air liquid

interface. A modified electrode chamber could be developed to enable the measurement of impedance with an electrode located at this interface. Observed changes in the impedance could then be investigated further using mutant strains as in this study to determine specific mechanisms resulting in impedance changes.

On a more applied level, the electrode used in this study should be developed further to detect the presence of *P. aeruginosa* in human sputum samples. As mentioned above, an alternative electrode assembly was developed for measurements in human sputum samples. However, this was a pragmatic design and would benefit from further development. Specifically, the support structure used to mount the electrode should be developed so that it fits within a typical sputum sample pot. Inconsistency between some of the measurements could have resulted from mechanical damage to the electrode surface and the screen printed connectors. Therefore, the design of the support structure should also protect the electrode from mechanical damage both during assembly and use. The electrode may also benefit from further characterisation using cyclic voltammetry.

In this study, the electrode-electrolyte interface was only explored through impedance spectroscopy. A powerful electrochemical technique that can be used to explore the electrode-electrolyte interface further is cyclic voltammetry (Bard and Faulkner 2001). By varying the potential across the electrode and measuring the current, a plot can be produced which indicates the potentials at which redox processes occur (Southampton Electrochemistry Group 2001). In the context of the study carried out here, cycle voltammetry would be useful for the following two reasons. Firstly, it would enable a greater understanding and characterisation of the electrode-electrolyte interface to be gained by cycling the electrode across a range of different potentials. In particular, cyclic voltammetry could have been used to further understand the reason behind phase shift seen occasionally prior to electrode conditioning (described in section 4.3.2). Secondly, cyclic voltammetry would have provided a clear indication of the redox potentials at which the phenazines discussed in section 5.4 undergo redox reactions with the electrodes described in this thesis. Future analysis of these aspects would provide more information on the electrode properties before and after conditioning and could inform a more optimum DC bias potential for the identification of the production of phenazine metabolites.

Normalisation of the impedance data resulting from the measurements is another key factor that should be explored in a future device. Two strategies could be employed for the detection of *P. aeruginosa* using the normalisation approach. Firstly, a low cost artificial



blanking media could be developed that mimics the electrochemical properties of a *P. aeruginosa* negative sputum sample. This approach could result in the specific identification of peaks in only the *P. aeruginosa* positive samples, in a similar manner to that found during the *in vitro* measurements. Alternatively, the measured sputum sample could be blanked against a previous sputum sample from the given patient known to be *P. aeruginosa* negative.

In conclusion, several avenues of exploration exist for further refinement of the electrode developed here. Notwithstanding this, the characteristic impedance changes caused by *P. aeruginosa* suggest that a clinically useful device could be developed that would allow more rapid detection in people with CF.

## **8 REFERENCES**

- Aaron SD, Ramotar K, Ferris W, Vandemheen K, Saginur R, Tullis E, Haase D, Kottachchi D, St. Denis M, Chan F (2004) Adult Cystic Fibrosis Exacerbations and New Strains of *Pseudomonas aeruginosa*. *American Journal of Respiratory and Critical Care Medicine* 169:811–815
- Archer NK, Mazaitis MJ, Costerton JW, Leid JG, Powers ME, Shirtliff ME (2011) *Staphylococcus aureus* biofilms. *Virulence* 2:445–459
- Bakare N, Rickerts V, Bargon J, Just-Nübling G (2003) Prevalence of *Aspergillus fumigatus* and other fungal species in the sputum of adult patients with cystic fibrosis. *Mycoses* 46:19–23
- Balfour-Lynn I, Elborn JS (2007) *Respiratory disease: infection. Cystic fibrosis*. Hodder Arnold, London, pp 137–157
- Bard AJ, Faulkner LR (2001) *Electrochemical methods: fundamentals and applications*. Wiley, New York
- Baron SS, Rowe JJ (1981) Antibiotic action of pyocyanin. *Antimicrob. Agents Chemother.* 20:814–820
- Barth AL, Pitt TL (1996) The high amino-acid content of sputum from cystic fibrosis patients promotes growth of auxotrophic *Pseudomonas aeruginosa*. *Journal of Medical Microbiology* 45:110–119
- Bayouhd S, Othmane A, Ponsonnet L, Ben Ouada H (2008) Electrical detection and characterization of bacterial adhesion using electrochemical impedance spectroscopy-based flow chamber. *Colloids and Surface A* 318:291–300
- Bekir K, Barhoumi H, Braiek M, Chrouda A, Zine N, Abid N, Maaref A, Bakhrouf A, Ouada HB, Jaffrezic-Renault N, Mansour HB (2015) Electrochemical impedance immunosensor for rapid detection of stressed pathogenic *Staphylococcus aureus* bacteria. *Environ Sci Pollut Res* 1–8
- Ben-Yoav H, Freeman A, Sternheim M, Shacham-Diamand Y (2011) An electrochemical impedance model for integrated bacterial biofilms. *Electrochim Acta* 56:7780–7786
- Bhatt JM (2013) Treatment of pulmonary exacerbations in cystic fibrosis. *Eur Respir Rev* 22:205–216
- Bilton D, Canny G, Conway S, Dumcius S, Hjelte L, Proesmans M, Tümmler B, Vavrova V, De Boeck K (2011) Pulmonary exacerbation: towards a definition for use in clinical trials. Report from the EuroCareCF Working Group on outcome parameters in clinical trials. *Journal of Cystic Fibrosis* 10:S79–S81
- Bjarnsholt T (2013) The role of bacterial biofilms in chronic infections. *APMIS* 121:1–58
- Bjarnsholt T, Alhede M, Alhede M, Eickhardt-Sørensen SR, Moser C, Kühl M, Jensen PØ, Høiby N (2013a) The in vivo biofilm. *Trends in Microbiology* 21:466–474
- Bjarnsholt T, Ciofu O, Molin S, Givskov M, Høiby N (2013b) Applying insights from biofilm biology to drug development — can a new approach be developed? *Nat Rev Drug Discov* 12:791–808

- Bockris JO, Reddy AKN (1998) Modern electrochemistry. Vol 1, Ionics. Plenum Press, New York, NY
- Bockris JO, Reddy AKN, Gamboa-Aldeco M (2000) Modern electrochemistry. Vol 2A, Fundamentals of electrochemistry. Plenum Press, New York, NY
- Bone S, Zaba B (1992) Bioelectronics. Wiley, Chichester; New York
- Brandel J, Humbert N, Elhabiri M, Schalk IJ, Mislin GLA, Albrecht-Gary A-M (2012) Pyochelin, a siderophore of *Pseudomonas aeruginosa*: Physicochemical characterization of the iron(III), copper(II) and zinc(II) complexes. Dalton Trans. 41:2820–2834
- Brett CMA, Brett AMO (1993) Electrochemistry : principles, methods, and applications. Oxford University Press, Oxford ; New York
- Brock TD, Madigan MT (2009) Biology of microorganisms. Pearson Benjamin Cummings, San Francisco
- Brutinel E, Gralnick J (2012) Shuttling happens: soluble flavin mediators of extracellular electron transfer in *Shewanella*. Applied Microbiology and Biotechnology 93:41–48
- Bryant JM, Grogono DM, Greaves D, Foweraker J, Roddick I, Inns T, Reacher M, Haworth CS, Curran MD, Harris SR, Peacock SJ, Parkhill J, Floto RA (2013) Whole-genome sequencing to identify transmission of *Mycobacterium abscessus* between patients with cystic fibrosis: a retrospective cohort study. Lancet 381:1551–1560
- Cady P (1975) Rapid automated bacterial identification by impedance measurement. In: Hedén C.-G., Illéni T. (eds) New approaches to the identification of microorganisms. Wiley, London, pp 74–79
- Chiarini L, Bevivino A, Dalmastrì C, Tabacchioni S, Visca P (2006) *Burkholderia cepacia* complex species: health hazards and biotechnological potential. Trends in Microbiology 14:277–286
- Connolly P, Shedden L (2010) A System and Method for Cell Characterisation. Patent application number: WO2009136157 (A3).
- Corrigan DK, Schulze H, Henihan G, Ciani I, Giraud G, Terry JG, Walton AJ, Pethig R, Ghazal P, Crain J, Campbell CJ, Mount AR, Bachmann TT (2012) Impedimetric detection of single-stranded PCR products derived from methicillin resistant *Staphylococcus aureus* (MRSA) isolates. Biosensors and Bioelectronics 34:178–184
- Costerton JW (2001) Cystic fibrosis pathogenesis and the role of biofilms in persistent infection. Trends in Microbiology 9:50–52
- Costerton JW, Stewart PS, Greenberg EP (1999) Bacterial Biofilms: A Common Cause of Persistent Infections. Science 284:1318–1322
- Cox CD (1986) Role of pyocyanin in the acquisition of iron from transferrin. Infect Immun 52:263–270

- Cox CD, Adams P (1985) Siderophore activity of pyoverdinin for *Pseudomonas aeruginosa*. *Infection and immunity* 48:130–138
- Cox MJ, Allgaier M, Taylor B, Baek MS, Huang YJ, Daly RA, Karaoz U, Andersen GL, Brown R, Fujimura KE, Wu B, Tran D, Koff J, Kleinhenz ME, Nielson D, Brodie EL, Lynch SV (2010) Airway Microbiota and Pathogen Abundance in Age-Stratified Cystic Fibrosis Patients. *PLoS ONE* 5:e11044
- Cystic Fibrosis Foundation (2012) Patient Registry Annual Data Report.
- Cystic Fibrosis Trust (2010) Laboratory Standards for Processing Microbiological Samples from People with Cystic Fibrosis.
- Cystic Fibrosis Trust (2011) Standards for the Clinical Care of Children and Adults with Cystic Fibrosis in the UK. 49
- Cystic Fibrosis Trust (2013) UK Cystic Fibrosis Registry Annual Data Report 2012.
- Déziel E, Lépine F, Milot S, He J, Mindrinos MN, Tompkins RG, Rahme LG (2004) Analysis of *Pseudomonas aeruginosa* 4-hydroxy-2-alkylquinolines (HAQs) reveals a role for 4-hydroxy-2-heptylquinoline in cell-to-cell communication. *PNAS* 101:1339–1344
- Dheilly A, Linossier I, Darchen A, Hadjiev D, Corbel C, Alonso V (2008) Monitoring of microbial adhesion and biofilm growth using electrochemical impedancemetry. *Appl Microbiol Biot* 79:157–164
- Dietrich LEP, Price-Whelan A, Petersen A, Whiteley M, Newman DK (2006a) The phenazine pyocyanin is a terminal signalling factor in the quorum sensing network of *Pseudomonas aeruginosa*. *Molecular Microbiology* 61:1308–1321
- Dietrich LEP, Price-Whelan A, Petersen A, Whiteley M, Newman DK (2006b) The phenazine pyocyanin is a terminal signalling factor in the quorum sensing network of *Pseudomonas aeruginosa*. *Mol. Microbiol.* 61:1308–1321
- Farrow M (2010) A Wound Infection Monitoring System. University of Strathclyde
- Farrow MJ, Hunter IS, Connolly P (2012) Developing a Real Time Sensing System to Monitor Bacteria in Wound Dressings. *Biosensors* 2:171–188
- Felice CJ, Valentinuzzi ME (1999) Medium and interface components in impedance microbiology. *Biomedical Engineering, IEEE Transactions on* 46:1483–1487
- Fifield FW (2000) Principles and practice of analytical chemistry. Blackwell Science, Oxford ; Malden, MA
- Firstenberg-Eden R, Eden G (1984) Impedance microbiology. Research Studies Press, England
- Fleischmann RD, Adams MD, White O, Clayton RA, Kirkness EF, Kerlavage AR, Bult CJ, Tomb JF, Dougherty BA, Merrick JM, et al (1995) Whole-genome random sequencing and assembly of *Haemophilus influenzae* Rd. *Science* 269:496–512

- Foster KR, Schwan HP (1989) Dielectric properties of tissues and biological materials: a critical review. *Crit Rev Biomed Eng* 17:25–104
- Fothergill JL, Panagea S, Hart CA, Walshaw MJ, Pitt TL, Winstanley C (2007) Widespread pyocyanin over-production among isolates of a cystic fibrosis epidemic strain. *BMC Microbiology* 7:45
- Friedheim E, Michaelis L (1931) Potentiometric Study of Pyocyanine. *J. Biol. Chem.* 91:355–368
- Garrett TR, Bhakoo M, Zhang Z (2008) Bacterial adhesion and biofilms on surfaces. *Progress in Natural Science* 18:1049–1056
- Geddes LA (1972) *Electrodes and the measurement of bioelectric events.* Wiley-Interscience, New York ; Chichester
- Gibson RL, Emerson J, McNamara S, Burns JL, Rosenfeld M, Yunker A, Hamblett N, Accurso F, Dovey M, Hiatt P, Konstan MW, Moss R, Retsch-Bogart G, Wagener J, Waltz D, Wilmott R, Zeitlin PL, Ramsey B (2003) Significant Microbiological Effect of Inhaled Tobramycin in Young Children with Cystic Fibrosis. *Am J Respir Crit Care Med* 167:841–849
- Gillum AM, Tsay EY, Kirsch DR (1984) Isolation of the *Candida albicans* gene for orotidine-5'-phosphate decarboxylase by complementation of *S. cerevisiae* *ura3* and *E. coli* *pyrF* mutations. *Mol. Gen. Genet.* 198:179–182
- Goddard AF, Staudinger BJ, Dowd SE, Joshi-Datar A, Wolcott RD, Aitken ML, Fligner CL, Singh PK (2012) Direct sampling of cystic fibrosis lungs indicates that DNA-based analyses of upper-airway specimens can misrepresent lung microbiota. *PNAS* 109:13769–13774
- van Gool K, Norman R, Delatycki MB, Hall J, Massie J (2013) Understanding the Costs of Care for Cystic Fibrosis: An Analysis by Age and Health State. *Value in Health* 16:345–355
- Gorby YA, Yanina S, McLean JS, Rosso KM, Moyles D, Dohnalkova A, Beveridge TJ, Chang IS, Kim BH, Kim KS, Culley DE, Reed SB, Romine MF, Saffarini DA, Hill EA, Shi L, Elias DA, Kennedy DW, Pinchuk G, Watanabe K, Ishii S, Logan B, Nealson KH, Fredrickson JK (2006) Electrically conductive bacterial nanowires produced by *Shewanella oneidensis* strain MR-1 and other microorganisms. *PNAS* 103:11358–11363
- Goss CH, Muhlebach MS (2011) Review: *Staphylococcus aureus* and MRSA in cystic fibrosis. *Journal of Cystic Fibrosis* 10:298–306
- Gow NAR, van de Veerdonk FL, Brown AJP, Netea MG (2012) *Candida albicans* morphogenesis and host defence: discriminating invasion from colonization. *Nat Rev Micro* 10:112–122
- Gralnick JA, Newman DK (2007) Extracellular respiration. *Molecular Microbiology* 65:1–11

- Greger R (2000) Cystic fibrosis. Channelopathies. Elsevier Science, Amsterdam, pp 227–253
- Grimnes S, Martinsen ØG (2008) Bioimpedance and bioelectricity basics. Academic, London
- Gross H, Loper JE (2009) Genomics of secondary metabolite production by *Pseudomonas* spp. *Nat. Prod. Rep.* 26:1408–1446
- Harrison (2007) Microbial ecology of the cystic fibrosis lung. *Microbiology* 153:917–923
- Harrison JJ, Ceri H, Yerly J, Stremick CA, Hu Y, Martinuzzi R, Turner RJ (2006) The use of microscopy and three-dimensional visualization to evaluate the structure of microbial biofilms cultivated in the Calgary Biofilm Device. *Biol Proced Online* 8:194–215
- Hassett DJ, Charniga L, Bean K, Ohman DE, Cohen MS (1992) Response of *Pseudomonas aeruginosa* to pyocyanin: mechanisms of resistance, antioxidant defenses, and demonstration of a manganese-cofactored superoxide dismutase. *Infect. Immun.* 60:328–336
- Hassett DJ, Sutton MD, Schurr MJ, Herr AB, Caldwell CC, Matu JO (2009) *Pseudomonas aeruginosa* hypoxic or anaerobic biofilm infections within cystic fibrosis airways. *Trends Microbiol.* 17:130–138
- Hause LL, Komorowski RA, Gayon F (1981) Electrode and Electrolyte Impedance in the Detection of Bacterial Growth. *IEEE T Bio-med Eng* 28:403–410
- Herigstad B, Hamilton M, Heersink J (2001) How to optimize the drop plate method for enumerating bacteria. *J Microbiol Meth* 44:121–129
- Hernandez ME, Newman DK (2001) Extracellular electron transfer. *Cellular and molecular life sciences* 58:1562–1571
- Holm A, Vikström E (2014) Quorum sensing communication between bacteria and human cells: signals, targets, and functions. *Front. Plant Sci.* 5:309
- Honeychurch KC (2012) 13 - Printed thick-film biosensors. In: Prudenziati M., Hormadaly J. (eds) *Printed Films*. Woodhead Publishing, pp 366–409
- Hughes E, Smith IM (1995) *Hughes electrical technology*. Longman Scientific & Technical ; Wiley, Harlow, England
- Hunter RC, Klepac-Ceraj V, Lorenzi MM, Grotzinger H, Martin TR, Newman DK (2012) Phenazine Content in the Cystic Fibrosis Respiratory Tract Negatively Correlates with Lung Function and Microbial Complexity. *American Journal of Respiratory Cell and Molecular Biology* 47:738–745
- Ip M, Lui SL, Poon VKM, Lung I, Burd A (2006) Antimicrobial activities of silver dressings: an in vitro comparison. *J Med Microbiol* 55:59–63
- Jorcín J-B, Orazem ME, Pébère N, Tribollet B (2006) CPE analysis by local electrochemical impedance spectroscopy. *Electrochimica Acta* 51:1473–1479

- Kessler E, Safrin M (2014) Elastinolytic and Proteolytic Enzymes. In: Filloux A., Ramos J.-L. (eds) *Pseudomonas Methods and Protocols*. Springer New York,
- de Kievit TR (2009) Quorum sensing in *Pseudomonas aeruginosa* biofilms. *Environmental Microbiology* 11:279–288
- Kim S, Yu G, Kim T, Shin K, Yoon J (2012) Rapid bacterial detection with an interdigitated array electrode by electrochemical impedance spectroscopy. *Electrochimica Acta* 82:126–131
- Kim T, Kang J, Lee JH, Yoon J (2011) Influence of attached bacteria and biofilm on double-layer capacitance during biofilm monitoring by electrochemical impedance spectroscopy. *Water Res* 45:4615–4622
- Kirchner S, Fothergill JL, Wright EA, James CE, Mowat E, Winstanley C (2012) Use of Artificial Sputum Medium to Test Antibiotic Efficacy Against *Pseudomonas aeruginosa* in Conditions More Relevant to the Cystic Fibrosis Lung. *Journal of Visualized Experiments*
- Kito N, Ohnishi Y, Kagami M, Ohno A (1974) Reduction by a Model of NAD(P)H. Construction of Electron Bridges. *Chemistry Letters* 3:353–356
- Klausen M, Heydorn A, Ragas P, Lambertsen L, Aaes-Jørgensen A, Molin S, Tolker-Nielsen T (2003) Biofilm formation by *Pseudomonas aeruginosa* wild type, flagella and type IV pili mutants. *Molecular Microbiology* 48:1511–1524
- Korgaonkar A, Trivedi U, Rumbaugh KP, Whiteley M (2013) Community surveillance enhances *Pseudomonas aeruginosa* virulence during polymicrobial infection. *PNAS* 110:1059–1064
- Koryta J (1991) *Ions, electrodes, and membranes*. Wiley, Chichester, UK
- K'Owino IO, Sadik OA (2005) Impedance Spectroscopy: A Powerful Tool for Rapid Biomolecular Screening and Cell Culture Monitoring. *Electroanalysis* 17:2101–2113
- Koza A, Hallett PD, Moon CD, Spiers AJ (2009) Characterization of a novel air–liquid interface biofilm of *Pseudomonas fluorescens* SBW25. *Microbiology* 155:1397–1406
- Krishna S, Miller LS (2012) Host-pathogen interactions between the skin and *Staphylococcus aureus*. *Curr Opin Microbiol* 15:28–35
- Kruppa M (2009) Quorum sensing and *Candida albicans*. *Mycoses* 52:1–10
- Langton Hewer SC, Smyth AR (2009) Antibiotic strategies for eradicating *Pseudomonas aeruginosa* in people with cystic fibrosis. In: The Cochrane Collaboration, Langton Hewer S.C. (eds) *Cochrane Database of Systematic Reviews*. John Wiley & Sons, Ltd, Chichester, UK,
- Langton Hewer SC, Smyth AR (2014) Antibiotic strategies for eradicating *Pseudomonas aeruginosa* in people with cystic fibrosis. *Cochrane Database of Systematic Reviews*. John Wiley & Sons, Ltd,



- Lapin C, Pryor JA (2007) *Physiotherapy. Cystic fibrosis*. Hodder Arnold, London, pp 407–420
- Lau GW, Hassett DJ, Ran H, Kong F (2004) The role of pyocyanin in *Pseudomonas aeruginosa* infection. *Trends in Molecular Medicine* 10:599–606
- Lemire JA, Harrison JJ, Turner RJ (2013) Antimicrobial activity of metals: mechanisms, molecular targets and applications. *Nat Rev Micro* 11:371–384
- Liberati NT, Urbach JM, Miyata S, Lee DG, Drenkard E, Wu G, Villanueva J, Wei T, Ausubel FM (2006) An ordered, nonredundant library of *Pseudomonas aeruginosa* strain PA14 transposon insertion mutants. *Proceedings of the National Academy of Sciences* 103:2833–2838
- Li C, Vandenberg K, Prabhulkar S, Zhu X, Schnepfer L, Methee K, Rosser CJ, Almeida E (2011) Paper based point-of-care testing disc for multiplex whole cell bacteria analysis. *Biosensors and Bioelectronics* 26:4342–4348
- Lim YW, Evangelista JS, Schmieder R, Bailey B, Haynes M, Furlan M, Maughan H, Edwards R, Rohwer F, Conrad D (2014) Clinical Insights from Metagenomic Analysis of Sputum Samples from Patients with Cystic Fibrosis. *J. Clin. Microbiol.* 52:425–437
- LiPuma JJ (2010) The Changing Microbial Epidemiology in Cystic Fibrosis. *Clin. Microbiol. Rev.* 23:299–323
- Littlewood J (2004) *Pseudomonas Aeruginosa Infection in People with Cystic Fibrosis: Suggestions for Prevention and Infection Control Report of the UK Cystic Fibrosis Trust Infection Control Group*. Cystic Fibrosis Trust, Bromley, UK
- Li X, Liu L, Liu T, Yuan T, Zhang W, Li F, Zhou S, Li Y (2013) Electron transfer capacity dependence of quinone-mediated Fe(III) reduction and current generation by *Klebsiella pneumoniae* L17. *Chemosphere* 92:218–224
- Lovley DR (2008) The microbe electric: conversion of organic matter to electricity. *Current Opinion in Biotechnology* 19:564–571
- Lyczak JB, Cannon CL, Pier GB (2002) Lung Infections Associated with Cystic Fibrosis. *Clin Microbiol Rev* 15:194–222
- Lynch SV, Bruce KD (2013) The Cystic Fibrosis Airway Microbiome. *Cold Spring Harb Perspect Med* 3:a009738
- Macdonald JR (1987) *Impedance spectroscopy : emphasizing solid materials and systems*. Wiley, New York
- Madeira A, dos Santos SC, Santos PM, Coutinho CP, Tyrrell J, McClean S, Callaghan M, Sá-Correia I (2013) Proteomic Profiling of *Burkholderia cenocepacia* Clonal Isolates with Different Virulence Potential Retrieved from a Cystic Fibrosis Patient during Chronic Lung Infection. *PLoS ONE* 8:e83065

- Mahenthalingam E, Baldwin A, Dowson C g. (2008) Burkholderia cepacia complex bacteria: opportunistic pathogens with important natural biology. *Journal of Applied Microbiology* 104:1539–1551
- Mahon CR, Lehman DC, Manuselis G (2015) *Textbook of diagnostic microbiology*. Elsevier, Maryland Heights, Missouri
- Mandon CA, Heyries KA, Blum LJ, Marquette CA (2010) Polyshrink™ based microfluidic chips and protein microarrays. *Biosensors and Bioelectronics* 26:1218–1224
- Marsili E, Baron DB, Shikhare ID, Coursolle D, Gralnick JA, Bond DR (2008a) Shewanella secretes flavins that mediate extracellular electron transfer. *Proc Natl Acad Sci U S A* 105:3968–3973
- Marsili E, Rollefson JB, Baron DB, Hozalski RM, Bond DR (2008b) Microbial Biofilm Voltammetry: Direct Electrochemical Characterization of Catalytic Electrode-Attached Biofilms. *Appl. Environ. Microbiol.* 74:7329–7337
- Mavrodi DV, Bonsall RF, Delaney SM, Soule MJ, Phillips G, Thomashow LS (2001) Functional Analysis of Genes for Biosynthesis of Pyocyanin and Phenazine-1-Carboxamide from *Pseudomonas aeruginosa* PAO1. *J. Bacteriol.* 183:6454–6465
- McGuigan L, Callaghan M (2014) The evolving dynamics of the microbial community in the cystic fibrosis lung. *Environ Microbiol* 17:16–28
- Merritt JH, Kadouri DE, O’Toole GA (2005) *Growing and Analyzing Static Biofilms*. *Current Protocols in Microbiology*. John Wiley & Sons, Inc.,
- Morrin A, Killard AJ, Smyth MR (2003) Electrochemical Characterization of Commercial and Home-Made Screen-Printed Carbon Electrodes. *Analytical Letters* 36:2021–2039
- Moulton S., Barisci J., Bath A, Stella R, Wallace G. (2004) Studies of double layer capacitance and electron transfer at a gold electrode exposed to protein solutions. *Electrochimica Acta* 49:4223–4230
- Mowat E, Paterson S, Fothergill JL, Wright EA, Ledson MJ, Walshaw MJ, Brockhurst MA, Winstanley C (2011) *Pseudomonas aeruginosa* Population Diversity and Turnover in Cystic Fibrosis Chronic Infections. *Am J Respir Crit Care Med* 183:1674–1679
- Muñoz-Berbel X, García-Aljaro C, Muñoz FJ (2008a) Impedimetric approach for monitoring the formation of biofilms on metallic surfaces and the subsequent application to the detection of bacteriophages. *Electrochim Acta* 53:5739–5744
- Muñoz-Berbel X, Godino N, Laczka O, Baldrich E, Muñoz FX, Campo FJ (2008b) Impedance-Based Biosensors for Pathogen Detection. In: Zourob M., Elwary S., Turner A. (eds) *Principles of Bacterial Detection: Biosensors, Recognition Receptors and Microsystems*. Springer New York, New York, NY, pp 341–376
- Muñoz-Berbel X, Muñoz FJ, Vigués N, Mas J (2006) On-chip impedance measurements to monitor biofilm formation in the drinking water distribution network. *Sensor Actuat B-Chem* 118:129–134

- Muñoz-Berbel X, Vigués N, Jenkins ATA, Mas J, Muñoz FJ (2008c) Impedimetric approach for quantifying low bacteria concentrations based on the changes produced in the electrode–solution interface during the pre-attachment stage. *Biosens Bioelectron* 23:1540–1546
- Muñoz-Berbel X, Vigués N, Mas J, Jenkins ATA, Muñoz FJ (2007) Impedimetric characterization of the changes produced in the electrode–solution interface by bacterial attachment. *Electrochem Commun* 9:2654–2660
- Nair D, Memmi G, Hernandez D, Bard J, Beaume M, Gill S, Francois P, Cheung AL (2011) Whole-Genome Sequencing of *Staphylococcus aureus* Strain RN4220, a Key Laboratory Strain Used in Virulence Research, Identifies Mutations That Affect Not Only Virulence Factors but Also the Fitness of the Strain. *J. Bacteriol.* 193:2332–2335
- Newman DK, Kolter R (2000) A role for excreted quinones in extracellular electron transfer. *Nature* 405:94–97
- Niessen J, Schröder U, Scholz F (2004) Exploiting complex carbohydrates for microbial electricity generation – a bacterial fuel cell operating on starch. *Electrochemistry Communications* 6:955–958
- Noble PA (1999) Hypothetical model for monitoring microbial growth by using capacitance measurements - a minireview. *J Microbiol Meth* 37:45–49
- Noble PA, Dziuba M, Harrison DJ, Albritton WL (1999) Factors influencing capacitance-based monitoring of microbial growth. *J Microbiol Meth* 37:51–64
- Oxoid (2014) Sputasol (Liquid) SR0233.  
[http://www.oxoid.com/UK/blue/prod\\_detail/prod\\_detail.asp?pr=SR0233](http://www.oxoid.com/UK/blue/prod_detail/prod_detail.asp?pr=SR0233)
- Pantosti A, Venditti M (2009) What is MRSA? *Eur Respir J* 34:1190–1196
- Paredes J, Becerro S, Arizti F, Aguinaga A, Del Pozo JL, Arana S (2012) Real time monitoring of the impedance characteristics of *Staphylococcal* bacterial biofilm cultures with a modified CDC reactor system. *Biosensors and Bioelectronics* 38:226–232
- Paredes J, Becerro S, Arizti F, Aguinaga A, Del Pozo JL, Arana S (2013) Interdigitated microelectrode biosensor for bacterial biofilm growth monitoring by impedance spectroscopy technique in 96-well microtiter plates. *Sensors and Actuators B: Chemical* 178:663–670
- Peleg AY, Hogan DA, Mylonakis E (2010) Medically important bacterial–fungal interactions. *Nat Rev Micro* 8:340–349
- Pemberon RM, Pittson R, Biddle N, Hart JP (2009) Fabrication of microband glucose biosensors using a screen-printing water-based carbon ink and their application in serum analysis. *Biosensors and Bioelectronics* 24:1246–1252
- Pierson LS, Pierson EA (2010) Metabolism and function of phenazines in bacteria: impacts on the behavior of bacteria in the environment and biotechnological processes. *Appl Microbiol Biotechnol* 86:1659–1670

- Pillariseti N, Williamson E, Linnane B, Skoric B, Robertson CF, Robinson P, Massie J, Hall GL, Sly P, Stick S, Ranganathan S, on behalf of the Australian Respiratory Early Surveillance Team for Cystic Fibrosis (AREST CF) (2011) Infection, Inflammation, and Lung Function Decline in Infants with Cystic Fibrosis. *American Journal of Respiratory and Critical Care Medicine* 184:75–81
- Pires L, Sachsenheimer K, Kleintschek T, Waldbaur A, Schwartz T, Rapp BE (2013) Online monitoring of biofilm growth and activity using a combined multi-channel impedimetric and amperometric sensor. *Biosensors and Bioelectronics* 47:157–163
- Poortinga AT, Bos R, Busscher HJ (1999) Measurement of charge transfer during bacterial adhesion to an indium tin oxide surface in a parallel plate flow chamber. *Journal of Microbiological Methods* 38:183–189
- Poortinga AT, Bos R, Busscher HJ (2001) Charge transfer during staphylococcal adhesion to TiNOX coatings with different specific resistivity. *Biophysical Chemistry* 91:273–279
- Price-Whelan A, Dietrich LEP, Newman DK (2006) Rethinking 'secondary' metabolism: physiological roles for phenazine antibiotics. *Nature chemical biology* 2:71–78
- Price-Whelan A, Dietrich LEP, Newman DK (2007) Pyocyanin alters redox homeostasis and carbon flux through central metabolic pathways in *Pseudomonas aeruginosa* PA14. *J. Bacteriol.* 189:6372–6381
- Proesmans M, Vermeulen F, Boulanger L, Verhaegen J, De Boeck K (2013) Comparison of two treatment regimens for eradication of *Pseudomonas aeruginosa* infection in children with cystic fibrosis. *Journal of Cystic Fibrosis* 12:29–34
- Rabaey K, Boon N, Siciliano SD, Verhaege M, Verstraete W (2004) Biofuel Cells Select for Microbial Consortia That Self-Mediate Electron Transfer. *Appl. Environ. Microbiol.* 70:5373–5382
- Ran H, Hassett DJ, Lau GW (2003) Human targets of *Pseudomonas aeruginosa* pyocyanin. *PNAS* 100:14315–14320
- Ratjen F, Döring G (2003) Cystic fibrosis. *The Lancet* 361:681–689
- Ratjen F, Munck A, Kho P, Angyalosi G (2010) Treatment of early *Pseudomonas aeruginosa* infection in patients with cystic fibrosis: the ELITE trial. *Thorax* 65:286–291
- Regelmann WE, Elliott GR, Warwick WJ, Clawson CC (1990) Reduction of Sputum *Pseudomonas aeruginosa* Density by Antibiotics Improves Lung Function in Cystic Fibrosis More than Do Bronchodilators and Chest Physiotherapy Alone. *Am Rev Respir Dis* 141:914–921
- Reguera G, McCarthy KD, Mehta T, Nicoll JS, Tuominen MT, Lovley DR (2005) Extracellular electron transfer via microbial nanowires. *Nature* 435:1098–1101
- Reguera G, Nevin KP, Nicoll JS, Covalla SF, Woodard TL, Lovley DR (2006) Biofilm and Nanowire Production Leads to Increased Current in *Geobacter sulfurreducens* Fuel Cells. *Appl. Environ. Microbiol.* 72:7345–7348

- Reid DW, Latham R, Lamont IL, Camara M, Roddam LF (2013) Molecular analysis of changes in *Pseudomonas aeruginosa* load during treatment of a pulmonary exacerbation in cystic fibrosis. *Journal of Cystic Fibrosis* 12:688–699
- Reis RS, Pereira AG, Neves BC, Freire DMG (2011) Gene regulation of rhamnolipid production in *Pseudomonas aeruginosa* – A review. *Bioresource Technology* 102:6377–6384
- Richards JCS, Jason AC, Hobbs G, Gibson DM, Christie RH (1978) Electronic measurement of bacterial growth. *J Phys E Sci Instrum* 11:560–568
- Richardson DJ (2000) Bacterial respiration: a flexible process for a changing environment. *Microbiology* 146:551–571
- Rigaud B, Morucci JP, Chauveau N (1996) Bioelectrical impedance techniques in medicine. Part I: Bioimpedance measurement. Second section: impedance spectrometry. *Crit Rev Biomed Eng* 24:257–351
- Rogers GB, Hart CA, Mason JR, Hughes M, Walshaw MJ, Bruce KD (2003) Bacterial Diversity in Cases of Lung Infection in Cystic Fibrosis Patients: 16S Ribosomal DNA (rDNA) Length Heterogeneity PCR and 16S rDNA Terminal Restriction Fragment Length Polymorphism Profiling. *J Clin Microbiol* 41:3548–3558
- Rosenstein BJ, Zeitlin PL (1998) Cystic fibrosis. *The Lancet* 351:277–282
- Rubin BK (2007) Mucus structure and properties in cystic fibrosis. *Paediatric respiratory reviews* 8:4–7
- Ryan KJ, Ray CG (2014) *Sherris medical microbiology*. McGraw-Hill Education Medical, New York
- Sawa T, Shimizu M, Moriyama K, Wiener-Kronish JP (2014) Association between *Pseudomonas aeruginosa* type III secretion, antibiotic resistance, and clinical outcome: a review. *Critical Care* 18:668
- Schelstraete P, Haerynck F, Van daele S, Deseyne S, De Baets F (2013) Eradication therapy for *Pseudomonas aeruginosa* colonization episodes in cystic fibrosis patients not chronically colonized by *P. aeruginosa*. *Journal of Cystic Fibrosis* 12:1–8
- Schindelin J, Arganda-Carreras I, Frise E, Kaynig V, Longair M, Pietzsch T, Preibisch S, Rueden C, Saalfeld S, Schmid B, Tinevez J-Y, White DJ, Hartenstein V, Eliceiri K, Tomancak P, Cardona A (2012) Fiji: an open-source platform for biological-image analysis. *Nat Methods* 9:676–682
- Schrott GD, Bonanni PS, Robuschi L, Esteve-Nuñez A, Busalmen JP (2011) Electrochemical insight into the mechanism of electron transport in biofilms of *Geobacter sulfurreducens*. *Electrochimica Acta* 56:10791–10795
- Sharma G, Rao S, Bansal A, Dang S, Gupta S, Gabrani R (2014) *Pseudomonas aeruginosa* biofilm: Potential therapeutic targets. *Biologicals* 42:1–7

- Sharp D, Gladstone P, Smith RB, Forsythe S, Davis J (2010) Approaching intelligent infection diagnostics: Carbon fibre sensor for electrochemical pyocyanin detection. *Bioelectrochemistry* 77:114–119
- Shedden L (2008) *The Intelligent Stent*. University of Strathclyde
- Shoseyov D (2006) Aspergillus Bronchitis in Cystic Fibrosis. *Chest* 130:222–226
- Sibley CD, Grinwis ME, Field TR, Eshaghurshan CS, Faria MM, Dowd SE, Parkins MD, Rabin HR, Surette MG (2011) Culture Enriched Molecular Profiling of the Cystic Fibrosis Airway Microbiome. *PLoS ONE* 6:e22702
- Sifri CD (2008) Quorum Sensing: Bacteria Talk Sense. *Clin Infect Dis.* 47:1070–1076
- Sismaet HJ, Webster TA, Goluch ED (2014) Up-regulating pyocyanin production by amino acid addition for early electrochemical identification of *Pseudomonas aeruginosa*. *Analyst* 139:4241–4246
- Smith AL, Doershuk C, Goldmann D, Gore E, Hilman B, Marks M, Moss R, Ramsey B, Redding G, Rubio T, Williams-Warren J, Wilmott R, Wilson HD, Yogev R (1999) Comparison of a  $\beta$ -lactam alone versus  $\beta$ -lactam and an aminoglycoside for pulmonary exacerbation in cystic fibrosis. *The Journal of Pediatrics* 134:413–421
- Solartron (1996) *1260 Impedance Gain-Phase Analyzer Operating Manual*.
- Southampton Electrochemistry Group (2001) *Instrumental methods in electrochemistry*. Ellis Horwood, Chichester
- Sriramulu DD, Lünsdorf H, Lam JS, Römling U (2005) Microcolony formation: a novel biofilm model of *Pseudomonas aeruginosa* for the cystic fibrosis lung. *J. Med. Microbiol* 54:667–676
- Stewart L, Ford A, Sangal V, Jeukens J, Boyle B, Caim S, Crossman L, Hoskisson PA, Levesque R, Tucker NP (2013) Draft genomes of twelve host adapted and environmental isolates of *Pseudomonas aeruginosa* and their position in the core genome phylogeny. *Pathogens and Disease* 71:20–25
- Stressmann FA, Rogers GB, Marsh P, Lilley AK, Daniels TWV, Carroll MP, Hoffman LR, Jones G, Allen CE, Patel N, Forbes B, Tuck A, Bruce KD (2011) Does bacterial density in cystic fibrosis sputum increase prior to pulmonary exacerbation? *Journal of Cystic Fibrosis* 10:357–365
- Sudbery PE (2011) Growth of *Candida albicans* hyphae. *Nat Rev Micro* 9:737–748
- Swords WE (2012) Quorum signaling and sensing by nontypeable *Haemophilus influenzae*. *Front Cell Infect Microbiol* 2:
- Taccetti G, Bianchini E, Cariani L, Buzzetti R, Costantini D, Trevisan F, Zavataro L, Campana S (2012) Early antibiotic treatment for *Pseudomonas aeruginosa* eradication in patients with cystic fibrosis: a randomised multicentre study comparing two different protocols. *Thorax* 67:853–859

- Valerius NH, Koch C, Høiby N (1991) Prevention of chronic *Pseudomonas aeruginosa* colonisation in cystic fibrosis by early treatment. *Lancet* 338:725–726
- Varshney M, Li Y (2009) Interdigitated array microelectrodes based impedance biosensors for detection of bacterial cells. *Biosensors and Bioelectronics* 24:2951–2960
- Voynow JA, Rubin BK (2009) Mucins, Mucus, and Sputum. *Chest* 135:505–512
- Wade DS, Calfee MW, Rocha ER, Ling EA, Engstrom E, Coleman JP, Pesci EC (2005) Regulation of *Pseudomonas* Quinolone Signal Synthesis in *Pseudomonas aeruginosa*. *J. Bacteriol.* 187:4372–4380
- Wang J, Pedrero M, Sakslund H, Hammerich O, Pingarron J (1996) Electrochemical activation of screen-printed carbon strips. *The Analyst* 121:345
- Wang Y, Newman DK (2008) Redox Reactions of Phenazine Antibiotics with Ferric (Hydr)oxides and Molecular Oxygen. *Environ. Sci. Technol.* 42:2380–2386
- Wang Y, Wilks JC, Danhorn T, Ramos I, Croal L, Newman DK (2011) Phenazine-1-Carboxylic Acid Promotes Bacterial Biofilm Development via Ferrous Iron Acquisition. *J. Bacteriol.* 193:3606–3617
- Watson D, MacDermot J, Wilson R, Cole PJ, Taylor GW (1986) Purification and structural analysis of pyocyanin and 1-hydroxyphenazine. *European Journal of Biochemistry* 159:309–313
- Webster TA, Sismaet HJ, Conte JL, Chan IJ, Goluch ED (2014) Electrochemical detection of *Pseudomonas aeruginosa* in human fluid samples via pyocyanin. *Biosensors and Bioelectronics* 60:265–270
- Wegener J, Sieber M, Galla HJ (1996) Impedance analysis of epithelial and endothelial cell monolayers cultured on gold surfaces. *Journal of biochemical and biophysical methods* 32:151–170
- Wiesemann HG, Steinkamp G, Ratjen F, Bauernfeind A, Przyklenk B, Döring G, von der Hardt H (1998) Placebo-controlled, double-blind, randomized study of aerosolized tobramycin for early treatment of *Pseudomonas aeruginosa* colonization in cystic fibrosis. *Pediatr. Pulmonol.* 25:88–92
- Wilson R, Sykes DA, Watson D, Rutman A, Taylor GW, Cole PJ (1988) Measurement of *Pseudomonas aeruginosa* phenazine pigments in sputum and assessment of their contribution to sputum sol toxicity for respiratory epithelium. *Infect. Immun.* 56:2515–2517
- Winsor GL, Lam DKW, Fleming L, Lo R, Whiteside MD, Yu NY, Hancock REW, Brinkman FSL (2011) *Pseudomonas* Genome Database: improved comparative analysis and population genomics capability for *Pseudomonas* genomes. *Nucleic Acids Res.* 39:D596–600
- World Health Organisation (2011) *Laboratory Methods for the Diagnosis of Meningitis Caused by Neisseria meningitidis, Streptococcus pneumoniae, and Haemophilus influenzae.*

- Xia X, Cao X, Liang P, Huang X, Yang S, Zhao G (2010) Electricity generation from glucose by a *Klebsiella* sp. in microbial fuel cells. *Applied Microbiology and Biotechnology* 87:383–390
- Yang L, Li Y, Griffis CL, Johnson MG (2004) Interdigitated microelectrode (IME) impedance sensor for the detection of viable *Salmonella typhimurium*. *Biosens Bioelectron* 19:1139–1147
- Yang L, Ruan C, Li Y (2003) Detection of viable *Salmonella typhimurium* by impedance measurement of electrode capacitance and medium resistance. *Biosens Bioelectron* 19:495–502
- Yarwood JM, Schlievert PM (2003) Quorum sensing in *Staphylococcus* infections. *J Clin Invest* 112:1620–1625
- Yoon SS, Hennigan RF, Hilliard GM, Ochsner UA, Parvatiyar K, Kamani MC, Allen HL, DeKievit TR, Gardner PR, Schwab U, others (2002) *Pseudomonas aeruginosa* Anaerobic Respiration in Biofilms:: Relationships to Cystic Fibrosis Pathogenesis. *Developmental cell* 3:593–603
- Yuan X-Z, Song C, Wang H, Zhang J (2010) *Electrochemical Impedance Spectroscopy in PEM Fuel Cells Fundamentals and Applications*. Springer-Verlag, London
- Zhang L, Zhou S, Zhuang L, Li W, Zhang J, Lu N, Deng L (2008a) Microbial fuel cell based on *Klebsiella pneumoniae* biofilm. *Electrochemistry Communications* 10:1641–1643
- Zhang T, Cui C, Chen S, Ai X, Yang H, Shen P, Peng Z (2006) A novel mediatorless microbial fuel cell based on direct biocatalysis of *Escherichia coli*. *Chemical Communications* 2257
- Zhang T, Cui C, Chen S, Yang H, Shen P (2008b) The direct electrocatalysis of *Escherichia coli* through electroactivated excretion in microbial fuel cell. *Electrochemistry Communications* 10:293–297
- Zikmund A, Ripka P, Krasny L, Judl T, Jahoda D (2010) Biofilm detection by the impedance method. 2010 3rd International Conference on Biomedical Engineering and Informatics (BMEI) 4:1432–1434



## **9 APPENDIX**

## 9.1 Appendix A: Biorepository Ethics Approval Form



Wednesday, 15 January 2014

Andrew Ward  
Dept of Biomedical Engineering  
Strathclyde University  
106 Rottenrow  
G4

Dear Andrew,

**Biorepository Application Number: 139**

**Study Title: Collection and use of surplus sputum samples from cystic fibrosis patients during hospital visits.**

On behalf of the NHS GG&C Biorepository Management Committee I am pleased to provide approval for the acquisition of tissue for the above research study. This approval is on the basis described in your application and supporting documents.

The committee would be grateful for an update on the progress of the use of the tissue and for information on the publications which arise from this work. At the end of the study Bio-repository staff may also contact you for this information.

In addition we would ask you to acknowledge the NHS GG&C Bio-repository in any publications.

Thank you for collaborating with the NHS GG&C Biorepository. We wish you every success with this work.

Yours sincerely,

A handwritten signature in black ink that reads 'James Going'.

James Going, MB PhD, MRCP, FRCPath  
Consultant Senior Lecturer in Pathology and Director of NHSGGC Biorepository  
cc Jane Hair, Fiona Graham

Dr James Going, MB PhD, MRCP, FRCPath  
University Pathology Unit  
L2b – 106  
Laboratory Medicine Building, Southern General Hospital  
Govan Road, Glasgow, G51 4TF

Tel: +44 (0)141 354 9437  
E-mail: [james.going@glasgow.ac.uk](mailto:james.going@glasgow.ac.uk)

## *Pseudomonas aeruginosa* Can Be Detected in a Polymicrobial Competition Model Using Impedance Spectroscopy with a Novel Biosensor

Andrew C. Ward<sup>1</sup>, Patricia Connolly<sup>1\*</sup>, Nicholas P. Tucker<sup>2</sup>

<sup>1</sup> Department of Biomedical Engineering, University of Strathclyde, Glasgow, United Kingdom, <sup>2</sup> Strathclyde Institute of Pharmacy and Biomedical Sciences, University of Strathclyde, Glasgow, United Kingdom

### Abstract

Electrochemical Impedance Spectroscopy (EIS) is a powerful technique that can be used to elicit information about an electrode interface. In this article, we highlight six principal processes by which the presence of microorganisms can affect impedance and show how one of these - the production of electroactive metabolites - changes the impedance signature of culture media containing *Pseudomonas aeruginosa*. EIS, was used in conjunction with a low cost screen printed carbon sensor to detect the presence of *P. aeruginosa* when grown in isolation or as part of a polymicrobial infection with *Staphylococcus aureus*. By comparing the electrode to a starting measurement, we were able to identify an impedance signature characteristic of *P. aeruginosa*. Furthermore, we are able to show that one of the changes in the impedance signature is due to pyocyanin and associated phenazine compounds. The findings of this study indicate that it might be possible to develop a low cost sensor for the detection of *P. aeruginosa* in important point of care diagnostic applications. In particular, we suggest that a development of the device described here could be used in a polymicrobial clinical sample such as sputum from a CF patient to detect *P. aeruginosa*.

**Citation:** Ward AC, Connolly P, Tucker NP (2014) *Pseudomonas aeruginosa* Can Be Detected in a Polymicrobial Competition Model Using Impedance Spectroscopy with a Novel Biosensor. PLoS ONE 9(3): e91732. doi:10.1371/journal.pone.0091732

**Editor:** Christophe Beloin, Institut Pasteur, France

**Received:** September 26, 2013; **Accepted:** February 14, 2014; **Published:** March 10, 2014

**Copyright:** © 2014 Ward et al. This is an open-access article distributed under the terms of the Creative Commons Attribution License, which permits unrestricted use, distribution, and reproduction in any medium, provided the original author and source are credited.

**Funding:** This work has been funded by the Engineering and Physical Sciences Research Council (www.epsrc.ac.uk, grant number: EP/F50036X/1) as part of an Engineering Doctorate. The funders had no role in study design, data collection and analysis, decision to publish, or preparation of the manuscript.

**Competing Interests:** The authors have declared that no competing interests exist.

\* E-mail: patricia.connolly@strath.ac.uk

### Introduction

Electrochemical Impedance Spectroscopy (EIS) has been investigated extensively as a tool for the detection of microbial attachment and biofilm formation [1–11]. However, few examples exist where this technology has been used in conjunction with a low cost screen printed sensor in a point of care device. One example is the use of EIS in conjunction with a low cost screen printed electrode to detect the level of moisture in chronic wounds, without the need to remove the dressing. This device minimises the need to disrupt the dressing unnecessarily therefore reducing patient discomfort and enhancing clinical practice decisions about dressing replacement [12]. These wound moisture sensors have also been investigated in the context of wound infection to determine if it is possible to detect different strains of *Staphylococcus aureus* growing in a suspension in Mueller-Hinton Broth with different concentrations of glucose [13]. In this study, it was found that specific impedance signatures could be discerned between control electrodes and those inoculated with *S. aureus* once growth increased above  $5 \times 10^7$  CFU/ml.

Impedance spectroscopy measures the resistance and reactance of an electrode in contact with an electrolyte across a spectrum of AC frequencies. A number of electrochemical processes affect these two measurements at different frequencies and these can be interpreted by a simple model called the Randles equivalent circuit [14,15] (figure 1A). The ability of the electrode to exchange electrons with the electrolyte is governed by the electrode material

and the composition of the media. The availability of the electroactive species at the electrode surface has an impact on the electron transfer rate across the interface (and therefore the impedance) in a diffusion dependant manner. Other processes which affect impedance include the dielectric properties of the electrolyte adjacent to the electrode and the resistance of the bulk electrolyte. The former is known as the double layer capacitance and is defined by the relationship between polar and non-polar molecules and structures in very close proximity to the electrode. The latter is defined by the number of ions and other charged compounds within the media that convey charge between the electrodes. We propose six potential mechanisms through which the electrode-electrolyte interface could be changed by the growth of microorganisms, thus influencing impedance in a characteristic manner. These are: the production of redox compounds [16–19]; the deposition of biofilm material on the electrode surface; charge transfer through the attachment of cells and microbial nanowires [6,20–23]; the presence of microbial cells in close proximity to the electrode surface; breakdown of nutrients within the electrolyte [24–26]; and the adsorption of proteins to the electrode surface [15,27] (figure 1B).

The impedance spectrum can be interpreted by analysing the reactance and resistance data directly from the measurement or by analysing the modulus or phase angle of the impedance (see supporting information S1 for an explanation of how these are derived). Numerous circuit models have been proposed to explain

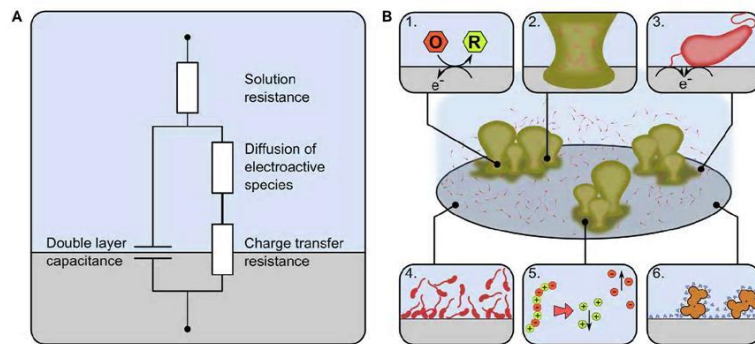


**Figure 1. Mechanisms through which microorganisms could affect the impedance.** (A) The impedance signature of a given electrochemical system is defined by the interplay of solution resistance, redox compounds, diffusion gradients and the electrolyte composition adjacent to the electrode surface. (B) Microorganisms could affect this impedance signature through: (1) production of electroactive secondary metabolites that facilitate a charge transfer at the electrode/electrolyte interface; (2) biofilm matrix attached to the electrode surface that affects capacitance and/or charge transfer; (3) direct microbial attachment, through pili, flagella and outer membrane proteins facilitating charge transfer; (4) Outer cell membrane contact at high cell densities that affect capacitance; (5) Breakdown of nutrients within the media reducing solution resistance; (6) Protein/macromolecule adsorption on the electrode surface influencing double layer capacitance. doi:10.1371/journal.pone.0091732.g001

the underlying processes that give rise to a particular impedance profile related to bacterial attachment and biofilm formation [1 3,6,8,11,28,29]. In this study we used the normalisation procedure discussed by Farrow (2012), which allows relative changes in the impedance over time to be analysed by dividing a parameter of interest against its corresponding value at the start of the experiment [30]:

$$IPN_{t=n} = \frac{IPA_{t=n}}{IPA_{t=0}}$$

Where  $IPN_{t=n}$  is the normalised impedance parameter of interest (i.e. reactance, resistance, impedance modulus or phase) and  $IPA_t$  is the absolute (as measured) impedance parameter. The aim of the normalised impedance parameter is to identify a characteristic signature that can be used to detect a specific microorganism. An example is the clinically important pathogen *Pseudomonas aeruginosa*.

*P. aeruginosa* is an opportunistic pathogen capable of inhabiting numerous environments, including the cystic fibrosis (CF) lung, burns patients and babies in hospital neonatal units [31–34]. Early detection of *P. aeruginosa* within the CF airway may be useful by enabling prompt treatment and prevention of further lung damage. *P. aeruginosa* produces numerous virulence factors such as pyocyanin, which plays a role in pathogenicity and host tissue damage. The virulence of pyocyanin has been shown in several studies to be multi-faceted, including the inhibition of ciliary beating and cellular respiration, induction of neutrophil apoptosis and depletion of cellular glutathione [35]. In this study, we have investigated the application of EIS to a label-less, low cost screen printed sensor for the detection of *P. aeruginosa* and have elucidated at least one of the causes for the observed changes in impedance.

We used a novel sensor to determine if it is possible to detect the presence of *P. aeruginosa* in a simple polymicrobial model with *Staphylococcus aureus*. *S. aureus* was used because it is also commonly

found within the CF airway [36]. The bacteria were cultured in an artificial sputum media (ASM) made with large quantities of mucin and DNA [37] designed to simulate conditions within the CF airway. EIS was used to sweep across a frequency spectrum from 100 mHz to 1 MHz with a custom built measurement chamber containing the electrode, which remained in-situ throughout the experiment.

## Results and Discussion

### Baseline Impedance Characteristics of the Electrodes show a High Initial Impedance Signature

Electrodes were designed with a working electrode that was much smaller than the counter electrode and constructed using thick film screen printing techniques with a carbon ink printed onto acetate. Carbon ink was used because of its low cost, which is an important driver for a point of care, disposable sensor. Silver chloride (Ag-AgCl) ink was also considered, however results from another study suggest that screen printed Ag-AgCl electrodes may affect bacterial growth [13]. The carbon nature of the electrodes resulted in very high magnitudes of impedance, with the impedance modulus ranging from 600 Ω at high frequency to 4.8 MΩ at 100 mHz. It was recognised that the high impedance might mask some of the impedance changes caused by the bacteria. This was traded off against the low cost of producing the sensors and the avoidance of Ag-AgCl ink in the electrode design. Therefore, in order to effectively analyse differences between inoculated and control samples, the normalisation procedure described above was used in conjunction with the phase angle and impedance modulus.

### *P. aeruginosa* is Specifically Detectable Alone, or as Part of Coculture with *S. aureus*

Impedance experiments were carried out to characterise the typical signatures resulting from microbial broths containing the *P. aeruginosa* strain PA14 and *S. aureus* strain RN4220, grown alone

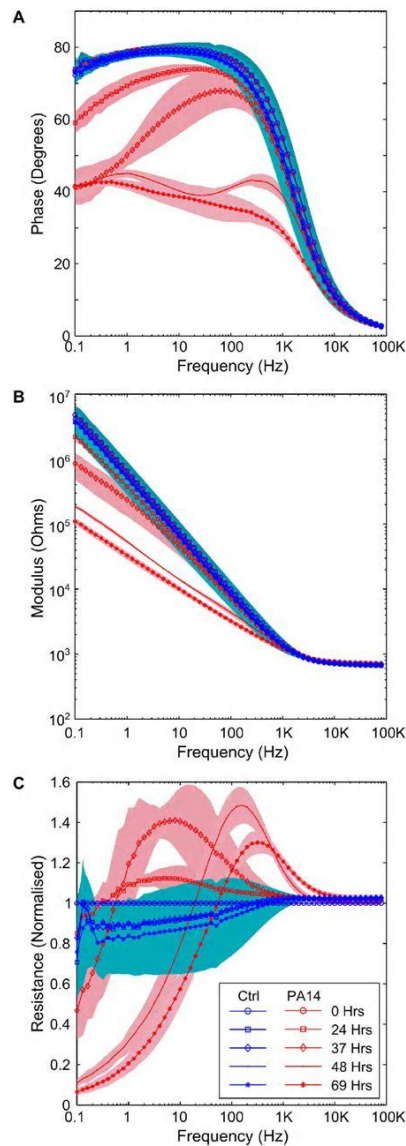


**Figure 2. Changes in the impedance resulting from *P. aeruginosa* PA14.** (A) phase plot, showing a drop in the absolute

phase angle as a result of microbial growth, (B) the final impedance modulus at low frequency is more than one and a half orders of magnitude lower than the starting impedance, (C) the normalised resistance shows a peak for the electrode chambers containing PA14 that is not present in the control data. Background shading and error bars represent  $\pm 1$  SD. PA14  $n = 4$ ; Neg Ctrl  $n = 5$ . doi:10.1371/journal.pone.0091732.g002

and together. Electrode chambers were inoculated in replicates of at least four with PA14, RN4220, a combination of the two, or left sterile as negative controls. For electrodes inoculated with *P. aeruginosa* or *S. aureus*, equal numbers of colony forming units (CFUs) were used for the starting density, between  $3 \times 10^8$  and  $5 \times 10^6$  CFU/ml. Measurements were taken periodically for a total of three days. After inoculation, the electrodes were placed in a microaerophilic environment, more representative of conditions within the lungs [37].

At 24 hours, changes in the phase angle and impedance modulus were clearly observable between the samples inoculated with PA14 and control samples (figure 2). Similar behaviour has been observed with other *P. aeruginosa* strains across multiple experiments, including PAO1 grown in LB, and J1385 and J1532: a non-mucoid and mucoid isogenic pair from a CF patient [38] (data not shown). The impedance modulus drops from 4.7 M $\Omega$  to 100 K $\Omega$  over that course of the experiment at low frequencies (0.1 Hz), where charge transfer and mass diffusion of electroactive compounds are the most dominant impedance processes. A drop in the phase angle from around 90 $^\circ$  in the electrodes containing PA14 cultures shows that the interface changes from one which has no electron transfer to one where a proportion of the current across the electrode-electrolyte interface is carried through electron transfer. Specifically, it can be seen that the growth of *P. aeruginosa* results in a current carried partly by the capacitance of the interface and partly by electron transfer at frequencies below 1000 Hz (after 24 hours). Corresponding changes are also observable in a complex plane plot, where an arc is evident at higher frequencies, indicative of the presence of a charge transfer resistance [14]. In contrast, the impedance signature of the negative controls remains constant throughout the experiment, with no deviation from a capacitive interface (i.e. an interface where no electron transfer occurs). Interestingly, a peak is visible in the normalised resistance data from the experiment (figure 2C). Peaks of this nature might be characteristic of *P. aeruginosa* and could be used as a powerful tool in a diagnostic device for the identification of different bacteria.

We decided to investigate the impact that the growth of *S. aureus* RN4220 would have upon the impedance signature, to determine if it would change in a similar manner to that seen with PA14. It was observed that the interface did not change significantly throughout the experiment, compared to the negative control, for either the raw impedance data or any of the normalised impedance data (figure 3). In order to test this further, *S. aureus* was grown in Tryptone Soya Broth (TSB) for 3 days in aerobic conditions. These growth conditions resulted in a cell density of  $5.58 \times 10^7$  CFU/ml at the end of the experiment compared to a starting cell density of  $1.47 \times 10^7$  CFU/ml. It was noted in a subsequent experiment that the cell density of *S. aureus* in a culture was higher (i.e.  $4.56 \times 10^8$  CFU/ml) if the media was vigorously disrupted with a 1 ml pipette prior to taking an aliquot for colony counting. As with the experiments using ASM, no change was found in the impedance when RN4220 was grown in TSB (data not shown).

Previously, investigators identified that changes in the impedance were a result of the breakdown of nutrients within the media

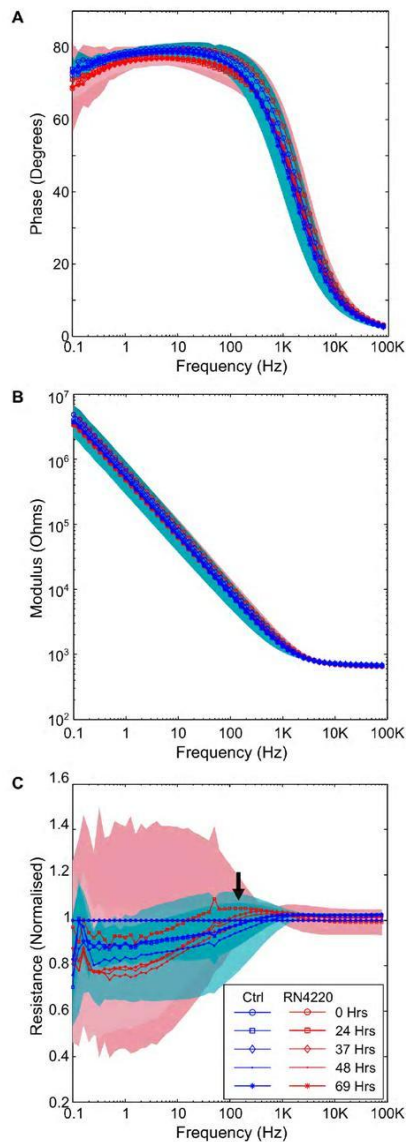


**Figure 3. Impedance changes as consequence of growth with *S. aureus* RN4220.** Shows that there is no discernible different in (A) the

phase, (B) the modulus and (C) the normalised reactance under the same conditions as those used for *P. aeruginosa* PA14. The arrow indicates a slight peak at 125 Hz at 24 hours moving to 400 Hz at later timepoints. Background shading represent  $\pm 1$  SD. RN4220  $n=4$ ; Neg Ctrl  $n=5$ . doi:10.1371/journal.pone.0091732.g003

[24–26], in a field that became known as impedance microbiology. When *S. aureus* was grown in ASM or TSB our sensor did not result in a significant change in impedance. This is probably because the impedance microbiology methods measure changes in the conductivity of the media, an effect not seen here due to the large baseline impedance. The large baseline impedance would also screen any small changes to the electrode-broth interface impedance that were caused by the bacteria. Although not significantly different, the normalised resistance plot shows that the samples containing *S. aureus* do differ in their impedance curve, with a slight peak visible after 37 hours at 400 Hz (figure 3C). An electrode with lower starting impedance might be more sensitive to these changes and enable a unique signature to be identified for *S. aureus*.

A more representative situation within the CF airway is a polymicrobial infection consisting of two or more microbial species [36]. In order to test the performance of the sensor in this context, measurements were taken with PA14 and RN4220 grown together at equal starting densities in the same electrode chamber, under microaerophilic conditions. As with the monoculture of *P. aeruginosa* alone, changes in the impedance between the negative control and the polymicrobial infection were observable after 24 hours in the impedance phase and modulus data (figure 4A and 4B). These changes were similar to those observed with PA14 alone and by the end of the experiment, the polymicrobial infection model and PA14 had a similar impedance curve. The normalised resistance data was also similar, suggesting that PA14 was responsible for the changes seen in the impedance (figure 4C).

To further understand the dynamics of the polymicrobial model, colony counting was carried out on an aliquot of the samples taken at 37 hours and 69 hours (table 1), which indicates the number of viable planktonic cells present. It can be seen that PA14 outcompetes RN4220 by the end of the experiment, at which point no RN4220 could be cultured from the electrode chambers. This supports other work that found *P. aeruginosa* results in reduced numbers of gram positive bacteria in a polymicrobial infection model [39]. At the 37 hour timepoint, it can also be seen that fewer viable RN4220 cells exist within the polymicrobial samples. In contrast, at 37 hours  $3.65 \times 10^5$  CFU/ml were present for RN4220, indicating that some viable cells remained in the presence of PA14, but no growth occurred.

#### Pyocyanin is Present in the Supernatant and Causes Changes in Impedance

It is well documented that a number of electroactive phenazine pigments are produced by *P. aeruginosa* [16,40,41]. One of these phenazines, pyocyanin has been studied extensively in several fields, from its effects as a virulence factor in a clinical context [35] to its use as a redox mediator in a glucose sensor [42]. We hypothesised that the green pigment observed in the media at the end of a 69 hours experiment was partly caused by the blue colour from the redox active phenazine, pyocyanin. To explore this further, after 69 hours the media was removed from the electrode chambers and filter sterilised. The supernatant was then added to an equal volume of methanol and the UV-visible spectrum was measured.

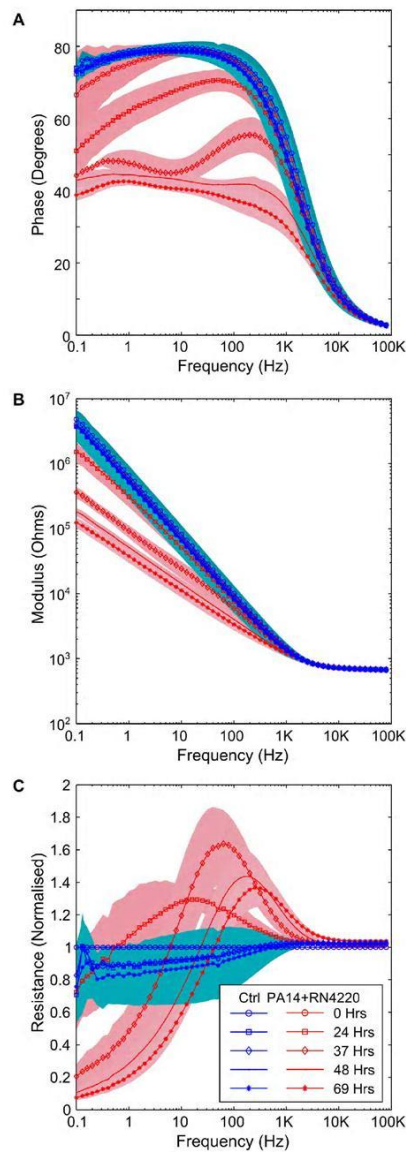


**Figure 4. Polymicrobial growth of *P. aeruginosa* and *S. aureus*.** When RN4220 and PA14 are grown together, the impedance is similar

to when PA14 is grown alone. (A) and (B) a change is clearly visible the overall phase angle and a drop in the impedance modulus, (C) the normalised resistance shows a peak, and a change in the peak frequency as a result of growth. Background shading represent  $\pm 1$  SD. Polymicrobial  $n=5$ ; neg ctrl  $n=5$ . doi:10.1371/journal.pone.0091732.g004

Peaks were observed in the UV-visible spectrum for media where PA14 was grown, either alone or as part of the polymicrobial infection model (figure 5). These changes were observed at 315 nm, 368 nm and 698 nm, and correspond to the absorbance peaks of pyocyanin found at 238 nm, 316 nm, 347 nm, 368 nm and 690 nm [43]. It is clear therefore from the UV-visible spectrum that pyocyanin is present within the ASM media following the growth of *P. aeruginosa* at 69 hours. We investigated the impact that pyocyanin had on the measured impedance by firstly measuring the impedance of pyocyanin alone in ASM at different concentrations, from 1000  $\mu$ M to 10  $\mu$ M. Only a slight change in the impedance was seen at low frequencies and high concentrations of pyocyanin (1000  $\mu$ M to approximately 500  $\mu$ M), which was unrepresentative of the changes observed when the impedance of a culture containing PA14 (alone or polymicrobial) was measured (data not shown). We reasoned that this could be because the pyocyanin existed in its oxidised form and therefore no reduced pyocyanin was available to balance the redox reaction at each electrode. Alternatively, pyocyanin could have been just one of multiple electroactive compounds that transferred electrons in a chain, with the compounds at an appropriate redox potential compared to the electrode causing the change in impedance. An alternative situation was explored, were pyocyanin was added directly to a late log culture of *P. aeruginosa* and *S. aureus* in order to assess the effect it had on the impedance.

Cultures of *P. aeruginosa* (PA14) and *S. aureus* (RN4220) were grown in ASM microaerophilically overnight to late log phase in 24 well plates. After measuring the impedance of the media, and the impedance of the late log phase cultures, pyocyanin was added to the cultures at concentrations of 100  $\mu$ M and 300  $\mu$ M and a further impedance measurement was immediately carried out. The results indicated a clear change in the impedance for each of the electrode chambers (figure 6), similar to the changes in phase observed through the growth of PA14 and the polymicrobial infection model. It was noticed when similar experiments were carried out in LB media that the blue pigment resulting from the addition of pyocyanin changed from blue to clear in all but the top layer of each of the cultures. On shaking, the pyocyanin was rapidly oxidised and returned to its original blue pigment, before gradually being reduced again. This was apparent after five minutes for the culture of *S. aureus* while *P. aeruginosa* took longer to lose its pigment and did so to a lesser degree.

These results indicate that pyocyanin plays a role in the observed impedance of PA14 when grown microaerophilically in ASM. Furthermore, it is clear that the presence of *S. aureus* leads to the reduction of pyocyanin in some manner and a consequent change in the impedance signature. It has been shown previously that pyocyanin is capable of non-enzymatically oxidising NADH in a  $2e^-$ ,  $2H^+$  reaction [44], and has more recently been explored in terms of the ability of phenazines to facilitate extracellular respiration through electron shuttling [40]. The reduction of pyocyanin by these mechanisms could explain how the microorganisms have the capacity to change the impedance.

The synthesis pathway of pyocyanin in *P. aeruginosa* is also responsible for the production of phenazine-1-carboxylic acid, 1-hydroxyphenazine, phenazine-1-carboxamide and 5-methylphenazine-1-carboxylic acid betaine [41,45-47]. Like pyocyanin,

these phenazines are redox active [16] and therefore could also have an impact upon the impedance signature. In order to explore the potential changes that a culture of *P. aeruginosa* unable to produce pyocyanin would have on the impedance, we explored the impedance signature of mutant strains of PA14 from the PA14NR set [48] and also the impedance of a double knockout mutant [47]. PA14ΔphzM a mutant that produces phenazine-1-carboxylic acid and 1-hydroxyphenazine and PA14ΔphzS is a mutant that produces phenazine-1-carboxylic acid and 5-methylphenazine-1-carboxylic acid betaine, were tested [46]. Whilst both strains were able to produce phenazine, neither of the strains were able to produce pyocyanin. In order to explore the impedance of *P. aeruginosa* when no phenazines were produced, we tested a strain where the phzA1-G1 and phzA2-G2 operons had been deleted [47]. A change in the impedance phase angle and modulus, and a peak in the normalised resistance were observed in data for both the PA14ΔphzM and PA14ΔphzS strains tested (figures 7A, C and 8A, C). The UV-visible spectra shows a peak clearly visible at 366 nm, suggesting the presence of phenazine-1-carboxylic acid [46]. No peak is present at 698 nm, confirming that no pyocyanin was produced (figure 7D and 8D). Although the PA14ΔphzM and PA14ΔphzS strains followed the same basic pattern as the wild type strain, a different impedance signature can clearly be seen, particularly in the phase angle and the normalised resistance. This shows that different combinations of phenazine compounds influence the electrode/electrolyte interface (figure 7E and 8E). In contrast, the PA14ΔphzA1-G1/A2-G2 mutant did not result in a significant impedance change in the phase and modulus data (figure 9A and B). A small peak in the normalised resistance data, different to the negative control, is clearly visible after 24 hours, although this is not of the same magnitude as the wild type or other mutants tested. This suggests a process other than electroactive transfer mediated by phenazines. Further investigation is required to explore the underlying mechanism leading to this peak.

**Microbial Attachment to the Electrode Surface may also have an Impact on Impedance**

Epifluorescent microscopy of the electrode surface was used in order to determine the extent to which *P. aeruginosa* is capable of attaching to the electrode surface. Coupons of the carbon electrode material were incubated aerobically for 48 hours in LB media. It can be seen that at the air-liquid interface, extensive biofilm formation on the carbon electrode surface is possible (figure 10A). This shows that *P. aeruginosa* has the capacity to attach to the electrode surface and form a biofilm. In contrast, incubating the electrode coupon at the bottom of a chamber resulted in some microbial attachment, but little biofilm formation (figure 10B). This could have been due to the viscous, thick media at the end of the experiment pulling biofilm away from the electrode surface

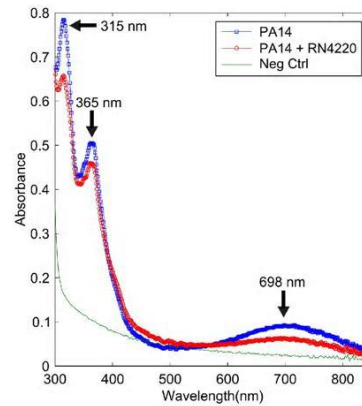


**Figure 5. UV-visible spectroscopy of the supernatant after 3 days showing typical spectrum.** At the end of experiments, the supernatant was taken from all samples and combined with 50% MeOH. The peaks highlighted by the arrows are similar to those found in pyocyanin, a redox active phenazine produced by *P. aeruginosa*. doi:10.1371/journal.pone.0091732.g005

when the cell was aspirated. The negative control indicates that there is no autofluorescence on the electrode surface (figure 10C).

We investigated the impedance signature of *P. aeruginosa* at the end of a 3 day microaerophilic incubation period in ASM, when the media within the electrode chamber was replaced with fresh media. Under these conditions, we noticed that the media at the end of the experiment was far less viscous and the biofilm formed at the air liquid interface was much more limited. Interestingly, we found that a small change in impedance could still be distinguished against control samples (figure 10D). This could suggest that microbial attachment to the electrode surface also plays a role in the observed impedance changes. However, it is interesting to note that the normalised resistance peak observed with PA14ΔphzA1-G1/A2-G2 (figure 9C) is different to the normalised resistance observed when the media is replaced (figure 10D). This could be related to the residual media and limited biofilm material attached to the electrode containing electroactive compounds produced by *P. aeruginosa* changing the impedance in addition to the effect observed with the PA14ΔphzA1-G1/A2-G2 mutant.

**Table 1. Indicative cell densities of planktonic cells at the end of the experiment and timepoints during the experiment.**

Sample Type	Cell Concentration (CFU/ml)		
	Initial (0 hrs)	37 Hrs mean (range)	69 Hrs mean (range)
PA14 Mono	3–5 × 10 <sup>6</sup>	6.5 × 10 <sup>6</sup> (5.4 × 10 <sup>6</sup> –7.3 × 10 <sup>6</sup> )	2.1 × 10 <sup>6</sup> (6.5 × 10 <sup>5</sup> –3.3 × 10 <sup>6</sup> )
RN4220 Mono	3–5 × 10 <sup>6</sup>	1.6 × 10 <sup>7</sup> (1.1 × 10 <sup>7</sup> –2.9 × 10 <sup>7</sup> )	3.1 × 10 <sup>7</sup> (4.9 × 10 <sup>6</sup> –7.2 × 10 <sup>7</sup> )
PA14 Poly	3–5 × 10 <sup>6</sup>	6.0 × 10 <sup>6</sup> (4.1 × 10 <sup>6</sup> –7.2 × 10 <sup>6</sup> )	8.5 × 10 <sup>7</sup> (5.9 × 10 <sup>6</sup> –1.0 × 10 <sup>8</sup> )
RN4220 Poly	3–5 × 10 <sup>6</sup>	3.7 × 10 <sup>5</sup> (6.8 × 10 <sup>4</sup> –1.4 × 10 <sup>6</sup> )	0

doi:10.1371/journal.pone.0091732.t001



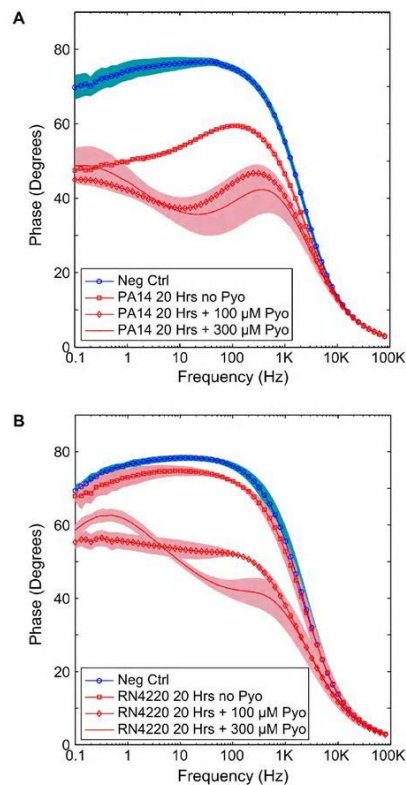


**Figure 6. Addition of Pyocyanin yields a distinct change in the impedance.** Adding the phenazine pigment pyocyanin to cultures of *P. aeruginosa* and *S. aureus* causes the impedance to change. (A) Change in impedance of PA14, which is similar to the change caused by growth in microaerophilic conditions. (B) Change in impedance of *S. aureus*, RN4220. Background shading represents  $\pm 1$  SD,  $n = 3$ . doi:10.1371/journal.pone.0091732.g006

### Conclusion

This article describes how *P. aeruginosa* could be detected using a low cost, disposable sensor. The technique can be applied with low cost sensors and microelectronic measurement equipment, making it potentially useful in different point of care diagnostic scenarios, such as monitoring of CF sputum. However, several challenges still need to be overcome in the translation of this technology from the laboratory to a point of care application. For example, in the case of CF, sputum samples are thick and viscous, requiring some form of homogenisation prior to measurement and a change in the redox state of the electroactive phenazines between expectoration and measurement might affect the sensitivity of the sensor. Future investigations will therefore focus upon device testing in real

clinical samples in order to identify and address potential detection problems.

### Materials and Methods

#### Media, Buffers and Microbial Strains

LB media (used to grow overnight cultures, for the adjustment of optical density at the start of each experiment and for epifluorescent microscopy) was made by mixing 1 g tryptone (order code: BPE1421, Fisher Scientific) 0.5 g yeast extract (order code: 92144, Fluka) and 0.5 g NaCl (order code: 31434, Sigma-Aldrich) with 100 ml of dH<sub>2</sub>O before autoclaving for 20 mins at 121°C. TSB (order code: CM0129, Fisher Scientific) was used as directed and autoclaved prior to use. 100 ml aliquots of ASM were produced following an adapted version of the protocol by Kirchner et al. (2012). Briefly, 400 mg DNA from fish sperm (order code: 74782, Sigma-Aldrich) and 500 mg of porcine mucin (order code: M2378, Sigma-Aldrich) were sterilised overnight in 2 ml of 100% EtOH. This was then poured into 50 ml of sterile dH<sub>2</sub>O. 25 mg of the specified amino acids, 1 ml egg yolk emulsion (order code: 17148, Sigma-Aldrich) and 500 mg NaCl was then added to the DNA and porcine mucin as described [37]. The pH of the media was tested and adjusted to 6.9 by aseptically taking small aliquots of media to measure the pH after adjusting with sterile 1 M Tris. Normal saline was used for electrode conditioning and was made in aliquots of 100 ml by mixing dH<sub>2</sub>O with 0.9 g NaCl. The strains used in this experiment are described in table 2. Mutants taken from a copy of the PA14NR transposon library [48] and were cultured for single colonies on LB agar plates containing 15 µg/ml of gentamicin.

**Electrode printing and preconditioning.** The electrode pattern consisted of a small working electrode (2 mm diameter) surrounded by a larger counter electrode (10 mm diameter). Electrodes were manufactured using thick film screen printing processes on a DEK 247 semi-automatic screen printing machine (DEK). This was achieved firstly by producing a mask for the electrode pattern. The electrodes were then screen printed onto acetate sheets suitable for a mono laser printer (order code: 9543383, Supplies Team). Electrodes were printed using Electro-dag PF407A carbon ink and were cured (after each printing cycle) in a box oven at 120°C for 30 minutes. A dielectric ink was hand painted over the track leading up to the working electrode with Gwent D2020823D2 and cured at 80°C for 30 minutes. After production, a 20 mm section of 15 ml centrifuge tube (order code: 11542293, Fisher Scientific) was mounted over the top of the electrode with Servisol silicone adhesive (order code: RE39W, Maplin), completing the electrode assembly (figure S1). An electrode conditioning procedure described by Wang et al. (1996) [49] was adapted as follows. 2 ml 0.9% NaCl made with dH<sub>2</sub>O was added to each electrode. Conditioning was carried out using a Solartron 1260 impedance gain/phase analyser and the Zplot/Zview software package. Using a 2 mm diameter platinum counter electrode (order code: PT007920, Goodfellow), both the working and counter carbon electrodes were DC biased at 2 volts and held there for 3 minutes, and then at -2 volts for a further 3 minutes. The electrode assemblies were sterilised by submerging in 70% EtOH for 10 minutes. Following this, the EtOH was allowed to fully evaporate in a sterile environment overnight.

**Microaerophilic chamber design.** A microaerophilic environment was created by using a lock 'n' lock plastic box (product number: HPL826M) modified with two 9 way D-sub connectors mounted through the sidewalls of the box (Order code: 674-0760 and 450-9258, RS components) to enable impedance measurements to be carried out without the need to remove the lid. The D-

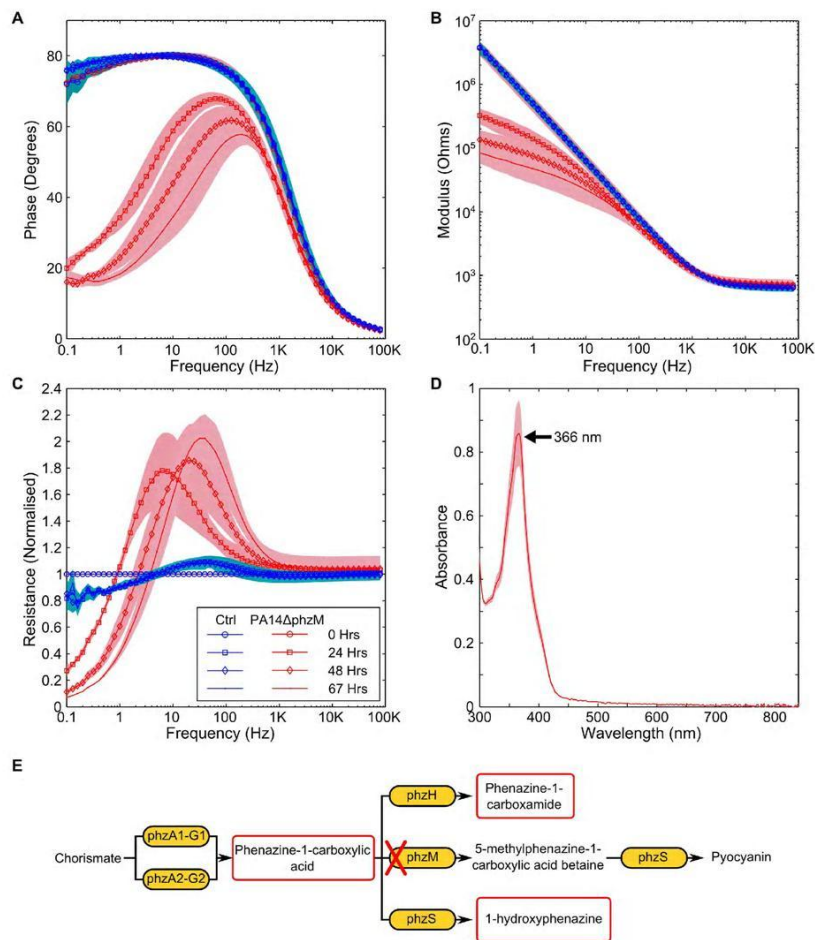


**Figure 7. Impedance changes caused by the PA14ΔphzM mutant.** Changes to the impedance spectrum can be clearly observed when a mutant of *P. aeruginosa*, unable to produce pyocyanin is measured. Changes to the (A) phase, (B) modulus and (C) normalised resistance are similar to those found in the PA14 wild type. (D) the UV-visible spectrum shows a peak at 367 nm, suggesting the presence of phenazine-1-carboxylic acid. (E) Indicates the biosynthesis pathway for phenazines and shows the effect that the phzM knockout is anticipated to have. Background shading represent  $\pm 1$  SD. PA14ΔphzM  $n = 3$ ; Neg Ctrl  $n = 3$ . doi:10.1371/journal.pone.0091732.g007

sub connectors were made airtight by sealing around the connectors on the inside of the box with Servisol silicone adhesive.

**Calculation of starting cell densities and electrode inoculation.** The number of PA14 and RN4220 CFUs at  $OD_{600}$  were determined through the production of a standard curve in a preparatory experiment. Overnight cultures of PA14

and RN4220 were grown in LB media and adjusted to an  $OD_{600}$  of 0.33 and 0.67 respectively, representing a cell density of approximately  $3 \times 10^8$  to  $5 \times 10^8$  CFU/ml. 1 ml of ASM media was then inoculated with 10  $\mu$ l of the OD adjusted media.

**Monoculture and polymicrobial experiments.** At the start of the experiment, nine sterile electrodes were connected,

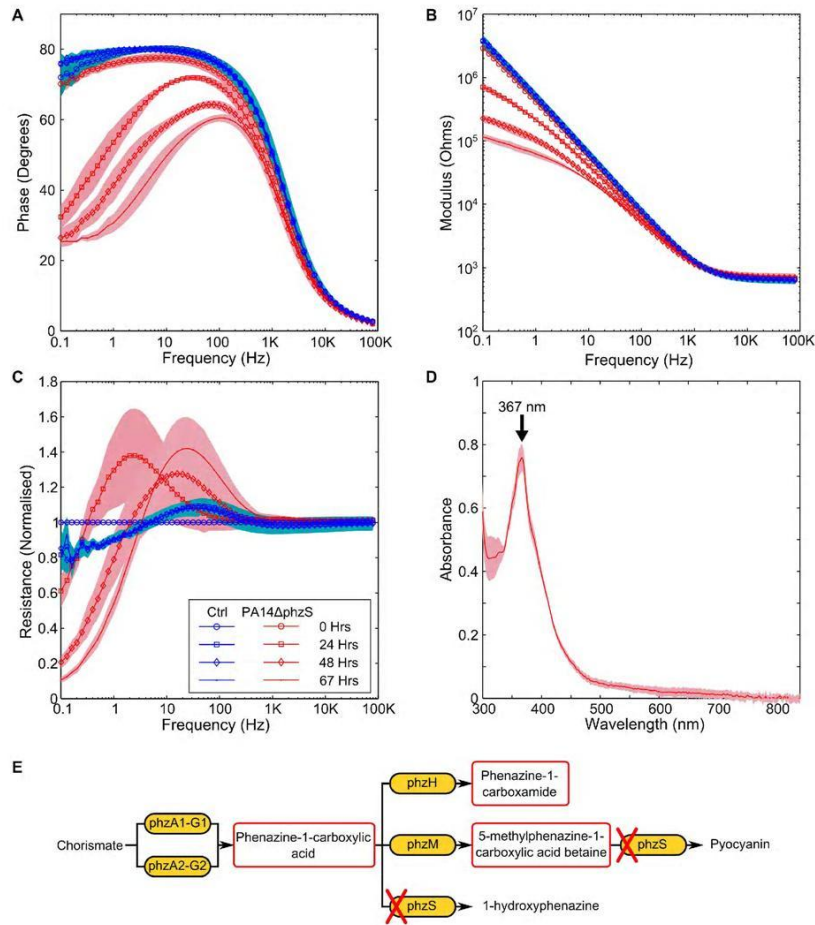


**Figure 8. Impedance changes caused by the PA14ΔphzS mutant.** Similar changes are observable in the (A) phase, (B) modulus and (C) normalised resistance to the wild type and the PA14ΔphzS mutant. (D) the presence of phenazine-1-carboxylic acid can also be seen. (E) Indicates the biosynthesis pathway for phenazines and shows the effect that the phzS knockout is anticipated to have. Background shading represent  $\pm 1$  SD. PA14ΔphzS  $n = 3$ ; Neg Ctrl  $n = 3$ . doi:10.1371/journal.pone.0091732.g008

inoculated and placed into each box, with up to 18 electrodes used in one experiment. At least four replicates of each sample (including negative control) were carried out. A microaerophilic environment was created using a Campygen gas generation pack (order code: 10108012, Fisher Scientific). Electrodes were then incubated at 37°C in a shaking incubator at 75 rpm for a maximum of three days.

**Impedance measurement.** All impedance measurements were carried out on a Solartron 1260 impedance gain/phase analyser in conjunction with the Zplot/Zview software package (Scribner Associates). Impedance measurements were carried out at the start of the experiment and then at least once every 24 hours for the duration of the experiment. The microaerophilic chamber was removed from the incubator and kept at room temperature for the duration of the measurements which typically lasted approx-

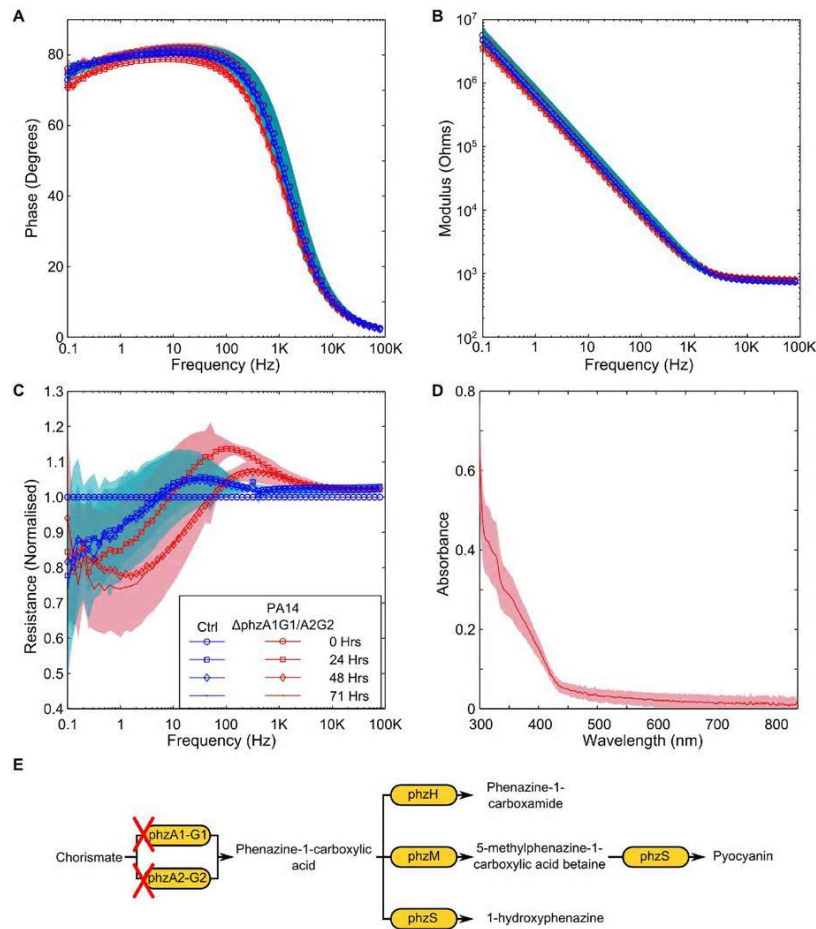


**Figure 9. Measurement of *P. aeruginosa* PA14 $\Delta$ phzA1-G1/A2-G2 double mutant.** (A and B) no significant different can be seen in the phase or modulus of the impedance. (C) a small difference in the normalised resistance can be seen, contrasted to the negative control. (D) The UV-visible spectrum indicates that the phenazines present in the wild type or other mutants tested are no present. (E) Indicates the point on the biosynthesis pathway that the double knockout is anticipated to affect. Background shading represent  $\pm$ 1 SD. PA14 $\Delta$ phzA1-G1/A2-G2  $n=4$ ; Neg Ctrl  $n=4$ . doi:10.1371/journal.pone.0091732.g009

imately 45 minutes per chamber and four minutes per electrode. The impedance measurements carried out in the experiment were made using a Solartron 1260 impedance analyser with an AC rms voltage of 200 mV between 0.1 Hz and 1 MHz. Impedance data analysis was carried out using Matlab r2012b (Mathworks).

**UV-Vis spectrum and associated protocol.** At the end of the experiment period, the supernatant was filter sterilised through 0.22  $\mu$ m syringe filter (Millipore) and then added to an equal

volume of methanol to fix the sample. The UV visible spectrum was then measured from 190 nm to 850 nm using a Thermofisher 2000x spectrophotometer. Data analysis of the UV-visible spectrum was carried out in Matlab r2012b (Mathworks).

**Exogenous pyocyanin measurements.** Pyocyanin purified from *P. aeruginosa* (order code: P0046, Sigma-Aldrich) was solubilised in 100% EtOH to create a 10x stock solution. This was then mixed with sterile dH<sub>2</sub>O for the measurements carried

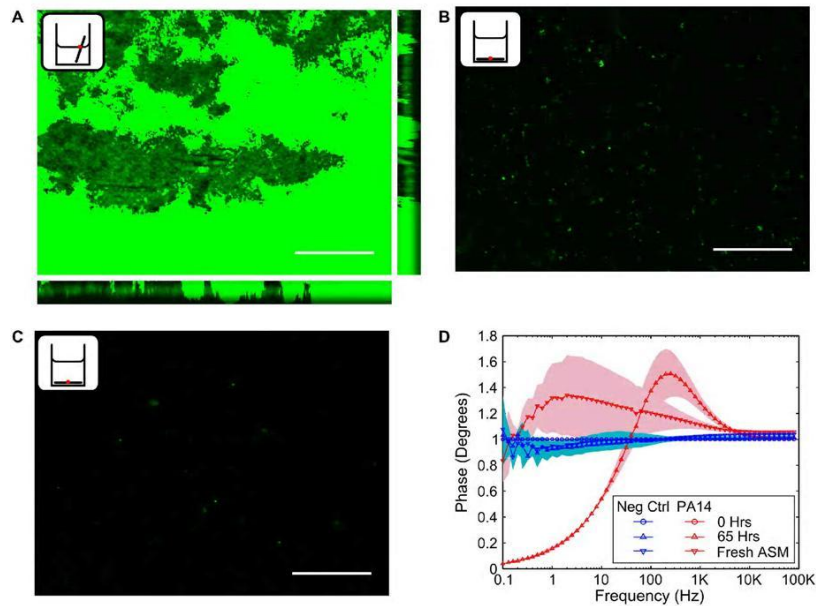


**Figure 10. Attachment of *P. aeruginosa* PA14 to the electrode surface could affect the impedance.** Electrode coupons were incubated in LB media (aerobic conditions) for 48 Hrs. (A) At the air-liquid interface, extensive biofilm formation can be seen indicating that *P. aeruginosa* will attach to the electrode surface. (B) Some limited microbial attachment can be seen on the electrode surface at the bottom of the a well after 48 hours. (C) Negative control showing that the electrode surface does not autofluoresce. (D) A small change can be observed in the impedance signature (contrasted to the negative control) at the end of a microaerophilic experiment when the media is exchanged with a fresh, sterile aliquot. Scale bars represent 50  $\mu$ m. Shading in (D) represents  $\pm 1$ SD,  $n = 3$ . doi:10.1371/journal.pone.0091732.g010

out using *S. aureus* and *P. aeruginosa*. 1 ml samples of *P. aeruginosa* and *S. aureus* (as monocultures) were grown overnight (20 hours) along with negative controls in 24 well plates. Following this, the samples were removed from the microaerophilic growth chamber and after initial impedance measurements, pycocyanin was added to aliquots of media to a final concentration of 100  $\mu$ M and 300  $\mu$ M. An impedance measurement was carried out at each concentration.

**Epifluorescent microscopy of electrode coupons.** Electrode coupons were manufactured in the same manner as the electrodes used in the experiment. The coupons were made by cutting electrodes into a shape compatible with incubation in a 24 well plate. After sterilising in 70% EtOH for 10 minutes, 1 ml of LB was added to each sample. For the positive control electrodes, the samples were positioned at an angle so that a portion of the coupon was out of the media, thus facilitating

**Table 2. Bacterial strains used in this study.**

Strain	Comment	Reference
RN4220	<i>S. aureus</i> wild type laboratory strain	[51]
PA14WT	<i>P. aeruginosa</i> wild type laboratory strain	[48]
PA14 $\Delta$ phz5	<i>P. aeruginosa</i> PA14 mutant from the PA14NR set (gene ID: 44099)	[48]
PA14 $\Delta$ phzM	<i>P. aeruginosa</i> PA14 mutant from the PA14NR set (gene ID: 40343)	[48]
PA14 $\Delta$ phzA1-G1/A2-G2	<i>P. aeruginosa</i> double knockout mutant	[47]

doi:10.1371/journal.pone.0091732.t002

biofilm growth at the air liquid interface. Samples were then inoculated with PA14 or left sterile as controls and incubated aerobically at 37°C, shaking at 75 rpm for 48 hours. Coupons were removed from the 24 well plate, aspirated and then stained with 5 µM of SYTO 9 (order code: S-34854, Life Technologies). Microscopy was carried out on a Zeiss Axio Imager Z1, with an exposure time of 750 ms per image. Brightness and contrast were made consistent across images and scales bars were added in Fiji image [50].

## Supporting Information

**Figure S1 Example of an assembled electrode chamber.** (TIFF)

## References

- Yang L, Li Y, Griffis CL, Johnson MG (2004) Interdigitated microelectrode (IME) impedance sensor for the detection of viable *Salmonella typhimurium*. *Biosens Bioelectron* 19: 1139–1147. doi:10.1016/j.bios.2003.10.009.
- Yang L, Ruan C, Li Y (2005) Detection of viable *Salmonella typhimurium* by impedance measurement of electrode capacitance and medium resistance. *Biosens Bioelectron* 19: 495–502. doi:10.1016/S0956-5663(03)00229-X.
- Muñoz-Berbel X, Muñoz EJ, Vigués N, Mas J (2006) On-chip impedance measurements to monitor biofilm formation in the drinking water distribution network. *Sens Actuators B Chem* 118: 129–134. doi:10.1016/j.snb.2006.04.070.
- Muñoz-Berbel X, Vigués N, Mas J, Jenkins ATA, Muñoz EJ (2007) Impedimetric characterization of the changes produced in the electrode solution interface by bacterial attachment. *Electrochem Commun* 9: 2654–2660. doi:10.1016/j.elecom.2007.08.011.
- Muñoz-Berbel X, Vigués N, Jenkins ATA, Mas J, Muñoz EJ (2008) Impedimetric approach for quantifying low bacteria concentrations based on the changes produced in the electrode solution interface during the pre-attachment stage. *Biosens Bioelectron* 23: 1540–1546. doi:10.1016/j.bios.2008.01.007.
- Bayoudh S, Othmane A, Ponsomet L, Ben Ouada H (2008) Electrical detection and characterization of bacterial adhesion using electrochemical impedance spectroscopy-based flow chamber. *Colloids Surf Physicochem Eng Asp* 318: 291–300.
- Dheilly A, Lénosier J, Darchen A, Hadjiev D, Corbel C, et al. (2008) Monitoring of microbial adhesion and biofilm growth using electrochemical impedanceometry. *Appl Microbiol Biotechnol* 79: 157–164. doi:10.1007/s00253-008-1404-7.
- Ben-Yoav H, Freeman A, Sernheim M, Shacham-Diamand Y (2011) An electrochemical impedance model for integrated bacterial biofilms. *Electrochimica Acta* 56: 7780–7786. doi:10.1016/j.electacta.2010.12.025.
- Kim T, Kang J, Lee JH, Yoon J (2011) Influence of attached bacteria and biofilm on double-layer capacitance during biofilm monitoring by electrochemical impedance spectroscopy. *Water Res* 45: 4615–4622.
- Kim S, Yu G, Kim T, Shin K, Yoon J (2012) Rapid bacterial detection with an interdigitated array electrode by electrochemical impedance spectroscopy. *Electrochimica Acta* 82: 126–131. doi:10.1016/j.electacta.2012.05.131.
- Muñoz-Berbel X, García-Aljaro C, Muñoz EJ (2008) Impedimetric approach for monitoring the formation of biofilms on metallic surfaces and the subsequent application to the detection of bacteriophages. *Electrochimica Acta* 53: 5739–5744. doi:10.1016/j.electacta.2008.03.050.
- McColl D, MacDougall M, Watret L, Connolly P (2009) Monitoring moisture without disturbing the wound dressing. *Wounds UK* 5: 94–99.
- Farrow MJ, Hunter IS, Connolly P (2012) Developing a Real Time Sensing System to Monitor Bacteria in Wound Dressings. *Biosensors* 2: 171–188. doi:10.3390/bios2020171.
- Bard AJ, Faulkner LR (2001) *Electrochemical methods: fundamentals and applications*. 2 edn. New York: Wiley.
- K'owino IO, Sadik OA (2005) Impedance Spectroscopy: A Powerful Tool for Rapid Biomolecular Screening and Cell Culture Monitoring. *Electroanalysis* 17: 2101–2113. doi:10.1002/elan.200503371.
- Wang Y, Newman DK (2008) Redox Reactions of Phenazine Antibiotics with Ferric (Hydroxides) and Molecular Oxygen. *Environ Sci Technol* 42: 2380–2386. doi:10.1021/es702290a.
- Wang Y, Kern SE, Newman DK (2010) Endogenous Phenazine Antibiotics Promote Anaerobic Survival of *Pseudomonas aeruginosa* via Extracellular Electron Transfer. *J Bacteriol* 192: 365–369. doi:10.1128/JB.01188-09.
- Liu GY, Nizer V (2009) Color me bad: microbial pigments as virulence factors. *Trends Microbiol* 17: 406–413. doi:10.1016/j.tim.2009.06.006.
- Marsili E, Baron DB, Shikhare ID, Coursolle D, Gralnick JA, et al. (2008) *Shewanella* secretes flavins that mediate extracellular electron transfer. *Proc Natl Acad Sci U S A* 105: 3968–3973. doi:10.1073/pnas.0710525105.
- Hernandez ME, Newman DK (2001) Extracellular electron transfer. *Cell Mol Life Sci* 58: 1562–1571.
- Reguera G, McCarthy KD, Mehta T, Nicoll JS, Tuominen MT, et al. (2005) Extracellular electron transfer via microbial nanowires. *Nature* 435: 1098–1101. doi:10.1038/nature03661.
- Poortinga AT, Bos R, Busscher HJ (2001) Charge transfer during staphylococcal adhesion to TiNOX coatings with different specific resistivity. *Biophys Chem* 91: 273–279. doi:10.1016/S0301-4622(01)00177-6.
- Marsili E, Rollefson JB, Baron DB, Hozacki RM, Boud DR (2008) Microbial Biofilm Voltammetry: Direct Electrochemical Characterization of Catalytic Electrode-Attached Biofilms. *Appl Environ Microbiol* 74: 7329–7337. doi:10.1128/AEM.00177-08.
- Cady P (1975) Rapid automated bacterial identification by impedance measurement. In: Hedén C-G, Illeni T, editors. *New approaches to the identification of microorganisms*. London: Wiley, 74–79.
- Firstenberg-Eden R, Eden G (1984) *Impedance microbiology*. England: Research Studies Press.
- Ur A, Brown D (1975) Monitoring of bacterial activity by impedance measurement. In: Hedén C-G, Illeni T, editors. *New approaches to the identification of microorganisms*. New York: Wiley.
- Moulton S, Barisci J, Bath A, Stolla R, Wallace G (2004) Studies of double layer capacitance and electron transfer at a gold electrode exposed to protein solutions. *Electrochimica Acta* 49: 4223–4230. doi:10.1016/j.electacta.2004.03.034.
- Paredes J, Becerro S, Arizti F, Aguinaga A, Del Pozo JL, et al. (2012) Real time monitoring of the impedance characteristics of *Staphylococcal* bacterial biofilm cultures with a modified CDC reactor system. *Biosens Bioelectron* 38: 226–232. doi:10.1016/j.bios.2012.05.027.
- Paredes J, Becerro S, Arizti F, Aguinaga A, Del Pozo JL, et al. (2013) Interdigitated microelectrode biosensor for bacterial biofilm growth monitoring by impedance spectroscopy (technique in 96-well microtiter plates). *Sens Actuators B Chem* 178: 663–670. doi:10.1016/j.snb.2013.01.027.
- Connolly P, Shedden L (2010) A System and Method for Cell Characterisation. Patent application number: WO2009136157 (A3).
- Hasset DJ, Sutton MD, Schurr MJ, Herr AB, Caldwell CC, et al. (2009) *Pseudomonas aeruginosa* hypoxic or anaerobic biofilm infections within cystic fibrosis airways. *Trends Microbiol* 17: 130–138. doi:10.1016/j.tim.2008.12.003.
- Ratjen F, Döring G (2003) Cystic fibrosis. *The Lancet* 361: 681–689. doi:10.1016/S0140-6736(03)12567-6.
- Jefferies JMC, Cooper T, Yam T, Clarke SC (2012) *Pseudomonas aeruginosa* outbreaks in the neonatal intensive care unit – a systematic review of risk factors and environmental sources. *J Med Microbiol* 61: 1052–1061. doi:10.1099/jmm.0.0448184.
- Branski LK, Al-Mousawi A, Rivero H, Jeschke MG, Sanford AP, et al. (2009) Emerging infections in burns. *Surg Infect* 10: 389–397. doi:10.1089/sur.2009.024.
- Lau GW, Hasset DJ, Ran H, Kong F (2004) The role of pyocyanin in *Pseudomonas aeruginosa* infection. *Trends Mol Med* 10: 599–606. doi:10.1016/j.molmed.2004.10.002.
- Harrison (2007) Microbial ecology of the cystic fibrosis lung. *Microbiology* 153: 917–923. doi:10.1099/mic.0.2006/004077-0.
- Kirchner S, Fothergill JL, Wright EA, James CE, Mowat E, et al. (2012) Use of Artificial Sputum Medium to Test Antibiotic Efficacy Against *Pseudomonas aeruginosa* in Conditions More Relevant to the Cystic Fibrosis Lung. *J Vis Exp*. Available: <http://www.jove.com/video/3837/use-artificial-sputum-medium-to-test-antibiotic-efficacy-against>. Accessed 26 September 2012.
- Stewart L, Ford A, Sangal V, Jenkins J, Boyle B, et al. (2013) Draft genomes of twelve host adapted and environmental isolates of *Pseudomonas aeruginosa* and their position in the core genome phylogeny. *Pathog Dis*. In press. doi:10.1111/2049-632X.12107.
- Korgaonkar A, Trivedi U, Rumbaugh KP, Whiteley M (2013) Community surveillance enhances *Pseudomonas aeruginosa* virulence during polymicrobial infection. *Proc Natl Acad Sci* 110: 1059–1064. doi:10.1073/pnas.1214550110.

40. Price-Whelan A, Dietrich LEP, Newman DK (2007) Pyocyanin alters redox homeostasis and carbon flux through central metabolic pathways in *Pseudomonas aeruginosa* PA14. *J Bacteriol* 189: 6372–6381. doi:10.1128/JB.00505-07.
41. Price-Whelan A, Dietrich LEP, Newman DK (2006) Rethinking 'secondary' metabolism: physiological roles for phenazine antibiotics. *Nat Chem Biol* 2: 71–78.
42. Ohfuji K, Sato N, Hamada-Sato N, Kobayashi T, Imada C, et al. (2004) Construction of a glucose sensor based on a screen-printed electrode and a novel mediator pyocyanin from *Pseudomonas aeruginosa*. *Biosens Bioelectron* 19: 1237–1244. doi:10.1016/j.bios.2003.11.010.
43. Watson D, MacDermot J, Wilson R, Cole PJ, Taylor GW (1996) Purification and structural analysis of pyocyanin and 1-hydroxyphenazine. *Eur J Biochem* 159: 309–313. doi:10.1111/j.1432-1033.1996.tb09869.x.
44. Kato N, Ohnishi Y, Kagami M, Ohno A (1974) Reduction by a Model of NAD(P)H. Construction of Electron Bridges. *Chem Lett* 3: 353–356.
45. Winsor GL, Lam DKW, Fleming L, Lo R, Whiteside MD, et al. (2011) *Pseudomonas* Genome Database: improved comparative analysis and population genomics capability for *Pseudomonas* genomes. *Nucleic Acids Res* 39: D596–600. doi:10.1093/nar/gkr369.
46. Mavrodi DV, Bonsall RF, Delaney SM, Soule MJ, Phillips G, et al. (2001) Functional Analysis of Genes for Biosynthesis of Pyocyanin and Phenazine-1-Carboxamide from *Pseudomonas aeruginosa* PAO1. *J Bacteriol* 183: 6454–6465. doi:10.1128/JB.183.21.6454-6465.2001.
47. Dietrich LEP, Price-Whelan A, Petersen A, Whiteley M, Newman DK (2006) The phenazine pyocyanin is a terminal signalling factor in the quorum sensing network of *Pseudomonas aeruginosa*. *Mol Microbiol* 61: 1308–1321. doi:10.1111/j.1365-2958.2006.03306.x.
48. Liberati NT, Urbach JM, Miyata S, Lee DG, Drenkard E, et al. (2006) An ordered, nonredundant library of *Pseudomonas aeruginosa* strain PA14 transposon insertion mutants. *Proc Natl Acad Sci* 103: 2833–2838.
49. Wang J, Pedrero M, Sakslund H, Hammerich O, Pingarron J (1996) Electrochemical activation of screen-printed carbon strips. *The Analyst* 121: 345. doi:10.1039/an9962100345.
50. Schindelin J, Arganda-Carreras I, Frise E, Kaynig V, Longair M, et al. (2012) Fiji: an open-source platform for biological-image analysis. *Nat Methods* 9: 676–682. doi:10.1038/nmeth.2019.
51. Nair D, Memmi G, Hernandez D, Bard J, Beaune M, et al. (2011) Whole-Genome Sequencing of *Staphylococcus aureus* Strain RN4220, a Key Laboratory Strain Used in Virulence Research, Identifies Mutations That Affect Not Only Virulence Factors but Also the Fitness of the Strain. *J Bacteriol* 193: 2332–2335. doi:10.1128/JB.00027-11.

# Development of a diagnostic device to detect different *Pseudomonas aeruginosa* phenotypes in medically relevant contexts

Andrew C. Ward, Nicholas P. Tucker, Patricia Connolly

**Abstract**— *Pseudomonas aeruginosa*, widely present in the environment, is well known for its ability to cause infection in immune compromised individuals. For example, *P. aeruginosa* is the leading cause of morbidity and mortality in patients with cystic fibrosis (CF). Here, we describe how Electrochemical Impedance Spectroscopy (EIS) can be used to detect the presence of four different strains of *P. aeruginosa*. Using a low cost, screen printed carbon electrode significant changes can be seen in impedance data in the presence of *P. aeruginosa* after 24 hours. Furthermore, through the use of a normalization technique whereby the phase angle of the impedance (a commonly used parameter) is divided by a starting measurement, it is possible to identify differences between a non-mucoid and mucoid strain of *P. aeruginosa*. Sensors based upon the techniques described here could be used in a number of healthcare scenarios, where there is a need for low cost, real time detection of *P. aeruginosa*, such as CF.

## I. INTRODUCTION

*Pseudomonas aeruginosa* is a medically important gram negative bacterium responsible for causing infection in immune compromised individuals. Chronic lung infections due to *P. aeruginosa* are the leading cause of morbidity and mortality in patients with cystic fibrosis (CF)[1]. Burns are also particularly vulnerable to colonization by *P. aeruginosa* [2] and there are a number of other groups who may succumb to the infection including pre-term babies [3]. *P. aeruginosa* infections have also been associated with blood stream infections (BSI). BSIs have a large economic burden, with the cost of a treatment estimated to be \$40, 000 per patient [4].

In CF patients, initial virulent strains of *P. aeruginosa* become rapidly host adapted, forming biofilms which make them resistant to eradication either by the host immune system or by antibiotics [5]. Virulent strains of *P. aeruginosa* are generally motile and planktonic whereas host adapted strains are sessile and produce large quantities of alginate. The virulent strains are often described as “non-mucoid”, in contrast to their alginate producing, “mucoid” counterparts. Early detection of the non-mucoid strain before the bacteria become host adapted may make it possible to eradicate *P. aeruginosa*, thus preventing chronic

colonisation [6]. A technique that enables real time detection of these two strains in a sample could therefore be clinically useful.

Electrochemical Impedance Spectroscopy (EIS) has been explored previously as a potential technique for monitoring or characterising *P. aeruginosa* [7]–[9]. Whilst much research has been carried out using EIS, the dependence upon labels (such as antibodies or DNA oligonucleotides) or expensive electrode materials and manufacturing techniques make application in low cost point of care devices challenging. In this study, we have combined the use of low cost, disposable screen printed carbon electrodes with EIS in order to detect the presence of *P. aeruginosa*. Previously, we have shown how *P. aeruginosa* is detectable in a polymicrobial competition model using a screen printed carbon electrode [10]. In other work, it has also been shown that screen printed silver chloride electrodes can be used to detect *S. aureus* in a microbial broth [11]. Screen printing has been applied previously as a basis for low cost sensors, such as the detection of moisture within a chronic wound [12], [13]. The technique has been granted an EU patent for its use in cell and bacterial recognition and patents owned by the University of Strathclyde are pending worldwide [14].

The impedance characteristics of an electrode-electrolyte interface are governed by a number of processes [15]. The concentration of charged molecules and solutes within the electrode affect the capacitance, the presence of redox active compounds can affect the charge transfer capabilities of the interface. The diffusion of any redox active compounds will also influence the rate of charge transfer, along with the concentration of these compounds within the media. The conductivity of electrolyte between the electrodes also has an impact upon the measured impedance at high frequencies. We hypothesize that it is possible to detect the presence of microorganisms by looking across the impedance spectrum for specific changes to the characteristics of the interface. In this study, we focus upon the impedance signature caused by *P. aeruginosa* and demonstrate differences in the impedance between non-mucoid and mucoid strains.

## II. METHODS

### A. Strains and Media

All experiments were performed in Lysogeny Broth (LB) media (described previously [10]). Two non-mucoid/mucoid strain pairs of *P. aeruginosa* were tested: J1385/J1532 and C1446/C1433. These are clinical isolates from CF sputum and were kindly provided by the UK Cystic Fibrosis Microbiology Consortium at the University of Edinburgh

This work has been funded by the Engineering and Physical Sciences Research Council (www.epsrc.ac.uk, grant number: EP/T50036X/1) as part of an Engineering Doctorate.

A. C. Ward is with the University of Strathclyde, Wolfson Building, 106 Rottenrow, Glasgow, G4 0NW, UK. (andrew.c.ward@strath.ac.uk).

N. P. Tucker is with the University of Strathclyde (nick.tucker@strath.ac.uk).

P. Connolly is with the University of Strathclyde (corresponding author. patricia.connolly@strath.ac.uk. Tel. 44 141 548 3034)



[16]. J1385 and C1426 are non-mucoid strains and J1532 and C1433 are mucoid strains. All measurements were replicated with four different samples for each strain. Final concentrations of *P. aeruginosa* at the end of the experiment were determined using the drop plate method [17], as described previously [10].

#### B. Electrode Manufacture and Normalization

Carbon electrodes were screen printed onto acetate, with a section of 15 ml centrifuge tube mounted on top of them [10]. The impedance measurements resulting from the experiment were normalized in order to distinguish differences in the impedance caused by *P. aeruginosa* [14]. This was achieved using the following equation:

$$IPN_{t=n} = \frac{IPA_{t=n}}{IPA_{t=0}}$$

Where  $IPN_{t=n}$  is the normalized impedance parameter of interest (i.e. reactance, resistance, impedance modulus or phase) and  $IPA_t$  is the absolute (as measured) impedance parameter.

#### C. Impedance Measurement and Growth Experiments

Electrodes chambers were sterilized in 70 % v/v ethanol and then inoculated in replicates of four with 10  $\mu$ l of bacterial broth containing approximately  $3.5 \times 10^9$  colony forming units (CFU) per milliliter of the strain of interest. Four electrodes were filled with sterile media as negative controls. Electrodes were incubated for 72 hours at 37°C in air. In order to prevent the samples drying out during the incubation period, the humidity was increased through the use of wet paper towel placed around the chambers. A plastic container was then placed over the electrodes to allow the humidity to increase. Impedance measurements were taken with a Solartron 1260 impedance analyzer with an AC potential of 200 mV<sub>rms</sub> from 1 MHz to 0.1 Hz at the start of the experiment and then once every 24 hours.

#### D. Statistical analysis

The Mann-Whitney test was used to compare the results against the negative control. Minitab was used for the statistical analysis. Statistical significance is defined here as  $P \leq 0.05$ .

TABLE 1. MEAN CHANGE IN IMPEDANCE MODULUS AT LOW FREQUENCY FOR EACH STRAIN. VALUES MARKED \* ARE SIGNIFICANTLY DIFFERENT TO THE NEGATIVE CONTROL.

Strain	Impedance Modulus at 0.1 Hz (Ohms)			
	0 Hours	24 Hours	50 Hours	72 Hours
Neg ( $n=4$ )	$4.51 \times 10^6$	$4.39 \times 10^6$	$4.20 \times 10^6$	$4.09 \times 10^6$
C1426 ( $n=4$ )	$5.27 \times 10^6$	$1.13 \times 10^6$ *	$5.28 \times 10^5$ *	$3.04 \times 10^5$ *
C1433 ( $n=4$ )	$4.73 \times 10^6$	$3.03 \times 10^5$ *	$2.00 \times 10^5$ *	$2.47 \times 10^5$ *
J1385 ( $n=4$ )	$4.98 \times 10^6$	$7.33 \times 10^5$ *	$2.95 \times 10^5$ *	$2.10 \times 10^5$ *
J1532 ( $n=4$ )	$5.58 \times 10^6$	$5.35 \times 10^5$ *	$2.87 \times 10^5$ *	$2.14 \times 10^5$ *

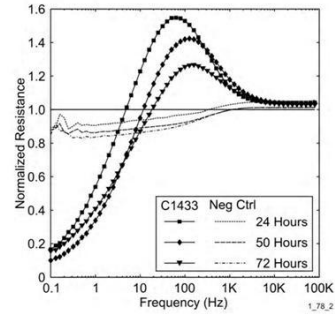


Figure 1. Example of normalized resistance peaks present in the mucoid strain C1433 over the course of the experiment. This peak was typical of both non-mucoid and mucoid strains. Data represents the mean from 4 measurements, error bars omitted for clarity.

### III. RESULTS

#### A. Growth of Bacteria during Experiment

After 24 hours, all strains of *P. aeruginosa* produced a change in the impedance resistance, reactance and associated normalized impedance parameters contrasted to the negative controls. Characteristic impedance peaks occurred in the normalized resistance data after 24 hours (figure 1). These are similar to those observed previously, with a different *P. aeruginosa* strain, PA14 [10].

A significant drop in the impedance modulus at low frequency could be seen with each of the strains contrasted to the negative control, indicating a decrease in the impedance of the sensor as a consequence of the growth of *P. aeruginosa* (table 1).

#### B. Non-mucoid vs. Mucoid Impedance Changes

The impedance signatures from each of the non-mucoid/mucoid pairs were compared to determine if it is possible to detect any difference between a virulent strain of *P. aeruginosa* and a host adapted strain. Comparison of the non-mucoid and mucoid mean data shows that a clear peak and trough pair are present in the data from the non-mucoid strain around 100 Hz, with a trough present between 1 KHz and 2.5 KHz (figure 2A). In contrast, only one peak is observable at 100 Hz for the mucoid strain, seen in the data for C1433 at 72 hours (figure 2B). Troughs are still visible in some of the data from the mucoid strains, as seen in mean data for J1532 and C1433 (figure 2B).

When the normalized phase angle at 100 Hz is analyzed, a clear difference is observable between the non-mucoid strains and mucoid strains. Specifically, it can be seen that the non-mucoid strains have a higher normalized phase angle than the mucoid strains (figure 3A and figure 3B). Furthermore, when the data from the two non-mucoid strains and the data from the two mucoid strains are pooled, there is a significant difference in the normalized phase angle at 24

hours and 48 hours ( $P = 0.0014$  and  $P = 0.0039$  respectively), although this difference disappears at later time points.

#### C. Post experiment cell density

Colony counting was carried out at the end of the experiment in order to determine the *P. aeruginosa* cell density within each of the electrode chambers. A similar concentration of cells was found across all strains (table 2), with the exception of J1532, where a slightly lower concentration was counted. This could have been related to the viscous media present at the end of the experiment which made it difficult to homogenize the sample and perform serial dilutions equally, thus possibly leading to an underestimate of the number of viable cells present.

#### IV. DISCUSSION

These results demonstrate that it is possible to detect the presence of four different strains of *P. aeruginosa*, all of which were clinical isolates originally from CF sputum. The carbon electrode has a high starting impedance, which could mask some of the impedance changes or reduce the sensitivity of the electrode. The drop in the modulus of impedance for electrodes inoculated with *P. aeruginosa* was found previously to be caused at least in part by a set of electroactive compounds produced by *P. aeruginosa* called phenazines [10]. These compounds fundamentally change the electrode-electrolyte interface to facilitate electron transfer that isn't possible in the control chambers. A similar effect could be occurring here, suggesting that clinical isolates could be detected through the same mechanism.

Whilst the experimental arrangement described here is far from the same as the composition of a clinical sample, it is interesting to note that slight but significant differences in impedance characteristics have been found between the non-mucoid and mucoid strains. The similarity between the bacterial cell densities of each strain at the end of the experiment suggest that the changes are not related to a difference in cell concentration. Furthermore, it is possible that the peaks observed in the normalized phase angle are caused by phenotype differences between the non-mucoid and mucoid strains. Specifically, the changes could be related to different concentrations of phenazine compounds produced by each of the strains.

TABLE 2. FINAL *P. AERUGINOSA* CELL DENSITIES DETERMINED THROUGH DROP PLATE COLONY COUNTING

Strain	<i>P. aeruginosa</i> cell density at 72 Hours (CFU/ml)		
	Mean	Min	Max
C1426 ( $n = 4$ )	$5.96 \times 10^9$	$5.20 \times 10^8$	$1.65 \times 10^{10}$
C1433 ( $n = 4$ )	$6.80 \times 10^9$	$1.68 \times 10^9$	$2.00 \times 10^{10}$
J1385 ( $n = 4$ )	$5.28 \times 10^9$	$1.55 \times 10^8$	$1.27 \times 10^{10}$
J1532 ( $n = 4$ )	$4.60 \times 10^8$	$7.00 \times 10^6$	$1.63 \times 10^9$

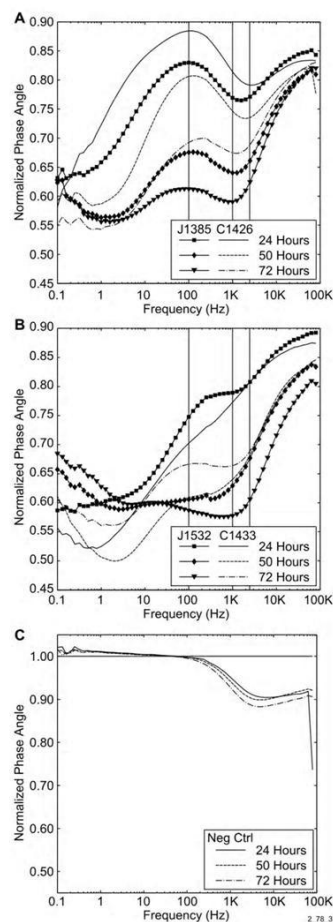


Figure 2. Comparison of the mean ( $n = 4$ ) normalised phase angle between non-mucoid and mucoid pairs across the frequency spectrum. (A) non-mucoid strains J1385 and C1426, showing a clear peak at approximately 100 Hz and a trough between 1 kHz and 2.5 kHz across all data points (black vertical lines). (B) Mucoid strains J1532 and C1433, showing that only one slight peak exists at 72 hours in the data from C1433. (C) Negative control showing the stability of the electrode over the course of the experiment. Results represent the mean from 4 replicates, error bars not included for clarity.

Alternatively, the differences could be caused by other phenotypic changes in the bacteria, such as an interaction between alginate produced by the mucoid strain and the electrode-electrolyte interface. Further investigation is required to identify the underlying cause for the impedance change between the non-mucoid and mucoid strains.

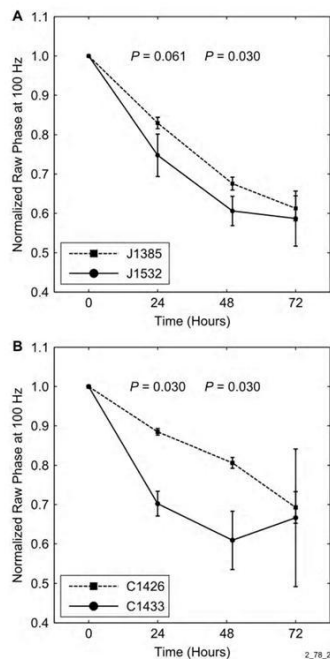


Figure 3. Comparison of the normalized phase angle between non-mucoid and mucoid pairs at 100 Hz. (A) J1385/J1532 pair and (B) C1426/C1433 pair. Error bars represent  $\pm 1$ SD,  $n = 4$ .

The measurement voltage of 200 mV<sub>rms</sub> used for the impedance measurement is greater than the magnitude over which the electrochemical cell behaves in a linear manner [15], [18]. However, at smaller measurement voltages, it was found that the low frequency (i.e. less than 1 Hz) impedance data were noisy making these potentials impractical for analysis (data not shown). This was probably caused by the limitations of the equipment given the high electrode impedance.

#### V. CONCLUSION

The experiments described here show how EIS, combined with a low cost screen printed sensor could be used to detect the presence of *P. aeruginosa*. The normalization procedure described can be used as a powerful technique to elucidate differences between *P. aeruginosa* strains, under laboratory conditions. Future development may lead to a sensor that is capable of detecting phenotypic changes in *P. aeruginosa* in clinically important samples, such as sputum from CF patients.

#### REFERENCES

- [1] G. Döring, P. Flume, H. Heijerman, J. S. Elborn, and for the Consensus Study Group, "Treatment of lung infection in patients with cystic fibrosis: Current and future strategies," *J. Cyst. Fibros.*, vol. 11, no. 6, pp. 461–479, Dec. 2012.
- [2] L. K. Branski, A. Al-Mousawi, H. Rivero, M. G. Jeschke, A. P. Sanford, and D. N. Herndon, "Emerging infections in burns," *Surg. Infect.*, vol. 10, no. 5, pp. 389–397, Oct. 2009.
- [3] J. M. C. Jefferies, T. Cooper, T. Yam, and S. C. Clarke, "Pseudomonas aeruginosa outbreaks in the neonatal intensive care unit - a systematic review of risk factors and environmental sources," *J. Med. Microbiol.*, vol. 61, no. Pt. 8, pp. 1052–1061, Jun. 2012.
- [4] A. M. Elward, C. S. Hollenbeak, D. K. Warren, and V. J. Fraser, "Attributable Cost of Nosocomial Primary Bloodstream Infection in Pediatric Intensive Care Unit Patients," *PEDIATRICS*, vol. 115, no. 4, pp. 868–872, Apr. 2005.
- [5] D. J. Hassett, M. D. Sutton, M. J. Schurr, A. B. Herr, C. C. Caldwell, and J. O. Matu, "Pseudomonas aeruginosa hypoxic or anaerobic biofilm infections within cystic fibrosis airways," *Trends Microbiol.*, vol. 17, no. 3, pp. 130–138, Mar. 2009.
- [6] P. Schelstraete, F. Haerynck, Van daele Sabine, S. Deseyne, and F. De Baets, "Eradication therapy for Pseudomonas aeruginosa colonization episodes in cystic fibrosis patients not chronically colonized by *P. aeruginosa*," *J. Cyst. Fibros.*, vol. 12, no. 1, pp. 1–8, Jan. 2013.
- [7] A. Dheilily, I. Linossier, A. Darchen, D. Hadjiev, C. Corbel, and V. Alonso, "Monitoring of microbial adhesion and biofilm growth using electrochemical impedanceometry," *Appl. Microbiol. Biotechnol.*, vol. 79, pp. 157–164, Mar. 2008.
- [8] T. Kim, J. Kang, J. H. Lee, and J. Yoon, "Influence of attached bacteria and biofilm on double-layer capacitance during biofilm monitoring by electrochemical impedance spectroscopy," *Water Res.*, vol. 45, pp. 4615–4622, 2011.
- [9] S. Kim, G. Yu, T. Kim, K. Shin, and J. Yoon, "Rapid bacterial detection with an interdigitated array electrode by electrochemical impedance spectroscopy," *Electrochimica Acta*, vol. 82, pp. 126–131, Nov. 2012.
- [10] A. C. Ward, P. Connolly, and N. P. Tucker, "Pseudomonas aeruginosa Can Be Detected in a Polymicrobial Competition Model Using Impedance Spectroscopy with a Novel Biosensor," *PLoS ONE*, vol. 9, no. 3, p. e91732, Mar. 2014.
- [11] M. J. Farrow, I. S. Hunter, and P. Connolly, "Developing a Real Time Sensing System to Monitor Bacteria in Wound Dressings," *Biosensors*, vol. 2, no. 4, pp. 171–188, May 2012.
- [12] D. McColl, B. Carlidge, and P. Connolly, "Real-time monitoring of moisture levels in wound dressings in vitro: An experimental study," *Int. J. Surg.*, vol. 5, no. 5, pp. 316–322, 2007.
- [13] D. McColl, M. MacDougall, L. Watret, and P. Connolly, "Monitoring moisture without disturbing the wound dressing," *Wounds UK*, vol. 5, no. 3, pp. 94–99, 2009.
- [14] P. Connolly and L. Shedden, "A System and Method for Cell Characterisation. Patent application number: WO2009136157 (A3)," WO2009136157 (A3), 28-Jan-2010.
- [15] J. R. Macdonald, *Impedance spectroscopy: emphasizing solid materials and systems*. New York: Wiley, 1987.
- [16] L. Stewart, A. Ford, V. Sangal, J. Jeukens, B. Boyle, S. Caim, L. Crossman, P. A. Hoskisson, R. Levesque, and N. P. Tucker, "Draft genomes of twelve host adapted and environmental isolates of *Pseudomonas aeruginosa* and their position in the core genome phylogeny," *Pathog. Dis.*, p. In press, 2013.
- [17] B. Herigstad, M. Hamilton, and J. Heersink, "How to optimize the drop plate method for enumerating bacteria," *J. Microbiol. Methods*, vol. 44, no. 2, pp. 121–129, 2001.
- [18] A. J. Bard and L. R. Faulkner, *Electrochemical methods: fundamentals and applications*, 2 edn. New York: Wiley, 2001.

### Appendix C: Mean normalised peak and trough data from in vitro experiments with non-mutant strains

This appendix describes the mean peak and trough data for the plots described in figures 7-12, 7-13 and 7-16. C = carbon electrode, C-cond = conditioned carbon electrode; Micro = Microaerophilic growth conditions, IS = *in situ*, NaN = no peak detected. Ten measurements were performed per frequency decade, therefore the absolute resolution of the peaks identified at higher frequencies could be increased if more measurements were performed at these frequencies.

Species	Strain	Electrode Type	Growth Media	Growth Conditions	In situ/ ex situ	Time (Hrs)	Normalised Resistance				Normalised Phase				Raw Phase				Thesis Figure
							Peak		Trough		Peak		Trough		Peak		Trough		
							Freq	Amp	Freq	Amp	Freq	Amp	Freq	Amp	Freq	Amp	Freq	Amp	
Neg Ctrl	Ctrl	C	LB	Aerobic	IS	24.00	NaN	NaN	79.40	1.08	2000.00	1.00	4470.00	1.00	6.31	82.20	NaN	NaN	Figure 4-2
Neg Ctrl	Ctrl	C	LB	Aerobic	IS	24 - fresh media	20.00	1.23	100.00	1.08	5.62	1.02	126.00	0.99	6.31	82.30	NaN	NaN	Figure 4-2
Neg Ctrl	Ctrl	C	LB	Aerobic	IS	24 - fresh media					316.00	0.99	4470.00	0.98					Figure 4-2
<i>P. aeruginosa</i>	PAO1 RHL GFP	C	LB	Aerobic	IS	24 - fresh media	50.10	1.26	89.10	1.07	126.00	0.94	1410.00	0.92	50.10	76.70	NaN	NaN	Figure 4-2
<i>P. aeruginosa</i>	PAO1 RHL GFP	C	LB	Aerobic	IS	24.00	126.00	2.55	70.80	1.08	NaN	NaN	14.10	0.26	501.00	45.40	12.60	20.80	Figure 4-2
Neg Ctrl	Ctrl	C	LB	Aerobic	IS	24.00	50.10	1.16	31600.00	1.00	282.00	0.98	282.00	0.98	28.20	80.20	14.10	80.20	Figure 4-3
Neg Ctrl	Ctrl	C	LB	Aerobic	IS	48.00	200.00	1.04	NaN	NaN	3.55	1.02	3.55	1.02	8.91	82.30	NaN	NaN	Figure 4-3

Species	Strain	Electrode Type	Growth Media	Growth Conditions	In situ/ ex situ	Time (Hrs)	Normalised Resistance				Normalised Phase				Raw Phase				Thesis Figure
							Peak		Trough		Peak		Trough		Peak		Trough		
							Freq	Amp	Freq	Amp	Freq	Amp	Freq	Amp	Freq	Amp	Freq	Amp	
Neg Ctrl	Ctrl	C	LB	Aerobic	IS	48- fresh media	158.00	1.11	NaN	NaN	11.20	0.98	11.20	0.98	20.00	8.03	NaN	NaN	Figure 4-3
<i>P. aeruginosa</i>	PAO1 RHL GFP	C	LB	Aerobic	IS	24.00	100.00	2.78	25100.00	1.00	0.50	0.45	0.20	0.40	398.00	52.60	8.91	26.10	Figure 4-3
<i>P. aeruginosa</i>	PAO1 RHL GFP	C	LB	Aerobic	IS	24.00							10.00	0.32					Figure 4-3
<i>P. aeruginosa</i>	PAO1 RHL GFP	C	LB	Aerobic	IS	48.00	100.00	2.47	NaN	NaN	0.50	0.42	0.20	0.39	398.00	50.70	11.20	21.50	Figure 4-3
<i>P. aeruginosa</i>	PAO1 RHL GFP	C	LB	Aerobic	IS	48.00							11.20	0.26					Figure 4-3
<i>P. aeruginosa</i>	PAO1 RHL GFP	C	LB	Aerobic	IS	48- fresh media	NaN	NaN	10.00	0.94	63.10	0.93	0.16	0.44	44.70	76.50	NaN	NaN	Figure 4-3
<i>P. aeruginosa</i>	PAO1 RHL GFP	C	LB	Aerobic	IS	48- fresh media							1260.00	0.88					Figure 4-3
Neg Ctrl	Ctrl	C - cond	LB	Aerobic	IS	24.00	NaN	NaN	7940.00	0.97	0.16	1.03	0.79	0.97	17.80	82.00	NaN	NaN	Figure 4-10
Neg Ctrl	Ctrl	C - cond	LB	Aerobic	IS	24.00					44.70	0.99							Figure 4-10
Neg Ctrl	Ctrl	C - cond	LB	Aerobic	IS	48.00	20.00	1.00	5010.00	0.93	0.16	1.05	0.50	0.98	10.00	82.40	NaN	NaN	Figure 4-10

Species	Strain	Electrode Type	Growth Media	Growth Conditions	In situ/ ex situ	Time (Hrs)	Normalised Resistance				Normalised Phase				Raw Phase				Thesis Figure
							Peak		Trough		Peak		Trough		Peak		Trough		
							Freq	Amp	Freq	Amp	Freq	Amp	Freq	Amp	Freq	Amp	Freq	Amp	
Neg Ctrl	Ctrl	C - cond	LB	Aerobic	IS	48.00					3.98	0.99	11.20	0.99					Figure 4-10
Neg Ctrl	Ctrl	C - cond	LB	Aerobic	IS	48.00					39.80	0.99	1000.00	0.99					Figure 4-10
Neg Ctrl	Ctrl	C - cond	LB	Aerobic	IS	48.00					2240.00	0.99							Figure 4-10
Neg Ctrl	Ctrl	C - cond	LB	Aerobic	IS	72.00	39.80	0.97	3.16	0.94	0.18	1.06	0.79	0.99	7.94	82.80	NaN	NaN	Figure 4-10
Neg Ctrl	Ctrl	C - cond	LB	Aerobic	IS	72.00			2510.00	0.92	2.82	1.00	63.10	1.00					Figure 4-10
Neg Ctrl	Ctrl	C - cond	LB	Aerobic	IS	72.00					2000.00	1.00							Figure 4-10
Neg Ctrl	Ctrl	C - cond	LB	Aerobic	IS	72 - fresh media	200.00	1.01	7940.00	0.99	NaN	NaN	10000.00	0.95	6.31	82.90	NaN	NaN	Figure 4-10
<i>P. aeruginosa</i>	PA14	C - cond	LB	Aerobic	IS	24.00	10.00	1.82	39800.00	0.96	0.16	0.68	0.40	0.67	100.00	71.30	NaN	NaN	Figure 4-10
<i>P. aeruginosa</i>	PA14	C - cond	LB	Aerobic	IS	24.00					251.00	0.89	1410.00	0.88					Figure 4-10
<i>P. aeruginosa</i>	PA14	C - cond	LB	Aerobic	IS	24.00					39800.00	0.93							Figure 4-10

Species	Strain	Electrode Type	Growth Media	Growth Conditions	In situ/ ex situ	Time (Hrs)	Normalised Resistance				Normalised Phase				Raw Phase				Thesis Figure
							Peak		Trough		Peak		Trough		Peak		Trough		
							Freq	Amp	Freq	Amp	Freq	Amp	Freq	Amp	Freq	Amp	Freq	Amp	
<i>P. aeruginosa</i>	PA14	C - cond	LB	Aerobic	IS	48.00	25.10	1.72	39800.00	0.94	0.16	0.63	0.40	0.62	126.00	66.50	NaN	NaN	Figure 4-10
<i>P. aeruginosa</i>	PA14	C - cond	LB	Aerobic	IS	48.00					316.00	0.84	2000.00	0.81					Figure 4-10
<i>P. aeruginosa</i>	PA14	C - cond	LB	Aerobic	IS	48.00					50100.00	0.89							Figure 4-10
<i>P. aeruginosa</i>	PA14	C - cond	LB	Aerobic	IS	72.00	25.10	1.42	39800.00	0.92	178.00	0.86	1780.00	0.82	79.40	69.40	NaN	NaN	Figure 4-10
<i>P. aeruginosa</i>	PA14	C - cond	LB	Aerobic	IS	72.00					39800.00	0.89							Figure 4-10
<i>P. aeruginosa</i>	PA14	C - cond	LB	Aerobic	IS	72 - fresh media	251.00	1.11	39800.00	1.00	0.18	0.96	1.78	0.93	15.80	78.30	NaN	NaN	Figure 4-10
<i>P. aeruginosa</i>	PA14	C - cond	LB	Aerobic	IS	72 - fresh media					20.00	0.95	2510.00	0.84					Figure 4-10
<i>P. aeruginosa</i>	PA14	C - cond	LB	Aerobic	IS	72 - fresh media					56200.00	0.91							Figure 4-10
Neg Ctrl	Ctrl	C - cond	ASM	Micro	IS	24.00	1580.00	1.02	12600.00	1.02	NaN	NaN	0.18	0.97	7.08	78.60	NaN	NaN	Figure 5-6; Figure 5-7
Neg Ctrl	Ctrl	C - cond	ASM	Micro	IS	24.00							4470.00	0.88					Figure 5-6; Figure 5-7

Species	Strain	Electrode Type	Growth Media	Growth Conditions	In situ/ ex situ	Time (Hrs)	Normalised Resistance				Normalised Phase				Raw Phase				Thesis Figure
							Peak		Trough		Peak		Trough		Peak		Trough		
							Freq	Amp	Freq	Amp	Freq	Amp	Freq	Amp	Freq	Amp	Freq	Amp	
Neg Ctrl	Ctrl	C - cond	ASM	Micro	IS	37.00	2000.00	1.03	0.63	0.88	NaN	NaN	0.18	0.98	7.08	79.00	NaN	NaN	Figure 5-6; Figure 5-7
Neg Ctrl	Ctrl	C - cond	ASM	Micro	IS	37.00			12600.00	1.02			5620.00	0.89					Figure 5-6; Figure 5-7
Neg Ctrl	Ctrl	C - cond	ASM	Micro	IS	48.00	2000.00	1.02	0.63	0.88	NaN	NaN	0.18	0.97	7.94	78.80	NaN	NaN	Figure 5-6; Figure 5-7
Neg Ctrl	Ctrl	C - cond	ASM	Micro	IS	48.00			10000.00	1.02			6310.00	0.88					Figure 5-6; Figure 5-7
Neg Ctrl	Ctrl	C - cond	ASM	Micro	IS	69.00	NaN	NaN	NaN	NaN	0.45	0.99	0.18	0.98	7.08	79.00	NaN	NaN	Figure 5-6; Figure 5-7
Neg Ctrl	Ctrl	C - cond	ASM	Micro	IS	69.00							5620.00	0.83					Figure 5-6; Figure 5-7
<i>S. aureus</i>	RN4220	C - cond	ASM	Micro	IS	24.00	100.00	1.06	0.79	0.91	2.00	0.98	1260.00	0.93	4.47	77.00	NaN	NaN	Figure 5-6; Figure 5-7
<i>S. aureus</i>	RN4220	C - cond	ASM	Micro	IS	24.00			39800.00	0.99									Figure 5-6; Figure 5-7
<i>S. aureus</i>	RN4220	C - cond	ASM	Micro	IS	37.00	501.00	1.04	25100.00	1.02	NaN	NaN	5620.00	0.86	6.31	77.10	NaN	NaN	Figure 5-6; Figure 5-7
<i>S. aureus</i>	RN4220	C - cond	ASM	Micro	IS	48.00	631.00	1.03	25100.00	1.01	NaN	NaN	6310.00	0.85	7.08	76.90	NaN	NaN	Figure 5-6; Figure 5-7



Species	Strain	Electrode Type	Growth Media	Growth Conditions	In situ/ ex situ	Time (Hrs)	Normalised Resistance				Normalised Phase				Raw Phase				Thesis Figure
							Peak		Trough		Peak		Trough		Peak		Trough		
							Freq	Amp	Freq	Amp	Freq	Amp	Freq	Amp	Freq	Amp	Freq	Amp	
<i>S. aureus</i>	RN4220	C - cond	ASM	Micro	IS	69.00	1260.00	1.02	0.79	0.75	0.40	1.00	0.22	0.99	6.31	76.90	NaN	NaN	Figure 5-6; Figure 5-7
<i>S. aureus</i>	RN4220	C - cond	ASM	Micro	IS	69.00			20000.00	1.01			6310.00	0.83					Figure 5-6; Figure 5-7
<i>S. aureus</i> + <i>P. aeruginosa</i>	RN4220 + PA14	C - cond	ASM	Micro	IS	24.00	15.80	1.29	NaN	NaN	224.00	0.92	1410.00	0.91	50.10	70.60	NaN	NaN	Figure 5-6; Figure 5-7
<i>S. aureus</i> + <i>P. aeruginosa</i>	RN4220 + PA14	C - cond	ASM	Micro	IS	37.00	63.10	1.63	31600.00	1.02	NaN	NaN	7.08	0.58	0.50	48.30	5.62	44.90	Figure 5-6; Figure 5-7
<i>S. aureus</i> + <i>P. aeruginosa</i>	RN4220 + PA14	C - cond	ASM	Micro	IS	37.00									200.00	55.50			Figure 5-6; Figure 5-7
<i>S. aureus</i> + <i>P. aeruginosa</i>	RN4220 + PA14	C - cond	ASM	Micro	IS	48.00	158.00	1.43	39800.00	1.01	NaN	NaN	35.50	0.53	0.63	44.50	50.10	41.70	Figure 5-6; Figure 5-7
<i>S. aureus</i> + <i>P. aeruginosa</i>	RN4220 + PA14	C - cond	ASM	Micro	IS	48.00									126.00	41.90			Figure 5-6; Figure 5-7
<i>S. aureus</i> + <i>P. aeruginosa</i>	RN4220 + PA14	C - cond	ASM	Micro	IS	69.00	251.00	1.36	31600.00	1.04	NaN	NaN	100.00	0.49	0.79	42.60	NaN	NaN	Figure 5-6; Figure 5-7
Neg Ctrl	Ctrl	C - cond	ASM	Aerobic	IS	14.00	NaN	NaN	NaN	NaN	31.60	0.99	25100.00	0.87	7.94	79.40	NaN	NaN	Figure 5-1
Neg Ctrl	Ctrl	C - cond	ASM	Aerobic	IS	24.00	1260.00	1.00	5010.00	1.00	NaN	NaN	NaN	NaN	6.31	78.80	NaN	NaN	Figure 5-1

Species	Strain	Electrode Type	Growth Media	Growth Conditions	In situ/ ex situ	Time (Hrs)	Normalised Resistance				Normalised Phase				Raw Phase				Thesis Figure
							Peak		Trough		Peak		Trough		Peak		Trough		
							Freq	Amp	Freq	Amp	Freq	Amp	Freq	Amp	Freq	Amp	Freq	Amp	
Neg Ctrl	Ctrl	C - cond	ASM	Aerobic	IS	38.00	1260.00	1.01	10000.00	1.01	2.00	0.98	6310.00	0.83	6.31	78.70	NaN	NaN	Figure 5-1
Neg Ctrl	Ctrl	C - cond	ASM	Aerobic	IS	48.00	1580.00	1.00	7940.00	1.00	1.78	0.99	7940.00	0.82	6.31	78.90	NaN	NaN	Figure 5-1
Neg Ctrl	Ctrl	C - cond	ASM	Aerobic	IS	65.00	2510.00	1.00	6310.00	1.00	1.78	0.99	5620.00	0.78	6.31	79.50	NaN	NaN	Figure 5-1
Neg Ctrl	Ctrl	C - cond	ASM	Micro	IS	14.00	NaN	NaN	1.00	0.97	3.98	0.99	0.18	0.98	10.00	80.10	NaN	NaN	Figure 5-1
Neg Ctrl	Ctrl	C - cond	ASM	Micro	IS	14.00							15800.00	0.94					Figure 5-1
Neg Ctrl	Ctrl	C - cond	ASM	Micro	IS	24.00	NaN	NaN	0.50	0.94	3.16	0.99	2.00	0.99	10.00	80.20	NaN	NaN	Figure 5-1
Neg Ctrl	Ctrl	C - cond	ASM	Micro	IS	24.00							17800.00	0.93					Figure 5-1
Neg Ctrl	Ctrl	C - cond	ASM	Micro	IS	38.00	15.80	1.00	63.10	0.99	0.56	1.00	20.00	0.99	10.00	80.10	NaN	NaN	Figure 5-1
Neg Ctrl	Ctrl	C - cond	ASM	Micro	IS	38.00					35.50	0.99	17800.00	0.93					Figure 5-1
Neg Ctrl	Ctrl	C - cond	ASM	Micro	IS	48.00	NaN	NaN	NaN	NaN	NaN	NaN	0.20	0.99	8.91	80.10	0.16	76.10	Figure 5-1

Species	Strain	Electrode Type	Growth Media	Growth Conditions	In situ/ ex situ	Time (Hrs)	Normalised Resistance				Normalised Phase				Raw Phase				Thesis Figure
							Peak		Trough		Peak		Trough		Peak		Trough		
							Freq	Amp	Freq	Amp	Freq	Amp	Freq	Amp	Freq	Amp	Freq	Amp	
Neg Ctrl	Ctrl	C - cond	ASM	Micro	IS	48.00							22400.00	0.92					Figure 5-1
Neg Ctrl	Ctrl	C - cond	ASM	Micro	IS	65.00	1000.00	1.01	3980.00	1.01	0.56	1.00	20000.00	0.91	7.94	79.90	NaN	NaN	Figure 5-1
<i>P. aeruginosa</i>	PA14	C - cond	ASM	Aerobic	IS	14.00	12.60	1.45	12600.00	0.99	282.00	0.90	2000.00	0.89	100.00	69.50	NaN	NaN	Figure 5-1
<i>P. aeruginosa</i>	PA14	C - cond	ASM	Aerobic	IS	14.00					8910.00	0.89							Figure 5-1
<i>P. aeruginosa</i>	PA14	C - cond	ASM	Aerobic	IS	24.00	3.16	1.39	NaN	NaN	178.00	0.92	2820.00	0.87	79.40	71.80	NaN	NaN	Figure 5-1
<i>P. aeruginosa</i>	PA14	C - cond	ASM	Aerobic	IS	38.00	126.00	1.54	NaN	NaN	1.41	0.54	0.20	0.51	2.24	42.70	7.94	42.40	Figure 5-1
<i>P. aeruginosa</i>	PA14	C - cond	ASM	Aerobic	IS	38.00							8.91	0.53	316.00	51.00			Figure 5-1
<i>P. aeruginosa</i>	PA14	C - cond	ASM	Aerobic	IS	48.00	200.00	1.40	31600.00	0.99	0.45	0.56	0.20	0.55	2.00	43.50	5.01	43.50	Figure 5-1
<i>P. aeruginosa</i>	PA14	C - cond	ASM	Aerobic	IS	48.00							6.31	0.55	224.00	48.80			Figure 5-1
<i>P. aeruginosa</i>	PA14	C - cond	ASM	Aerobic	IS	65.00	126.00	1.37	39800.00	1.00	0.45	0.56	0.22	0.56	200.00	54.70	NaN	NaN	Figure 5-1

Species	Strain	Electrode Type	Growth Media	Growth Conditions	In situ/ ex situ	Time (Hrs)	Normalised Resistance				Normalised Phase				Raw Phase				Thesis Figure
							Peak		Trough		Peak		Trough		Peak		Trough		
							Freq	Amp	Freq	Amp	Freq	Amp	Freq	Amp	Freq	Amp	Freq	Amp	
<i>P. aeruginosa</i>	PA14	C - cond	ASM	Aerobic	IS	65.00					447.00	0.73	1780.00	0.71					Figure 5-1
<i>P. aeruginosa</i>	PA14	C - cond	ASM	Micro	IS	14.00	10.00	1.80	12600.00	1.01	7940.00	0.96	44700.00	0.95	70.80	68.70	NaN	NaN	Figure 5-1
<i>P. aeruginosa</i>	PA14	C - cond	ASM	Micro	IS	24.00	25.10	1.72	31600.00	1.00	NaN	NaN	NaN	NaN	141.00	62.20	NaN	NaN	Figure 5-1
<i>P. aeruginosa</i>	PA14	C - cond	ASM	Micro	IS	38.00	251.00	1.45	31600.00	1.01	0.40	0.51	35.50	0.43	0.63	39.70	56.20	34.40	Figure 5-1
<i>P. aeruginosa</i>	PA14	C - cond	ASM	Micro	IS	38.00									282.00	35.50			Figure 5-1
<i>P. aeruginosa</i>	PA14	C - cond	ASM	Micro	IS	48.00	316.00	1.38	39800.00	1.01	0.63	0.51	89.10	0.38	0.79	40.40	200.00	29.60	Figure 5-1
<i>P. aeruginosa</i>	PA14	C - cond	ASM	Micro	IS	48.00									316.00	29.60			Figure 5-1
<i>P. aeruginosa</i>	PA14	C - cond	ASM	Micro	IS	65.00	251.00	1.50	39800.00	1.01	NaN	NaN	35.50	0.38	0.40	36.40	44.70	30.20	Figure 5-1
<i>P. aeruginosa</i>	PA14	C - cond	ASM	Micro	IS	65.00									355.00	32.80			Figure 5-1
<i>C. albicans</i>	SC5314	C - cond	ASM	Micro	IS	24.00	200.00	1.10	0.50	0.84	1.41	0.98	3980.00	0.88	7.08	78.80	NaN	NaN	Figure 5-19

Species	Strain	Electrode Type	Growth Media	Growth Conditions	In situ/ ex situ	Time (Hrs)	Normalised Resistance				Normalised Phase				Raw Phase				Thesis Figure
							Peak		Trough		Peak		Trough		Peak		Trough		
							Freq	Amp	Freq	Amp	Freq	Amp	Freq	Amp	Freq	Amp	Freq	Amp	
<i>C. albicans</i>	SC5314	C - cond	ASM	Micro	IS	24.00			25100.00	1.03									Figure 5-19
<i>C. albicans</i>	SC5314	C - cond	ASM	Micro	IS	39.00	200.00	1.10	NaN	NaN	NaN	NaN	4470.00	0.88	6.31	79.10	NaN	NaN	Figure 5-19
<i>C. albicans</i>	SC5314	C - cond	ASM	Micro	IS	48.00	158.00	1.09	0.63	0.84	1.00	0.98	5010.00	0.88	6.31	79.10	NaN	NaN	Figure 5-19
<i>C. albicans</i>	SC5314	C - cond	ASM	Micro	IS	48.00			15800.00	1.03									Figure 5-19
<i>C. albicans</i>	SC5314	C - cond	ASM	Micro	IS	71.00	126.00	1.09	0.40	0.84	NaN	NaN	6310.00	0.88	5.62	79.30	NaN	NaN	Figure 5-19
<i>C. albicans</i>	SC5314	C - cond	ASM	Micro	IS	71.00			12600.00	1.03									Figure 5-19
Neg Ctrl	Ctrl	C - cond	ASM	Micro	IS	24.00	158.00	1.06	31600.00	1.03	NaN	NaN	0.18	0.98	6.31	79.30	NaN	NaN	Figure 5-19
Neg Ctrl	Ctrl	C - cond	ASM	Micro	IS	24.00							5010.00	0.88					Figure 5-19
Neg Ctrl	Ctrl	C - cond	ASM	Micro	IS	39.00	NaN	NaN	39800.00	1.03	0.50	0.99	0.20	0.99	5.01	79.50	NaN	NaN	Figure 5-19
Neg Ctrl	Ctrl	C - cond	ASM	Micro	IS	39.00							5010.00	0.88					Figure 5-19

Species	Strain	Electrode Type	Growth Media	Growth Conditions	In situ/ ex situ	Time (Hrs)	Normalised Resistance				Normalised Phase				Raw Phase				Thesis Figure
							Peak		Trough		Peak		Trough		Peak		Trough		
							Freq	Amp	Freq	Amp	Freq	Amp	Freq	Amp	Freq	Amp	Freq	Amp	
Neg Ctrl	Ctrl	C - cond	ASM	Micro	IS	48.00	NaN	NaN	31600.00	1.03	0.56	0.99	0.20	0.98	5.62	79.50	NaN	NaN	Figure 5-19
Neg Ctrl	Ctrl	C - cond	ASM	Micro	IS	48.00							5010.00	0.88					Figure 5-19
Neg Ctrl	Ctrl	C - cond	ASM	Micro	IS	71.00	NaN	NaN	31600.00	1.03	0.50	0.99	0.18	0.98	5.62	79.40	NaN	NaN	Figure 5-19
Neg Ctrl	Ctrl	C - cond	ASM	Micro	IS	71.00							5620.00	0.88					Figure 5-19
<i>P. aeruginosa</i>	PA14	C - cond	ASM	Micro	IS	24.00	15.80	1.68	31600.00	1.03	251.00	0.88	0.20	0.56	100.00	69.40	NaN	NaN	Figure 5-21
<i>P. aeruginosa</i>	PA14	C - cond	ASM	Micro	IS	24.00							3160.00	0.82					Figure 5-21
<i>P. aeruginosa</i>	PA14	C - cond	ASM	Micro	IS	39.00	79.40	1.61	31600.00	1.03	NaN	NaN	NaN	NaN	200.00	57.20	NaN	NaN	Figure 5-21
<i>P. aeruginosa</i>	PA14	C - cond	ASM	Micro	IS	48.00	251.00	1.55	31600.00	1.03	3.55	0.51	0.20	0.41	3.98	41.70	89.10	34.60	Figure 5-21
<i>P. aeruginosa</i>	PA14	C - cond	ASM	Micro	IS	48.00							70.80	0.43	631.00	38.40			Figure 5-21
<i>P. aeruginosa</i>	PA14	C - cond	ASM	Micro	IS	72.00	251.00	1.51	39800.00	1.03	NaN	NaN	20.00	0.37	0.50	34.80	22.40	30.30	Figure 5-21

Species	Strain	Electrode Type	Growth Media	Growth Conditions	In situ/ ex situ	Time (Hrs)	Normalised Resistance				Normalised Phase				Raw Phase				Thesis Figure		
							Peak		Trough		Peak		Trough		Peak		Trough				
							Freq	Amp	Freq	Amp	Freq	Amp	Freq	Amp	Freq	Amp	Freq	Amp			
<i>P. aeruginosa</i>	PA14	C - cond	ASM	Micro	IS	72.00										562.00	34.10			Figure 5-21	
<i>P. aeruginosa</i> + <i>C. albicans</i>	PA14 + SC5314	C - cond	ASM	Micro	IS	24.00	20.00	1.76	NaN	NaN	316.00	0.89	3160.00	0.85	126.00	68.90	NaN	NaN			Figure 5-20
<i>P. aeruginosa</i> + <i>C. albicans</i>	PA14 + SC5314	C - cond	ASM	Micro	IS	39.00	79.40	1.58	31600.00	1.02	708.00	0.80	2000.00	0.79	200.00	59.50	NaN	NaN			Figure 5-20
<i>P. aeruginosa</i> + <i>C. albicans</i>	PA14 + SC5314	C - cond	ASM	Micro	IS	48.00	251.00	1.48	NaN	NaN	2.82	0.56	56.20	0.48	3.16	45.00	70.80	38.70			Figure 5-20
<i>P. aeruginosa</i> + <i>C. albicans</i>	PA14 + SC5314	C - cond	ASM	Micro	IS	48.00									501.00	40.90					Figure 5-20
<i>P. aeruginosa</i> + <i>C. albicans</i>	PA14 + SC5314	C - cond	ASM	Micro	IS	70.00	316.00	1.44	31600.00	1.03	0.28	0.45	39.80	0.40	0.45	34.90	56.20	32.20			Figure 5-20
<i>P. aeruginosa</i> + <i>C. albicans</i>	PA14 + SC5314	C - cond	ASM	Micro	IS	70.00									447.00	33.40					Figure 5-20
<i>C. albicans</i>	SC5314	C - cond	TSB+YE	Aerobic	IS	24.00	126.00	0.99	2510.00	0.98	2000.00	1.01	89.10	1.00	5.62	79.20	NaN	NaN			Figure 5-16; Figure 5-17; Figure 5-18
<i>C. albicans</i>	SC5314	C - cond	TSB+YE	Aerobic	IS	48.00	631.00	0.99	3160.00	0.99	NaN	NaN	NaN	NaN	5.62	79.20	NaN	NaN			Figure 5-16; Figure 5-17; Figure 5-18

Species	Strain	Electrode Type	Growth Media	Growth Conditions	In situ/ ex situ	Time (Hrs)	Normalised Resistance				Normalised Phase				Raw Phase				Thesis Figure
							Peak		Trough		Peak		Trough		Peak		Trough		
							Freq	Amp	Freq	Amp	Freq	Amp	Freq	Amp	Freq	Amp	Freq	Amp	
<i>C. albicans</i>	SC5314	C - cond	TSB+YE	Aerobic	IS	72.00	501.00	0.98	2000.00	0.98	NaN	NaN	NaN	NaN	4.47	79.60	NaN	NaN	Figure 5-16; Figure 5-17; Figure 5-18
Neg Ctrl	Ctrl	C - cond	TSB+YE	Aerobic	IS	24.00	39800.00	0.99	0.40	0.78	0.16	1.08	79.40	1.00	7.08	79.50	NaN	NaN	Figure 5-16; Figure 5-17; Figure 5-18
Neg Ctrl	Ctrl	C - cond	TSB+YE	Aerobic	IS	24.00					224.00	1.00	11200.00	0.94					Figure 5-16; Figure 5-17; Figure 5-18
Neg Ctrl	Ctrl	C - cond	TSB+YE	Aerobic	IS	48.00	NaN	NaN	NaN	NaN	NaN	NaN	12600.00	0.91	7.94	79.60	NaN	NaN	Figure 5-16; Figure 5-17; Figure 5-18
Neg Ctrl	Ctrl	C - cond	TSB+YE	Aerobic	IS	72.00	NaN	NaN	0.25	0.73	NaN	NaN	12600.00	0.92	7.08	80.20	NaN	NaN	Figure 5-16; Figure 5-17; Figure 5-18
<i>H. influenzae</i>	HI680	C - cond	HTM	Micro	IS	24.00	631.00	1.02	2.00	0.90	2.51	0.98	2820.00	0.88	7.08	79.40	NaN	NaN	Figure 5-8
<i>H. influenzae</i>	HI680	C - cond	HTM	Micro	IS	24.00			25100.00	1.01									Figure 5-8
<i>H. influenzae</i>	HI680	C - cond	HTM	Micro	IS	48.00	1000.00	1.02	2.00	0.89	2.82	0.98	3160.00	0.87	7.08	79.50	NaN	NaN	Figure 5-8



Species	Strain	Electrode Type	Growth Media	Growth Conditions	In situ/ ex situ	Time (Hrs)	Normalised Resistance				Normalised Phase				Raw Phase				Thesis Figure	
							Peak		Trough		Peak		Trough		Peak		Trough			
							Freq	Amp	Freq	Amp	Freq	Amp	Freq	Amp	Freq	Amp	Freq	Amp		
<i>H. influenzae</i>	HI680	C - cond	HTM	Micro	IS	72.00	3160.00	1.02	0.79	0.82	NaN	NaN	3980.00	0.86	5.62	80.40	NaN	NaN	Figure 5-8	
<i>H. influenzae</i>	HI680	C - cond	HTM	Micro	IS	72.00			12600.00	1.01										Figure 5-8
Neg Ctrl	Ctrl	C - cond	HTM	Micro	IS	24.00	79.40	1.03	0.63	0.89	0.36	1.01	0.18	1.01	5.62	81.00	NaN	NaN	Figure 5-8	
Neg Ctrl	Ctrl	C - cond	HTM	Micro	IS	24.00			7940.00	1.02			5620.00	0.96						Figure 5-8
Neg Ctrl	Ctrl	C - cond	HTM	Micro	IS	48.00	NaN	NaN	NaN	NaN	NaN	NaN	0.22	1.02	4.47	81.30	NaN	NaN	Figure 5-8	
Neg Ctrl	Ctrl	C - cond	HTM	Micro	IS	48.00							6310.00	0.96					Figure 5-8	
Neg Ctrl	Ctrl	C - cond	HTM	Micro	IS	72.00	NaN	NaN	0.79	0.84	0.36	1.03	0.22	1.02	3.98	81.50	NaN	NaN	Figure 5-8	
Neg Ctrl	Ctrl	C - cond	HTM	Micro	IS	72.00							5010.00	0.95					Figure 5-8	
<i>H. influenzae</i>	HI 680	C - cond	HTM	Micro	IS	24.00	NaN	NaN	NaN	NaN	6.31	0.98	5010.00	0.85	15.80	80.70	NaN	NaN	Figure 5-9	
<i>H. influenzae</i>	HI 680	C - cond	HTM	Micro	IS	48.00	2000.00	1.03	NaN	NaN	NaN	NaN	5010.00	0.83	14.10	80.90	NaN	NaN	Figure 5-9	

Species	Strain	Electrode Type	Growth Media	Growth Conditions	In situ/ ex situ	Time (Hrs)	Normalised Resistance				Normalised Phase				Raw Phase				Thesis Figure
							Peak		Trough		Peak		Trough		Peak		Trough		
							Freq	Amp	Freq	Amp	Freq	Amp	Freq	Amp	Freq	Amp	Freq	Amp	
Neg Ctrl	Ctrl	C - cond	HTM	Micro	IS	24.00	0.63	0.90	2.00	0.89	3.16	0.99	0.22	0.95	15.80	81.10	NaN	NaN	Figure 5-9
Neg Ctrl	Ctrl	C - cond	HTM	Micro	IS	24.00	1260.00	1.03					4470.00	0.87					Figure 5-9
Neg Ctrl	Ctrl	C - cond	HTM	Micro	IS	48.00	2000.00	1.02	NaN	NaN	NaN	NaN	5010.00	0.81	12.60	81.20	NaN	NaN	Figure 5-9
<i>H. influenzae</i>	HI 680	C - cond	HTM	Micro	ES	72.00	63.10	1.03	12.60	1.02	7.08	1.01	56.20	1.00	20.00	80.40	NaN	NaN	Figure 5-10; Figure 5-11
<i>H. influenzae</i>	HI 680	C - cond	HTM	Micro	ES	72.00					6310.00	1.07	63100.00	1.06					Figure 5-10; Figure 5-11
Neg Ctrl	Ctrl	C - cond	HTM	Micro	ES	72.00	100.00	1.01	1580.00	1.00	4470.00	1.05	56.20	1.01	15.80	81.10	NaN	NaN	Figure 5-10; Figure 5-11
Neg Ctrl	Ctrl	C - cond	HTM	Micro	ES	72.00	15800.00	1.00					44700.00	1.04					Figure 5-10; Figure 5-11
Neg Ctrl	Ctrl	C - cond	TSB	Aerobic	IS	24.00	NaN	NaN	NaN	NaN	NaN	NaN	12600.00	0.92	7.08	80.10	NaN	NaN	Figure 5-3
Neg Ctrl	Ctrl	C - cond	TSB	Aerobic	IS	48.00	NaN	NaN	NaN	NaN	NaN	NaN	11200.00	0.87	7.08	80.50	NaN	NaN	Figure 5-3
Neg Ctrl	Ctrl	C - cond	TSB	Aerobic	IS	70.00	NaN	NaN	NaN	NaN	NaN	NaN	10000.00	0.87	5.62	80.80	NaN	NaN	Figure 5-3

Species	Strain	Electrode Type	Growth Media	Growth Conditions	In situ/ ex situ	Time (Hrs)	Normalised Resistance				Normalised Phase				Raw Phase				Thesis Figure
							Peak		Trough		Peak		Trough		Peak		Trough		
							Freq	Amp	Freq	Amp	Freq	Amp	Freq	Amp	Freq	Amp	Freq	Amp	
<i>S. aureus</i>	RN4220	C - cond	TSB	Aerobic	IS	24.00	NaN	NaN	NaN	NaN	NaN	NaN	5620.00	0.92	4.47	80.30	NaN	NaN	Figure 5-3
<i>S. aureus</i>	RN4220	C - cond	TSB	Aerobic	IS	48.00	25100.00	1.05	NaN	NaN	NaN	NaN	7080.00	0.91	5.01	80.30	NaN	NaN	Figure 5-3
<i>S. aureus</i>	RN4220	C - cond	TSB	Aerobic	IS	70.00	NaN	NaN	NaN	NaN	NaN	NaN	6310.00	0.91	5.01	80.40	NaN	NaN	Figure 5-3
Neg Ctrl	Ctrl	C - cond	TSB	Aerobic	ES	72.00					14100.00	0.98	5010.00	0.98	11.20	80.90	NaN	NaN	Figure 5-4; Figure 5-5
<i>S. aureus</i>	RN4220	C - cond	TSB	Aerobic	ES	72.00	63.10	1.12	39800.00	0.99	0.56	0.98	0.36	0.98	11.20	79.60	NaN	NaN	Figure 5-4; Figure 5-5
<i>S. aureus</i>	RN4220	C - cond	TSB	Aerobic	ES	72.00					2.82	0.98	1.12	0.98					Figure 5-4; Figure 5-5
<i>S. aureus</i>	RN4220	C - cond	TSB	Aerobic	ES	72.00	1580.00	1.03	7940.00	1.03	56200.00	1.02	708.00	0.95					Figure 5-4; Figure 5-5
<i>H. influenzae</i>	HI 680	C - cond	ASM	Micro	ES	72.00	25.10	1.04	5010.00	0.95	7.94	0.99	0.16	0.99	12.60	81.70	NaN	NaN	Figure 5-12
<i>H. influenzae</i>	HI 680	C - cond	ASM	Micro	ES	72.00					3550.00	1.04	3.55	0.99					Figure 5-12
<i>H. influenzae</i>	HI 680	C - cond	ASM	Micro	ES	72.00							39.80	0.99					Figure 5-12

Species	Strain	Electrode Type	Growth Media	Growth Conditions	In situ/ ex situ	Time (Hrs)	Normalised Resistance				Normalised Phase				Raw Phase				Thesis Figure
							Peak		Trough		Peak		Trough		Peak		Trough		
							Freq	Amp	Freq	Amp	Freq	Amp	Freq	Amp	Freq	Amp	Freq	Amp	
Neg Ctrl	Ctrl	C - cond	ASM	Micro	ES	72 - Starting measurement	50.10	1.00	6310.00	0.94	4470.00	1.04	63.10	1.00	12.60	82.60	NaN	NaN	Figure 5-12
Neg Ctrl	Ctrl	C - cond	ASM	Micro	ES	72 - Starting measurement							50100.00	1.00					Figure 5-12
Neg Ctrl	Ctrl	C - cond	ASM	Micro	ES	72 - Fresh Media	63.10	1.02	6310.00	0.95	4470.00	1.04	79.40	1.00	11.20	82.50	NaN	NaN	Figure 5-12
Neg Ctrl	Ctrl	C - cond	ASM	Micro	ES	72 - Fresh Media							56200.00	0.99					Figure 5-12
<i>H. influenzae</i>	HI 680	C - cond	ASM	Micro	ES	72.00	NaN	NaN	6310.00	0.93	3980.00	1.04	0.50	0.99	17.80	81.60	NaN	NaN	Figure 5-13; Figure 5-14
<i>P. aeruginosa</i>	PA14	C - cond	ASM	Micro	ES	72.00	25.10	1.74	39800.00	0.94	39800.00	0.99	NaN	NaN	70.80	64.20	NaN	NaN	Figure 5-13; Figure 5-14
<i>P. aeruginosa</i> + <i>H. influenzae</i>	PA14 + HI680	C - cond	ASM	Micro	ES	72.00	15.80	1.73	39800.00	0.94	39800.00	0.99	0.16	0.50	63.10	67.30	NaN	NaN	Figure 5-13; Figure 5-14
<i>P. aeruginosa</i> Mutant	PA14 delta PhzA1G1 /A2G2	C - cond	ASM	Micro	IS	24	100.00	1.13	39800.00	1.02	1.58	0.97	1780.00	0.87	7.08	78.80	NaN	NaN	Figure 5-31
<i>P. aeruginosa</i> Mutant	PA14 delta PhzA1G1 /A2G2	C - cond	ASM	Micro	IS	48	316.00	1.07	1	0.78	2.00	0.98	2510.00	0.84	7.08	80.40	NaN	NaN	Figure 5-31
<i>P. aeruginosa</i> Mutant	PA14 delta PhzA1G1 /A2G2	C - cond	ASM	Micro	IS	48			3.16E+04	1.02									Figure 5-31

Species	Strain	Electrode Type	Growth Media	Growth Conditions	In situ/ ex situ	Time (Hrs)	Normalised Resistance				Normalised Phase				Raw Phase				Thesis Figure	
							Peak		Trough		Peak		Trough		Peak		Trough			
							Freq	Amp	Freq	Amp	Freq	Amp	Freq	Amp	Freq	Amp	Freq	Amp		
<i>P. aeruginosa</i> Mutant	PA14 delta PhzA1G1 /A2G2	C - cond	ASM	Micro	IS	72	316.00	1.08	3.16E+04	1.02	NaN	NaN	2240.00	0.86	5.01	80.80	NaN	NaN	Figure 5-31	
Neg Ctrl Mutant	Ctrl	C - cond	ASM	Micro	IS	24	31.60	1.06	794.00	1.02	44700.00	0.93	10000.00	0.92	14.10	80.50	NaN	NaN	Figure 5-31	
Neg Ctrl Mutant	Ctrl	C - cond	ASM	Micro	IS	48	31.60	1.05	631.00	1.02	39800.00	0.92	7940.00	0.91	12.60	80.40	NaN	NaN	Figure 5-31	
Neg Ctrl Mutant	Ctrl	C - cond	ASM	Micro	IS	48			15800.00	1.02										
Neg Ctrl Mutant	Ctrl	C - cond	ASM	Micro	IS	72	31.60	1.05	1260.00	1.01	0.40	0.99	0.25	0.99	12.60	80.10	NaN	NaN	Figure 5-31	
Neg Ctrl Mutant	Ctrl	C - cond	ASM	Micro	IS	72					35.50	0.98	20.00	0.98					Figure 5-31	
Neg Ctrl Mutant	Ctrl	C - cond	ASM	Micro	IS	72							20000.00	0.90						
Neg Ctrl	Ctrl	C - cond	LB	Aerobic	IS	24.00	NaN	NaN	NaN	NaN	31600.00	0.93	7080.00	0.90	7.08	80.20	NaN	NaN	Figure 4-12; Figure 4-13; Figure 4-14	
Neg Ctrl	Ctrl	C - cond	LB	Aerobic	IS	50.00	6310.00	1.01	20000.00	1.01	NaN	NaN	5010.00	0.90	7.94	80.10	NaN	NaN	Figure 4-12; Figure 4-13; Figure 4-14	

Species	Strain	Electrode Type	Growth Media	Growth Conditions	In situ/ ex situ	Time (Hrs)	Normalised Resistance				Normalised Phase				Raw Phase				Thesis Figure
							Peak		Trough		Peak		Trough		Peak		Trough		
							Freq	Amp	Freq	Amp	Freq	Amp	Freq	Amp	Freq	Amp	Freq	Amp	
Neg Ctrl	Ctrl	C - cond	LB	Aerobic	IS	72.00	6310.00	1.01	0.63	0.83	0.36	1.01	5010.00	0.88	7.08	80.20	NaN	NaN	Figure 4-12; Figure 4-13; Figure 4-14
Neg Ctrl	Ctrl	C - cond	LB	Aerobic	IS	72.00			15800.00	1.01									Figure 4-12; Figure 4-13; Figure 4-14
<i>P. aeruginosa</i>	C1426	C - cond	LB	Aerobic	IS	24.00	15.80	1.32	25100.00	1.08	112.00	0.89	2820.00	0.79	50.10	69.60	NaN	NaN	Figure 4-12; Figure 4-13; Figure 4-14
<i>P. aeruginosa</i>	C1426	C - cond	LB	Aerobic	IS	24.00					56200.00	0.83							Figure 4-12; Figure 4-13; Figure 4-14
<i>P. aeruginosa</i>	C1426	C - cond	LB	Aerobic	IS	50.00	25.10	1.43	31600.00	1.06	0.20	0.60	0.79	0.59	70.80	63.10	NaN	NaN	Figure 4-12; Figure 4-13; Figure 4-14
<i>P. aeruginosa</i>	C1426	C - cond	LB	Aerobic	IS	50.00					126.00	0.81	2000.00	0.73					Figure 4-12; Figure 4-13; Figure 4-14
<i>P. aeruginosa</i>	C1426	C - cond	LB	Aerobic	IS	50.00					44700.00	0.82							Figure 4-12; Figure 4-13; Figure 4-14

Species	Strain	Electrode Type	Growth Media	Growth Conditions	In situ/ ex situ	Time (Hrs)	Normalised Resistance				Normalised Phase				Raw Phase				Thesis Figure
							Peak		Trough		Peak		Trough		Peak		Trough		
							Freq	Amp	Freq	Amp	Freq	Amp	Freq	Amp	Freq	Amp	Freq	Amp	
<i>P. aeruginosa</i>	C1426	C - cond	LB	Aerobic	IS	72.00	79.40	1.46	39800.00	1.05	0.18	0.56	0.89	0.54	79.40	54.00	0.16	40.60	Figure 4-12; Figure 4-13; Figure 4-14
<i>P. aeruginosa</i>	C1426	C - cond	LB	Aerobic	IS	72.00					178.00	0.70	1260.00	0.67					Figure 4-12; Figure 4-13; Figure 4-14
<i>P. aeruginosa</i>	C1433	C - cond	LB	Aerobic	IS	24.00	63.10	1.55	31600.00	1.04	63100.00	0.87	0.56	0.52	89.10	53.70	0.22	39.20	Figure 4-12; Figure 4-13; Figure 4-14
<i>P. aeruginosa</i>	C1433	C - cond	LB	Aerobic	IS	50.00	126.00	1.42	39800.00	1.03	NaN	NaN	2.00	0.50	63.10	47.00	1.58	38.80	Figure 4-12; Figure 4-13; Figure 4-14
<i>P. aeruginosa</i>	C1433	C - cond	LB	Aerobic	IS	72.00	158.00	1.26	39800.00	1.03	141.00	0.67	1.78	0.56	56.20	51.40	NaN	NaN	Figure 4-12; Figure 4-13; Figure 4-14
<i>P. aeruginosa</i>	C1433	C - cond	LB	Aerobic	IS	72.00							631.00	0.66					Figure 4-12; Figure 4-13; Figure 4-14
<i>P. aeruginosa</i>	J1385	C - cond	LB	Aerobic	IS	24.00	20.00	1.37	31600.00	1.04	100.00	0.83	1580.00	0.77	50.10	65.00	NaN	NaN	Figure 4-12; Figure 4-13; Figure 4-14

Species	Strain	Electrode Type	Growth Media	Growth Conditions	In situ/ ex situ	Time (Hrs)	Normalised Resistance				Normalised Phase				Raw Phase				Thesis Figure
							Peak		Trough		Peak		Trough		Peak		Trough		
							Freq	Amp	Freq	Amp	Freq	Amp	Freq	Amp	Freq	Amp	Freq	Amp	
<i>P. aeruginosa</i>	J1385	C - cond	LB	Aerobic	IS	24.00					56200.00	0.85							Figure 4-12; Figure 4-13; Figure 4-14
<i>P. aeruginosa</i>	J1385	C - cond	LB	Aerobic	IS	50.00	79.40	1.41	39800.00	1.05	126.00	0.68	1.41	0.56	56.20	52.60	0.71	44.10	Figure 4-12; Figure 4-13; Figure 4-14
<i>P. aeruginosa</i>	J1385	C - cond	LB	Aerobic	IS	50.00							1120.00	0.64					Figure 4-12; Figure 4-13; Figure 4-14
<i>P. aeruginosa</i>	J1385	C - cond	LB	Aerobic	IS	72.00	158.00	1.34	39800.00	1.04	89.10	0.61	1.58	0.56	39.80	48.30	0.79	43.60	Figure 4-12; Figure 4-13; Figure 4-14
<i>P. aeruginosa</i>	J1385	C - cond	LB	Aerobic	IS	72.00							891.00	0.59					Figure 4-12; Figure 4-13; Figure 4-14
<i>P. aeruginosa</i>	J1532	C - cond	LB	Aerobic	IS	24.00	50.10	1.76	39800.00	1.05	NaN	NaN	NaN	NaN	126.00	58.10	NaN	NaN	Figure 4-12; Figure 4-13; Figure 4-14
<i>P. aeruginosa</i>	J1532	C - cond	LB	Aerobic	IS	50.00	126.00	1.45	39800.00	1.02	NaN	NaN	2.82	0.59	20.00	47.90	1.78	46.60	Figure 4-12; Figure 4-13; Figure 4-14



Species	Strain	Electrode Type	Growth Media	Growth Conditions	In situ/ ex situ	Time (Hrs)	Normalised Resistance				Normalised Phase				Raw Phase				Thesis Figure
							Peak		Trough		Peak		Trough		Peak		Trough		
							Freq	Amp	Freq	Amp	Freq	Amp	Freq	Amp	Freq	Amp	Freq	Amp	
<i>P. aeruginosa</i>	J1532	C - cond	LB	Aerobic	IS	72.00	200.00	1.33	39800.00	1.03	15.80	0.60	5.01	0.60	0.36	50.20	3.98	47.60	Figure 4-12; Figure 4-13; Figure 4-14
<i>P. aeruginosa</i>	J1532	C - cond	LB	Aerobic	IS	72.00							631.00	0.58	14.10	48.10			Figure 4-12; Figure 4-13; Figure 4-14